AN INVESTIGATION INTO THERMALLY INDUCED STRUCTURAL MODIFICATIONS IN ISOTACTIC POLYPROPYLENE AND ITS BLENDS WITH AMORPHOUS TERPOLYMERS

A THESIS SUBMITTED BY

Stuart Fyfe Brown B.Sc.

in partial fulfilment of the requirements of

The Council for National Academic Awards

for the award of

DOCTOR OF PHILOSOPHY

Dundee Institute of Technology

1992

This thesis is dedicated to my mum and dad

with love and thanks.

DECLARATION

I hereby declare that the work presented in this thesis was carried out by me at Dundee Institute of Technology, except where due acknowledgement is made, and has not been submitted by me for any other degree.

Signed [redacted]

Date 1/5/92

CONTENTS

CHAPTER 3

CHAPTER 4

CHAPTER 5

CHAPTER 6

ACKNOWLEDGEMENTS

I would like to take this opportunity to pay very special thanks to Dr David A. Ross who as Head of Department in the Molecular and Life Sciences Department has provided me with laboratory facilities in which to complete this reseach. Also as my supervisor he has been a source of untiring enthusiasm, motivation and friendship, as well as providing technical guidance and inspiration throughout this research and, for this, I reiterate my sincere gratitude.

Thanks must also go to my second supervisor Dr David H. Bremner with whom I have had many interesting discussions and who, along with Dr David A. Ross and his wife Lyn, have painstakingly helped in the proof reading of this manuscript and, for that, I thank them.

Special thanks must also be extended to the Tayside Polypropylene Group which consists of Amoco, William Halley Ltd, Scott and Fyfe Ltd and Don and Low Plc, who have helped to fund this work and, in particular, Alexander Mackay, one of the founders of the Group, who has shown an active interest in the project.

Several people have been very helpful in the sharing of their expertise in various disciplines and for this I express my sincere thanks. These include the Chief Technician of the Molecular and Life Sciences Department, Mr Mike G. Black, whose knowledge of the equipment in the Department was of great help on numerous occasions; Mr Harry Staines of the Department of Mathematics and Computer Studies at Dundee Institute of Technology, who provided guidance in the statistical analysis of results; Dr Patrick Tollin and Dr Fred Hubbard of the Department of Physics at the University of Dundee for their guidance in x-ray diffraction methods; Dr Alan Wernick of the Chemistry Department at Napier Polytechnic for use of the hot-stage polarising microscope; Dr Oliver Howarth of the Centre For Nuclear

Magnetic Resonance at the University of Warwick for providing ^{13}C-nmr facilities for the analysis of fractionated polypropylene; and Dr Steve Holding of RAPRA Technology Ltd for providing molecular weight data for various samples using his high temperature GPC equipment.

Finally, I would like to express my very special gratitude to my mum and dad for all their support and tolerance throughout this project and my girlfriend Karen for her encouragement and understanding of the demands that such work had on my time.

AN INVESTIGATION INTO THERMALLY INDUCED STRUCTURAL MODIFICATIONS IN ISOTACTIC POLYPROPYLENE AND ITS BLENDS WITH AMORPHOUS TERPOLYMERS

Stuart Fyfe Brown B.Sc.

ABSTRACT

Isotactic polypropylene undergoes rearrangement of its ternary helical structure when rapidly quenched from the molten state. This is an important area since cooling from the molten state is a fundamental aspect of a typical industrial extrusion process.

Studies were carried out on a range of commercial isotactic polypropylene samples and quench induced structural changes were investigated using FTIR, DSC, x-ray diffraction, SEM and hot-stage polarised microscopy. Results showed clear evidence of induced structural disorder attributable to the formation of conformationally disordered isotactic helices (or smectic phase) which, depending on the degree of quenching, resulted in either a biphasic or triphasic system. Results also showed that differences in the degree of quenching exist between various commercial grade polypropylenes.

DSC studies on the samples quenched rapidly from the molten state revealed the presence of a double melting endotherm. Further DSC investigations using controlled quenching rates *in situ* showed that multiple peaks were caused by progressive reorientation of the metastable disordered phase towards a higher crystalline order, and that they were dependent on both the DSC quench rate and the heating rate subsequent to quenching.

Stepwise downward annealing studies using DSC showed that each step induced crystallite cluster formation which resulted in a discontinuous multiple endothermic melting profile, whose individual peaks occurred at a consistent point above the corresponding temperature of annealing and the relative percentage of the total ΔH_f for each peak in the melting profile was found to be highly dependent on molecular weight and stereoregularity.

Solvent extraction of a particular commercial polypropylene sample yielded fractions which, when characterised by GPC and ^{13}C-nmr, clearly showed that fractionation had been achieved on the basis of molecular weight and stereoregularity. Studies on these fractions using stepwise downward annealing gave insights into the role of molecular weight/stereoregularity in the overall thermal behaviour of polypropylene.

Studies were also carried out on isotactic polypropylene/amorphous terpolymer blends using a similar range of techniques. Results showed a remarkable degree of compatibility in the blends and an "intrinsically determined" morphology dependent on terpolymer structure and blend ratio. The effect of temperature on the infrared spectroscopy of the blends, in particular, showed an interesting relationship between the onset temperature of structural breakdown and the blend composition.

CHAPTER 1

1.0 GENERAL INTRODUCTION TO POLYPROPYLENE

1.0 GENERAL INTRODUCTION TO POLYPROPYLENE

1.1. HISTORY OF POLYPROPYLENE

Polypropylene, one of the world's most widely used and youngest commercial synthetic polymers is the product of modern polymer scientific research. Unlike other widely used polymers such as polyvinyl chloride, polystyrene and the acrylics, it was invented after Staudinger, Mark and Carothers had demonstrated the existence of macromolecules.

The use of the word "polypropylen" was probably first documented in two articles by A.M. Butlerov in 1876 and 1879 in the German publication den Annalen der Chemie[1]. He obtained tetramers and pentamers by the addition of sulphuric acid to propylene[2,3]. At about the same time a French chemist called Prunier obtained a polypropylene polymer which was liquid but which had no practical use.

Although low molecular weight amorphous polypropylene, which had been prepared by the use of boron trifluoride with a hydrogen fluoride activator, was used as a viscosity index improver and as a lubricating oil during the Second World War, no significant advances were made in the development of polypropylene until the late 1940's when C.M Fontana of the Mobil Oil Co. obtained polypropylene having a very broad molecular weight distribution (600 to 830,000). This cationically polymerised polypropylene was produced[5-8] at a temperature of -44°C but due to excessive hydride transfer a highly branched structure was obtained which showed no signs of crystallisation.

Attempts had been made by Breil in Zeigler's laboratory to polymerise propylene but since the pressure did not decrease as dramatically as it did when ethylene was used,

it was concluded that no reaction took place. On this occasion he recorded that "propylene cannot be converted into high molecular weight polypropylene". As a result Zeigler never included polypropylene in any patent applications at that time.

Zeigler attempted to produce polypropylene again in May 1954 using a new reactor. Subsequent to this, however, Wright of Petrochemicals succeeded in producing polypropylene using a pilot plant but because he wrongly assumed that Zeigler had already covered polypropylene in a previous patent, he did not make any application himself.

During this same period Natta, who had been asked by Zeigler to limit his studies to HDPE, directed his assistant Chini to prepare crystalline polypropylene. The date was March 11, 1954. Natta applied for a patent beating Zeigler by just ten days. He published his findings[9] in 1955.

Hogan and Banks of Phillips Petroleum Co., however, had discovered polypropylene at least two years previously whilst working on a project to convert light olefins into high octane fractions in gasoline by dimerisation-trimerisation etc. They were investigating the modification of the NiO-silica-alumina catalyst system with a second transition metal promoter (chromium ion) when something unexpected happened. This discovery was recorded on June 5, 1951 as follows:-

Subject: Synthesis of normally solid polymer from propylene

Earliest Conception Date: June 5 1951

"In the polymerisation of propylene over commonly used catalysts, such as phosphoric acid and nickel on silica-alumina, the polymer produced is liquid and contains little if any solid polymer.

However, it has been discovered that using a catalyst prepared by impregnating silica-alumina with chromia and nickel oxide, a considerable amount of the product is a white solid, and since a low polymerization temperature is used, this solid is no doubt completely olefinic and is therefore a unique solid material. This solid material has a tacky, latex-like nature."

A battle for the patent was to ensue.

1.1.1. Battle For The Patent

In 1958, the U.S. Patent Office had declared an interference proceeding[10] following the initial filing of a Phillips patent application in January 1953 and similar applications by other companies in the early 1950's. This was destined to be long and costly to those involved.

Contesting the patent were Phillips, DuPont, Montecatini, Standard Oil of Indiana, and Hercules (although due to late discovery dates, Hercules was dropped from the interference in 1964).

In 1972, the patent was assigned to Montecatini[11] (now known as Montedison) who were representing Professor Natta of Milan. Phillips, DuPont and Standard Oil of Indiana filed an appeal against this decision which resulted in a Civil Court trial to be held in 1977-78 in the Federal Court of Delaware. This court outlined its decision in a 200 page document that the patent on crystalline polypropylene should be awarded to Hogan and Banks of Phillips[12] in January 1980. In spite of appeals by the losing parties to the Federal Appeals Court in 1982, the decision of the lower court was sustained. The Supreme Court refused to review this decison and on March 15, 1983

U.S Patent 4,376,851 was assigned to Phillips Petroleum Company[13] with a single claim, "Normally solid polypropylene, consisting essentially of recurring propylene units, having a substantial crystalline polypropylene content". It should be stated that the losing parties have appealed once more the latest decision of the court.

The court, then, awarded the patent to Hogan and Banks on the basis that they recognised, in 1951 and 1952, that they had produced polypropylene using a chromic acid - alumina/silica catalyst system and made a patent application describing how the polymer was produced and stated a practical use for it.

1.2 MANUFACTURE OF POLYPROPYLENE

The development of the petrochemical industry is probably the greatest single contributing factor in the growth of the polymer industry with the two industries having a remarkable degree of interdependence.

Polypropylene is by and large a by-product of the petrochemical industry. The abundance of propene and ethylene monomer feedstock from the refinery distillation and cracking of naptha coincided with an ever increasing boom in worldwide polymerisation research. Naptha cracking provides the scientists with the alkene gases which can be used as monomers or intermediates for polymerisation.

The typical manufacturing process for polypropylene involves five main steps. These are outlined in the following sections.

1.2.1 Polymerisation

There are four main ways in which polypropylene can be polymerised. These are described in the following sections.

1.2.1.1 Slurry in Hydrocarbon Process

The slurry in hydrocarbon process was used to produce isotactic polypropylene in 1957 by Montecatini[14]. Polymerisation takes place in an inert hydrocarbon such as hexane or heptane in which the monomer and atactic polymer (by-product) are soluble but in which the isotactic polymer (product) is not. These solvents are chosen on the basis that they will not poison the catalyst or react with it in any way that might be detrimental to the polymerisation.

The polymerisation rate is proportional to the amount of $TiCl_3$ and the monomer concentration[15] and can be controlled by varying temperature and pressure. In this process the dissolution of atactic polymer increases the viscosity and thereby limits the heat transfer in the reactor.

1.2.1.2 Slurry In Liquid Propylene (Bulk) Process

This process differs from the slurry process in so far as the diluent is the propylene monomer itself rather than some other solvent hydrocarbon. In this system the polymer is insoluble in the monomer[16]. Fast rates of polymerisation are obtained in this system where the presence of a liquid monomer and relatively high temperatures requires extremely high pressures. The partial solubility of atactic material in the

liquid monomer makes it possible to separate atactic from isotactic polymer by simple filtration. If the atactic polymer is not adequately removed then the tensile strength of the resultant polymer may be reduced to some extent.

1.2.1.3 Solution Process

In this process it is possible to sustain sufficiently high temperatures so that the polymer product dissolves in the liquid diluent thus eliminating the problem of polymer build-up on the reactor. After the reaction is complete the polymer is precipitated from solution into a non-solvent giving a finely divided polymer product. In the case of polypropylene, cyclohexane can be used as the solvent and by using an alcohol such as methanol as a non-solvent it is possible to accomplish the catalyst deactivation and the removal of catalyst residues simultaneously.

1.2.1.4 Gas Phase Process

A gas-phase, fluidised bed process was developed initially for high density polyethylene in the 1960's and was first commercialised in 1968 at Union Carbide's Seadrift Plant in Texas[4]. This process is known as the Unipol Process.

The first use of this technology for polypropylene polymerisation was in the late 1980's at this same plant. It involves the combination of the Unipol Process with Shell Chemical's high activity catalyst and produces a full range of homopolymers and copolymers.

The system consists of a fluidised-bed reactor, a cycle gas blower and a cycle gas cooler into which catalyst, propylene and other reactants are fed continuously. Granular polypropylene and a small amount of catalyst are situated in a vertical fluidised bed through which monomer gas is circulated. No mechanical stirring is necessary for mixing in this system.

The product is removed in a granular form directly from the reactor. The reaction gas is circulated back to the reactor whilst the resin is discharged and purged of residual hydrocarbons before being removed for pelletisation.

1.2.2 Removal Of Atactic Material

The polymerisation of polypropylene results in a product which is a mixture of atactic and isotactic polymer. End product requirements dictate the amount of atactic material that will be acceptable. In moulding it is possible to use a polypropylene with quite a high atactic content but for products such as fibres and films the high tensile strength associated with high crystallinity material means that the atactic content must be low. It is therefore necessary to remove the undesireable atactic material from the polypropylene. This can be achieved by filtration or centrifugation of the atactic material which has been dissolved in the hydrocarbon reaction medium.

1.2.3 Removal Of Catalyst Residues

Catalyst traces can be detrimental to polymer properties such as heat and light stability, colour, and electrical properties. It is therefore necessary to remove them as far as possible from the polymer and this can be carried out by the deactivation and solubilising of catalyst residues using alcohols, acids, bases or complexing agents[17]. It is important that all of the catalyst residue is treated and to do this effectively the

agent used should be capable of penetrating the polymer. This is necessary, as one which only washed the surface of the polymer would leave a lot of residue within the polymer itself. Agents that are commonly used are methanol and n-butanol which can sufficiently wet the polymer and are relatively inexpensive.

1.2.4 Addition Of Stabilisers

Polypropylene is inherently prone to thermal oxidation and ultraviolet degradation. For this reason it is essential to add antioxidants and UV stabilisers in order to prolong the life of the polymer. Antioxidants such as the phenol alkane type, Topanol CA ([1,1,3-tris-(4-hydroxy-2-methyl-5-t-butylphenyl)] butane) tend to give optimum stability during processing[18]. For protection against exposure to sunlight it is common to use hindered amine stabilisers and nickel compounds.

The choice of stabiliser must be based on its lack of toxicity especially when the polymer is to be used for packaging. Effective light stabilisers must also be chosen carefully especially if the product is to be used in an outdoor environment in a country with a hot and sunny climate. The stabiliser must not react in any way with the processing equipment and in particular must not weaken it by corrosive action.

1.2.5 Polypropylene Pelletising

Polypropylene is usually sold to processors in the form of pellets which contain stabilisers, additives or pigments. This form allows easy storage, conveying and continuous feeding into processing machinery. The polypropylene from the polymerisation reactor is normally in the form of fine powder. This is mixed with the necessary stabilisers and additives which modify its properties. It is then melted, homogenised and extruded into a ribbon or strands before it is granulated.

Granulation either takes place as it cools when emerging from the extruder or after it has been cooled. Different granule sizes can be produced depending on the buyers demands.

1.2.6 Coordination Catalysts and Polymerisation Mechanism

1.2.6.1 Coordination Catalysts

In recent years a large number of polypropylene manufacturers have developed catalyst systems based on the heterogenous catalysts of the type first used by Zeigler and Natta. These are known as coordination catalysts and are capable of being stereoselective towards structure and give high yields.

The basic Zeigler-Natta catalyst is obtained by reducing aluminium metal with titanium chloride according to the redox reaction:-

$$Al + 3TiCl_4 \longrightarrow AlCl_3 . (TiCl_3)_3$$

If these catalysts are ball-milled through conversion of alpha and beta forms of the Al-Ti salt into the less orderly delta form, the activity of the catalyst is increased several fold[19]. The effect is to increase the surface area[20] from a few m^2/g up to 40-60 m^2/g and even to 150 m^2/g resulting in the aforementioned proportional increase of the catalyst activity toward polymerisation.

The continuous development of these catalysts over the years has led to catalysts of improved activity and stereospecificity. Thus the so called second and third generation catalysts have emerged on the polymerisation scene.

Item	Catalyst Generation		
	First	Second	Third
Main Catalyst Co-catalyst	$TiCl_3$ $AlEt_2Cl$	$TiCl_3$ $AlEt_2Cl$	$MgCl_3$ $AlEt_3$
Catalyst Yield (kg) of PP/g of catalyst	0.5 - 2.0	2.0 - 5.0	8.0 - 15.0
Products (%)	88 - 95	95	95
Powder Particle Size Distribution	Broad to Narrow	Narrow	Broad
Average Particle Size Polymer Powder μ	250	250	350

Table 1.0 Information regarding 1st, 2nd and 3rd generation Zeigler-Natta catalysts.

Using first generation catalysts it was necessary to remove catalyst residues and atactic material. This step was simplified after the emergence of the second generation catalysts and is almost completely eliminated when using third generation catalysts.

The third generation catalyst has magnesium chloride as a support. By using intricate prilling techniques the same catalyst can be capable of producing spherically shaped particles thus making it possible to eliminate the last operation of extrusion and pelletisation too. Details of these catalyst systems are shown in Table 1.0.

1.2.6.2 Polymerisation Mechanism

Much work has been undertaken[20] in an attempt to elucidate the chemical nature of the Zeigler-Natta catalysts but despite this the chemistry at the catalyst surface is relatively unknown. The treatment with AlR_2Cl, where R is an alkyl group, is thought to alkylate the surface titanium sites. The active site is assumed to be a monoalkylated titanium(3^+) ion attached to the crystal by Ti-Cl-Ti bridges[21].

The propylene molecule coordinates to the titanium atom adjacent to the Ti-C sigma bond on which the growing polymer chain is attached whilst growth of the chain results from insertion of the coordinated olefin into the Ti-C bond. The proposed site for isotactic polymerisation on the surface of a $TiCl_3$ crystal is shown in Figure 1.0.

The propylene molecule coordinates to the titanium atom adjacent to the Ti-C sigma bond on which the growing polymer chain is attached whilst growth of the chain results from insertion of the coordinated olefin into the Ti-C bond. The proposed site for isotactic polymerisation on the surface of a $TiCl_3$ crystal is shown in Figure 1.0.

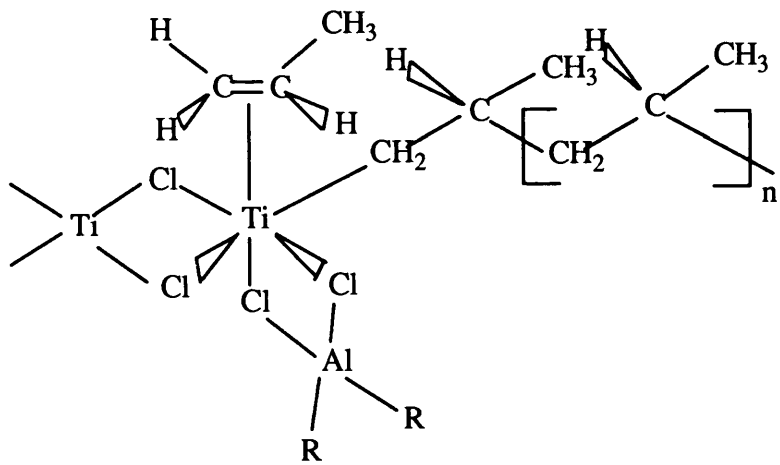

Figure 1.0 Proposed site for isotactic polymerisation of propylene on the surface of a $TiCl_3$ crystal. The growing polymer chain extends to the right.

The remarkable stereoregularity of these propylene polymerisation catalysts is attributed to the steric environment of the active metal centre. Insertion of the propylene molecule at the active site can result in the possibility of two products ie. α-CH_2 product or the α-$CH(CH_3)$ product (see Figure 1.1).

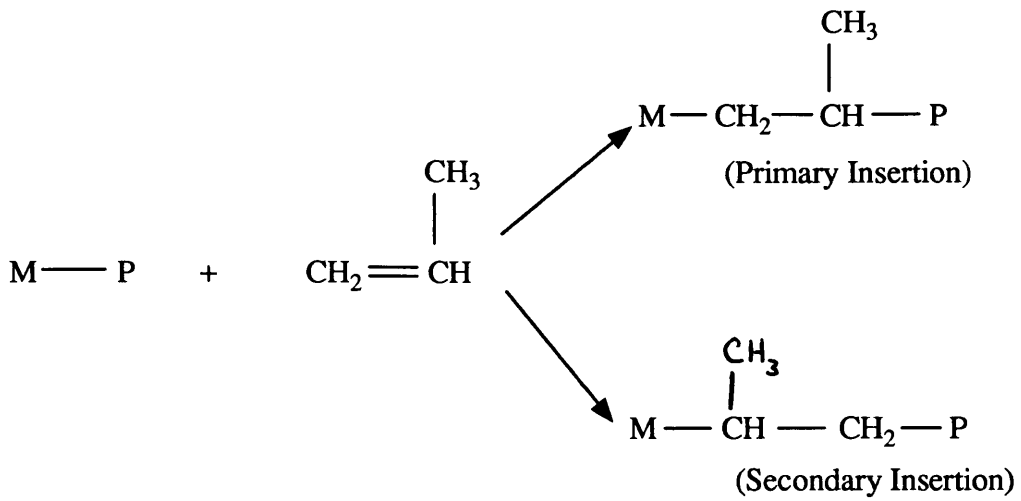

Figure 1.1 Polyinsertion in polypropylene where M is the transition metal and P is the growing chain bonded to M.

These possible forms result from the process of primary or secondary insertion respectively[22]. The α-CH_2 product is sterically less demanding therefore the outcome is more likely to be a polymer chain containing propylene units linked head-to-tail. Four arrangements can result from this head to tail linking of the propylene monomer units (see Figure 1.16).

For the propagation of isotactic polypropylene, the steric environment is very important and must be such that the steric interactions between the methyl group of the propylene and the transition metal ligands are preferentially selective to isotactic orientation of the methyl groups in the growing polymer chain.

The steric properties of the ligands on either side of the transition metal must be different from one another so that the incoming monomer is sterically constrained in such a way that it consistently approaches the activated metal-carbon bond from the same side[22].

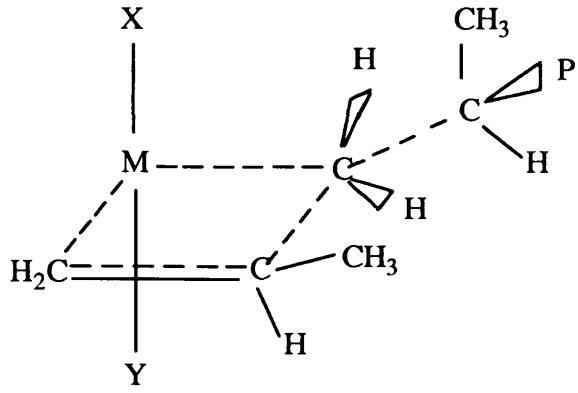

Figure 1.2 Possible transition state complex in the isotactic polymerisation of propylene.

In Figure 1.2 above, it is assumed that the Y-ligand is sterically more demanding than the X-ligand.

The homogenous catalyst system, $VCl_4/AlEt_2Cl$ has been found to favour the syndiotactic polymerisation of polypropylene[23]. It is thought that the mechanism relies on strong methyl-methyl interactions which force the incoming propylene unit into a configuration which is always opposite to the last unit added.

1.3 GENERAL PROCESSING OF POLYPROPYLENE

Polypropylene, being a thermoplastic, has to be heated into the molten state in order to be processed. The melt characteristics of high viscosity yet strongly non- Newtonian behaviour are typical of thermoplastics such as polypropylene. The low power consumption and process temperatures are added attributes when compared to the processing of other materials such as metals[24].

The polymer is altered to the desired shape or form once in the molten state and can only solidify when the heat has been conducted away. The low thermal conductivity of the polymer means that both the product design and the productivity of the process can be quite complex.

Most processing operations involve the use of melt temperatures in the range 210 - 250°C and because of the tendency of polypropylene to oxidise, heating times are normally kept to a minimum[18].

Polymer materials, such as polypropylene, have proved especially amenable to a variety of molding and extrusion techniques. In particular the following principal processing and fabricating operations for thermoplastics now enable products and components of many complex shapes and sizes to be mass produced on a very large scale.

1.3.1 Moulding Techniques

Moulding is one of the oldest known methods of polymer processing[25]. In almost all moulding operations some pressure and heat is applied to make the polymer flow into a preferred form. Dimensional stability, then, is conferred by cooling or further

heating[26]. Because thermoplastics have to be cooled below the melting temperature (T_m) before removal from the mould, it is usually necessary to carry out a sequence of heating, pressurised flow and pressurised cooling.

There are two main types of thermoplastic moulding:-

1.3.1.1 Compression Moulding

This is probably the oldest method of polymer processing, the earliest use being in the early 19th century when Hancock utilised it as a technique for moulding rubber[27].

A compression mould consists of two parts, a female part and a male part which come together when the mould is closed. When temperature and pressure are applied, the material is forced to flow into the cavity where it becomes a homogenous mass. The excess material which ensures that the cavity is properly full is squeezed out between the mating surfaces of the mould in a thin film known as flash which is easily removed once the mould is cooled.

To allow the expulsion of gases or trapped air from the mould, it must be opened for an instant prior to fully closing. If this gaseous matter is not released then the product will possess undesireable qualities associated with porosity. A diagram of a compression mould and press is shown in Figure 1.3.

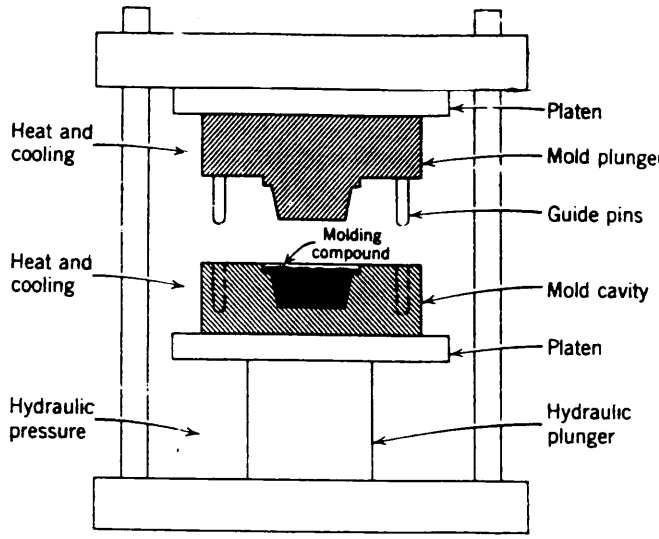

Figure 1.3 Diagram of a compression moulding press and mould.

1.3.1.2 Injection Moulding

Compression moulding of a thermoplastic resin involves heating and then cooling of the mould but such materials are often more efficiently moulded by injection of the molten material into a mould. Injection moulding is a major processing operation for manufacturing plastics and is steadily replacing the more customary compression moulding.

Injection moulding is characterised by a high production rate and a high degree of automation along with a reduction in the amount of scrap[28]. It is a cyclic process whereby the polymer is automatically fed by means of screw or ram along a heated barrel, through the nozzle, sprue, runner system and gate into a mould. This system helps control the distribution of the melt and ensures that flow paths to the farthest points of the mould are approximately equal.

As with compression moulding, provision must be made for the air that the cavity initially contains to be vented. A gap of 25μm width at the edge is generally adequate. Guiding pins on the mould facilitate the correct positioning of the join in order that this venting be carried out.

In order to achieve the balance between minimising the residual stress and maximising the cooling rate, the mould is kept at a constant temperature by circulating either oil or water through cooling channels.

The mould is separated into two halves by the use of an ejector plate on which are situated ejector pins. This ejector plate is automatically activated when the mould slightly opens and is retracted when the mould closes. Stripper rings may be used to distribute the force produced by ejector pins. This helps to minimise the risk of mould buckling, especially in thin-walled moulds which are particularly susceptible to distortion of this kind. Figure 1.4 shows the main components of a compression mould.

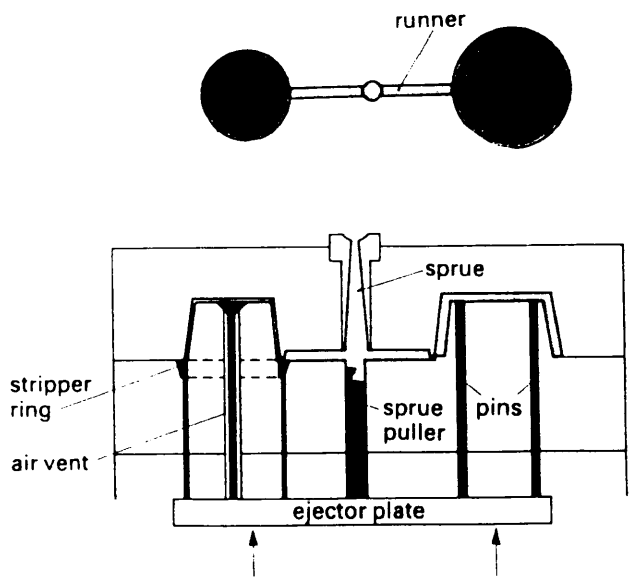

Figure 1.4 Diagram showing components of an injection mould.

Subsequent to this process the parts of the mould are clamped together again, a further quantity of molten material is charged and the cycle is repeated. The success of the whole process is highly influenced by the melt rheology of the material as it will only fill the complete cavity if it possesses the appropriate flow properties during the moulding cycle. This, however, can pose a dilemma as although low melt viscosity is desirable, in order to achieve it use of high injection temperatures is necessary which lead to longer cycle times and lower production rates. Moulding and product design therefore must be planned in such a manner as to take into account the polymer flow patterns, orientation and crystallisation effects, all of which contribute to the final product properties.

The solution to this problem requires information from several scientific and engineering disciplines including machine and mould design, fluid mechanics, rheology, reaction engineering, heat transfer, polymer science and process control[28].

The machinery used in injection moulding processing of thermoplastics falls into three categories:-

1. The ram injection type
2. The in-line screw injection type
3. The out-line screw injection type

Schematic daigrams of these machines are shown in Figure 1.5.

(a)

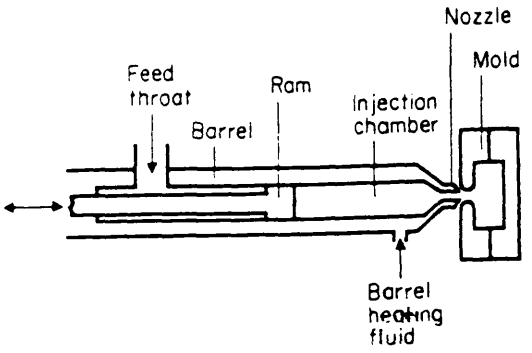

(b)

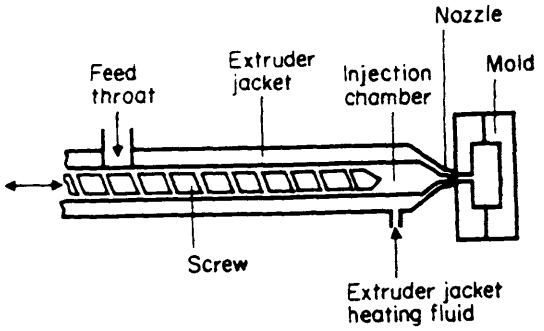

(c)

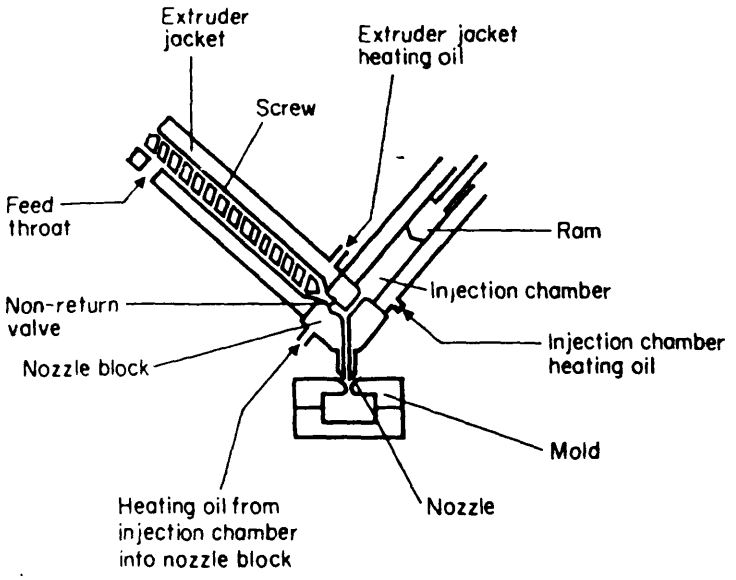

Figure 1.5 Schematic diagram of (a) ram injection extruder (b) in-line screw injection extruder and (c) out-line screw extruder.

Ram type machines are becoming less common nowadays due to polymer homogenising difficulties and lack of uniform temperature distribution. It is also difficult to meter accurately the shot size due to the fact that metering is on a volume basis and any variation in the density of the material will alter the shot weight.

Other problems associated with the ram type are that in compressing the material which is in a variety of forms (solid granules/viscous melt) the pressure at the nozzle can vary quite considerably from cycle to cycle. In some systems a "torpedo" is used to split up the mass of material in the barrel and improve the heat transfer. This can also cause a significant pressure drop in the system. The flow properties of the melt are pressure sensitive and because of this these erratic inconsistencies in pressure tend to amplify the problem of variability in successful uniform filling of the mould.

Using the in-line screw type of machine or preferably the out-line screw type, these problems can be overcome. In the latter, raw material is fed into the first barrel where it is plasticised by an extruder screw and fed through a non-return valve into the other barrel. A plunger in the second barrel then forces the melt through a nozzle and into the mould. This results in overall superior homogenisation because the melt has to pass through a small opening connecting the two barrels. The shot size can be metered more accurately since the volume of material fed to the second barrel can be controlled by a limit switch on its plunger. There is also no need for the torpedo on the main injection cylinder.

Injection moulding, then, is quite versatile and any three dimensional shape that can be extracted from a steel cavity when it opens into two or more parts can be made by this process. Although this excludes hollow or re-entrant parts, many difficult features

such as internal threads[24] or intersecting holes can be made using unscrewing or sliding cores attatched to the main mould.

1.3.2 Extrusion Techniques

Extrusion is defined[28] as "a continuous process in which polymeric materials, through heat or reaction and deformation, are changed to a viscous form, mixed, pumped, pressurised and shaped."

Although the process will vary depending on which type of product is being made, in general it consists of feeding the polymer (usually in the granular form) from a hopper into a heated barrel where a screw conveyor known as the extruder carries the material forward, compacting, compressing and melting it with the aid of external heaters and the friction of the viscous flow. The resultant melt is then forced under pressure through a screen pack and breaker plate which is situated between the screw and die and which filters out dirt and unfused polymer lumps from the melt. Ultimately the melt is extruded through a shaped die into the desired form ie. sheet, tube, rod, or perhaps an extrusion of more complicated form. On its exit from the die the melt is quenched either by use of chill rollers, water quench tank or air cooling. This solidifies the polymer and gives it some degree of dimensional stability making it manageable in order that other operations can be carried out further on in the process.

1.3.2.1 Importance Of Screw Design

It is well known that polymer melts do not behave as Newtonian fluids and the rheological behaviour of polypropylene is very complex. It is necessary to optimise the screw design in order to obtain the best mixing and homogenisation of the melt. This is because most of the energy that melts the thermoplastic during extrusion results from mechanical work on the material.

In this section two screw types will be discussed, the Conventional Archimedean Screw and the Barrier Flighted Screw.

(a) The Conventional Screw Type

The start of melting in an extrusion process is determined by screw geometry, operating conditions and physical properties of the polymer. The polymer is carried through the solids conveying section from the hopper by the motion of the rotating screw. It becomes increasingly compressed and compacted together and the resultant friction and conducted heat form a melt on top of the packed polymer known as the gel point. This is a noteable point as it is where the pressure first begins to rise rapidly in the extruder.

Both solid and melted polymer co-exist along the length of the screw. The situation inside the barrel, then, is one of a solid bed of polymer adjacent to the screw on the low pressure side of the channel, a melt pool of polymer on the high pressure side of the channel and a film of melted polymer which is mainly in the flight clearance and whose thickness increases along the channel as more and more solid polymer is melted off the solid bed.

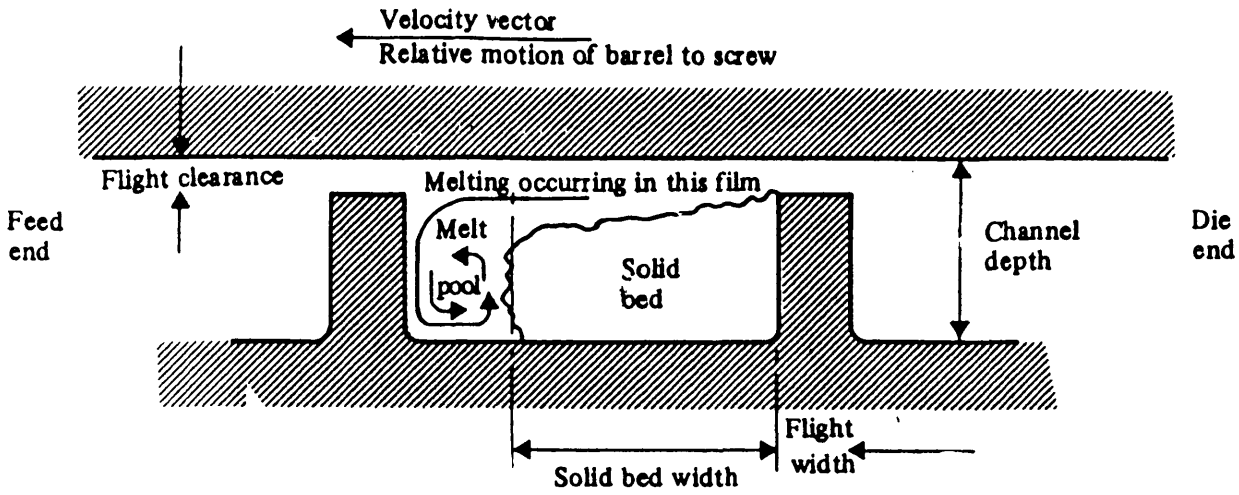

Figure 1.6 Schematic diagram showing melting of the polymer in a conventional screw.

The melt pool gradually increases in volume as the solid material is melted and the melt pool pressure forces the solid bed to the low pressure side of the channel. If melting of the solid bed is incomplete in the extruder then solid material will reach the die head and cause undesireable fluctuations of output, pressure and melt temperature.

If the channel depth is reduced gradually over the melting section of the screw it is possible to improve the rate of melting of material ie. the solid bed material is pushed against the heated barrel wall which, along with the shearing action of the screw and friction within the solid, rapidly decreases the amount of solid bed material as it is spread over the gradually increasing screw width. If, however, the channel width becomes too small, this can lead to fracturing of the solid due to excess melt pool pressure. This can cause large reductions in the melting rate as it now becomes dependent on thermal diffusivity which in turn means that it is possible for solid material to enter the screw.

The conventional screw design has some associated disadvantages. Firstly the melting rate determines the output from the extruder which means that less solid material is able to come into contact with the barrel wall as the material moves down the channel. This leads to a decrease in the melting rate in the later sections of the screw. Also, fracture of the solid bed tends to occur in the later sections of the screw due to excess pool pressure. This in turn causes fluctuations in output and temperature in the metering zone which can be transmitted to the die. A schematic diagram of the conventional screw is shown in Figure 1.6.

(b) Barrier Flighted Screws

The barrier flighted screws have a flight running along the entire length of the melting section. Only molten material can pass over the small clearance and therefore the solid material can no longer mix with the molten material and interfere with the quality of the extrudate. The solids conveying section is designed and operates in the same way as that of a conventional screw.

There are two types of barrier flighted screws, namely the parallel and spiral barrier screws.

(i) Parallel Barrier

The parallel barrier screw melting section is designed so as to keep the melt pool and the solid bed materials apart by use of a secondary flight. The solid bed channel becomes more and more shallow until it has a depth equal to that of the secondary flight clearance at the end of the melting zone where it is blended into the metering zone of the screw. On the other hand the secondary melt channel progressively becomes deeper until it reaches the end of the melting zone where it is blended into the metering zone of the screw.

The secondary flight clearance is designed in a way which allows the melt film formed at the solid bed/hot barrel wall interface to pass over the flight into the next melt channel. The solid material remains in the main channel whilst the melt material moves down the channel. The process continues as fresh material comes into contact with the barrel wall. During this process the solids channel, melt channel, main flight and secondary flight widths remain constant whilst the melt channel depth is increased at such a rate as to accommodate the increasing volume of the melted material. A schematic diagram of a parallel barrier screw is shown in Figure 1.7.

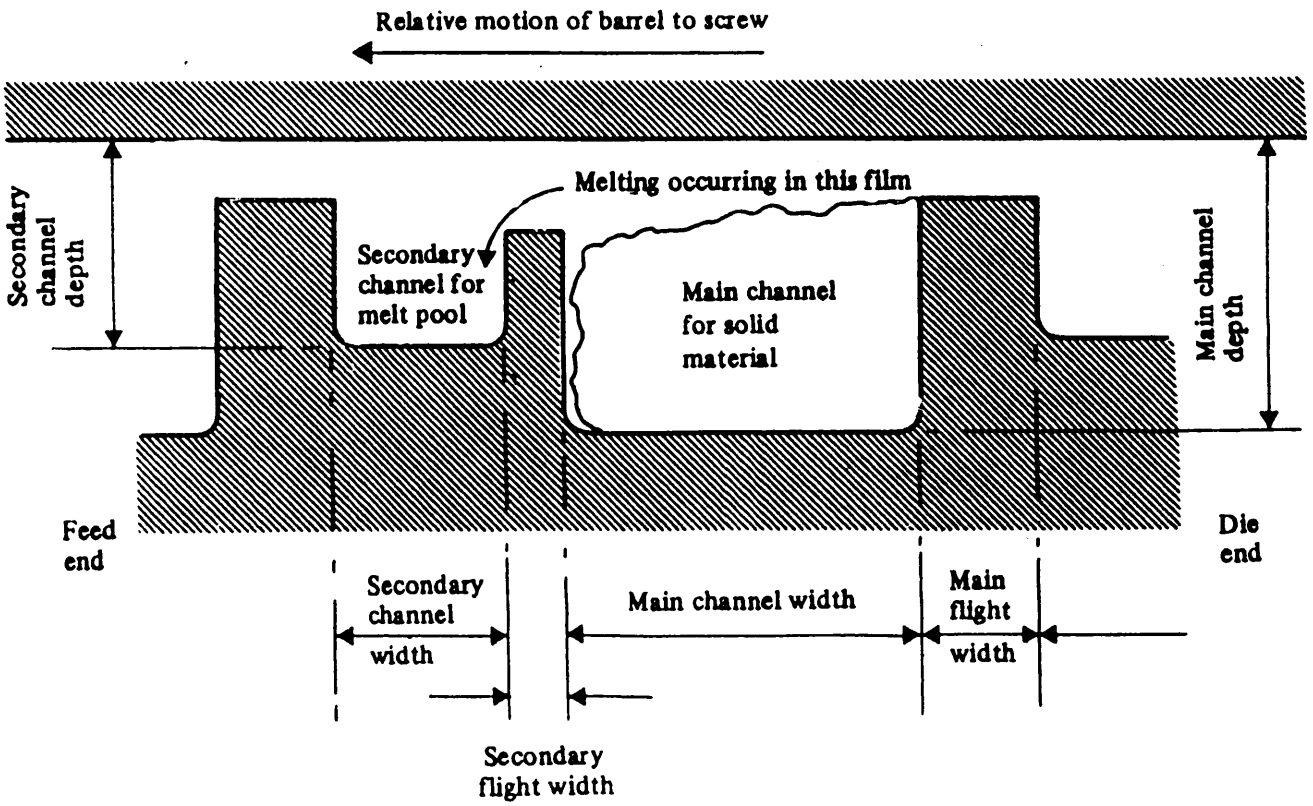

Figure 1.7 Schematic diagram showing polymer melting in a parallel barrier screw.

(ii) Spiral Barrier

The spiral barrier is basically a secondary flight which starts near to the gel point and finishes when melting is assumed to be complete. As with the parallel barrier, the solids conveying method is similar to that of the conventional screw. The design is also similar to the parallel barrier in that it works on the principle of separating the solid and molten material allowing only molten material to reach the metering zone. The melt film is formed at the solid bed material/hot barrel wall interface and is dragged across the channel by the relative motion of the rotating screw and the barrel. The spiral barrier allows the melt film to pass and be collected in the following channel aided by the scraping action of the main flight. The solids channel, as before, becomes progressively narrow whilst the melt channel becomes increasingly wider until it approaches the same width as the screw channel.

The spiral barrier flight should reduce the tendency of the solid bed to fracture and will also allow an increase in output by tending to retain solid material within the melting section of the screw. This enables the use of higher speeds before the onset of surging than in conventional screws.

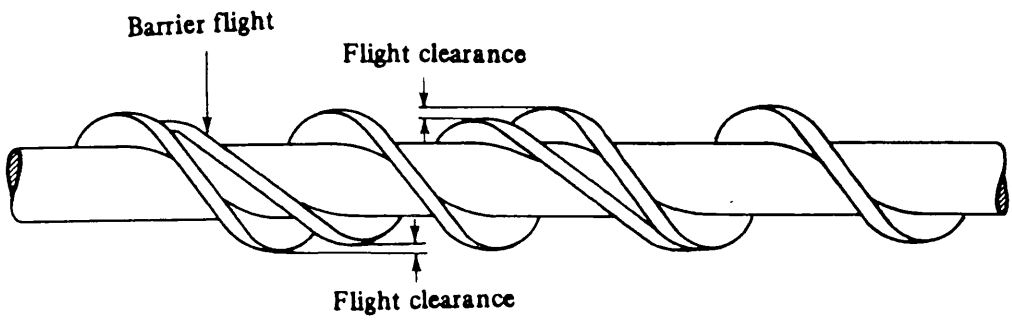

Figure 1.8 Schematic diagram of a spiral barrier

It does have its disadvantages though because as the melting proceeds, the area of melt pool contact with the barrel wall increases and this can lead to excess shear causing undesirable temperature increases in the melt pool temperature. A schematic diagram of a spiral barrier screw is shown in Figure 1.8.

1.3.2.2 Slit-Film Extrusion Process

Slit-film extrusion is an example of a commonly used process in the production of polypropylene fibres and twines. After extrusion the polymer melt enters the die head through a small hole about the size of a one pence piece. The pressure from the extruder enables the polymer to spread across the die face where it is forced out of the die lips. Figure 1.9 shows a diagram of a flat die for tape extrusion.

(a) Chill Rolls

As the extrudate exits the die head it is wound onto the chill rolls (or in some cases into a water quench bath). The chill rolls are highly polished rollers which are kept cold by circulating water at a fast rate through them. They should generally be as cold as possible in order to produce maximum cooling at big temperature differences. This is necessary as the cooling of the polymer determines the flatness of the film and therefore must be uniform[29]. The high speed flow of water helps to minimise temperature differences along the chill roll surface.

At the back of the chill roll is the air knife. This blows air onto the film and ensures that the film web passes the same cooling distance on the chill roll. This is essential because it facilitates the absolute flatness of the film. The air knife (Figure 1.10) also blows air onto the edges of the melt and fixes the melt to the roll at the edges therefore preventing shrinkage.

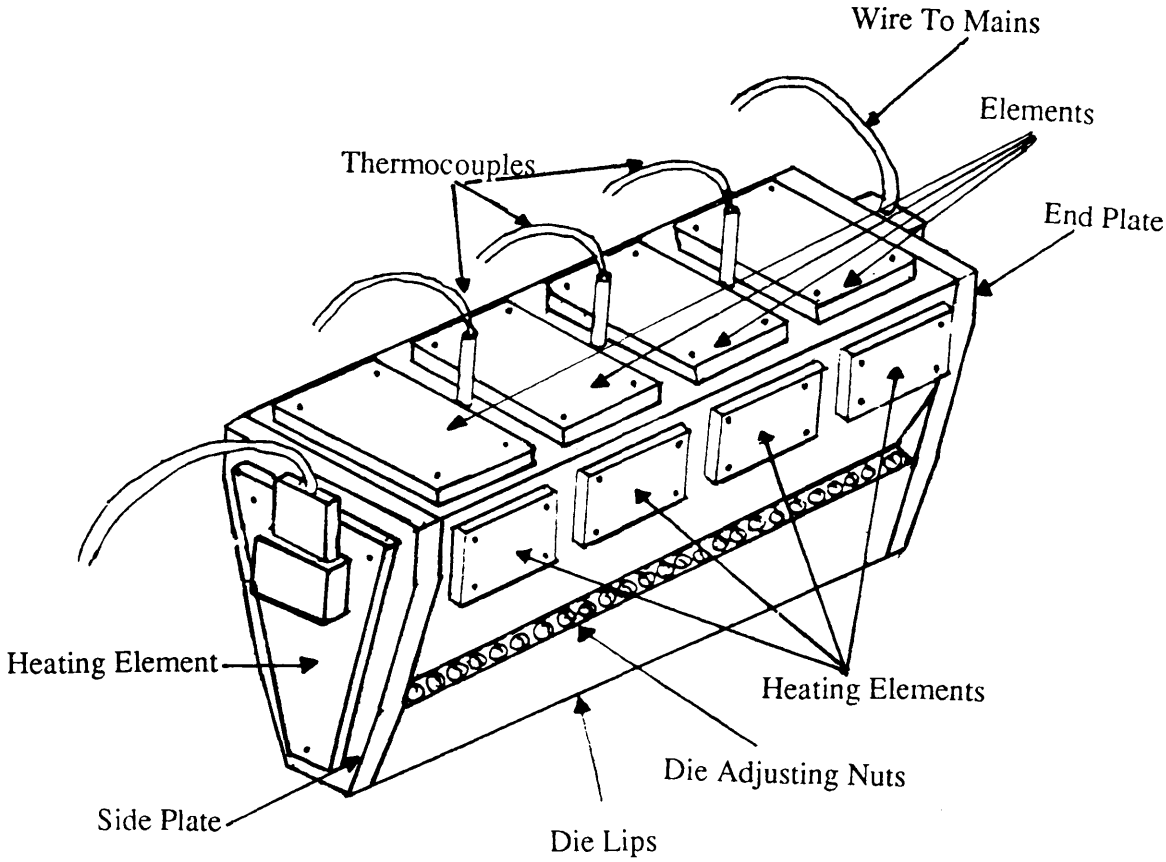

Figure 1.9 Schematic diagram of flat die in the extrusion process.

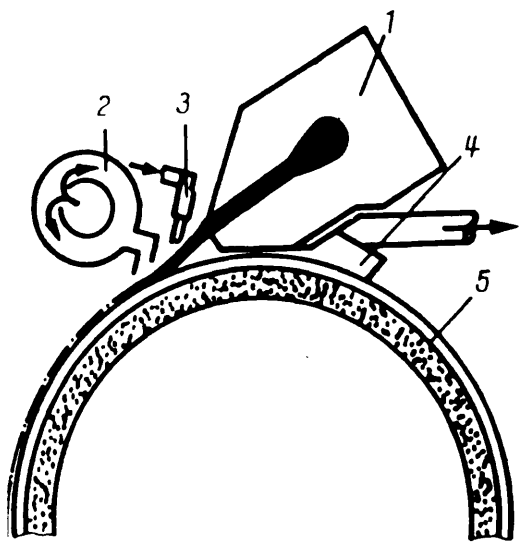

Figure 1.10 Schematic diagram showing the arrangement of air knives. 1. Slit die; 2. Air knives; 3. Air nozzles; 4. Suction nozzles; and 5. Chill roll.

The advantage of chill rolls over water quench baths is that the only time water can get onto the sheet and cause the tape to become curled or lumpy is if the chill rolls are sufficiently cold to induce condensation. On the other hand, if the circulating water is not cold enough or the circulating system is blocked, the film will become sticky and hot causing snarl at blades and/or breakages further along the process line.

(b) Slitting And Drawing

The unit consists of cutting blades being exactly the same distance between each other, typically of 8 -10mm. These blades cut the sheet into individual tapes. Each tape is separated by a comb just before the first draw stand. At the front of each draw stand just under the leading roll with a nip roll on top there is an aspirator which is continuously on throughout the production. Its role is to suck in any tapes that have suffered breakages and feed them to waste or to a shredding unit from which they can be fed back into the hopper for reprocessing. A diagram of the slitting unit is shown in Figure 1.11.

The draw rolls stretch the tapes causing molecular orientation which give the tape the desired mechanical properties. This also regulates the tex of the material (weight in grams of 1000 metres) therefore if the draw roll speed is increased the tex of the material will decrease and vice versa. The draw ratios for polypropylene tapes are typically between 6 and 9:1. The tapes are then heated by passing them through an oven. As efficiency of heat transfer in the polymer is very low, heating zones are often rather long and occupy considerable floor space. The tapes also must be carried unsupported perhaps over several metres during the critical drawing period. A diagram of the draw rollers and oven is shown in Figure 1.12.

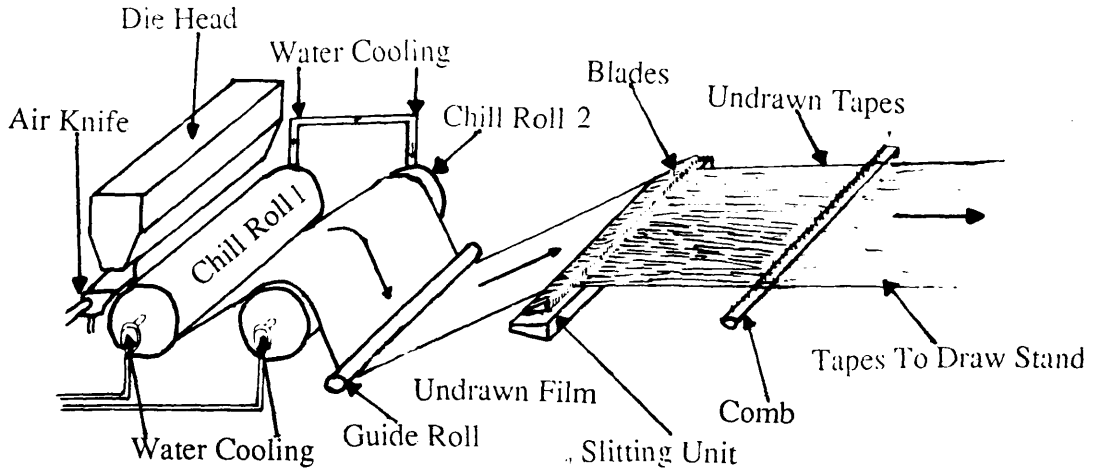

Figure 1.11 Diagram showing tape slitting unit.

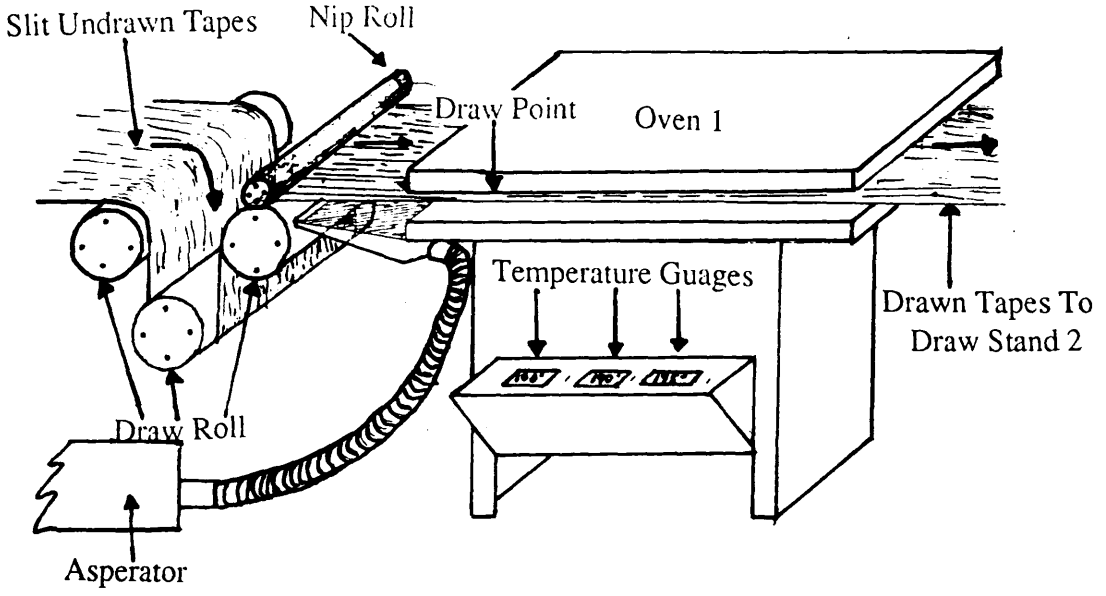

Figure 1.12 Diagram showing the draw roller and oven.

An alternative technique is to heat the tapes by heating the rolls themselves. The temperature of the rolls may be controlled accurately and drawing may be carried out more efficiently and in a smaller space than say an oven. The comparative capital costs of these heated rolls, however, may be high.

As the tape leaves draw stand one and passes through the oven it enters draw stand two which is set at a higher speed. This variation in roll speed stretches the tape from a width of circa 8 mm to circa 3 mm. The tape then passes into yet another oven, and onto the final draw stand from which it is passed onto the winders.

(c) Fibrillation Of The Tapes

An added feature to this process is that a fibrillator (Figure 1.13(a)) can be fitted between the second draw stand and oven. The tapes run through a nip roll and into the pin roll which scratches the tape so as to cut small slits in it (Figure 1.13(b)). They then pass through a second set of nip rolls before entering the oven and continuing onto the last draw stand (output rolls).

The degree of fibrillation is determined by the linear speed of the film, the roll speed and the depth of penetration. To make textile fibre of uniform fibril size the spacing of the teeth have to be of controlled configuration. Fibrillation of tape has the effect of adding to the tenacity of the tape and the product is often used in secondary carpet backings.

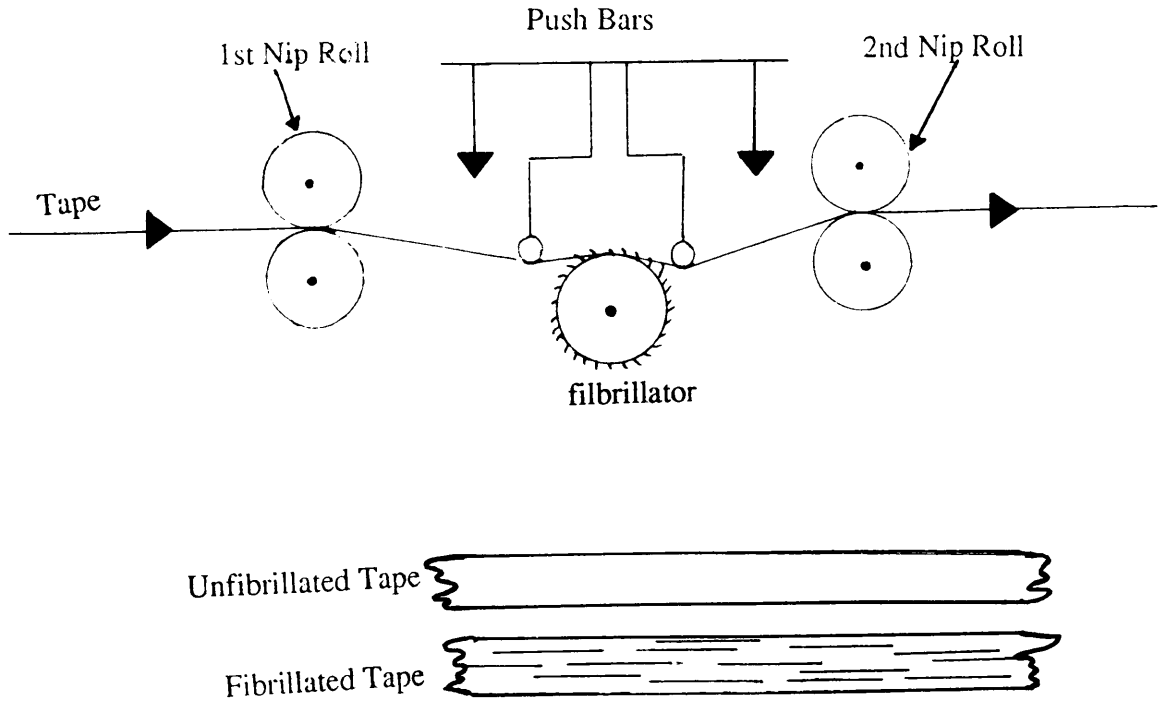

Figure 1.13 Diagram showing the fibrillator and fibrillated tape.

(d) Wind-Up

The wind-up mechanism consists of loading the tape or fibre onto spools or reels which measure between 300 and 600 mm in diameter. The machinery is normally automated and programmable so that it can be adapted to the type of product being produced. The film should be wound at the expected storage temperature to avoid shrinkage or post-crystallisation problems. It is not uncommon for some producers to store the wound up material in large annealing ovens before it is sold and distributed.

1.3.2.3 Blown Film Extrusion

Blown film extrusion is another method of processing polypropylene into sheet form which can subsequently undergo additional treatment such as slitting and fibrillation etc. in order to transform it into the desired end product.

In this process the molten polymer is extruded as before except in this instance it is forced through a ring shaped annular die around a mandrel. The melt rises vertically and is expanded circumferentially by the rising air pressure. The bubble is sealed at one end by the mandrel and at the other end by a nip roll.

The polymer is generally cooled by the use of air jets which are situated below the bubble. It can also be cooled using water in which case the molten polymer is extruded vertically downwards rather than upwards so that the water can run down the film.

The extruded melt is clear in appearance before it cools. As it cools it crystallises and becomes cloudy. The transition line between the molten (clear) and crystalline (cloudy) material is known as the "frost line".

Blown film production is an example of biaxial tensile flow. This occurs as the polymer is stretched in two dimensions with the air bubble acting to orientate in the hoop direction whilst the action of the nip roll orientates the film in the machine direction thus giving the tape desirable mechanical properties. In the manufacture of flat extruded tape, biaxial orientation can only be carried out using hooks inside a temperature controlled oven in which a widening and a drawing tension can be exerted but this type of technology can be expensive to install.

The blow up ratio (ie bubble diameter: die diameter) can be as high as 4 or 5:1 but more typically for polypropylene[26] is about 2:1. The greater the ratio then the further the film travels before being properly cooled and there is also a further decrease in molecular orientation produced inside the die. These factors can lead to deteriorations in the mechanical properties of the film. A schematic diagram of the blown-film extrusion process is shown in Figure 1.14.

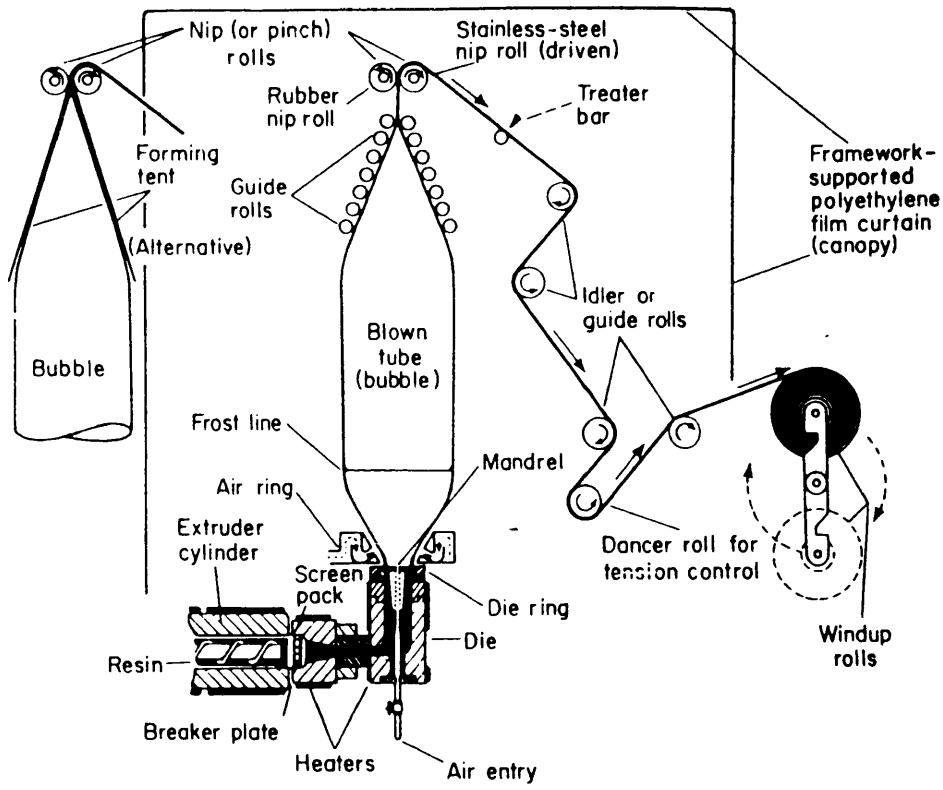

Figure 1.14 Schematic diagram of the blown-film extrusion process.

1.3.3 Other Forms Of Polypropylene Processing And Fabrication

Although the main forms of polypropylene processing have been discussed, it is a very versatile material and can be processed in many different ways. Some of these are discussed briefly below:-

1.3.3.1 Blow Moulding

This type of extrusion is used to make hollow articles. The continuous tubing is blown vertically downward out of an annular nozzle and into a mould[30]. In this type of moulding it is also possible to use an injection moulding machine rather than extruding the polymer. This is known as injection blow moulding.

1.3.3.2 Rotational Moulding

Used to mould large hollow objects, this process is more laborious than blow moulding. A powder is charged into the mould where it is melted. The mould is then biaxally rotated[25]. This gives the inside walls of the mould a uniform polymer coating. The mould is then cooled, opened and the solid, hollow object removed.

1.3.3.3 Thermoforming

In this process softened polymer is sucked or air pressurised into the male or female mould[31]. Again, the mould is cooled, opened and the finished article removed.

1.3.3.4 Calendering

Continuous sheets of polymer are manufactured using this method[25]. Thick sheets are passed under pressure through pairs of highly polished rolls. Temperature, pressure and rotation speed are carefully monitored. Different surface finishes can be generated using this technique ie. high gloss finishes, embossed designs and marbling.

1.3.3.5 Sintering

Here the polymer is compressed into a sinter under high pressure and then heated in such a way as to melt only the surface layers[30]. The polymer particles coalesce and the finished article usually contains porous channels. They can be used as filter supports or as products requiring large surface areas.

1.3.3.6 Welding

Plastics tend to be amenable to welding due to their low melting characteristics. The polymer is softened until tacky and then two surfaces are brought together e.g. plastic tubing. Welding can occur between two polymers (autogenous welding) where it forms its own seam, with the welded seam of another material (heterogenous welding) or by friction welding where the melting is encouraged by the friction and pressure applied to the two surfaces being welded[30].

1.3.3.7 Machining

Turning, drilling, grinding, milling and planing can also be applied to thermoplastics[31] but because of the relatively low melting temperatures, low thermal conductivies and low moduli of polymeric materials it is unfortunately quite easy to deform the material with the cutting tool.

1.4 POLYPROPYLENE STRUCTURE

1.4.1 Stereoregularity

In the growing vinyl polymer chain three bonds of the carbon atom at the radical end are in one plane and the unpaired electron can be described as being on either side of the plane. Therefore any incoming monomer unit can approach the radical from either side of this plane (Figure 1.15).

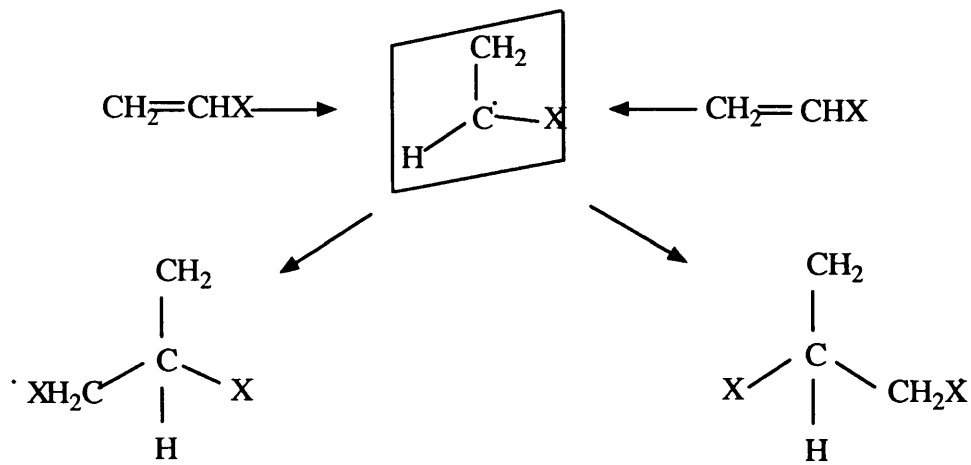

Figure 1.15 Addition Polymerisation: Formation Of Asymmetric Centres.

Once the incoming monomer has been attached, the carbon atom which was planar in the radical becomes the centre of a tetrahedron and has four different groups attached to it. It is thus said to be an asymmetric carbon atom. The two products in this case are the same and are actually mirror images or optical isomers[32].

In 1932 Staudinger[33] suggested that polymers of monosubstituted ethylene (or vinyl polymers) such as polystyrene and poly (vinyl acetate) lacked crystallinity due to the irregularity of configuration in these asymmetric atoms. When Alfry and

co-workers[34] polymerised styrene at various temperatures, the resultant fractions were found to differ in physical properties. These differences were attributed by Huggins[35] to the different configuration of the asymmetric atoms.

Schildknecht and co-workers[36,37] noted that when isobutyl vinyl ether was polymerised slowly and at low temperatures in the presence of boron trifluoride etherate, the resultant polymer was more brittle and possessed crystallinity. This increased crystallinity was attributed to enhanced ordering in the configuration although the nature of the orderly arrangement was not clear at the time.

Probably the most significant development in the theory of polymer regularity came in 1955 when Natta and co-workers[9,38-40] in Milan, Italy published a series of articles detailing examinations carried out on polymers derived from propylene by the x-ray diffraction technique. They found that a few of the polymers showed a much higher regularity in their structure than the rest. This occurred mainly in those which were prepared from the monomer using an aluminium trialkyl-titanium chloride catalyst (otherwise known as a Zeigler catalyst after its discoverer Karl Zeigler of Muelheim, Germany) or by means of a chromium trioxide-silica alumima catalyst.

Natta distinguished four main types of stereoregular polymer which can be described by means of Fischer projection. Another way of representing these forms and which is probably the easiest way to describe the difference in regularity is by taking the polymer and stretching out all the chains. By doing this it is easy to see how the methyl substituent lies above or below the plane with respect to nearest neighbour methyl groups. Both means of illustration of the different tactic forms are shown in Figure 1.16.

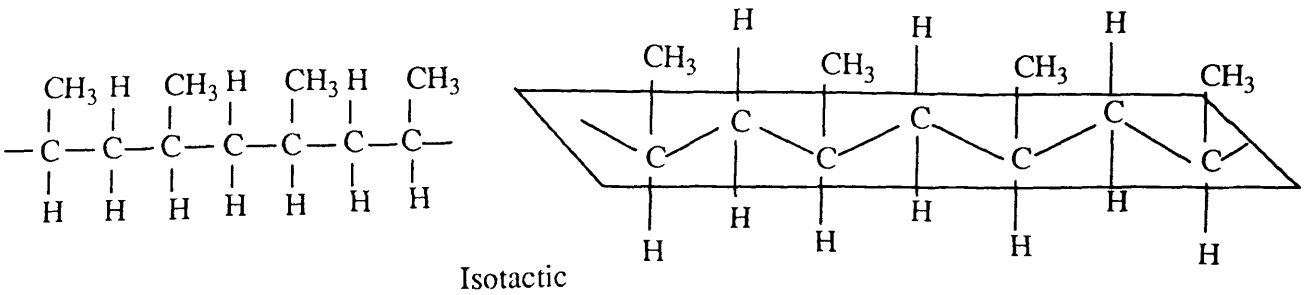

Isotactic

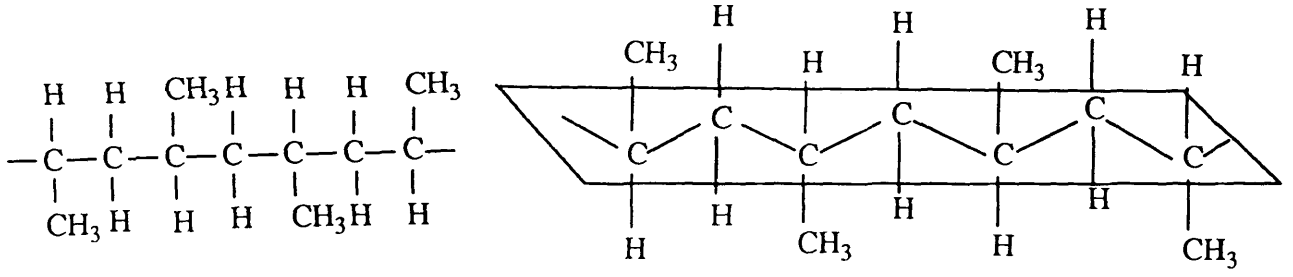

Syndiotactic

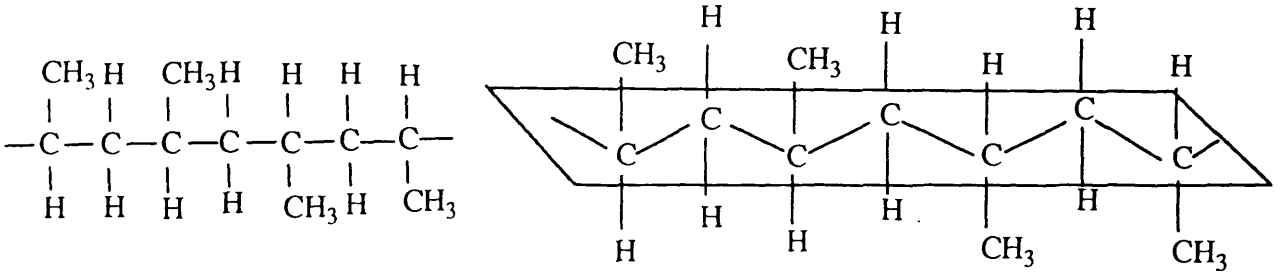

Stereoblock

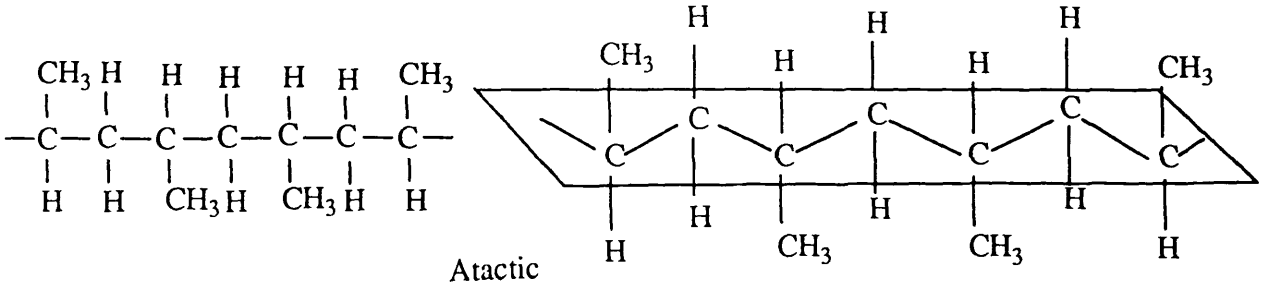

Atactic

Fischer Projection

Planar Representation

Figure 1.16 Schematic representation of tactic forms in polypropylene.

If all the methyl (or R groups) on the alternate asymmetric carbon atoms are on the same side of the plane then the polymer is said to be *isotactic*. If the methyl (or R groups) are alternating on either side of the plane then it is said to be *syndiotactic*. If the methyl (or R groups) are arranged at random on either side of the plane then it is said to be *atactic* and if the methyl (or R groups) are in isotactic blocks on either side of the plane then they are called *stereoblock* polymers.

On the advice of his wife, Natta used the term "tacticity" to describe the configuration of these polymers. The term "tactic" is taken from the Greek word "tactikos" meaning "placed in order". The prefixes "iso", "syndio" and "a" mean "same", "two together" and "without" respectively[41].

Strictly speaking the tertiary carbon atoms in polyolefin chains are not asymmetric in the sense that a simple organic molecule possesses asymmetry because two of their substituents are similarly built and consist of practically infinite polymer sequences[20]. Thus, although the specification if the generally accepted symbols R and S cannot be directly applied to these pseudo asymmetric atoms, using D and L to designate configuration of tertiary carbon atoms in polyolefin chains is common practice. It should be stressed that no particular meaning is associated with this designation other than to distinguish between similarly situated substituents. In the light of this the various forms would be recognised as follows:-

Isotactic - DDDDDD or LLLLLL...
Syndiotactic - DLDLDLDL...
Atactic - DLDDLLLDLLDDDDDLLDDLLL...
Stereoblock - DDDDLLLLDDDDLLLL...

The effect of stereoregularity on properties is striking and in general an increase in tacticity coincides with a marked increase in crystallinity. Thus highly isotactic polymers are often brittle, high melting solids whereas atactic polymers are soft, rubbery, low melting solids or even syrupy liquids.

Instead of being entirely isotactic or entirely syndiotactic or completely atactic it is likely that a polymer will have segments of considerable length which are isotactic and which are alternating with segments which are atactic. Similarly, syndiotactic and atactic or syndiotactic and isotactic may occur in the same polymer.

1.4.2 Conformation

Conformational aspects of any polymer in the crystalline state are highly dependent on chain configuration. The expression "conformation" is always used with respect to a single bond and refers to arrangements related to rotation about this single primary bond[30]. Such conformations may also be called microconformations. In a macromolecule there are many microconformations and hence the macromolecule adopts an overall macroconformation which in turn determines the shape of the molecule.

Configuration, on the other hand, refers to arrangements fixed by chemical bonding which cannot be altered except through primary bond breaking[41]. Terms such as "head to tail", "d and l" and "cis and trans" refer to the configuration of a chemical species. Polymer properties are equally dependent on both conformation and configuration.

1.4.2.1 Geometrical Equivalence

Natta and co-workers[42,43] postulated that there is geometric equivalence of structural units along a tactic chain with regard to an axis which allows us to define exactly the possible types of geometrical symmetry that a linear molecule may achieve in the crystalline state.

Factors determining the conformation in the crystalline state can be classified into two kinds, the intermolecular effect (the way in which the chains are packed) and the intramolecular effect (interactions between atoms in the same chain)[44].

In isotactic polypropylene there are at least three different crystalline modifications (α, β, γ)[45] all containing 3_1 helices and having the same value of chain axis but different modes of packing of the chains. Of these phases, the α-form is the most stable crystalline phase and also the most widely studied.

Syndiotactic polypropylene has the 4_1 conformation. It exhibits local symmetry[45] with each structural unit being repeated into the next one by a twofold axis centred on a CH_2 group perpendicular to the screw axis. Figure 1.17 shows the helical forms of both isotactic and syndiotactic polypropylene.

The conformations 3_1 and 4_1 are so called because in isotactic and syndiotactic polypropylene it takes three and four propylene monomeric units respectively to complete one turn of the helix.

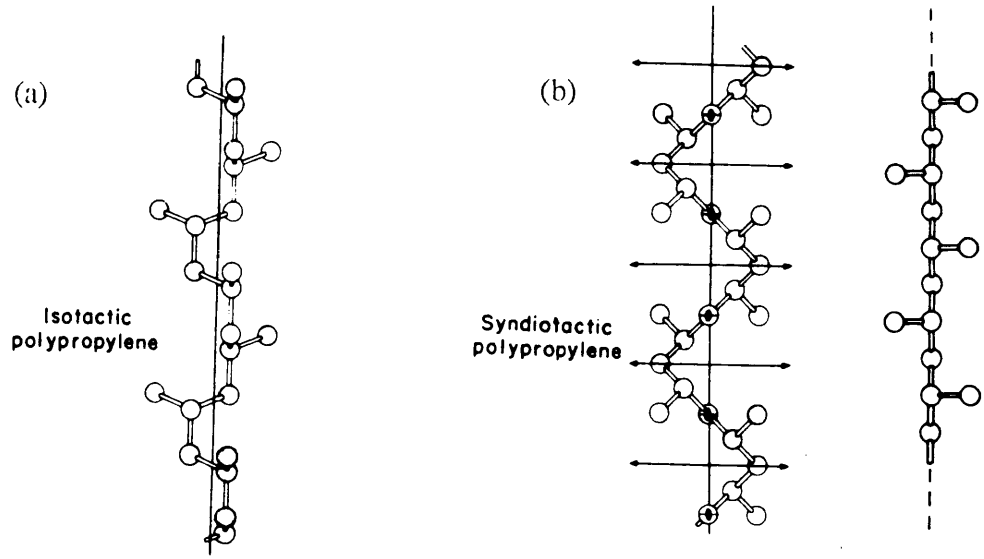

Figure 1.17 Diagram showing (a) the 3_1 helix in isotactic polypropylene and (b) the 4_1 helix in syndiotactic polypropylene.

1.4.2.2 Mode Of Packing Of Polymer Chains

The close packing principle states that if the cell and symmetry are given then the packing of the molecules can be found from the condition of equality of intermolecular distances of atoms of one kind. This is a consequence of minimum free energy.

Provided that distances between neighbouring atoms of different molecules cannot become less than the van der Waals distances then the close packing principle implies that the minima in the multi-dimensional energy surface are close to the minima of the multi-dimensional volume surface[45].

As far as polymers are concerned the principle of close packing becomes easier to apply than in the case of the low molecular weight organic compounds. This problem is made easier due to the following simplifications:-

1. The known chain conformation allows the determination of the structure along at least one of the identity periods of the crystal ie. the chain axis.

2. The symmetry elements of an isolated chain which are allowed in a crystal are preserved. This situation arises, for example, when atoms which belong to different structural units of the same chain (but which are geometrically equivalent) can be matched with corresponding atoms belonging to neighbouring chains.

1.4.3 Role Of Molecular Weight Distribution

Most of the unique properties associated with macromolecules stem from the fact that they have a distribution of exceptionally high molecular weights around an average value. Although factors such as molecular flexibility, interchain hydrogen bonding, molecular composition, crystallinity, cross linking and many others play an important part in their properties, the fact that polymers have a high molecular weight is the all important reason for the rich tapestry of properties found in naturally occurring and synthetic polymers.

The statistical nature of the polymerisation process will inevitably produce some form of distribution of molecular sizes. It is extremely difficult to manufacture a truly monodisperse polymer in which every molecule has the same molecular weight. Since most commercial polymers are polydisperse and this disparity influences the properties of the polymer then it is necessary to view the system in terms of the molecular weight distribution and the average molecular weight (M). There are

several averages associated with molecular weight but the most useful ones are the number average molecular weight ($\bar{M}_n$) and the weight average molecular weight ($\bar{M}_w$) which is biased toward large molecules.

1.4.3.1 Number Average Molecular Weight

The number average molecular weight is given by:-

$$\bar{M}_n = \Sigma N_i M_i / \Sigma N_i$$

where N_i is the number of molecules of molecular weight M_i. The $\bar{M}_n$ value is the average molecular weight of the polymer based on the number of polymer chains present. Number average molecular weights of commercial polymers usually[25] lie in the range 10,000 - 100,000 but can, in some cases, be lower or higher than this range. If they have low $\bar{M}_n$ (ie <10,000) then the properties of these polymers tend to be under developed.

1.4.3.2 Weight Average Molecular Weight

The weight average molecular weight is given by:-

$$\bar{M}_w = \Sigma N_i M_i^2 / \Sigma N_i M_i$$

The $\bar{M}_w$ is the average molecular weight based on the weight of polymer molecules present which, in turn, is more closely related to the length/size of the molecule.

1.4.3.3 Polydisperity

By inspection of the expressions for $\overline{M}_w$ and $\overline{M}_n$ and from the fact that heavier molecules contribute more to $\overline{M}_w$ than light ones, the value of $\overline{M}_w$ is always greater than $\overline{M}_n$ except for the situation where all polymer chains have exactly the same molecular weight (ie $\overline{M}_w = \overline{M}_n$; the hypothetical monodisperse polymer).

The ratio $\overline{M}_w/\overline{M}_n$ is known as the polydispersity index and is a convenient indicator of the "breadth" of the distribution of chain lengths in a polymer and is extensively used for this purpose.

Other quantities are known but are used less than $\overline{M}_n$ and $\overline{M}_w$. These include the viscosity average molecular weight ($\overline{M}_v$) which is less than or equal to $\overline{M}_w$ and greater than $\overline{M}_n$; and the higher averages of $\overline{M}_z$ and $\overline{M}_{z+1}$. Equations showing their relationship with the weight and number of chains present in the polymer are given below:-

$$\overline{M}_v = \{\Sigma N_i M_i^{1+\alpha}/\Sigma N_i M_i\}^{1+\alpha}$$

$$\overline{M}_z = \Sigma N_i M_i^3/\Sigma N_i M_i^2 \qquad \overline{M}_{z+1} = \Sigma N_i M_i^4/\Sigma N_i M_i^3$$

1.4.3.4 Effect of Molecular Weight on Properties

Changing the molecular weight and/or the molecular weight distribution can have a significant effect on the properties of the polymer. For example, in polypropylene its molecular weight distribution has been considered critical for its application and processing[46]. If $\overline{M}_n$ is low then the chain interactions are relatively small and the chains can move easily with respect to one another under an applied stress.

Conversely, if there are a high number of chains then there is increased chain entanglement and greater resistance to movement under an applied stress. Also if the molecular weight is low there is less chance of the polymer being able to crystallise than if it had a high molecular weight, hence the increase in melting point to a maximum value as the molecular weight increases.

The polydispersity also has a marked effect on the properties of the polymer. For example, if the distribution consists of much low molecular weight material then the polymer will be "soft" will have low tensile strength and will degrade and melt at lower temperatures. However, it will have favourable qualities too such as high impact strength and ease of processing. By controlling the molecular weight, a compromise between desirable and undesirable properties can be achieved. Figure 1.18 shows a typical molecular weight distribution for polymers.

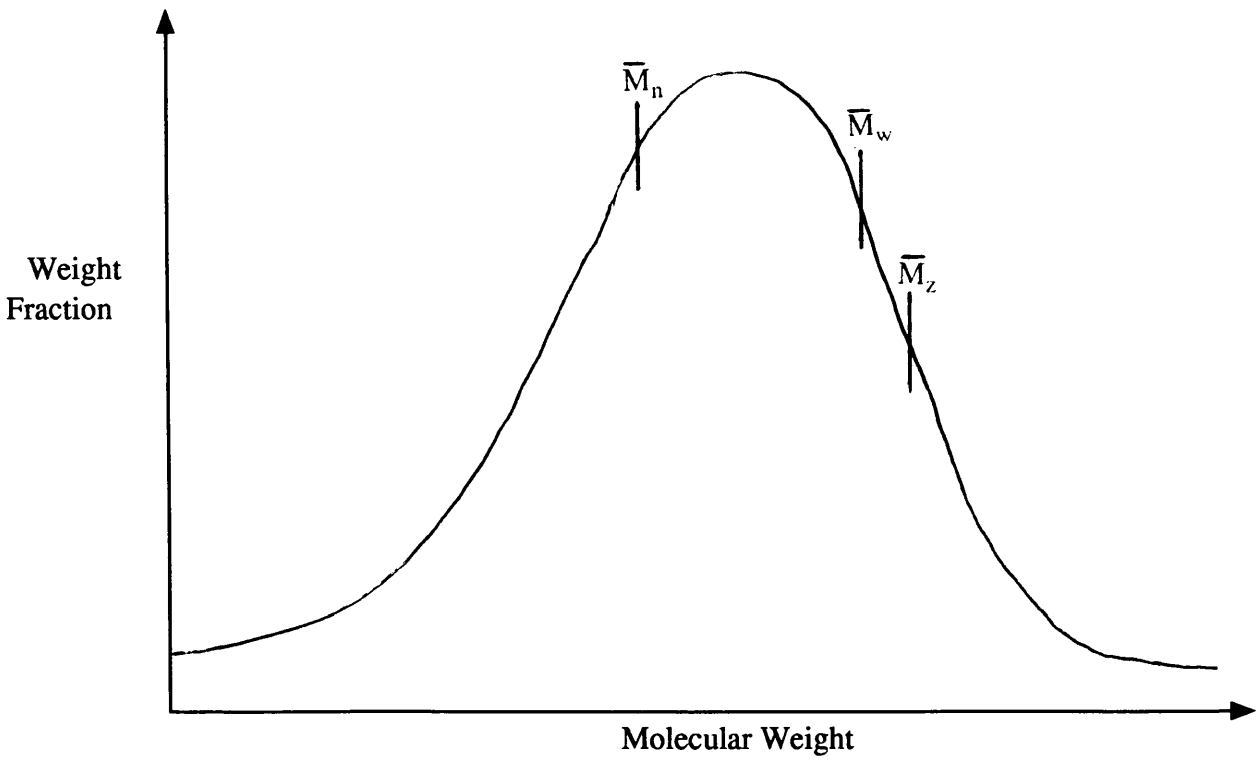

Figure 1.18 Diagram of a typical molecular weight distribution for polymers.

1.4.4 Polymorphism In Crystalline Polypropylene

It is well known[47,48] that isotactic polypropylene crystallises with a 3_1 helix chain conformation in at least three polymorphic forms: α, monoclinic; β, hexagonal; and γ, triclinic. The α-form, the most stable form, was discovered by Natta and Corradini[43] who have carried out extensive studies on its structure. The β-form was discovered by Keith and co-workers[49] and is usually found alongside the α-form in polypropylene. The existence of the γ-crystalline modification was reported soon after the elucidation of the more common α-phase[48]. The presence of a δ-phase was also described in this paper although work by Natta[50] discussing an infrared absorption band at 11.53μ which is characteristic for syndiotactic polypropylene was also clearly present in the δ-phase of polypropylene confirming earlier suspicions that the identity of this modification was closely linked to that of syndiotactic polypropylene.

1.4.4.1 α-Modification Of Polypropylene

The α-modification is the primary crystalline form of isotactic polypropylene and is the form most widely used in industry. It is obtained easily by crystallisation from the melt or solution at atmospheric pressure. Its structure consists of isomorphous 3_1 helices which are disposed in layers parallel to the ac plane with each right-handed helix being followed by a layer of left-handed helices along the b-direction[51]. A number of structural determinations have been carried out on this phase especially by Natta and Corradini[43] and Turner-Jones[52].

Natta and Corradini proposed a monoclinic unit cell having the following parameters in the C2/c space group:

$a = 6.65 \pm 0.05$ Å

$b = 20.96 \pm 0.15$ Å

$c = 6.50 \pm 0.05$ Å

$\beta = 99.33° \pm 1.00$

They found that there was statistical disorder in the up and down positioning of the chains. The degree of order is known to change and the structure of the α-phase of isotactic polypropylene as described by Hisoka and Seto[53] shows that there are two limiting modifications, α_1 and α_2 which can be obtained by different thermal treatments. The α_1 modification is considered to have up and down chains randomly distributed throughout the cell and is obtainable by rapid cooling from the melt. The α_2 form is characterised by a degree of order in the up and down positioning of the chains. The α_1 form can be transformed into the α_2 form by heating the polymer. This $\alpha_1 \rightarrow \alpha_2$ transition takes place at annealing temperatures of >150°C.

1.4.4.2 β-Modification of Polypropylene

The β-phase can occur at levels of only a few percent in commercial samples of isotactic polypropylene. Crystallising the polymer within a narrow temperature range (100-130°C) is usually required to obtain this phase and nucleating agents such as the quinacridone dyestuff (Permanent Red E3B) can be used to promote high levels of β-phase crystal growth[54]. Although the structure of β-phase polypropylene has been a subject of debate it is widely thought to be hexagonal in character. This hexagonal phase is probably induced by means of an epitaxial growth mechanism with the nucleating agent acting as epitaxial growth sites.

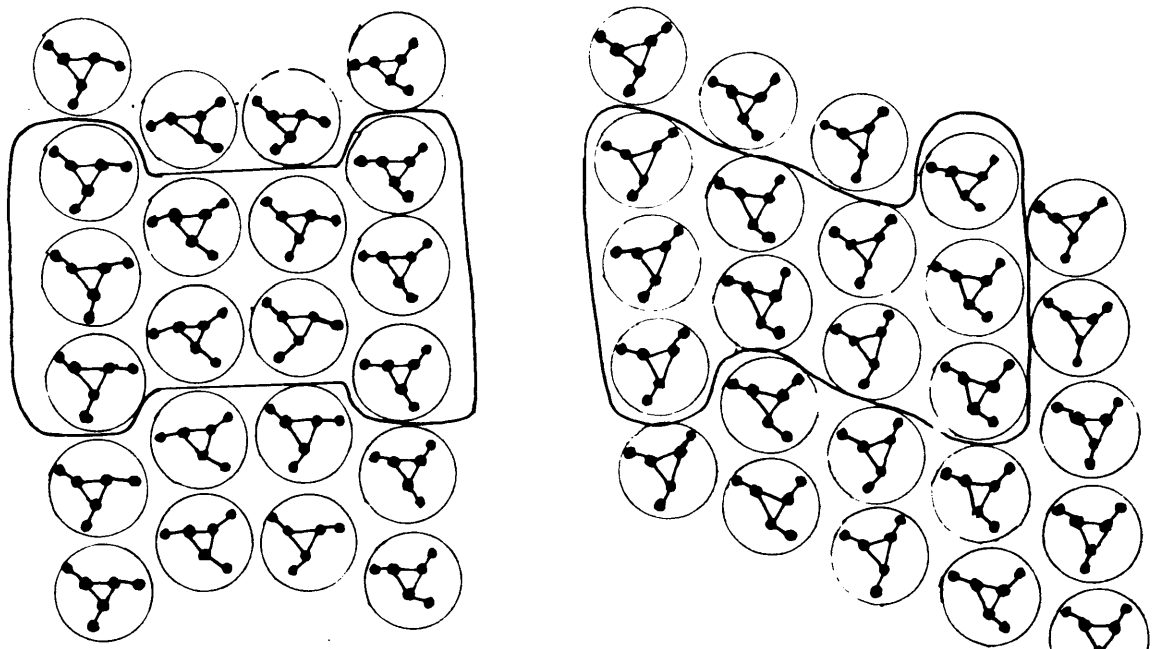

(a) α-Form (b) β-Form

Figure 1.19 (a) Alpha and (b) beta phase chain packing in isotactic polypropylene.

The β-form is readily converted back to the α-form on heating above 130°C. Figure 1.19 shows alpha and beta chain packing in isotactic polypropylene.

1.4.4.3 γ-Modification of Polypropylene

The γ-phase of isotactic polypropylene is often observed in small proportions in association with the α-phase. In the case of low molecular weight fractions of isotactic polypropylene, melt crystallisation can give rise to a mixture of α- and γ-phase material.

Depending on the cystallisation conditions the γ-form can be stable or meta-stable. For long chains[47] crystallisation under elevated pressure is the only known method for obtaining 100% stable γ-form. High temperature annealing can cause the $\alpha \rightarrow \gamma$-phase transition in the metastable form whereas the stable form must be melted and recrystallised before any change of phase will occur. The γ-phase can also be obtained using new homogenous catalytic systems for which future applications may be envisaged[55]. Turner-Jones[56] noticed that when small amounts of co-monomer units (4 - 10% ethylene or 1-butene) are introduced into the polymer then promotion of γ-phase crystallinity is observed in the resultant copolymer.

In an article by Lotz and co-workers[57] the γ-phase unit cell geometry is said to be similar to that of the α-phase and that the triclinic cell geometry of the γ-phase as proposed by Morrow and Newman[58] (unit cell dimensions a = 6.54, b = 21.40, c = 6.50Å, α = 89°, β = 99.6°, γ = 99°) appears to arise from the monoclinic α-phase (unit cell dimensions a = 6.65, b = 20.78, c = 6.50Å, β = 99°) by a simple shear along the a-axis. However, subsequent conformational analysis on the γ-crystal structure has failed to reveal a local minimum in the energy.

Recently Meille and co-workers[55] have proposed a novel crystal architecture based on low temperature x-ray diffraction data for this phase which exhibits non-parallel axes, although the development of this novel architecture is largely open to future contributions.

1.4.4.4 Smectic Polypropylene

Polypropylene forms a conformationally disordered phase when rapidly quenched from the molten state. The nature of this phase is discussed in more detail in section 4.1.1.

1.5 POLYPROPYLENE PROPERTIES AND END USES

The most outstanding feature of polypropylene is its versatility. With a specific gravity of 0.90 - 0.91 it is the least dense of all the commercial plastics[59,60]. It has the highest chemical resistance amongst polyolefins being resistant to most acids, alkalis and polar solvents. It is, however, susceptible to environmental stress cracking when subjected to concentrated sulphuric acid and chromic acid. Isotactic polypropylene has a relatively high softening point and hence a higher maximum service temperature (ie mouldings have been sterilised in hospitals for over 1000 hours at 135°C in both wet and dry conditions without severe damage). Its hydrophobic nature makes it resistant to moisture and because it is indigestible by insects and pests as well as a poor surface for the growth of micro-organisms it is ideally suited as a storage material in most environments.

Polypropylene is a hydrocarbon and as such it will ignite when exposed to a flame. However, when it melts it draws away from the flame and exhibits self-extinguishing tendencies. It has good electrical properties and is useful as an insulator in both wet and dry environments. Having the lowest thermal conductivity of all the commercial polymers, it has a reputation as being the warmest fibre in this respect. Polypropylene can be degraded fairly rapidly by unprotected exposure to sunlight so it is therefore necessary to use UV stabilising agents to prolong its life in that sort of environment.

Polypropylene fibres have many applications in a variety of products and hence must be strong as well as exhibiting the desirable properties mentioned above. Wet tensile properties are equal to those in the dry state and fibres can be made with different tenacities depending on the product requirements. Typical tensile strengths of 58,000 - 69,000 p.s.i. for staple polypropylene fibre[61] can be expected. The fibres generally

have excellent elastic recovery properties and have a high toughness index indicative of a tough abrasion resistant fibre.

These commendable properties show that polypropylene is an easily processed polymer with almost limitless potential for use as products in almost every domestic and industrial situation. It would be impossible to list all the products obtained from polypropylene so for convenience, products from the main markets are described below.

(a) Ropes and Twines

Polypropylene is dominant in the ropes and twines market due to its superior properties to conventional natural materials. The type of rope or twine required naturally depends on the environment in which it is to be used ie. it may require good UV stability, high tensile strength and abrasion resistance as well as being water resistant.

One of the problems with polypropylene in this market, however, is its susceptibility to fusion at high temperatures. An interesting way of alleviating this problem is to blend polypropylene with polyester to lengthen the lifetime of the rope. Another feature of polypropylene is that it floats in water which makes it applicable as docking ropes for small boats, the benefit being that because the rope floats it has less chance of becoming entangled in the propellors of the boat. It is also widely used in agriculture for baling hay. The product can be tailored so that it eventually degrades under exposure to direct sunlight.

(b) Intermediate Bulk Containers And Packaging

Most consumers nowadays expect their goods to be wrapped in some form of plastic film or covering. Polypropylene sacking and film packaging have been very successful in this area. The advantages of polypropylene sacking and bags are their strength, rot resistance, acid/alkali resistance and light weight. The sacks can be woven, sheet or clear film and can be used to store almost all materials from fruit to powdered chemicals.

(c) Carpets

Polypropylene is used on a large scale in the carpet industry. The advantage of using polypropylene as a carpet pile yarn are that it is cheap, the fibres are bulky and it is readily available in a wide range of spun-dyed colours. It is, however, not very resilient. To help combat this, polypropylene can be blended with wool to different extents which increases the resilience of the product as well as increasing its price competitiveness with other popular products such as the nylon/wool blends.

Polypropylene is also used in carpet backing which helps give the carpet good dimensional stability. Also the polypropylene will not rot or develop undesirable smells after prolonged use. This makes it ideal for use in the bathroom or kitchen environments.

These factors coupled with its high tensile strength, low static build-up, resistance to acids and alkalis as well as being relatively light makes it very competitive as an alternative to other synthetics in the carpet industry.

(d) Geotextiles and Cement Reinforcement

The civil engineering profession has benefited from developments in product design in polypropylene. Major roads have failed because of the contamination of the base layers with subsoil material and polypropylene can be used as a filter allowing the rain water through whilst preventing the movement of soil particles. Another application of geotextiles is in grass airfields. These airfields become extremely muddy with heavy use in wet weather. The use of polypropylene webbing to support the grass root system gives a considerable degree of protection and encourages the formation of a consistent surface. In the Netherlands, 5,500 tonnes of polypropylene have been used to stabilise the sea bed in the Dutch flood protection programme.

Polypropylene is also useful in the refinement of cement. Cuttings of fibrillated polypropylene are added to concrete mix. The main incentives for the use of polypropylene/cement composites are the low fibre content, low cost, improved impact resistance and ease of fabrication. A very satisfactory bond is formed between the irregular networks of fibrillated polypropylene and cement. This is quite different from the physico-chemical adhesion between cement and hydrophilic fibre such as asbestos and glass. Polypropylene/concrete composites have been used to replace rock ballast in the harbour wall at St. Hellier, Jersey and plans for the full commercial scale up of such products are at an advanced stage.

(e) Non-woven Products

Using non-woven extrusion technology in which polypropylene is extruded through two dies consisting of many holes in order to produce molten filaments which are layed on top of each other, it is possible to produce polypropylene cloth. The handle or softness of this cloth can be varied from a very coarse cloth which can be used in geotextile applications to a very soft cloth which can be used in products such as protective clothing, sanitary towels, nappies and tea bags.

1.6 ECONOMIC OUTLOOK FOR POLYPROPYLENE

A recent survey of the European plastics industry shows that it is growing faster than the European economy as a whole[62]. This statement also reflects the general state of the polypropylene industry.

The economic outlook for polypropylene is based on the stability of its main source in Western Europe, that is, crude oil. Crude oil is the basic material from which naptha comes and although many feared that the recent crisis in the Middle Eastern Gulf states would cause great instability in the worldwide petroleum markets, it is widely believed that it will have little long term effect on oil prices. This, of course, is a relief for the polypropylene industry as its price and costs are closely related to the price of crude oil and thus subject to the many complexities associated with the petrochemical industry.

The naptha from crude oil is used to produce ethylene in steam crackers, a process of which propylene monomer is a co-product. At present 70% of feedstocks for ethylene and propylene in Western Europe come from cracking of naptha. Other sources of propylene include refining and from natural gas.

In Western Europe 70% of propylene produced is a co-product of ethylene production and hence the relationship between crude oil prices and ethylene is often used as an indication of propylene prices. For the next few years at least this is expected to be reflected in the following equation[63] :-

Ethylene Price (US$/te) = Oil Price (Brent Crude US$/bbl) *x 25*

Propylene demand is growing faster than that of ethylene and the current price ratio of propylene to ethylene is 0.8 which is expected to increase slightly over the next year or so. The propylene to ethylene price ratio has grown from around 0.4 to 0.8 over the last 25 years and depending on the industrial climate, has tended to fluctuate around the latter value. Demand for propylene is governed by demand for polypropylene which currently accounts for approximately 48% of propylene chemical usage[64]. This figure is expected to rise to some degree over the next decade at the expense of other commodity chemicals produced from propylene. These include acrylonitrile, oxo-alcohols, cumene, phenol and propylene oxide.

The production of propylene and hence its supply can be controlled by the severity of cracking ie the temperature at which the cracking process is carried out. At high temperatures the formation of ethylene is preferred and at low temperatures more

propylene is produced. This means that if all crackers in Europe were to switch to low severity cracking an extra 1.4 million tonnes of propylene could be produced[62]. This fact allows the supply of propylene for the polypropylene industry to be managed with more flexibility.

The projected figures[64] for the sources of polypropylene feedstocks in 1995 compared to what they were in 1986 are shown in Table 1.1.

	Millions of Tonnes		
Year	Crackers	Refineries	Imports
1986	6.08	1.10	0.15
1995	6.80	1.60	0.40

Table 1.1 Projected figures for polypropylene feedstock sources versus the 1986 figures.

The imports value for 1995 is a high estimate and in actual fact is likely to be lower than this due to increased capacity caused by investment into steam cracking plants during the mid 1980's.

Between 1980 and 1988 propylene capacity was outgrown by demand and subsequently producers reaped the benefits of increased margins at the end of the 1980's. This shortage in propylene supply caused by an 11% growth per annum in demand for polypropylene against a backdrop of capacity growth at 6% per annum stimulated investment in plant building. Consequently there has recently been an oversupply of polypropylene. This, however, is beginning to settle down and as debottlenecking of existing stocks is coming to an end producers of polypropylene are

now looking to push through price rises in order to once again increase margins and make greater profits whilst stocks at their lowest levels since the beginning of the year[65].

The projected estimates for the unconstrained market size for polypropylene in Western Europe[66] are shown in Table 1.2.

Millions of Tonnes		
1990	1995	2000
3.75	5.30	7.80

Table 1.2 Projected estimates for the unconstrained market size for polypropylene in Western Europe.

Again these estimates may prove to be reduced considerably due to the effects of the environmental lobby and, in particular, the growth in recycling technology in the polypropylene industry.

Polypropylene is probably the most price competitive of all the commodity polymers. The cost base has been continually reduced in real terms throughout the last 25 years and is finding more and more end uses. Being cheap to make and relatively light in weight allows low costs of distribution which helps to keep the price of polypropylene similar throughout the world markets.

The polypropylene industry seems to be ready for the challenges of the 1990's and beyond and investments by companies such as BASF, Shell and Himont into polymerisation technology coupled with recent catalyst developments has opened up a wealth of opportunities to reduce costs.

The single European market situation in 1992 will have little effect on the polypropylene market because most large companies producing polypropylene operate in more than one of the European Community member countries. If anything, costs may be reduced due to increased ease of distribution and decrease in tariffs between the member countries. The U.K. Gross Domestic Product may be increased in which case demand is likely to keep on rising.

If crude oil prices do increase, as might be expected, increases in raw material costs may cause some problems but it is believed that process and product developments together with a shift to fewer and larger polypropylene producers will enhance the ability of polypropylene to remain competitive in world markets.

CHAPTER 2

2.0 EXPERIMENTAL TECHNIQUES

2.0 EXPERIMENTAL TECHNIQUES

2.1 INFRARED SPECTROSCOPY

2.1.1 Theory Of Infrared Spectroscopy

Infrared (IR) spectroscopy is a non-destructive technique and can be used for almost any material as long as it is composed of, or contains, compounds rather than pure elements. The samples can be solids, liquids or gases and can be recorded in solution, as neat liquids, films, mulled with mineral oil or incorporated in a KBr disc.

The infrared region of the electromagnetic spectrum can be divided into three main areas:-

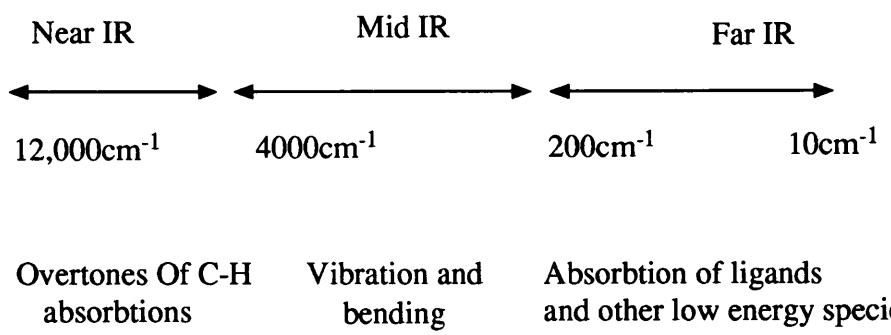

Figure 2.0 Diagram showing the infrared region of the electromagnetic spectrum.

Although the IR region of the electromagnetic spectrum is quite broad most spectrometers operate in the mid IR region (5000 - 400cm^{-1}) which is of most interest to organic chemists.

The two main fundamental vibrations for molecules are stretching, which is characterised by an increase or decrease in the atomic distance between atoms with the atoms remaining in the same bond axis; and bending in which the position of the atom changes relative to the original bond axis.

For a molecule to absorb IR radiation there must be a change in the electric dipole of the molecule caused by an interaction between the electric dipole of the vibrating molecule and the oscillating vector of incident electromagnetic radiation. For the various stretching and bending vibrations of the bonds to take place the incident radiation must be of an appropriate frequency. When energy is absorbed by the molecule the amplitude of the vibration is increased. This energy is released as heat when the molecule reverts from the excited state to the original ground state. Forces within the nuclei of the constituents of the molecule are assumed to be similar to massless springs which restore bond lengths or angles to certain equilibrium values.

In a Cartesian co-ordinate system each mass requires three co-ordinates (x,y,z) to define its position and it can be said that it has three independent degrees of freedom of motion; the x-direction, y-direction and the z-direction. The molecule, therefore, has 3N degrees of freedom, where N is the number of atoms in the molecule. Once the three degrees of freedom for translations of the centre of gravity of the molecule and the three rotational degrees of freedom which specify the molecular orientation about the centre of gravity are subtracted, this leaves 3N-6 possible fundamental vibrational modes that may give rise to an absorption in the IR spectrum (or 3N-5 for a linear molecule which only has two independent rotational degrees of freedom) although not all will do so. Some of the various stretching and bending vibrations that can take place in a molecule are shown in Figure 2.1.

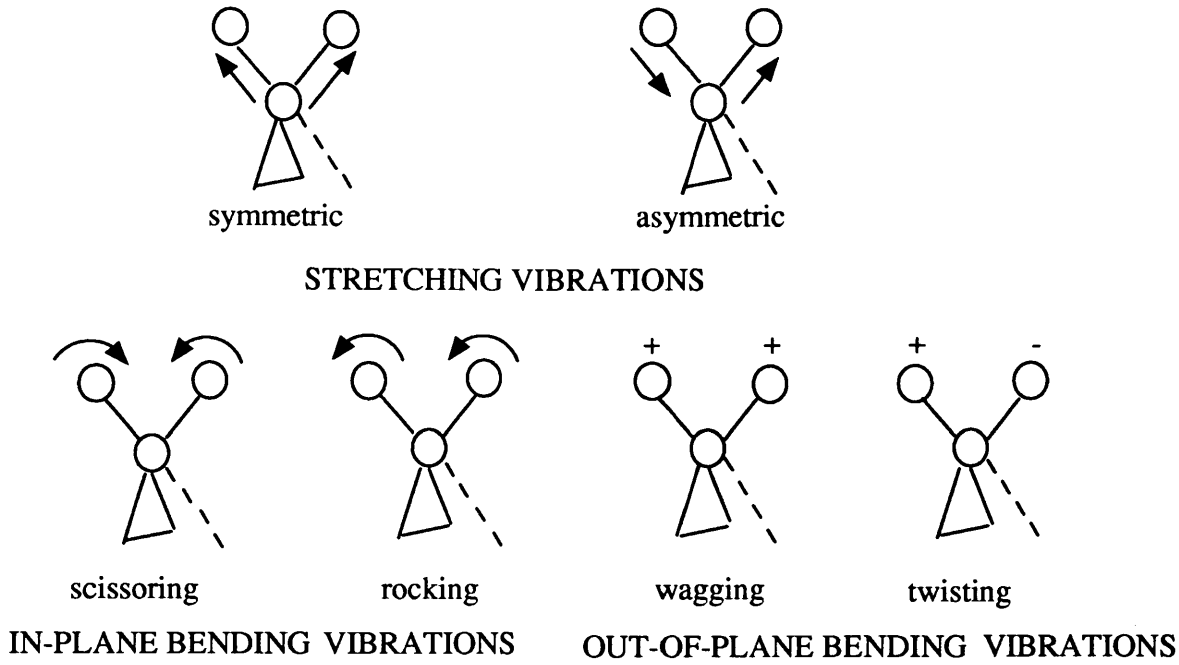

Figure 2.1 Schematic diagram showing stretching and bending vibrations in molecules. + and - signs signify vibrations perpendicular to the plane of the paper.

2.1.2 Vibrations In Long Chain Molecules

The number of degrees of freedom associated with polymer molecules is different from small molecules. The three translational modes which result in translation of the whole chain may be disregarded and so may the mode corresponding to rotation round the z-axis (chain axis) giving 3N-4 modes. Two other rotational type modes give rise to genuine modes because of the constraint applied to each repeating unit of an infinite chain by units on either side. So, for infinite polymers of well defined conformation, N now refers to the number of nuclei per translationally equivalent structural unit ie. $-CH_2-CH_2-$ for polyethylene. In the case of polypropylene N = 27, in other words there are 9 atoms per chemical repeat unit and three units from a translationally equivalent repeat unit.

Group theory can be a powerful tool for identifying vibrations. This method can be used in identifying and catagorising the vibrations of a molecule and thus to determine whether or not they are IR active. The associated theory of this analysis is well documented[67-69].

Unlike most crystalline organic molecules, polymers can contain both crystalline and amorphous regions. Annealing can lead to higher degrees of crystallinity and depending on the degree of crystallinity, the IR spectra of the polymer may reflect vibrational transitions associated with irregular chain conformations, presumably in the amorphous regions and in the case of polyethylene these can be found in the 1300cm^{-1} region. Similar behaviour occurs in the 1200 - 800cm^{-1} region for polypropylene. Specific infrared theories related to structural aspects of isotactic polypropylene will be discussed in section 4.2.

2.1.3 Infrared Spectroscopic Methods

In the field of IR spectroscopy there are two main instruments of analysis. The first of these is the conventional dispersive infrared spectrometer and the second is the more modern Fourier Transform Infrared Spectrophotometer.

2.1.3.1 Conventional Dispersive Infrared Spectrometer

The conventional dispersive IR spectrometer consists of a double beam of infrared radiation stemming from a common light source. This source is the Nernst glower, a moulded rod containing electrically heated rare earth oxides such as zirconium oxide, yttrium oxide and erbium oxide. The source illuminates both the sample and the reference sides. At this stage the relative intensity of light transmitted (and therefore absorbed) is measured by the photometer. Optical prisms or diffraction gratings can

be used to produce monochromated light from the broad spectrum of light emitted at the source. The gratings consist of a number of equally spaced grooves which allows light of only one wavelength at a time to undergo constructive interference. Light of different wavelengths can be obtained by rotating the grating relative to the light source. Thus a whole range of wavelengths can be sequentially scanned. This part of the instrument, known as the monochromator, ensures that only a narrow spectral region is transmitted to the detector at any one time.

The light passes to the detector and is of uniform intensity for both sample and reference if there is no sample present. When a sample is introduced the intensity of light from the sample side is decreased due to the sample absorbing in that particular wavelength. The reference side will be of relatively high intensity. Most detectors are thermal detectors in which incident light varies the electromotive force (emf) in the thermocouples. Such a detector may consist of a piece of blackened gold foil welded to two dissimilar metals chosen to give a large thermoelectric emf.

The information from the detector is amplified so as to present the sample to reference comparison from the photometer on the ordinate of the recorder in the form of % transmittance versus wavelength (or wavenumber). A schematic diagram of a conventional dispersive IR spectrometer is shown in Fig 2.2.

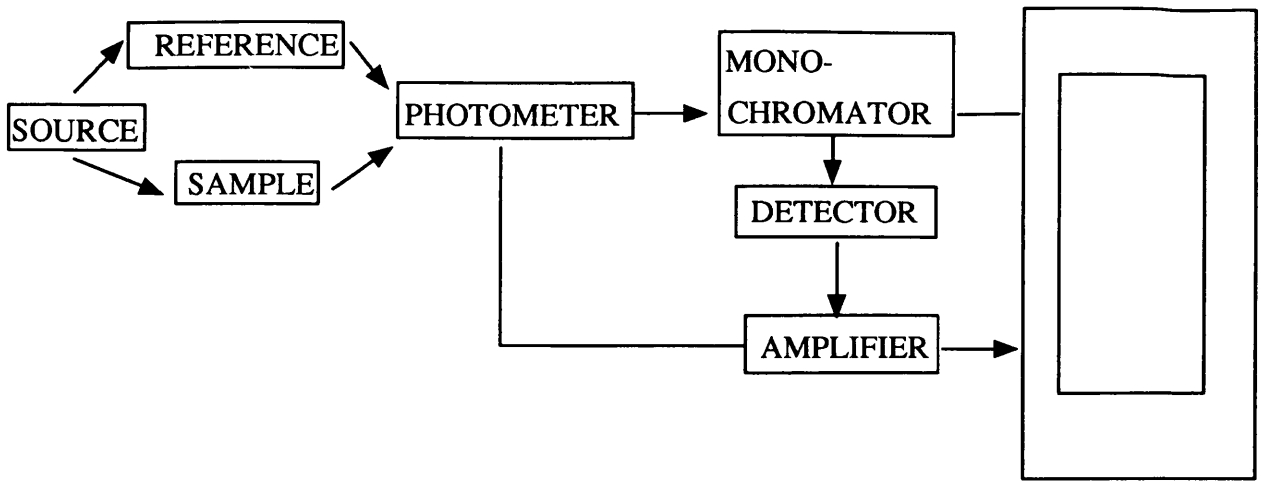

Figure 2.2 Schematic diagram of a conventional dispersive infrared spectrometer.

2.1.3.2 Fourier Transform Infrared Spectroscopy

The development of Fourier transform infrared spectroscopy (FTIR) has opened up a variety of new applications for IR spectroscopy in general. The method is based around a different optical system to that of the conventional dispersive spectrometer. In dispersive instruments, a spectrum is recorded by continuous scanning of the spectrum at successive frequencies, whilst in FTIR the entire frequency range of interest is passed simultaneously through an interferometer which produces an output signal containing all these frequencies.

The most important component of the FTIR instrument is the interferometer which was developed by Michelson[70], the father of visible light interferometry and receiver of the Nobel Prize for physics in 1907. The basic construction of the Michelson interferometer instrument is shown diagramatically in fig 2.3.

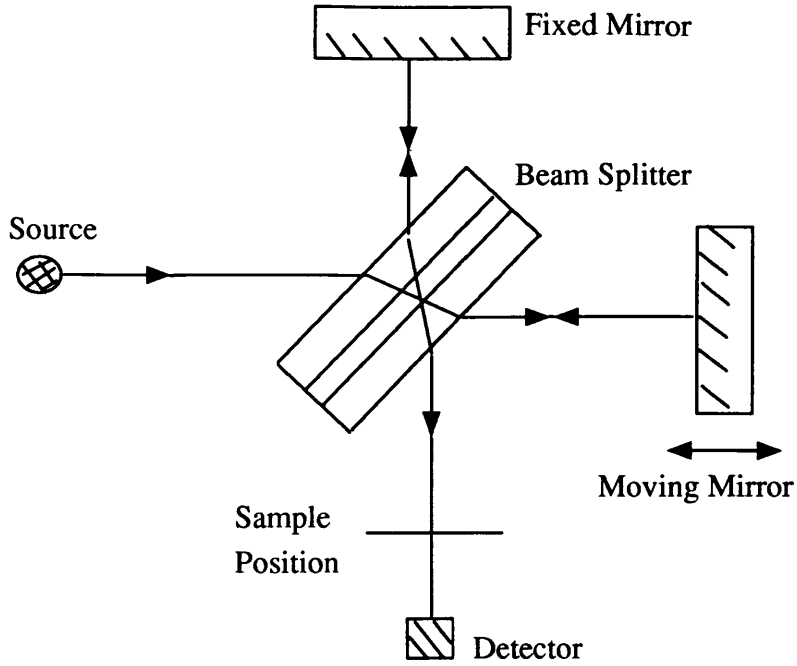

Figure 2.3 Schematic diagram of a Michelson interferometer.

Two mirrors (one stationary and one moveable) and a beam splitter are the main features of the interferometer. Collimated light from the source is incident at 45° on the thin dielectric beam splitter. The beam amplitude divides the light, half going to the fixed mirror and half going to the moveable mirror. The beams return to the beam splitter and recombine to produce interference effects. The beam is then passed through the sample and onto the detector.

When the stationary and moving mirrors are equidistant from the beam splitter, the reflected beams are in-phase and hence all wavelengths interfere constructively. As the moveable mirror moves away from the position of zero path difference, destructive interference will occur.

The quantitative way in which this signal varies, as the condition for interference within the interferometer is varied, is called an interferogram and is an oscillatory pattern which is a representation of the spectral distribution of the absorption signal reaching the detector.

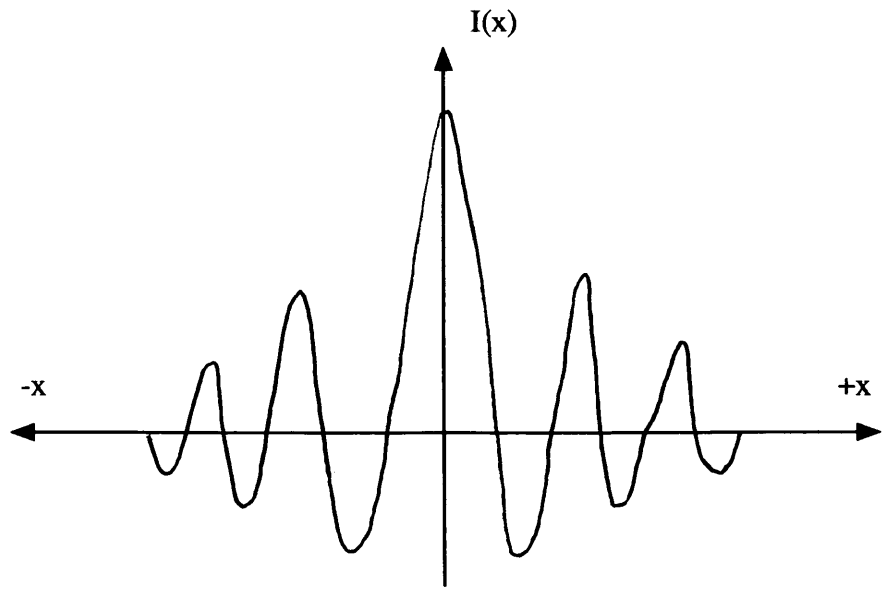

Figure 2.4 Diagram of an interferogram.

From this interferogram the spectrum can be obtained as a function of frequency by a mathematical procedure known as Fourier transform[71]. Although this procedure is time consuming and complicated, small and powerful computers can be combined with an interferometer in a single unit to produce the transformed spectrum in a relatively short time.

The spectrum is derived from the Fourier transform of the form:-

$$G(v) = \int_{x-}^{x+} I(x)\cos 2\pi vx \, dv$$

where G(v) is the spectral distribution at given frequency (v). I(x) is the range of

intensity values at different path lengths(x), at which the transform is carried out to give the spectral intensity at given frequency.

The beam from a helium/neon laser follows the IR beam through the interferometer. The system uses the laser beam to track the distance that the moving mirror travels (optical path distance) and to determine when to take a data point. The detectors in FTIR spectrophotometers are typically lithium tantalate or temperature stabilised fast recovery deuterated triglycine sulphate (FR-DTGS).

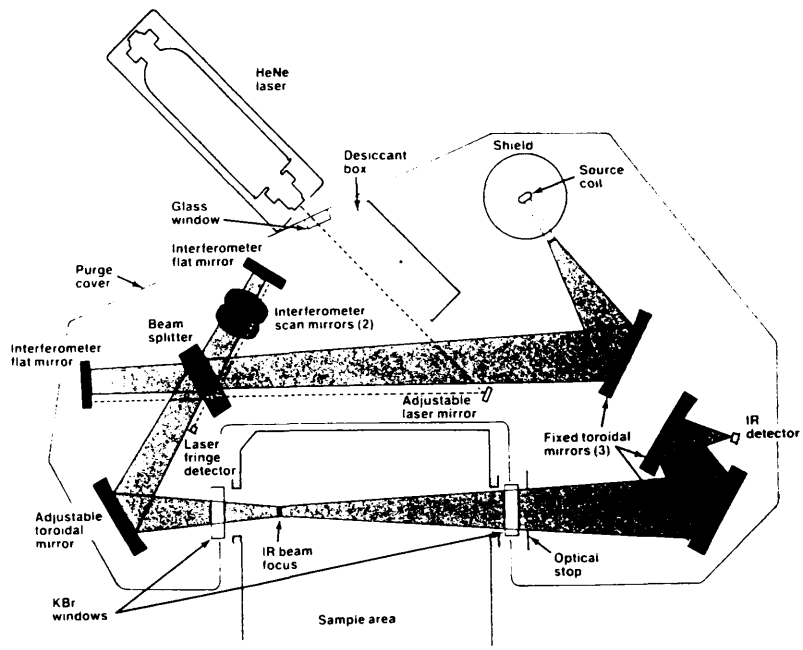

Figure 2.5 Diagram showing the optical system in the Perkin-Elmer 1640 Model FTIR.

2.1.3.3 Comparison Of FTIR Over Conventional Dispersive IR Instruments

The FTIR has a number of advantages over the conventional dispersive IR. Around 1950, Fellget[72] recognised that information from all spectral elements is measured simultaneously with an interferometer. This is known as *Fellget's Advantage* or the *Multiplex Advantage* and differs from conventional IR in that it overcomes the problems of having to scan sequentially.

During the same period, Jaquinot[72] discovered that, as the interferometer does not use restricting narrow entrant and exit slits during processing as in dispersive instruments, the solid angle of radiant power accepted from the source is correspondingly much larger. This advantage is known as the *Jaquinot Advantage* or the *Throughput Advantage*. The combination of these two advantages leads to much improved signal-to-noise ratios of the FTIR over that of the dispersive IR having the same resolution and scanning rate.

All the benefits associated with the microprocessor are also credited to most FTIR systems. These include the ability to store a large amount of spectroscopic data on the hard or soft disks, normalisation of IR spectra, the ability to carry out mathematical operations on spectra such as derivatisation, spectral subtraction and expansion of spectral ranges in order to improve analytical accuracy. Care must be taken, however, to understand fully the implications of the various software manipulations that can be carried out on the spectra.

One disadvantage of FTIR instruments is that if CO_2 or H_2O builds up in the sample compartment during a scan then because the background becomes different from the recorded background, then the CO_2 and H_2O traces will show up on the resultant

spectrum. This problem is not present in the dispersive instrument because the dualbeam system means that the reference beam effectively subtracts the background for each point on the curve as the scan proceeds.

2.1.4 Instrumentation

All spectra were run on a Perkin-Elmer Model 1640 FTIR Spectrophotometer. The system is based on the single beam scanning Michelson interferometer with sealed and dessicated optics containing a germanium coated potassium bromide beam splitter.

The source of infrared radiation is a temperature stabilised heated wire operating at 1300K with a beam size at focus of 8mm. It has an abscissa range of 7800 to 350cm^{-1} with an accuracy of 0.01cm^{-1} using a helium/neon laser reference.

The signal-to-noise is typically better than 2800/1 peak-to-peak for one minute data acquisition at 4cm^{-1} resolution over the range 2200 to 2000cm^{-1} and the ordinate precision is typically limited by the resolution but is thought to be better than 0.1%. The scan time is 4 seconds at 4cm^{-1} resolution (which ranges from 2 to 64cm^{-1}). The detector is a temperature stabilised fast recovery deuterated triglycine sulphate (FR-DTGS) type detector.

The Perkin-Elmer 1640 model has a Motorola 68010-based dedicated data handling controller with built-in 9 inch cathode ray tube and membrane keyboard. It has multiple spectrophotometer memories, interactive graphics, spectral subtraction and full data handling with FLAT, SMOOTH, ABEX, T/A, AUTEX and JCAMP data export. A 5.25 inch floppy disk drive is also present which allows storage and data management of spectral data and methods.

2.2 DIFFERENTIAL SCANNING CALORIMETRY

Thermal analysis has been established as an analytical technique since its inception in the late 1700's. The generic name "thermal analysis" covers a range of experimental techniques in which measurements are made of a property that changes as the temperature changes. The range of instrumentation has come a long way since the development of the first calorimetric[73] and differential thermal analysis techniques. Nowadays this includes highly sensitive machines capable of carrying out thermal investigations on a material, such as thermogravimetric analysis, electrical thermal analysis, thermomechanical analysis and effluent gas analysis.

In the studies described in this thesis thermal analysis has been carried out using differential scanning calorimetry (DSC) and this will be discussed in more detail in chapter 4.

2.2.1 Theory Of DSC

Since most chemical and physical changes are accompanied by changes in enthalpy, it is possible to use a technique based on the detection of heat changes. The simplest technique for measuring this difference in temperature is differential thermal analysis (DTA) and because of its strong similarities to DSC in both equipment and application it is convenient to discuss both techniques under the same heading.

DTA involves the measurement of a difference in temperature between sample and reference material whilst both are subjected to the same heating programme. In "classical" DTA two thermocouples connected in opposition are placed within the sample and an inert reference material which are contained in the symmetrical

cavities surrounded by a single block which acts as a heat sink. If there are no transitions then the temperature of both sample and reference should be identical and no signal is recorded. If an endothermic event occurs in the sample it will result in the temperature of the sample (Ts) lagging behind that of the reference (Tr). The thermocouples measure the temperature difference (ΔT) = Ts-Tr and when plotted against Tr this gives a negative signal on the recorder, as shown in Figure 2.6 (convention in DTA is that negative signals represent an endothermic transition whereas in DSC the endothermic transition is represented by a positive signal on the recorder).

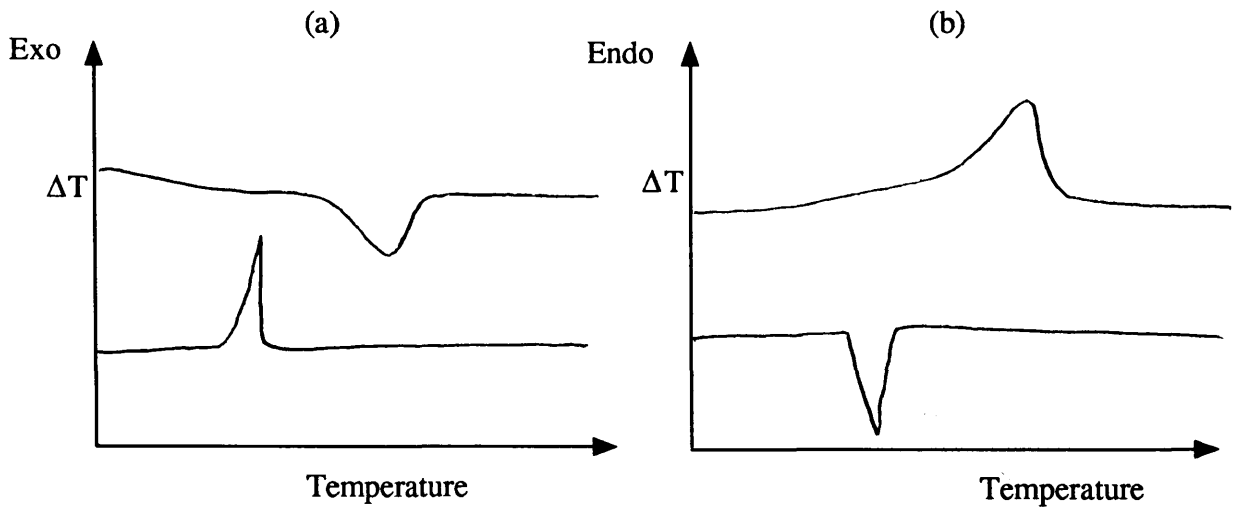

Figure 2.6 Recorder signals showing endothermic and exothermic responses for (a) DTA; and (b) DSC.

An exothermic transition in the sample is characterised by a decrease in transfer of heat to the sample in comparison with the reference and results in a positive exothermic response. The area under the curve in DSC is related to the enthalpy (ΔH)

change but in DTA, because the sample constitutes part of the heat flow path to the surrounding furnace, the actual temperature difference for a given enthalpy change will depend upon the thermal properties of the sample, thus making the peak area sample dependent and therefore unquantifiable in DTA.

For accuracy in the measurement of physical and chemical changes in a sample using DTA, optimisation of the reference material is very important. It should be chosen for its thermal inertness over the temperature range of interest, its similarity in thermal conductivity and heat capacity to the sample and it should not react in any way with the sample, the sample holder or the thermocouple. The use of reference materials often causes problems in obtaining reproducible thermal paths between heat source and sensors and are notoriously difficult to pack consistently in the sample and reference cavities.

A slight variation on this technique which helps to overcome the main disadvantage of the dependency of enthalpy on thermal properties of the sample in DTA, is known as Boersma DTA or heat-flux DSC and was first described by Boersma[74] in 1955. In this adaptation of DTA the differential thermocouples are no longer positioned directly in the sample and reference, but instead are attached to the thermally conducting bases on which the sample and reference pans are placed. This means that the enthalpy of transition now acts upon a fixed thermal resistance and consequently the peak area can be related to the change in enthalpy by a calibration factor. Although this overcomes the main disadvantage of DTA, the output signal response is usually slower.

"Real" DSC, as developed by Perkin-Elmer, USA, differs from the DTA techniques in so much as it uses a different measurement principle[75]. The theory of operation is based on the exclusive Perkin-Elmer "null-balance" DSC principle. The system

consists of sample and reference sides which are heated at a predetermined rate by a single main furnace but each is also maintained at the programmed temperature by a seperate subsidiary heater. Energy absorbed or evolved by the sample is compensated by adding or subtracting an equivalent amount of electrical energy to a heater located in the sample holder. As the energy per unit time is continually monitored throughout the run, any variation in thermal behaviour results in automatic adjustment of heater power in order to keep the sample holder temperature equal to that of the reference holder. This provides an equivalent electrical signal which is made directly in milliwatts and which is therefore a true electrical energy measurement of peak areas. This type of thermal analysis is also known as power compensated DSC and is distinctly different to heat-flux DSC in which the magnitude of peaks depends directly on the magnitude of the thermal constants in the system. These constants are known to vary as a function of temperature, thus making true calorimetric readings difficult. DSC, then, provides a way of directly measuring the energy involved in a transition and is therefore considered superior in its ability to measure true calorimetric transitions. Figure 2.7 shows diagrams of the various thermal analysis equipment.

Throughout any particular DSC run, atmospheric and external block temperatures can be controlled . To control the atmospheric conditions, inert gases such as helium and nitrogen are commonly used and are fed continuously through both sample and reference cavities in order to promote a non-oxidative environment. Conversely, if an oxidative environment is desired then it can be achieved by feeding oxygen through the system.

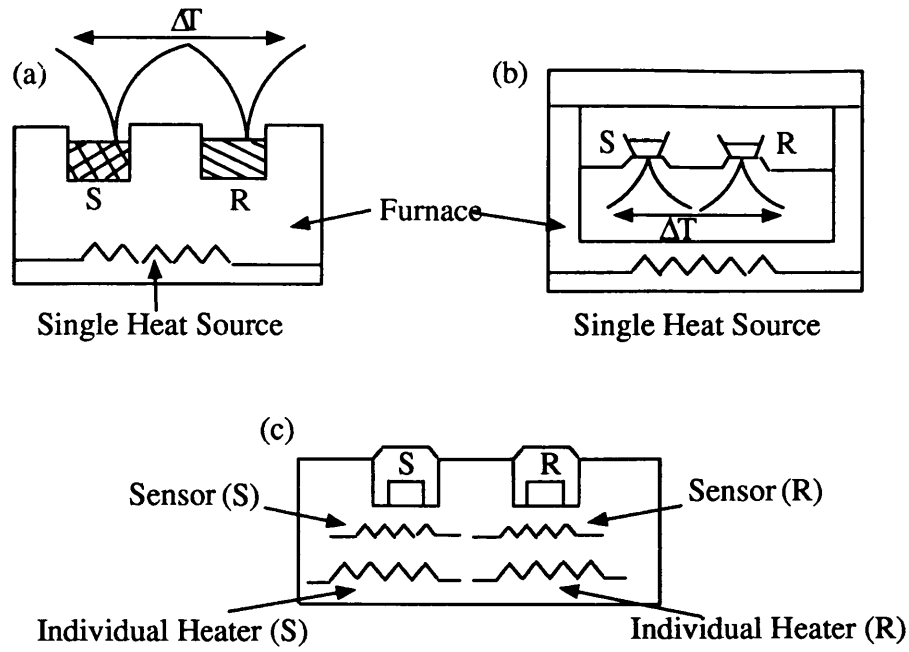

Figure 2.7 Schematic diagrams showing (a) Classical DTA (b) Boersma DTA and (c) Power Compensated DSC.

Controlling the external block temperature helps to keep constant any heat loss to the environment thus increasing reproducibility. This can be achieved by running water through the block (or liquid nitrogen when working at sub-ambient temperatures). This process also helps the furnace to cool quicker from high temperatures.

2.2.2 Application Of DSC To Polymers

Application of DSC to the study of polymers has been very successful. Any thermal transition in a polymer which involves an enthalpy change of sufficient magnitude can be studied using DSC. Since thermal transitions which occur in a polymer have

significant bearing on the way in which it may be processed and on its end-product properties, then it is important to have a method by which its thermal transitions can be easily and reproducibly studied using relatively small samples.

A typical DSC curve showing the main transitions in a semicrystalline polymer is shown in Figure 2.8.

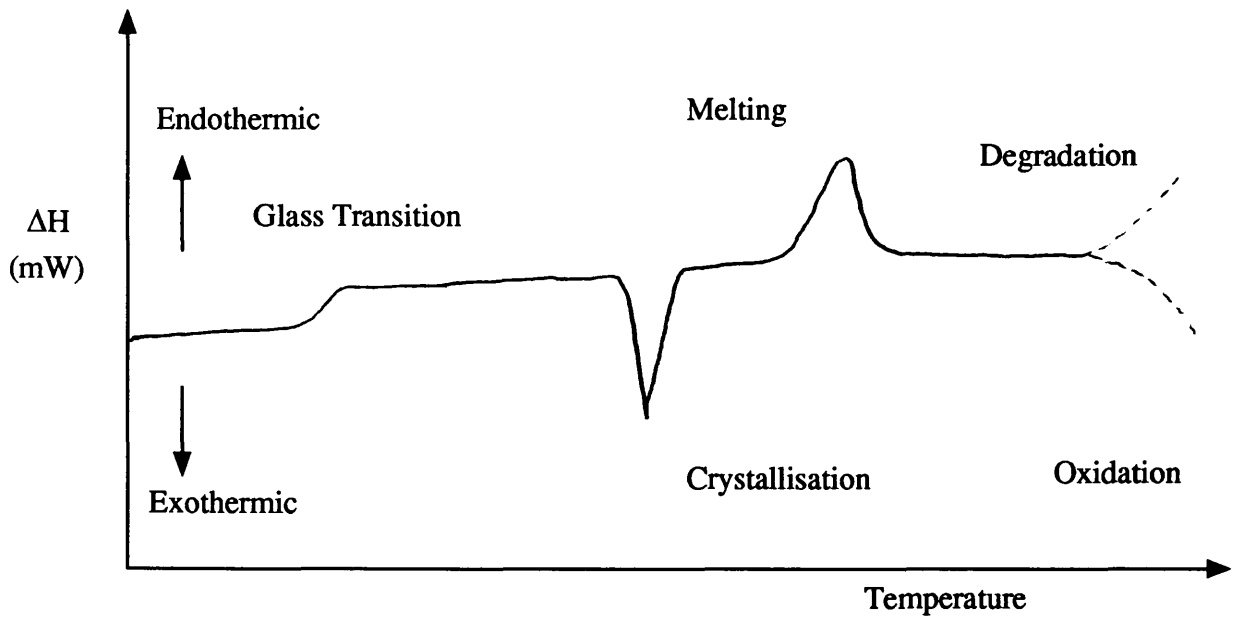

Figure 2.8 Diagram of a typical DSC curve for a semicrystalline polymer.

DSC is commonly used to measure first order transitions, such as crystalline melting and crystallisation in polymers which exhibit sizeable enthalpy changes. Second order phase transitions, such as the glass transition, are accompanied by a change in heat capacity but little, if any, change in ethalpy. This event is characterised by discontinuity in the baseline.

Many studies on different aspects of polymer structure and thermal behaviour have been carried out using DSC data. Such studies have been carried out on quantities such as tacticity[76-78] using crystallisation and glass transition data. Morphological

investigations[79,80] and phase transitions in polymers have been extensively studied and oxidative stability[81], specific heat[82,83], crystallisation kinetics[84] and crystallinity content in polymers[85] are examples of the range of information that can be obtained from thermal transitions in the polymer using DSC. This information, along with countless other applications, has led to a greater understanding of many aspects of polymer behaviour. The development of DSC and other thermal analysis methods, then, has been an invaluable asset to the polymer scientist.

2.2.3 DSC Instrumentation

All DSC measurements in this study were carried out using a Perkin-Elmer DSC-7 Model which operates under the power compensated temperature null balance principle (measuring energy directly and not differential temperature).

The DSC cell consists of independent dual furnaces constructed of platinum-iridium alloy with independent platinum resistance heaters and temperature sensors. The system was calibrated against indium and zinc run at 10°C/minute in a nitrogen atmosphere with an external block temperature of ~10°C ie. cold running water. For sub-ambient operation, calibration was repeated for an external block temperature of -110°C.

The calorimetric precision is better than ±0.1% with temperature precision and accuracy to within ±0.1°C. Heating and cooling rates range from 0.1°C/minute to 200°C/minute in 0.1°C increments. These values are based on running 4-8 mg samples of indium at 5°C/minute on a calibrated instrument. The standard unit allows operation from ambient to 730°C. This range may be extended to -170°C using the Perkin-Elmer sub-ambient cooling accessory.

Control of the furnace atmosphere was employed throughout using nitrogen as a purge gas. Other gases may be used depending on atmospheric requirements eg. argon, helium, carbon dioxide, oxygen, or other inert or non-corrosive gases.

The system is linked to an Epson personal computer and is operated using Perkin-Elmer DSC-7 thermal analysis software packages which allow storage and manipulation of the thermal data. The computer is linked to a Hewlett-Packard Colourpro Plotter with multiple pen operation for generation of colour plots.

2.3 X-RAY DIFFRACTION

X-rays were discovered in 1895 by the German physicist Roentgen[86], who named them as such due to their unknown nature. In 1912 von Laue[87] proposed that x-rays could be diffracted by crystals. The interaction of this electromagnetic radiation with matter is a complex subject which requires knowledge of many aspects of modern physics.

2.3.1 X-Ray Generation

By bombarding a metal target with high energy electrons emitted from a heated filament held at a highly negative potential (20-60 kV), it is possible to produce electromagnetic radiation of very short wavelength known as x-rays. These x-rays are emitted when the photons produced by the electron bombardment of the target decelerate, thus leading to the emission of a large fraction of energies which lie within the x-ray range.

Another process which takes place, and which is important for analytical purposes, is the ejection of an electron from an inner shell of a target atom by the accelerated bombarding electron. When this happens, an electron from a higher shell falls into the lower shell, releasing energy in the form of an x-ray. The significance of this is that if the target material is made of a single pure element eg. copper, then it is possible to create x-rays which are monoenergetic (have the same wavelength). The most useful x-ray component, due to the high intensity obtained, is that which is emmitted when electrons fall from the second electron shell (L) into the first electron shell (K) and is known as the K_α x-ray . The x-ray generation is carried out in an evacuated tube to prevent scattering by gas atoms. The x-ray radiation ultimately passes through a window which is transparent to the required component.

2.3.2 X-Ray Diffraction

Laue showed that x-rays passed through a crystal resulted in a differaction pattern which was characteristic of the regular crystal structure. Bragg[88] studied the reverse experiment, in which the beam of x-rays was reflected from the plane face of a crystal. The intensity of the diffracted beam was then measured as a function of the angle of diffraction by means of an ionising chamber. From this, information can be obtained on the crystal structure of the sample. Bragg's interpretation of his results led to the derivation of the well known relationship for the occurrence of a reflection:-

$$n\lambda = 2d\sin\theta$$

where d is the spacing between planes, θ is the angle between the x-ray beam and the plane, λ is the wavelength of the x-ray beam and n is an integer > 0.

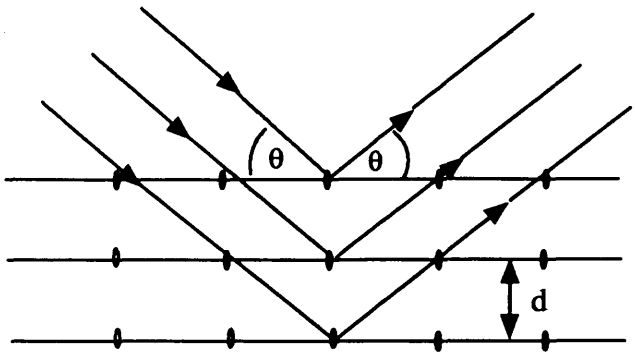

Figure 2.9 Diagram showing interference of X-rays reflected by successive planes of regularly spaced atoms.

If the crystal is composed of parallel planes of regularly arranged atoms, then the Bragg Condition will be observed (Figure 2.9).

2.3.3 Measurement Of Diffracted X-Rays

There are two main methods of measurement pertaining to x-ray diffraction; powder photography and powder diffractometry. The word "powder" refers to a sample containing a large number of randomly oriented crystals of the same kind.

(i) Powder Photography

When the sample is bombarded by the collimated beam of x-rays it will produce a series of diffracted x-rays which correspond to characteristics of the crystal structure. If a photographic film is placed around the sample being being bombarded, then a series of spots will be recorded. Since disorientation occurs in all directions in the powder sample, a line pattern is obtained ie. all the associated spots join up. The cylindrical positioning of the photographic film in order to trap all diffracted x-rays is known as a Debye-Scherrer Camera and the resultant photographic halos are called

Debye-Scherrer rings. From the positioning of these rings a value for the d-spacings and Bragg angles can be obtained, giving information on the crystal lattice. A schematic diagram the Debye-Scherrer Camera is shown in Figure 2.10.

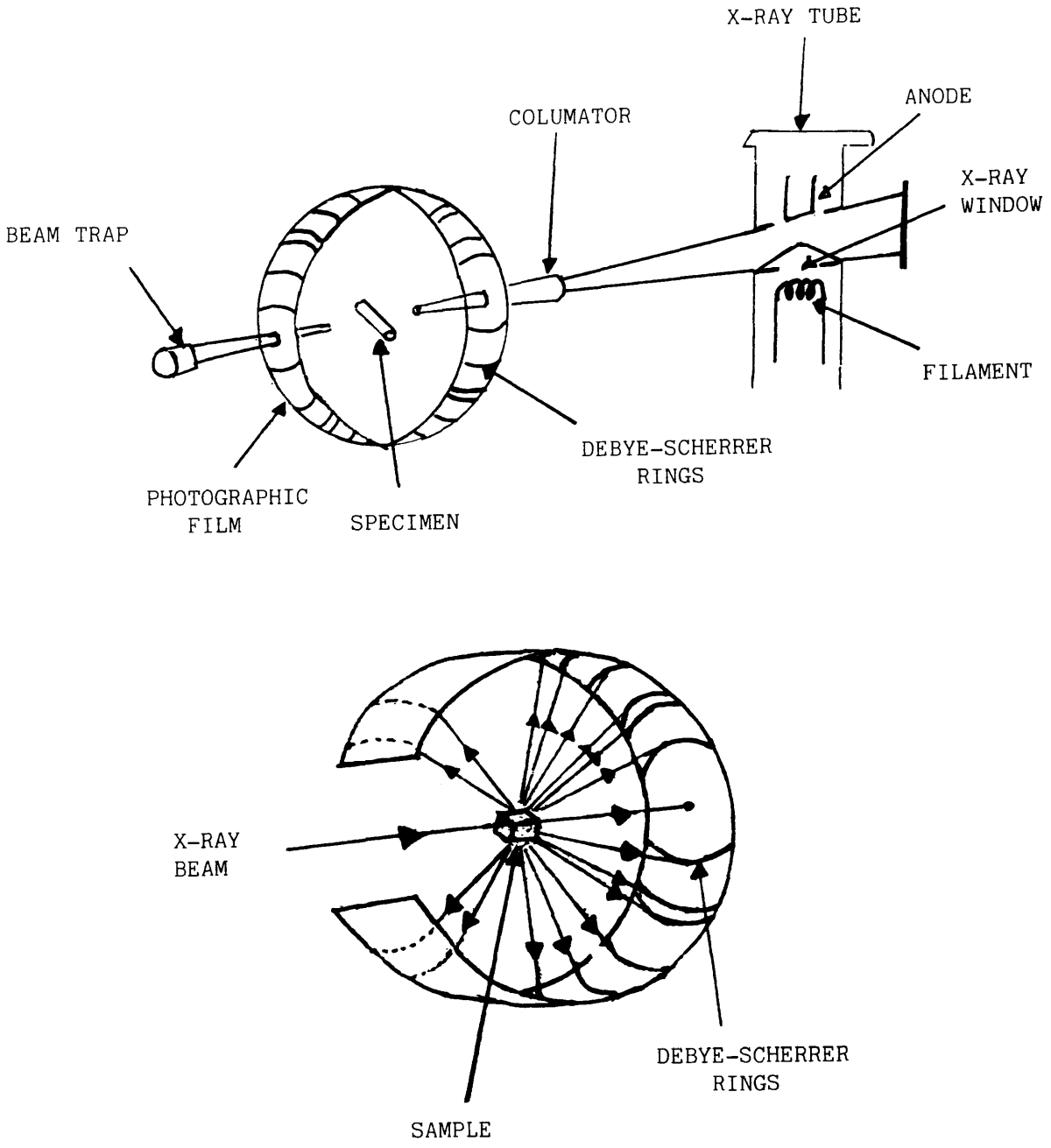

Figure 2.10 Schematic diagram of the Debye-Scherrer Camera.

(ii) Powder Diffractometry

The powder diffractometer is basically an x-ray counter. The most common arrangement is shown in Figure 2.11.

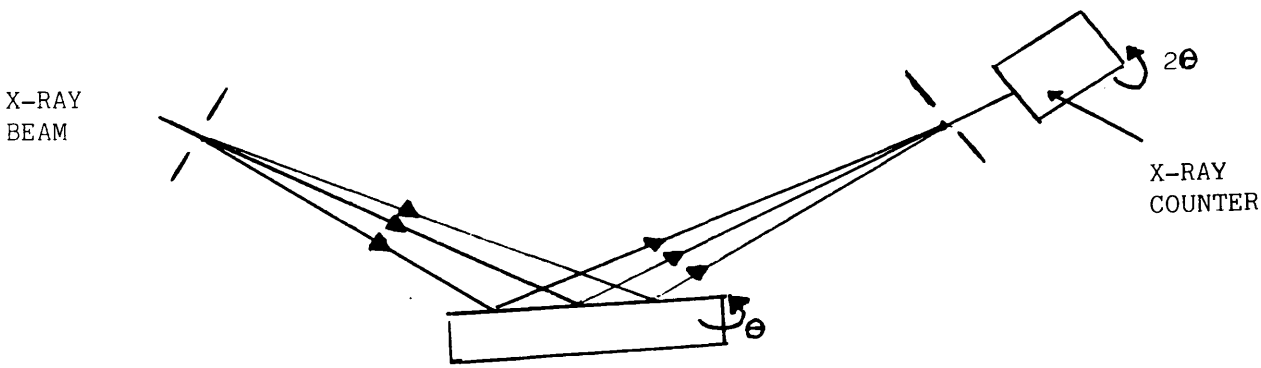

Figure 2.11 Schematic diagram of a powder diffractomer.

In this system the sample is mounted with its surface parallel to the bed of the sample mount. When the x-ray beam collides with the sample whilst it is slowly rotated, a multiplicity of Bragg reflections are excited.

The counter is carefully positioned so that it moves in synchronisation with the sample as it is rotated. This allows the counter to record only those reflections which occur when the lattice planes are parallel to the sample surface. In order for this to work successfully, the counter must be rotated through twice the angle in which the

sample turns (or in otherwords, 2θ). This means that the diffraction peaks will be observed at those positions for which the planes lying parallel to the surface adhere to Bragg's law:-

$$2d_{hkl}\sin\theta_{hkl} = \lambda$$

Since values are known for λ, and $2\theta_{hkl}$ can be read from the counter setting, it is possible to calculate the d-spacings. The counter gives a signal which is proportional to the intensity of the x-rays that it is receiving. This signal is amplified and displayed on a meter and/or a chart recorder giving a plot of intensity versus 2θ. A typical crystalline polypropylene diffractogram can be seen in Figure 2.12.

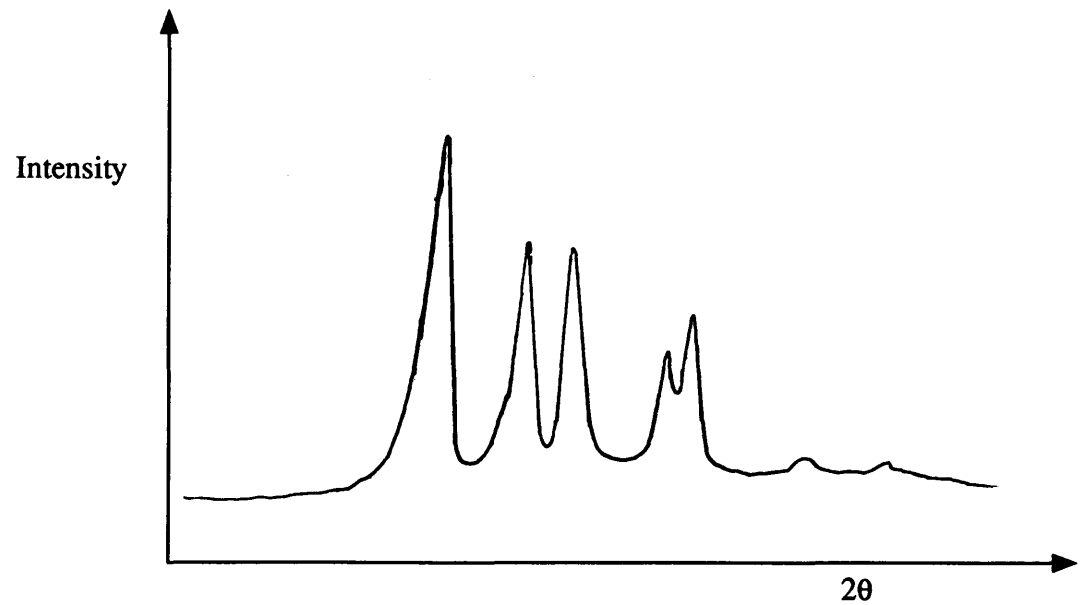

Figure 2.12 Diagram showing typical powder diffractometer X-ray peaks for polypropylene.

2.3.4 Application Of X-Ray Diffraction To Polymers

Since polymers are rarely purely crystalline in nature, the x-ray photographs or diffractograms will be affected by the amorphous scattering. This results in diffuse halos being observed in powder photographs, and a broad underlying amorphous background in the case of the powder diffractogram. Despite these inherent difficulties associated with the application of x-ray diffraction to polymers, the technique has been widely used, providing the polymer scientist with much valuable information on polymer structure.

Information on polymer molecular orientation, crystallite size and degree of crystallinity have been well investigated and other structural information such as unit cell dimensions and measurements of helical structures in particular have been very useful[89]. In polymers which contain more than one morphological phase, x-ray diffraction can be used[47,48,90] to establish which forms are present in a particular sample.

The determination of crystallinity of polymers by x-ray methods is useful, although for all quantitative studies by x-rays it is necessary to analyse the complete diffraction pattern into separate amorphous and crystalline components. This is often difficult due to the diffuse nature of the amorphous scattering and the tendency for some of the crystalline intensity peaks to be rather broad. Nevertheless, the technique provides data which can be used comparatively but which inevitably involves the judgement of the observer and therefore lacks some objectivity.

X-ray diffraction can also be used to evaluate crystallite sizes. For a large perfect crystal the reflections are sharp and well defined. In polymers, however, because the crystallites tend to be a distribution of relatively small sizes, the reflections are more

diffuse in nature. This information, although diffuse, can be used to estimate the mean crystallite size. This measurement is carried out by taking the peak width (β) at half-peak height. This is related to the dimension of the crystal by the expression:-

$$\beta = (0.9\lambda\sec\theta)/t$$

where λ is the x-ray wavelength, θ the Bragg angle and t the dimensions of the crystal normal to the set of diffracting planes. It must be stressed, however, that the values obtained by this method should be considered as minimum values due to the possibility of line broadening effects for a variety of reasons which are inherent to the technique such as camera conditions and beam divergence.

2.3.5 Instrumentation

All x-ray diffraction work was carried out in the Physics Department of the University of Dundee.

(i) Photographic Method

All x-ray powder photographs were taken of specimens hanging from a glass fibre mounted in a Debye-Scherrer camera of diameter 114.6 mm with the film in the Straumanis arrangement. The x-rays used were Cu K_α radiation produced using a nickel filter and sealed x-ray tube in a Phillips PW1010 1000 Watt generator.

(ii) Diffractometer method

All samples were run on a Phillips PW1050 X-ray Diffractometer fitted with a curved graphite single crystal monochromator with an entry slit of 1°.

The system was run at 30 mA, 40 kV with full scale deflection on the chart recorder (F.S.D. = 4×10^2). The x-rays used were Cu K_α with a wavelength (λ) of 1.5418 and were detected using a sealed xenon gas detector.

2.4 GEL PERMEATION CHROMATOGRAPHY (GPC)

2.4.1 Theory Of GPC

GPC is considered by many to be the most valuable technique for the molecular weight characterisation of polymers. Since the introduction of the term gel permeation chromatography by Moore[91] in 1964, columns containing porous crosslinked polystyrene gels covering a wide range of pore sizes have been used for the separation of high polymers in order to determine molecular weight distributions. These columns can be either metal or glass, and can range in diameter from a few millimetres to a few centimetres, and in length from a few centimetres to several metres. As well as crosslinked polystyrene or other crosslinked copolymers, column packings can consist of silica gel or glass, which also give good separation and which have high mechanical strength and durability at elevated temperatures.

GPC is basically a separation technique based on molecular size (hence its other common name, *size exclusion chromatography*), which involves the passage of a mobile liquid phase through a column containing the stationary phase ie. the crosslinked gel. The mobile phase is normally an organic solvent, where polymer samples are concerned (or water for biological systems), and is pumped continuously through the column at a predetermined rate. The degree of separation, or column efficiency, increases with increasing length of the column, but associated with this is the problem of increased throughput and analysis time.

The polymer sample is dissolved in the solvent being used as the mobile phase, and is introduced at the injection port of the system which commonly has a syringe and needle type entry. Also available, however, is the automatic multiport valve system

which is useful for high temperature injections. The injection port will normally hold an accurate amount of solution in a loop and any solution in excess of this amount will exit the injection port via an overflow facility. It may be necessary to filter the solution before injection, to remove any foreign bodies or aggregates which may block pores if allowed into the column.

Once the injection port is loaded, a valve is opened and the accurate amount of solution is introduced into the mobile phase. As it progresses through the column, separation occurs by preferential penetration of the different sized molecules into the pores of the gel. The smaller molecules are able to permeate more easily into the pores of the gel and therefore have a longer path length through the column. The larger molecules have less pore volume available into which they can enter and thus have a shorter path length through the column. The molecules exit the column in inverse order of size, with the largest molecules eluting first followed by the smaller molecules.

Detection is often carried out using a differential refractometer, but many other methods can be used either singly or in various combinations. Such methods include infrared detectors, viscosity detectors, UV detectors and low angle laser light scattering (LALLS) measurements. The refractive index detector will monitor any changes in refractive index between the reference cell containing stationary solvent and the sample cell through which the mobile phase (same solvent as reference cell) passes. If there is no polymer present in the mobile phase then a stable baseline will be produced but as soon as the dissolved polymer enters the sample cell in the detector the differential between reference and sample cells is recorded due to the difference in refractive index between the pure solvent (reference) and the polymer solution (sample). The greater the concentration of polymer then the larger the signal. Normally a system will have a constant flow rate and therefore the volume passing

through the system per unit of time will be known. This means that the recorder will respond at a specific time for a particular molecular weight.

2.4.1.1 Calibration

In order for this method to work efficiently, it is necessary to calibrate the system with standard samples of known molecular weight and a narrow molecular weight distribution, these having been predetermined using an independent method such as LALLS, viscometry or osmometry. The narrow standard calibration technique is valuable for comparison purposes and is usually carried out over a wide molecular weight range. A plot of log molecular weight versus retention time for the calibration standards is constructed, allowing the calculation of molecular weight values for polymers of unknown molecular weight distribution to be carried out with respect to retention time (Figure 2.13).

Care must be taken when using this technique as major errors can result from a poor calibration due to the use of a log scale. For example, a 1% change in retention time can result in an 8-20% change in molecular weight.

Another method of calibration is with broad standards where only two inputs are required, $\overline{M}n$ and $\overline{M}w$. These are determined from absolute methods, such as those mentioned above, for a known broad molecular weight distribution standard.

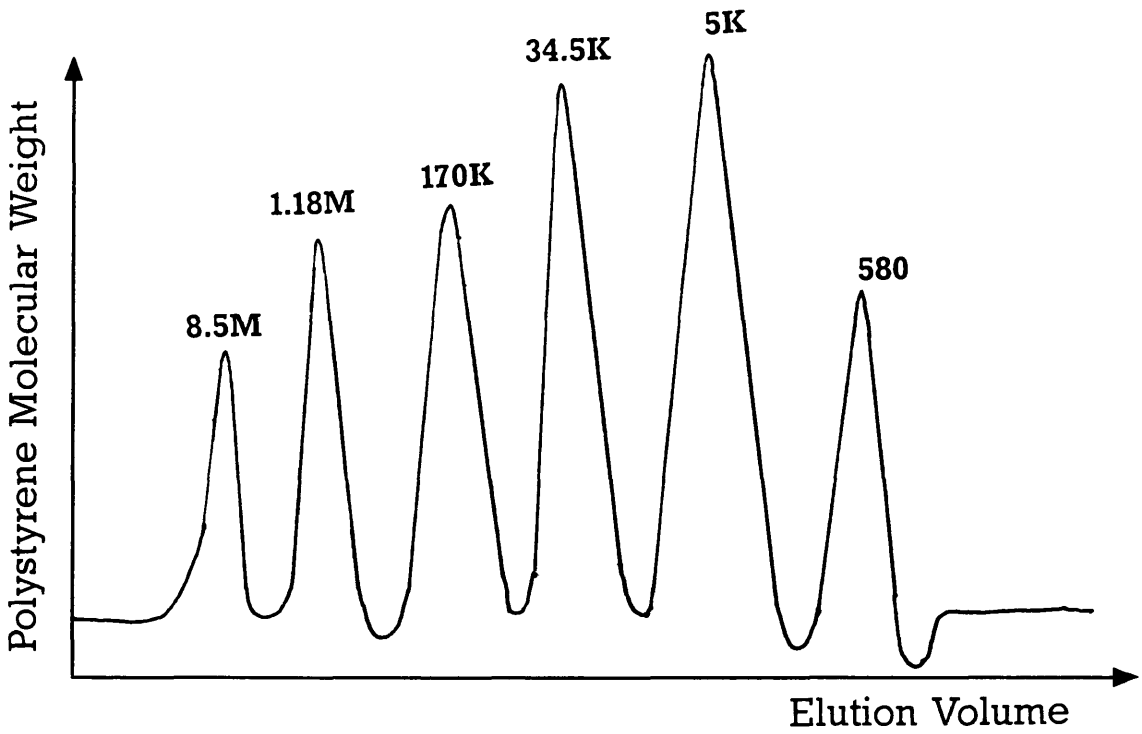

Figure 2.13 Diagram showing narrow molecular weight distribution polystyrene standards separated using a crosslinked polystyrene gel for GPC calibration.

The most common, and possibly most useful, calibration method for polymers is the Universal calibration. This method also uses narrow molecular weight distribution standards, but requires hydrodynamic information on the polymer in the form of the Mark-Houwink[92] constants. Polystyrene or poly(methyl methacrylate) are two of the few commercially available polymer standards with a series of molecular weights with narrow molecular weight distribution.

If the Mark-Houwink constants for any other polymers are also known, then based on hydrodynamic volume considerations, it is possible to obtain the molecular weight averages for those polymers. If polystyrene standards are used in the calibration (Figure 2.13) for example, it is possible to obtain molecular weight data on a polypropylene sample if Mark-Houwink constants are known for both polymers.

The hydrodynamic volume of a particular polymer can be expressed as the product of the molecular weight (M) and the intrinsic viscosity ([η]). It has been established that a plot of log intrinsic viscosity multiplied by molecular weight (log [η]M) versus retention volume (V_R) (or retention time) for different polymers results in the separate calibration curves merging into a single plot. This provides the basis for Universal calibration and assumes that retention is caused exclusively by size exclusion of the polymer molecules.

The intrinsic viscosity [η] is derived from the measured viscosity of the polymer in solution and is related to its molecular weight through an empirical equation which was proposed by several workers[93-95] and is known by various combinations of their names though most commonly as the Mark-Houwink equation[92] :-

$$[\eta] = K\bar{M}_v^{\alpha}$$

where $\bar{M}v$ is the viscosity average molecular weight, and K and α are constants for a given polymer/solvent/temperature system. For two different polymers, then, the following relationship holds:-

$$[\eta_1]M_1 = [\eta_2]M_2$$

Substituting the Mark-Houwink relationship the following equation is obtained:-

$$K_1M_1^{\alpha+1} = K_2M_2^{\alpha+1}$$

Rearrangement of this equation finally yields the following equation shown overleaf:-

$$M_1 = [K_2/K_1.M_2^{\alpha_1+1}]^{1/(\alpha_2+1)}$$

or in logarithmic form:-

$$\ln M_1 = 1/(\alpha+1) \ln K_2/K_1 + (\alpha_2+1)/(\alpha_1+1) \ln M_2$$

From this it can be seen that if molecular weight information for polymer 1 and Mark-Houwink constants for both polymers are known, it is possible to derive

molecular weight information for polymer 2. Values for K and α are tabulated for various polymers and temperature/solvent systems in the literature[96].

2.4.1.2 High Temperature GPC

At high temperatures, the theory and equipment for GPC is fundamentally the same. It is an extension of the GPC technique which is necessary when working with polymers such as polyethylene and polypropylene which are insoluble at room temperature. Complete dissolution of these polymers normally requires the use of di or trichlorobenzene as the solvent at temperatures of 130 to 150°C for most commercially avialable systems. For operation at temperatures above this it is necessary to modify the system. Titterton[97] argues that, for the analysis of polypropylene, GPC must be carried out at a temperature above its crystalline melting point in order that all polymer aggregates are eradicated from the solution and that it is necessary to use silica-based column packing at these temperatures. This is because the normal crosslinked polystyrene gel column packings are susceptible to swelling under these conditions and can cause problems of "viscous fingering" or in extreme cases even chain scission in the molecule, due to the reduction in gel interstitial space. In particular, this problem arises for samples whose molecular

weights are ~10^7 plus and it can result in deviations form the "true" molecular weight distribution. These deviations are in the form of apparently more low molecular weight polymer being detected whilst the real cause is due to "viscous fingering" or chain scission resulting in longer retention times for the affected high molecular weight polymer. This phenomenon is represented schematically in Figure 2.14.

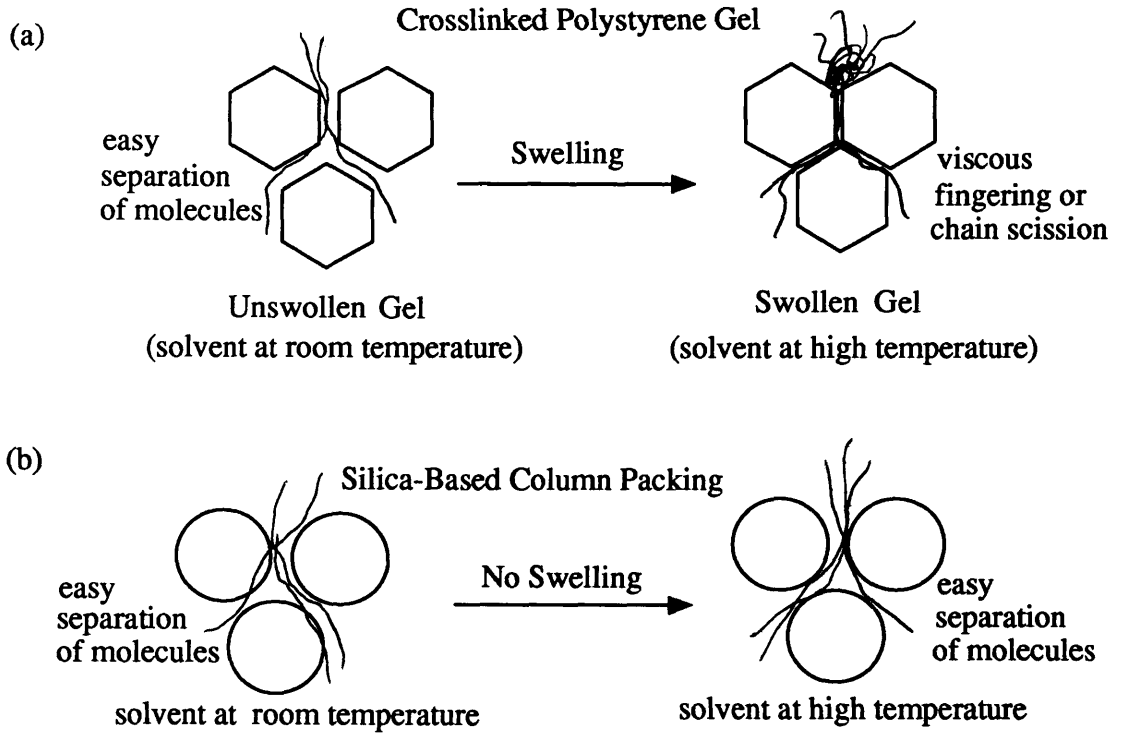

Figure 2.14 Diagram showing the effect of temperature on (a) cross-linked polystyrene and (b) silica-based GPC column packing materials.

At ICI, Titterton uses long columns (4-6 feet) with slow flow rates and wide bore stainless steel tubing. All columns and associated tubing is thoroughly insulated with kaolin wool and heated tape. The injection port is fully automatic and is kept at the same temperature as the rest of the system, as are the solvent reservoirs. All this helps to minimise heat loss (or cold spots) and improve resolution with minimal pressure effects.

Holding[98] argues that as long as the dissolution times for the polymer at temperatures above the crystalline melting temperature are adequate, then the polymer will be completely dissolved, without aggregates, and will remain in solution even when injected into a system operating at 140-150°C. RAPRA results have shown that the crosslinked polystyrene-based gel column packings have remained stable for several months operation at 150°C.

Regardless of which system is used, it is of utmost importance to keep the columns and all associated tubing well insulated and at a constant temperature, as any "cold spots" in the system can lead to increased viscosity or crystallisation of the solute which in turn, can slow down or block the flow in the system.

The type of detector must also be considered when operating at high temperatures. Refractive index is very sensitive to temperature changes and hence is susceptible to problems of unstable baselines at elevated temperatures. However, if the system is well insulated a reasonable level of baseline stability can be obtained up to temperatures of 140-150°C. Other detectors are normally more suitable for high temperature work and these include the use of fibre optics or infrared detectors.

2.4.2 Other Uses Of GPC In Polymer Science

Apart from general molecular weight analysis of polymers, GPC has been used in a number of applications such as determination of chain length in single crystals, polymer interactions in solution, research on polymerisation mechanisms, reactive degradation studies and evaluation of the possibility of processing polymers.

With continued research into the development of more sensitive detectors and more efficient column packings with higher resolutions and faster throughput times, it is likely that an ever increasing number of applications will become available for GPC as a technique in the future.

2.4.3 Instrumentation

All molecular weight measurements were carried out by RAPRA Technology Ltd on their modular high temperature GPC system. The columns used were two P.L. Gel 10 micron mixed bed type columns of 30cm length. The system was run at a temperature of 140°C with a flow rate of 1.0 ml/minute, using 1,2-dichlorobenzene containing anti-oxidant as a solvent system.

The detector was an infrared type (3.4 microns) and the system was calibrated using the Universal calibration method with narrow molecular weight distribution polystyrene as the standards. Mark-Houwink constants for the system were obtained from the literature. Each sample was run in duplicate.

2.5 POLARISED LIGHT MICROSCOPY

2.5.1 Theory Of Polarised Light Microscopy

The polarised light form of optical light microscopy is probably the most widely used when it comes to observing polymer specimens. Others include transmission microscopy, phase contrast microscopy, interference microscopy and dark field microscopy.

As its name suggests, polarised light microscopy uses polarised light obtained by passing incident light through polarising filters. These filters allow only that portion of light whose vibrations lie within a certain plane to pass through. This light is known as plane polarised light and with the development of "Polaroid" material, which is basically made from polymer sheets in which the chain molecules have been aligned into a parallel orientation by mechanical stretching, it has become relatively easy to produce plane polarised light.

The polarising filter, or polariser, is inserted into the illuminating system beneath the specimen so that it is illuminated with plane polarised light. A second polariser, known as the analyser, is placed above the specimen and is usually located somewhere in the eyepiece lens system.

If the two polarisers are positioned in such a way that their polarising planes are parallel, then the light will be transmitted without any alteration. If, however, the second polariser has its polarising planes at 90° to the first polariser then they are said to be at "cross polars" and consequently no light can pass through the microscope. If a specimen is present and light is still unable to pass through then this specimen is said to be optically isotropic. On the other hand, if a specimen is optically active, beam splitting and interference phenomena occur which rotate the light and allow it to pass through the microscope. When this situation arises, the specimen is said to be optically anisotropic. Figure 2.15 illustrates schematically the above phenomena.

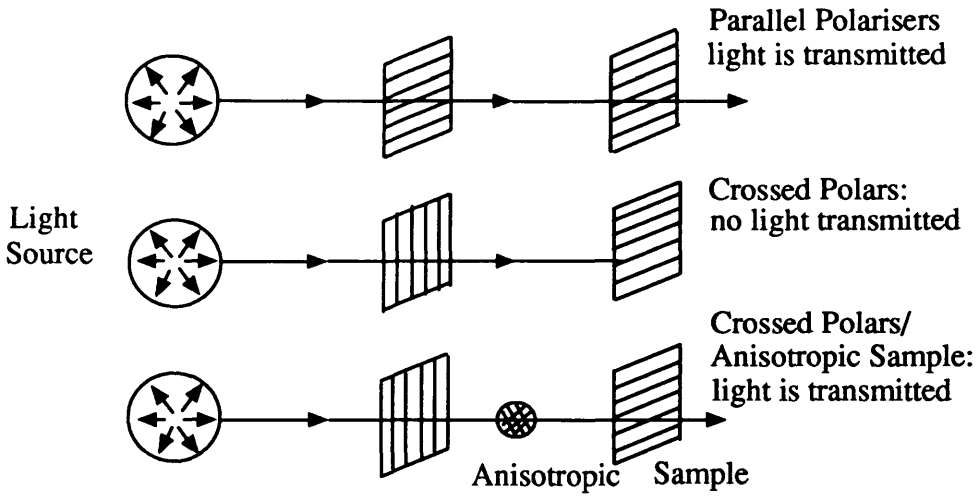

Figure 2.15 Schematic diagram showing the effect of polariser positioning and sample anisotropy on transmittence of incident light.

In an isotropic transparent material the optical properties are the same in all directions whereas in an anisotropic material the optical properties are a function of direction and result in polarised light. Provided the specimen molecule is optically anisotropic, the incident light which is already plane polarised will interact with it in such a way as to result in its becoming elliptically polarised. Such specimens will appear bright or even coloured against a dark background thus enabling the polarising microscope to be used in a qualitative way to image ordered regions in the specimen.

2.5.2 Applications To Polymers

In the application of polarised light microscopy to polymers, advantage can be taken of the ability of the semi-crystalline nature of some polymers to rotate the plane of polarised light. The most common structural feature of semi-crystalline polymers which can be viewed using a polarising microscope is the spherulite. The spherulite is a three dimensional spherically shaped morphological unit of semi-crystalline polymers in which plates grow radially from the nucleus with the chain direction of

each plate perpendicular to the direction of growth. Branching occurs during plate growth with both the regions between the plates and the interspherulitic regions consisting of non-polymeric and uncrystallisable/amorphous material. Spherulitic growth is shown schematically in Figure 2.16.

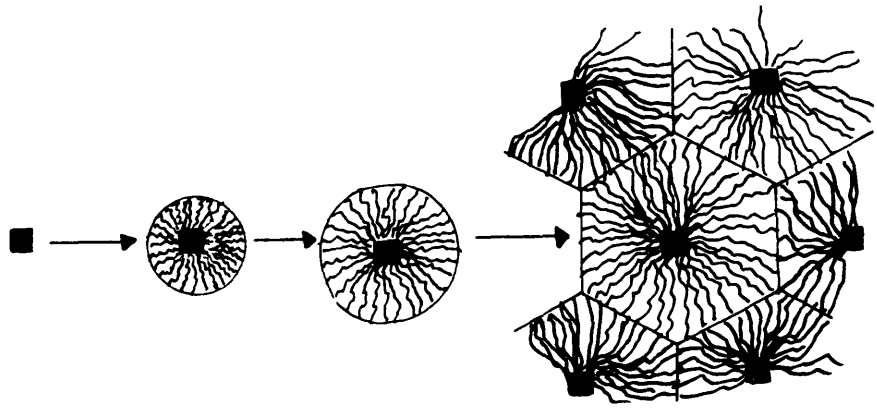

Figure 2.16 Schematic diagram showing spherulitic growth from the nuclei.

Within these uncrystallisable regions are components known as tie molecules which extend from one plate to another and which distribute mechanical stress[99,100] throughout the material. Another feature of polymer morphology is the existence of lamellae, the exact nature of which is not known but which are believed to be one of the basic anisotropic units giving rise to spherulitic anisotropy.

Information on a dimensionless quantity known as birefringence can be obtained using polarised light microscopy. Birefringence is the difference between the refractive index in two orthogonal directions. In the birefringent spherulite there are two main refractive indices, one in the radial direction and one in the tangential. In polypropylene the spherulite takes on the appearance of a Maltese Cross[101]. If the radial refractive index is higher than the tangential then the spherulite is said to exhibit positive birefringence (and vice versa for negative birefringence). Using a

birefringent accessory plate, it is possible to check the birefringence. If the optical path length of the birefringent accessory plate adds or subtracts from the optical path length of the specimen then there will be an associated change in the polarisation colours produced.

Birefringence can be used to examine the orientation, stress or form in the polymer specimen. If, for example, polymer molecules are orientated, then the magnitude of birefringence will become greater. If stress is applied to the polymer, the bonds will become stretched or deformed resulting in a change in polarisability and hence a birefringent effect associated with the principal stress axis. If dealing with rubbery polymers, care must be taken not to confuse stress birefringence with orientation birefringence because in this case it may just be an entropy elastic effect being observed rather than an energetic elastic effect. Form birefringence can occur if the polymer consists of two or more phases with different refractive indices. Keith and Padden[49] used polarised light spectroscopy and birefringence studies to identify four distinct types of spherulite in polypropylene.

As well as the aforementioned textural information, the polarising microscope can be used to monitor thermal transitions in polymers. This requires the use of a temperature controlled hot-stage. The polymer is melted between two glass slides on the hot-stage to remove any orientation effects. It can be crystallised at a controlled rate in order to give the replicate samples a common thermal history. Once crystallised the polymer sample can be reheated at a controlled heating rate until it melts. This can be observed by the disappearance of any birefringence and the subsequent dark field background. Similarly, the crystallisation process can be observed during controlled cooling of the polymer. Here the appearance of spherulite

nuclei marks the onset of crystallisation and the subsequent spherulitic growth can be imaged. In many cases microscopic determination of melting and crystallisation phenomenon in polymers can be very accurate.

2.5.3 Instrumentation

All polarised light microscopy was carried out at Napier Polytechnic, Edinburgh on a Nikon OPTIPHOT microscope with the UFX-IIA photomicrographic attachment. The photographs themselves were taken using a Nikon FX-35DX detachable camera.

Polymer samples were melted between two glass slides on the Linkam Hot-Stage and Controller before being cooled at a predetermined rate. The Linkam Hot-Stage was also equipped with a Linkam Videotext overlay VTO 232 facility.

2.6 SCANNING ELECTRON MICROSCOPY

2.6.1 Introduction

Scanning Electron Microscopy (SEM) has been commercially available as a technique for studying the materials at a considerably higher resolution than any other microscopic techniques[102] since about 1965. Although its layout is similar to that of Transmission Electron Microscopy (TEM) in which the specimen is illuminated with a static beam of radiation and subsequently focussed by a lens system in order to produce a magnified image, it is actually very different in its principle of operation.

Unlike TEM, the lens system in SEM is used in order to produce a very fine focussed beam of electrons which can probe successive points on the specimen, exciting the material and causing it to emit low energy secondary electrons and a variety of other radiations. These radiations are collected at the detector to produce a signal which in turn modulates the brightness of the beam of the display cathode ray tube (CRT). The electron beam and the CRT spot are both scanned using a rectangular set of straight lines known as a raster and as such there is an exact point-to-point correspondence between the raster on the specimen surface and the raster on the CRT screen. Each point detected from the specimen follows the last one so rapidly that they join up to produce a line across the screen. When this line is moved rapidly down the screen as it scans the specimen, the human eye is able to perceive a complete image of the specimen. In this way, then, an image of the specimen is progressively built up as a time sequence of points on the CRT screen.

The instrument can be set at different degrees of magnification and gives a considerably improved depth of field and resolution over a conventional optical microscope with the image appearing almost three-dimensional. Once the required image is produced, it can be recorded photographically for analysis. A schematic diagram of an SEM can be seen in Figure 2.17.

Ultra high resolution SEM known as Scanning Transmission Electron Microscopes (STEM) have been developed in which electrons are transmitted through thin specimens as in TEM but which are capable of resolving single atoms.

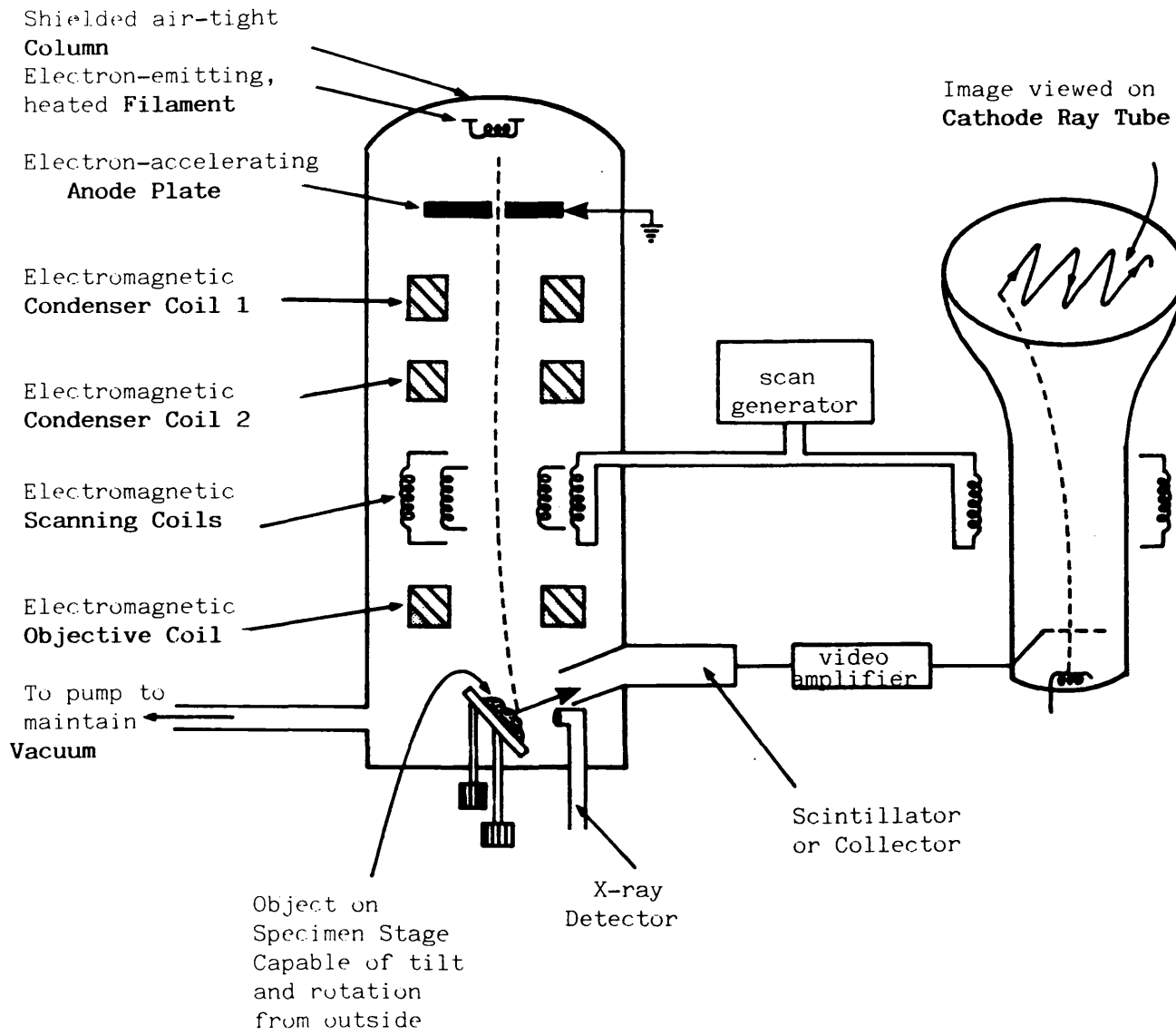

Figure 2.17 Schematic diagram of the scanning electron microscope.

2.6.2 Use of SEM In Polymer Science

As a characterisation tool for polymers, SEM has been very useful, particularly for high resolution topographical and morphological investigations[103]. One of the main problems associated with SEM analysis of polymers, however, is that they are generally very poor conductors of electricity and hence image distortions can arise due to electric charge building up on the specimen from the high energy electron beam which then interacts with the incoming electron beam and electrons which produce the signal. To overcome this problem it is necessary to sputter coat the specimen with a conductive material such as gold, which is commonly used due to its ability to produce secondary electrons on bombardment with high energy electrons and because it is easy to vapour deposit. Another problem with SEM investigations of polymers is the appearance of artefacts. These can be foreign objects which have somehow become present on the polymer surface, or modifications to the polymer surface which have been caused during sample preparation or during examination by the bombarding high energy beam of electrons.

Sample preparation, then, plays an important part in the degree of success in SEM investigation into polymers. Preparation procedures which are employed before gold sputter coating, such as selective etching[104], are often necessary when carrying out morphological studies. This procedure is useful in so much as it provides a surface profile of the polymer by effectively etching out those components of the polymer morphology which are succeptible to attack from the etchant leaving only those components that are required to be seen. This preparation procedure has been useful in revealing information about the internal structure, such as resolution of individual spherulites and their distribution. SEM has been used in a wide variety of applications to polymers but most commonly in the study of fibre morphology,

surface fractures and fibre composites. This has provided valuable information on fibre orientation, surface damage through wear and degree of adhesion in polymer composites.

2.6.3 Instrumentation

All SEM investigations were carried out on a JOEL JSM-T100 Scanning Electron Microscope with resolution 8 nm (25kV W.D. 12 mm) and magnification 50X ~ 100,000X (W.D. 12 mm), 35X ~ 75,000X (W.D. 20 mm, digital display), 15X ~ 30,000X (W.D. 48 mm) with secondary electron and back-scattered electron image modes.

The electron optics system consists of a cartridge exchange system gun filament with a built in filament monitor and an accelerating voltage of 5-15-25 kV (3 steps). The lens system is 3-stages made up of a 2-stage condenser and 1-stage objective. The astigmatism correction is an 8-pole electromagnetic X-Y method (2-stage exchange) with Astigmatism Finder and the image shift is ± 10μm in all directions with joystick control.

The instrument has a eucentric specimen stage with the following specifications:-

Specimen Shift	
Horizontal:	X = 10 mm
	Y = 20 mm
Tilt:	-40° ~ +90°
Working Distance (W.D.):	12, 20, 48 mm

The specimen size is 10 mm diameter x 10 mmH (standard) which is exchanged by specimen draw-out.

The display unit has full frame scanning, selected area scanning, line modulation and Y-modulation (YMD). The display tube is a 9-inch CRT for both observation and photography. The Scanning Image Photographic Device allows photographic recording of images and uses an automatic camera with manual shutter built-in.

The system is evacuated using an oil rotary vacuum pump with a working pressure of better than 7×10^{-4} Pa. Polymer films were made electrically conductive by coating with a thin layer of gold using a Polaron E500C-PS3 Sputter Coater.

2.7 NUCLEAR MAGNETIC RESONANCE (NMR)

2.7.1 Theory Of Nmr

The nmr technique utilises the property of nuclear spin. Since atoms such as ^{1}H, ^{13}C and ^{19}F, have an odd number of protons and/or neutrons in the nucleus, then it is possible for them to spin with non-zero angular momentum.

When placed in an external magnetic field, these spinning nuclei, which exhibit a magnetic dipole, assume certain allowed orientations or discrete energy levels with respect to this external field. The number of levels available for occupation depends on the overall spin of the nucleus. Transition from one spin state to another will result in an energy change.

Since the number of possible orientations is given by:-

$$2I+1$$

where I is the spin angular quantum number, then for a nucleus of spin I=1/2, such as ^{1}H or ^{13}C, the number of spin orientations will be 2 (ie. one lower energy state corresponding to spin aligned with the external magnetic field and a higher energy state corresponding to spin opposed to the external magnetic field). Figure 2.18 shows such behaviour schematically.

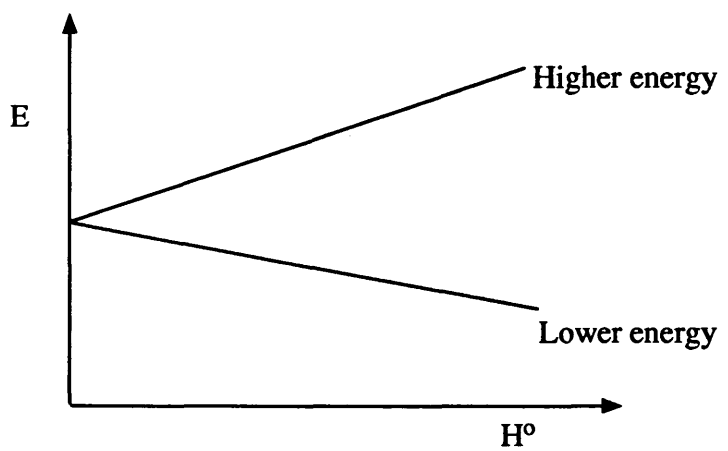

Figure 2.18 Energy levels involved in nmr.

The energy difference between the two states increases with increasing magnetic field. Since $E = h\upsilon$, where E is energy, h is Planck's constant (6.626×10^{-34} J/s) and υ is the frequency then given that $E \alpha H^{\circ}$ it follows that $\upsilon \alpha H^{\circ}$.

The spin motion of a proton is precessional or in otherwords similar to a spinning top in motion. When the hydrogen nucleus, for example, is placed between the poles of a magnetic field and electromagnetic radiation supplied, the nucleus will move from the lower energy state to a higher energy state (Figure 2.19).

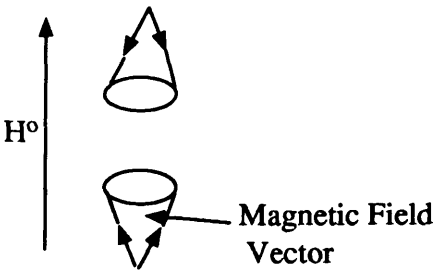

Figure 2.19 Nuclei moving to a higher energy state with increasing magnetic field.

The electromagnetic radiation required for this transition lies in the radiofrequency region of the spectrum. When the frequency of this radiation exactly matches the precessional frequency of the proton, the proton will move from the lower to the higher energy state. When this occurs, the two are said to be in resonance. For a magnetic field of 1.4 tesla the frequency for hydrogen resonance is 60 MHz. When the energy is released and the proton relaxes back to the lower energy state, the absorption of the energy involved can be detected.

If all hydrogen atoms resonated at the same value of magnetic field and radiofrequency energy, then nmr would be of little use to the chemist as a means of elucidating structure of organic molecules. However, resonance of the hydrogen atoms will vary according to their chemical environment. Normally the radiofrequency source has a fixed frequency and the magnetic field is varied, thus protons come to resonance at different values of the applied magnetic field. The spectral difference in the transition frequencies between two such chemically non-equivalent nuclei is referred to as the chemical shift.

Electrons in the bonds themselves act as magnets which oppose the applied magnetic field. The greater the electron density of the chemical bonds involved then the greater will be the size of the secondary (2^{o}) opposing field (Figure 2.20). This is known as the shielding effect.

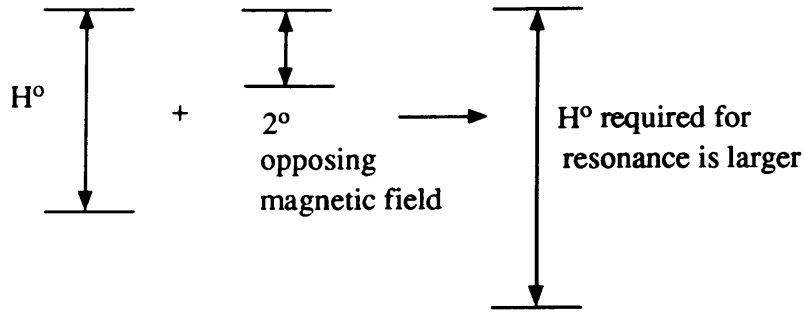

Figure 2.20 Schematic diagram showing effect of the opposing 2° magnetic field.

The variation of the required field is actually quite small and in order to overcome this, all values of chemical shift are quoted with reference to an internal standard such as the commonly used tetramethylsilane (TMS).

2.7.2 ^{13}C-Nmr And Its Application To Polymers

^{13}C-nmr has been of interest to many chemists and physicists alike probably due to the fact that carbon is the most fundamental atom in nature and life. ^{13}C behaves in a similar way to ^{1}H in nmr but in comparison has much weaker magnetic properties. It has a low natural abundance compared to ^{12}C and hence very sensitive equipment must be used to measure it. However, its low abundance also means that the chances of finding two adjacent ^{13}C atoms is very small and this renders the ^{13}C -^{13}C spin coupling negible therefore leaving only the couplings with protons to be considered.

In order to obtain reasonable levels of sensitivity it is necessary to involve the use of very large and powerful magnets. The signals produced in the ^{13}C-nmr spectra are generally narrower than those produced by proton nmr which allows a more detailed analysis of structural features. Since carbon is rarely found on the surface of a

molecule, as hydrogen is, intermolecular interactions become less of a problem and the applicability of the technique to structural elucidation in large molecules such as polymers is enhanced.

Although techniques such as ^{1}H-nmr and solid state nmr are useful in the study of polymers, ^{13}C-nmr is probably the most widely used. Many authors have found it particularly suited to the determination of polymer stereostructure[105,106] since the chemical shifts associated with each nuclear environment make it possible to determine the tactical purity of a polymer sample. This application is discussed in section 4.7.4.2 where it has been used to determine the stereostructure of various isotactic polypropylene fractions.

^{13}C-nmr has also been applied to the determination of polymer phase morphology which, in the case of polypropylene, involves the study of the α, β and γ crystalline phases[107,120]. Other applications to polymer science include the determination of co-monomer distrubutions in copolymers[108] and examination of catalyst behaviour[20] in polymerisation systems.

CHAPTER 3

3.0 EXPERIMENTAL PROCEDURES

3.0 EXPERIMENTAL PROCEDURES

3.1 INTRODUCTION

Unless otherwise stated in chapters 4 or 5, the experimental procedures outlined in this section were consistently used throughout the duration of the project.

3.2 SAMPLE PREPARATION

3.2.1 Preparation Of Polymer Film Specimens

Thin film specimens of polymer were prepared for analysis by melting and pressing pellets of the polymer between two sheets of a metal substrate (either aluminium or copper sheets of 0.051mm and 0.1mm thickness respectively) in heated platens contained within the confines of an hydraulic press.

The pellets were melted at 200°C and held at that temperature for a period of approximately 2 minutes under an applied pressure of 10-15 tons. This destroyed any previous thermomechanical history associated with the polymer and produced films which possessed similar pre-quench thermal histories.

3.2.2 Quenching Of Molten Films

Films possessing different post-quench thermal histories were obtained by releasing the pressure after 2 minutes melting time and quenching by rapidly plunging the sandwiched molten polymer directly into the appropriate quench medium. The film was held in the quench medium for approximately 1 minute to allow complete temperature equilibration.

The following quench media were used:-

Quench Medium	Temperature (°C)
Warm Water	50
Air	20
Ice Water	0
Ice/Salt Water	-18
Dry Ice/Acetone	-50
Dry Ice/Acetone	-110
Liquid Nitrogen	-190

Table 3.0 Quench media and corresponding temperatures for quench baths used throughout the project.

Samples were removed from the quench medium, separated from the metal substrate, towel dried and stored at room temperature ready for analysis. Polymer samples of low isotactic content which were "tacky" in nature and consequently difficult to remove from the metal substrate after hot pressing, were melted under a smaller load and for shorter melt times. Removal from the metal substrate was often carried out in the quench medium so that the film remained less "tacky" in nature.

3.3 ANNEALING OF FILM SAMPLES

Annealing of film samples was carried out at the appropriate temperature in an evacuated oven. The film samples being annealed were contained individually in glass vials before being introduced to the oven. To ensure the exclusion of oxygen and thus minimise the risks of film oxidation, the oven was flushed with dry nitrogen gas and evacuated several times

before annealing. The gas inlet of the oven was connected to a dry nitrogen source and after the appropriate annealing time, the pressure was released by introducing nitrogen gas into the evacuated oven, again helping to guard against sample oxidation.

3.4 PREPARATION OF POLYMER POWDERS

3.4.1 Grinding Of Polymer Pellets

Grinding small quantities of polymer pellets in a Waring blender produced powders of a fine particle size. By the intermittent introduction of liquid nitrogen into the blender, it was possible to cool the polymer below its glass transition temperature (T_g). This had the effect of increasing the brittleness of the polymer and hence the ease of grinding. Cooling the polymer in this way also helped preserve the inherent crystallinity of the polymer, since below the T_g temperature, fracture is more likely to occur in the frozen amorphous zones or glass regions of the polymer. The resultant powder consisted of a distribution of particle sizes which were separated into specific sizes using laboratory seives.

3.4.2 Polymer Powders By Precipitation

Another method which was effective in producing small particle size powders from pellets was precipitation of the polymer from solution into a non-solvent. The polymer pellets were dissolved in 1,2-dichlorobenzene at 140°C and the resultant hot solution was dropped slowly by Pasteur pipette into a large excess of methanol being constantly stirred at 0°C by use of a magnetic stirring device. The precipitated polymer was then filtered using a Buchner filter under vacuum and washed several times with methanol. The filtered polymer, which was in the form of a "cake" consisting of small particle sizes, was cut up into small pieces and thoroughly dried in a vacuum oven until all traces of solvent had been removed. Once dry, the small "cake" pieces were gently ground into a fine powder using a mortar and pestle.

3.5 PREPARATION OF POLYMER BLENDS

Polymer blends used throughout the project were prepared in one of two ways:-

(i) ***Co-Extrusion*:** Blends were prepared by Shell Chemicals UK, Carrington. Different compositions of polypropylene and amorphous terpolymer poly-α-olefins were blended together by co-extrusion in a laboratory extruder.

(ii) ***Co-precipitation:*** Blends were prepared by dissolving the various blend compositions in 1,2-dichlorobenzene and co-precipitating the polymers into a non-solvent according to the method described in section 3.4.2. After rotory evaporation of the filtrate, a negligible quantity of residue thought to consist of oligomers, soluble organic stabilisers and other impurities was recovered.

From results, there appeared to be no significant differences between blends prepared by either method.

3.6 FOURIER TRANSFORM INFRARED SPECTROSCOPY

3.6.1 General Procedure

Film specimens were prepared for infrared spectroscopic analysis by placing them in a film holder which could be mounted in the sample chamber of the FTIR instrument. In some cases where the specimen was of very low isotacticity and thus unable to form a coherent film, it was necessary to cast a film onto sodium chloride plates.

A scan of the background atmosphere was taken prior to the introduction of the sample to the film holder. In general, both background and film samples were scanned 16 times over the range 1300 - 700cm^{-1} at a resolution of 4cm^{-1}.

Unless special annealing treatments were to be performed on the film samples, they were run within one to two hours of hot pressing and were accepted or rejected on the basis of the bands of interest having a peak intensity[109] equivalent to a transmission in the region of 20-30%.

The infrared data collected from the polymer samples were stored on floppy disks from which it was possible to plot out a hard copy of each file for analysis purposes.

3.6.2 High Temperature Infrared Analysis

High temperature infrared analysis was carried out using a Specac Variable Temperature Cell and the associated Automatic Temperature Controllers. This accessory permitted infrared analysis over the temperature range ambient to 250°C.

It was necessary to record a background scan with the empty variable temperature cell mounted in the infrared sample chamber. Infrared spectra of film samples were recorded in the temperature range 30°C to 200°C throughout the study.

For operating temperatures above room temperature, evacuation of the system was necessary in order to minimise heat exchange between the heated cell and the environment. Recording infrared spectra of film samples above ambient temperatures involved increasing the temperature of the film to the appropriate point and allowing equilibration before scanning the sample 4 times. Large numbers of infrared spectra were recorded and conveniently stored on floppy disk for subsequent analysis.

3.7 DIFFERENTIAL SCANNING CALORIMETRY

3.7.1 Sample Encapsulation

There were four main forms of polymer sample used in DSC analysis throughout the project; films, pellets, powders and discs (with the most widely used form being film samples). Small flat circular discs, the same size as the sample pans, were punched from the films. When pellets were used, in order to ensure a flat base and good thermal contact with the base of the pan, they were sliced with a razor blade. Powder samples could simply be placed in the pan and sealed. Those samples which were low in isotacticity and which formed neither films or powders had to be shaped into discs for encapsulation.

In general, samples of 5-10 mg were weighed and encapsulated in Perkin-Elmer "old type" standard aluminium pans. These had the advantage of being thin and flat giving good all round thermal contact and were particularly well suited to the analysis of film samples. Unless otherwise stated, samples were run at 10°C/min in the range 30°C to 200°C.

3.7.2 Preliminary Steps Before Use Of DSC

Before starting a specific DSC programmed run, some preliminary steps were followed. To help burn off any residues or moisture in the sample furnace, the system was programmed to remain isothermal for 15-20 minutes at 500°C, with the cooling water and nitrogen purge gas flowing (the flow rate of the purge gas was set at 20 cm^3/min).

Calibration of the system was monitored by running indium and zinc standards and the resultant melting onsets and transition energies of these standards were compared against the literature values. If significant differences between obtained values and literature values was observed the system was recalibrated until agreement was reached.

3.8 X-RAY DIFFRACTION

X-ray diffraction of polymer samples was carried out by staff in the Physics Department of Dundee University as described in section 2.3.5.

3.9 GEL PERMEATION CHROMATOGRAPHY

Molecular weight measurements of polymers used throughout the project were carried out using high temperature gel permeation chromatography by staff at RAPRA Technology Ltd as described in section 2.4.3.

3.10 HOT-STAGE POLARISED LIGHT MICROSCOPY

Hot-stage polarised light microscopy observations were carried out in the Chemistry Department at Napier Polytechnic, Edinburgh. Polymer samples were melted between thin glass slides on a hot-stage and observations, taken at cross-polars, during crystallisation from this molten state were recorded by photography. Details of specific thermal treatments of the samples during this process are given in sections 4.7.3.9 and 5.2.1.1.2.

3.11 SCANNING ELECTRON MICROSCOPY

3.11.1 Preparation Of Samples For Analysis

Film samples were etched for 60 minutes at 80°C in a saturated chromic acid solution (containing 4 parts concentrated sulphuric acid to 1 part water). The films were removed and washed thoroughly with distilled water before being dried under vacuum for eight hours at 50°C.

These films were mounted on 10 x 10 mm aluminium cylindrical stubs and made electrically conductive by coating with gold, typically between 100 and 300Å thick. This was administered using a Polaron E5000-PS3 Sputter Coater. To ensure good electrical contact between the gold coated polymer film and the aluminium stub, a conducting silver paint was used to connect the two surfaces.

3.11.2 Operation Of The Scanning Electron Microscope

Sample stubs were mounted in the specimen holder and secured in position by tightening two screws around the edge of the rim which helped ensure good electrical contact.

Once the specimen holder had been placed into the SEM chamber, the electron beam was set by careful manipulation of the filament high tension. Scanning was commenced and the image was obtained by adjustment of the brightness, contrast, magnification and focus controls. Once the required image had been located on the screen, it was recorded by photography. Best results were obtained by varying the focus and astigmatism controls to obtain the sharpest image.

3.12 FRACTIONATION OF POLYMERS BY STEPWISE SOLVENT EXTRACTION

Fracionation of polymer samples was carried out in order to obtain samples which were made up of different molecular weight/tacticity fractions. This was achieved by stepwise extraction of the polymer samples in a series of solvents of increasing boiling points.

3.12.1 Sample Preparation

The polymer samples used for fractionation were converted from the pellet form into the powdered form by the methods detailed in section 3.4. The powdered polymer form allowed greater ease of wetting of the polymer and hence helped to optimise fractionation. Accurately weighed amounts of polymer were placed in paper extraction thimbles and a plug of glass wool was inserted to prevent spillage of the powder.

3.12.2 Solvents And Extraction Times

Solvents used throughout the fractionation procedure and their associated extraction times are shown in Table 3.1.

Solvent	Boiling Point(°C)	Extraction Time(Hours)
Diethyl Ether	34.6	8
n-Pentane	36.0	8
n-Hexane	69.0	8
n-Heptane	98.0	9
Toluene	110.0	11
n-Octane	126.0	17

Table 3.1 Solvents, associated boiling points and extraction times used in fractionation.

Prior to use, all solvents were purified by distillation and, in order to reduce the risk of oxidation, the solvents were thoroughly degassed by bubbling a stream of nitrogen gas through them for at least half an hour before use.

3.12.3 Extraction Apparatus

Two fractionation procedures were investigated in this study:-

(a) Soxhlet Extraction

A twin necked 500ml round bottomed flask was filled with approximately 300ml of degassed solvent. Nitrogen gas was connected to one neck of the flask and constantly bubbled through the solvent for the duration of the extraction. The Soxhlet extraction chamber and condenser were connected to the other neck of the flask. The extraction chamber was jacketed with cotton wool in order to help minimise heat exchange and keep the solvent in this chamber as hot as possible. Without specially adapted heated Soxhlet equipment, however, it was impossible to keep the solvent in this chamber at a temperature near its boiling point.

(b) Fractionation By Reflux

Thimbles containing the polymer were kept vertical in a wide-necked round bottomed flask containing degassed solvent. A condenser was attached and the system was flushed with nitrogen in order to expel any air present. A balloon containing nitrogen gas was attached to a tap and connected to the top of the condenser. The tap was fully opened in order to provide a positive nitrogen pressure inside the system.

The solvent was brought to boiling point and, as the polymer was now in direct contact with the boiling solvent, soluble material at that particular temperature was able to pass through the paper extraction thimble and remain in solution.

3.12.4 Recovery Of Fractionated Polymer

Once the extraction for one particular solvent was complete, the thimble containing unextracted polymer was removed from the flask and washed with fresh hot solvent in order to recover any soluble material absorbed by the paper thimble.

The thimble and unextracted polymer were dried thoroughly in a vacuum oven before being weighed. Once dry, the thimble containing the unextracted polymer was again placed in the wide-necked round bottomed flask and the whole extraction procedure repeated with a higher boiling solvent.

The extracted polymer, which remained in solution, was recovered by evaporating off the solvent using a rotory evaporator. The last traces of solvent were removed by thorough drying in a vacuum oven before weighing.

3.12.5 Oxidation Of Fractions

Due to the high temperatures of the boiling solvents and in spite of the precautions taken, oxidation occurred occasionally. This was monitored by infrared spectroscopy of the fractions.

3.13 DENSITY MEASUREMENTS

Densities of polymer samples used throughout the project were measured according to a flotation method as discussed by other authors[110,111]. This involved floating a polymer sample in a mixture of ethylene glycol dimethyl ether and 2-ethoxyethanol (densities of 0.867 and 0.930 g/ml respectively).

Densities of various mixtures of the two solvents were obtained by weighing them at 20°C in a 50ml density bottle standardised using distilled water. To obtain the density of the various mixtures of the two solvents, the weight of each mixture in the density bottle was divided by the density of the distilled water (0.9986 g/ml) in the density bottle at 20°C. The results were plotted on a graph of density versus percent mixture and a linear relationship was obtained.

3.13.1 Measurement Of Polymer Densities

Film samples were cut into square shapes of $1cm^2$ and placed in a measuring cylinder with a known volume of ethylene glycol dimethyl ether, the low density solvent, in which they sank to the bottom. The higher density solvent, 2-ethoxyethanol, was added to the measuring cylinder by burette and the two solvents allowed to mix. Additions were continued until the polymer film began to float. The percentage mixture at this point was calculated and fed into the computer calibration graph to obtain a density value for that particular mixture and hence the floating polymer film.

3.14 CARBON-13 NUCLEAR MAGNETIC RESONANCE

^{13}C-nmr spectra were recorded by staff at the Centre For Nuclear Magnetic Resonance at the University of Warwick using a Bruker spectrometer at 120°C with an operating frequency of 100.62Hz. Samples were prepared by dissolving 10% by weight of polymer into a

thoroughly degassed 1,2-dichlorobenzene (90% vol)/toluene-d8 (10% vol) solution at 140°C. These solutions were transferred into heated 5 mm Nmr tubes recommended for high field, multiple scan FT-nmr experiments.

Toluene-d8 was used as the internal lock for the system and the pulse angle for protonated carbons in the polymer was 50°. The pulse time was 6 microseconds and spacing between each pulse was 1.65 seconds. The number of scans, or transients, accumulated varied according to each sample.

CHAPTER 4

INVESTIGATIONS INTO THERMALLY INDUCED STRUCTURAL CHANGES IN ISOTACTIC POLYPROPYLENE HOMOPOLYMER

All quoted results in this chapter have estimated error values of:

Density	± 1%
FTIR APRA	± 0.2%
DSC Temperature	± 0.1%
DSC Enthalpy	± 0.1%

4.0 INVESTIGATIONS INTO THERMALLY INDUCED STRUCTURAL CHANGES IN ISOTACTIC POLYPROPYLENE HOMOPOLYMER

4.1 INTRODUCTION

Various studies are reported in this section concerning the behaviour of polypropylene under different thermal treatments. Fourier transform infrared spectroscopy (FTIR) and differential scanning calorimetry (DSC) were used to investigate thermally induced changes in polypropylene homopolymer structure and complimentary techniques such as wide angle x-ray diffraction (WAXD), scanning electron microscopy (SEM) and density measurements provided additional information on the treated samples.

Fractionation of the polypropylene homopolymer was undertaken in order to provide fractions of different molecular weight/tacticity composition for analysis. In addition to other techniques already mentioned, hot stage polarised light microscopy and ^{13}C-nmr were used in these studies.

4.1.1 Quenching Of Polypropylene Rapidly From The Melt

The quenching of isotactic poypropylene from its molten state gives rise to a structural reorganisation which is strongly dependent on quenching conditions. By rapid quenching at sufficiently low temperatures it is possible to obtain a biphasic system in which no crystallisation has taken place. This biphasic system consists of one phase which is totally amorphous and another which is structurally disordered and generally accepted by most authors[112-114] to be intermediate in nature between the amorphous and crystalline phases.

This second phase has been variously described in the literature by several authors. Natta[112] termed the structure as being "smectic" suggesting that it is comprised of chains in the parallel 3_1 helical conformation, as they are in the crystalline phase, but that disorder exists in packing of these chains perpendicular to their axes with right- and left-handed helices occurring at random. The relative displacements and orientations of the neighbouring chains do not appear to be completely random, thus indicating a structure which possesses a degree of order higher than that of an ideal nematic liquid crystalline phase in which the only degree of order is the molecular parallelism. A second structure was proposed by Miller[113] who described the quenched form as a paracrystal in which the edges of the unit cells are distorted in both length and direction. Gailey and Ralston[114] suggested an even higher degree of order existed and proposed a structure composed of very small (50-100 Å) hexagonal cystals. Gezovich and Geil[115] agreed with this view reporting that the "ball-like" structures they had observed were basic morphological units of the quenched form consisting of imperfect hexagonal crystallites.

A nodular smectic phase was observed on the surface of rapidly quenched polypropylene samples by Hsu and Geil[116] who suggested that the smectic phase crystallises from the glassy state at circa -20°C. Bodor and co-workers[117] assumed that the quenched form contained microcrystals of monoclinic polypropylene, arguing that crystal size line broadening in the x-ray analysis of this phase was responsible for the characteristic diffuse halo x-ray diffraction pattern. McAllister and co-workers[118] suggested that the quenched form contains approximately 60% amorphous material and that the remainder of the sample is constructed of chain helices arranged in a square array with cubic or tetragonal symmetry. Wunderlich and Grebowicz[119] described the quenched phase as a conformationally disordered crystal or "condis crystal".

More recently, in high-resolution solid-state ^{13}C-Nmr studies reported by Gomez and co-workers[120], the local packings of 3_1 helices in the β-form of polypropylene corresponded well with those of polypropylene in the quenched state. Corradini and co-workers[121], on the other hand, concluded that the mesomorphic form of polypropylene is not composed of small β-form crystals, but is much more disordered with the chains existing in bundles which exhibit parallelism of the chain axes with roughly 3_1 helices and an average interchain distance of 6.0Å. The local correlations between chains are more likely to resemble those which characterise the crystal structure of the monoclinic form, as opposed to those characterising the structure of the hexagonal form.

If polypropylene is quenched at a temperature higher than 70°C no smectic phase is obtained and the system, which is again biphasic, is made up of an uncrystallisable amorphous phase and a monoclinic crystalline phase. Quenching polypropylene at intermediate temperatures therefore produces a triphasic system consisting of an amorphous phase, a smectic phase and a monoclinic crystalline phase. The relative amounts of each phase formed is crucially dependent on the temperature of quenching; thus the lower the quench temperature, the larger the fraction of the smectic phase produced.

At room temperature, the smectic phase is stable for long periods of time, but can be readily transformed to the monoclinic crystalline phase simply by heating at temperatures above 70°C[122,123]. This transition to the crystalline form requires a significant amount of structural reorganisation leading to dimensional instability which in turn can affect mechanical properties. Consequently, studies investigating mechanical behaviour of the quenched form of polypropylene have been carried out[111,124].

4.2 STRUCTURAL DETERMINATION OF ISOTACTIC POLYPROPYLENE USING INFRARED SPECTROSCOPY

Infrared spectroscopy has been widely used for the determination of structure in isotactic polypropylene. Much of the work has concentrated on the crystallinity and stereoregularity of polypropylene through the study of crystallinity or helix bands in the infrared spectra. Natta and co-workers[9] described the relative intensities of bands found in unfractionated, amorphous and molten polypropylene between 1330 and 675 cm^{-1} using polarised infrared spectroscopy. They found that most of the differences between the infrared spectrum of the crystalline and non-crystalline polypropylene disappeared on melting of the crystalline product and reappeared after cooling the melted sample.

Abe and Yanagisawa[125] studied the thermal resistance properties of polypropylene using polarised infrared spectroscopy. They postulated that, from measurements of the melting behaviour, some spectral bands could be called "crystallinity sensitive" bands and others "amorphous" bands. They also proposed that the ratio of the optical densities of bands near 1000 and 970 cm^{-1} might be used as a measure of crystallinity. Heinen[126], using a similar procedure, noted that certain bands such as those near 1450, 1370, 1171, 978 and 890 cm^{-1} seemed to be independent of temperature whereas those near 1329, 1305, 1223, 1106, 1048, 1003, 944, 904, and 846 cm^{-1} either increased or decreased in intensity at higher temperatures. He concluded that these bands are temperature sensitive and connected with the degree of crystallinity. Using the band at 1171 cm^{-1} as an internal thickness standard and the band at 846 cm^{-1} as a crystallinity sensitive band Heinen[126] investigated, for the first time, the relationship between absorbance ratio A846/A1171 and the density of polypropylene homopolymer and its fractions in order to determine the crystallinity of the polymer.

Majer[127] used infrared absorption bands at 973 and 1245 cm^{-1} as internal thickness standards and densimetric calibration to obtain crystalline content with a precision of ±7% crystallinity.

From infrared studies on supposedly 100% isotactic and 100% atactic polypropylene samples, Luongo[128] published the first quantitative study seeking to relate isotacticity to infrared absorption band intensity. Showing that displacement towards the 1156 cm^{-1} position occurred in the 1171 cm^{-1} band as the percentage atactic material in the polymer increased, Luongo cautioned Heinen's use of this band[126]. In his studies Luongo made use of the absorption bands at 974 and 995 cm^{-1} showing that the ratio of these bands was a function of the isotacticity of the sample. This led him to establish a calibration curve relating the absorbance ratio to isotactic content, using physical mixtures of the supposedly completely isotactic and atactic polypropylene.

In a review by Krimm[129], it was argued that since the isotactic index was closely related to the crystallinity of the sample, thermal history effects would determine the outcome of the measurements. Brader[130] attempted to overcome this problem by annealing his samples in Carbowax at 160°C. However, his procedure failed to exclude oxygen and therefore the results were affected by problems associated with sample oxidation. Hughes[131] prevented sample oxidation in his experiments by annealing at 165°C for 3 hours in an argon atmosphere in order to fully develop the isotactic material into infrared active ternary helices. McDonald and Ward[132], in earlier experiments involving the comparison of the infrared spectra of partially deuterated polypropylenes with those of isotactic polypropylene, concluded that several infrared absorption bands are specific to the helical structure. They further concluded that the infrared spectrum cannot distinguish either crystallinity or tacticity *per se* but only a chain configuration state, since crystallinity is related to both

inter-molecular packing and helical conformation. Other authors[133,134] had also noted this, showing that the intense band at 995 cm^{-1} as well as those at 1170 and 841 cm^{-1} are related to the actual conformation rather than the crystallinity of the polymer.

The appearance of each isotactic helix band in the infrared spectrum of polypropylene is dependent on the length of the isotactic sequences in the polymer. The critical sequence lengths or effective regular sequence lengths (J_{eff}) above which each band will appear[20] are shown in Table 4.O.

Helix Band (cm^{-1})	J_{eff} (monomer units)
841	13-15
973	5
998	11-12
1167	---

Table 4.0 Effective regular sequence lengths (J_{eff}) for the appearance of the helix bands in the infrared spectrum of isotactic polypropylene.

Other ratios that have been used as indices of isotacticity are A998/A1460 (Spectral degree of isotacticity [α]); A998/A973 (Macrotacticity [M]); and A841/A973.

4.3 THE EFFECT OF RAPID QUENCHING FROM THE MELT ON ON THE IR SPECTRA OF SEVERAL COMMERCIAL ISOTACTIC POLYPROPYLENE HOMOPOLYMERS

An attempt was made in the present study to use infrared absorption ratios to investigate changes induced in commercial polypropylene by rapid quenching from the molten state into quench baths of various temperatures (see section 3.2.2).

Polypropylene samples used were highly isotactic and any change in the intensity of the infrared helix bands induced by rapid quenching was therefore considered to be due to the formation of the conformationally disordered smectic phase. Since the 841 and 998 cm^{-1} bands are sensitive to such changes, they were used to monitor the degree of structural change in polypropylene samples with respect to the temperature of quenching. The bands at 973 and 1167 cm^{-1} are relatively insensitive to such changes and could therefore be used as internal thickness reference bands.

The absorption ratios used in this study were as follows:-

A841/A973; A841/A1167; A998/A973; and A998/A1167.

These ratios have proved to be useful in the construction of calibration curves with respect to ^{13}C-nmr triad tacticities of polypropylene samples of varying isotactic content[109]. Due to their linearity the A841/A973 and A998/A973 ratios provide the best calibration curves. The corresponding calibration curves with the 1167 cm^{-1} internal standard contain more scattering and lack sensitivity in the important higher isotacticity regions.

4.3.1 Experimental

Two studies were carried out involving several commercially available isotactic polypropylene homopolymers which are commonly used by industrial processers in Tayside. Samples were pressed into films and quenched from the molten state using the procedures detailed in section 3.2. Infrared spectra of these films were recorded over the 1300 - 700cm^{-1} spectral range according to the procedure described in section 3.6.1. Molecular weight and density characterisation data for these polypropylenes is shown in Table 4.1.

Supplier	Grade	Density	$\bar{M}n$	$\bar{M}w$	$\bar{M}w/\bar{M}n$
ICI	GSE18	0.903	61610	376400	6.970
ICI	GYE41	0.903	51935	23250	4.610
ICI	GWE23	0.903	72525	442250	6.098
ICI	GXE35	0.903	58825	317850	5.403
SHELL	PLZ772	0.905	21205	199500	9.408
SHELL	JY6100	0.905	57810	477600	8.262
SHELL	KY6100	0.905	56215	438150	7.794
SHELL	LY6100	0.905	55020	436050	7.925
AMOCO	50103	0.900	70625	433250	6.135
AMOCO	50202	0.900	69190	454850	6.574
NESTE	UB3249F	0.900	76430	405100	5.300

Table 4.1 Polypropylene characterisation data.

4.3.2 Fourier Transform Infrared Absorption Peak Ratio Analysis (FTIR APRA)

The infrared spectrum of isotactic polypropylene between 1300 and 700cm^{-1} contains twelve bands, many of which overlap, making the study of integrated absorbance values difficult. For this reason it was found to be more convenient to study band height or intensity of the band of interest.

In a recent study[109] concerning infrared spectroscopic determination of polypropylene stereoregularity, Burfield and Loi indicated that FTIR absorbance values were significantly affected by computerised data processing methods such as "smoothing" or "flattening" of the infrared spectra, a method that is often used in order to obtain a common baseline for all absorbtion peaks. In this study no such manipulation of the raw data was undertaken and all spectra were analysed manually.

Infrared spectra were plotted onto graph paper and appropriate baselines were drawn for the absorption bands of interest. A typical example of baseline values for each band is given in Table 4.2 (although it was sometimes necessary to stray from these positions due to unstable sloping baselines)and spectra showing the infrared region of interest are shown in Figure 4.0.

Absorption Band (cm^{-1})	Baseline (cm^{-1})
841	930 - 780
973	1030 - 930
998	1030 - 930
1167	1230 - 1125

Table 4.2 Baseline parameters for the infrared absorption bands of interest.

Once the baseline had been constructed, a vertical line was drawn from the peak maximum to meet the baseline. The number of boxes on the graph representing the length of the vertical line from the peak maximum to the baseline were counted and converted to a value for absorption. This procedure was followed for each absorption band of interest.

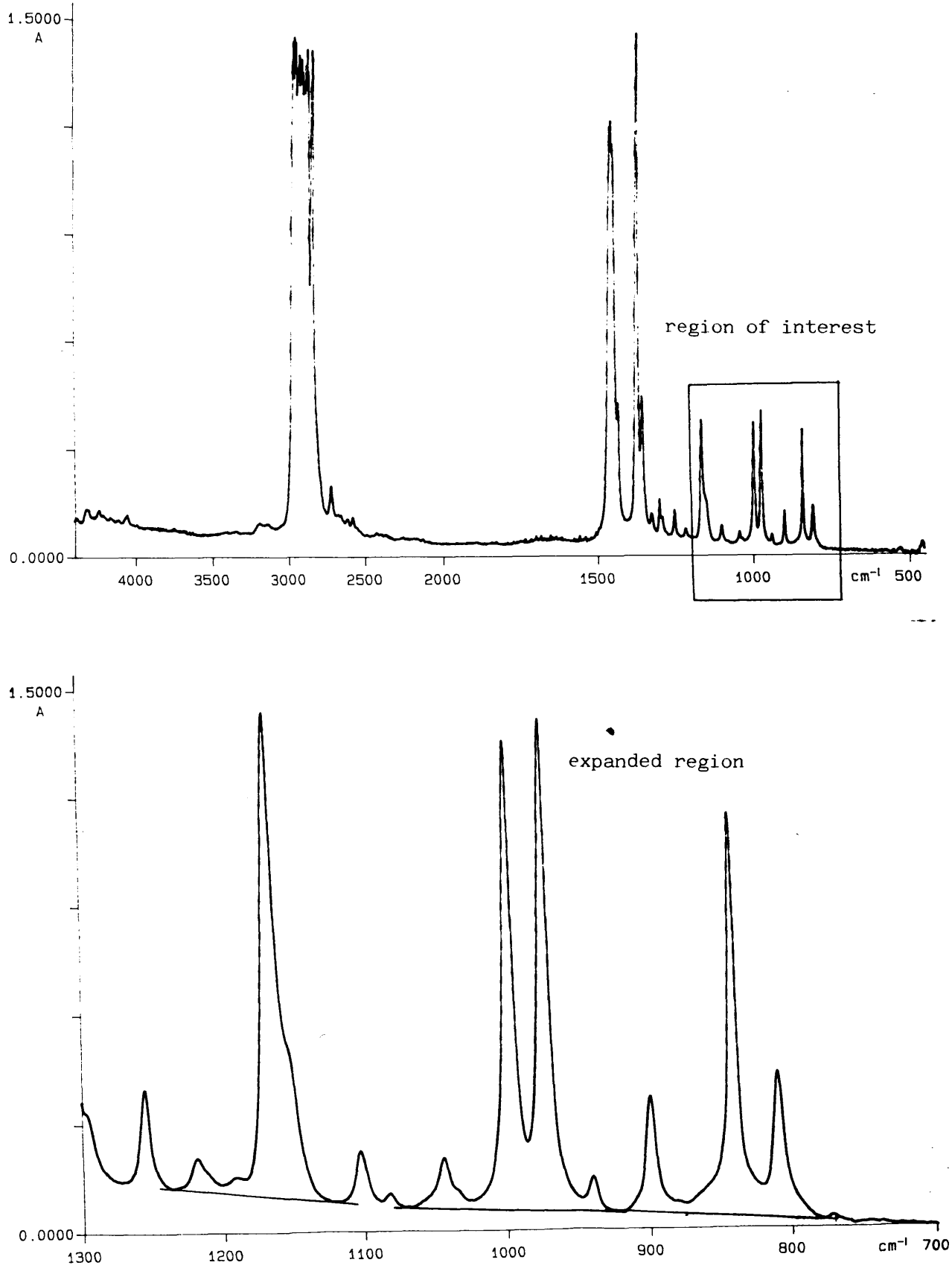

Figure 4.0 FTIR spectra showing the region of interest. (a) Full absorbance spectra (b) Expanded region

4.3.3 Preliminary Investigation

The aim of this preliminary study was to investigate the use of infrared spectroscopy as a means of detecting changes induced by rapid quenching from the melt of commercial polypropylene samples. Other techniques, including x-ray diffraction, density measurements and scanning electron microscopy were utilised in order to confirm that structural changes had actually taken place. Polypropylene samples and quench media used are shown in Table 4.3(a) and 4.3(b).

Quench Medium	Quench Temperature (°C)
Air	20
Ice/water	0
Ice/salt water	-18
Dry ice/acetone	-50
Liquid nitrogen	-190

Table 4.3(a) Quench media and corresponding temperatures used in the preliminary study.

Supplier	Grade
ICI	GSE18
ICI	GYE41
SHELL	PLZ772

Table 4.3(b) Commercial polypropylene samples used in the preliminary study.

Film thickness plays an important role in the extent of infrared transmission through the polypropylene films. The most reproducible measurements[112] for the ratios used in this study were found to be in the infrared transmittance range of 20-30% and consequently only films exhibiting this degree of transmittance were accepted for analysis.

In order to avoid any potential room temperature annealing effects which can lead to a slow post-quench increase in ratio values, sample spectra were recorded immediately after quenching. For each quench temperature and each polypropylene type, 10 replicate samples were prepared and analysed.

4.3.3.1 Oxidative Degradation Of Samples

Polypropylene has numerous tertiary carbon atoms and as such is susceptible to oxidative degradation. Hot pressing and annealing at high temperatures can accelerate this process and therefore monitoring of the films for signs of oxidation was carried out by checking for infrared carbonyl and unsaturation bands at 1715 and 1640 cm^{-1} respectively. In some cases, O-H stretch was exhibited at around 3400 cm^{-1} in the oxidised samples.

4.3.3.2 Metal Substrates For Pressing Of Films

Gezovich and Geil[115] found that they obtained a completely smectic/amorphous system in polypropylene quenched from the melt into media at temperatures up to 20°C using an aluminium substrate, whereas with a glass substrate they obtained 50% monoclinic crystalline form and 50% smectic form. Vittoria and Perullo[135] have shown that they obtained only the smectic and amorphous phases with thin copper foil

substrates at 0°C but when the thickness of the substrate was increased, the monoclinic phase began to appear at the expense of the smectic phase.

In the present study, two metal substrates (aluminium and copper foil) were investigated for use in the hot pressing of polypropylene films. Aluminium foil (0.051mm thick) was the thinner of the two but has the poorer thermal conductivity. Copper foil, on the other hand, has very good thermal conductivity but was thicker (0.1mm thick).

To test the effect of the substrate on the degree of quenching, densities of the polypropylene films, quenched at different temperatures, were measured and a graph of density versus quench temperature plotted for each substrate. The graph showing the effect of quench temperature and substrate on the density of the GSE18 polypropylene sample is shown in Figure 4.1.

Density values of the quenched films decrease with decreasing quench temperature indicating a corresponding drop in crystallinity. Although copper has the more favourable thermal conductivity of the two substrates, there appears to be little difference in the density values regardless of which substrate is used. In this study aluminium foil was used for all pressing of polypropylene films.

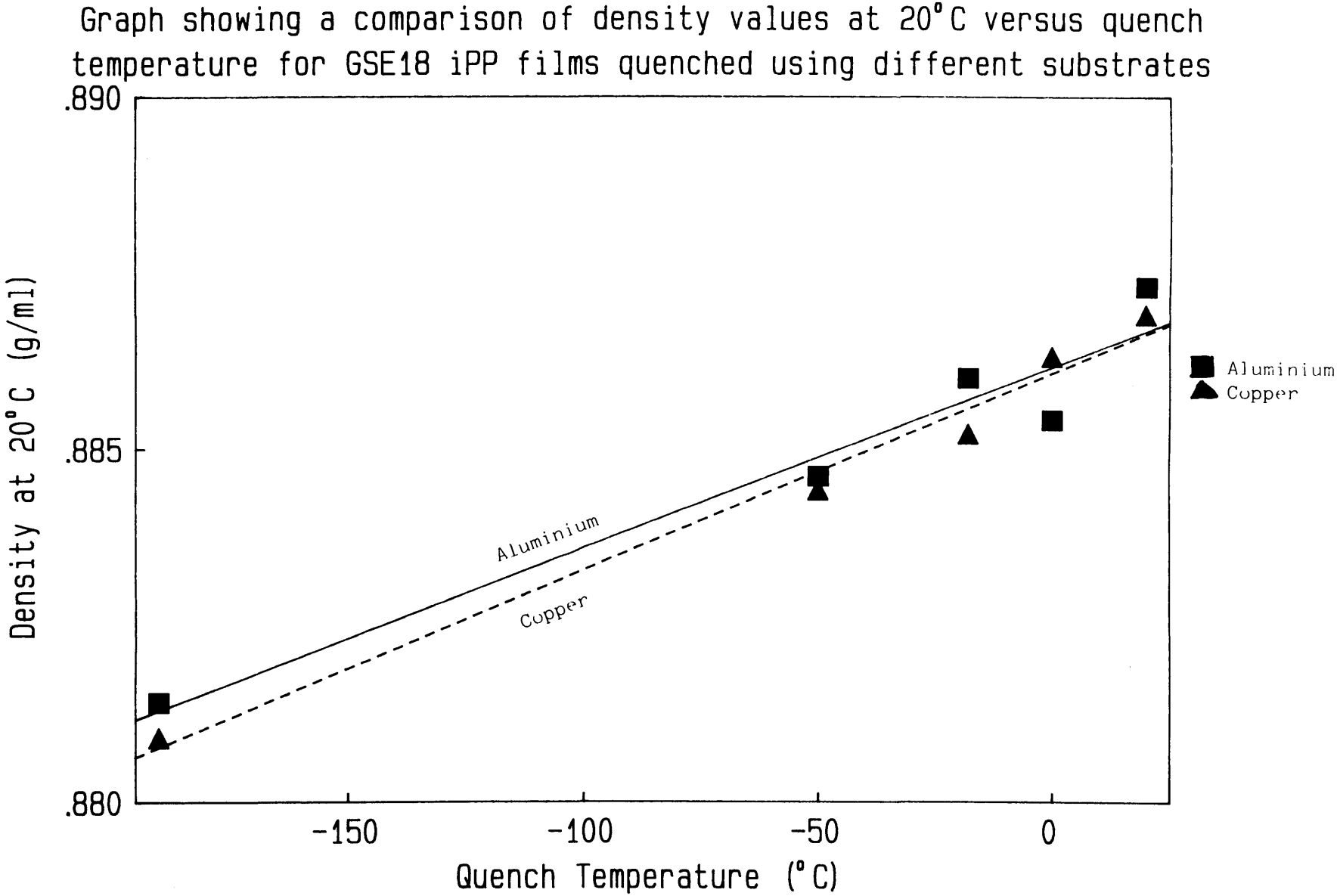
Graph showing a comparison of density values at 20°C versus quench temperature for GSE18 iPP films quenched using different substrates
.890
.885
.880
Density at 20°C (g/ml)
-150
-100
-50
0
Quench Temperature (°C)
Aluminium
Copper
Aluminium
Copper

Figure 4.1

4.3.3.3 FTIR APRA Results

Comparison of absorption ratios within each sample with respect to quench temperature are shown in Tables 4.4 - 4.6.

Sample = GSE18

Quench Temp(°C)	Ratios			
	A841/A973	A841/A1167	A998/A973	A998/A1167
20	0.7366	0.8127	0.8726	0.9627
0	0.7133	0.8042	0.8550	0.9640
-18	0.6772	0.7935	0.8207	0.9632
-50	0.6931	0.8013	0.8381	0.9702
-190	0.6913	0.7929	0.8364	0.9570

Table 4.4 Mean absorption ratio results for GSE18 at each quench temperature.

Sample = GYE41

Quench Temp(°C)	Ratios			
	A841/A973	A841/A1167	A998/A973	A998/A1167
20	0.7905	0.8303	0.9384	0.9856
0	0.7352	0.8079	0.8853	0.9736
-18	0.7465	0.8065	0.8944	0.9678
-50	0.7201	0.8059	0.8741	0.9771
-190	0.7597	0.8051	0.9047	0.9666

Table 4.5 Mean absorption ratio results for GYE41 at each quench temperature.

Sample = PLZ772

Quench Temp(°C)	Ratios			
	A841/A973	A841/A1167	A998/A973	A998/A1167
20	0.7759	0.8203	0.9055	0.9571
0	0.7083	0.8041	0.8494	0.9644
-18	0.7500	0.8109	0.8861	0.9582
-50	0.7030	0.8018	0.8443	0.9631
-190	0.7396	0.8064	0.8755	0.9549

Table 4.6 Mean absorption ratio results for PLZ772 at each quench temperature.

4.3.3.4 Comments On Results

From statistical analysis of variance and Scheffé's "s" test (Appendix 1) on these results the following general statements can be made about the polypropylene samples used in the study:-

(i) There are statistically significant differences in values for a given infrared absorption ratio and quench temperature between the GSE18, GYE41 and PLZ772 polypropylene grades.

(ii) For a given polypropylene grade, infrared absorption ratio values vary and are dependent on quench temperature.

(iii) Samples quenched at a temperature below 0°C have statistically similar infrared absorption ratio values which are significantly different to those quenched above 0°C.

From this, the conclusion is that infrared absorption peak ratio analysis does detect quench induced differences in the structure of polypropylene and the above points will be expanded on in the discussion.

4.3.3.5 Wide Angle X-Ray Diffraction (WAXD) Of Quenched Films

The effect of rapid quenching from the melt on the samples was apparent in the WAXD patterns of quenched films. Samples which had been rapidly quenched below 0°C showed diffuse halos characteristic of the WAXD pattern for smectic polypropylene.

X-ray photographs of polypropylene samples which have been (i)quenched and annealed, (ii) quenched at -50°C and (iii) quenched at -190°C are shown in Figure 4.2.

WAXD powder diffractograms also showed differences in samples quenched at different temperatures. These are shown in Figure 4.3 for the quenched and annealed sample and the samples quenched at -50°C and -190°C respectively.

4.3.3.6 Scanning Electron Microscopy Of Quenched Films

Quenched films were prepared for scannning electron microscopy by chromic acid etching and gold sputter coating (section 3.11). Electron micrographs of the surface of GSE18 films are shown below in Figure 4.4 for a quenched and annealed film and the -50 and -190°C quenched films respectively.

Scanning electron microscopy of the quenched films proved difficult due to annealing effects on the film during etching and many films prepared for analysis by this method had to be disregarded.

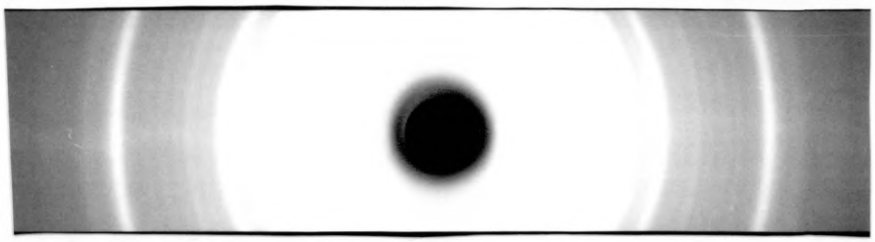

Quenched and annealed

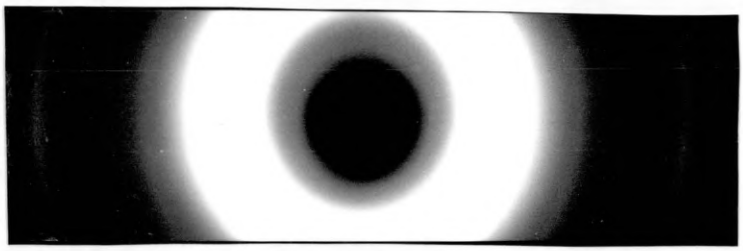

-50°C Quench

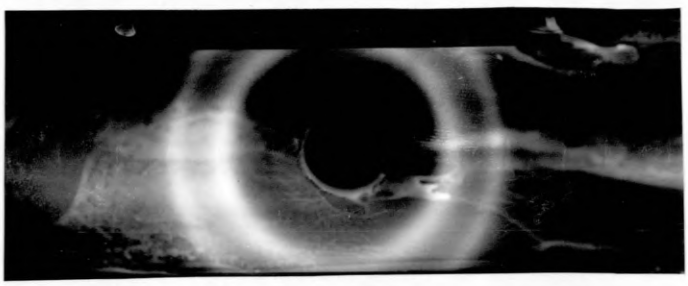

-190°C Quench

Figure 4.2 X-ray photographs of GSE18 polypropylene quenched from the melt at different temperatures

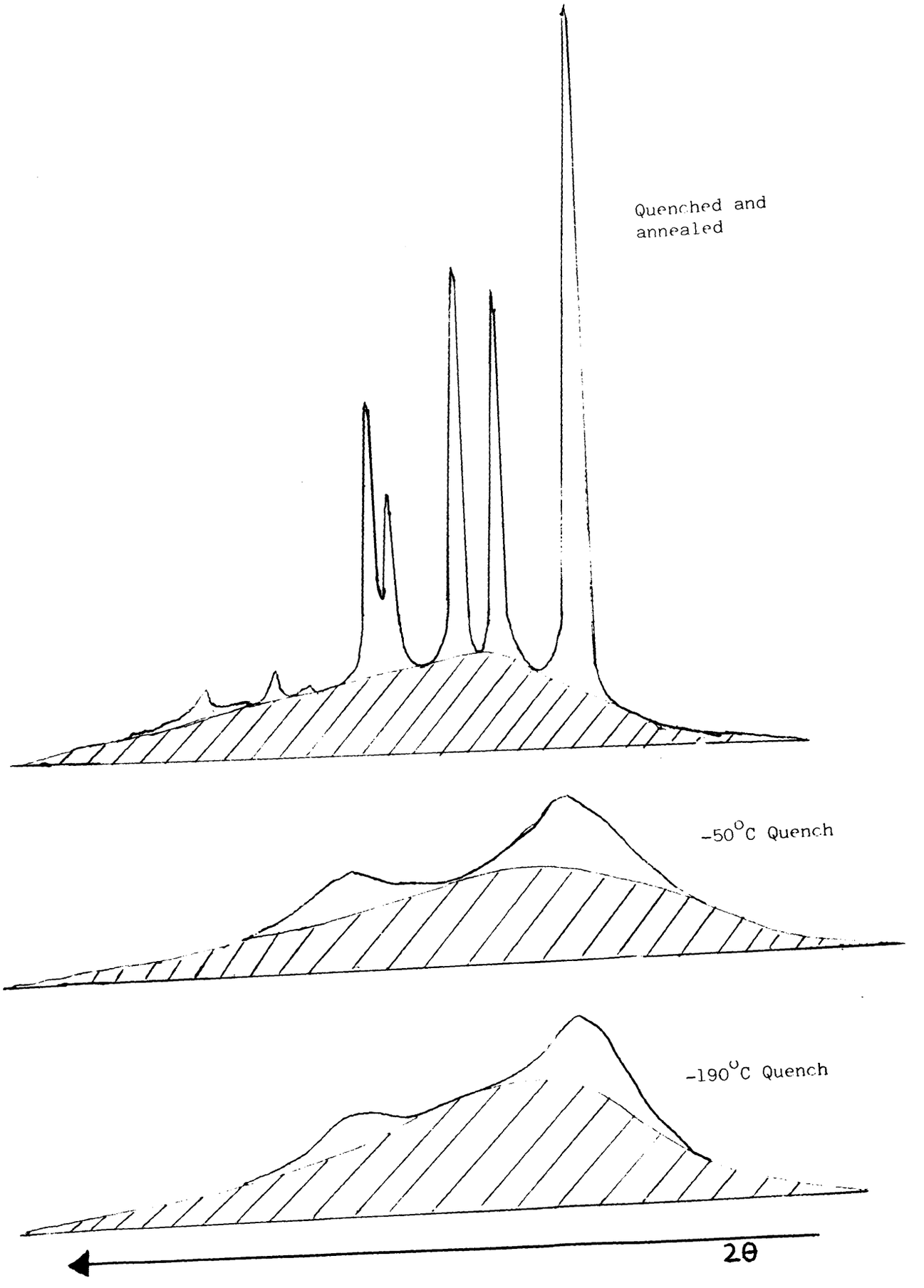

Figure 4.3 X-ray diffractograms of GSE18 polypropylene quenched from the melt at different temperatures

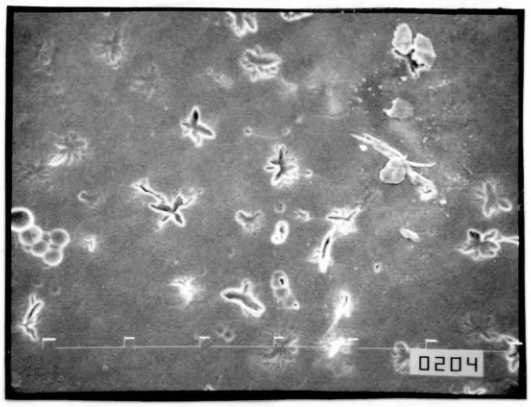

Quenched and annealed

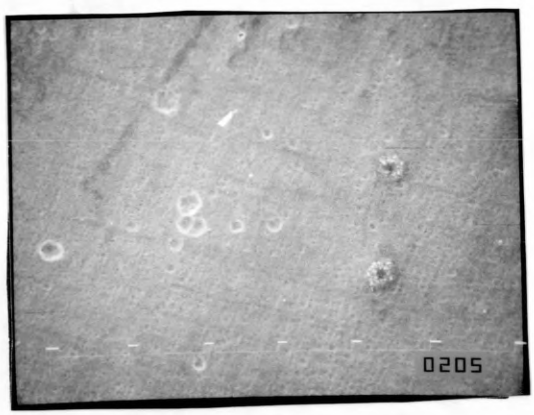

-50°C Quench

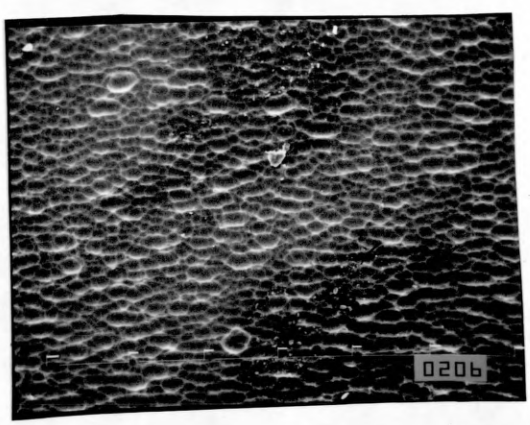

-190°C Quench

Figure 4.4 SEM photographs of GSE18 polypropylene quenched from the melt at different temperatures

4.3.3.7 Density And Crystallinity Of Quenched Samples

Percentage crystallinity was calculated for the GSE18, GYE41 and PLZ772 polypropylene samples for each quench temperature from density measurements (section 3.13) using the following equation:-

$$X_c = d_c/d_q.(d_q - d_a)/(d_c - d_a) \times 100$$

where X_c= percentage crystallinity of the sample

d_q= density of the quenched sample

d_c= ideal density[136] of crystalline polypropylene (0.936 g/ml)

d_a= ideal density[136] of amorphous polypropylene (0.856 g/ml)

The results for the mean densities and percentage crystallinities for the quenched samples are shown in Table 4.7.

	GSE18		GYE41		PLZ772	
Quench Temp(°C)	Mean Density	% Cryst^y	Mean Density	% Cryst^y	Mean Density	% Cryst^y
20	0.8873	41.27	0.8893	43.81	0.8880	42.16
0	0.8854	38.85	0.8873	41.27	0.8869	40.76
-18	0.8860	39.62	0.8858	39.36	0.8853	38.72
-50	0.8846	37.83	0.8851	38.47	0.8851	38.47
-190	0.8814	33.72	0.8820	34.49	0.8819	36.71

Table 4.7 Mean Density and percentage crystallinity values for each polypropylene grade as a function of quench temperature.

The figures stated for percentage crystallinity are in fact incorrect because the equation used is based on the two-phase crystalline-amorphous model but in the quenched films it is likely that there will be smectic, crystalline and amorphous phases present and in some cases a two-phase smectic-amorphous system. In order to calculate the exact percentage crystalline material present, information is required on the exact mass of one of these phases. Once this is known, the percentage of the other two can be calculated due to the fact that the three phases are linked by the expression:-

$$X_c + X_{sm} + X_a = 1$$

The calculation of actual percentage contents of each phase requires long exposure times during x-ray analysis to obtain information on the crystalline phase or complex sorption measurements to obtain information on the amorphous phase. Since the measurements being made in this study were relative to one another, it was not thought to be necessary to carry out these time consuming procedures.

The "pseudo" crystallinity values obtained are useful as an internal comparison guide and indicate that as the quench temperature is decreased a corresponding decrease in crystallinity is observed in the polypropylene films. These results appear to show a difference between the behaviour of the three polymer grades as far as density is concerned, indicating that quenching has much the same effect on the polymer for each particular quench temperature but to a different extent depending on sample grade. A graph of apparent crystallinity versus quench temperature is shown in Figure 4.5.

Figure 4.5

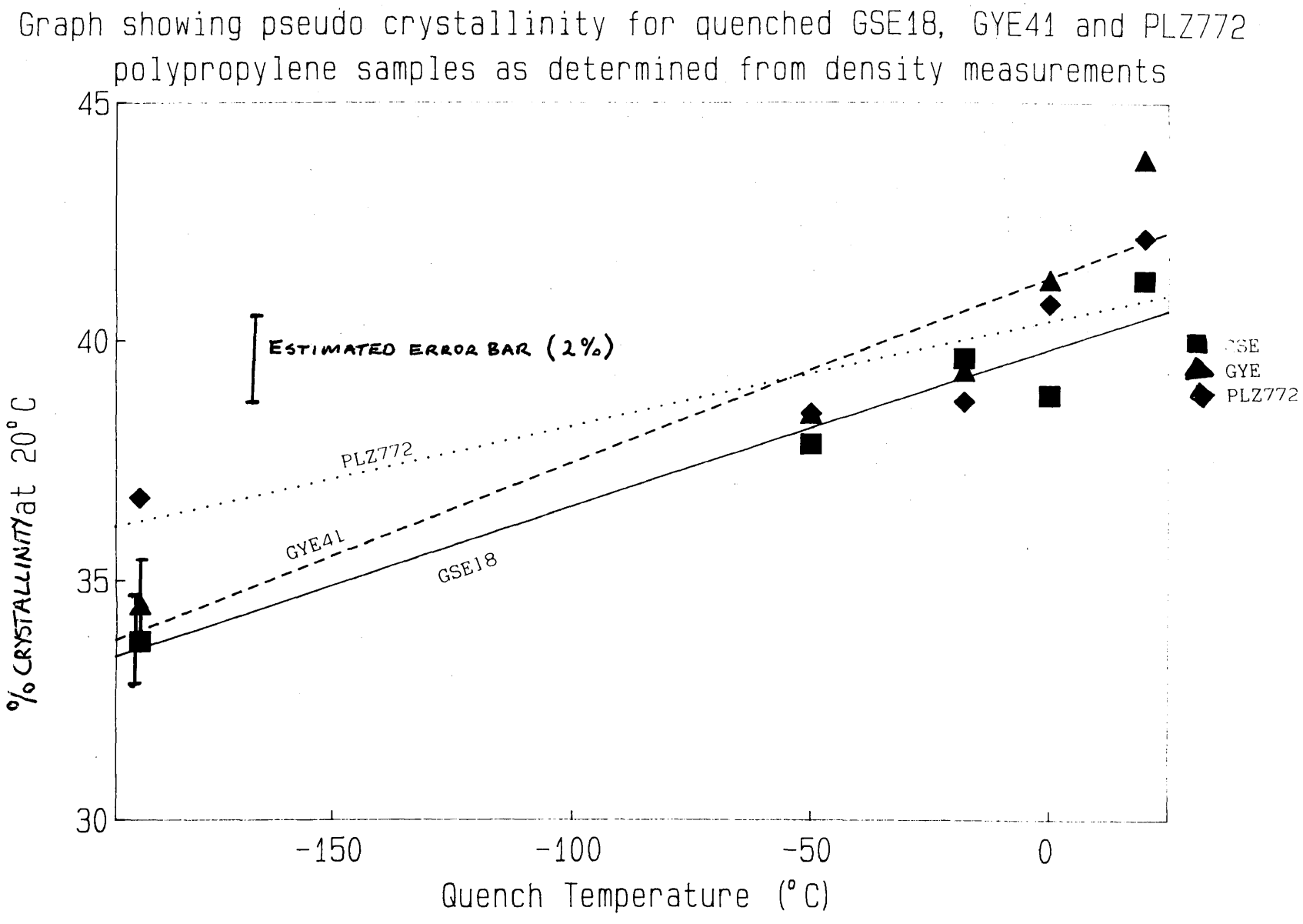
Graph showing pseudo crystallinity for quenched GSE18, GYE41 and PLZ772 polypropylene samples as determined from density measurements
45
40
35
30
% CRYSTALLINITY at 20°C
ESTIMATED ERROR BAR (2%)
PLZ772
GYE41
GSE18
GSE
GYE
PLZ772
-150
-100
-50
0
Quench Temperature (°C)

4.3.3.8 Effect Of Annealing

Annealing was carried out on liquid nitrogen quenched film samples as a means of examining recovery from the quenched state. Two temperatures of annealing were investigated; ambient temperature (25°C) and high temperature (140°C). Annealing was carried out according to the procedure detailed in section 3.3.

(i) Ambient Temperature Annealing

Films were annealed at 25°C for a period of 10 days during which they were removed at various times in order to obtain their infrared spectra. Three spectra were recorded during the first day, three on the second day and thereafter one each day for the remaining 8 days. Figure 4.6 shows the plot for the A998/A973 absorption ratio against annealing time for the liquid nitrogen quenched sample annealed at 25°C although behaviour was similar regardless of which ratio was used.

(ii) High Temperature Annealing

For films annealed at 140°C over 10 days the profile was different. This time there was a rapid increase in ratio value which reached a maximum after which it remained constant for the rest of the 10 day annealing period. This suggests a substantial rearrangement of chain molecules from the smectic to the crystalline phase during annealing. In the latter stages of annealing, some samples had absorption ratio values which appeared to be higher than expected. Infrared spectroscopic investigation of such samples revealed the presence of carbonyl and unsaturated bands indicating that oxidative degradation had occurred. The plot of the A998/A973 absorption ratio versus annealing time for the high temperature annealing is also shown in Figure 4.6. The infrared spectrum showing oxidative degradation which was present in some samples at the later stages of annealing is shown in Figure 4.7

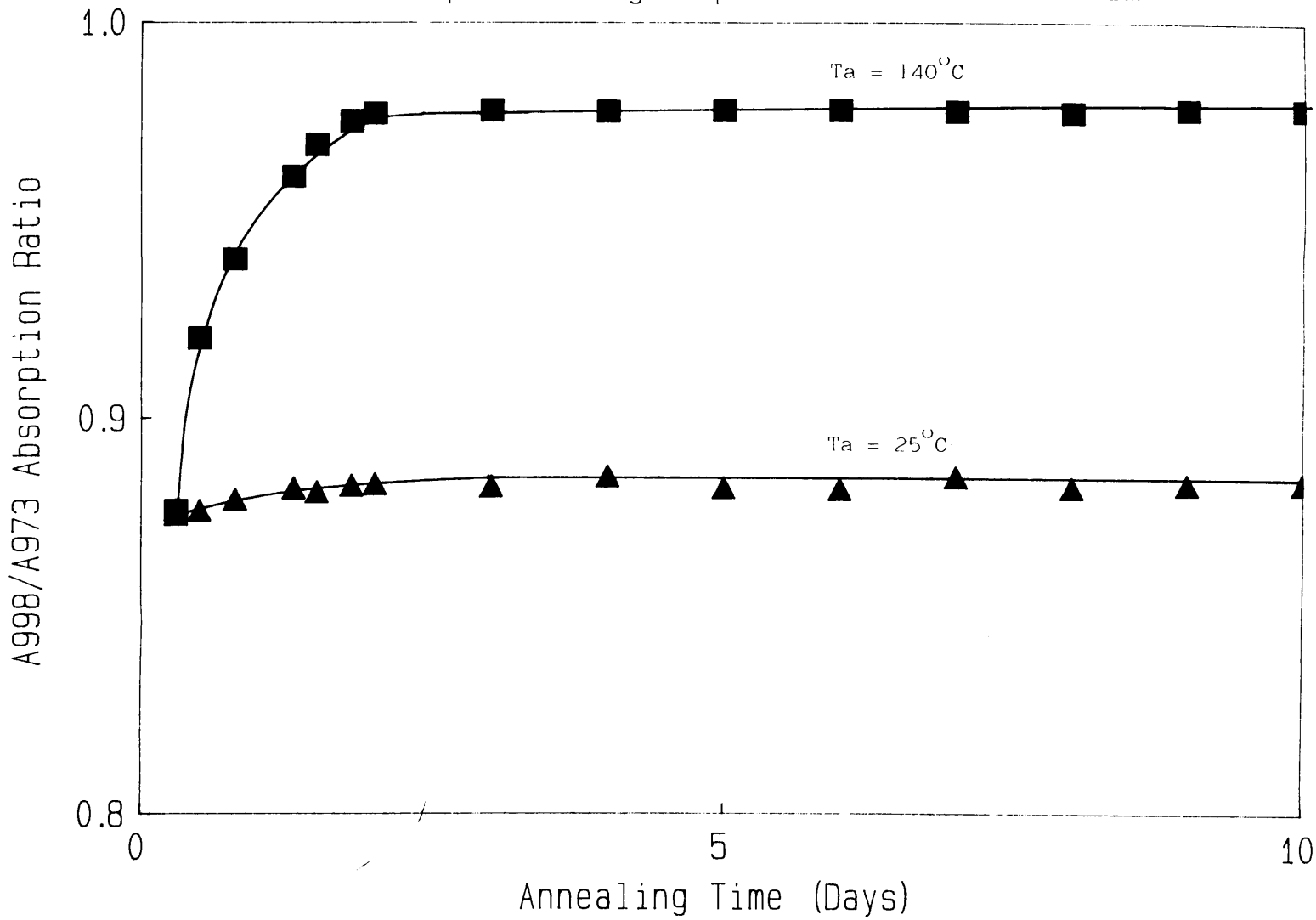
Graph showing the effect of annealing on the A998/A973 FTIR Absorption Ratio
of a liquid nitrogen quenched GSE18 iPP film
1.0
0.9
0.8
A998/A973 Absorption Ratio
Ta = 140°C
Ta = 25°C
0
5
10
Annealing Time (Days)

Figure 4.6

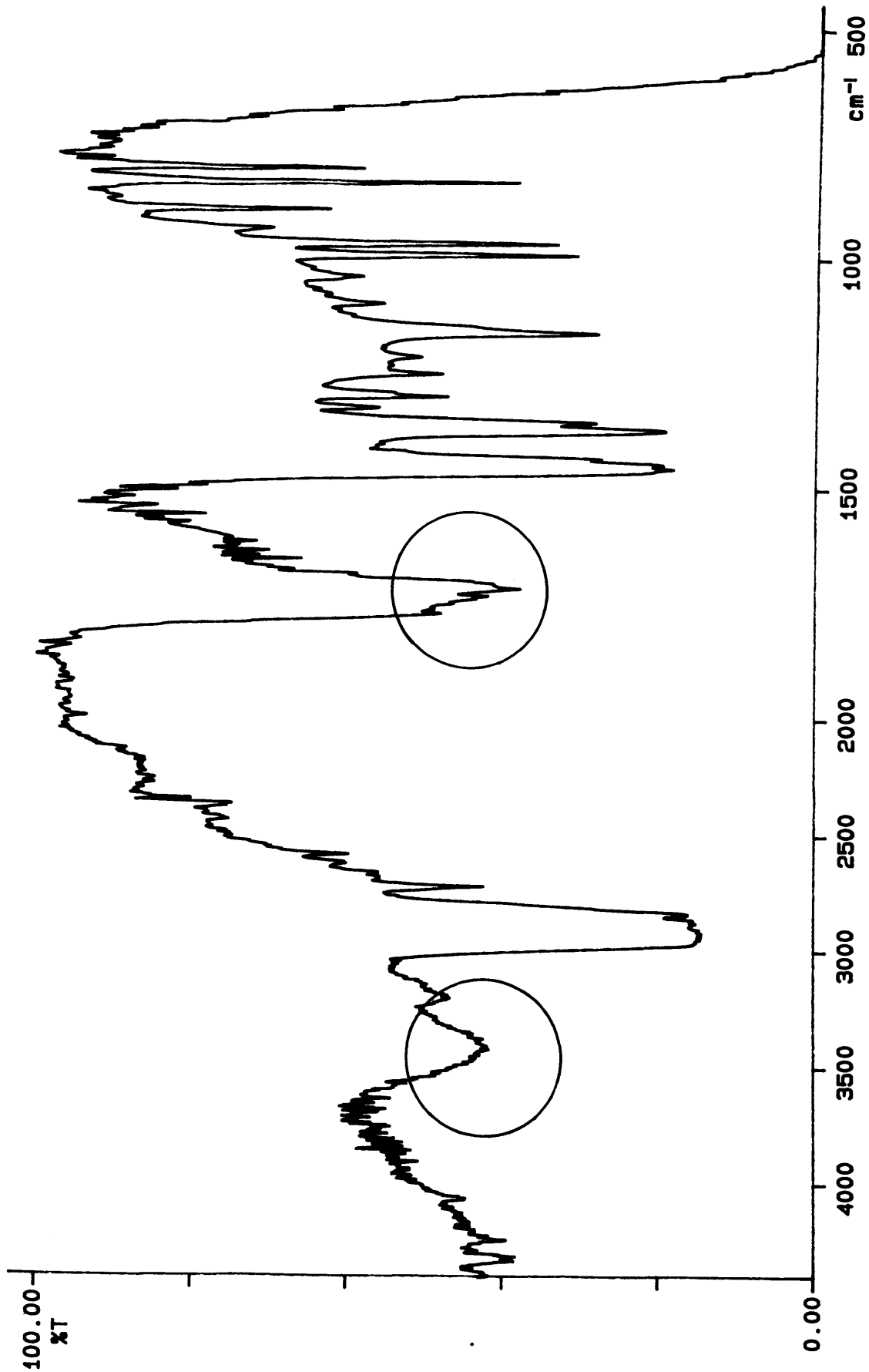

Figure 4.7 Infrared spectrum of an oxidised polypropylene sample. Main regions indicative of sample oxidation are circled.

4.3.4 Detailed Investigation

Having established that changes in structure due to various degrees of quenching from the melt had taken place in the GSE18, GYE41 and PLZ772 polypropylene samples, a study was set up to further investigate the use of infrared spectroscopy in the detection of quench induced behavioural differences between several commonly used commercial polypropylenes samples.

Sample preparation and scanning procedures were based on those used in the preliminary investigation, the only differences being that 5 replicates, in the quench range of -50 to 50°C, were used this time and that the study was extended to include a wider range of commercial samples. The polypropylene samples and quench temperatures used in this study are shown in Tables 4.8(a) and 4.8(b).

Quench Medium	Quench Temp(°C)
Warm water	50
Air	20
Ice/water	0
Dry ice/acetone	-50

Table 4.8(a) Quench media and corresponding temperatures used in the detailed study.

Supplier	Grade
SHELL	JY6100
SHELL	KY6100
SHELL	LY6100
ICI	GWE23
ICI	GXE35
AMOCO	50103
AMOCO	50202
NESTE	UB3249F

Table 4.8(b) Commercial polypropylene samples used in the detailed study.

4.3.4.1 FTIR APRA Results

Results comparing mean FTIR absorption ratios within each samples type with respect to quench temperature are shown in Tables 4.9 - 4.17.

Sample = Amoco 50103

Quench Temp(°C)	Ratios			
	A841/A973	A841/A1167	A998/A973	A998/A1167
50	0.6960	0.7932	0.8491	0.9676
20	0.7559	0.8214	0.8728	0.9484
0	0.6857	0.7935	0.8134	0.9418
-50	0.6255	0.7837	0.7602	0.9541

Table 4.9 Mean absorption ratio results for Amoco 50103 at each quench temperature.

Sample = Amoco 50202

Quench Temp(°C)	Ratios			
	A841/A973	A841/A1167	A998/A973	A998/A1167
50	0.7378	0.8070	0.8536	0.9454
20	0.7464	0.8167	0.8639	0.9452
0	0.6722	0.7646	0.8022	0.9133
-50	0.7442	0.8161	0.8505	0.9342

Table 4.10 Mean absorption ratio results for Amoco 50202 at each quench temperature.

Sample = GWE23

Quench Temp(°C)	Ratios			
	A841/A973	A841/A1167	A998/A973	A998/A1167
50	0.7321	0.8300	0.8494	0.9635
20	0.7435	0.8123	0.8530	0.9325
0	0.6434	0.7785	0.7713	0.9517
-50	0.6226	0.7661	0.7699	0.9473

Table 4.12 Mean absorption ratio results for GWE23 at each quench temperature.

Sample = GXE35

Quench Temp(°C)	Ratios			
	A841/A973	A841/A1167	A998/A973	A998/A1167
50	0.6898	0.8092	0.8147	0.9555
20	0.7272	0.7970	0.8576	0.9404
0	0.6415	0.7843	0.7863	0.9466
-50	0.7090	0.7896	0.7847	0.9352

Table 4.13 Mean absorption ratio results for GXE35 at each quench temperature.

Sample = UB3249F

Quench Temp(°C)	Ratios			
	A841/A973	A841/A1167	A998/A973	A998/A1167
50	0.6769	0.8073	0.7955	0.9506
20	0.7112	0.7970	0.8323	0.9329
0	0.6630	0.7872	0.7733	0.9169
-50	0.6824	0.7865	0.7492	0.9253

Table 4.14 Mean absorption ratio results for UB3249F at each quench temperature.

Sample = JY6100

Quench Temp(°C)	Ratios			
	A841/A973	A841/A1167	A998/A973	A998/A1167
50	0.7049	0.8116	0.8339	0.9605
20	0.7631	0.8202	0.8748	0.9363
0	0.6904	0.7963	0.8295	0.9565
-50	0.6539	0.7709	0.8154	0.9447

Table 4.15 Mean absorption ratio results for JY6100 at each quench temperature.

Sample = KY6100

Quench Temp(°C)	Ratios			
	A841/A973	A841/A1167	A998/A973	A998/A1167
50	0.7418	0.8264	0.8633	0.9643
20	0.7718	0.8202	0.8819	0.9363
0	0.7200	0.8034	0.8559	0.9514
-50	0.6760	0.7963	0.7626	0.9457

Table 4.16 Mean absorption ratio results for KY6100 at each quench temperature.

Table 8 Sample = LY6100

Quench Temp(°C)	Ratios			
	A841/A973	A841/A1167	A998/A973	A998/A1167
50	0.7171	0.8200	0.8298	0.9495
20	0.7767	0.8082	0.8876	0.9396
0	0.6970	0.7894	0.8415	0.9541
-50	0.6333	0.7517	0.7808	0.9151

Table 4.17 Mean absorption ratio results for LY6100 at each quench temperature.

4.3.4.2 Comments On Results

Analysis of variance and Scheffé's "s" test (Appendix 1) were also carried out on these results and the statements made about the results in section 4.3.3.4 were reinforced. Again, a difference in behaviour between infrared absorption values for different polymer grades at different quench temperatures was observed.

Further statistical analysis of the results using Tukey's Pairwise Comparison Procedure (Appendix 2) was carried out in order to examine more closely the differences in behaviour between polymer grades. The results of this comparison are shown in Table 4.18 The table shows polymer grade pairs with the lowest raw data infrared absorption ratio value on the right hand side of the slash in a Tukey Pairwise Comparison with the polymer grade being compared on the left. For example, the A841/A973 ratio for the 50°C quench shows that the UB3249F grade has the lowest value for this ratio and is similar to all other grades apart from the KY6100 from which it differs significantly.

Quench Temp(°C)	A841/A973	A841/A1167	A998/A973	A998/A1167
50	KY6100/ UB3249F	No Difference	KY6100/ UB3249F	No Difference
20	KY6100/ UB3249F LY6100/ UB3249F	No Difference	No Difference	No Difference
0	KY6100/ GXE35 KY6100/ GWE23 KY6100/ UB3249F	No Difference	JY6100/ GWE23 KY6100/ GWE23 LY6100/ GWE23 KY6100/ UB3249F LY6100/ UB3249F KY6100/ GXE35	No Difference
-50	50202/ GWE23 GXE35/ GWE23 50202/ 50103 GXE35/ 50202 50202/ LY6100 GXE35/ LY6100 50202/ JY6100 50202/ KY6100	50202/ LY6100	50202/ UB3249F JY6100/ UB3249F 50202/ 50103 50202/ KY6100 50202/ GWE23 50202/ LY6100 50202/ GXE35	No Difference

Table 4.18 Tukey's Pairwise Comparison for each ratio at each quench temperature.

4.3.5 Discussion

4.3.5.1 Preliminary Investigation

The preliminary studies (section 4.3.3) showed that the structure of commonly used commercial isotactic polypropylene homopolymers was markedly affected when samples were rapidly quenched from the molten state into quench baths of various temperatures. Density values for the quenched samples were found to decrease linearly with quench temperature (Figure 4.1) from a value of circa 0.9 g/ml for a highly crystalline annealed sample to a value of 0.8814 g/ml for a sample quenched from the melt into liquid nitrogen. This decrease in density is attributed to the formation, to greater or lesser extents, of a conformationally disordered smectic phase. A similar linear relationship for density of quenched polypropylene samples versus quench temperature was obtained by Vittoria and Perullo[135].

From the many clearly defined Debye-Scherrer lines in the WAXD photographic results (Figure 4.2) of the quenched and annealed film sample, it is apparent that a high degree of order in the packing of the chain molecules exists in this sample. For the sample quenched at -50°C, the Debye-Scherrer lines are not so distinct and have become more diffuse in nature. This indicates a structural change in the polymer in which a considerable fraction of chain molecules have become conformationally disordered. In this state, a triphasic smectic, crystalline and amorphous phase composition exists. The x-ray photograph for the sample quenched at -190°C shows only two diffuse Debye-Scherrer lines caused by quench induced structural changes. In this case virtually all chain molecules have become conformationally disordered and the system can be considered to consist of only the smectic and amorphous phases. Similarly, WAXD diffractograms (Figure 4.3) show a corresponding

decrease in peak resolution with decreasing quench temperature. At least seven clearly defined peaks are detected in the quenched and annealed samples, whilst only two broad peaks are detected for the samples quenched at -50^{0}C and -190°C. These differences in the x-ray analysis of samples of various monoclinic/smectic/amorphous compositions is in general agreement with many other authors[111,113,116,137,138] and confirms that quenching into the various media leads to induced structural changes in isotactic polypropylene.

Scanning electron microscopy has also shown differences in structure between samples quenched at different temperatures from the melt. Electron micrographs (Figure 4.4) clearly show a spherulitic morphology for the quenched and annealed samples, whilst the samples quenched at temperatures below zero exhibit a nodular type morphology similar to that described by Hsu and Geil[119].

Examination of the infrared absorption ratios at different stages of annealing for both ambient temperature annealing (25°C) and high temperature annealing (140°C) reveals a degree of recovery from the quenched state, to a greater or lesser extent, in the liquid nitrogen quenched samples (Figure 4.6). For the ambient temperature annealing, a small initial increase takes place over the first two days before reaching a constant maximum. At the higher annealing temperature, the maximum is reached much more quickly and occurs at a ratio value considerably higher than that of the ambient temperature annealed sample. These results suggest that even at ambient temperature there is a partial post-quench recovery, with the 3_1 helices striving to rearrange into an energetically more favourable structural arrangement from the disordered state. Annealing at high temperature allows the quenched sample to recover to a greater, if not full, extent. The degree of recovery from the quenched state, then, seems to be more dependent on annealing temperature than annealing time.

Statistical analysis of FTIR APRA results for GSE18, GYE41 and PLZ772 samples quenched rapidly from the melt into quench baths of various temperatures, revealed that certain structural changes with these polymer can be detected using this method. Results show that quench temperature has an effect on the infrared absorption ratios used in the study and suggest that, although differences exist to some extent between samples quenched below 0°C, they tend to be erratic and difficult to define. It can be said however, with some statistical degree of certainty that in general, significant differences exist between those samples quenched above 0°C and those quenched below it. Furthermore, the results indicate that differences in behaviour of the rapidly quenched samples exist between different polypropylene manufacturers and grades. Since this preliminary study involved only three different grades, a second study evaluating the use of infrared spectroscopy as a means of monitoring structural behaviour of a wider range of commonly used commercial polypropylene samples when rapidly quenched from the molten state was undertaken.

4.3.5.2 Detailed Investigation

Statistical analysis of the results from the detailed study reinforced those obtained for the preliminary study and again similar differences were revealed in the absorption ratio values which indicated a dependency of structure on quench temperature. This time, the analysis concentrated on the detection of differences in behaviour between different polypropylene manufacturers and grades. Tukey's Pairwise Comparison was carried out on the results in an attempt to determine which grades were more or less affected by the quench conditions.

Differences between the polypropylene manufacturers and grades were detected more easily by the A841/A973 and A998/A973 ratios but very poorly by the A841/A1167 or A998/A1167 ratios, although the reason for this is unclear. The 973 cm^{-1} band is thought to be representative of very short helices (5 monomer units) or non-helical material[20,109]. This band is a major feature in infrared spectra of both molten isotactic polypropylene and atactic polypropylene which strongly supports this argument. Using this band as an internal reference is justified, as it is unlikely to be affected by rapid quenching from the melt and can be considered to be independent of structure.

The 1167 cm^{-1} band, on the other hand, has a certain amount of ambiguity surrounding it[128]. This band has been used in the past[126] as an internal reference in the investigation of the relationship between absorption ratio and density of polypropylene (in early studies on crystallinity determination) and later as an internal thickness reference band in studies on the infrared spectroscopic determination of stereoregularity in polypropylene[109]. It may have been, with hindsight, a poor choice of internal reference band for this study. Tadokoro and coworkers[134] assigned the 1167 cm^{-1} as a helix band which was sensitive to changes in conformation. If this is the case then this casts doubt on it's use as a reference band in this study, as it would have been expected to behave in much the same way as the 998 and 841 cm^{-1} bands as the quench temperature was decreased. This may account for the apparent lack of sensitivity in this study to quench induced structural changes observed in absorbance ratios using the 1167 cm^{-1} band as the denominator. Due to the uncertainty involved in the 1167 cm^{-1} band and its lack of sensitivity in detecting differences between sample manufucturers/grades, the A841/A973 and A998/A973 absorption ratios have been used for this purpose.

(i) Differences Between Polypropylene Manufacturers/Grade Using The A841/A973 Infrared Absorption Ratio

Tukey's Pairwise Comparison Procedure results (Table 4.18) show statistically significant differences between the most affected (lowest ratio value) polypropylene type at each particular quench temperature and the rest of the polypropylene grades for the same quench (Appendix 2).

50°C Quench: The Neste UB3249F grade polypropylene had the lowest value for this ratio and quench and was found to differ significantly from only the Shell KY6100 grade.

20°C Quench: Again the Neste UB3249F grade was found to be the most affected grade at this quench and differed significantly from both Shell KY6100 and Shell LY6100 grades at this ratio and quench temperature.

0°C Quench: At this quench temperature, ICI GXE35 had the lowest value for this ratio and was found to be significantly different in behaviour from the Shell KY6100 grade. The next most affected grade at this quench temperature was ICI GWE23 which was similar in behaviour to all other grades but was also significantly different from the Shell KY6100 grade. The third most affected manufacturer/grade at this quench temperature was Neste UB3249F which, again, was significantly different in behaviour to the Shell KY6100

-50°C Quench: ICI GWE23 was the most affected grade at this quench and was found to differ in behaviour from the Amoco 50202 and ICI GXE35 grades but not significantly from any other manufacturer/grade. The second and third most affected grades were the Amoco 50103 and Shell LY6100 grades which once again differed

from the Amoco 50202 and ICI GXE35. The fourth and fifth most affected grades at this quench temperature were the Shell JY6100 and Shell KY6100 which differed in behaviour from the Amoco PSL grade but not significantly from any other manufacturers/grades.

(ii) Differences Between Polypropylene Manufactures/Grade Using The A998/A973 Infrared Absorption Ratio

50°C Quench: As for the A841/A973 absorption ratio, Neste UB3249F was the most affected grade for this ratio and quench temperature and once more was significantly different from the Shell KY6100 grade.

20°C Quench: Tukey's Pairwise Comparison failed to reveal any significant differences between manufacturers/grades at this quench temperature. This was unexpected, as significant differences were found between grades for this quench temperature for the A841/A973 ratio. This may be due to a difference in sensitivity of the 841 and 998 cm^{-1} bands respectively or it may be possible that the shorter isotactic helices, as measured by the 998 cm^{-1} band, were not affected as much at this quench temperature as the longer helices.

0°C Quench: The most affected grade at this quench temperature was the ICI GWE23 grade which was found to differ significantly from the Shell JY6100, Shell KY6100 and Shell LY6100 grades. The second most affected grade was Neste UB3249F which significantly differed from the Shell KY6100 and Shell LY6100 grades. The third most affected grade at this quench was the ICI GXE35 grade which significantly differed from the Shell KY6100 grade. It is interesting to note that the

three polymer grades with the lowest values for this ratio and quench temperature are the same grades that were the most affected for the corresponding quench temperature using the A841/A973 ratio, although the order of susceptibility is different. Again, this may be due to shorter helices being less affected by the quench temperature.

-50 Quench: Neste UB3249F was the most affected grade at this quench temperature and ratio and was found to be significantly different form the Amoco 50202 and Shell JY6100 grades. The second to sixth most affected grades were the Amoco 50103, Shell KY6100, ICI GWE23, Shell LY6100 and ICI GXE35 and all were significantly different in behaviour at this quench temperature and ratio from the Amoco 50202 grade.

From these results it can be seen that there is little detectable behavioural differences between sample manufacturers/grades at the higher quench temperatures, but as the quench temperature is reduced, with the exception of the 20°C quench for the A998/A973 ratio, there is a general increase in the number of differences being observed.

At the 50°C quench temperatures both ratios reveal the Neste UB3249F grade as the most affected by the quench temperature and the Shell KY6100 as the least affected. This is also the case for the A841/A998 ratio at the 20°C quench, but in this case the Neste UB3249F is also significantly different from the Shell LY6100 grade. For the 0°C quench temperature both ratios reveal ICI GXE35, ICI GWE23 and Neste UB3249F as the most affected samples at that quench, and again for the A841/A973 ratio the Shell KY6100 is the least affected grade. For the A998/A973 ratio at this quench temperature, Shell KY6100 is again amongst the least affected grades as are the Shell JY6100 and Shell LY6100 grades. At the -50°C quench temperature, with the exception of the Neste UB3249F for the A841/A973 ratio, all sample

manufacturers/grades are involved in significant differences. The Amoco 50202 sample appears to be the least affected at this temperature for either ratio and to some extent so is the ICI GXE35 grade.

For quench temperatures above O°C, then, the Neste UB3249F grade is in general the most affected with the Shell KY6100 and LY6100 being the least affected. At the 0°C quench temperature, the Neste UB3249F, ICI GXE35 and ICI GWE23 are the most affected with the three Shell grades KY6100, LY6100 and JY6100 being the least affected. At the -50°C quench temperature, all grades with the exception of Neste UB3249F for the A841/A973 ratio are significantly affected with the Amoco 50202 being the least affected followed by the ICI GXE35 and the Shell JY6100 grades.

These results show that differences between the behaviour in different sample grades are occurring and that certain grades act differently when quenched above 0°C compared to their behaviour below it. The general trends between both ratios are similar, but there are some differences. These may be due to differences in sensitivity to changes in helical content in the polypropylene samples between the 998 and 841 cm^{-1} bands or in otherwords, as previously mentioned, a difference in susceptibility of the shorter and longer helices to different degrees of quenching. It may also be possible, however, that drawing of baselines may be a contributing factor and as the 998 and 973 cm^{-1} absorption bands lie close together and share the same baseline it is probably more wise to view the results from the ratio of these two bands as the most reliable.

In summary, this study has shown that infrared spectroscopy can, detect structural changes in commercial polypropylenes. Furthermore, it can detect differences in behaviour for a given quench between different polypropylene grades. This is

important as it may have implications in polypropylene processability. When polypropylene is extruded, it is quenched either by air, water bath or chill rolls which means that the resultant structure is dependent on the temperature of the quench medium. This study has shown that changes in polypropylene structure can be detected at quench temperatures as high as 50°C and that differences between polypropylene grades exist even at temperatures as high as this, which is within the temperature range of quench tanks used in commercial extrusion plants.

Infrared absorption peak ratio analysis is perhaps not the most ideal method for quantifying structural changes in commercial polypropylenes induced by rapid quenching from the molten state. It requires the preparation of many film samples and time consuming manual analysis of spectra. The technique is subject to human judgement in the drawing of baselines and therefore tends to lack some objectivity. Other methods which are absolute, such as ^{13}C-nmr or X-ray diffraction techniques, may prove to be more useful.

4.4 MELTING BEHAVIOUR OF ISOTACTIC POLYPROPYLENE

Thermal analysis techniques such as DTA and DSC have previously proved to be very useful in the study of isotactic polypropylene providing much information on melting, crystallisation and the effects of thermal history on the structure of the polymer.

Ke[139] noted a single melting peak for polypropylene and estimated the heat of fusion to be 15.4 cal/g. Previous thermal history of the polymer, however, can affect the melting profiles of polypropylene and this phenomenon has been of great interest to many authors, some of whom have noted a transition which appears as an exothermic peak and which has been attributed to the crystallisation of α-form polypropylene

from the smectic phase. In studies of isotactic polypropylene quenched from the melt and annealed over a range of temperatures, Fichera and Zannetti[123] found two peaks in the melting endotherm of their heat-treated samples, one forming the main melting endotherm with the other being a small endothermic transition which increases in intensity and peak temperature up to a maximum of 140°C where it finally coincides with the main melting endotherm. They also
observed an exothermic peak in the "as-quenched" sample which becomes diminished as the annealing temperature increases.

Hsu and Geil[116] noted a small but broad exothermic peak at circa 80°C in the DSC thermogram of polypropylene. This had previously been observed by Gailey and Ralston[114] who showed, using DTA, that both peak area and position of this exotherm increases as the heating rate is raised. They reported a value of 2.3 cal/g for this transition. Fichera and Zannetti[123] reported a similar value of 4 cal/g for the heat of conversion for the smectic to monoclinic transition. De Candia and co-workers[111] observed this exothermic peak in thermally annealed samples at circa 107°C and found that it disappears in samples which have been annealed at temperatures greater than 90°C. They also noticed a small endotherm, first observed by Fichera and Zannetti[123], at a temperature corresponding to the temperature of annealing and which has a maximum peak value at about 20°C above it. It was proposed that this endotherm is due to small crystals formed during heating of the sample from the quench temperature to room temperature.

Another feature of polypropylene melting endotherms is the presence, in many cases, of more than one peak. Using stepwise annealing at increasing temperatures, Pae and Sauer[140] found that the final melting point of the polypropylene increases in temperature and if the final anneal temperature was close to 160°C, a double endotherm is observed in the process. They also showed that multiple endotherms

can be obtained if stepwise annealing is carried out for decreasing temperatures with the number of peaks being greater than or equal to the number of annealing temperatures.

Some authors[80,141] have shown that double peaks in the melting profiles of polypropylene are due to the presence of more than one crystalline form such as that caused by the $\beta \rightarrow \alpha$ form transition whilst others[142-144], by appropriate choice of temperature of crystallisation (ie. $130°C < T_c < 150°C$) have obtained double peaks in the melting profile of isotactic polypropylene.

Recently, Passingham and co-workers[145] re-evaluated the occurrence of multiple endotherms in polypropylene, showing that their development stems mainly from the α-crystalline regions with minimal influence from other crystalline forms such as the β-form of polypropylene. Furthermore, they suggested that although the thermograms exhibit multiple peak profiles only two genuine endotherms may be present and that the appearance of the multiple peaks is modified by recrystallisation processes.

In the present studies various induced thermal histories in polypropylene were investigated using DSC and are reported in the following sections.

4.5 EFFECT OF RAPID QUENCHING FROM THE MELT ON THE DSC MELTING ENDOTHERM OF POLYPROPYLENE

4.5.1 Experimental

The purpose of this study was to examine the effect of rapid quenching from the melt into different quench baths at various temperatures on the DSC melting endotherms of polypropylene. This study was carried out on the same film samples as used in

section 4.3.3 (details of which can be found in Tables 4.3(a) and 4.3(b)).

Film samples (circa 5mg) were prepared in triplicate by encapsulation in aluminium sample pans according to procedures outlined in section 3.7. Each sample was run from 30°C to 200°C at a heating rate of 10°C/min and held at this temperature before controlling the crystallisation of the sample by cooling at a rate of 10°C/min. This procedure was repeated 5 times on the same sample in order to study the effect of thermal cycling on the quench induced thermal history of the polypropylene samples. Melting and crystallisation profiles were recorded at all stages of thermal cycling for later analysis.

4.5.2 Results

4.5.2.1 Smectic → Monoclinic Transition

A small but broad exothermic transition was observed at about 80°C in the DSC thermogram of the rapidly quenched polypropylene samples of all grades (Figures 4.8 and 4.9). This has been attributed to the smectic → monoclinic crystalline phase transition. This feature in the thermogram of the quenched samples was found to disappear after subsequent thermal cycles.

4.5.2.2 DSC Melting (T_m) Results

The mean DSC data for the melting of quenched samples of GSE18, GYE41 and PLZ772 polypropylene for each thermal cycle at each quench temperature are shown in Tables 4.19 - 4.21. Figure 4.10 shows typical melting profiles of the 1st runs for polypropylene samples over the range of quench temperatures. Figure 4.11 shows a typical melting profile for the 2nd to 5th DSC runs.

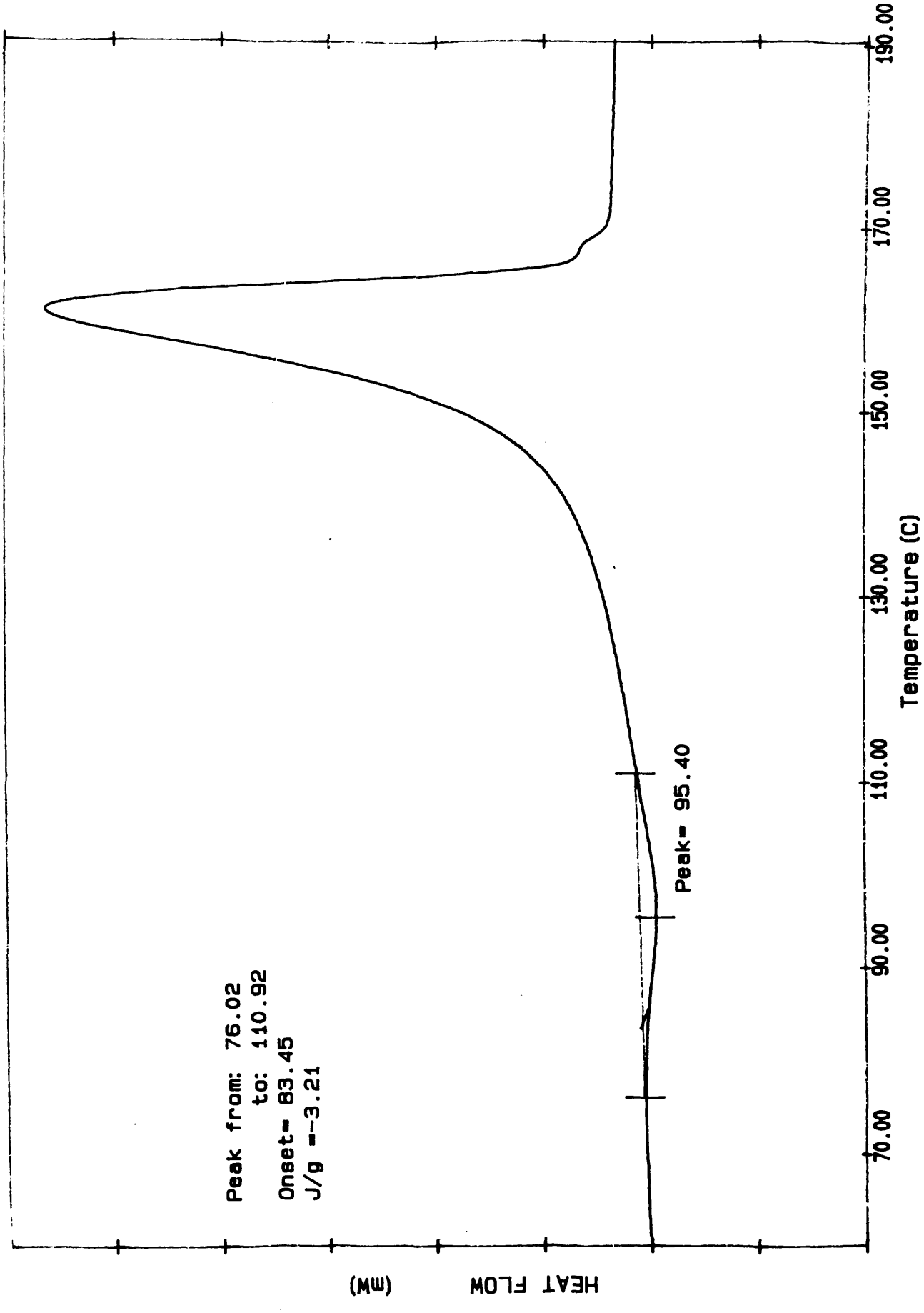

Figure 4.8 DSC melting endotherm of polypropylene rapidly quenched from the melt into liquid nitrogen

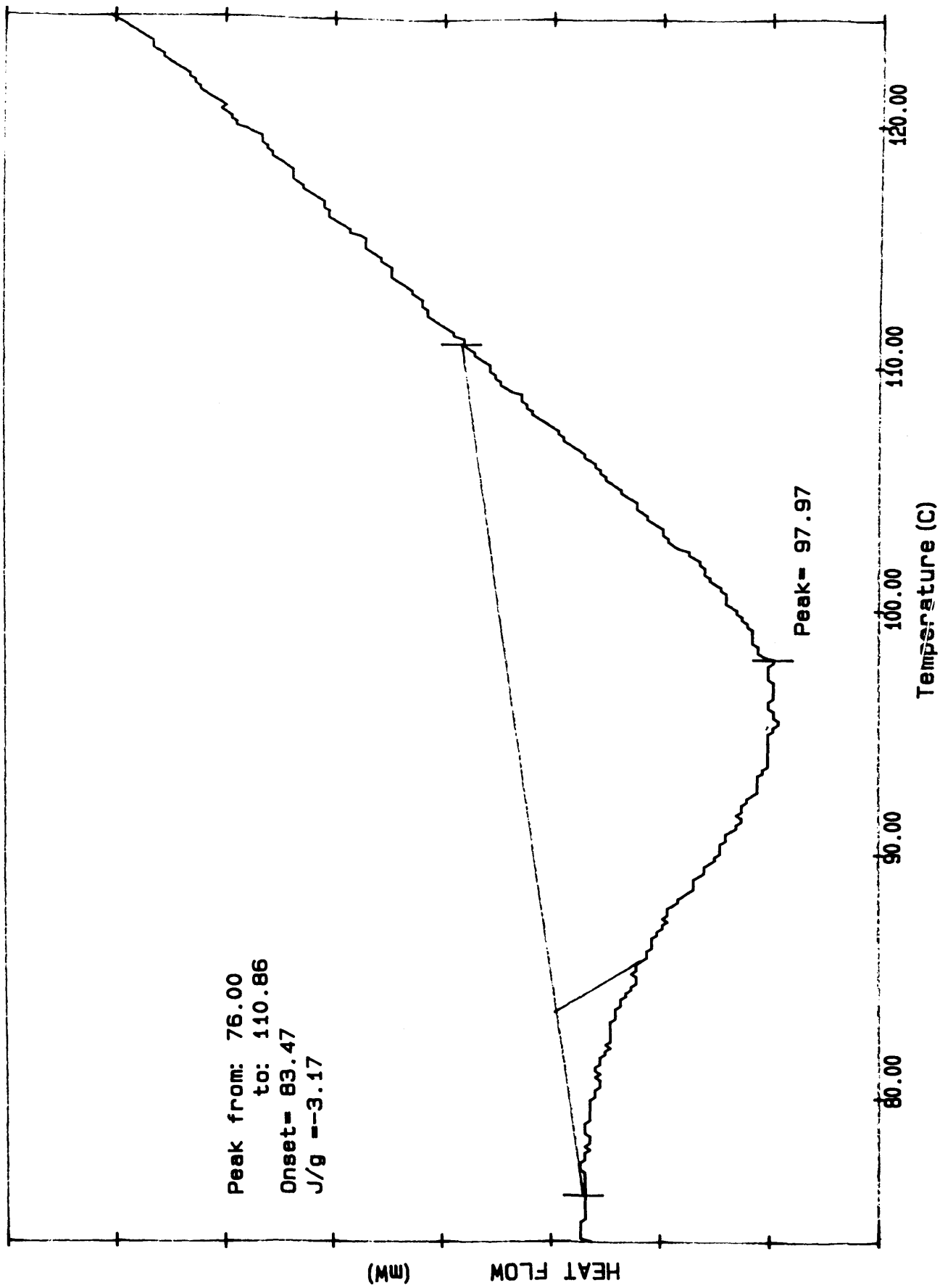

Figure 4.9 DSC thermogram showing the smectic → monoclinic exothermic transition

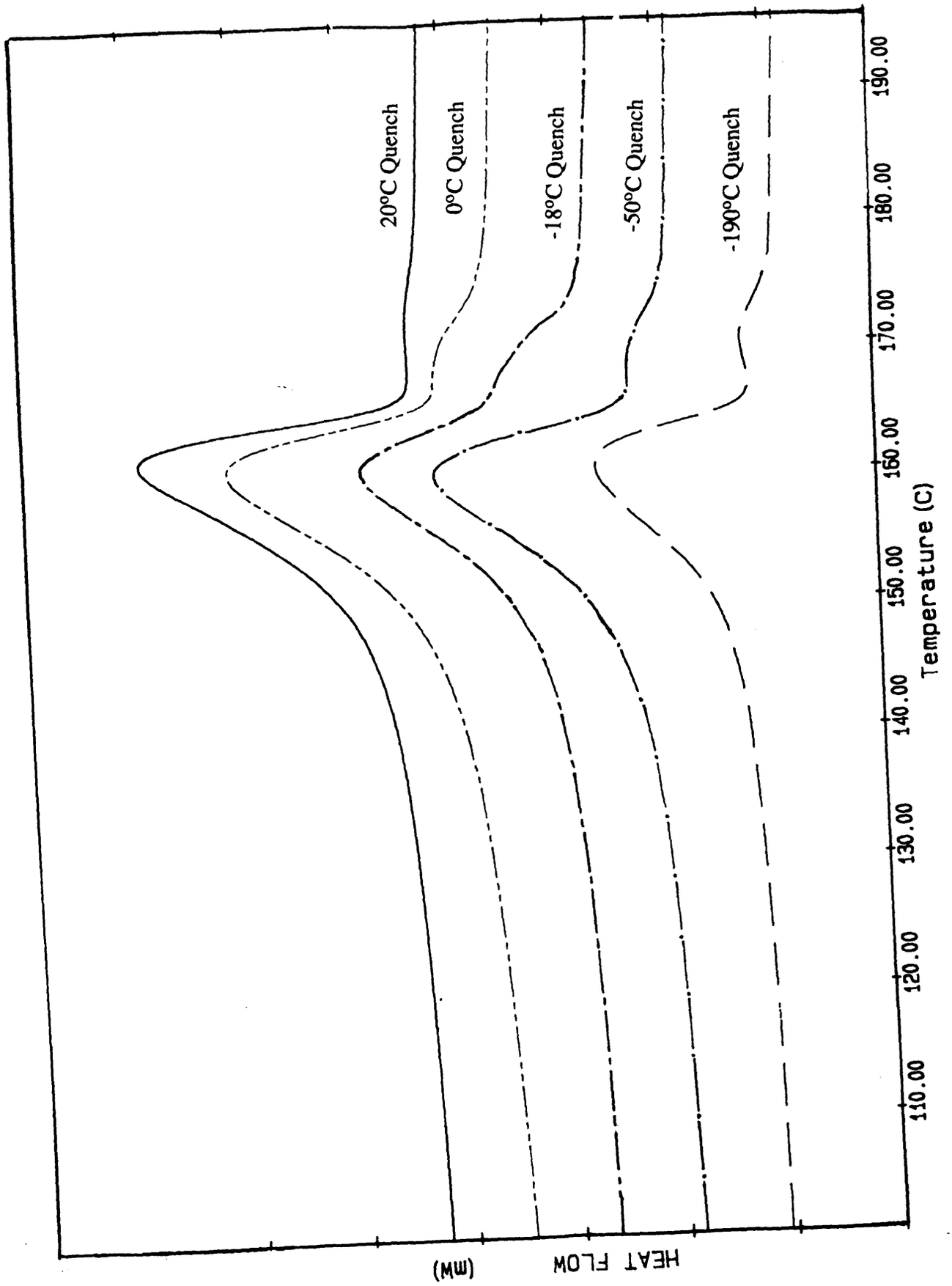

Figure 4.10 DSC thermogram showing the first run, melting endotherms of GSE18 polypropylene quenched from the melt into different quenched media

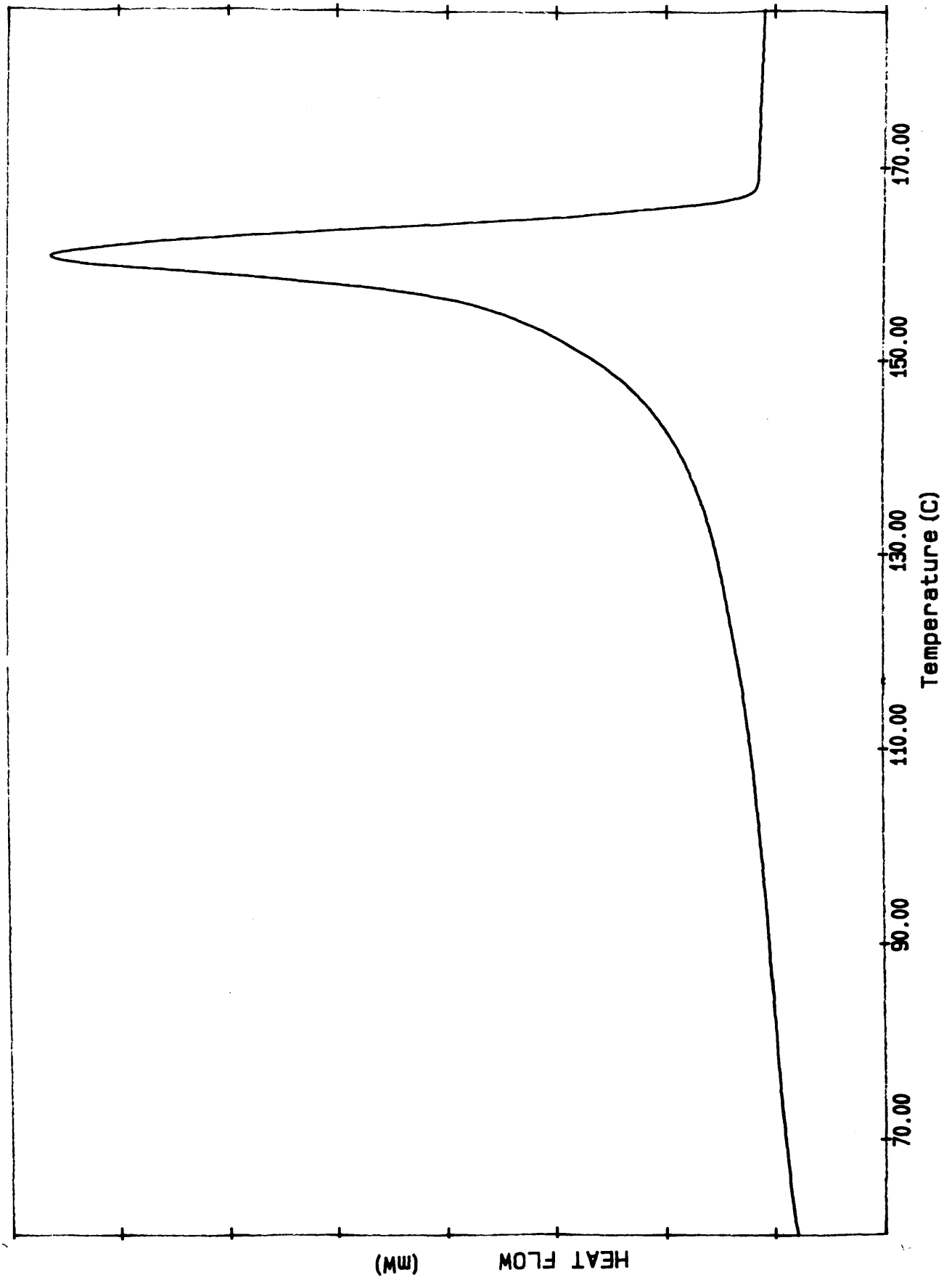

Figure 4.11 Typical DSC melting endotherm for polypropylene - heat cycles 2-5

Sample = GSE18

Quench Temp(°C)	DSC Cycle	T_m Onset (°C)	T_m Main Peak(°C)	ΔH_f (J/g)
20	**1**	**148.17**	**161.36**	**123.40**
	2	153.39	159.35	130.59
	3	153.32	159.33	128.69
	4	153.35	159.24	129.56
	5	153.36	159.19	127.92
0	**1**	**147.13**	**160.49**	**100.67**
	2	153.50	159.07	114.41
	3	153.43	159.00	114.17
	4	153.37	158.93	114.37
	5	153.41	158.89	114.17
-18	**1**	**147.72**	**160.38**	**90.01**
	2	153.34	159.12	109.85
	3	153.24	159.02	110.84
	4	153.24	159.00	108.35
	5	153.17	158.96	108.13
-50	**1**	**147.45**	**160.06**	**85.83**
	2	153.14	158.82	110.84
	3	153.20	158.89	110.79
	4	153.18	158.82	110.58
	5	153.08	158.81	109.08
-190	**1**	**146.93**	**160.27**	**117.92**
	2	152.65	158.32	118.81
	3	152.57	158.28	118.56
	4	152.57	158.24	118.21
	5	152.46	158.20	117.70

Table 4.19 Mean melting data for GSE18 with first runs in bold type.

Sample = GYE41

Quench Temp(°C)	DSC Cycle	T_m Onset (°C)	T_m Main Peak(°C)	ΔH_f (J/g)
20	**1**	**150.47**	**162.19**	**108.18**
	2	156.04	160.19	120.38
	3	156.02	160.18	120.17
	4	155.98	160.18	121.68
	5	155.94	160.15	122.33
0	**1**	**150.68**	**162.36**	**96.67**
	2	156.09	160.08	123.32
	3	156.06	160.55	122.50
	4	156.03	160.55	122.10
	5	156.00	160.52	121.88
-18	**1**	**150.35**	**163.15**	**101.39**
	2	156.01	160.48	110.85
	3	155.33	159.76	110.74
	4	155.32	159.75	111.36
	5	154.12	159.07	107.39
-50	**1**	**148.97**	**162.06**	**113.16**
	2	155.18	159.67	130.38
	3	155.16	159.89	129.31
	4	155.17	159.87	129.37
	5	155.18	159.83	129.83
-190	**1**	**150.71**	**163.73**	**131.17**
	2	156.06	160.82	127.23
	3	155.76	160.61	126.14
	4	155.73	160.55	125.92
	5	155.77	160.58	125.99

Table 4.20 Mean melting data for GYE41 with first runs in bold type.

Sample = PLZ772

Quench Temp(°C)	DSC Cycle	T_m Onset (°C)	T_m Main Peak(°C)	ΔH_f (J/g)
20	**1**	**149.09**	**162.11**	**107.56**
	2	155.12	160.24	117.34
	3	154.56	159.87	117.69
	4	154.44	159.67	117.15
	5	154.36	159.53	116.92
0	**1**	**149.01**	**160.80**	**89.41**
	2	154.13	160.09	118.17
	3	154.03	159.64	118.08
	4	154.00	159.44	119.91
	5	154.05	159.04	121.09
-18	**1**	**148.73**	**162.33**	**120.49**
	2	156.04	161.02	130.88
	3	155.66	160.91	128.52
	4	155.48	160.83	127.31
	5	155.48	160.77	127.06
-50	**1**	**148.97**	**161.34**	**101.67**
	2	156.25	161.31	123.40
	3	155.49	160.74	122.62
	4	155.20	160.53	121.04
	5	154.92	160.36	120.75
-190	**1**	**151.19**	**162.39**	**105.46**
	2	155.24	160.59	123.00
	3	154.78	159.73	121.50
	4	154.58	160.03	122.52
	5	154.14	159.63	121.78

Table 4.21 Mean melting data for PLZ772 with first runs in bold type.

4.5.2.3 DSC Crystallisation Results

Mean DSC data for the crystallisation runs during thermal cycling of the GSE18, GYE41 and PLZ772 samples are shown in Tables 4.22 - 4.24. Typical DSC crystallisation exotherms for the three polypropylene grades crystallised from 200°C at 10°C/min are shown in Figure 4.12.

Sample = GSE18

Quench Temp(°C)	DSC Cycle	T_c Onset (°C)	T_c Main Peak(°C)	$-\Delta H_c$ (J/g)
20	1	117.88	112.84	100.53
	2	117.68	112.65	100.44
	3	117.62	112.56	100.39
	4	117.57	112.47	100.50
	5	117.49	112.39	100.55
0	1	117.95	112.89	91.91
	2	117.86	112.86	90.13
	3	117.77	112.74	90.15
	4	117.73	112.66	90.00
	5	117.63	112.58	89.90
-18	1	117.30	111.80	85.64
	2	117.30	111.70	85.70
	3	117.35	111.79	85.80
	4	117.32	111.72	85.75
	5	117.26	111.67	85.73
-50	1	117.36	112.47	84.09
	2	117.31	112.34	84.06
	3	117.17	112.01	83.94
	4	117.23	112.06	83.97
	5	117.25	112.11	83.86
-190	1	116.84	111.77	87.48
	2	116.57	111.42	87.49
	3	116.45	111.31	87.36
	4	116.37	111.20	87.77
	5	116.32	111.15	87.46

Table 4.22 Mean crystallisation data for GSE18.

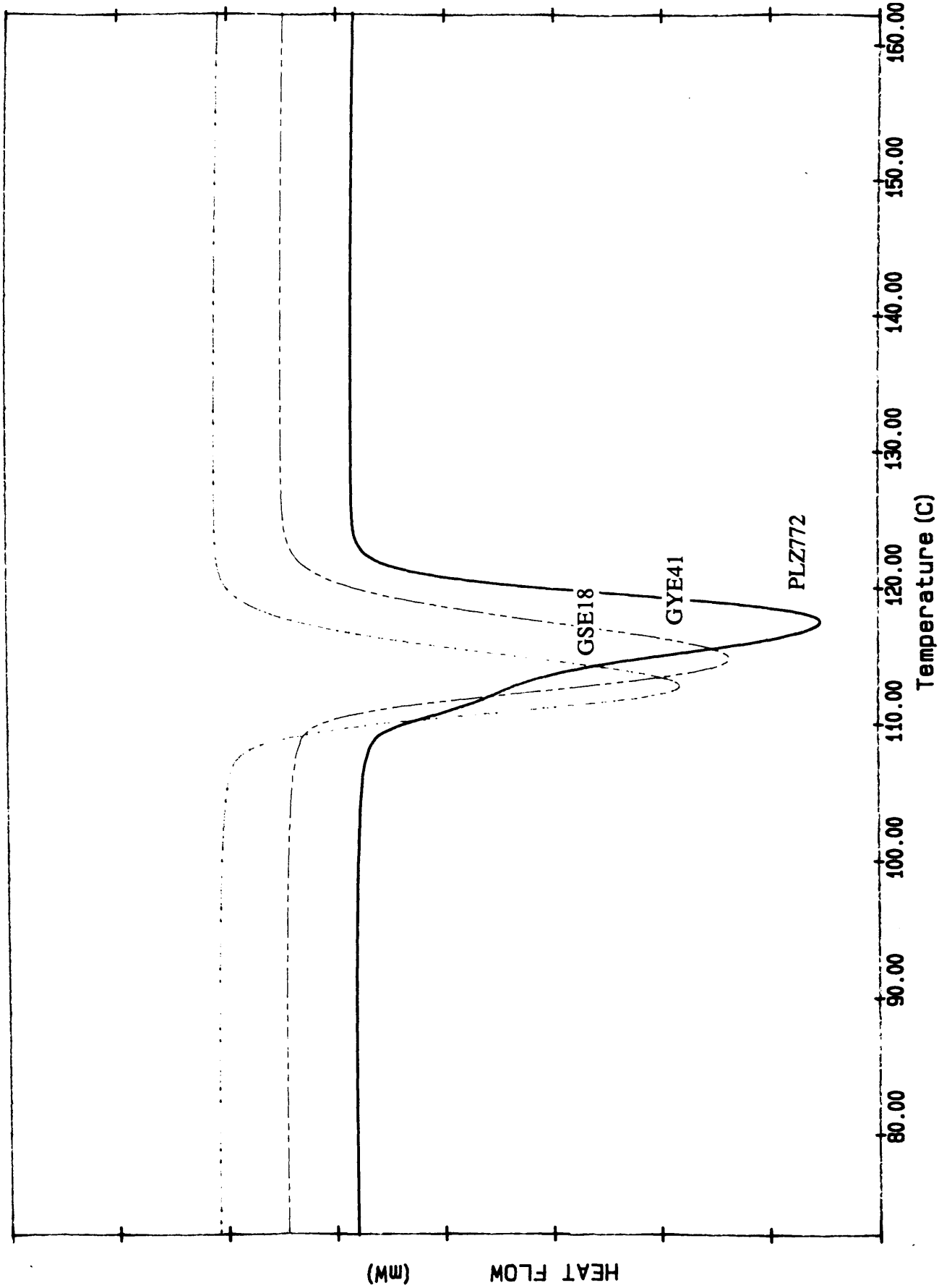

Figure 4.12 Typical DSC crystallisation exotherms for GSE18, GYE41 and PLZ772

Sample = GYE41

Quench Temp(°C)	DSC Cycle	T_c Onset (°C)	T_c Main Peak(°C)	$-\Delta H_c$ (J/g)
20	1	119.60	114.79	94.74
	2	119.55	114.78	94.69
	3	119.58	114.78	94.63
	4	119.58	114.75	94.57
	5	119.56	114.73	94.46
0	1	119.87	114.89	95.13
	2	119.74	114.80	95.15
	3	119.68	114.74	95.34
	4	119.65	114.71	95.32
	5	119.69	114.79	95.21
-18	1	119.85	114.99	102.95
	2	119.83	114.89	102.85
	3	119.33	114.39	102.76
	4	119.31	114.37	102.73
	5	119.30	114.38	102.77
-50	1	120.30	115.29	99.24
	2	120.38	115.34	99.21
	3	120.38	115.36	99.19
	4	120.40	115.41	99.24
	5	120.38	115.42	99.18
-190	1	119.81	114.99	102.66
	2	119.79	114.61	100.77
	3	119.73	114.50	100.85
	4	119.77	114.44	100.68
	5	119.52	114.40	100.79

Table 4.23 Mean crystallisation data for GYE41.

Sample = PLZ772

Quench Temp(°C)	DSC Cycle	T_c Onset (°C)	T_c Main Peak(°C)	$-\Delta H_c$ (J/g)
20	1	121.97	119.33	93.78
	2	121.50	118.50	92.25
	3	121.23	117.86	92.90
	4	121.02	117.49	92.70
	5	120.86	117.20	92.70
0	1	122.22	119.52	91.73
	2	121.58	118.90	91.18
	3	121.14	118.66	90.72
	4	120.84	118.33	90.23
	5	121.37	118.63	90.23
-18	1	123.37	120.43	99.31
	2	123.29	120.30	99.19
	3	122.82	119.86	98.78
	4	122.74	119.76	98.76
	5	122.54	119.75	96.84
-50	1	123.17	120.29	96.45
	2	122.84	119.86	96.17
	3	122.62	119.60	95.89
	4	122.34	119.26	95.72
	5	122.18	119.08	95.47
-190	1	122.02	118.83	97.55
	2	121.59	117.48	97.01
	3	121.34	118.74	96.48
	4	120.64	117.99	95.99
	5	120.32	117.71	95.73

Table 4.24 Mean crystallisation data for PLZ772.

4.5.3 Discussion

4.5.3.1 DSC Melting Of Quenched Isotactic Polypropylene Films

In the DSC analysis of polymers, the baseline is expected to rise linearly with temperature due to the heat capacity of the sample. If a thermal change in the

polymer takes place then, provided the magnitude of the change is sufficient to be detected, it will manifest itself as a deviation from this linear condition. In this study, the fusion endotherms of isotactic polypropylene film samples quenched rapidly from the melt into various quench media (Table 4.3(a)) exhibited more than one such deviation from the baseline. It is believed that the occurrence of more than one peak in this case is a direct consequence of the quench induced thermal history of the polypropylene since all samples had been provided with a common thermal history by holding at 200°C for 5 minutes prior to quenching.

A common feature amongst all the DSC thermograms of the quenched polypropylene samples was a small but broad exothermic peak at circa 80°C. It is well known[111,114,116,123] that the presence of this exotherm in the thermogram of quenched isotactic polypropylene is characteristic of the smectic → monoclinic phase transition and is due to a predominantly intramolecular transformation in the quenched polypropylene involving the recoiling of molecular segments possessing various lengths and different ternary helix spiralisation. A typical value for the heat of crystallisation for this transition was found to be circa 3.0 J/g which suggests that a significant amount of ternary helices in the polypropylene samples had been converted to the conformationally disordered smectic phase during quenching. This result is in agreement with the diffuse halo effect observed in the WAXD results in section 4.3.3.5.

Analysis of variance on data recorded for melting onset, main melting peak and heat of fusion (ΔH_f) for the three polypropylene grades used showed no significant difference in these parameters with respect to quench temperature. There was, however, a significant difference between the melting data for the first DSC run and that of subsequent runs. Melting onsets, main melting peaks and ΔH_f values differed slightly depending on sample grade but otherwise the above behaviour was common

to all sample grades. The average values for the 1st and 2nd to 5th thermal cycles for each sample grade across all quench temperatures is shown in Table 4.25. Note the slight differences in melting data between sample grades.

Sample Grade	DSC Cycle	T_m Onset (°C)	T_m Main Peak(°C)	ΔH_f Range (J/g)
GSE18	1	147.68	160.51	85.83 - 123.40
	2 - 5	153.15	158.87	108.13 - 130.59
GYE41	1	150.24	162.70	96.67 - 131.71
	2 - 5	155.65	160.16	107.39 - 130.38
PLZ772	1	149.40	161.79	89.41 - 120.49
	2 - 5	154.90	160.12	116.92 - 130.88

Table 4.25 Mean melting data values for 1st and 2nd to 5th thermal cycles for each sample grade across all quench temperatures.

For each grade the melting onset of the 1st run was 4 to 8°C lower than that of the 2nd to 5th thermal cycles and the main peak temperature of the 1st run in every case was 1 to 3°C higher than the 2nd to 5th thermal cycles. The ΔH_f values were less consistent across the samples but in every case there was a significantly lower ΔH_f value for the first run compared to that of the 2nd to 5th thermal cycles. In general, the data for the 2nd to 5th cycles was consistent throughout and values were characteristic for each polypropylene grade.

Another salient feature of the DSC melting profiles of the quenched polypropylene films was the occurrence of a reproducible double endotherm in the 1st run (Figure 4.10) which consisted of a large main melting peak and a smaller shoulder/peak at a higher temperature (circa 170°C). As the quench temperature decreased the relative intensity of this second peak increased.

The endothermic profile of the samples for the 2nd to 5th thermal cycles (Figure 4.11) was markedly different from that of the 1st run. There was no smectic → monoclinic transition exothermic phase transition, melting was much sharper with a higher onset value and heat of fusion, and there was no evidence of a second peak or shoulder at circa 170°C.

These results not only confirm the presence of smectic material in the quenched polypropylene films and its transformation to the monoclinic phase on subsequent thermal cycling, but they also reveal information on other structural reorganisations taking place during the 1st melting cycle of the quenched polypropylene. This is supported by the lower melting onsets and ΔH_f values. Also the fact that the main melting peak in the 1st cycles was relatively higher than that of the 2nd to 5th cycles, is indicative of a broader melting range possibly caused by a correspondingly broad distribution of crystallite sizes.

The relatively lower melting onsets and ΔH_f values for the 1st run may be explained by the effect that rapid quenching from the melt has on the apparent crystallinity of the polypropylene (section 4.3.3.7). Since rapid quenching induces disorder in the conformation of the ternary helices and consequently in the close packing of the molecules, this leads to a corresponding decrease in the crystallinity of the sample and hence lower energy requirements for the onset of melting. This is in agreement with Fatou[146] who suggested that low values of ΔH_f in quenched polypropylene were due to the effects of thermal treatment and, as a consequence, the crystallinity of the sample.

Previous studies on the thermograms of quenched polypropylene have shown that subsequent annealing can lead to the occurrence of multiple endotherms. Fichera and Zanetti[123] observed this phenomenon in samples annealed at temperatures above 70°C. Corradini and co-workers[144] investigated the double endotherm obtained using different heating rates on samples annealed at 125°C and 165°C respectively. They attributed the double peak obtained to an $\alpha_1 \rightarrow \alpha_2$-modification transition. This transition was better resolved at low heating rates (2.5°C/min) in the sample annealed at 125°C. In their studies on the double peak phenomena in polypropylene samples crystallised at different temperatures, Guerra and co-workers[143] concluded that for samples crystallised at 135-140°C or above, a recrystallisation occurred during heating which was essentially dependent on heating rate.

Some authors[58,80,147] have attributed the double peak phenomenon to the presence of different crystalline species many of which have centred on the study of double peaks in β-phase polypropylene. Various heating rates have been studied and results show that the recrystallisation process is complex since it can lead to the formation of both β- and α-phase crystals. Other studies[148] on the effect of orientation and annealing on the melting and recrystallisation process in polypropylene have observed multiple peaks in the thermogram. Degradation of the polypropylene[79] can also lead to the occurrence of double peaks in the DSC melting thermograms.

It seems that multiple peaks in polypropylene are related to the presence of different crystalline species, different disordered crystals, or different crystal sizes or degrees of perfection, and may result from a process of recrystallisation. Many studies, however, observed the smaller peak on the low temperature side of the main melting peak[79,123,143,144]. In the present study the minor peak occurred at the high temperature side of the main melting peak.

From x-ray work (section 4.3.3.4) it is clear that the structure of the quenched samples is monoclinic in origin, with various amounts of smectic material present depending on degree of quenching and that no β-phase material had been formed. If β-phase material had been involved in the double peak in this case then it would have been expected to be in very small amounts and to melt at a temperature lower than that of the main melting peak. This effectively rules out the possibility of different crystalline species being involved in the occurrence of the double peak. A comparison of the x-ray diffractogram of the α-phase (monoclinic) and the β-phase (hexagonal) polypropylene is shown in Figure 4.13

No orientation was present in the samples and this was apparent from the continuous circular Debye-Scherrer lines in the x-ray photographs of the samples (had they been oriented, then a discontinuous line with reflections only at certain points on the halo would be observed). This discounts any orientation effects that may have led to the appearance of the double endotherm.

Samples were monitored for oxidative degradation using infrared spectroscopy (section 4.3.3.1) and only those samples which showed no signs of any such degradation were selected for analysis. Had degradation been a factor in the occurrence of the double peaks then this would have appeared as a double peak in the 2nd to 5th thermal cycles also. For these reasons, degradation effects could not possibly have been involved.

The most probable explanation for the occurrence of this double endotherm lies in the recrystallisation process. When films are quenched rapidly from the melt, it is thought that the resultant structure consists of smectic material and possibly a distribution of small disordered monoclinic crystallites. It is feasible that these disordered crystallites rearrange themselves during heating at 10°C/min. They

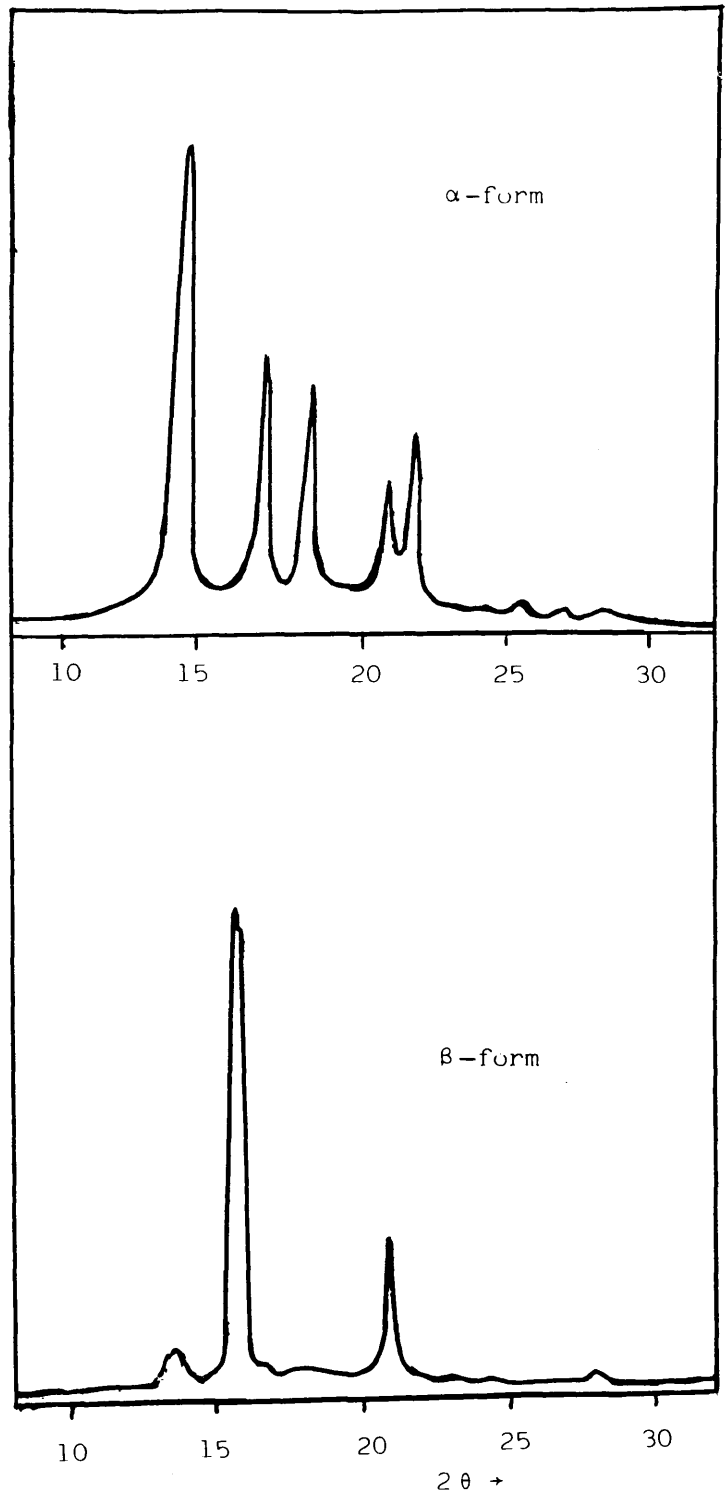

Figure 4.13 X-ray diffractograms of the α and β-forms of isotactic polypropylene

undergo a process of partial melting and subsequent recrystallisation, resulting in a greater degree of perfection. This continues throughout the distribution of crystallite sizes. This recrystallised distribution of crystallites forms the main melting peak in the thermogram. However, this does not fully explain the origin of the higher melting peak, the relative intensity of which appears to increase with the extent of quenching of the polypropylene films. It may be that an interaction between a portion of the smectic material which crystallises from the monoclinic phase transforms more easily from the α_1 modification to the higher order, lower free energy α_2 modification than the rest of the crystallite distribution in the quenched polypropylene samples. This would explain the slightly higher melting temperature of the second peak. Also, since the amount of smectic material increases with increasing extent of quenching then this may account for the increased intensity of the higher melting peak.

In the 2nd to 5th runs this process does not occur since the slow crystallisation rate prior to melting does not allow the formation of the smectic phase and results in a distribution of relatively large crystallites. These in turn exhibit quite a sharp melting range which is intermediate between that of the main melting peak and the higher melting peak in the 1st heat cycle of the quenched polypropylene films.

4.5.3.2 Crystallisation Between Melt Cycles

Crystallisation of the samples at the end of the 1st melting cycle was carried out at 10°C/min after holding the samples isothermally in the melt at 200°C for 5 minutes prior to cooling. This procedure was repeated after each heating cycle. It is thought that this treatment is sufficient to erase the majority of, if not all, nucleation sites characteristic of the previous thermal history. For this reason, as was expected, there were no significant differences in crystallisation onsets, peaks or heats of crystallisation (ΔH_c) for samples with respect to quench temperature.

It was interesting to note, however, that there was a difference in crystallisation onset and peak temperatures between polypropylene grades. Burfield and Doi[78] established a correlation between isotacticity and crystallisation onset temperatures in polypropylene. These results, then, indicate such a difference in isotacticity between the three polypropylene grades used and may account for the differences in melting onset data between the grades as shown in Table 4.25.

4.6 CONTROLLED QUENCHING BY DSC

Investigations into the effect of rapid quenching of polypropylene on the DSC melting profiles were extended in this study to *in situ* quenching of the polypropylene samples within the DSC furnace itself. This procedure was carried out in an attempt to emulate the quenching phenomenon in a more controlled environment.

4.6.1 Experimental

GSE18 polypropylene film samples (circa 5mg) were encapsulated in aluminium pans according to the procedure outlined in section 3.7. Samples were heated under a nitrogen atmosphere at 10°C/min to a final temperature well above the melting temperature of the polypropylene and held isothermal at this temperature for 5 minutes before quenching at a predetermined rate to 30°C. It was believed that this isothermal period would destroy any remaining nuclei which were characteristic of previous thermal treatments and provide all samples with a common thermal history prior to the quenching process. Following this, the samples were heated at 10°C/min from 30°C to 200°C in order to examine the effect of the particular thermal treatment on the subsequent melting profile of the polypropylene. The effect of several thermal treatments were investigated in this study.

4.6.2 Results

4.6.2.1 Quenching From 200°C At 200°C/Minute

Samples were heated at 10°C/min to 200°C and held at this temperature for 5 minutes before quenching at a controlled rate of 200°C/minute to 30°C. The sample was then heated at 10°C/minute from 30°C to 200°C. The resultant thermogram from this procedure consisted of four melting peaks and was highly reproducible. A typical melting profile for polypropylene treated in this way is shown in Figure 4.14 with each peak being designated a number. These numbers will be referred to throughout this study for each characteristic peak.

4.6.2.2 Effect of Holding At 200°C For Different Times

Triplicate samples were heated to 200°C as above and allowed to remain at this temperature for 5, 10, 15 or 30 minutes before quenching at 200°C/min to 30°C. The samples were then heated through their melting range as before to 200°C. Mean melting data for these DSC runs is presented in Table 4.26 and the associated melting profiles are shown in Figure 4.15.

Isothermal Time(Mins)	Main T_m Onset(°C)	ΔH_f (J/g)	Peak Number	Peak Temp(°C)
5	150.43	82.53	1 2 3 4	142.14 146.40 158.45 162.45
10	150.05	82.87	1 2 3 4	142.21 146.80 159.04 161.58
15	149.73	83.64	1 2 3 4	142.07 146.41 158.09 162.47
30	150.24	85.57	1 2 3 4	141.95 146.47 157.85 162.55

Table 4.26 Mean melting data for samples held at 200°C at for different isothermal melt times before quenching at 200°C/min.

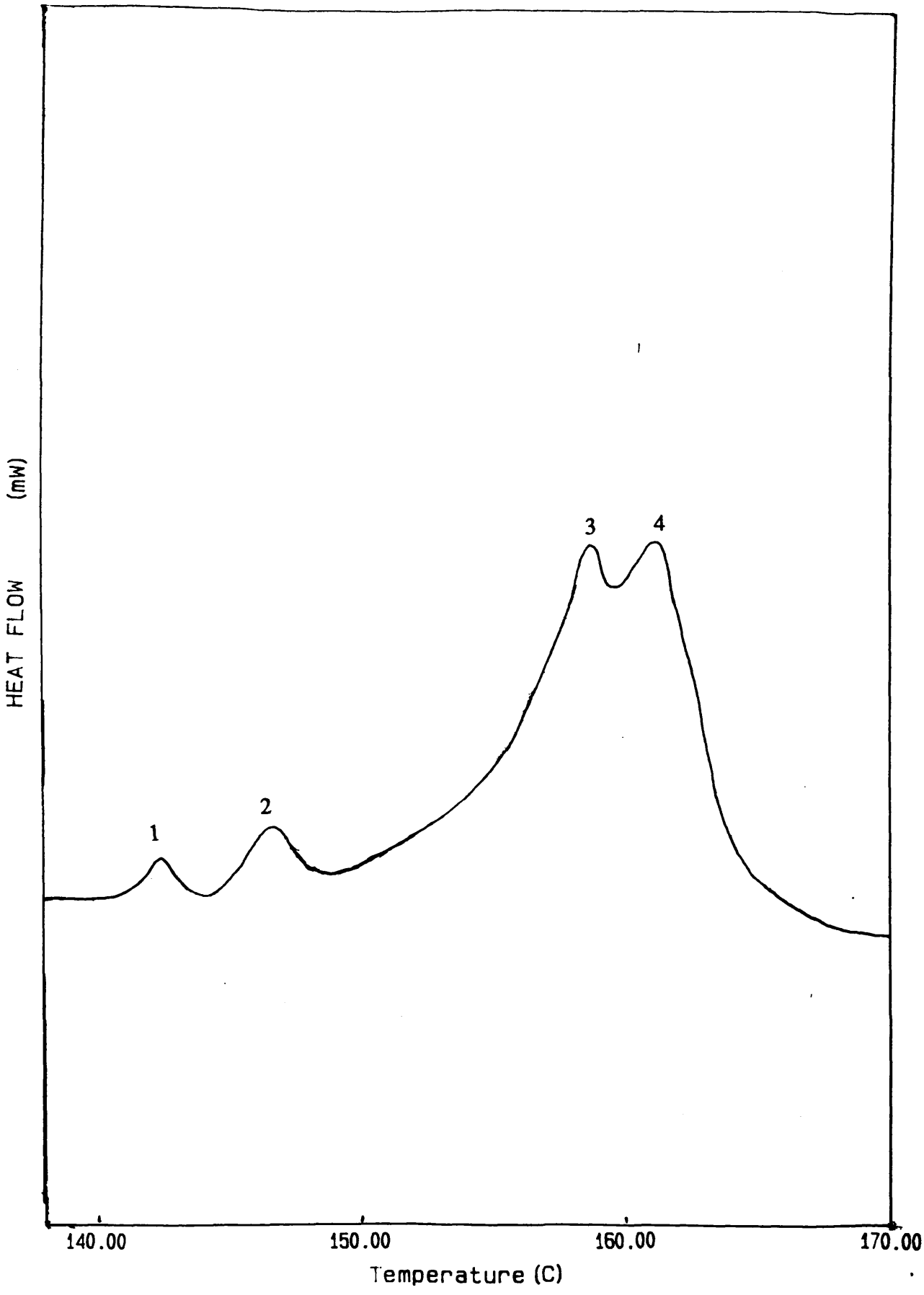

Figure 4.14 Typical melting thermogram for isotactic polypropylene subsequent to successive downward annealing treatment

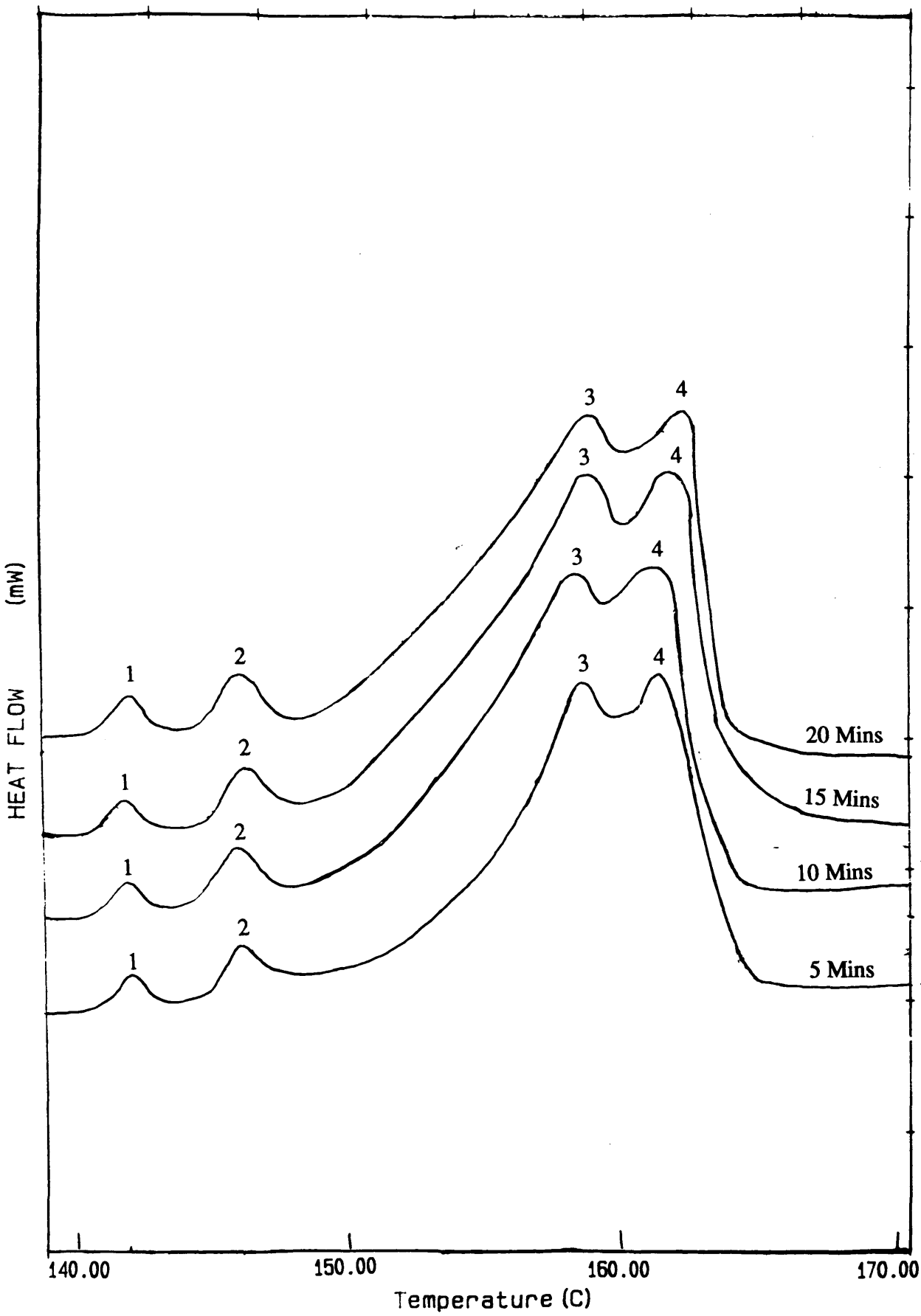

Figure 4.15 DSC melting profiles for polypropylene samples held in the melt for different times prior to quenching at 200°C/min

4.6.2.3 Effect Of Different Heating Rates

Triplicate samples were heated to 200°C at 10°C/min and held isothermal for 5 minutes before quenching at a rate of 200°C/min. Samples were then heated from 30°C to 200°C at different heating rates. Heating rates investigated were 1, 5, 10, 20 and 30°C. Mean melting data for these runs are presented in Table 4.27 and associated melting profiles are shown in Figure 4.16.

Heating Rate(°C/min)	Main T_m Onset(°C)	ΔH_f (J/g)	Peak Number	Peak Temp(°C)
1	158.84	223.50	1 2 3 4	--- --- 156.97 165.30
5	149.37	82.16	1 2 3 4	--- 146.26 155.96 161.71
10	151.07	88.05	1 2 3 4	142.33 146.55 158.41 162.14
20	150.34	88.29	1 2 3 4	--- --- 158.60 ---
30	151.38	90.07	1 2 3 4	--- --- 160.33 ---

Table 4.27 Mean melting data for samples quenched from 200°C to 30°C and then heated at different rates to 200°C.

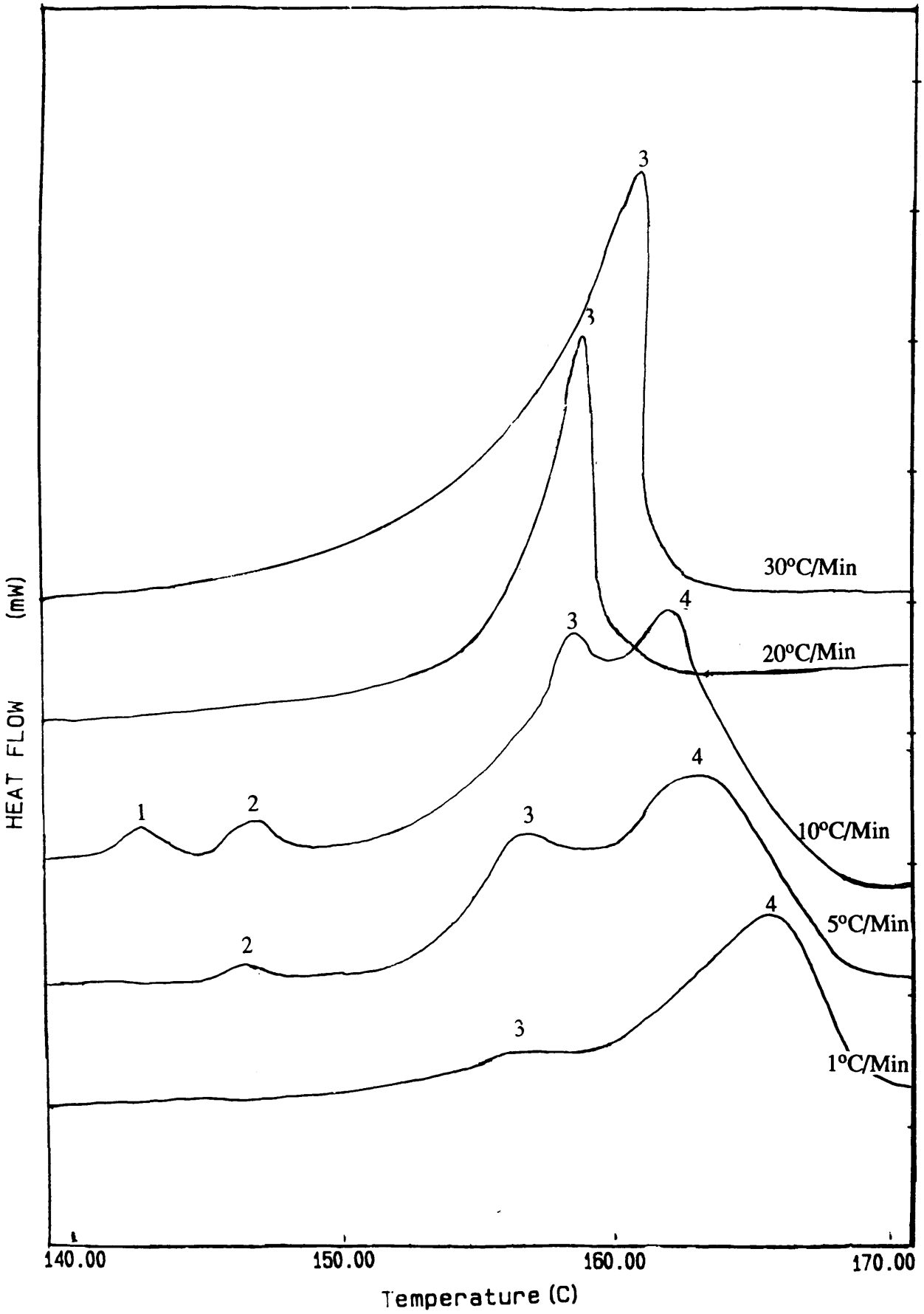

Figure 4.16 DSC melting profiles for polypropylene samples melted at different heating rates subsequent to quenching at 200°C/min

4.6.2.4 Effect Of Different DSC Quench Rates

Triplicate samples were heated to 200°C at 10°C/min and held isothermal for 5 minutes before cooling at DSC quench rates of 350, 300, 250, 200, 150, 20, 15, 10 and 5°C/min. Mean melting data for these DSC runs are presented in Table 4.28 overleaf and associated melting profiles are shown in Figure 4.17.

Quench Rate(°C/min)	Main T_m Onset(°C)	ΔH_f (J/g)	Peak Number	Peak Temp(°C)
5	155.21	84.11	1 2 3 4	--- --- 159.66 ---
10	153.27	104.22	1 2 3 4	--- --- 158.47 161.54
15	153.03	95.43	1 2 3 4	--- 144.72 158.70 161.69
20	152.95	94.11	1 2 3 4	--- 144.56 158.59 161.60
150	151.32	93.18	1 2 3 4	142.75 149.63 158.67 161.91
200	150.60	82.46	1 2 3 4	142.06 146.54 157.73 161.68
250	150.44	80.44	1 2 3 4	142.33 147.11 157.07 161.49
300	150.52	82.42	1 2 3 4	142.55 146.65 157.06 161.56
350	151.40	86.14	1 2 3 4	142.41 147.21 157.59 162.08

Table 4.28 Mean melting data for samples quenched at different cooling rates

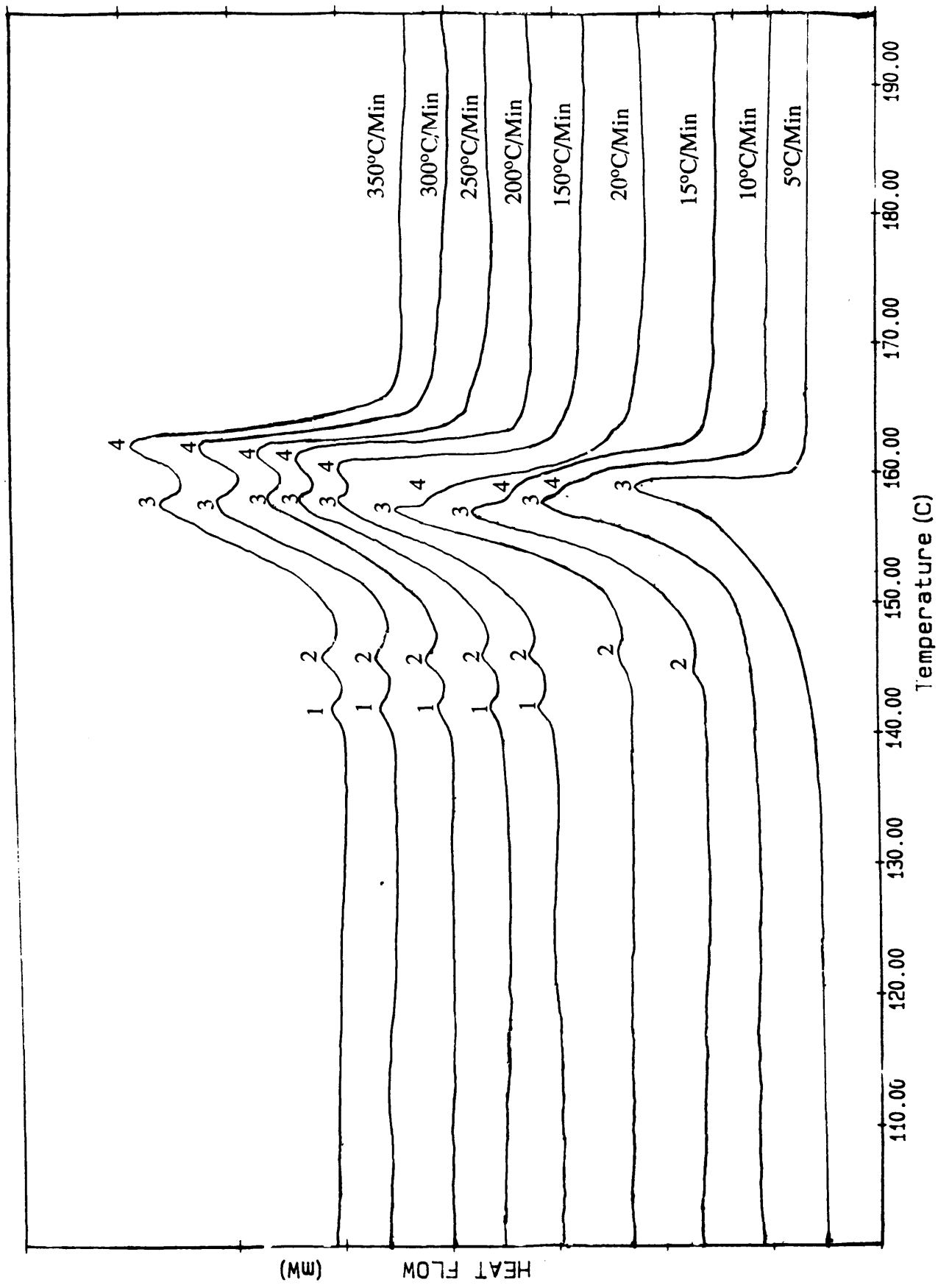

Figure 4.17 DSC melting profiles for polypropylene samples quenched at different rates from 200°C

4.6.2.5 Effect Of Annealing On Multiple Peaks

Samples were heated to 200°C at 10°C/min and held isothermal for 5 minutes before quenching at a rate of 200°C/min in the DSC to induce structural changes in the polypropylene which were reflected in the four peaks observed its subsequent DSC melting profile.

Samples were then run at 10°C/min to a predetermined annealing temperature (T_a) and held isothermal for 5 minutes. After this annealing period, the samples were heated at 10°C/min from T_a to 200°C and the resultant thermogram recorded. Annealing was carried out at 10°C intervals from 30°C to 150°C and 3 replicates were run for each anneal temperature. Main peak melting onsets and heat of fusion were similar throughout and so only the relative mean positions of each peak in the melting profile are presented in Table 4.29 for each annealing temperature. The relative intensities of each peak with respect to the corresponding peak in a previous anneal are shown in the table by the designation of a symbol. These symbols are as follows:-

+ = Intensity of the peak has increased relative to that of the corresponding peak at the previous annealing temperature.
/ = Intensity of the peak has remained constant relative to that of the corresponding peak at the previous annealing temperature.
- = Intensity of the peak has decreased relative to that of the corresponding peak at the previous annealing temperature.

The effect of annealing temperature on melting profiles is shown in Figure 4.18 overleaf.

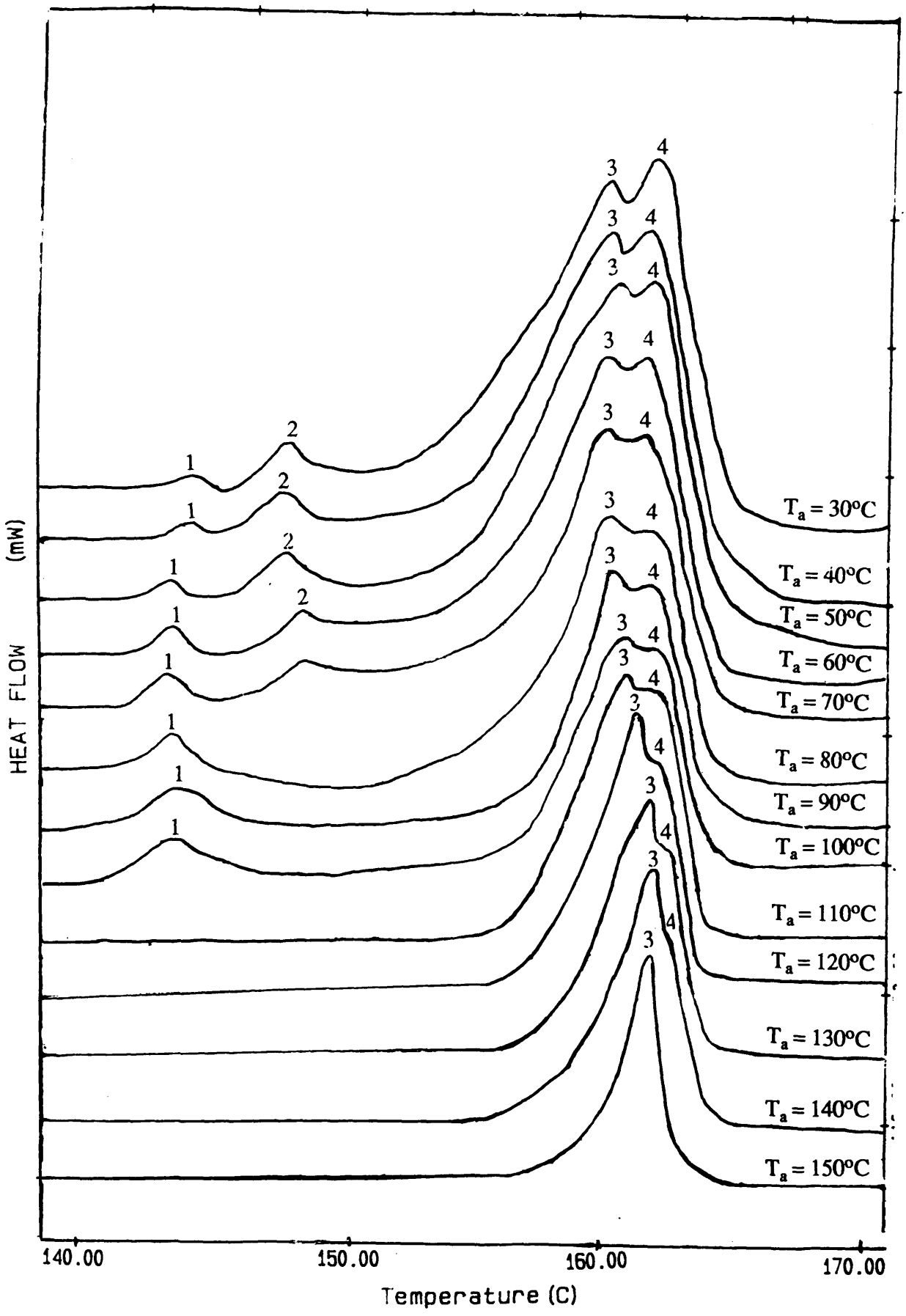

Figure 4.18 Effect of annealing temperature on DSC profiles of polypropylene quenched at 200°C/min

T_a(°C)	Peak 1 (°C)	Peak 2 (°C)	Peak 3 (°C)	Peak 4 (°C)
30	142.20	146.43	156.47	163.63
40	141.60-	146.44-	156.64+	163.71/
50	141.72/	148.47-	157.50+	162.25/
60	141.65/	149.32-	157.43+	161.73/
70	141.86-	147.91-	157.80+	163.46/
80	141.64-	---	158.34+	163.21-
90	142.33-	---	158.45+	162.66-
100	141.61-	---	158.42+	162.44-
110	---	---	158.71+	164.06-
120	---	---	158.66+	163.15-
130	---	---	158.97+	162.10-
140	---	---	159.23+	161.47-
150	---	---	160.36+	---

Table 4.29 Mean melting data for samples quenched at 200°C/min and then annealed at different temperatures.

4.6.3 Discussion

4.6.3.1 Direct Control Of Quenching During DSC Studies

Results discussed in the section 4.5.3 have shown that it is possible to obtain more than one peak in the melting profile of polypropylene samples by rapid quenching from the molten state into quench baths at various temperatures. In this section a study was undertaken to investigate the use of cooling the samples quickly in the DSC furnace itself.

Samples were provided with a common thermal history by heating to 200°C at 10°C/min and holding isothermal for 5 minutes prior to controlled quenching. Quenching the samples from this isothermal melt temperature at 200°C/min was found to produce samples which on remelting at 10°/min exhibited four distinct highly reproducible peaks in the melting profile. These peaks typically occurred at temperatures of around 142°, 146°, 158° and 162°C respectively. In the thermogram of these thermally treated samples there was no evidence of an exothermic peak at around 80°C which meant that the degree of quenching was insufficient to induce the conformationally disordered smectic phase although it was clear from the thermogram that disorder of some sort was present in the DSC quenched polypropylene crystallites.

X-ray diffraction carried out on a polypropylene sample quenched in this manner corroborated the absence of the smectic phase and the sample was found to consist of only the α-crystalline (or monoclinic) material. The x-ray diffractogram also discounted the possibility of any other polymorph of polypropylene being responsible for the curious melting profile of the quenched samples. This result is in good agreement with Passingham and co-workers[145] who recently carried out a similar

study in which they found 3 reproducible peaks in polypropylene samples on quenching at a rate of 320°C/min in the DSC. X-ray examination of their quenched samples showed that they were entirely composed of monoclinic material, and although one of their samples did exhibit a very small peak representative of the β-phase of polypropylene, it was considered to be present in such slight amounts that its effect, if any, on the resultant melting thermogram would be inconsequential. They explained the origin of this triple endotherm in terms of the formation of different helix lengths during the quenching process as determined from infrared data. In the present study, infrared spectroscopy of the samples subsequent to thermal treatment was attempted. However, due to their opaque nature very poor spectra were obtained and consequently they were of no use for analysis purposes.

Investigations into the quadruple melting peaks phenomenon were undertaken by subjecting films to various thermal treatments in an attempt to further understand the structural changes taking place.

4.6.3.2 Effect Of Holding Isothermally In The Melt At 200°C For Different Times.

This study was undertaken in order to assess the efficiency of erasing any previous thermomechanical history of the polypropylene by holding the sample isothermally in the melt at 200°C for 5 minutes prior to DSC quenching at 200°C/min.

From the results presented in Table 4.26 and from corresponding melting profiles shown in Figure 4.15, it is evident that holding isothermally at 200°C for different times has very litte effect on the occurrence or positioning of the four peaks in the melting profiles of polypropylene subsequent to quenching at 200°C/min. From this it can be concluded that 5 minutes isothermal at 200°C is sufficient to erase any

persistent nucleation sites characteristic of previous thermal or mechanical treatments.

4.6.3.3 Effect Of Different Heating Rates

The effect of different heating rates on the appearance of the melting profiles of samples quenched at 200°C/min from an isothermal melt temperature of 200°C was studied. From results presented in Table 4.27 and associated melting profiles shown in Figure 4.16, it is apparent that heating rate plays an important role in the appearance of the multiple peaks in the resultant endotherms.

At very low heating rates, such as 1°C/min, two broad peaks were observed, one of low intensity occurring at around 157°C with the second peak being the main melting peak and occurring at 165°C. At a heating rate of 5°C/min, three broad peaks were obtained. The first of these peaks was of low intensity and had its maximum at 146°C. The second peak was of higher intensity and occurred at 156°C and the third peak was the main melting peak which occurred at 162°C. At a heating rate of 10°C/min, the customary four peaks were observed and occurred at temperatures of 142°, 146°, 158° and 162°C respectively. Films heated at rates of 20 and 30°C/min exhibited only one peak which was relatively sharp and occurred at 159 and 160°C respectively.

Various studies[58,143,144,148-151] have shown that altering the heating rate can have a marked effect on the number of peaks resolved in the DSC melting thermograms of polypropylene. In this study, it appears that for very slow or very fast heating rates there is a tendency towards a single endotherm, albeit a much broader one at the very low heating rates. With a very slow heating rate, the main melting peak occurs at a higher temperature. This is also true for the faster heating rates although to a lesser extent. An intermediate heating rate of 10°C/min seems to be ideal for the resolution

of four peaks in the melting endotherm of the DSC quenched polypropylene films. Passingham and co-workers[145] observed three reproducible peaks at a heating rate of 20°C/min in their polypropylene samples but did not investigate any other heating rates. Had they run their samples at a slower heating rate then it is possible that more peaks may have been resolved.

Since x-ray diffractograms of films quenched at 200°C/min showed only the presence of the α-crystalline modification and the fact that the samples were unoriented and showed no signs of oxidation then the origin of the multiple peaks is obviously due to some other phenomenon. It is thought that the origin of the multiple peaks may be attributed to a recrystallisation process similar to that discussed in section 4.5.3 involving the melting of metastable crystallites followed by renewed crystallisation to more perfect crystallites. It is also proposed that the best heating rate for the study of this phenomenon is an intermediate heating temperature of 10°C/min.

At heating rates higher than this, the crystallites which are in a disordered state due to fast quenching, are not given sufficient time to undergo recrystallisation and hence the constant competition between melting and recrystallisation results in a single endotherm at a temperature of circa 160°C. At very slow rates, the small disordered crystallites have more than sufficient time to achieve greater perfection and crystal thickening. Also, at slow heating rates the magnitude of the DSC signal is very poor and the melting and recrystallisation is not detected by discontinuities in the baseline. This results in a distribution of crystallites of greater perfection melting together at a higher temperature. The 10°C/min heating rate is slow enough to allow the partial melting and recrystallisation but fast enough to exhibit a signal in the DSC thermogram.

Passingham and co-workers[145] postulated that the occurrence of more than two peaks in the thermogram of DSC quenched polypropylene is misleading and that only two peaks are genuine claiming that their triple endotherm was merely a double peak with an overlying exotherm due to recrystallisation between peaks 2 and 3. Using a model previously suggested by Corradini and coworkers[151], Guerra and co-workers[149] discussed the idea of a continuum of intermediate α-modifications between two limiting α_1 and α_2-modifications. It is thought that the behaviour of polypropylene samples in the present study conforms to this model which considers that a layer of isoclined macromolecules in the ac plane is succeeded by a double layer of anticlined macromolecules with probability 1 - p. In this model the α_2 limiting structure has a value of p = 1 and the α_1 limiting disordered structure corresponds to p = 0.5. It suggests that it is possible for a continuum of different structures to exist between that of the limiting disordered α_1-modification and the ordered limiting α_2-modification.

In this study, it is thought that the DSC quenched samples consist of disordered crystallites of the limiting α_1-modification which undergo reorganisation through various α-modifications between the α_1 and α_2 limiting modifications. These modifications undergo partial melting and recrystallisation until they acheive a stucture of higher order comparable to that of the α_2 limiting structure which subsequently melts at a higher temperature.

4.6.3.4 Effect Of Different Quench Rates

Different quench rates from an isothermal melt temperature of 200°C were investigated in order to assess their role in the occurrence of multiple peaks in the subsequent melting of the polypropylene films at 10°C/min. Quench rates of 350°,

300°, 250°, 200°, 150°, 20°, 15°, 10° and 5°C/min were used. Results presented in Table 4.27 and melting profiles shown in Figure 4.17 show that the melting profile is undoubtedly affected by different quench rates.

Samples quenched at 350°, 300°, 250°, 200° and 150°C/min exhibited four distinct peaks in their subsequent melting profiles. These occurred at circa 142°, 147°, 157° and 162°C respectively. Samples quenched at 20°C and 15°C/min respectively, showed only three peaks although peak 3 had been shifted to a slightly higher temperature and had begun merging with peak 4. At quench rates of 10°C/min no lower temperature peaks existed and the merging of peak 3 with peak 4 became even more enhanced. At the slowest quench rate of 5°C/min, only a relatively sharp solitary peak, occurring at circa 160°C, remained.

It is assumed that the greater the degree of quenching, then the more disorder or imperfection exists amongst the crystallites. Due to the absence of any exothermic peak at 80°C and the fact that the x-ray photographs show no diffuse halos, the degree of quenching is not sufficient to induce the formation of the smectic phase, even at a rate of 350°C/min. At the faster quench rates the intensity of peak 4 compared to peak 3 seems to be relative higher although the peak positions are not altered. The intensity difference, however, decreases with decreasing quench rates. At quench rates of 350° to 150°C/min, it is proposed that disorder in the crystallite structures is induced to a greater extent and hence a larger degree of structural reorganisation is exibited as the $\alpha_1 \rightarrow \alpha_2$ transition proceeds. At quench rates of 20°C and 15°C/min there is only one lower melting peak at 145°C and the main melting peak occurs at 159°C with a shoulder peak at circa 162°C. At a 10°C/min quench rate no low temperature peaks are present and the main peak at 159°C and shoulder at 162°C now

appear to resemble a single peak. At the 5°C/min quench rate no low temperature peaks exist and the high temperature shoulder (peak 4) has merged with peak 3 to form a single relatively sharp discrete endotherm at 160°C.

This behaviour at the lower quench rates suggests that as the quench rate becomes slower, the crystallites have more time to crystallise and the degree of disorder in the resultant polypropylene becomes less. As this happens, there is less requirement for recrystallisation as more of the crystallites are in a state of higher order. At the very slow cooling rates, the crystallites do not undergo any detectable recrystallisation on subsequent melting and thus produce a single melting endotherm typical of the fusion of crystallites closer in structure to the α_2 limiting modification.

4.6.3.5 Effect Of Annealing On Multiple Peaks

Samples which had been quenched at 200°C/min from an isothermal melt temperature of 200°C were heated to a predetermined annealing temperature (T_a) and held isothermal for 5 minutes before recommencing heating through the melting temperature of the polypropylene. Annealing was carried out at 10°C intervals over the temperature range of 30 to 150°C.

The results in Table 4.29 and Figure 4.18 show the effect that annealing has on the appearance of multiple peaks in the melting profile of the DSC quenched polypropylene samples. For low annealing temperatures, ie 30-70°C, four distinct peaks were observed in the melting profile. As T_a increased from 30-70°C it was seen that the intensity of peak 3 increased at the expense of peak 2. Peak 2 became absent in the samples annealed above 70°C and peaks 3 and 4 became less resolved at annealing temperatures in the range 80-100°C, whilst peak 1 became broader and slightly less intense in nature. Samples annealed at temperatures in the 110-140°C

range exhibited no low temperature peaks and peak 4 became progressively more shoulder-like until finally at an annealing temperature of 150°C the subsequent melting endotherm consisted of a relatively sharp single melting peak.

The very low annealing temperatures (30-50°C) seem to have little effect on the four peaks observed in the melting profile. As T_a is increased through the range 50-70°C, however, the corresponding increase in peak 3 at the expense of peak 2 suggests that annealing is alleviating some of the disorder in the DSC quenched structure. As T_a is further increased, the degree of disorder in the structure becomes less and this results in a corresponding decrease in the recrystallisation process during the heating run, which in turn leads to the simultaneous decrease in intensity and increase in broadness of peak 1 with the disappearance of peak 2. Also peak 3 becomes shifted to a slightly higher temperature and begins to merge with peak 4. At annealing temperatures above 110°C, the crystallites have had ample time to further perfect themselves and even less recrystallisation is necessary. This is apparent in the disappearance of both the low temperature peaks. This is also synonymous with the greater depletion of individual peaks 3 and 4 as they tend towards a single endotherm. At an annealing temperature of 150°C, all the disordered limiting α_1-modification crystallites have achieved greater perfection with the $\alpha_1 \rightarrow \alpha_2$ transition at an advanced stage. This results in a single melting peak at 160°C.

The annealing process, then, leads to progressive perfection as T_a is increased. This supports the argument that various stages of order exist between the α_1 limiting modification and the ordered α_2 limiting modification. It is also evident that at all annealing temperatures some degree of structural reorganisation is occurring. As the annealing temperature is increased, the kinetics of the $\alpha_1 \rightarrow \alpha_2$ transition become enhanced as disordered crystallites undergo recrystallisation at a faster rate.

4.7 FRACTIONATION OF ISOTACTIC POLYPROPYLENE HOMOPOLYMER

4.7.1 Introduction

It is well known that the composition of isotactic polypropylene can be considered as consisting of a distribution of both molecular weight and stereoregularity[152]. In isotactic polypropylene, it can be said that some molecules have very high degree of stereoregularity, some practically none and others have stereoregularity intermediate between the two extremes. A distribution of chain lengths also exists leading to a wide variation in molecular weight and since there appears to be some degree of correlation between these two characteristics[152], it is possible to fractionate a sample of highly isotactic polypropylene into different component parts of the molecular weight/tacticity distribution.

Many early fractionation studies[153,154] were principally concerned with the determination of molecular weight distributions in the whole polymer but with the emergence of gel permeation chromatography the use of polymer fractionation for this purpose has become increasingly obsolete.

Natta and co-workers[155] were amongst the first to investigate the separation of polypropylene on the basis of stereoregularity. By studying the solubility of polypropylene in various solvents having different boiling points and using Soxhlet type extraction apparatus to carry out the fractionation they discovered that it was possible to fractionate on the basis of stereoregularity as well as molecular weight. They found that boiling diethyl ether removed low molecular weight material which showed no signs of crystallinity in the x-ray diffraction studies. Using n-alkane solvents of C_5 to C_8 they noted that the fractions soluble in each solvent increased

progressively in x-ray crystallinity and intrinsic viscosity. Based on these studies they defined the terms atactic, stereoblock and isotactic polypropylene and with this it became customary to regard the atactic fraction as that which is soluble in boiling diethyl ether, stereoblock as being insoluble in boiling diethyl ether but soluble in boiling n-heptane and isotactic as the fraction which is insoluble in both boiling diethyl ether and n-heptane.

In stepwise extraction experiments using n-alkane solvents, fractionation on the basis of different molecular weights and isotacticities was confirmed by other authors[152,156]. Kissin[20] discussed the origin of the differences in degree of stereoregularity in polyolefin fractions in terms of a model which considers the existence of a continuous (or quasi-continuous) distribution of active catalytic centres in Zeigler-Natta catalysis with respect to their stereospecificity.

Studies[157,20] involving fractionation of polypropylene using successive extraction with n-alkane solvents found that the resultant fractions had different ^{13}C-nmr pentad tacticities thus providing further evidence that separation was on the basis of tacticity as well as molecular weight.

In the present study fractionation of an isotactic polypropylene was carried out in order to obtain fractions of different molecular weight/tacticity composition. The success of the fractionation procedure is appraised and the fractions obtained have been used (section 4.8) to investigate the role of molecular weight/tacticity in the thermal behaviour of polyproypylene.

4.7.2 Experimental

Pellets of GSE18 polypropylene were ground (using a Waring blender in the presence of liquid nitrogen according to the procedure described in section 3.4.1.) to produce a fine powder with a particle size in the range 150 to 250 microns.

Samples (circa 5g) were put in paper thimbles and placed into the fractionation apparatus. As previously mentioned in section 3.12.3, two fractionation procedures were investigated. Fractions thus obtained were characterised for molecular weight and tacticity using gel permeation chromatography, ^{13}C-nmr, density measurements, DSC melting and crystallisation, optical microscopy and infrared spectroscopy.

Also, using a stepwise annealing procedure similar to that developed by Pae and Sauer[140] on the obtained fractions, the role of molecular weight/tacticity on the thermal behaviour of polyproyplene was investigated.

4.7.3 Results

4.7.3.1 Investigative Fractionation Procedure

Fractionation was carried out according to the procedure described in section 3.12.3(a). Solvents and extraction times for this procedure are shown in Table 3.1. The fractionation was carried out in triplicate under the same conditions and results for the weight of each fraction obtained are shown in Table 4.30

Fraction	Extraction Time (Hrs)	Fraction Weight (%)			IR Oxidation
		1	2	3	
Ether	8	0.85	1.04	0.61	-
Pentane	8	0.79	0.54	0.91	+
Hexane	8	2.35	2.75	1.76	-
Heptane	9	12.68	10.20	14.34	+
Toluene	11	23.11	30.72	27.20	+
Octane	17	55.30	52.45	53.38	+
Losses		4.92	2.30	1.80	

Table 4.30 Fraction weight (%) for three extracted GSE18 polypropylene samples by Soxhlet extraction (+ and - signs indicate the presence or absence of oxidation respectively).

4.7.3.2 Fractionation By Reflux

Samples were fractionated according to the improved procedure of extraction under reflux as described in section 3.12.3(b). Results for the fractionation of three separate samples are shown in Table 4.31.

Fraction	Extraction Time (Hrs)	Fraction Weight (%)			IR Oxidation
		1	2	3	
Ether	8	3.29	3.41	3.21	-
Pentane	8	1.43	1.22	1.48	-
Hexane	8	2.90	2.98	2.81	-
Heptane	9	5.56	5.28	5.47	-
Toluene	11	63.50	63.44	62.18	-
Octane	17	20.83	21.82	22.08	-
Losses		2.49	1.85	2.77	

Table 4.31 Fraction weight (%) for three extracted GSE18 polypropylene samples by reflux extraction.

4.7.3.3 Molecular Weight Determination Of Fractions

Molecular weight averages were obtained for each fraction by high temperature gel permeation chromatography (GPC) at 140°C. All GPC measurements were carried out by RAPRA Technology Ltd. under the conditions described in section 2.4.3. Table 4.32 shows molecular weight averages for each fraction and Figures 4.19 - 4.22 show the relationship between the molecular weight averages and the extraction temperature for each fraction.

Fraction	$\bar{M}_n/10^3$	$\bar{M}_w/10^3$	$\bar{M}_z/10^3$	$\bar{M}_p/10^3$	$\bar{M}_w/\bar{M}_n$
Ether	8.76	53.74	318.00	28.36	6.14
Pentane	9.69	34.04	86.17	29.12	3.72
Hexane	10.97	72.15	226.45	55.19	6.58
Heptane	14.48	83.09	271.50	58.88	5.74
Toluene	9.16	40.74	160.70	24.27	4.45
Octane	48.38	189.85	399.50	148.40	3.93
GSE18	61.61	376.40	1083.50	240.05	6.97

Table 4.32 Molecular weight averages and distribution for GSE18 polypropylene fractions and homopolymer.

Figure 4.19

Graph showing the relationship between $\bar{M}n$ and temperature of fractionation for GSE18 polyproylene fractions

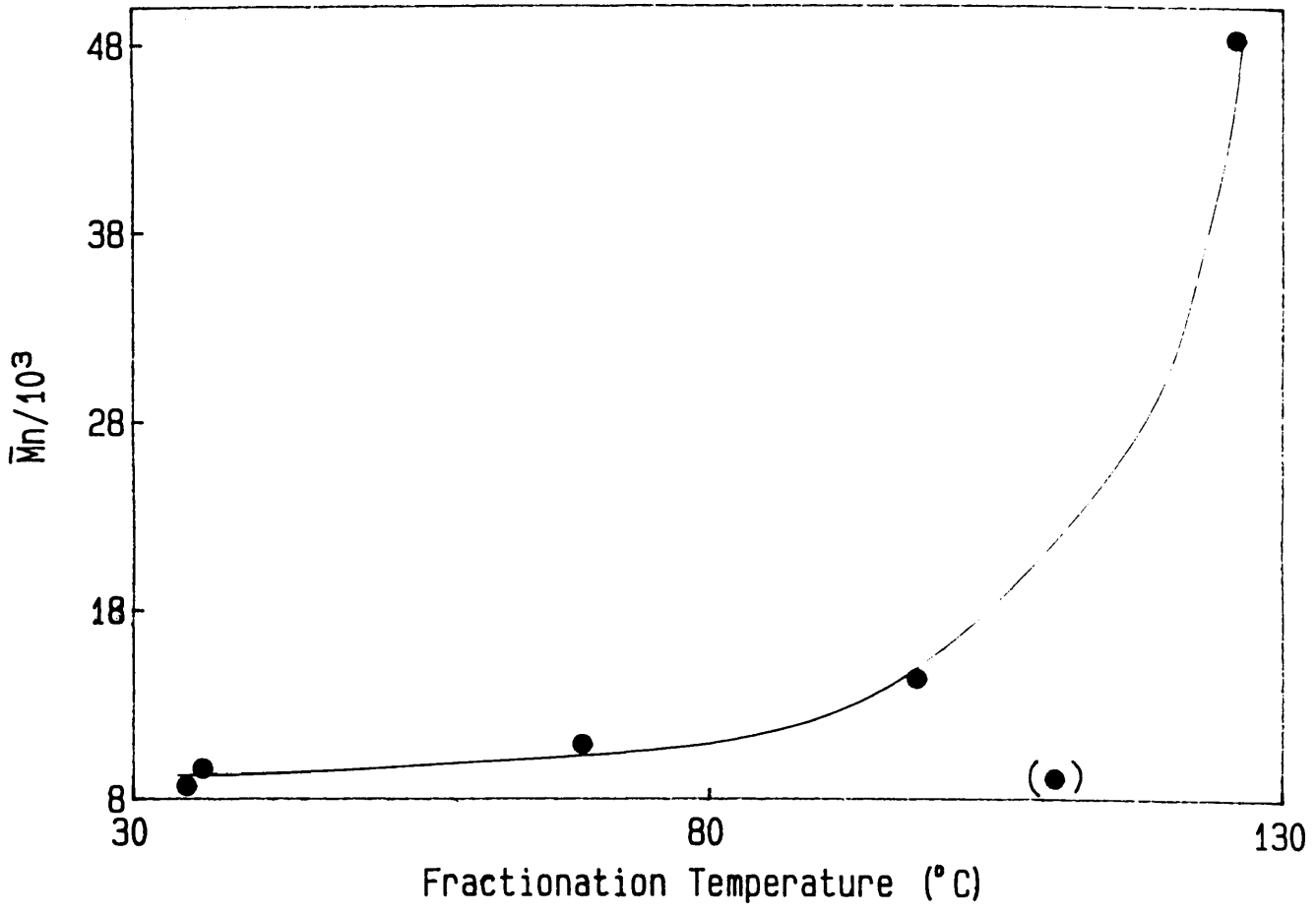

Figure 4.20

Graph showing the relationship between $\bar{M}w$ and temperature of fractionation for GSE18 polypropylene fractions

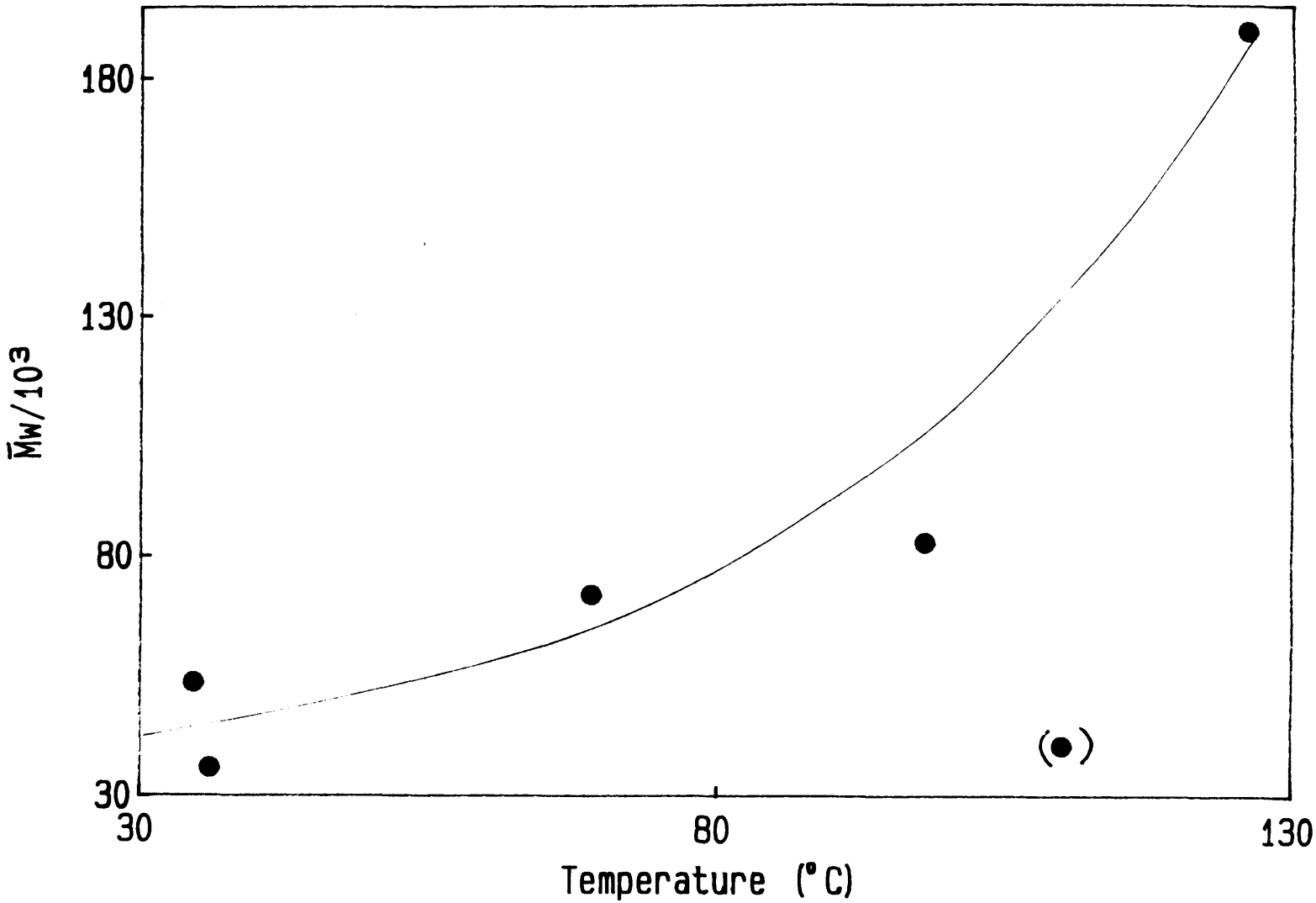

Figure 4.21

Graph showing the relationship between $\bar{M}z$ and temperature of fractionation for GSE18 polypropylene fractions

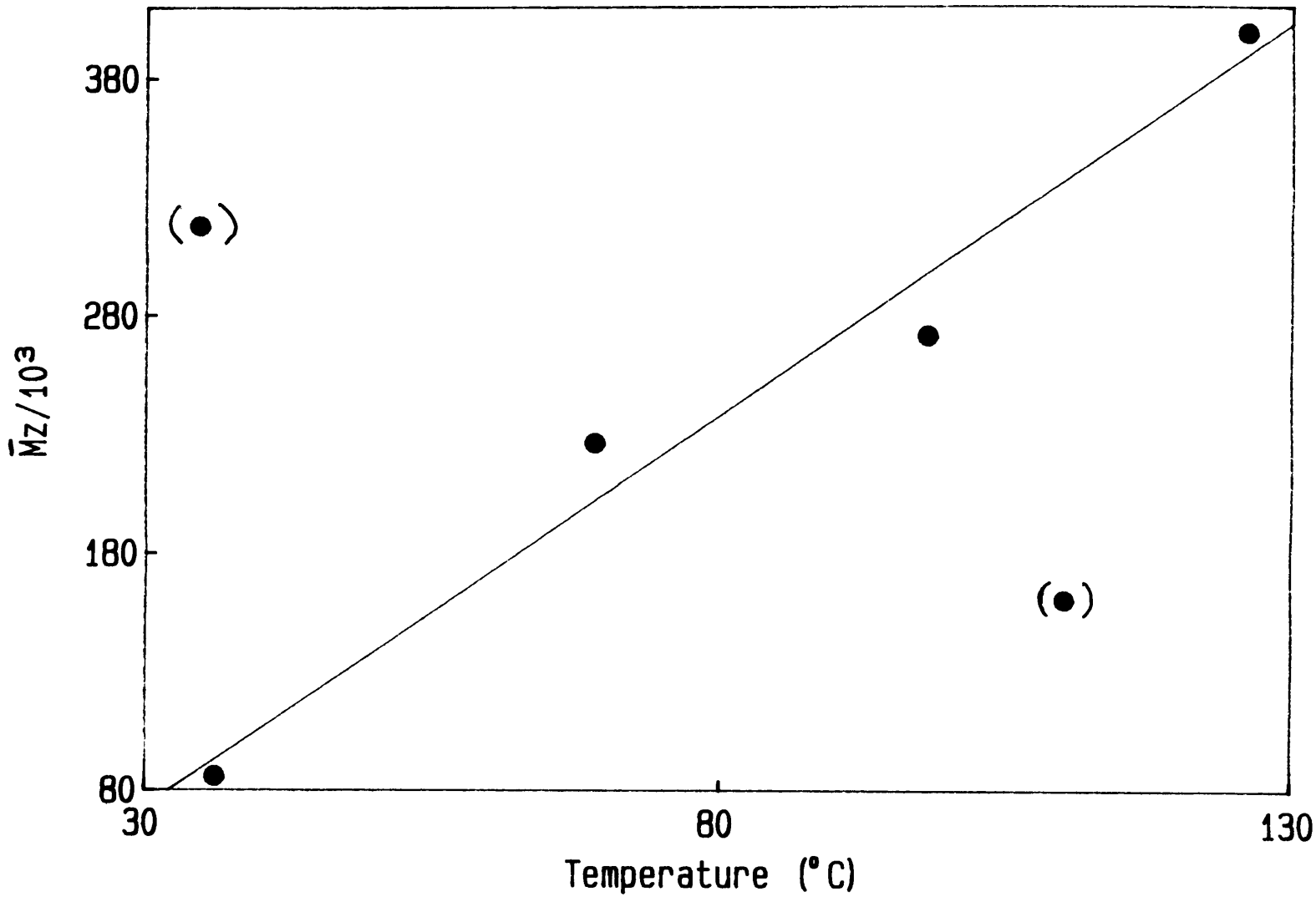

Figure 4.22

Graph showing the relationship between $\bar{M}p$ and temperature of fractionation for GSE18 polypropylene fractions

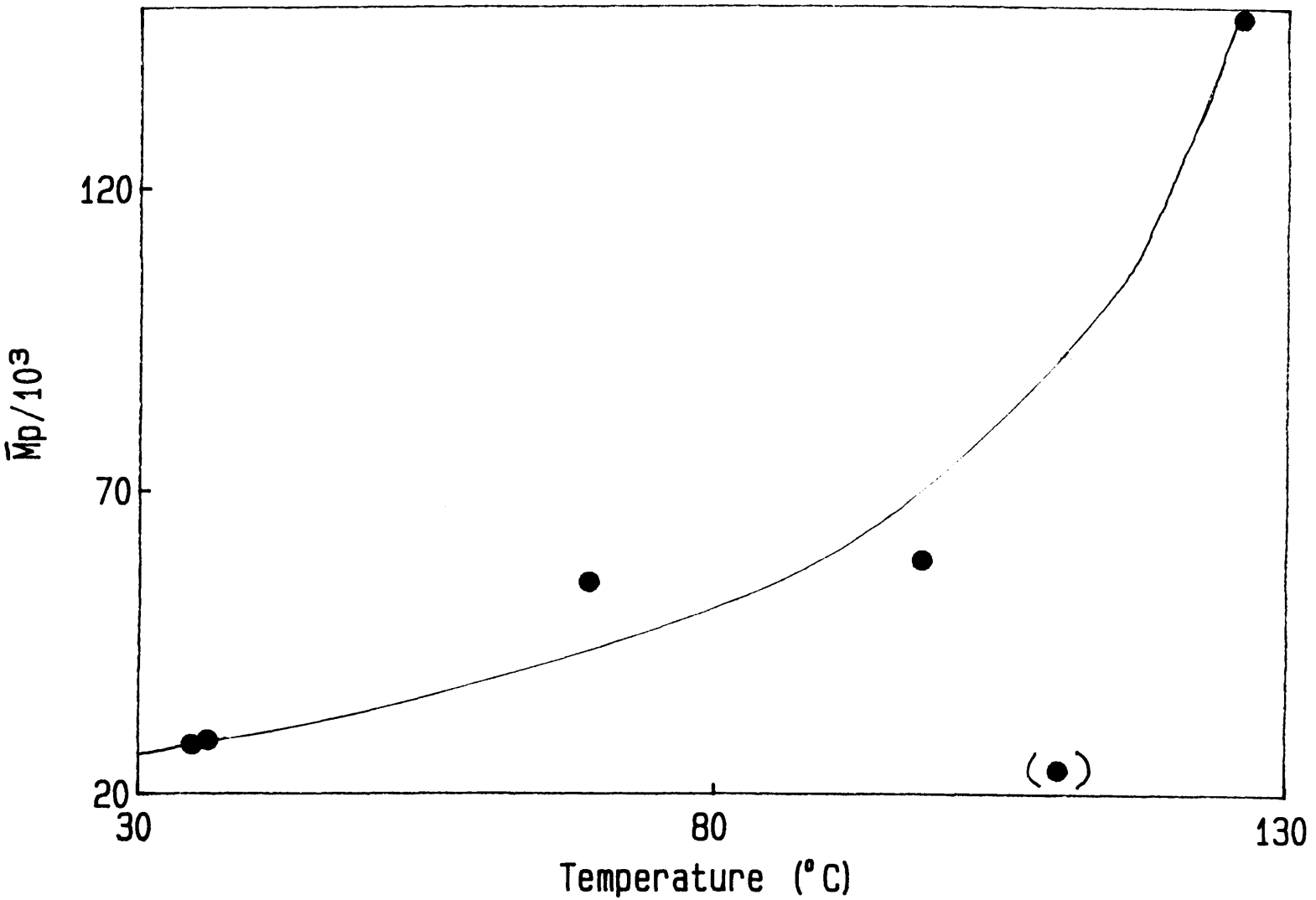

4.7.3.4 ^{13}Carbon Nuclear Magnetic Resonance (^{13}C-nmr)

In order to assess the relative degrees of isotacticity of each fraction, ^{13}C-nmr spectra of the obtained polypropylene fractions were recorded according to the conditions described in section 3.14. Relative peak areas for the methyl (CH_3) and methylene (CH_2) regions of the spectra were calculated for each fraction from the ^{13}C-nmr integrals and values were assigned to pentad[105] and tetrad[106] stereosequences respectively. Tables 4.33 and 4.34 show ^{13}C-nmr pentad and tetrad sequence distributions for the methyl and methylene regions respectively for the fractions and homopolymer. Figures 4.23 - 4.25 show the effect of fractionation on the ^{13}C-nmr spectra of the methyl, methylene and methine regions as the isotactic content of the fractions increases.

Methyl Region (CH_3)

Fractn	*mmmm*	*mmmr*	*rmmr*	*mmrr*	*mmrm* + *rmrr*	*mrmr*	*rrrr*	*mrrr*	*mrrm*
Ether	0.106	0.096	0.053	0.128	0.165	0.048	0.160	0.138	0.064
Pentane	0.161	0.092	0.035	0.133	0.133	0.045	0.166	0.138	0.076
Hexane	0.362	0.119	0.030	0.127	0.079	0.043	0.098	0.075	0.067
Heptane	0.497	0.104	---	0.104	0.052	0.017	0.050	0.050	0.074
Toluene	0.924	0.029	---	0.024	---	---	0.012	---	---
Octane	0.967	---	---	0.013	---	---	---	---	---
GSE18	0.864	0.029	0.009	0.023	0.012	0.011	0.018	0.018	0.018

Table 4.33 Pentad sequence distribution for each fraction and original homopolymer in the methyl region of the ^{13}C-nmr spectra.

Methylene Region (CH_2)

Fraction	*mrm*	*rrr*	*mrr*	*mmr*	*rmr*	*mmm*
Ether	0.043	0.167	0.287	0.059	0.325	0.057
Pentane	0.035	0.152	0.276	0.064	0.350	0.064
Hexane	0.013	0.093	0.062	0.150	0.054	0.584
Heptane	0.016	0.074	0.023	0.090	0.023	0.752
Toluene	---	---	0.016	0.021	0.021	0.920
Octane	---	---	0.022	---	---	0.978
GSE18	---	0.021	0.011	0.032	0.032	0.889

Table 4.34 Tetrad sequence distribution for each fraction and original homopolymer in the methylene region of the ^{13}C-nmr spectra.

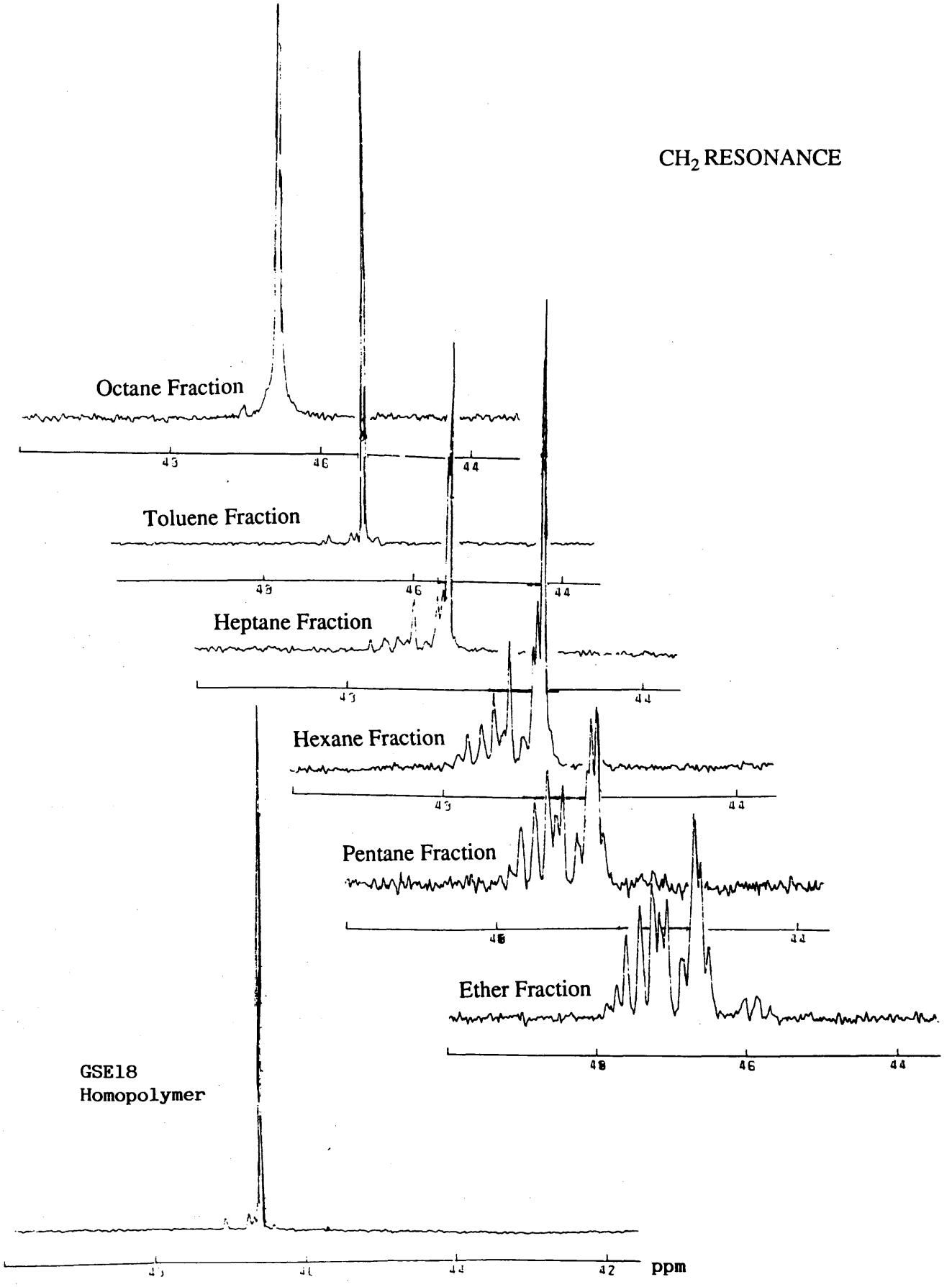

Figure 4.23 ^{13}C-Nmr spectra showing the methylene region for the GSE18 polypropylene fractions and homopolymer

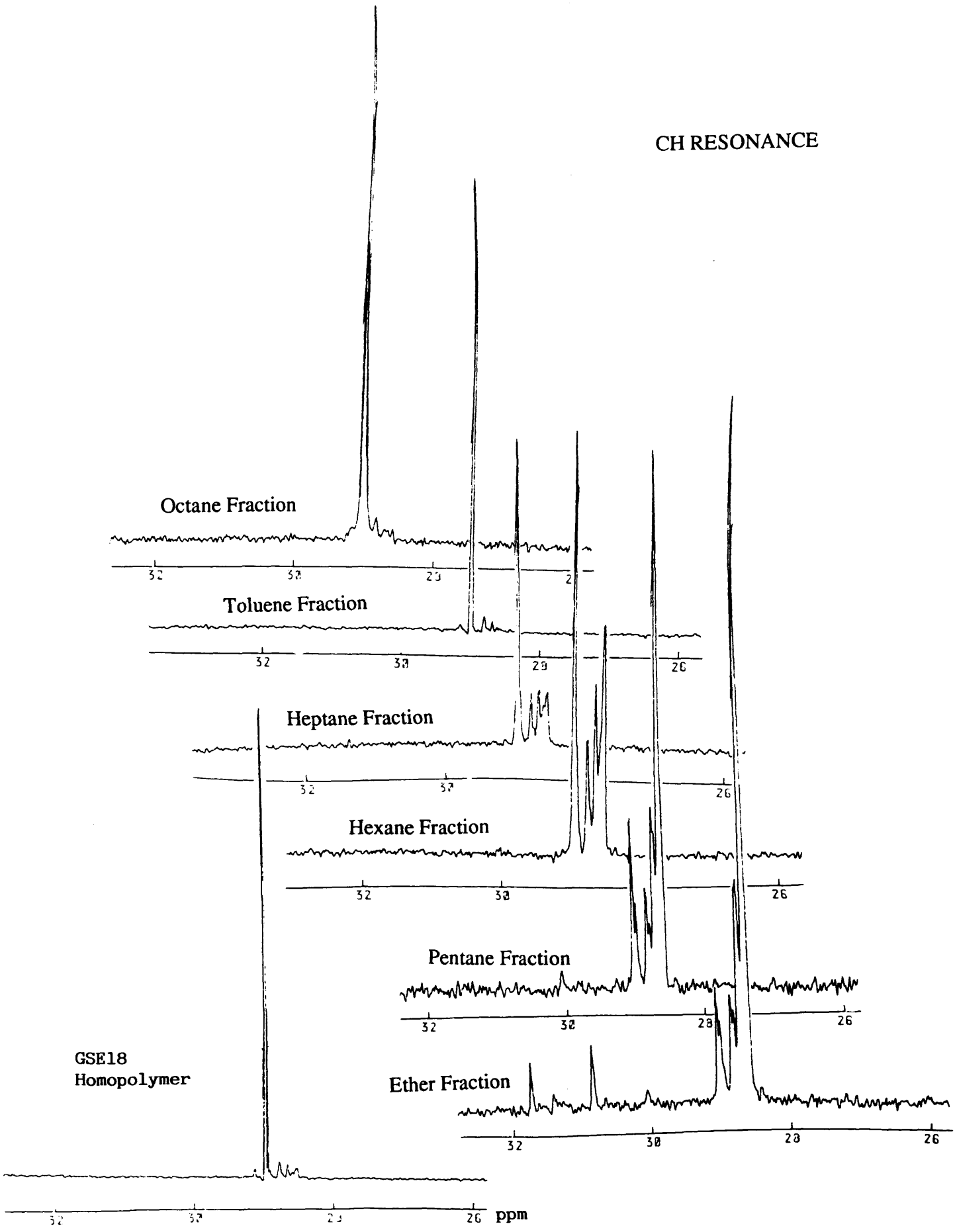

Figure 4.24 ^{13}C-Nmr spectra showing the methine region for the GSE18 polypropylene fractions and homopolymer

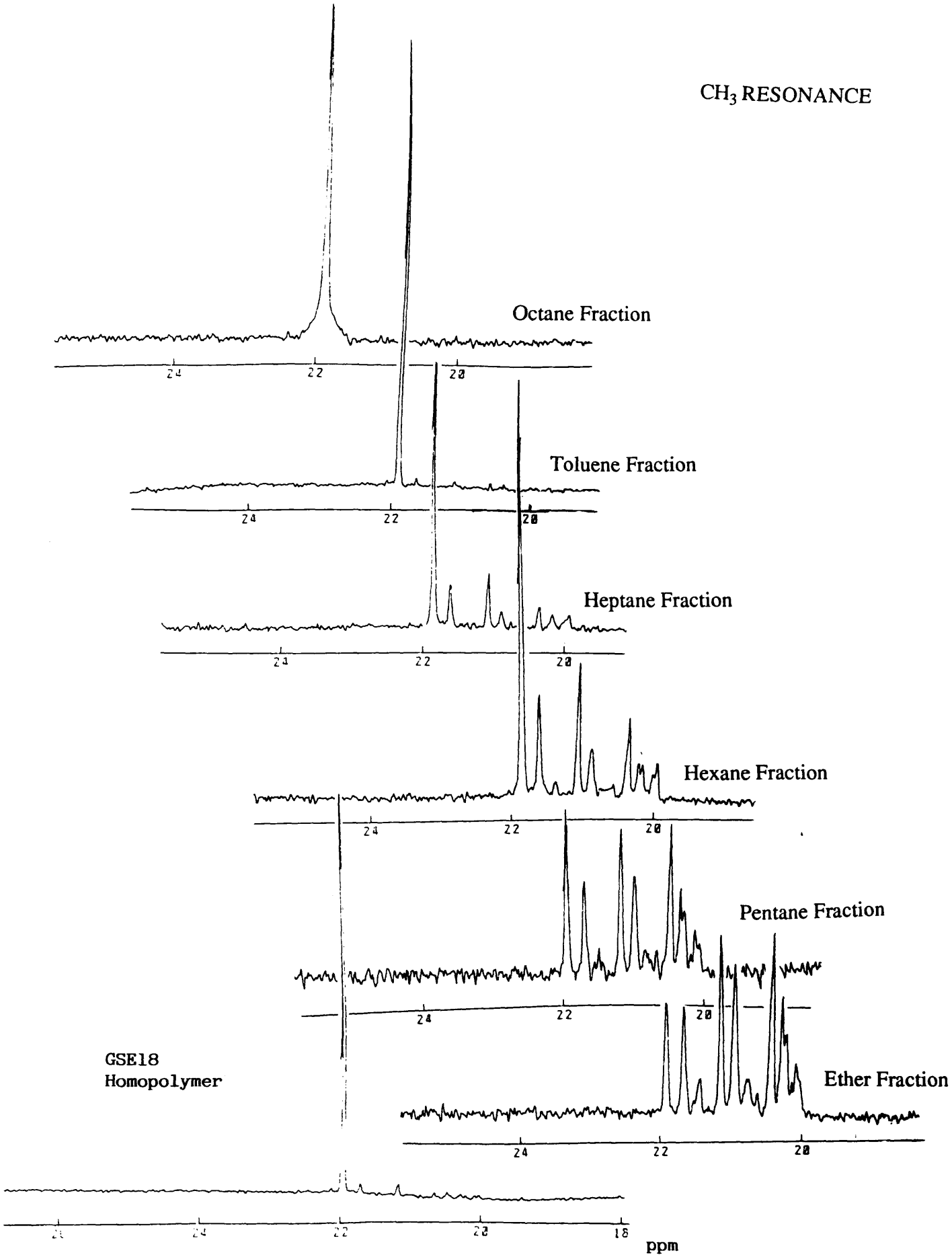

Figure 4.25 ^{13}C-Nmr spectra showing the methyl region for the GSE18 polypropylene fractions and homopolymer

4.7.3.5 Fourier Transform Infrared Spectroscopy

Infrared spectra of fractions which had been annealed at 80°C for 2 hours (section 3.3) were recorded according to the procedure described in section 3.6.1. All fractions were prepared as films for this analysis except the ether fraction which, due to its "tacky" nature, had to be cast from solution onto sodium chloride plates.

Spectra were analysed using the FTIR APRA technique (section 4.3.2). For the same reasons as discussed in section 4.3.5.2, the 1167 cm^{-1} band was not used as a reference band and only the A998/A973 and A841/A973 ratios were used for analysis purposes.

FTIR APRA results for each fraction are presented in Table 4.35 and infrared spectra for each fraction are shown in Figures 4.26 - 4.31.

	Ratio	
Fraction	A998/A973	A841/A973
Ether	0.187	0.236
Pentane	0.243	0.276
Hexane	0.418	0.362
Heptane	0.611	0.594
Toluene	0.852	0.699
Octane	0.881	0.734

Table 4.35 FTIR APRA results for the fractionated GSE18 polypropylene.

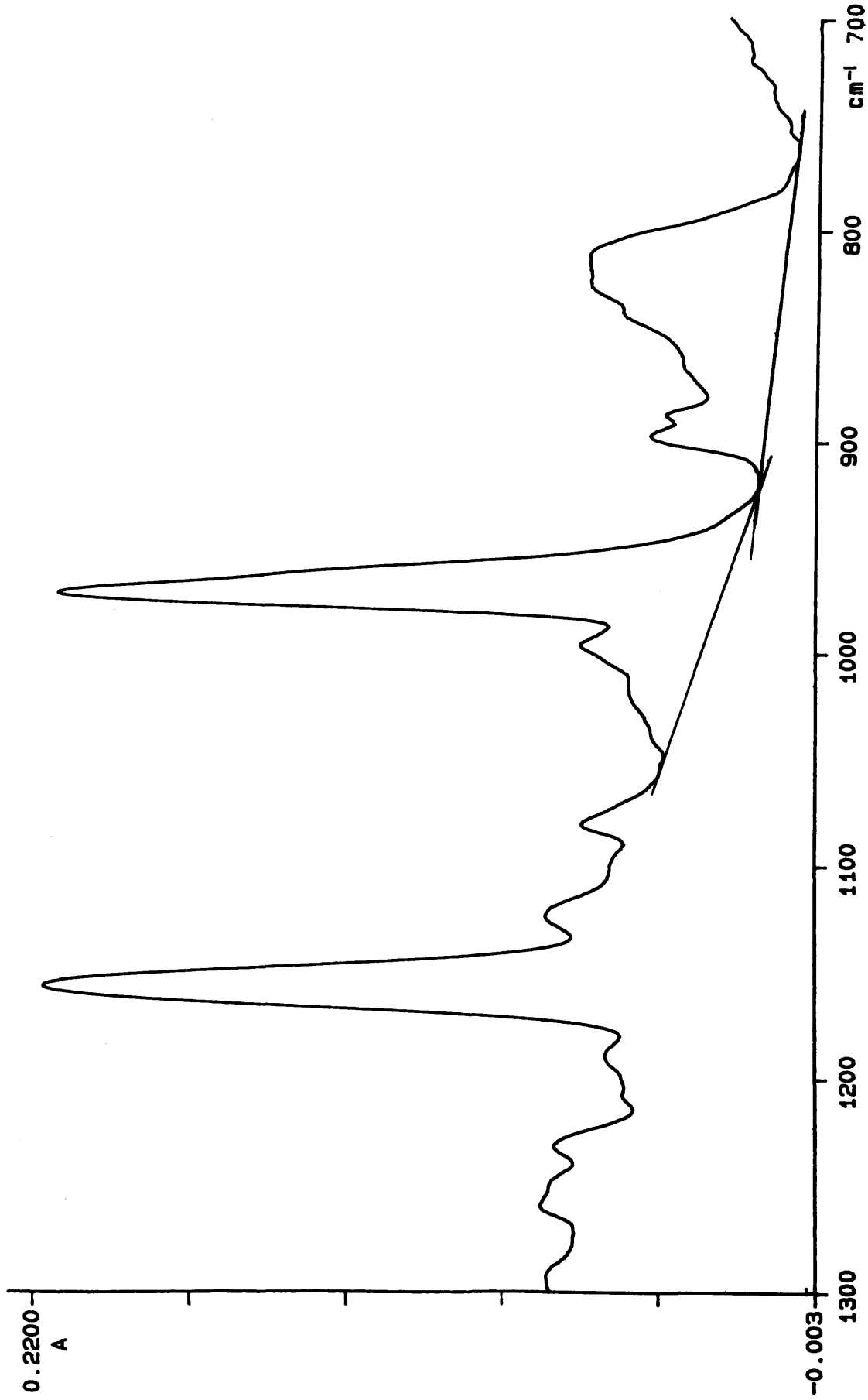

Figure 4.26 FTIR spectrum showing the 1300–700 cm^{-1} region for the GSE18 polypropylene ether fraction

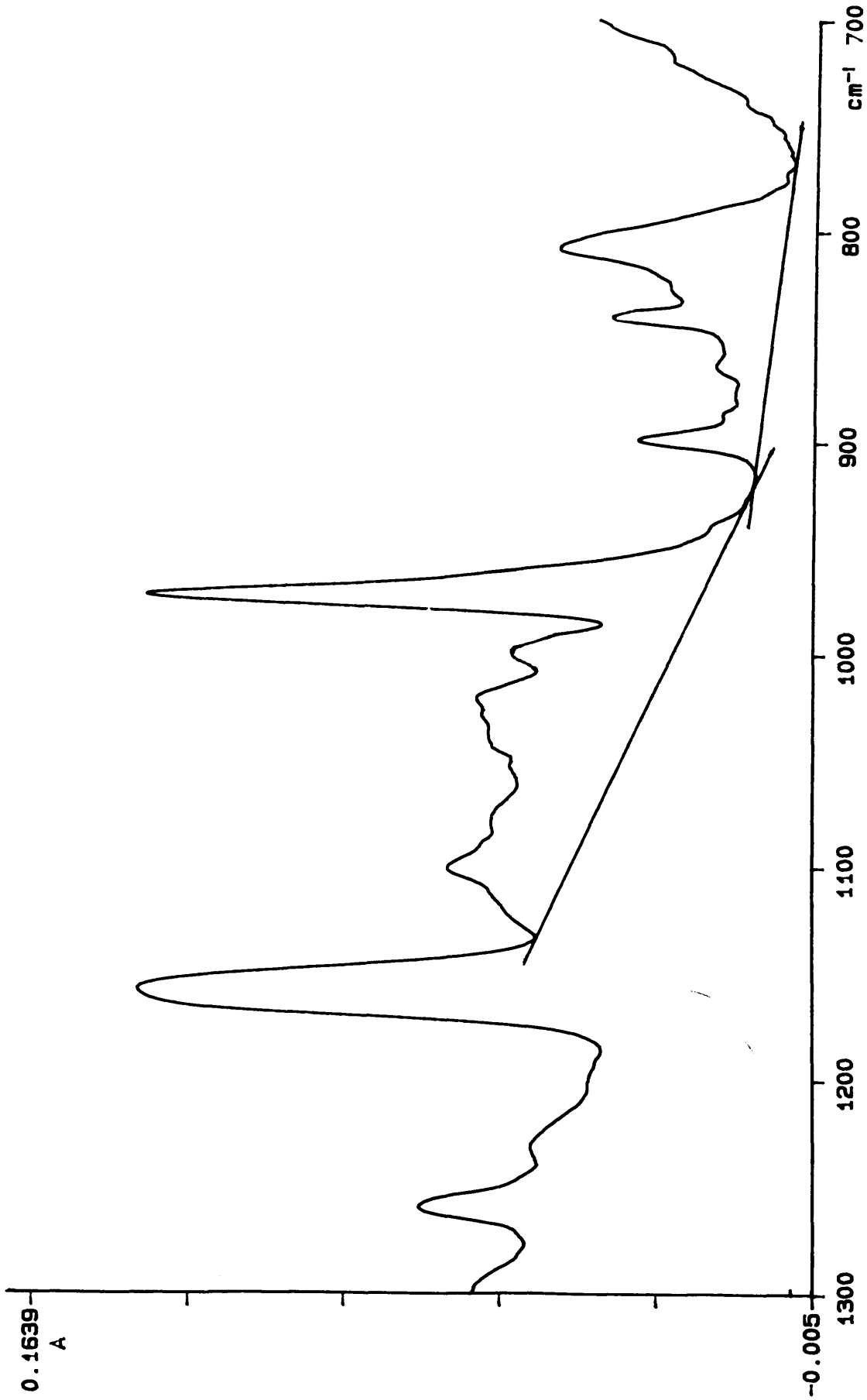

Figure 4.27 FTIR spectrum showing the 1300 - 700 cm^{-1} region for the GSE18 polypropylene pentane fraction

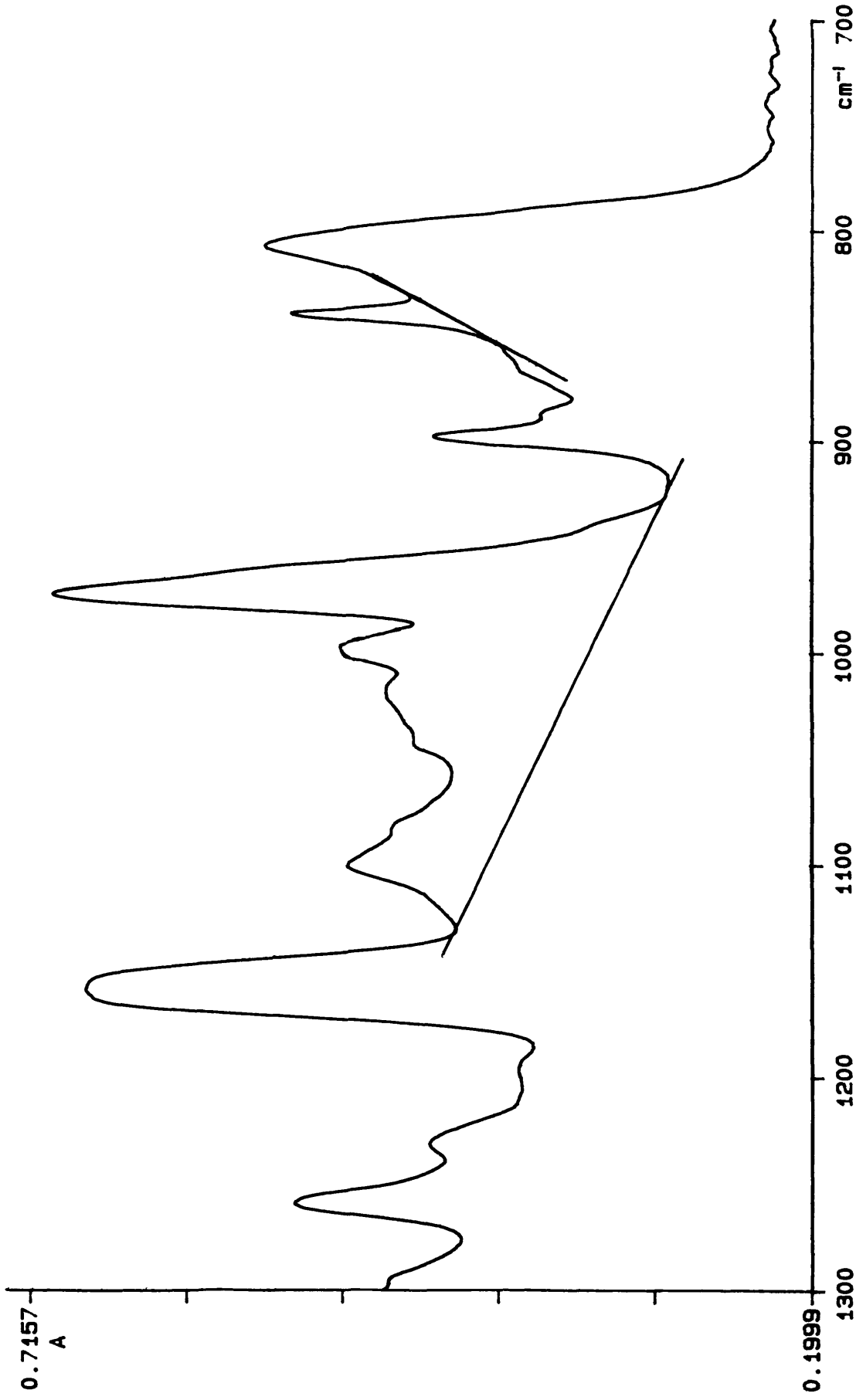

Figure 4.28 FTIR spectrum showing the 1300 - 700 cm^{-1} region for the GSE18 polypropylene hexane fraction

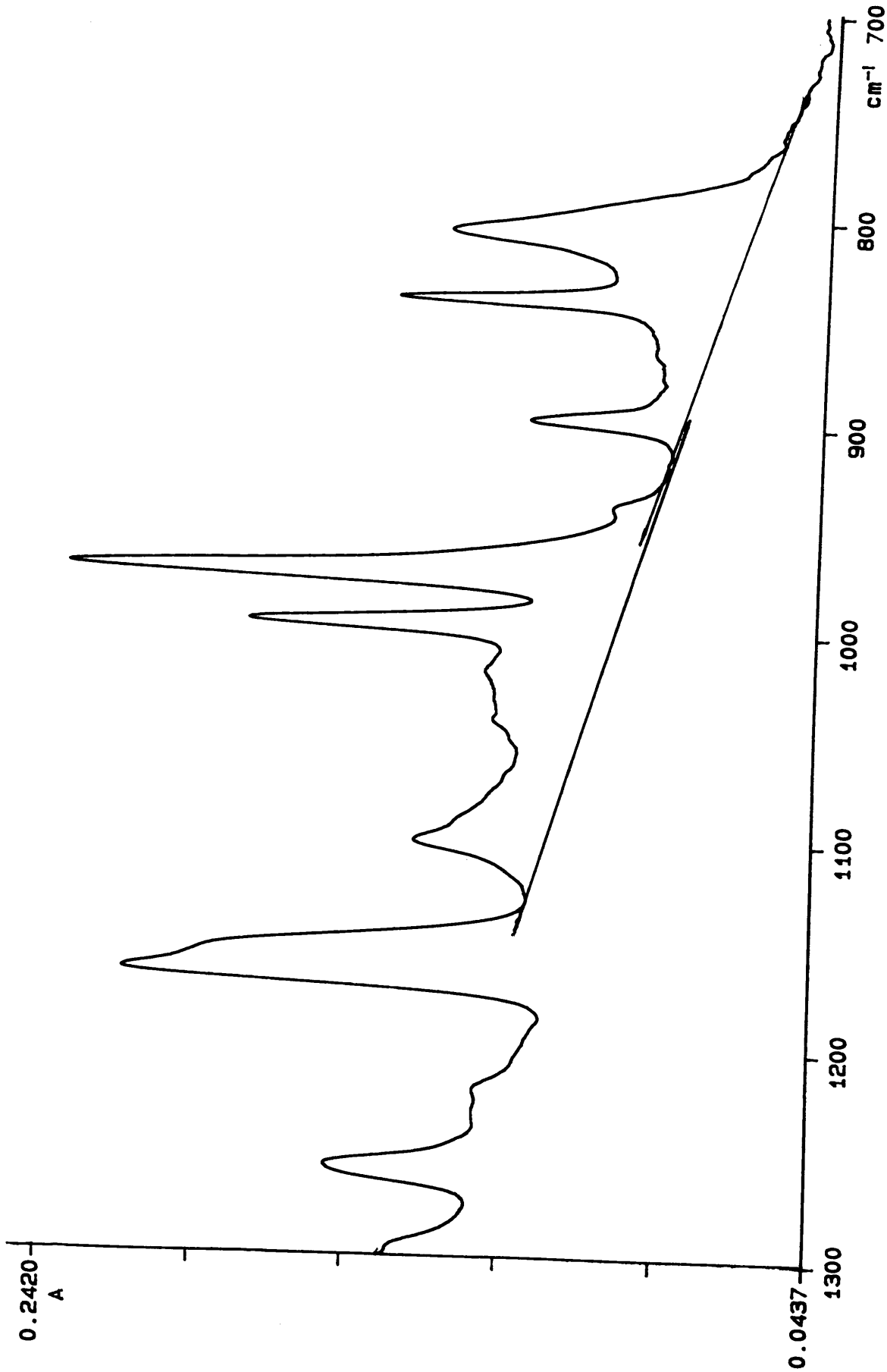

Figure 4.29 FTIR spectrum showing the 1300 - 700 cm^{-1} region for the GSE18 polypropylene heptane fraction

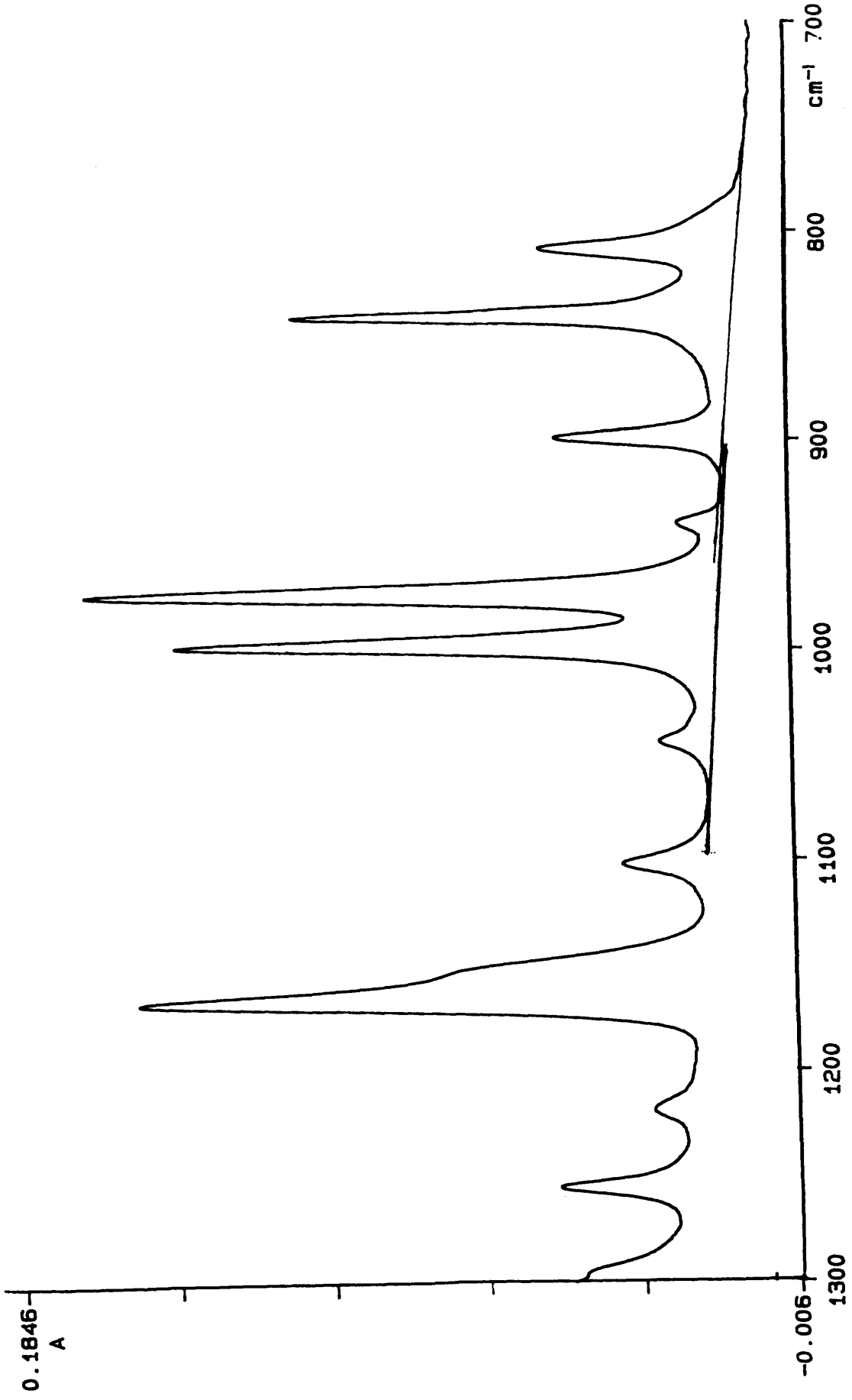

Figure 4.30 FTIR spectrum showing the 1300 - 700 cm^{-1} region for the GSE18 polypropylene toluene fraction

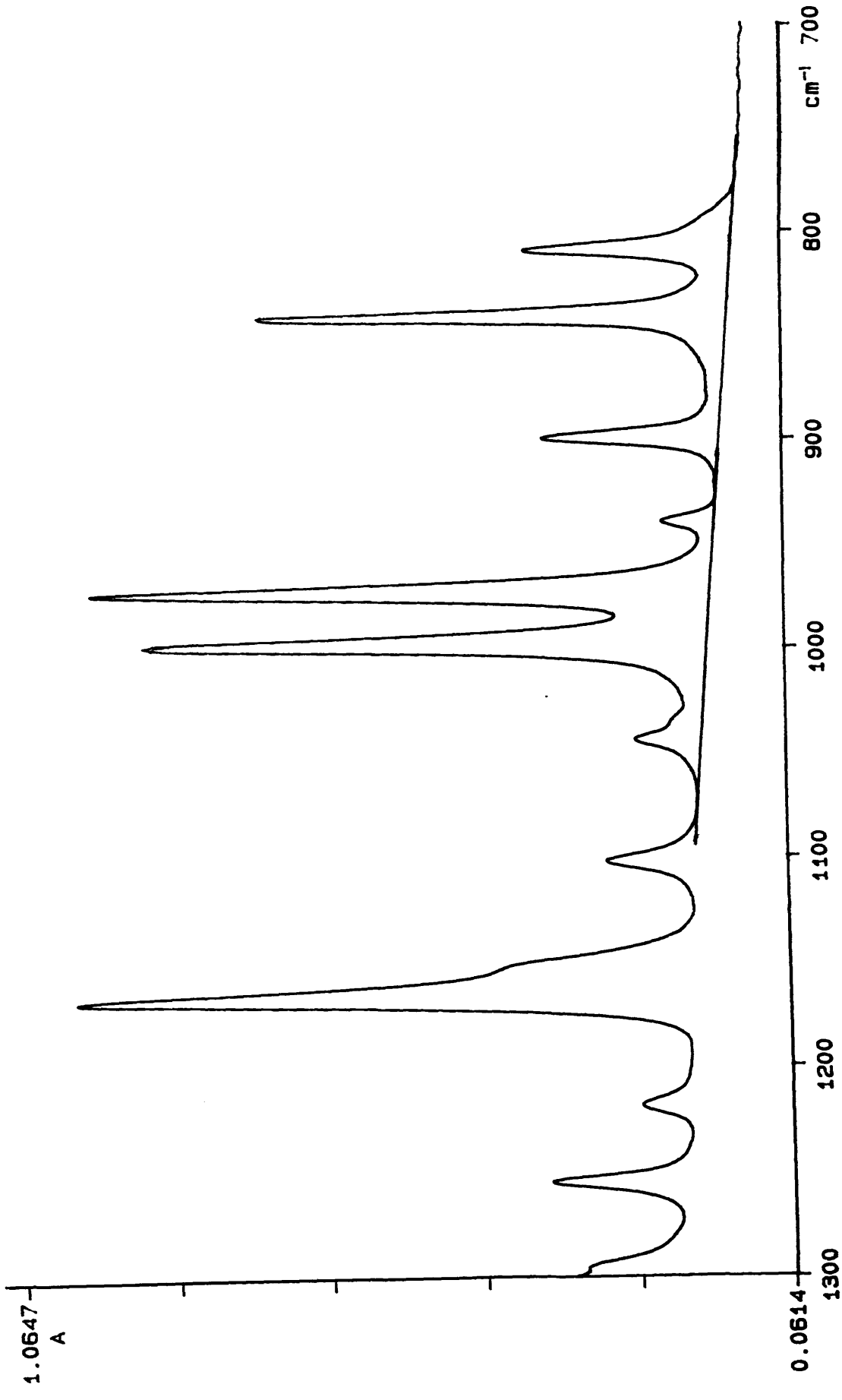

Figure 4.31 FTIR spectrum showing the 1300 - 700 cm^{-1} region for the GSE18 polypropylene octane fraction

4.7.3.6 Density Measurements

Samples of the obtained fractions which had been annealed at 80°C for two hours in an inert atmosphere (section 3.3) were measured in triplicate for density at 20°C according to the flotation method described in section 3.13.1. These density values were converted to a value for percentage crystallinity using the two-phase crystalline amorphous model previously described in section 4.3.3.7. Results for mean densities and their associated percentage crystallinities are presented in Table 4.36. Figure 4.32 shows a graph of percentage crystallinity versus extraction temperature for each fraction.

Fraction	Mean Density(g/ml)	% Crystallinity
Ether	---	---
n-Pentane	0.8677	15.78
n-Hexane	0.8774	25.08
n-Heptane	0.8971	49.24
Toluene	0.9153	72.49
n-Octane	0.9158	73.14

Table 4.36 Mean densities and associated percentage crystallinity values.

4.7.3.7 DSC Melting And Crystallisation

DSC melting and crystallisation data were obtained for the fractions according to procedures described in section 3.7. Samples of 5-10 mg were encapsulated in triplicate for DSC analysis (the less tactic samples, such as the ether, pentane and hexane fractions, required weights at the higher end of this range to facilitate an adequate signal in the DSC).

Figure 4.32

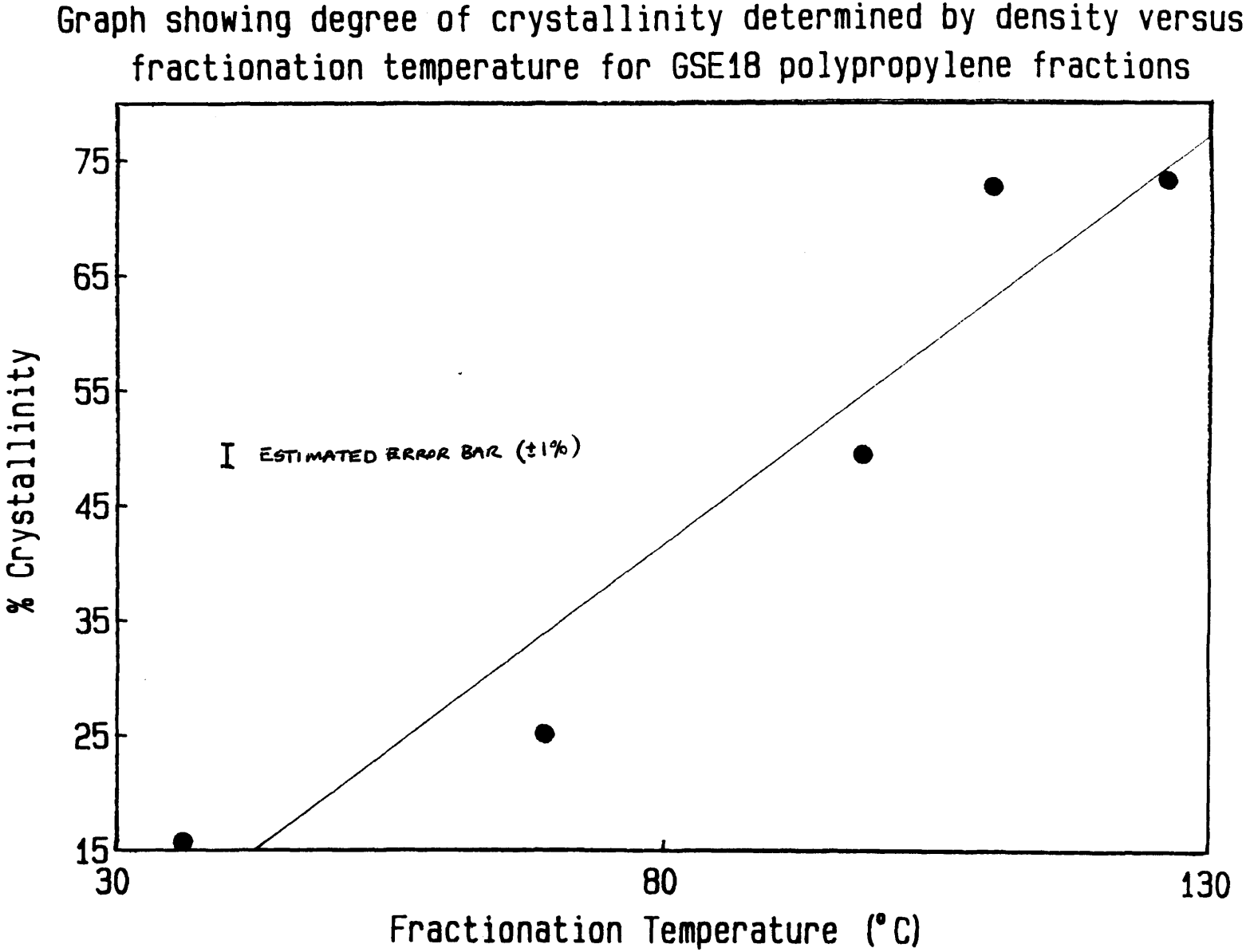
Graph showing degree of crystallinity determined by density versus fractionation temperature for GSE18 polypropylene fractions
% Crystallinity
75
65
55
45
35
25
15
I ESTIMATED ERROR BAR (±1%)
30
80
130
Fractionation Temperature (°C)

The ether fraction was uncrystallisable in nature and, in effect, behaved as a viscous liquid. For this reason there was no deviation from the baseline which sloped continually upwards as a consequence of the sample heat capacity. Mean melting and crystallisation results for the fractions are shown in Table 4.37. DSC crystallinity was calculated for each fraction from the heat of fusion data using the following equation:-

$$X_c = \Delta H_{f*}/\Delta H_f$$

where ΔH_{f*} is the measured DSC heat of fusion and ΔH_f is the heat of fusion for a supposedly 100% crystalline polypropylene which has a value[85] of 146.5 J/g. A graph showing crystallinity as a function of fractionation temperature for the fractions is shown in Figure 4.33.

Fraction	T_m(°C) Onset	T_m(°C) Peak	ΔH_f (J/g)	T_c(°C) Onset	T_c(°C) Peak	$-\Delta H_c$ (J/g)	% Cryst^y
Ether	---	---	---	---	---	---	---
Pentane	74.94	84.41	20.57	56.65	48.91	27.26	14.04
Hexane	92.75	108.08	17.77	77.95	63.91	20.26	13.52
Heptane	127.66	145.41	52.43	108.85	103.72	54.28	35.78
Toluene	146.21	160.58	108.03	118.06	113.92	86.83	73.74
Octane	146.88	159.66	127.66	117.84	112.89	95.47	87.14

Table 4.37 DSC melting and crystallisation data and associated percentage crystallinities for GSE18 polypropylene fractions.

Figures 4.34 and 4.35 show melting and crystallisation profiles respectively for the GSE18 polypropylene fractions and Figures 4.36 - 4.41 show graphs of melting and crystallisation data versus temperature of fractionation.

Figure 4.33

Graph showing degree of crystallinity determined by DSC heat of fusion versus fractionation temperature for GSE18 polypropylene fractions

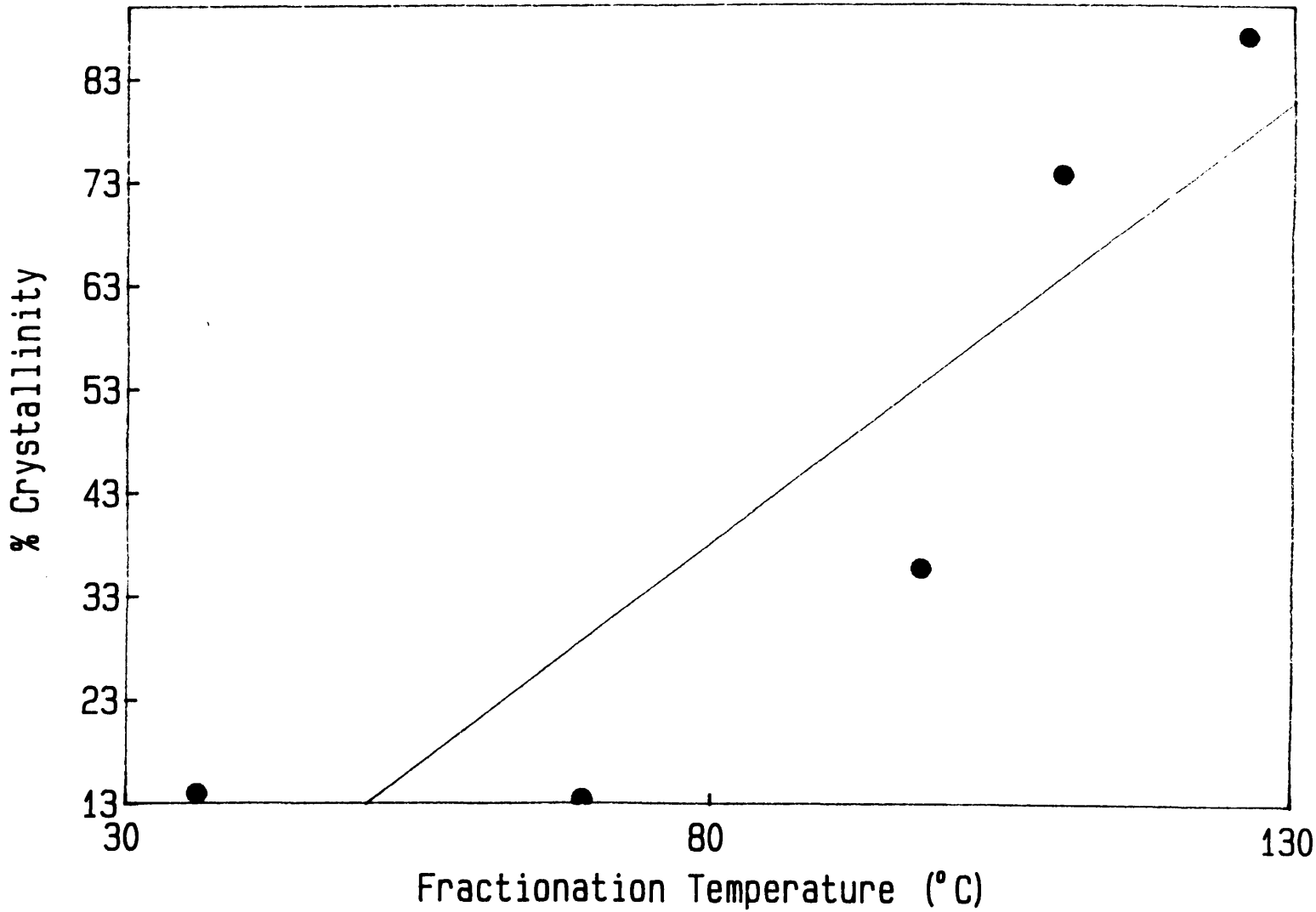

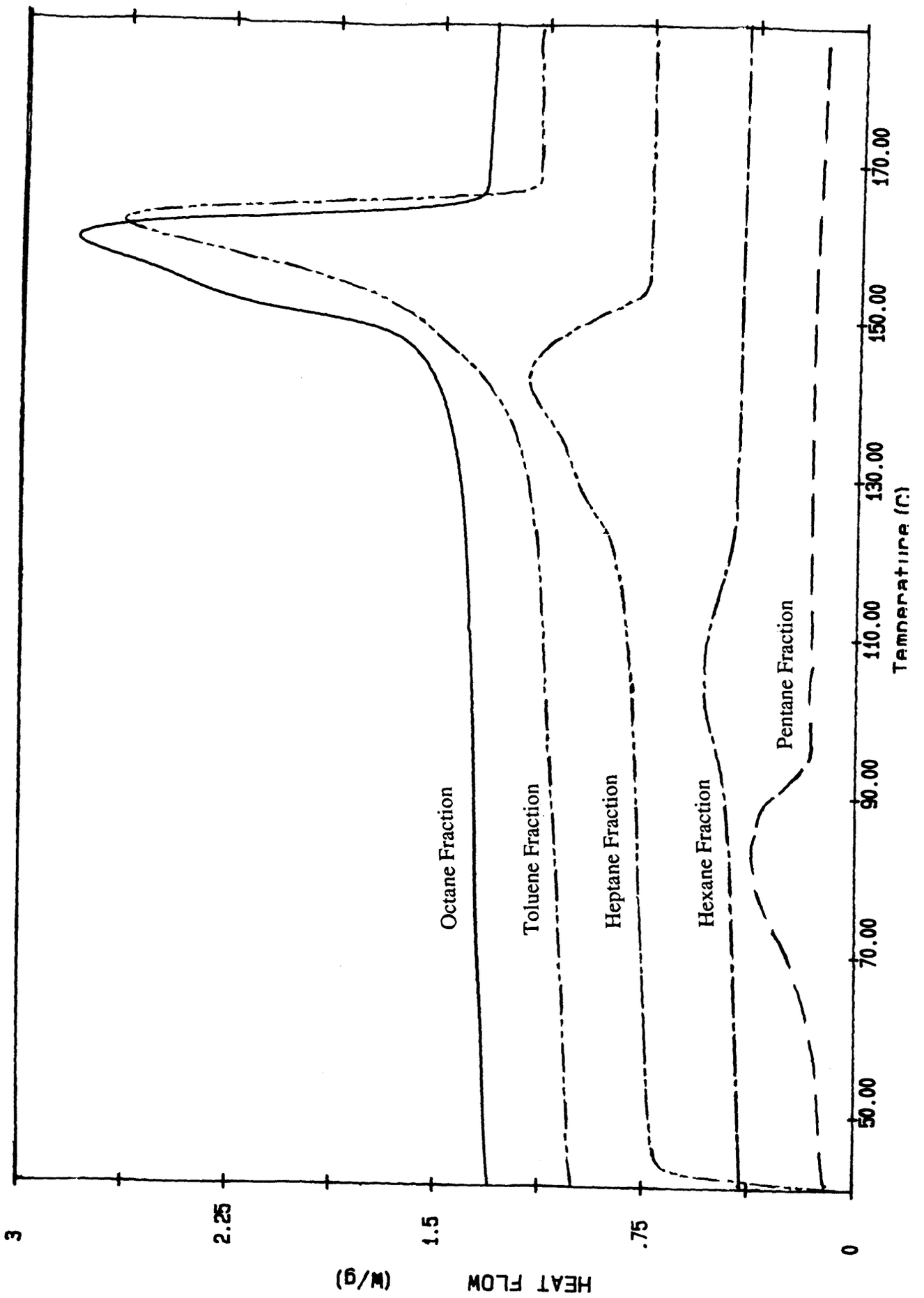

Figure 4.34 DSC melting profiles for the GSE18 polypropylene fractions

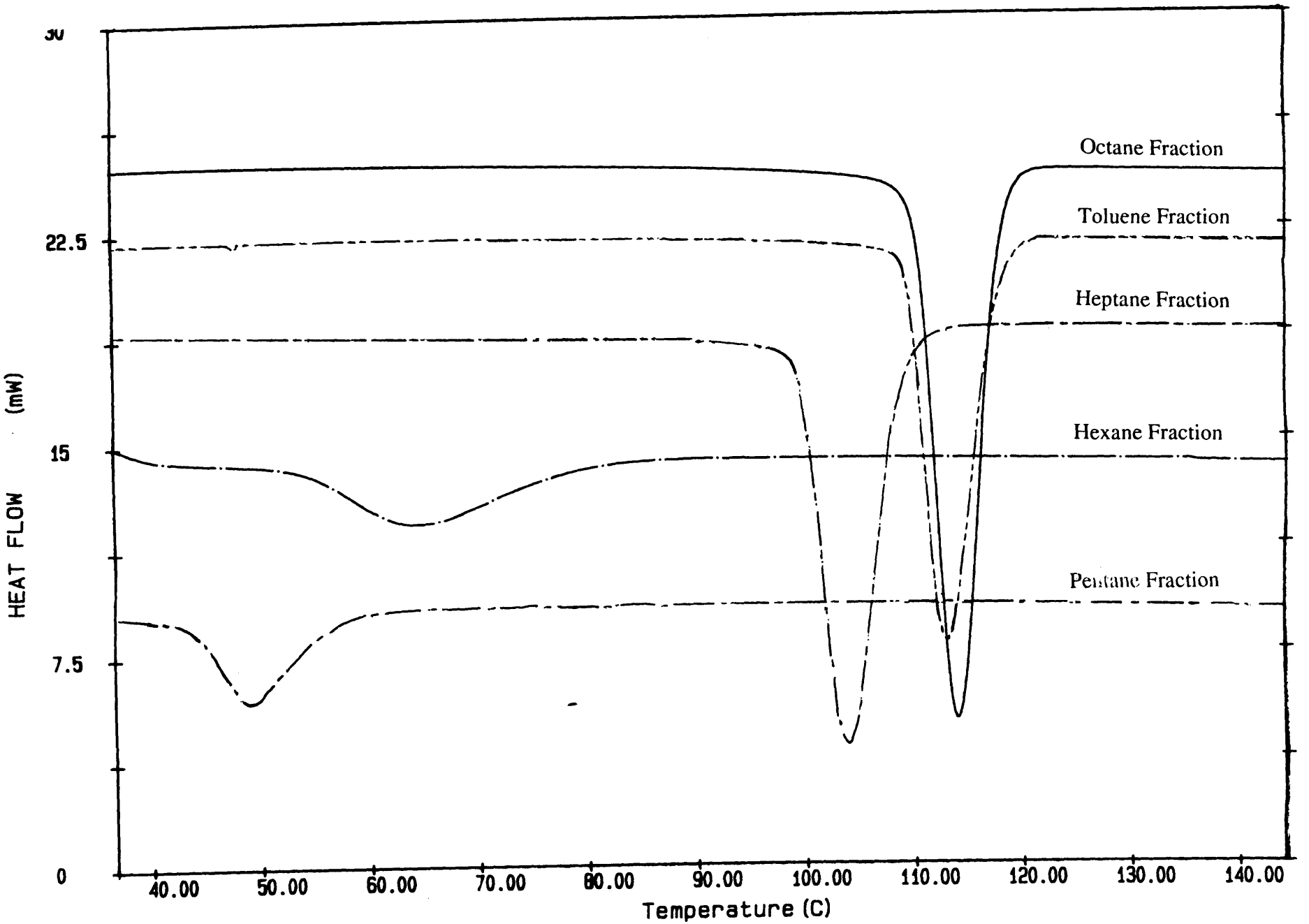

Figure 4.35 DSC crystallisation profiles for the GSE18 polypropylene fractions

Figure 4.36

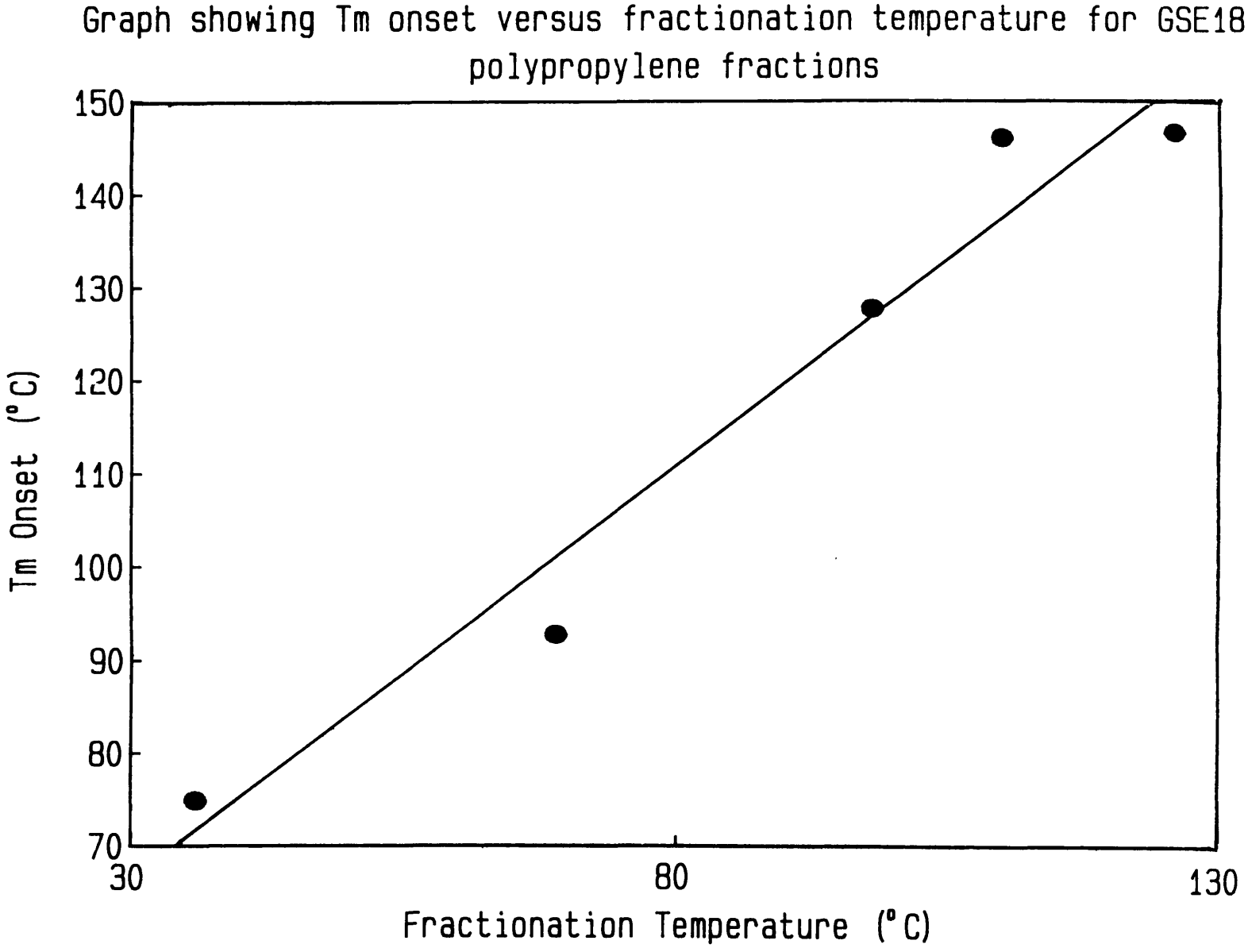
Graph showing Tm onset versus fractionation temperature for GSE18 polypropylene fractions
Tm Onset (°C)
150
140
130
120
110
100
90
80
70
30
80
130
Fractionation Temperature (°C)

Figure 4.37

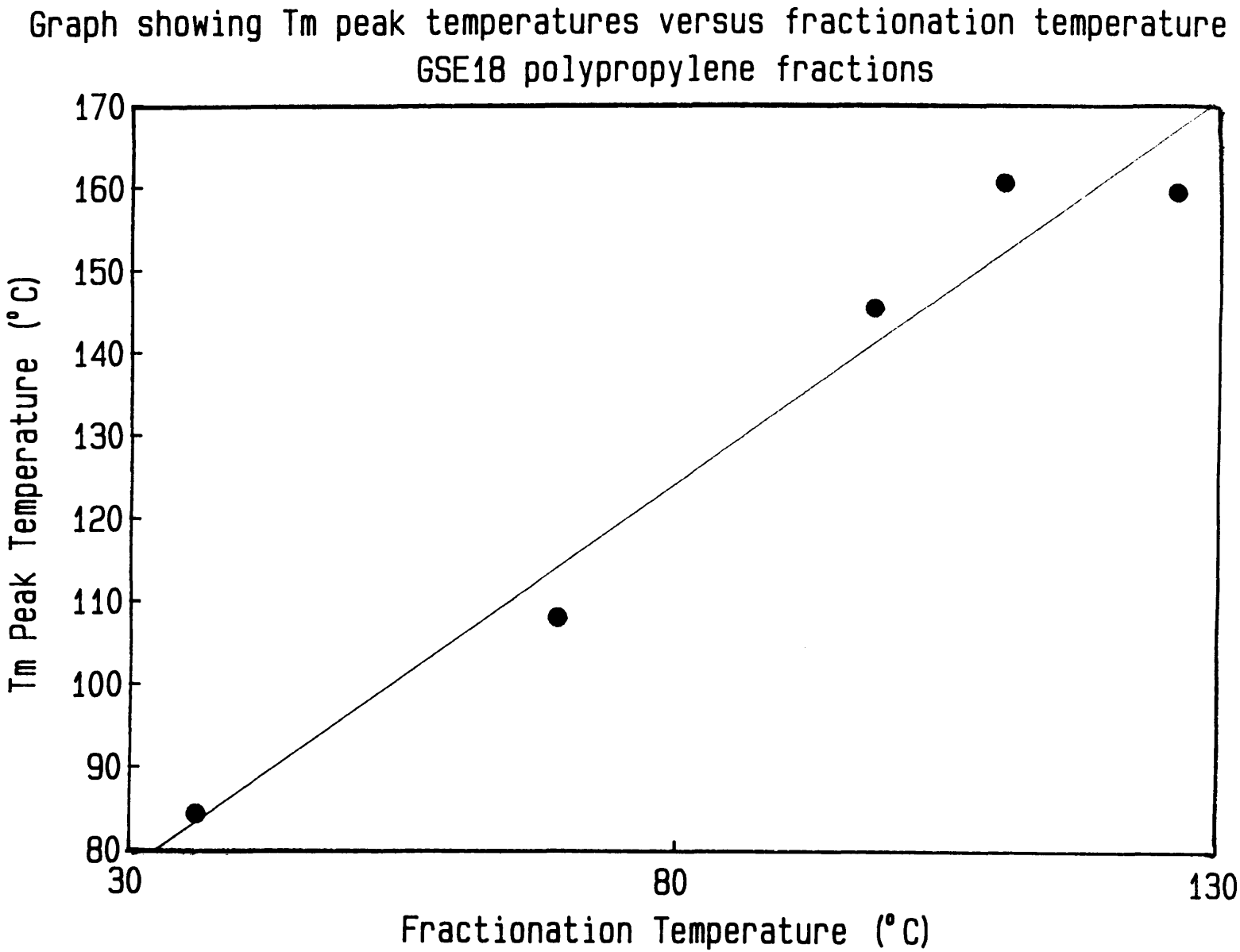
Graph showing Tm peak temperatures versus fractionation temperature for GSE18 polypropylene fractions
Tm Peak Temperature (°C)
170
160
150
140
130
120
110
100
90
80
30
80
130
Fractionation Temperature (°C)

Figure 4.38

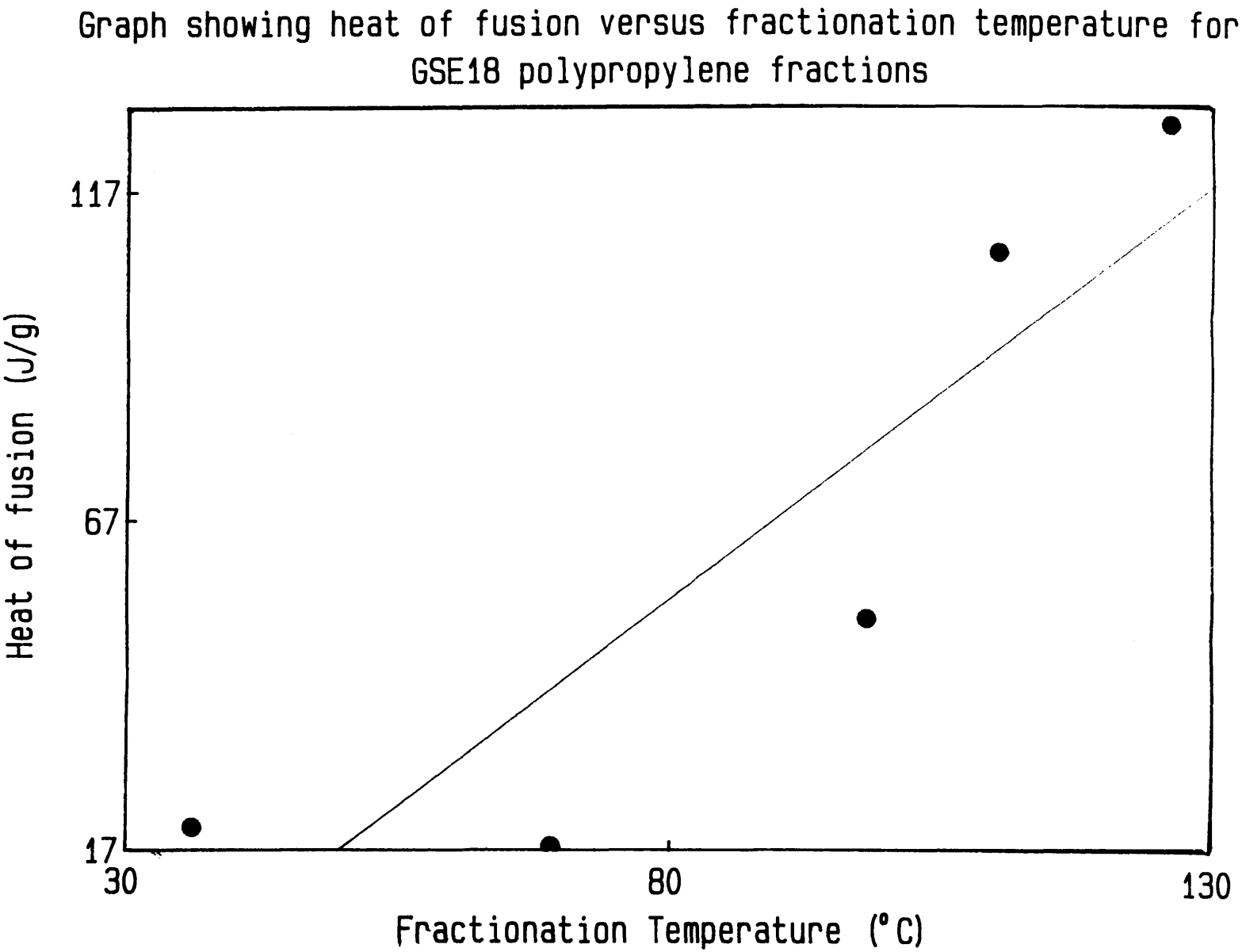
Graph showing heat of fusion versus fractionation temperature for GSE18 polypropylene fractions
Heat of fusion (J/g)
117
67
17
30
80
130
Fractionation Temperature (°C)

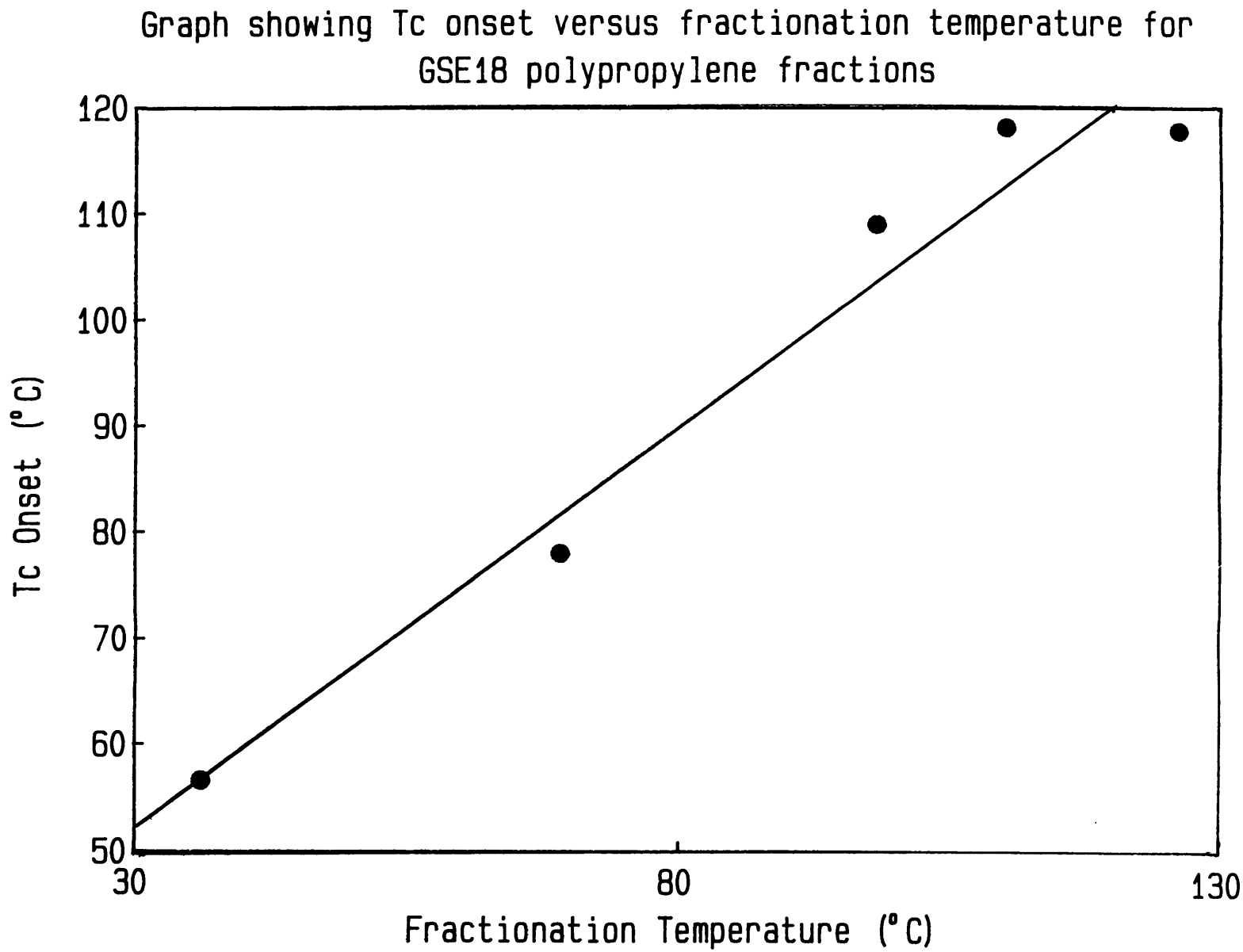
Graph showing Tc onset versus fractionation temperature for GSE18 polypropylene fractions
120
110
100
90
80
70
60
50
Tc Onset (°C)
30
80
130
Fractionation Temperature (°C)

Figure 4.39

Figure 4.40

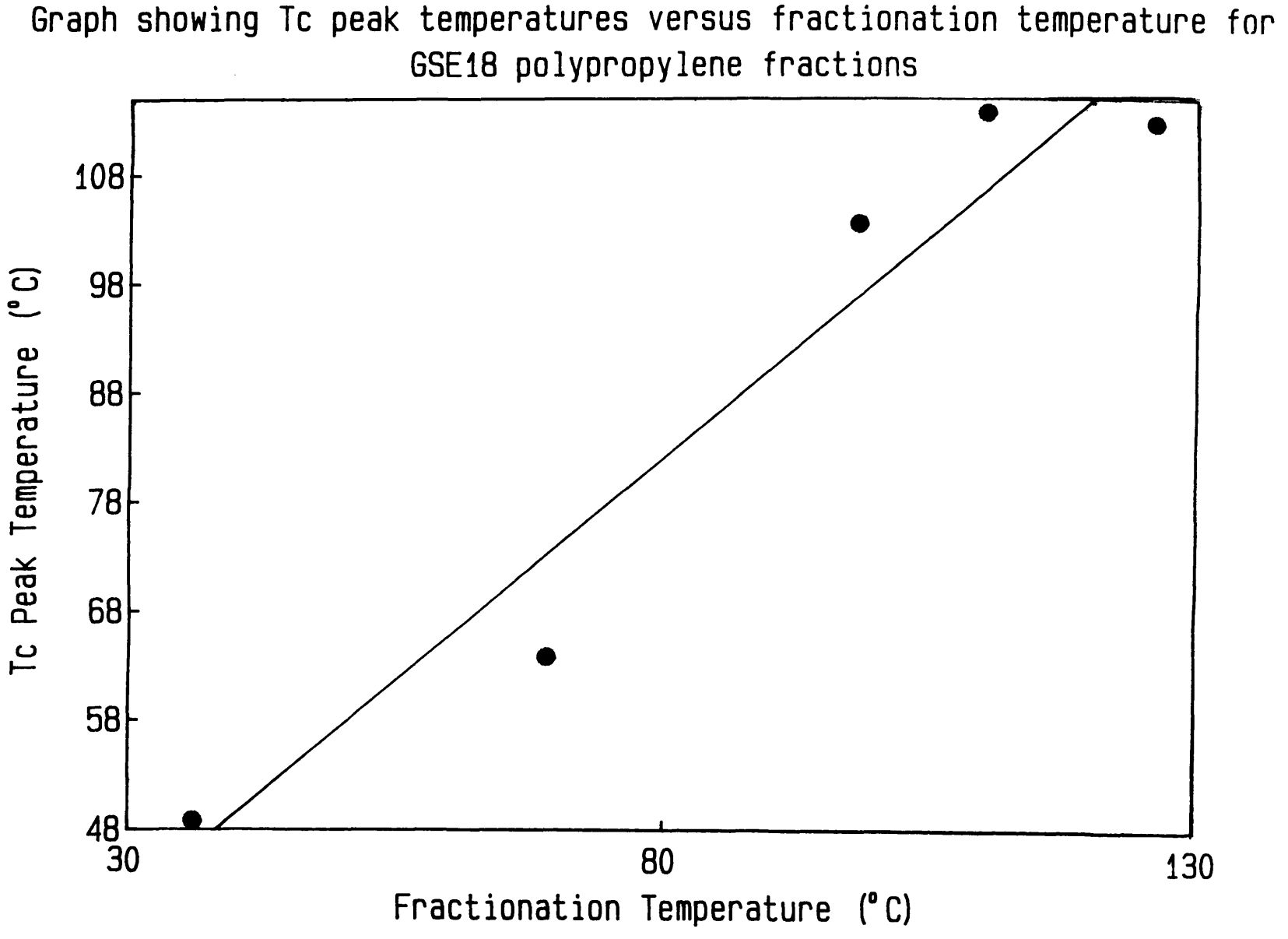
Graph showing Tc peak temperatures versus fractionation temperature for GSE18 polypropylene fractions
Tc Peak Temperature (°C)
108
98
88
78
68
58
48
30
80
130
Fractionation Temperature (°C)

Figure 4.41

Graph showing heat of crystallisation versus fractionation temperature for GSE18 polypropylene fractions

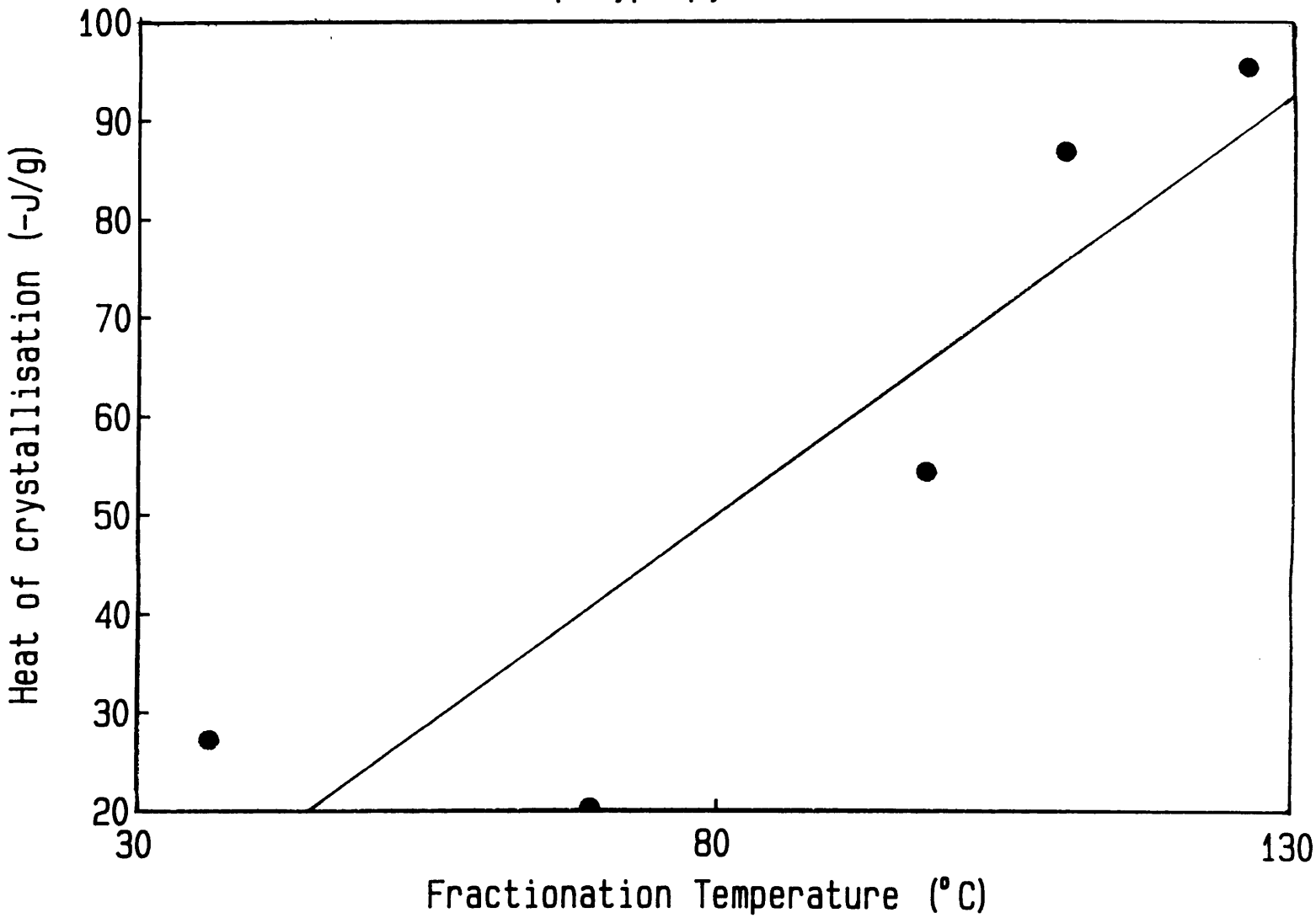

4.7.3.8 X-Ray Diffraction

Wide angle x-ray diffraction was carried out on the GSE18 polypropylene fractions (excluding the pentane fraction) under the conditions detailed in section 2.3.5. The x-ray crystallinities (Table 4.38) were calculated using the following equation:-

$$X_c = A_c/(A_c + A_a) \times 100$$

where X_c is the x-ray crystallinity, A_c is the area under the peaks caused by crystalline diffractions and A_a is the area under the broad curve caused by amorphous scattering. Areas were obtained by planimetry. Figure 4.42 shows a graph of x-ray crystallinity versus fractionation temperature.

Fraction	% Crystallinity
Ether	0.00
Pentane	---
Hexane	22.73
Heptane	35.55
Toluene	46.59
Octane	50.31

Table 4.38 X-ray crystallinity of GSE18 polypropylene fractions by planimetry.

Graph showing degree of crystallinity measured by x-ray diffraction versus fractionation temperature for GSE18 polypropylene fractions

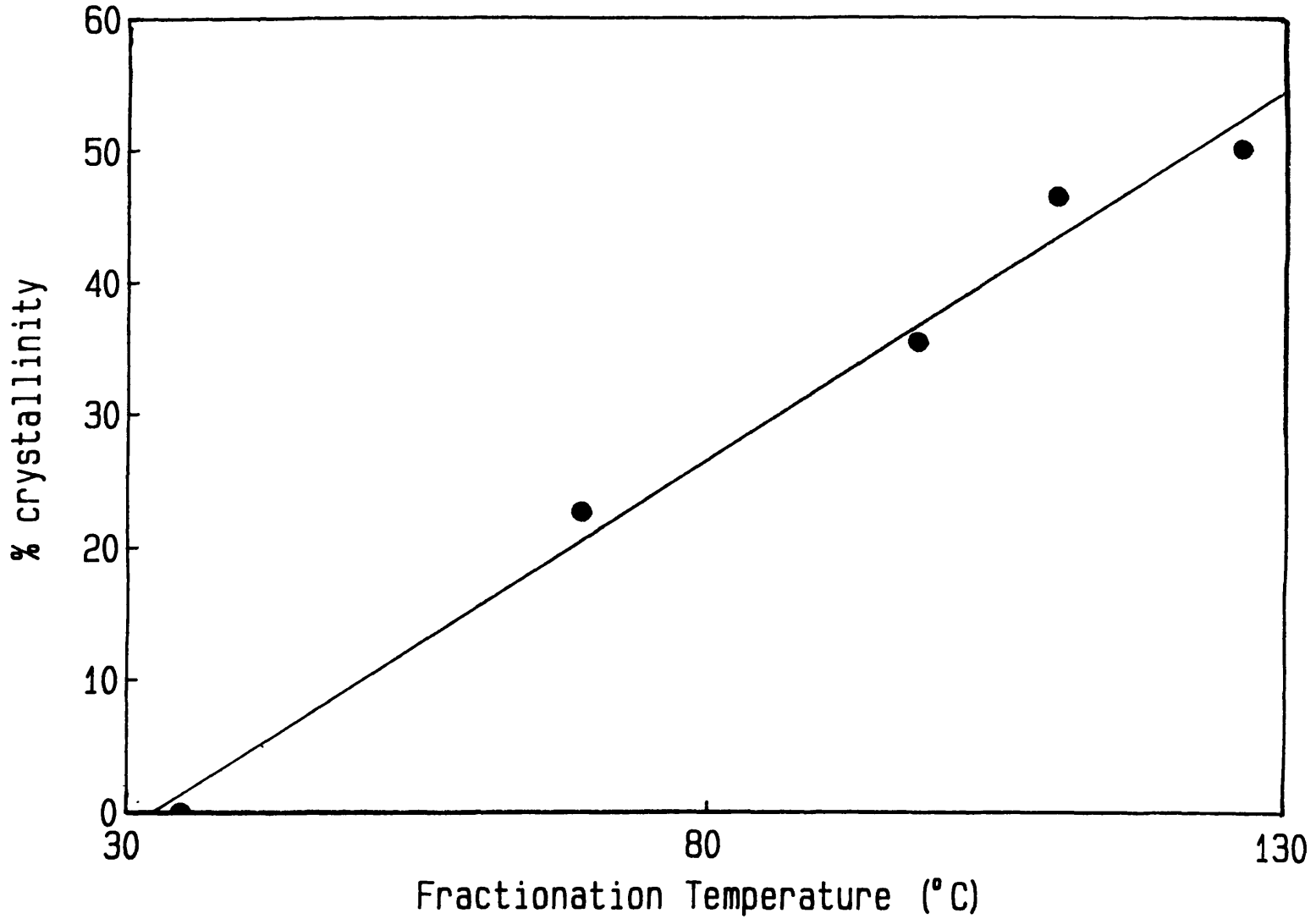

Figure 4.42

The main diffraction angles for each fraction are presented in Table 4.39 and x-ray diffraction profiles for these fractions are shown in Figures 4.43 and 4.44.

Fraction	Diffraction Angle 2θ (degrees)							
Ether	---	16.50	---	---	---	---	---	---
Pentane	---	---	---	---	---	---	---	---
Hexane	14.15	16.85	18.30	18.80	20.25	21.30	21.90	25.50
Heptane	14.30	17.10	18.40	18.80	20.20	21.30	22.00	25.60
Toluene	14.10	16.90	---	18.75	---	21.25	21.90	25.60
Octane	14.40	17.30	---	18.85	---	21.50	22.20	26.10

Table 4.39 X-ray diffraction angles for GSE18 polyproylene fractions.

4.7.3.9 Hot-Stage Polarised Light Microscopy

Hot-stage polarised light microscopy investigations were carried out at cross-polars on the polypropylene fractions according to the procedure in section 3.10. Samples were heated to 200°C at a rate of 20°C/min and held isothermally in the melt for 5 minutes prior to cooling at 10°C/min to the point where the onset of spherulitic growth first became apparent by the visible formation of nuclei. The temperature at which this occurred was taken as the microscopic crystallisation onset temperature (T_c). Optical micrographs of each fraction are shown in Figures 4.45 - 4.49 for samples at:-

(i) Crystallisation onset (T_c)

(ii) Isothermal at T_c for 30 seconds

(iii) Isothermal at T_c for 1 minute

(iv) Isothermal at T_c for 2 minutes

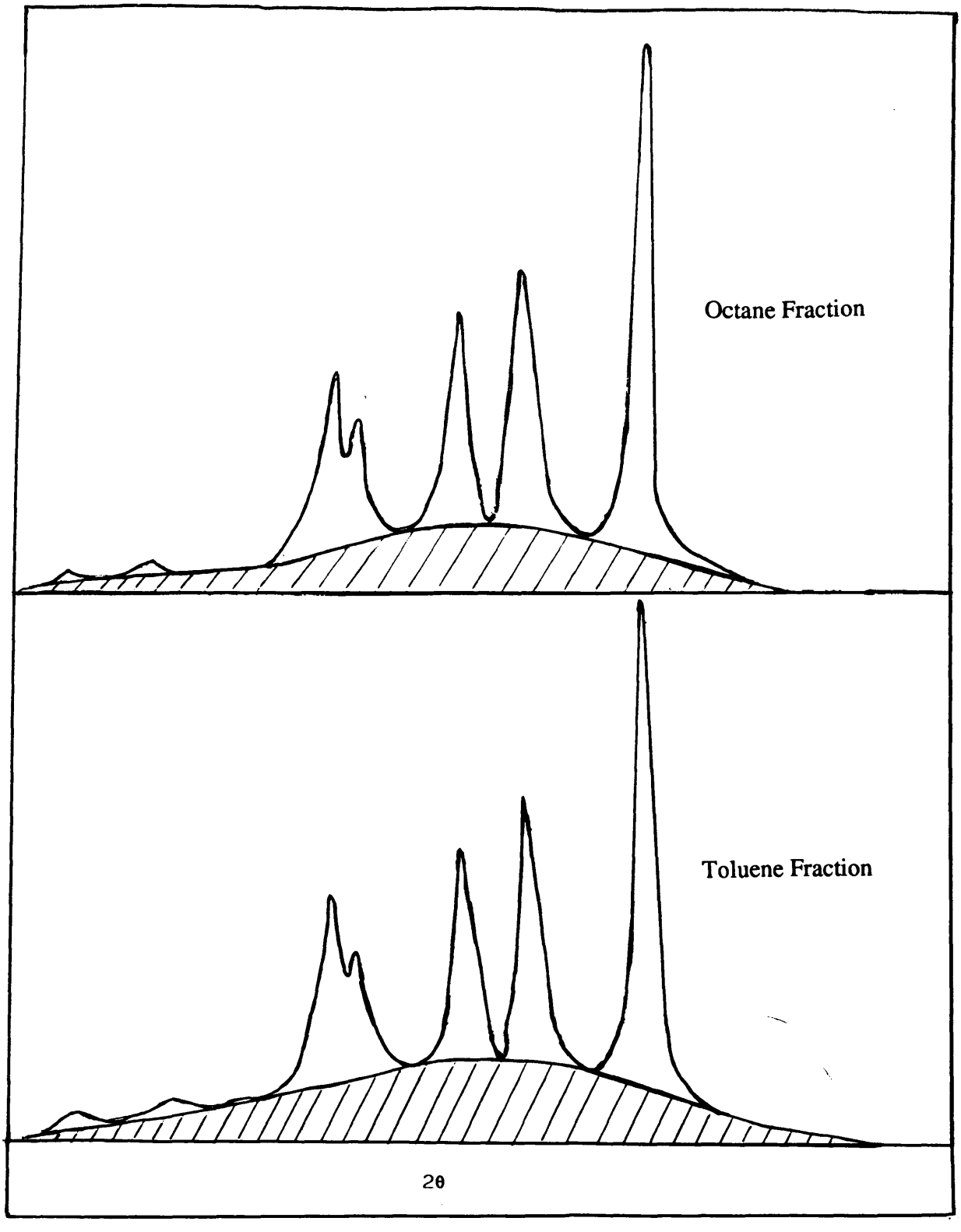

Figure 4.43 X-ray diffractograms for the octane and toluene fractions

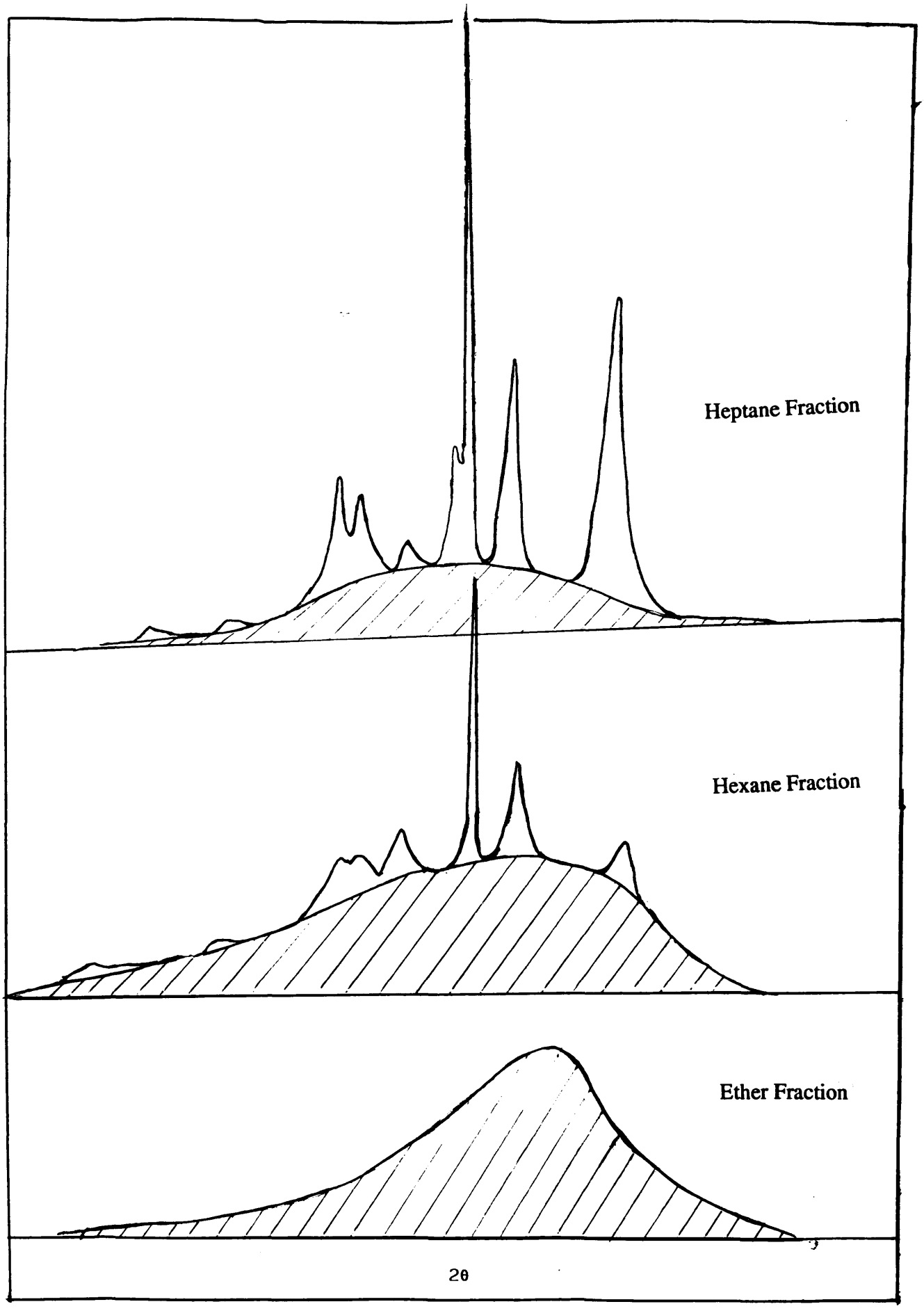

Figure 4.44 X-ray diffractograms for the heptane, hexane and ether fractions

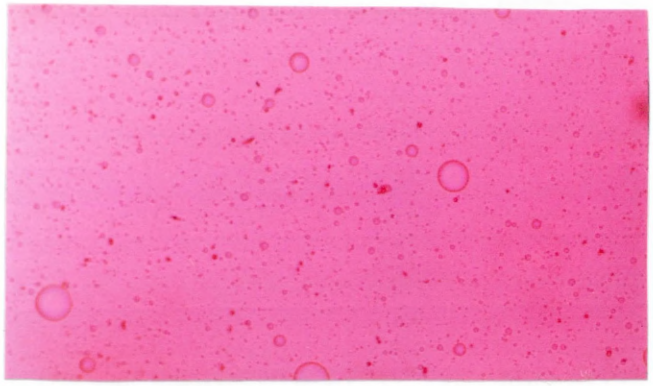

Ether Fraction at 30°C

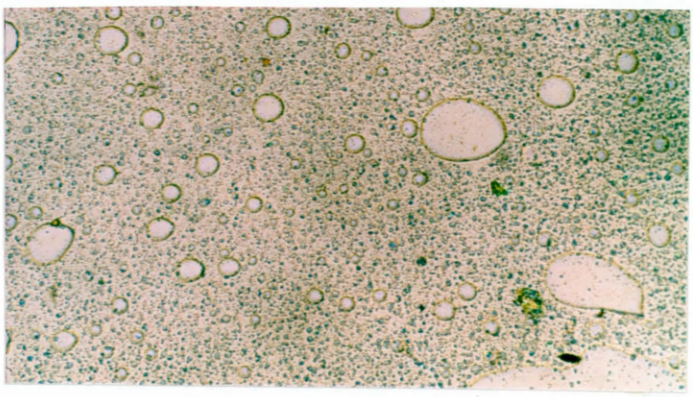

Pentane Fraction at 30°C

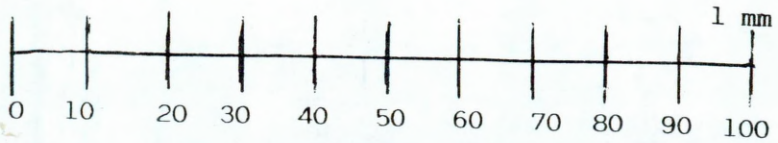

Figure 4.45 Optical micrographs of the ether and pentane fractions at 30°C

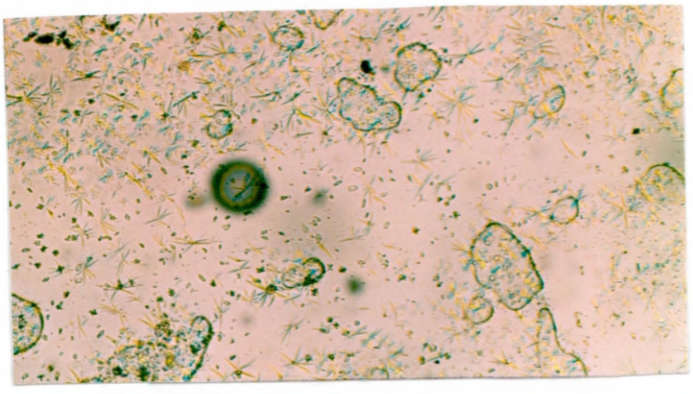

Crystallisation onset (87°C)

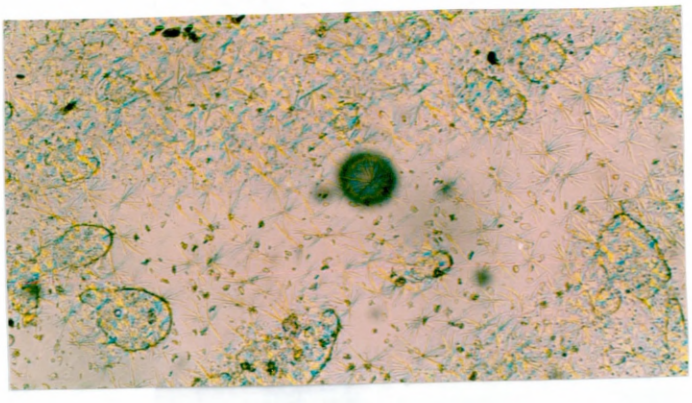

30 seconds at 87°C

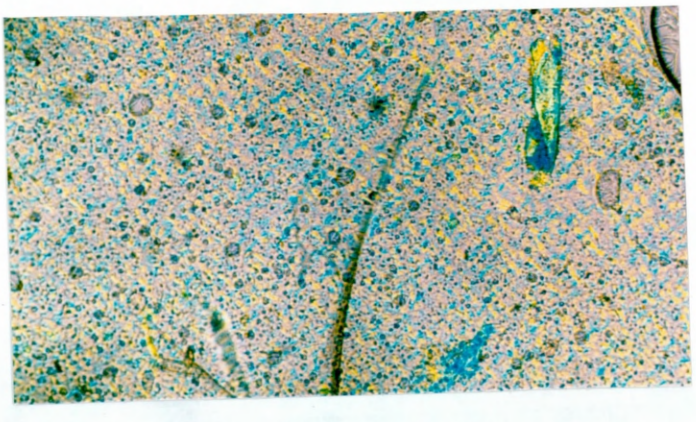

1 minute at 87°C

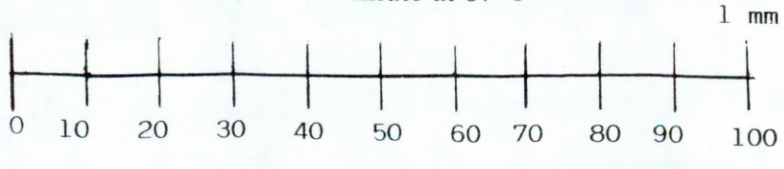

Figure 4.46 Optical micrographs of the hexane fraction at different stages of spherulitic growth

Heptane Fraction

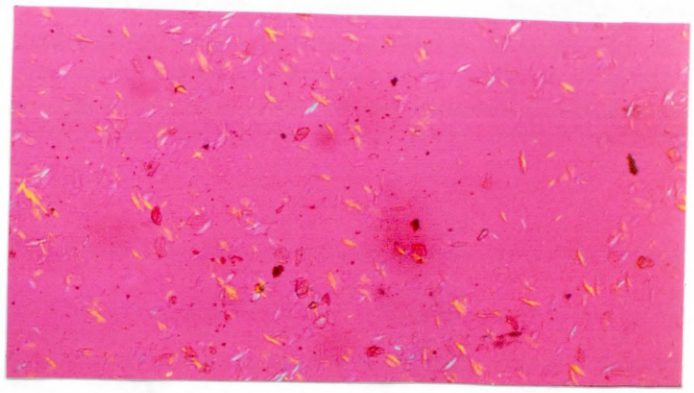

Crystallisation onset (113°C)

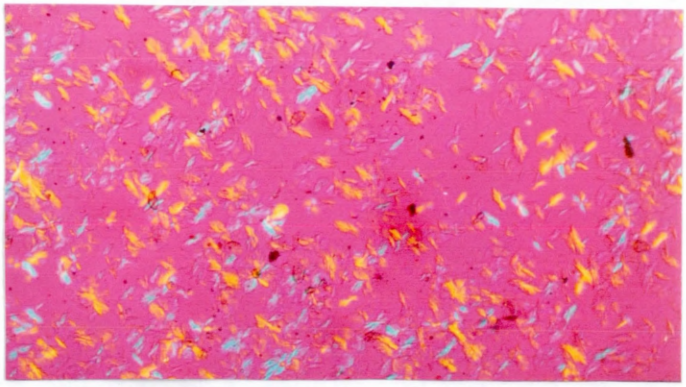

30 seconds at 113°C

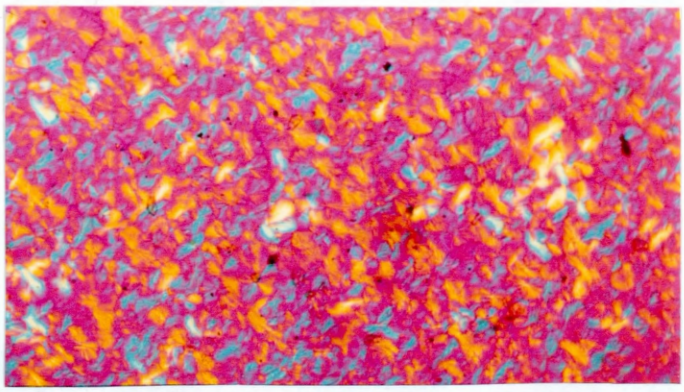

1 minute at 113°C

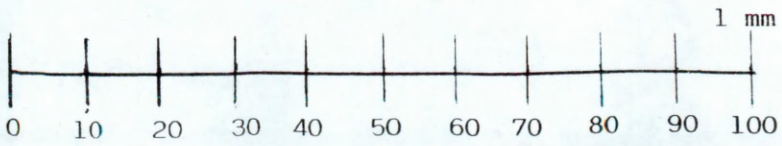

Figure 4.47 Optical micrographs of the heptane fraction at different stages of spherulitic growth

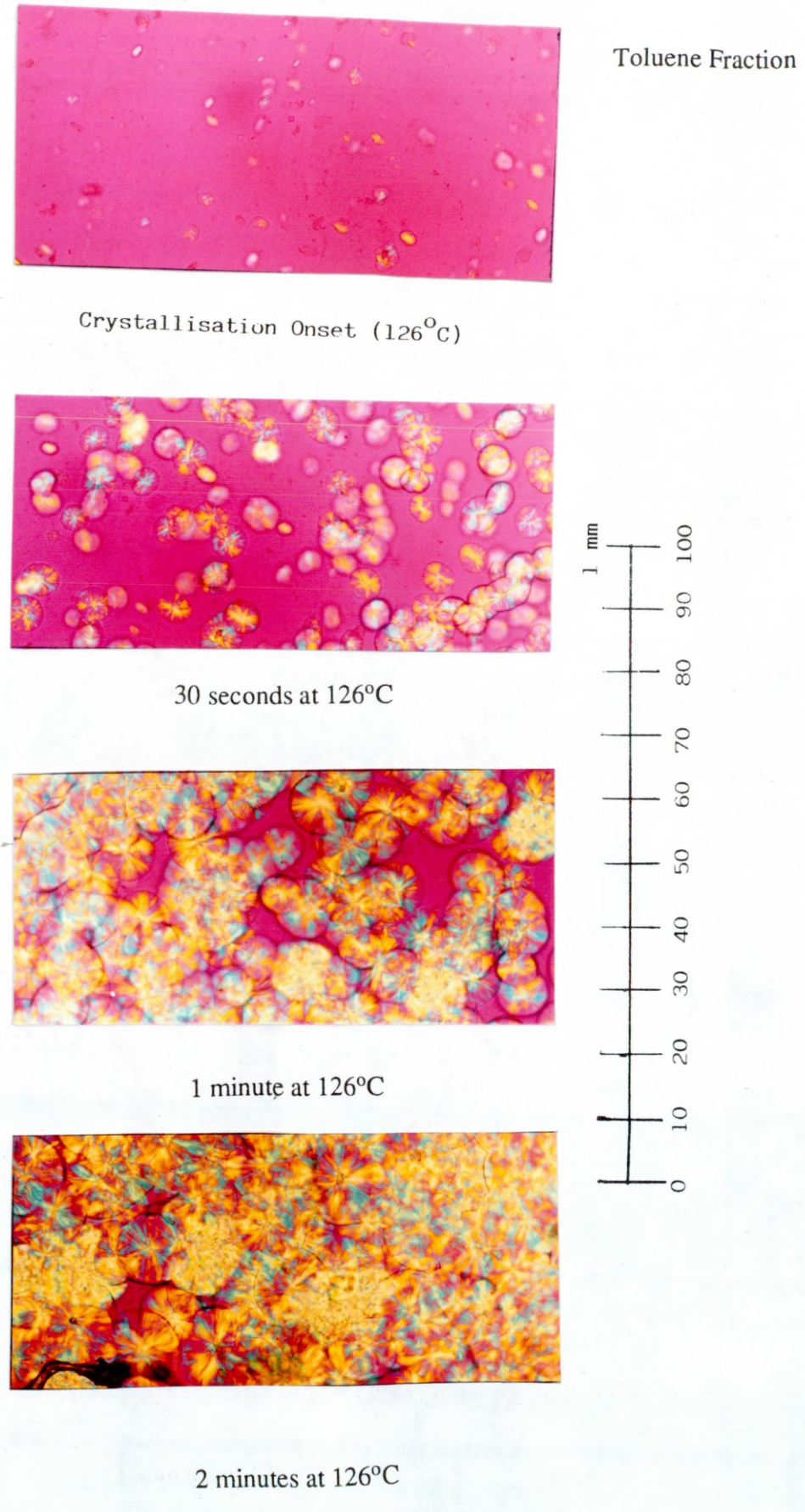

Figure 4.48 Optical micrographs of the toluene fraction at different stages of spherulitic growth

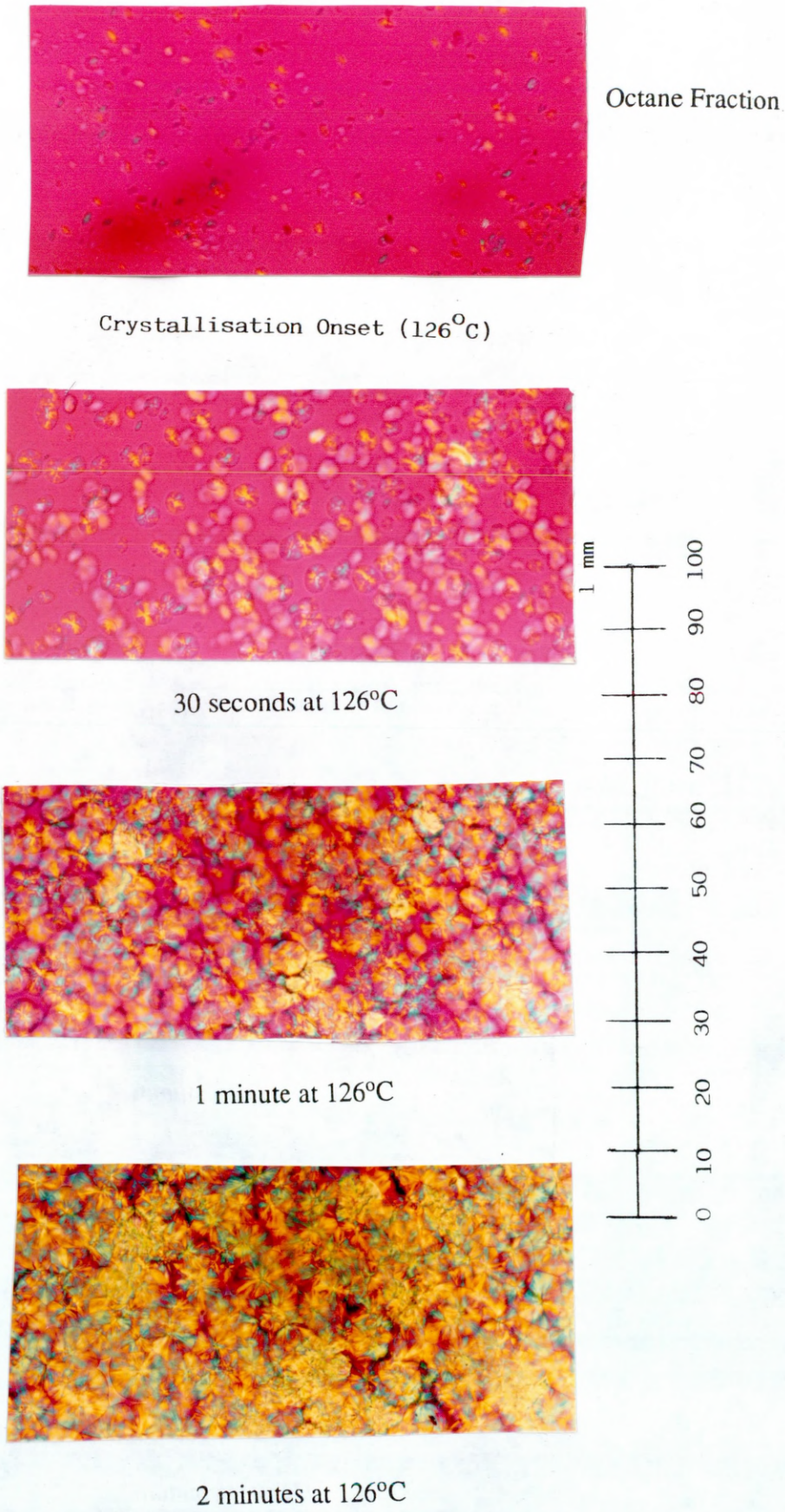

Figure 4.49 Optical micrographs of the octane fraction a different stages of spherulitic growth

4.7.4 Discussion

The investigative fractionation study proved useful as it highlighted certain fundamental problems associated with the Soxhlet fractionation technique. These included inconsistent yields of fractionated polymer and quality of the fractions which, to a great extent had undergone a substantial degree of oxidative degradation during extraction (Table 4.30).

The poor reproducibility of obtained fractions may be attributed to variations in the fractionation temperature. Since the Soxhlet extraction technique relies on condensed solvent vapour for the dissolution of material in the extraction zone, it is almost impossible to control the exact temperature of the fractionating solvent without the use of specially adapted heating jackets strapped around the system. This inevitably leads to inconsistent results and it also means that fractionation is not taking place at the boiling point of the fractionating solvent.

The additional problem of oxidation occurred when polymer which had been fractionated by condensed solvent (warm) was suddenly released into boiling solvent (hot) by the Soxhlet mechanism. Since the system is believed to have been insufficiently deoxygenated, then this ultimately led to sample oxidation and hence poor quality of obtained fractions.

Another problem was the loss of lower boiling, volatile solvent in the form of escaped vapour which leaked to the atmosphere and meant that extra solvent had to be added to the system from time to time. This resulted in the cooling of the boiling solvent and hence interrupted the extraction and became another source of inconsistency. These problems exposed the Soxhlet extraction method as being of little value as a reliable and reproducible procedure for the preparative fractionation of polypropylene.

The investigative study did, however serve as a valuable exercise and provided a fundamental base on which to develop a more efficient and improved system.

The development of an improved fractionation procedure centred around solving three outstanding problems:-

(i) Exclusion of oxygen from the system
(ii) Containment of volatile vapour
(iii) Consistency of extraction temperature

The exclusion of oxygen from the system was achieved by extensive degassing of the extraction solvents, flushing of the system with dry nitrogen and operating a closed system under a constant positive internal nitrogen atmosphere. All connecting joints were greased in order to minimise leakages of nitrogen gas and solvent vapours.

In order to obtain a consistent extraction temperature, the paper thimble containing the powdered polypropylene was placed directly into the extracting solvent. Once this solvent had reached its boiling point, the temperature of the extraction could go no higher and as long as the boiling temperature was maintained, the extraction would be carried out at a constant temperature. This meant that all molecules which were soluble in a particular solvent system at its boiling temperature were extracted (and not just a fraction of them as in the Soxhlet extraction method which was plagued with inconsistencies in extraction temperature).

When the results of each extraction system are compared for a 5 mg powdered sample of GSE18 polypropylene (Tables 4.30 and 4.31) it can be seen that the lower boiling solvents such as ether, pentane and heptane extracted more polypropylene fraction using the reflux method than in the corresponding extraction using the Soxhlet

method. The heptane fraction using the reflux method was virtually half that obtained using the Soxhlet method.

A possible explanation for this lies in the temperature of extraction. In the Soxhlet method the temperature of extraction for the low boiling solvent is not sufficiently high to extract all the molecules which would be soluble in the corresponding boiling solvent. This means that for the Soxhlet extraction, the molecules which should have been extracted by the ether, pentane and hexane solvents are only being extracted by hot heptane. This results in a misleading increase in the fraction of heptane soluble material. However, in the fractions obtained by the reflux method, since all molecules which are truly soluble in the boiling ether, pentane and hexane solvents have been extracted, there is no overspill of soluble polypropylene into the heptane extraction and hence the decrease in the yield for this fraction using the reflux method.

The reflux method results clearly show that the majority of the polypropylene molecules were soluble in boiling toluene. The temperature of the toluene in the extraction chamber of the Soxhlet equipment, however, was less than the boiling point and as a consequence, was insufficiently high to extract all of the polypropylene molecules which were truly extractable in boiling toluene. This resulted in the Soxhlet method incorrectly showing the polypropylene to be predominantly made up of octane soluble material.

The overall degree of reproducibility over the three extractions was superior using the reflux extraction procedure. Due to the precautions taken to exclude oxygen from the system, the quality of the extracted polyproplene, at least as far as oxidative degradation is concerned, was markedly improved over that of fractions obtained by the Soxhlet fractionation procedure.

4.7.4.1 Molecular Weight Of Fractions

Determination of molecular weight using high temperature GPC was a crucial step in the appraisal of the quality of the polymer fractions being extracted in the reflux fractionation technique. Results shown in Table 4.32 clearly indicate that, in general, molecular weight averages such as $\overline{M}_n$, $\overline{M}_w$, $\overline{M}_z$ and $\overline{M}_p$ increase in value with the corresponding increase in fractionation temperature. Figures 4.19 - 4.22 show that the molecular weight averages for each fraction increase in an almost exponential manner as a function of fractionation temperature except for the $\overline{M}_z$ values which show a linear relationship.

The toluene and ether fractions, however, deviate from this situation. The ether fraction deviates only slightly and has $\overline{M}_w$ and $\overline{M}_z$ values which are slightly higher than expected. The toluene fraction, however, deviates by a significant amount, having values for $\overline{M}_n$, $\overline{M}_w$, $\overline{M}_z$ and $\overline{M}_p$ much lower than expected. Results of other qualitative measurements for this fraction such as density, crystallinity, melting, crystallisation, ^{13}C-nmr and infrared spectroscopy, show no real deviation from the expected trends and thus cast doubt over the authenticity of the GPC data for this fraction.

The polydispersity ratios ($\overline{M}_w/\overline{M}_n$) for the fractions do not exhibit a simple correlation with respect to fractionation temperature. This suggests that another factor such as tacticity may be involved in the fractionation of the polypropylene. If, in some cases long chain atactic molecules were being extracted preferentially over short chain isotactic molecules, then this would definitely have implications for the polydispersity or molecular weight distribution of the resultant fraction. This scenario may also explain the higher than expected $\overline{M}_w$, $\overline{M}_z$ and $\overline{M}_w/\overline{M}_n$ values for the ether fraction.

From the GPC results (with exception of the toluene fraction) it is quite clear that fractionation of the polypropylene has progressed, at least, on the basis of molecular weight which increases in an exponential manner with respect to fractionation temperature.

An unexpected feature of this experiment, however, was that the molecular weight data for the GSE18 homopolymer was higher than that of the corresponding values for any of the fractions. The reason for this is unclear but it may be feasible that some form of thermal chain breakdown of the highest molecular weight chains has occurred during fractionation. The fact that the $\bar{M}_w$ and $\bar{M}_z$ values appear to show the highest relative values, and are more representative of higher molecular weights, supports this argument.

4.7.4.2 ^{13}Carbon Nuclear Magnetic Resonance

The ^{13}C-nmr spectrum of polypropylene with a high isotactic content is very simple and consists of only three peaks which are assigned to the methyl (CH_3), methine (CH) and methylene (CH_2) carbon atoms at circa 21.9, 28.9 and 46.6 ppm respectively. Each of these peaks are sensitive to changes in the stereoregularity of the polymer. This is clearly indicated in Figures 4.23 - 4.25.

From the various regions of the ^{13}C-nmr spectra of polypropylene, a progressive increase in spectral splitting is observed as the fractionation temperature becomes lower thus indicating the occurrence of a less stereoregular structure. Although this increase in the number of peaks for the fractions extracted in the lower boiling solvents is common to all three spectral regions, the signal assigned to the methyl carbons (Figure 4.25) provides the best stereochemical splitting and is considered to

be the most useful for quantitative measurements of the polypropylene stereostructure. Although the methylene region (Figure 4.23) does provide a considerable degree of stereochemical splitting, it tends to exhibit a sizeable amount of peak overlap for important stereochemical resonances. This introduces an element of ambiguity and therefore makes it less reliable than the methyl region for the purposes of stereostructure evaluation in polypropylene[20]. The methine region (Figure 4.24) is less sensitive to changes in the stereochemical environment and consequently is not widely used in the determination of polypropylene stereostructure[106].

Bovey[158] used a meso(*m*) and racemic (*r*) nomenclature to distinguish between consecutive monomer pairs with either the same (*m*) or opposite (*r*) configurations. For example, the tetrad sequences *mmm*, *mrm* and *rrr* would correspond to the following:-

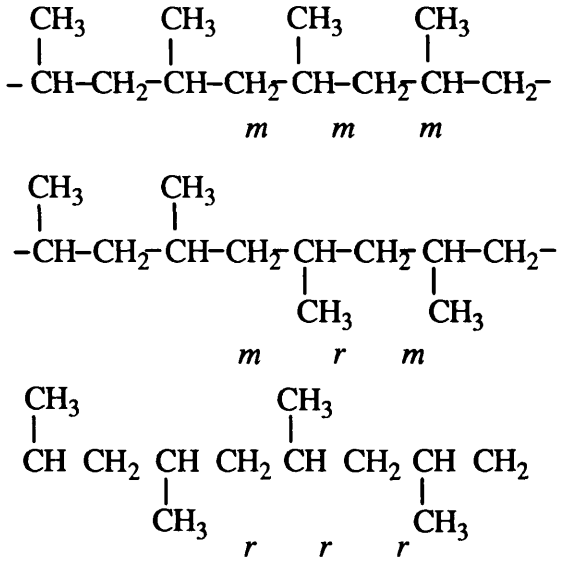

This nomenclature has been widely used[105,106,157-160] to express all possible stereochemical sequences of the same length using either diads, triads, tetrads pentads or heptads. Different diads, triads etc. are assigned to particular peaks in the ^{13}C-nmr

spectrum of polymers based on information obtained from chemical shift calculations[105,159] and the ^{13}C-labelling of model compounds[160]. Figure 4.50 shows the generally accepted assignments of pentad stereosequences[105] in the methyl region and tetrad stereosequences[106] in the methylene region of the ^{13}C-nmr spectrum of polypropylene.

The values for each stereosequence (Tables 4.33 and 4.34) were determined by calculation of the relative peak areas from the ^{13}C-nmr integrals. From results presented in Table 4.33 for the methyl region of the spectra, it is clear that as the fractionation temperature increases, the concentration of *mmmm* istotactic pentad stereosequences increases indicating an increase in the isotacticy of the polypropylene fractions with fractionation temperature. At the same time, a corresponding progressive decrease in the concentration of non-isotactic and less regular pentad stereosequences such as *rrrr*, *mrrm*, *mrrr*, *mrmr*, *mmrm* + *rmmr*, and *rmmr* is observed. For the fraction extracted by boiling toluene and octane, the isotactic *mmmm* pentad is the most dominant stereosequence with very little contribution from other pentad sequences.

It is perhaps interesting to note that from the ^{13}C-nmr methyl cluster of peaks for the supposedly atactic ether fraction and the pentane fraction there is a relatively large amount of sydiotactic *rrrr* pentad resonance contribution to the overall stereoregularity interspersed in a distribution of stereoblock sequences[155]. This was also the case in results reported by Kawamura and co-workers[157] for fractionation studies investigating the two-site model for polypropylene polymerisation.

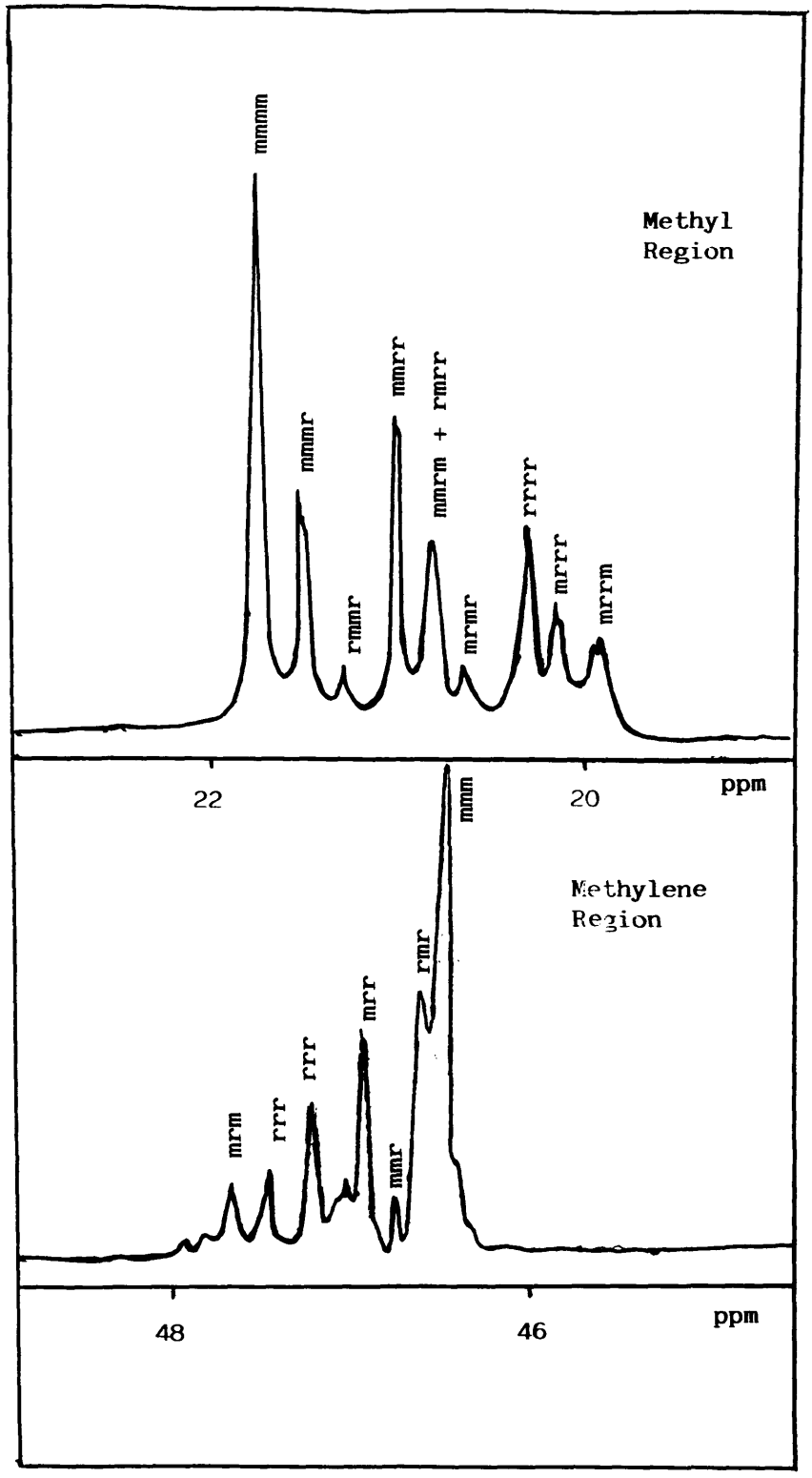

Figure 4.50 ^{13}C-Nmr pentad and tetrad stereosequences for the methyl and methylene regions of isotactic polypropylene respectively

The ^{13}C-nmr pentad sequence distribution for the GSE18 homopolymer indicates a predominantly isotactic stereostructure with small amounts of various other pentad sequences interspersed throughout which correspond to structural irregularities expected in the polymerisation of polypropylene.

The methylene tetrad stereosequence distribution was also investigated for the GSE18 polypropylene fractions (Table 4.34) and was found to exhibit similar trends to those found in the methyl pentad sequence distribution. As previously mentioned, however, insufficient resolution of peaks in this region introduces an element of ambiguity and from the results it can be see that there is quite a poor correlation with the methyl resonances for the polypropylene fractions extracted at the lower boiling temperatures. For this reason, the more reliable *mmmm* methyl pentad stereosequence was used for purposes of assigning isotacticity values to the various fractions.

The ^{13}C-nmr results coupled with the GPC results have shown quite conclusively that fractionation has proceeded on the basis of stereostructure as well as molecular weight.

4.7.4.3 Fourier Transform Infrared Absorption Peak Ratio Analysis (FTIR APRA)

FTIR APRA results for the polypropylene fractions annealed at 80°C provided further evidence of the involvement of tacticity in the reflux fractionation procedure. As previously discussed, the use of infrared absorption bands at 841 and 998 cm^{-1} for the elucidation of polypropylene stereostructure is well established[109,131,132,161]. Table 4.35 shows results for the A998/A973 and A841/A973 absorption ratios obtained from the infrared spectra of the GSE18 polypropylene fractions. Both ratios show a steady increase in value as the temperature of the fractionation increases. This

suggests that the proportion of conformationally regular helical sequences present in the polypropylene fractions becomes higher as the fractionation progresses. This result is in agreement with the ^{13}C-nmr results in section 4.7.4.2.

An associated problem with the infrared analysis, however, is the lack of baseline stability in the spectra of fractions extracted by the lower boiling solvents. This leads to difficulties in the reproducible construction of reliable baselines which in turn causes a decrease in objectivity. Nevertheless, the decrease in the peak intensities of the 998 and 841 cm^{-1} helix bands is clearly visible from the spectra of the fractions in Figures 4.26 - 4.31. Furthermore, the results give a linear correlation with the ^{13}C-nmr *mmmm* methyl pentad stereosequence results (Figure 4.55).

As previously mentioned in section 4.7.3.5, the band at 1167 cm^{-1} was omitted as a reference band for this study. It appears that, from the progressive shifting of this band towards a peak at 1156 cm^{-1} for the fractions extracted by the lower boiling solvents, the exclusion of this band as an internal reference band was a wise decision.

4.7.4.4 Measurement Of Crystallinity

The measurement of the degree of crystallinity is one of the most useful parameters for the characterisation of a semi-crystalline polymer. Amongst other factors, the degree of crystallinity is dependent on the degree of regular configuration in the polymer.

The GSE18 polypropylene fractions were analysed for degree of crystallinity using three methods, namely, density[136], DSC and x-ray diffraction[85].

(i) **Density measurements**

Density measurements were carried out on the polypropylene fractions using the floatation method at 20°C and the results were converted to values reflecting the degree of crystallinity using the two-phase crystalline/amorphous model (section 4.3.3.7).

The degree of crystallinity, according to this method, increased linearly with respect to the temperature of fractionation (Figure 4.32) which suggests that the fractionation proceeds on the basis of stereostructure with the highly crystalline isotactic fraction becoming soluble only in the higher boiling solvents.

(ii) **DSC Melting And Crystallisation**

DSC melting and crystallisation results presented in Table 4.36 show that the molecular weight/tacticity fractions posses different thermal behaviour.

Melting onsets, melting peaks and heats of fusion all show a linear increase in value with respect to fractionation temperature (Figures 4.36 - 4.38), as does the corresponding degree of crystallintity which was calculated from the heat of fusion results (Figure 4.33). It is apparent from these results that as fractionation proceeds, the fractions obtained possess a higher degree of crystallinity which leads to higher energy requirements for melting.

By the same token, the samples crystallise at a faster rate in the fractions obtained by extraction at a higher boiling temperature. Data for the crystallisation onset, crystallisation peak and heat of crystallisation all exhibit a linear relationship with the temperature of fractionation (Figures 4.39 - 4.41). This confirms the conclusions of

Burfield and Doi[78] who proposed that a direct correlation exists between isotacticity and crystallisation onset temperature in polypropylene. Furthermore, the relationship between the heat of crystallisation and ^{13}C-nmr tacticity is well defined which was not the case in the study conducted by Burfield and Doi. Figures 4.51 and 4.52 show a linear relationship between % crystallinity of the polypropylene fractions obtained in this study and the crystallisation onset and heat of crystallisation respectively. These relationships show that there is a clear dependence of crystallisation onset and heat of crystallisation on the inherent crystallinity of the polypropylene fractions. Such relationships can be represented by the following expressions:-

(a) % crystallinity = $0.93T_c - 41$

(b) % crystallinity = $0.01\Delta H_c + 0.013$

Additionally, the relationship between *mmmm* pentad tacticity and crystallisation onset, is also linear (Figure 4.53) and is represented by the expression:-

(c) Isotacticity = $0.01T_c - 0.54$

Since isotacticity and crystallinity are closely related, this further supports the proposals of Burfield and Doi[78] that a relationship exists between polypropylene tacticity.

Graph showing the relationship between % crystallinity (by density) and crystallisation onset temperature for GSE18 polypropylene fractions

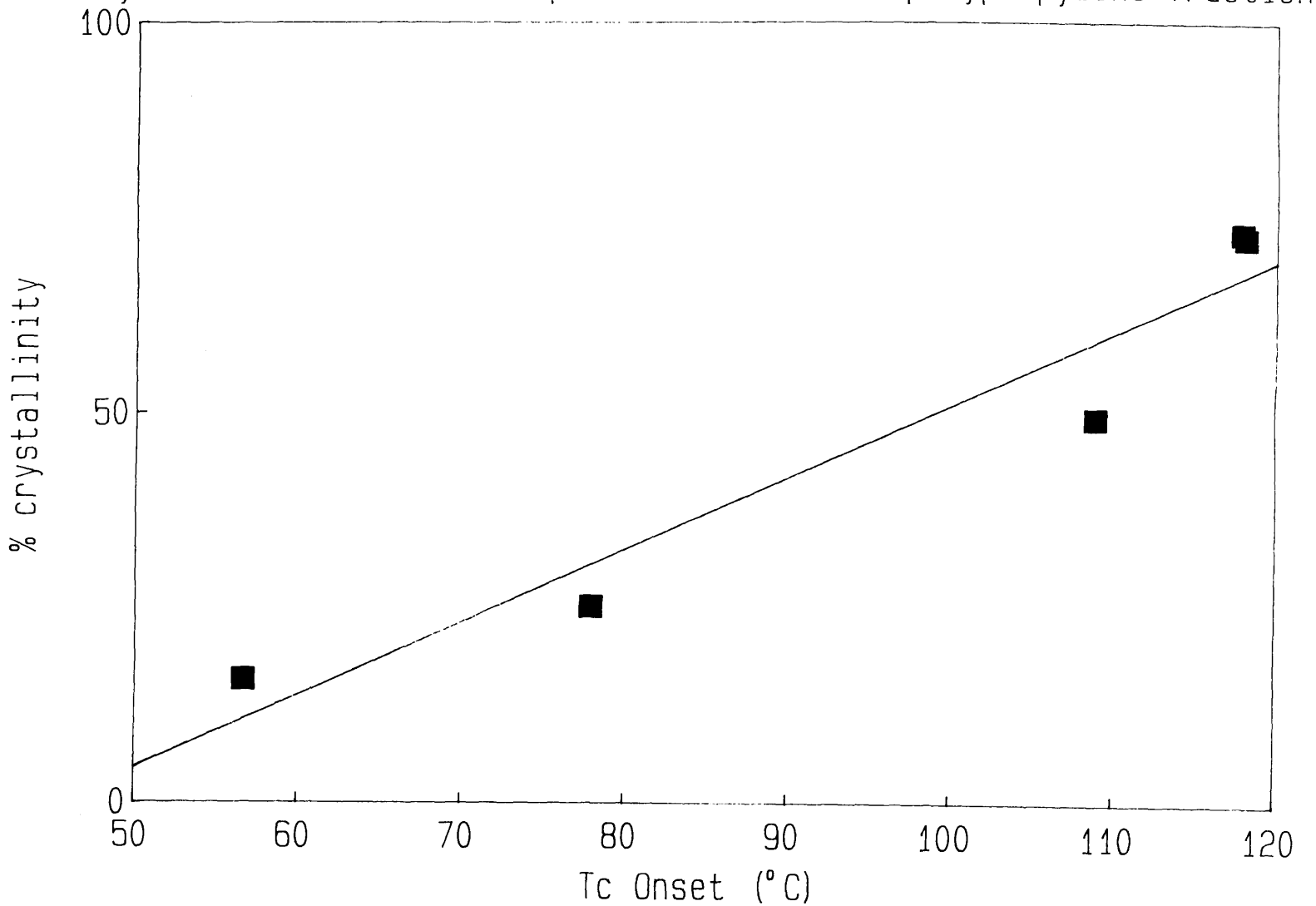

Figure 4.51

Figure 4.52

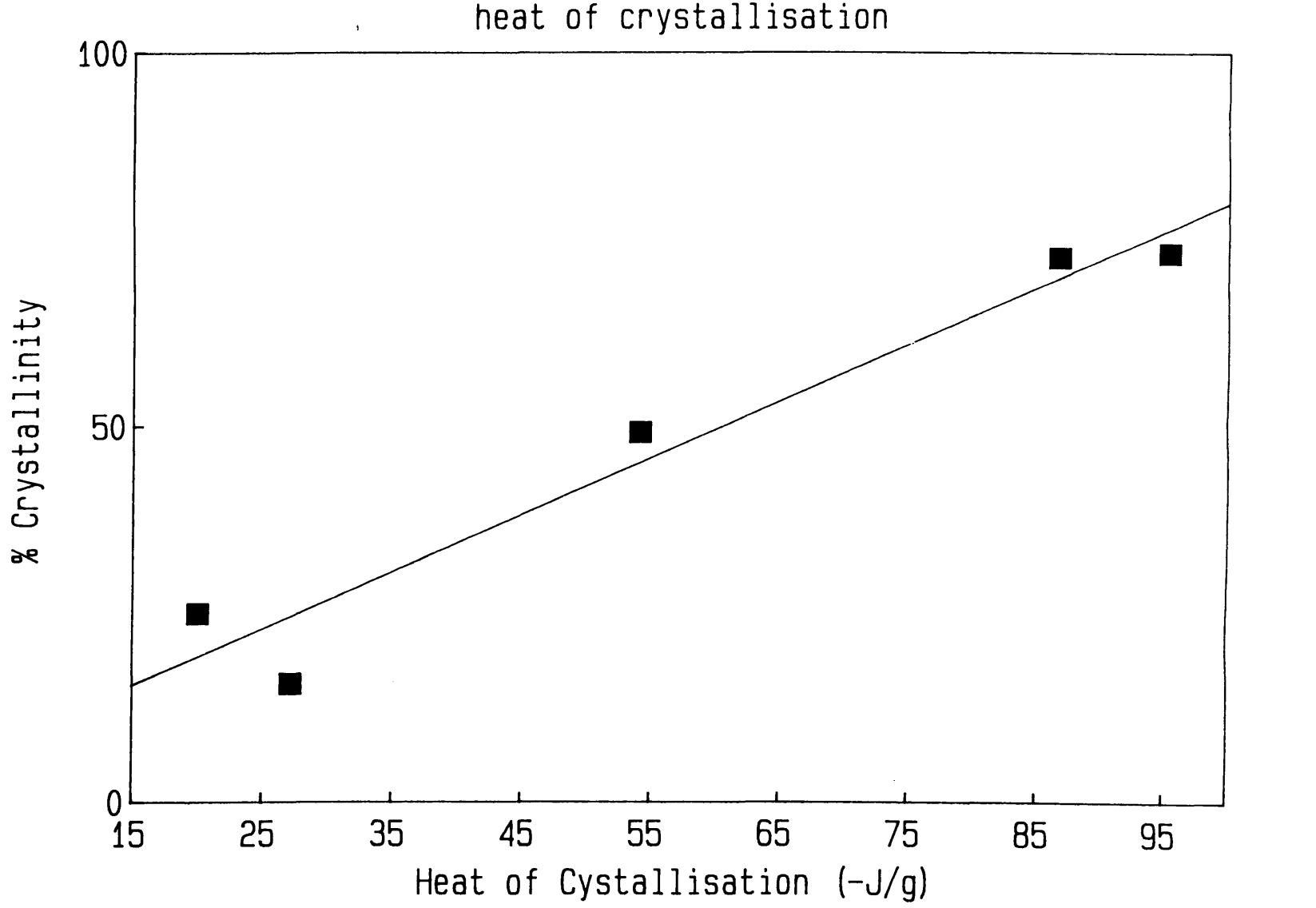
Graph showing the relationship between % crystallinity (by density) and heat of crystallisation
100
50
0
% Crystallinity
15
25
35
45
55
65
75
85
95
Heat of Cystallisation (-J/g)

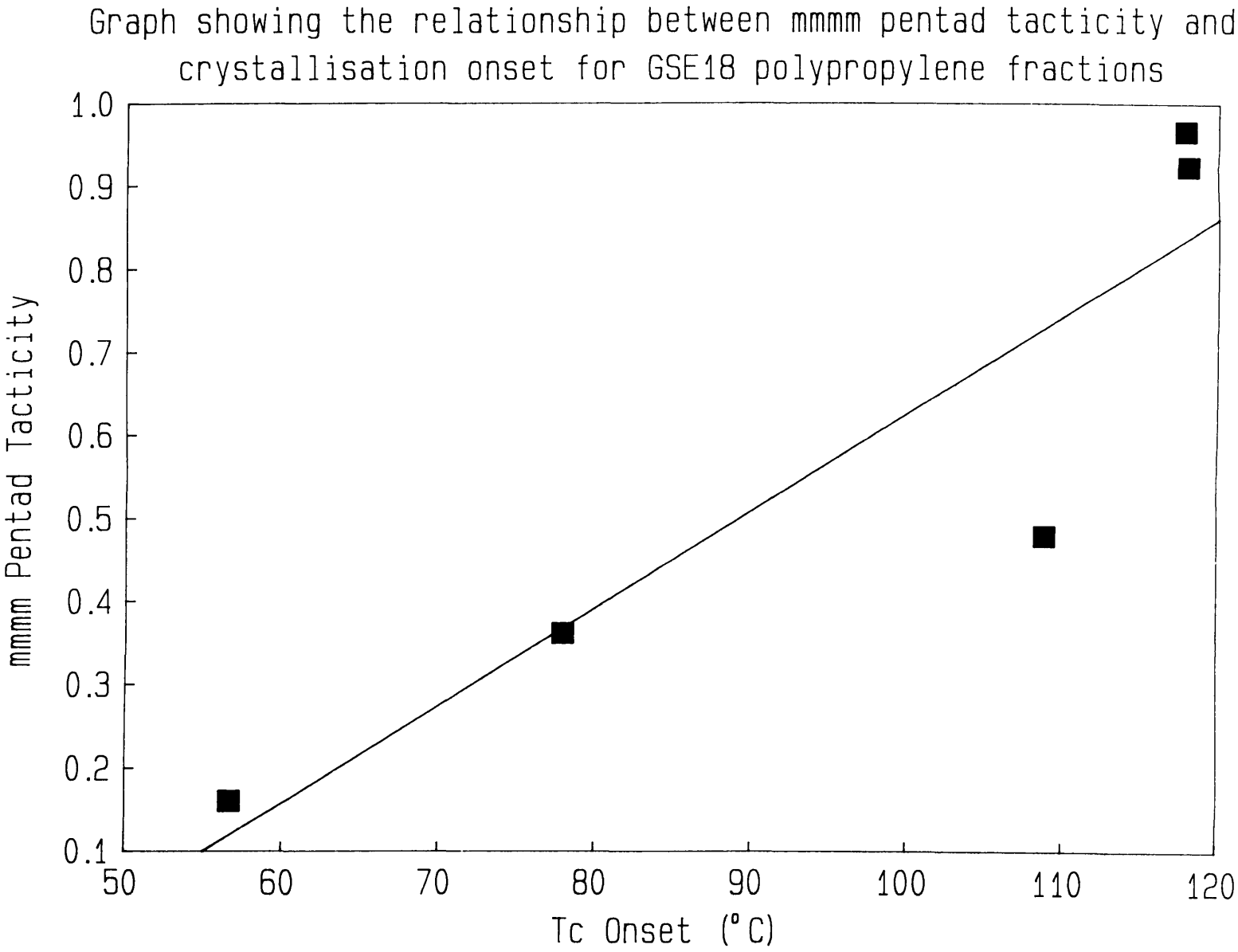
Graph showing the relationship between mmmm pentad tacticity and crystallisation onset for GSE18 polypropylene fractions
mmmm Pentad Tacticity
1.0
0.9
0.8
0.7
0.6
0.5
0.4
0.3
0.2
0.1
50
60
70
80
90
100
110
120
Tc Onset (°C)

Figure 4.53

(iii) Wide Angle X-ray Diffraction

From the diffractograms presented in Figures 4.43 and 4.44, it can be seen that there are clear differences in the degree of x-ray crystallinity of the polypropylene fractions. The diffractogram of the ether fraction exhibited only one broad peak which is characteristic of the amorphous scattering associated with atactic polypropylene and indicative of very little, if any, crystallisable material. Unfortunately, there was insufficient pentane fraction at the time of analysis and therefore no x-ray data was obtained for this fraction. The results from the other fractions, however, did provide enough information to establish a trend (Figure 4.42).

The hexane and heptane fractions showed an increase in crystallinity over the ether fraction. The hexane fraction showed poor resolution of the peaks expected for polypropylene thus suggesting that a only a small amount of crystallisable material was present.

The peaks for the heptane fraction were better resolved, although a relatively large amount of amorphous scattering was still apparent. Both hexane and heptane fractions exhibited considerable band narrowing and increased intensity of the peak at 2θ equal to circa 18.30°. Peak splitting was also exhibited in this region which was very slight in the hexane fraction but more resolved in the heptane fraction with the appearance of a peak at 2θ equal to around 18.80°. This peak corresponds with the main peak at 2θ equal to 18.80° observed in the diffractogram of the more crystalline fractions.

A possible explanation for the shifting to a lower 2θ value, band narrowing and increased intensity of this band is that it may be caused by a decrease in size or imperfections in the crystallites for the hexane and heptane fractions. So, although the

packing of the chains is fundamentally the same, there are more atoms in that particular reflecting plane and hence the difference in the scattering causing this peak to occur. Both fractions also exhibit a small peak at 2θ equal to circa 20.00° which may be indicative of the presence of a small amount of β-phase polypropylene[162]. However, as there is no evidence of the more intense β-phase x-ray diffraction peak at 2θ equal to circa 16.00° (which would be more likely to appear if any β-phase material was present), then it is unlikely that the β-phase is responsible for this peak. It may be that impurities may be to blame instead.

The diffractogram of the toluene and octane fractions which are believed to be of higher crystallinity and tactic regularity, exhibit main peaks at 2θ equal to 14.10°, 17.00°, 18.80°, 21.20°, 22.00° and 26.00°. The peak at 14.10° becomes more intense in the toluene and octane fractions compared to that of the corresponding peak in the hexane and heptane fractions. The peak at circa 18.30° exhibited in the hexane and heptane fractions disappears in the diffractograms of the toluene and octane fractions and the broader, less intense peak at circa 18.80 becomes the major peak in this region. The degree of amorphous scattering in the toluene and octane fractions is much less than the hexane and heptane fractions and consequently a higher degree of crystallinity is observed.

The results calculated from the relative areas under the peaks for the amorphous and crystalline regions as measured by planimetry, show a linear increase in crystallinity with respect to fractionation temperature which again confirms the role of stereostructure and crystallinity in the reflux fractionation procedure.

The three methods used for the determination of the degree of crystallinity show considerable differences in values between each method (Table 4.40). This, however, is unimportant as each technique has its associated flaws which determine the

outcome of the results. Density measurements are highly dependent on temperature, DSC is dependent on scanning rate and x-ray is dependent on exposure times. The important point is that they all show a linear increase with respect to the temperature of fractionation of the GSE18 polypropylene and therefore collectively corroborate the argument that stereostructure, as well as molecular weight, is a factor in the stepwise solvent extraction of polypropylene by reflux fractionation.

Fraction	Degree Of Crystallinity		
	Density	X-ray Diffraction	DSC
Ether	---	0.00	---
Pentane	15.78	---	14.04
Hexane	25.08	22.73	13.52
Heptane	49.24	35.55	35.78
Toluene	72.49	46.59	73.74
Octane	73.14	50.31	87.14

Table 4.40 Comparison of results for methods of degree of crystallinity determination.

4.7.4.5 Polarised Light Microscopy

Hot-stage polarised light microscopy was used to study the crystallisation process in the GSE18 polypropylene fractions. Figures 4.45 - 4.49 show optical micrographs of the polypropylene fractions at the crystallisation onset temperature (T_c); isothermal at T_c for 30 seconds; isothermal at T_c for 1 minute; and, in the case of the toluene and octane fractions, isothermal at T_c for 2 minutes.

Samples were melted and held at 200°C in order to destroy any persistent nuclei. At this temperature there were no signs of any crystalline structures in the melt and therefore it was assumed that the effects of previous thermal histories had been erased. Since all samples were cooled from this temperature at 10°C/min, it is also assumed that any differences between the spherulitic morphologies of the crystallising fractions is attributed to structural characteristics and not a consequence of previous thermal treatment.

From the optical micrographs in Figures 4.45, it is clear that the fraction extracted by boiling ether shows no signs of crystallisation which is consistent with the x-ray results for this fraction. The pentane fraction shows very little evidence of crystallisation and it is very difficult to say whether any spherulitic growth has taken place although the crystallisation onset as indicated by the appearance of colour in the optical micrograph was considered to be around 64°C. DSC results (section 4.7.3.7) for this fraction suggest that crystallisable material is present and from its melting data and density it is considered to have a crystalline content of circa 14-15%. The optical micrograph for this fraction is fairly poor and thus has a degree of ambiguity surrounding it.

The hexane fraction (Figure 4.46) first shows signs of spherulitic growth at circa 87°C. The growing spherulites are primitive and needle-like in character. After 30 seconds at 87°C, an increase in the spherulite concentration is observed and merging of the spherulites occurs. After 1 minute at 87°C, it is difficult to pick out individual spherulites but it is quite clear that the spherulitic morphology observed consists of small poorly formed spherulites interspersed in a predominantly amorphous environment which is indicated by the pink background. This would explain the high

amorphous scattering and low crystallinity observed for this fraction in the x-ray diffraction results and perhaps the band narrowing of the peak at 2θ equal to circa 18.30°.

The onset of spherulitic growth in the fraction extracted by boiling heptane (Figure 4.47) occurs at circa 113°C where, although thicker in nature than those observed for the hexane fraction, poorly formed needle-like spherulites appear. Many more nucleation sites develop after 30 seconds at 113°C and after 1 minute at this temperature the spherulite concentration has become such that they merge into one another. Again, the small poorly formed spherulites are dispersed in the pink coloured amorphous background, although to a lesser extent than in the hexane fraction. This is also in agreement with x-ray results where the relative amorphous scattering is less than that of the hexane fraction and the growth of the peak at 2θ equal to circa 18.80° indicates a tendency towards a more crystalline morphology.

The toluene fraction (Figure 4.48) shows its first signs of spherulitic nucleation at circa 126°C where, even at this stage, evidence of the well developed characteristic circular shape of spherulites in highly crystalline polypropylene is observed. After 30 seconds at 126°C the characteristic Maltese cross develops in the spherulites which, in fractions up until now, has been relatively poorly defined. After 1 minute at this temperature there is a marked increase in growth and nucleation and after two minutes the spherulites have become very numerous and are noticeably larger than those of previous fractions. Another feature of the crystallisation of this phase is the decrease of the pink amorphous background.

A similar onset temperature and growth pattern for polypropylene extracted by boiling octane (Figure 4.49) was observed in the optical micrographs, although in this case the concentration of nuclei was visibly higher and as a consequence the size to

which the spherulites could grow before merging was reduced. After 2 minutes at 126°C, there was a very high concentration of well developed spherulites with very little amorphous background. This also corroborates the x-ray results.

No attempt was made to determine birefringence for the spherulites obtained in the fractions and so no information was obtained about which of the four distinct types of spherulites as identified by Keith and Padden[49] were present. It can be said, however, that the differences in spherulitic morphologies between the fractions confirms the low degree of crystallinity in polypropylene extracted by low boiling solvents where poorly formed imperfect spherulites were found to exist and the high degree of crystallinity in the fractions extracted by the higher boiling solvents where a greater degree of perfection in the development of the spherulitic morphology was apparent.

Crystallisation onset temperatures obtained by hot-stage polarised light microscopy in this study are much higher than those determined by DSC for the same samples. This indicates that DSC is insufficiently sensitive to detect the earliest onset of crystalline nucleation in the polymer. The crystallisation onset temperatures obtained by microscopy, then, can be assumed to be more accurate. A comparison of results obtained for crystallisation onsets by both methods are shown in Table 4.41.

	Crystallisation Onset Temperature	
Fraction	DSC	Polarised Light Microscopy
Ether	---	---
Pentane	56.56	64.00
Hexane	77.95	87.00
Heptane	108.85	113.00
Toluene	118.06	126.00
Octane	117.84	126.00

Table 4.41 Crystallisation onset temperatures as obtained by DSC and polarised light microscopy.

4.7.4.6 Correlations With ^{13}C-nmr

Since ^{13}C-nmr is considered to be a powerful and reproducible technique for the characterisation of polymer stereostructure, it was useful to examine the relationships between the *mmmm* methyl pentad tacticities and results from the various other techniques used in this study for the characterisation of the polypropylene fractions.

(i) Molecular Weight

Figure 4.54 shows a linear relationship between the molecular weight averages and ^{13}C-nmr *mmmm* methyl pentad tacticities with correlation coefficients from least squares linear regression of 0.945, 0.973 and 0.984 for $\overline{M}_n$, $\overline{M}_w$ and $\overline{M}_p$ respectively.

This, again, shows that the fractionation was based on both molecular weight and stereoregularity and that a degree of interdependence is apparent between the two parameters.

(ii) FTIR Absorption Peak Ratio Analysis

The linear relationships observed in Figure 4.55 for the A998/A973 and A841/A973 FTIR absorption ratios with respect to ^{13}C-nmr *mmmm* methyl pentad tacticities shows that the concentration of helical material associated with the 998 and 841 cm^{-1} infrared bands increases with the stereoregularity of the polypropylene fractions. Given that stereoregularity is a precondition for the formation of regular 3_1 helices in polypropylene, then it is not surprising that such a linear relationship (correlation coefficients of 0.987 and 0.961 for A998/A973 and A841/A973 absorption ratios respectively) exists between the two characterisation methods for the fractionated

polypropylene. Similar correlations between ^{13}C-nmr *mm* triad tacticities and the above infrared ratios were described by Burfield and Doi[109].

(iii) Density Measurements

Since the degree of stereoregularity increases with increasing fractionation temperature, it was expected that the crystalline density of the polypropylene fractions would do likewise and this, in fact, is the case. It was also expected, therefore, that because the crystallinity and hence density of a polymer is related to the close packing of the molecules which in turn, is related to the stereoregularity of the polymer, that a linear relationship between density and ^{13}C-nmr *mmmm* methyl pentad tacticities would exist. Such a relationship is shown in Figure 4.56 (correlation coefficient equal to 0.974) for the fractionated polypropylene, once more confirming the basis of the fractionation.

(iv) DSC Melting And Crystallisation

Melting onsets and melting peaks for the polypropylene fractions show a linear relationship with *mmmm* methyl pentad tacticities having correlation coefficients of 0.945 and 0.923 respectively (Figure 4.57). Again this would be expected as the higher the isotacticity of the fractions then the higher the crystallinity and hence temperature of melting. This relationship is also reflected in the ΔH_f results shown in Figure 4.58 (correlation coefficient of 0.971).

Crystallisation onsets and peak values for the polypropylene fractions also exhibited a linear relationship (Figure 4.59) with respect to *mmmm* methyl pentad tacticities (correlation coefficients of 0.910 and 0.903 repectively). This relationship is in good agreement with results published by Burfield and Doi[78]. The relationship between

$-\Delta H_c$ and *mmmm* methyl pentad tacticities is again linear having a correlation coefficient of 0.954 which confirms a higher degree of crystallinity or stereoregularitiy for the fractions obtained at higher boiling temperatures (Figure 4.58).

(v) X-ray Crystallinity

Degree of crystallinity calculated from x-ray diffraction results show reasonable correlation (correlation coefficient of 0.954) with the ^{13}C-nmr *mmmm* methyl pentad tacticities (Figure 4.60). This, once more, was expected and again shows that the fractionation has been carried out on the basis of crystallinity which in turn depends on molecular weight and stereoregularity.

Graph showing mmmm methyl pentad tacticities versus molecular weight average for GSE18 polypropylene fractions

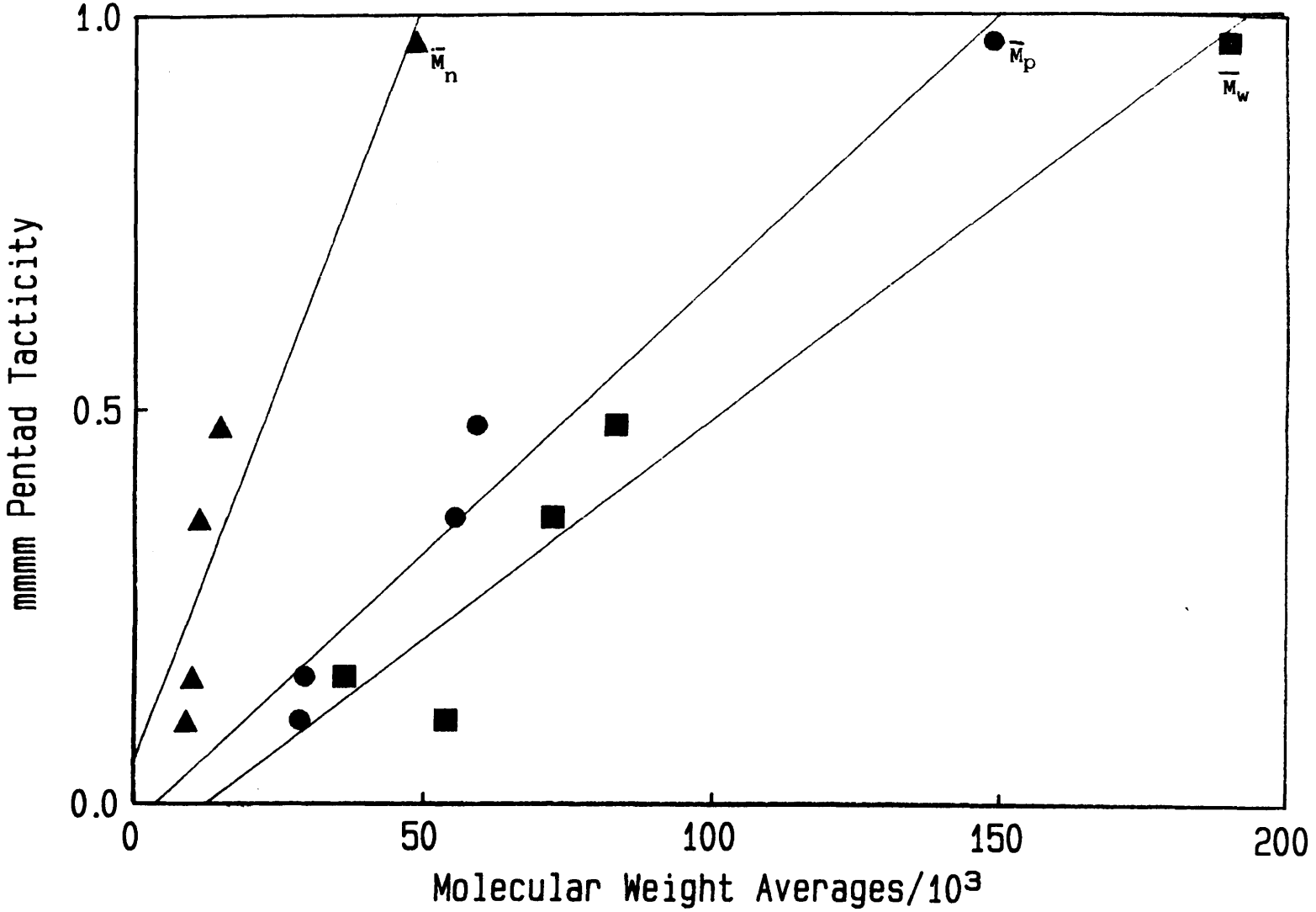

Figure 4.54

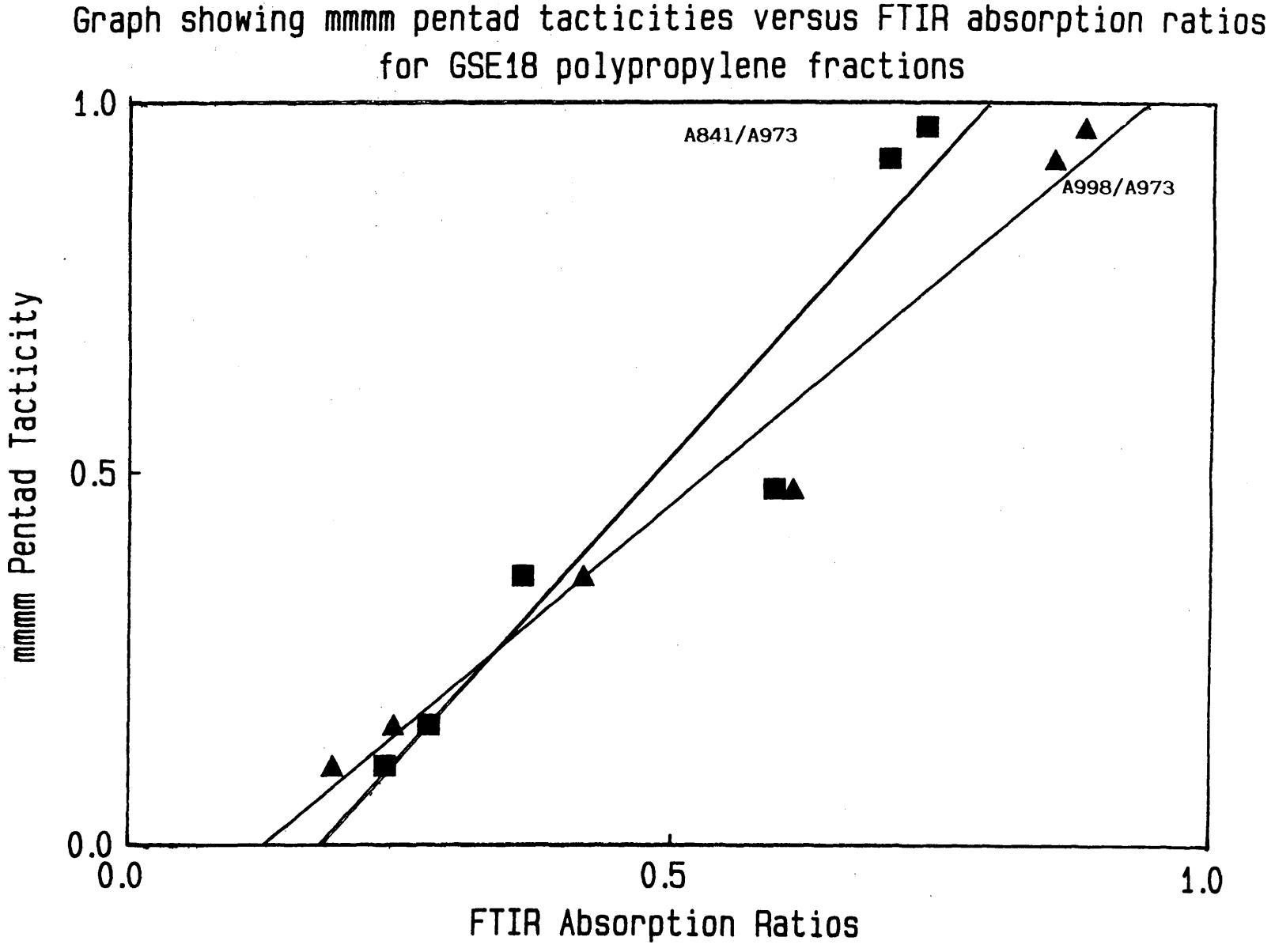
Graph showing mmmm pentad tacticities versus FTIR absorption ratios
for GSE18 polypropylene fractions
1.0
0.5
0.0
0.0
0.5
1.0
mmmm Pentad Tacticity
FTIR Absorption Ratios
A841/A973
A998/A973

Figure 4.55

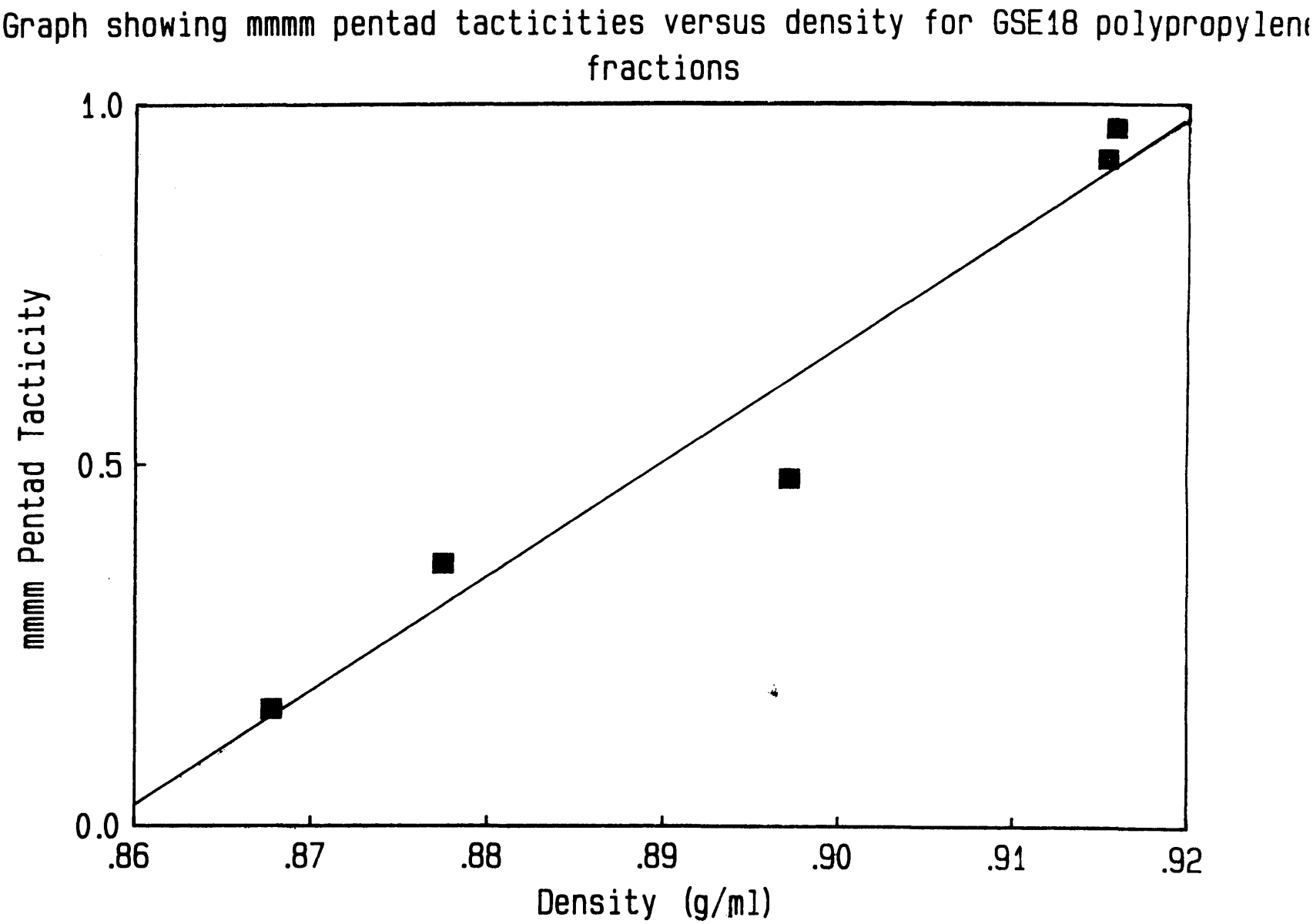
Graph showing mmmm pentad tacticities versus density for GSE18 polypropylene fractions
1.0
0.5
0.0
mmmm Pentad Tacticity
.86
.87
.88
.89
.90
.91
.92
Density (g/ml)

Figure 4.56

Figure 4.57

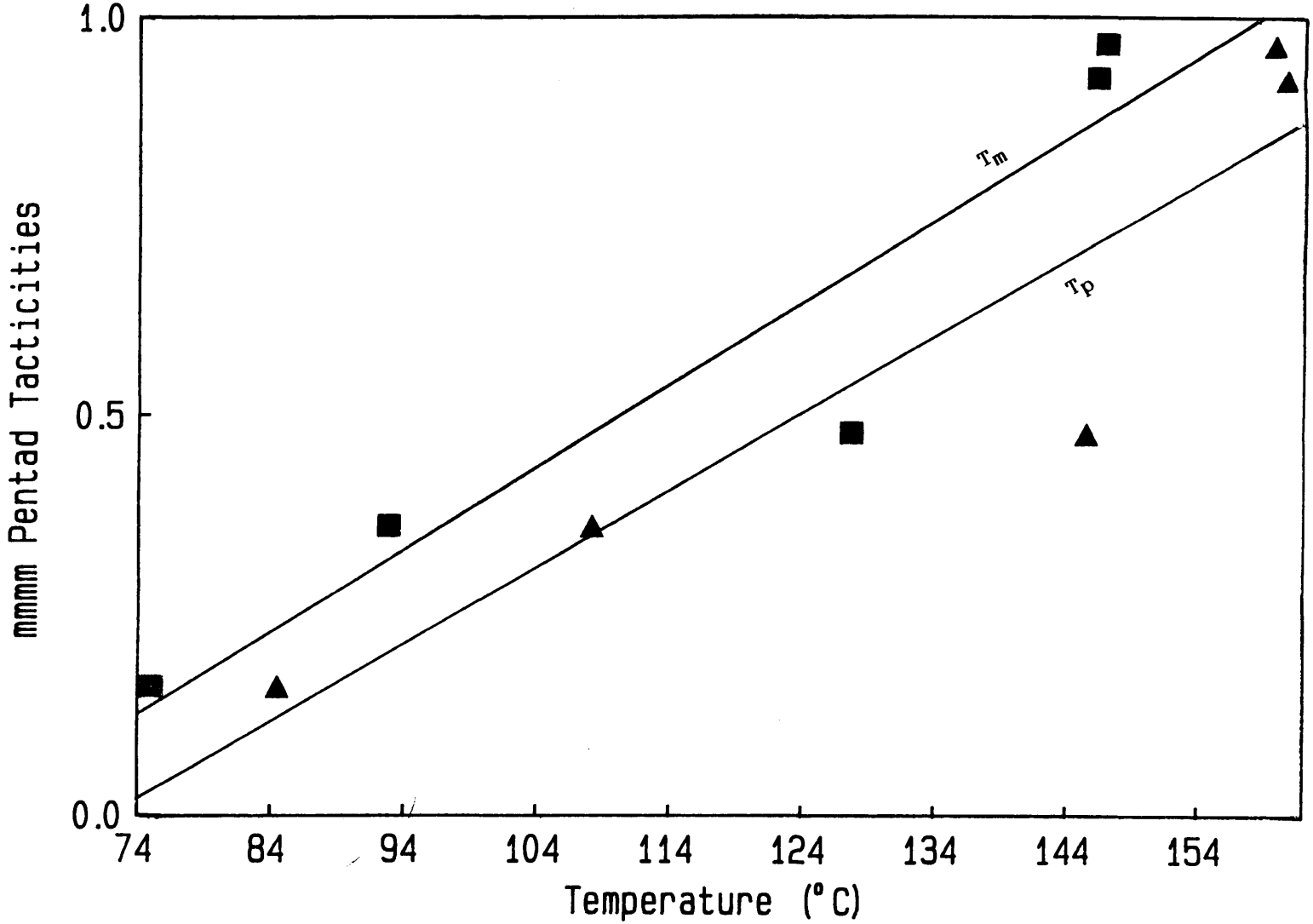
Graph showing mmmm pentad tacticities versus DSC melting data for GSE18 polypropylene fractions
mmmm Pentad Tacticities
1.0
0.5
0.0
74
84
94
104
114
124
134
144
154
Temperature (°C)
T_m
T_p

Graph showing mmmm pentad tacticities versus DSC heat of transition data for GSE18 polypropylene fractions

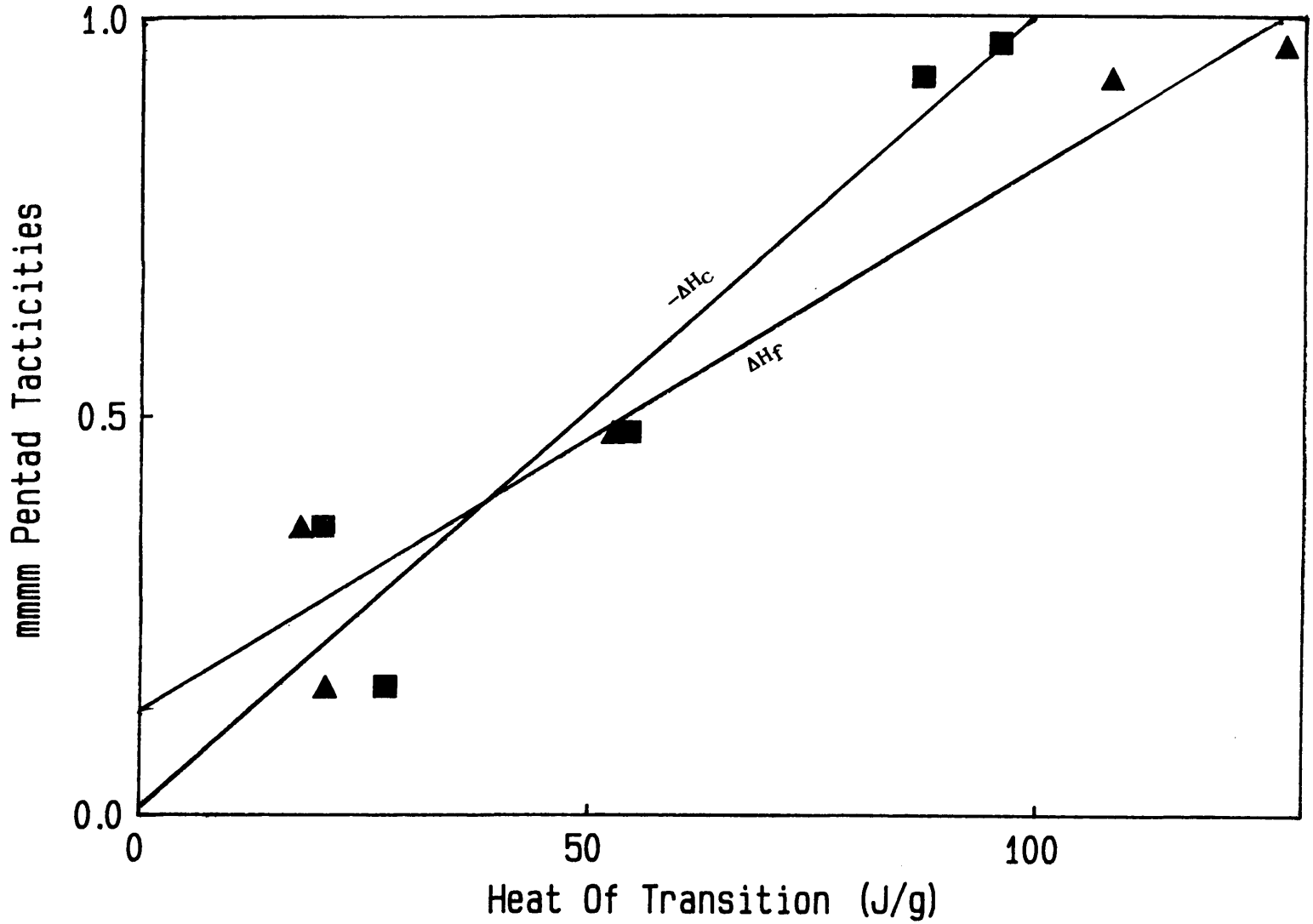

Figure 4.58

Figure 4.59

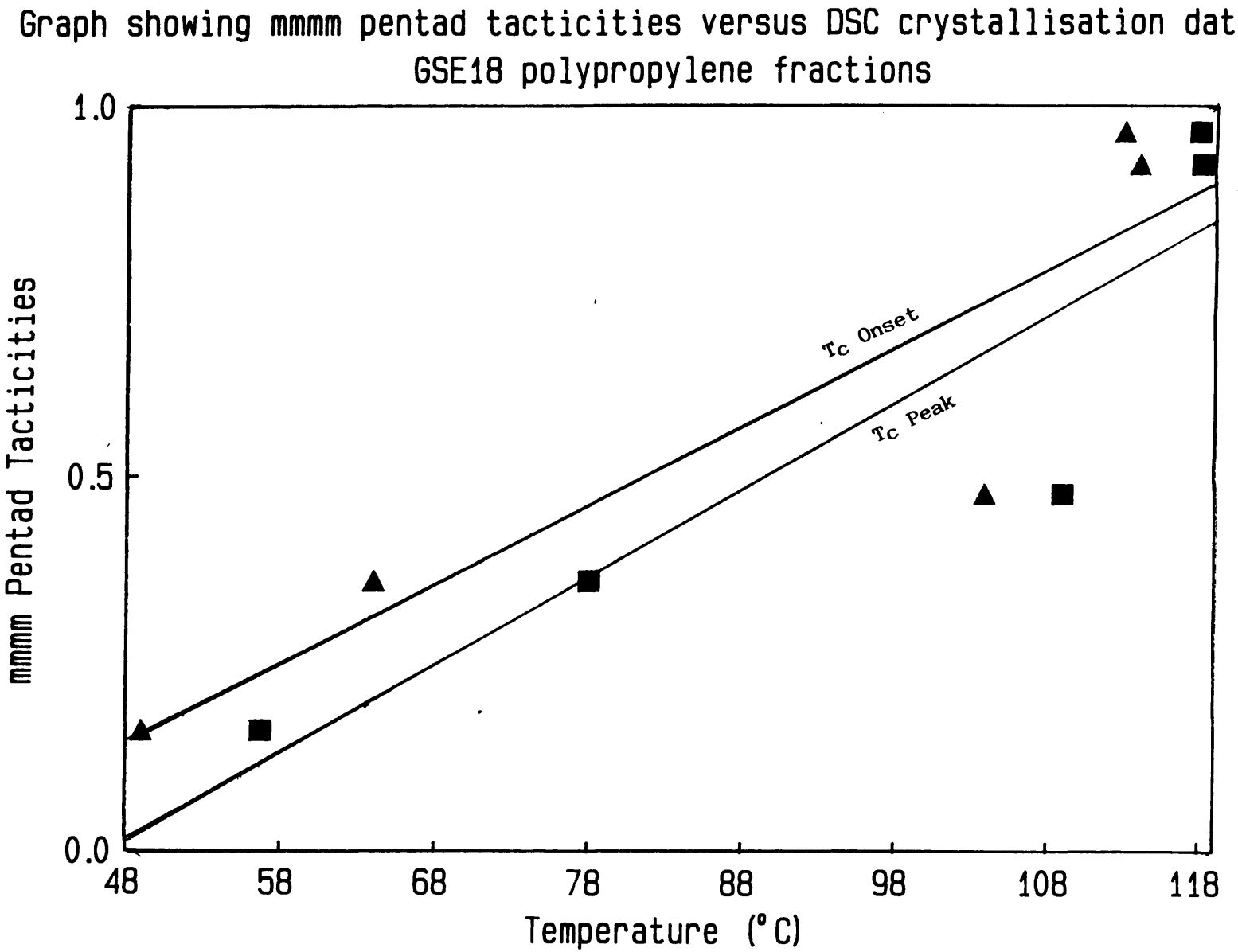
Graph showing mmmm pentad tacticities versus DSC crystallisation data for GSE18 polypropylene fractions
1.0
0.5
0.0
mmmm Pentad Tacticities
Tc Onset
Tc Peak
48
58
68
78
88
98
108
118
Temperature (°C)

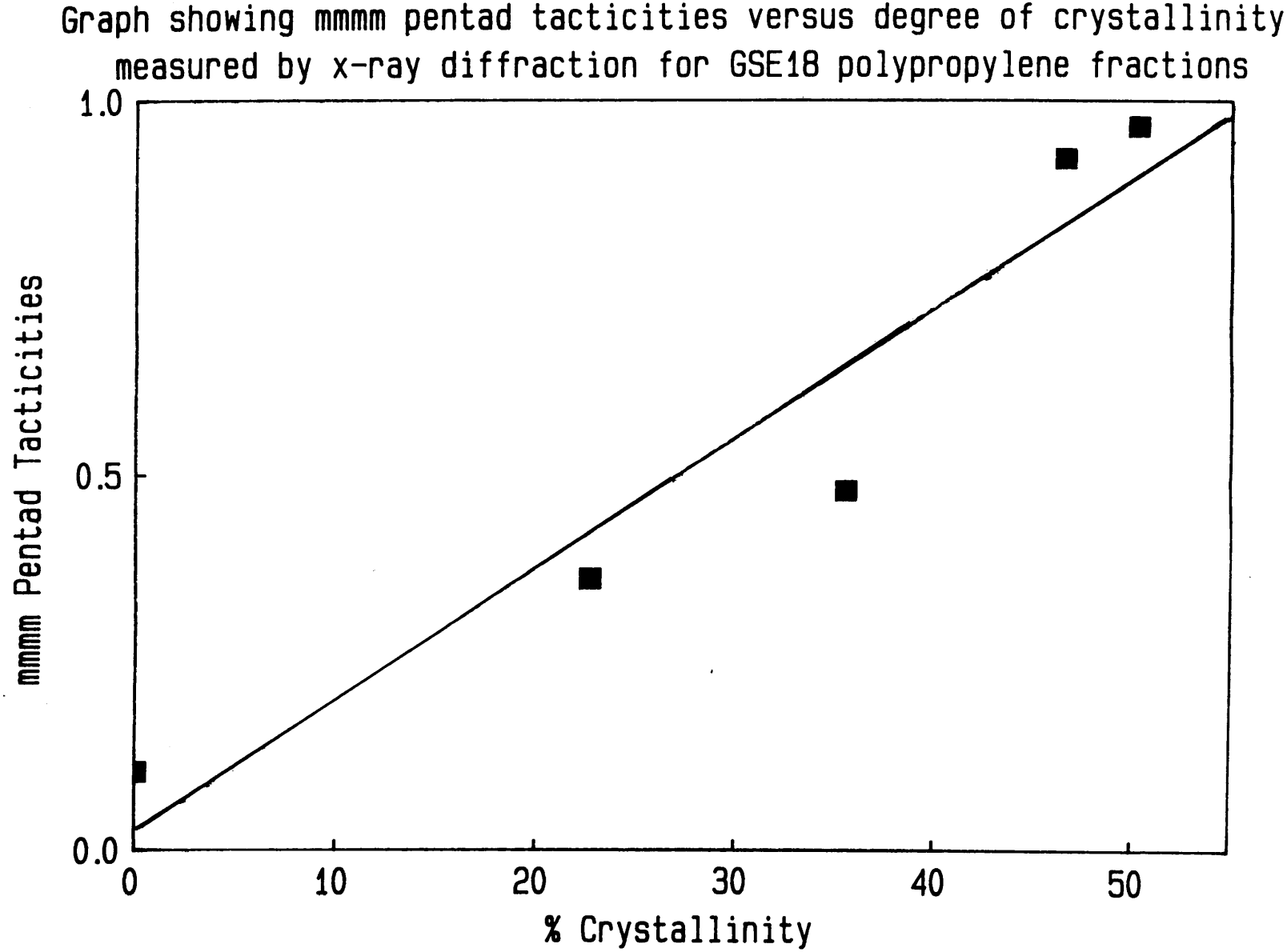
Graph showing mmmm pentad tacticities versus degree of crystallinity
measured by x-ray diffraction for GSE18 polypropylene fractions
mmmm Pentad Tacticities
1.0
0.5
0.0
0
10
20
30
40
50
% Crystallinity

Figure 4.60

4.8 THERMAL BEHAVIOUR OF GSE18 POLYPROPYLENE FRACTIONS

The effect of thermal treatment on the GSE18 polypropylene fractions was investigated in order to establish the role of molecular weight/tacticity in the formation of multiple peaks in the DSC thermograms of polypropylene. To obtain well defined reproducible multiple peaks in the DSC thermograms of the polypropylene fractions, a stepwise downward annealing procedure similar to that reported by Pae and Sauer[140] was used.

4.8.1 Stepwise Downward Annealing

Samples of 5-10 mg were encapsulated for DSC analysis according to procedures detailed in section 3.7.1. These samples were heated to 200°C at 200°C/min and held isothermally in the melt for 5 minutes in order to erase any persistent nuclei from previous thermal or mechanical treatment and to provide each sample with a common thermal history. After this isothermal melt period, the sample was cooled at 200°C/min to a temperature of 70°C and held for a period of 3 minutes before heating at 10°C/min to 160°C. The sample was again held at this temperature for 5 minutes before rapidly cooling at 200°C/min to 70°C. After holding at 70°C for 3 minutes the sample was heated at 10°C/min to 150°C, held for 5 minutes and then cooled at 200°C/min back to 70°C. This procedure was repeated at 10°C intervals for progressively decreasing annealing temperatures down to a final annealing temperature of 120°C. After the final annealing temperature, the sample was cooled at 200°C/min to 30°C and a DSC thermogram was then recorded at 10°C/min from 30°C to 200°C. The resultant melting thermogram exhibited at least five reproducible peaks for the GSE18 polypropylene homopolymer. A schematic diagram of the stepwise downward annealing procedure is shown in Figure 4.61.

Different combinations of this procedure produce melting thermograms with various numbers of peaks with correspondingly varied relative intensities. Figure 4.62 shows a series of melting endotherms for a GSE18 polypropylene homopolymer which was annealed at successively decreasing temperatures, as above, from 160°C but with a different amount of annealing steps before recording the thermogram from 30°C to 200°C. These annealing steps are shown in Table 4.42

Curve Number	Anealing Steps (°C)				
1	160,	150,	140,	130,	120
2	160,	150,	140,	130	---
3	160,	150,	140,	---	---
4	160,	150,	---	---	---
5	160,	---	---	---	---

Table 4.42 Stepwise downward annealing to different degrees for GSE18 polypropylene homopolymer.

Although the possible annealing combinations are many and varied, it was decided that decreasing annealing temperatures at 10°C intervals between 160°C and 120°C inclusively would be used for the study of the polypropylene fractions.

Analysis of the resultant thermograms was carried out by examination of the areas under the multiple peaks as a fraction of the area under the total endotherm. This was facilitated by a DSC software program for calculating partial areas. An example of a sample which was annealed in a successively downward manner and examined for partial areas is shown in Figure 4.63.

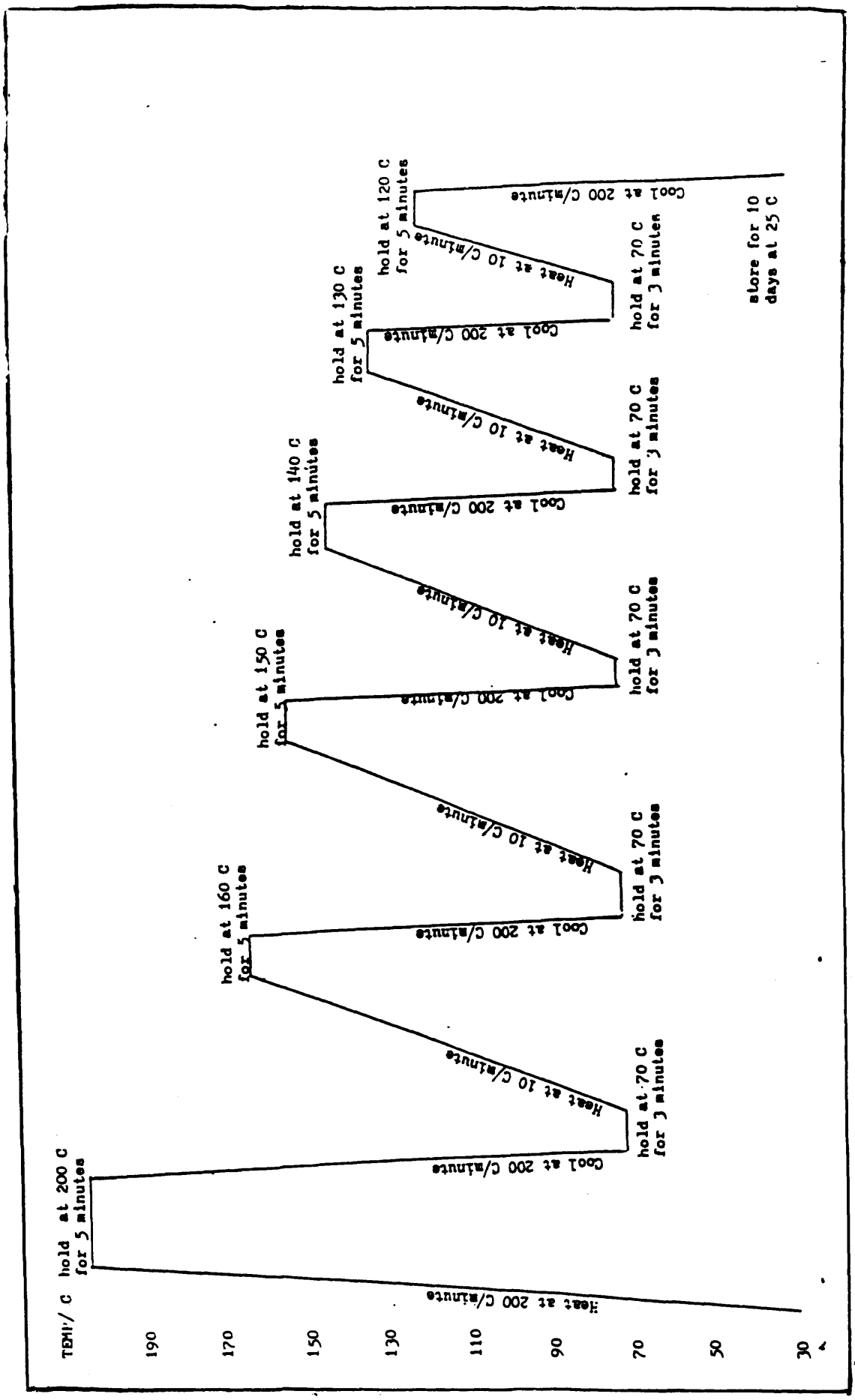

Figure 4.61 Schematic diagram showing the stepwise downward annealing procedure

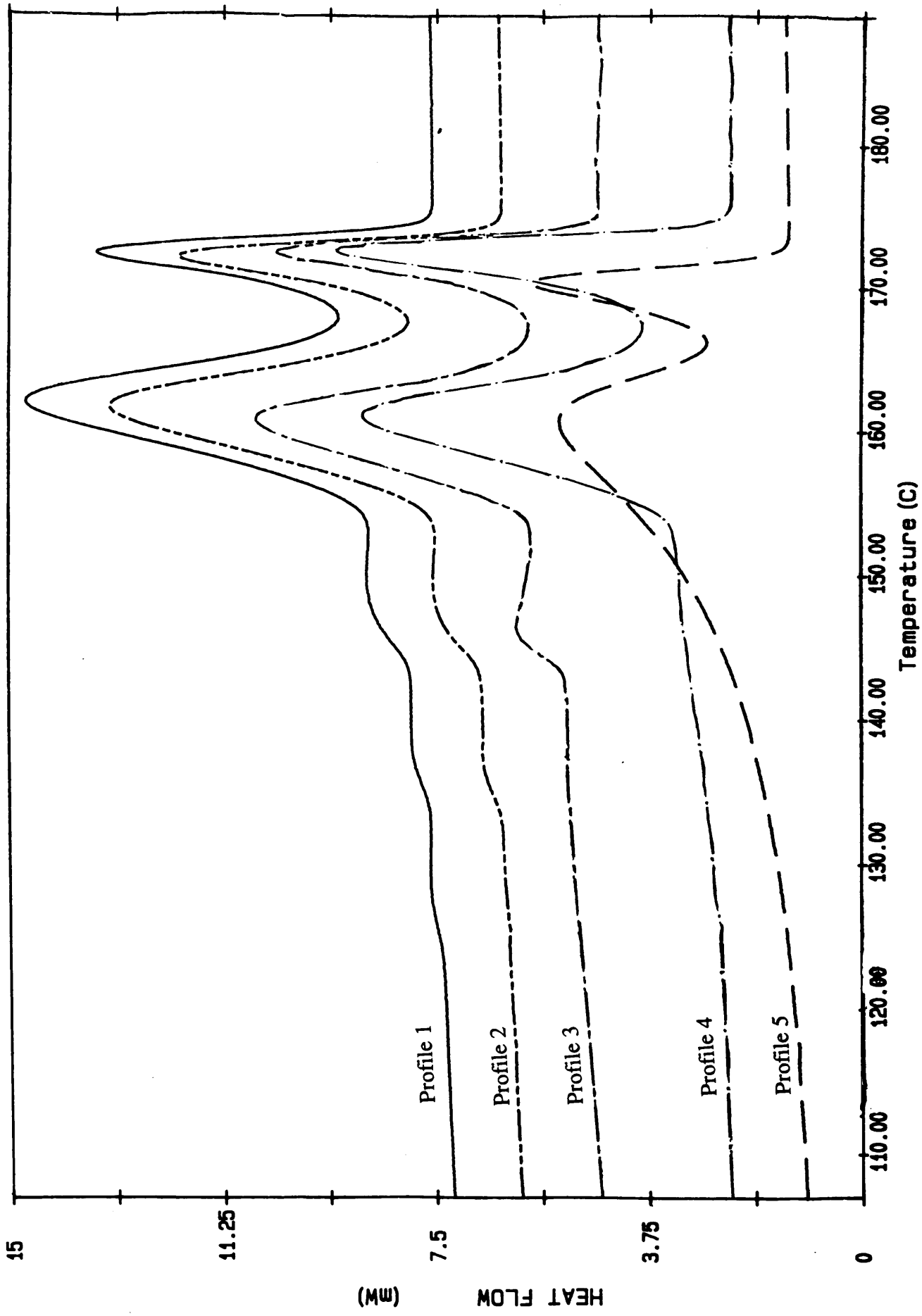

Figure 4.62 DSC melting endotherms of GSE18 polypropylene annealed in a successively downward fashion to differing degrees

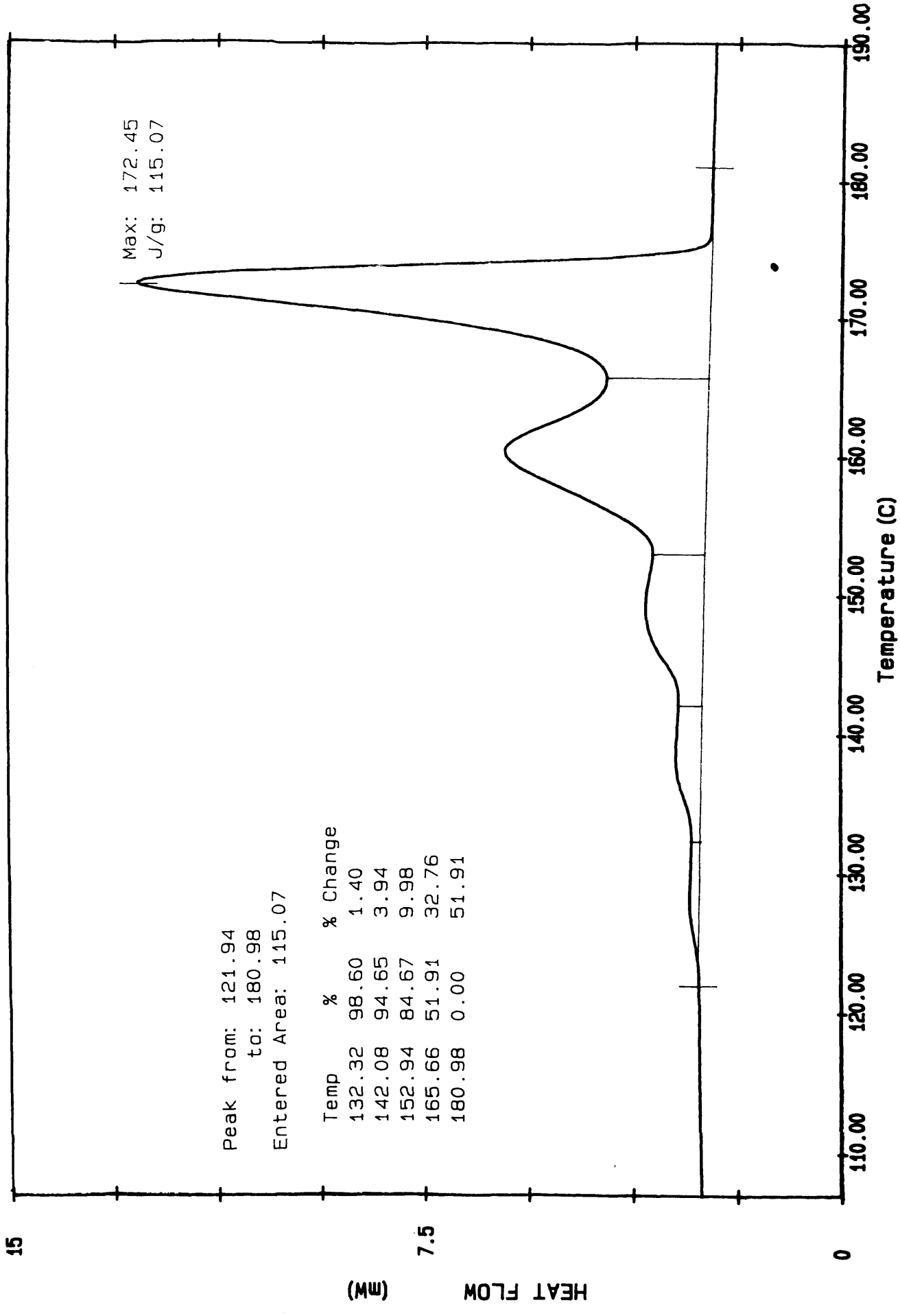

Figure 4.63 DSC profile showing partial areas analysis for a successively downward annealed GSE18 polypropylene sample

Triplicate samples of the GSE18 polypropylene fractions were annealed and analysed in this way and the results for the mean areas and peak positions are presented in Tables 4.43 and 4.44 respectively. Typical melting thermograms of the fractions subsequent to the stepwise downward annealing procedure are shown in Figure 4.64. The ether and pentane fractions are not shown as it was difficult to obtain an adequate signal in the DSC for them. Figure 4.65 shows the hexane and heptane fractions on a larger scale.

	Total	Partial Areas									
	ΔH_f	1		2		3		4		5	
Fraction	(J/g)	%	Area	%	Area	%	Area	%	Area	%	Area
Ether	---	---	---	---	---	---	---	---	---	---	---
Pentane	---	---	---	---	---	---	---	---	---	---	---
Hexane	10.10	94.80	9.58	5.20	0.53	---	---	---	---	---	---
Heptane	37.27	18.80	7.01	12.32	4.59	19.26	7.18	33.16	12.36	16.45	6.13
Toluene	128.43	3.48	4.47	5.08	6.52	9.48	12.18	28.00	35.96	53.90	69.22
Octane	133.48	1.59	2.12	4.41	5.89	9.05	12.08	28.78	38.42	56.15	74.95

Table 4.43 Mean partial areas of each peak for each fraction as a percentage of the mean total heat of fusion (ΔH_f).

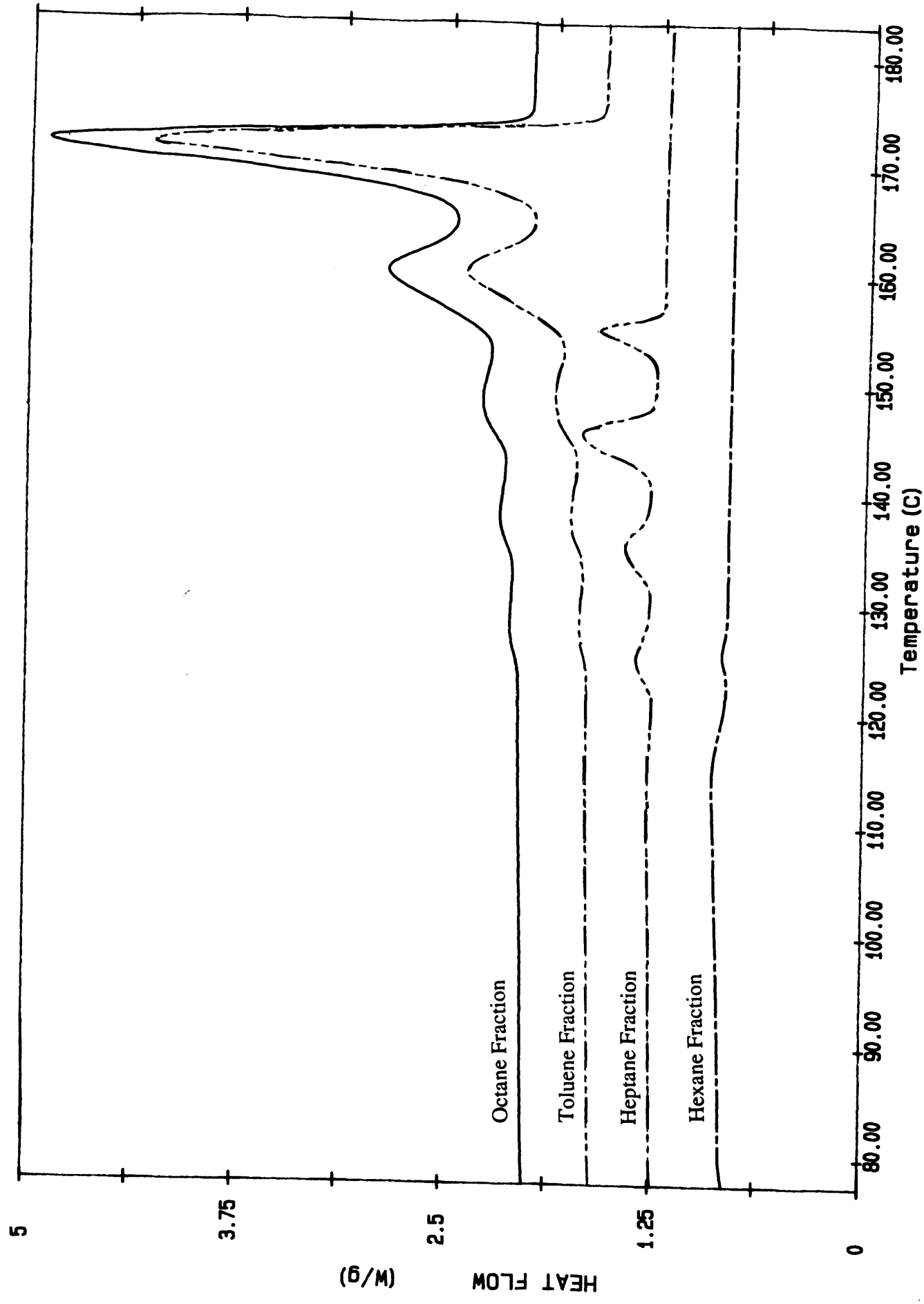

Figure 4.64 Typical melting thermograms of the GSE18 polypropylene fractions subsequent to the stepwise downward annealing procedure

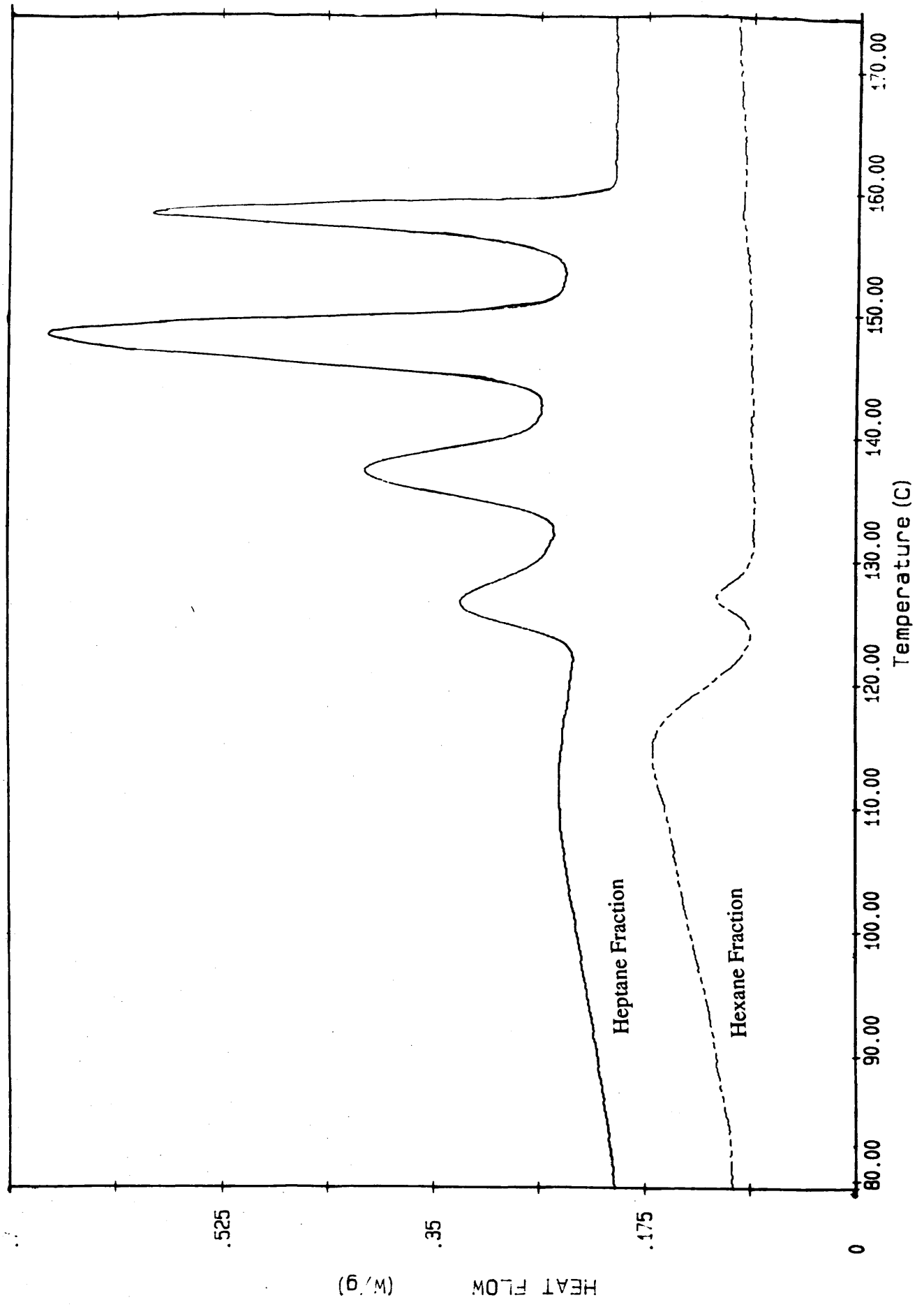

Figure 4.65 Melting profiles for successively downward annealed hexane and heptane fractions shown on a larger scale

Fraction	Peak Temperature (°C)				
	1	2	3	4	5
Ether	---	---	---	---	---
Pentane	---	---	---	---	---
Hexane	113.89	136.31	---	---	---
Heptane	112.14	126.47	137.13	148.07	158.12
Toluene	128.46	138.09	148.60	160.27	171.72
Octane	129.93	138.66	148.60	160.33	171.73

Table 4.44 Mean peak temperatures in the melting thermograms of successively downward annealed fractions.

4.8.2 Discussion

4.8.2.1 Thermal Behaviour Of The Fractions

When stepwise downward annealing is carried out on GSE18 homopolymer according to the procedure shown schematically in Figure 4.61, five peaks of increasing intensity are observed in the subsequent melting profile. The position of the peaks are approximately 10°C higher than the annealing temperature (T_a). Using a similar annealing procedure on an ethylene-butene copolymer, Gray and Casey[163] obtained six separate peaks for samples annealed at successively decreasing temperature intervals of 10°C and twelve peaks for those annealed at decreasing temperature intervals of 5°C. The occurrence of these peaks was attributed to discontinuous crystallite distributions which are formed as a result of the annealing temperature.

In the GSE18 polypropylene homopolymer sample annealed in this manner (Figure 4.63), the peak at circa 172°C is obtained as a result of annealing at 160°C. If the

polymer had been allowed to cool slowly without interuptions, then a corresponding continuous distribution of crystallite size and/or perfection would have been obtained. However, since the polypropylene had been cooled rapidly from the liquid state at 200°C to 70°C and held there for 3 minutes prior to heating at 10°C/min to T_a= 160°C (a temperature at which a large proportion of polypropylene molecules are in the liquid state), crystallites of higher order which are not molten at this temperature are able to rearrange themselves to obtain an even higher degree of perfection. This produces a discrete cluster of crystallite sizes and/or perfections which have obtained a greater stability at this temperature, hence the reason for the melting of these crystallites at circa 10°C higher than T_a. When cooled from 160°C to 70°C no change occurs in the crystallites characteristic of the 160°C anneal whilst the molten material crystallises with a broad distribution of crystallite sizes and perfections. During the next annealing step of T_a = 150°C, crystallites which would normally have melted at a temperature a few degrees higher than T_a are able to grow in size and perfection so that they too form a cluster of crystallites of greater order and perfection which are characteristic of T_a= 150°C and which melt at a temperature at about 10°C higher than T_a.

This process occurs for each successively decreasing annealing temperature. From Figure 4.63 it is quite clear that the largest proportion of crystallites in the GSE18 polypropylene homopolymer achieve perfection at the highest annealing temperature with the remaining crystallites achieving perfection to a lesser extent at each successively decreasing T_a. If the polymer had been allowed to crystallise without any special annealing procedure, the melting profile would have been much broader than the individual peaks obtained by stepwise downward annealing and would have exhibited only one peak which would have had its maximum[140] at circa 160°C.

The stepwise downward annealing procedure, then, provides information about the crystallite distribution in the sample under analysis. For the GSE18 polypropylene homopolymer under these conditions it can be seen that a large proportion of the polymer is capable of achieving a very high degree of perfection on annealing at 160°C. This reflects the high isotacticity and molecular weight of the polypropylene (*mmmm* = 0.864; $\overline{M}_n$= 61610, $\overline{M}_w$= 376400). It has relatively few crystallites which achieve greater perfection at the lower annealing temperatures.

The discontinuous crystallite size model can also be applied to a variation on this annealing procedure detailed in Table 4.42 and shown in Figure 4.62. For profile 1, the situation is similar to that described for Figure 4.63. For profile 2, it can be seen that there are no crystallites which have achieved greater perfection in order to form a distinct peak at circa 130°C and hence it is assumed that these crystallites have melted gradually, thus showing an inclining baseline only. For profile 3, no annealing has taken place at 120°C or 130°C and hence no crystallite clusters of improved perfection and size have been formed which melt at 130°C and 140°C respectively, and again, only an inclining baseline characteristic of gradual continuous melting is observed. Since annealing was carried out at T_a = 160°, 150° and 140°C, peaks appear at circa 172°, 160° and 150°C repectively which are characteristic of the associated crystallite clusters of improved quality for the annealing temperatures. For profile 4, there were only two annealing temperatures ie. 160 and 150°C and consequently only two peaks were obtained, one corresponding to T_a = 150°C and the other to T_a= 160°C. There were no distinct peaks at 130, 140 or 150°C, only an inclining baseline, again, indicative of continuous gradual melting. For profile 5, only one annealing temperature was used. It may have been expected to obtain only one peak at circa 172°C for this anneal but this was not the case and two peaks were exhibited. The reason for this is that only a certain portion of the polypropylene is still in the solid state at this temperature and therefore only those crystallites in the

solid state can grow and perfect themselves. On remelting of the polypropylene after this anneal, a broad melting peak characteristic of the crystallite distribution which was molten at the annealing temperature of 160°C and a peak at circa 172°C were obtained. The broad lower temperature peak has its maximum at circa 160°C but its melting onset occurs at a much lower temperature indicative of a broad distribution of crystallite sizes formed on cooling.

If the annealing time had been longer[140] then it is possible that a larger and broader peak would have been obtained at circa 172°C as molten crystallites nucleated on the existing crystallistes and thickening of lamellae occurred. At the same time the peak at 160°C would have become less intense and shifted to a lower value.

If the discontinuous crystallite distribution model is applied to the molecular weight/tacticity fractions for the stepwise downward annealing procedure at decreasing annealing temperature intervals of 10°C between 160°C and 120°C inclusively (Figures 4.64 and 4.65), then using the GSE18 homopolymer as a reference, information can be obtained on the role of molecular weight/tacticity in the thermal behaviour of the polymer under these conditions.

The profile of the octane fraction which is of relatively high molecular weight and isotacticity (*mmmm* = 0.967; $\overline{M}_n$= 48380, $\overline{M}_w$= 189850) exhibited five peaks whose positions are shown in Table 4.44. Results presented in Table 4.43 show the area under each peak as a percentage of the total ΔH_f for each particular sample profile. For the octane fraction, 56.15% of the total ΔH_f is accounted for by the melting of crystallites which have achieved the highest degree of perfection at T_a = 160°C. The corresponding value for the toluene (*mmmm* = 0.924; molecular weight averages thought to be erroneous for this fraction) is 53.90%. The octane fraction has 28.78% of its total ΔH_f accounted for by the melting of crystallite clusters achieving

perfection at T_a= 150°C whereas the toluene fraction has a corresponding value of 28.00%. In all cases for the remaining peaks, the toluene fraction has a greater proportion of crystallites achieving perfection at each individual T_a. This shows the octane fraction, which contains the highest proportion of crystalline material and has the highest molecular weight, as the fraction most capable of producing the highest percentage of highly ordered crystallites and suggests that the melting profiles subsequent to successive downward annealing are sensitive to the molecular weight/tacticity composition of the polymer. This behaviour is seen throughout the range of polypropylene fractions.

The heptane fraction (*mmmm* = 0.497; $\overline{M}_n$= 14480, $\overline{M}_w$= 83090) exhibits five peaks (Figure 4.65) which have their maximums at values lower than those of the toluene and octane fractions. There are no peaks which correspond to T_a= 160°C since at this temperature all molecules for this fraction were in the liquid state and therefore were unable to undergo enhancement of the crystallite perfection. The peak at 158.12°C corresponds with the melting of crystallites formed at T_a= 150°C. The melting of the crystallites achieving perfection at this temperature accounts for only 16.45% of the total ΔH_f for the fraction which is relatively small compared to the corresponding amount for the toluene and octane fractions. As well as occurring at a lower temperature, the peak is also less intense and narrower than the corresponding peak for toluene and octane fractions, thus indicating a relatively small amount of crystallites achieving perfection at this temperature which occur in a narrower distribution. The peak at around 148°C is attributed to the melting of crystallite clusters characteristic of T_a= 140°C. Again, this has its maximum at a lower temperature than the corresponding peak for the toluene and octane fractions and is also narrower. The area under this peak constitutes the largest portion of the total ΔH_f for the heptane fraction with 33.16% being attributed to the melting of crystallites characteristic of this annealing temperature.

The peaks at 137.13 and 126.47°C are due to T_a= 130°C and 120°C respectively and, again, have a lower peak temperature and are narrower in profile than the corresponding peaks for the octane and toluene fractions. These peaks account for 19.26 and 12.32% of the total ΔH_f respectively. The broad peak at 112.14°C is attributed to a broad distribution of very small poorly formed crystallites which remain in the molten state even at the lowest annealing temperature of 120°C. For this reason, they are unable to perfect themselves to any significant degree and hence exhibit a broad melting range at a low temperature. The melting of these crystallites accounts for 18.80% of the total ΔH_f of the fraction.

The hexane fraction (*mmmm* = 0.362; $\overline{M}_n$= 10970, $\overline{M}_w$= 72150) exhibits only two peaks and shows no response to annealing temperatures of 160°, 150°, 140° or 130°C since at these temperatures all the molecules are in the molten state. Only the peak at 136.31°C, which is very small and broad relative to the same peak for all other fractions, can be attributed to the melting of crystallites which have achieved a higher degree of order due to annealing at 120°C and accounts for 5.20% of the total ΔH_f. Even at 120°C most of the polymer molecules are in the liquid state and therefore unable to form crystallites of greater stability and perfection. This is evident from the broad melting peak at 113.89°C which accounts for 94.80% of the total ΔH_f for this fraction. The pentane and ether fractions gave very poor signals for this annealing procedure and were therefore disregarded.

From these results, it can be seen that differences exist in the thermal behaviour of the fractions subsequent to the stepwise downward annealing procedure. The octane fraction which is highly isotactic and has a relatively high molecular weight, exhibits a higher percentage of crystallites which melt at circa 160°C and 172°C than any other fraction. The toluene fraction also exhibits a large degree of crystallites which

melt at the higher temperatures after annealing, but not as much as the octane fraction. The toluene fraction does, however, exhibit a higher proportion of crystallites melting at temperatures associated with the intermediate and lower annealing temperatures.

The heptane fraction contains a relatively small proportion of crystallites which are capable of achieving a high degree of perfection and stability at annealing temperatures of 150°C and 160°C and consequently most crystallites tended to achieve perfection at the intermediate and lower annealing temperatures for this fraction.

The hexane fraction had no crystallites capable of achieving perfection at temperatures above T_a= 120°C. If the hexane and heptane fractions had been annealed at further decreasing temperatures, then it is possible that crystallite clusters associated with these annealing temperatures would be formed. Admittedly, however, no attempt was made at annealing temperatures less than 120°C.

It is evident, then, that the nature and number of peaks obtained for this particular annealing procedure is highly dependent on the molecular weight/tacticity element of polypropylene. The clusters capable of melting at temperatures of circa 172°C occur only in the highly isotactic/high molecular weight fractions and a relatively larger portion of the crystallite clusters capable of melting at the lower temperatures are found in the fractions of lower stereoregularity and molecular weight.

The GSE18 polypropylene homopolymer exhibits the majority of its crystallite clusters achieving higher order at the annealing temperatures of 160°C and 150°C but not to the same degree as the toluene and octane fractions. It also shows that it contains a sizeable amount of crystallites capable of forming clusters at the intermediate and low annealing temperatures. This result is not entirely unexpected as the homopolymer is considered to be representative of all fractions mixed together.

CHAPTER 5

5.0 BLENDS OF ISOTACTIC POLYPROPYLENE WITH AMORPHOUS POLY-α-OLEFIN TERPOLYMERS

All quoted results in this chapter have estimated error values of:

Density	± 1%
FTIR APRA	± 0.2%
DSC Temperature	± 0.1%
DSC Enthalpy	± 0.1%

5.0 BLENDS OF ISOTACTIC POLYPROPYLENE WITH AMORPHOUS POLY-α-OLEFIN TERPOLYMERS

5.1 INTRODUCTION

Polymer blends have become more and more attractive industrially as economically viable substitutes for more expensive existing materials. They are capable of providing properties as good as, if not better than, the material they are replacing. The pattern of properties possessed by polymer blends can often be better than just those exhibited by the component parts.

One of the most common methods of improving the properties of polypropylene in order to make it more competitive in markets where newer synthetic polymers or already existing polyolefins are successful, is to modify it by composing blends with suitable polymers in order to obtain the desired performance characteristics.

The majority of polypropylene blends are concerned with the modification of impact strength at low temperatures and this has been achieved using various elastomers including polyisobutylene[164], polyisoprene[165] and natural rubber[166]. The most effective blends for this application, however, have been with ethylene-propylene (EPR) copolymers[167] and ethylene-propylene-diene (EPDM) terpolymers[168].

Most blend systems involving two or more polymers are immiscible due to low entropies of mixing and this results in an inhomogeneous mixture which can have high interfacial tension and consequently poor adhesion between components which in turn, leads to depleted mechanical properties. To overcome this problem of inhomogeneity, immiscible polymers can be melted in the presence of interfacially active substances which "compatabilise" the different polymer phases. Another

method of "compatibilising" immiscible blends is by "chemical mixing". This involves optimising conditions of copolymerisation in order to obtain tailored copolymers whose phase morphologies are virtually independent of processing parameters and are only dictated by the block length distribution. Lohmar and Meyer[169] termed the blend morphologies of the "compatibilised" material as being "extrinsically determined" (dependent on exterior parameters) and "intrinsically determined" (phase morphologies which are determined by the system itself) respectively.

In the present study, isotactic polypropylene blends with amorphous poly-α-olefin terpolymers were investigated. The terpolymers used in this study (under the trade name of Vestoplast) are specifically ethylene-propylene-butene-1 terpolymers which are high in propylene content and are tailor made by copolymerising the ethylene, propylene and butene-1 monomer gases at low pressure in the presence of a Zeigler-Natta catalyst. Variations in the process parameters such as temperature, choice of catalyst and monomer feed can be made in order to produce products which have well defined softening points, melt viscosity, crystallinity and hardness characteristics. Figure 5.0 shows the polymerisation of polypropylene compared to that of poly-α-olefins.

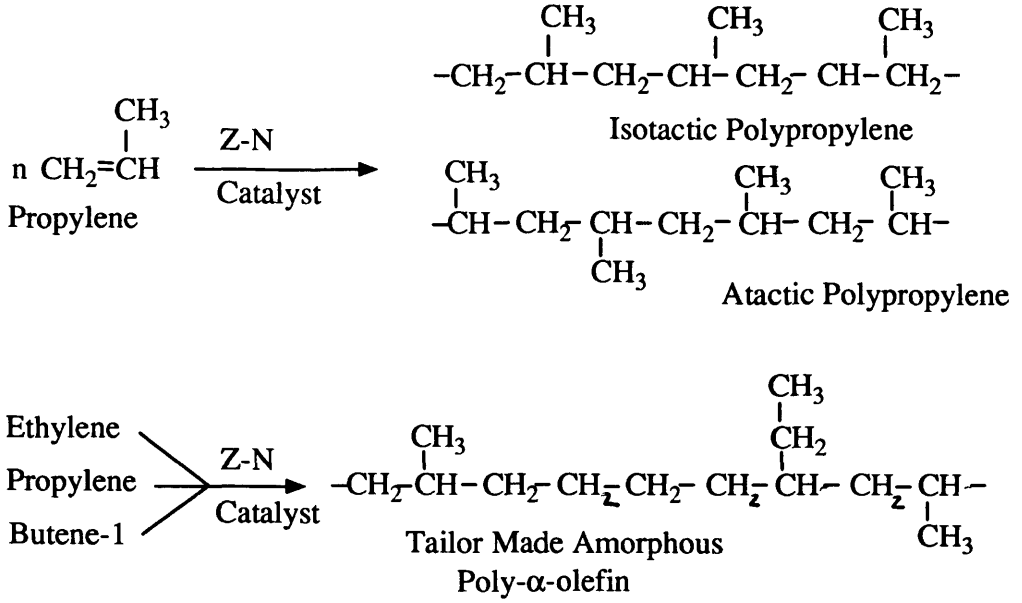

Figure 5.0 Scheme showing polymerisation of amorphous poly-α-olefins.

Amorphous terpolymers of this type variously used in this study were Vestoplast 703, 708 and 750 (abbreviated in this thesis to Vest703, Vest708 and Vest750 respectively). The first digit in the number code refers to the composition of the terpolymer and in this case the number "7" indicates that it is high in propylene content. The last two digits describe the viscosity of the polymer measured at 190°C. The manufacturer's (Hüls) specifications for physical properties of the three grades above are shown in Table 5.0.

Property	Vest703	Vest708	Vest750
Melt viscosity at 190°C	3000	8000	50000
Softening point, ring and ball (°C)	125	105	110
Density at 23°C (g/cm^3)	0.87	0.87	0.87
Molecular weight ($\bar{M}_v$)	35000	45000	70000
Intrinsic viscosity (100 ml/g)	0.45	0.55	0.85

Table 5.0 Manufacturer's specification[170] for physical properties for the amorphous poly-α-olefin terpolymers used in this study.

The isotactic polypropylene used to compose blends was a commercial grade polypropylene manufactured by Shell ($\bar{M}_n$= 68545, $\bar{M}_w$= 342100). Blends were prepared in the ratios of Shell:Vest, 25:75, 50:50 and 75:25 weight percent by procedures described in section 3.5. Investigations into the nature of the blends were carried out using a variety of techniques, including, DSC, infrared spectroscopy, density measurements, GPC, hot-stage polarised light microscopy and x-ray diffraction.

The effect of rapidly quenching the blends from the molten state was assessed and infrared spectroscopy was used to monitor changes in the helical content of the resultant structures. High temperature infrared spectroscopy was used to monitor the temperatures of helical extinction in the blends.

The blends were also subjected to the stepwise downward annealing procedure described in section 4.8.1 in order to study their thermal behaviour in terms of crystallite distribution and associated melting.

5.2 EXPERIMENTAL

5.2.1 Characterisation Of The Blends

Characterisation of the Shell:Vest blends was carried out in order to establish the effect of amorphous poly-α-olefin terpolymers on the structure, miscibility and general behaviour of the resultant polymer system. The blend involving Vest703 terpolymer was the most widely studied with the blends involving Vest708 and Vest 750 being used for comparative purposes.

5.2.1.1 Miscibility Of The Components

DSC and hot-stage polarised microscopy were used in order to assess the miscibility of the two components in the blend involving the Vest703 terpolymer.

5.2.1.1.1 Differential Scanning Calorimetry

Equal weights of the unblended Shell isotactic polypropylene (iPP) and Vest703 were encapsulated in 50μl aluminium DSC sample pans according to procedures described in section 3.7.

The unblended components were heated to 200°C and held for 5 minutes before recording the cooling run at a rate of 10°C/min to 30°C. Whilst in the liquid state at 200°C, the two components were able to mix by flowing into one another. The heating and cooling cycle was repeated 14 times with the degree of melt blending increasing after each cycle. Crystallisation data at various stages throughout the 14 heat/cool cycles are shown in Table 5.1. Figure 5.1 shows the corresponding DSC crystallisation profiles.

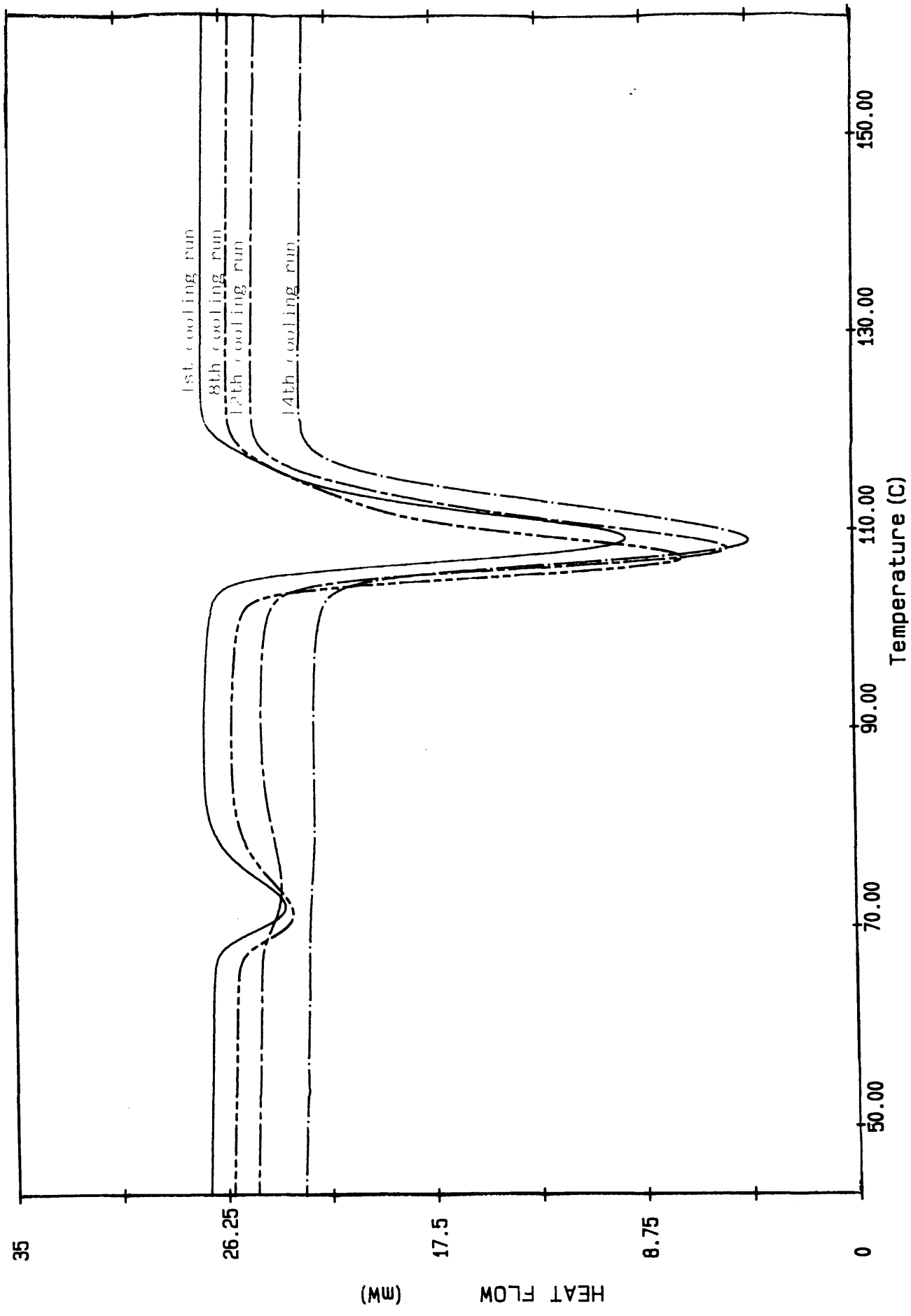

Figure 5.1 DSC crystallisation profiles of Shell : Vest703 at various stages of co-crystallisation

Cooling Run No.	Peak 1 T_c Onset (°C)	Peak 1 $-\Delta H_c$ (J/g)	Peak 2 T_c Onset (°C)	Peak 2 $-\Delta H_c$(J/g)
1	78.47	8.73	115.12	47.32
8	78.96	8.38	112.76	47.83
12	83.36	4.06	114.70	49.30
14	---	---	116.25	52.01

Table 5.1 Crystallisation data for various stages in the heat/cool cycles for the two components (iPP and Vest703) of the blend in the same sample pan.

5.2.1.1.2 Hot-Stage Polarised Light Microscopy

Equal weights of the two components (iPP and Vest703) were placed between two glass microscope slides and melted at 200°C for 5 minutes on the hot-stage. At this temperature the components were in the liquid state and could therefore undergo a certain degree of "self-mixing" before being cooled at 10°C/min to 30°C. Crystallisation was monitored at cross-polars by polarised light microscopy. The heat/cool cycle was repeated several times and results were recorded by photography. Optical micrographs showing the crystallised blend at different stages of the "self-mixing" process are shown at two magnifications in Figures 5.2 - 5.5.

Co-crystallisation
Run 1

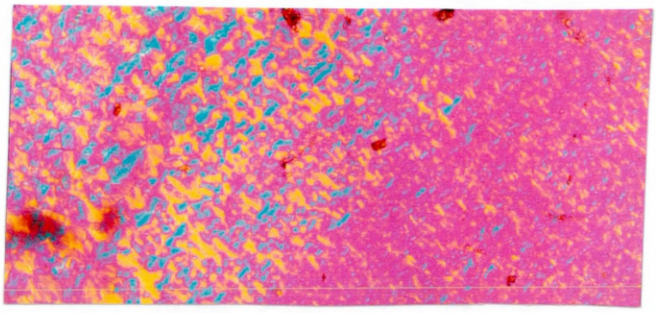

Low Magnification

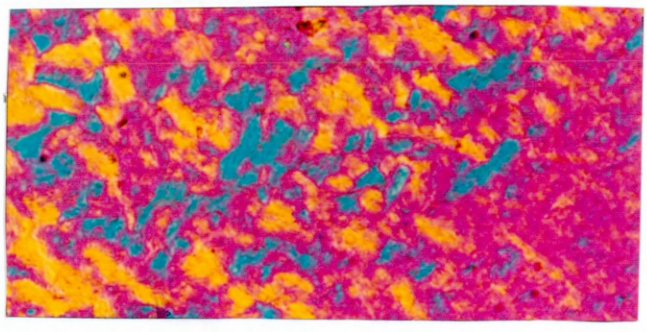

High Magnification

Figure 5.2 Optical micrographs showing spherulites of the Shell : Vest703 blend at high and low magnifications after the 1st co-crystallisation run

Co-crystallisation
Run 8

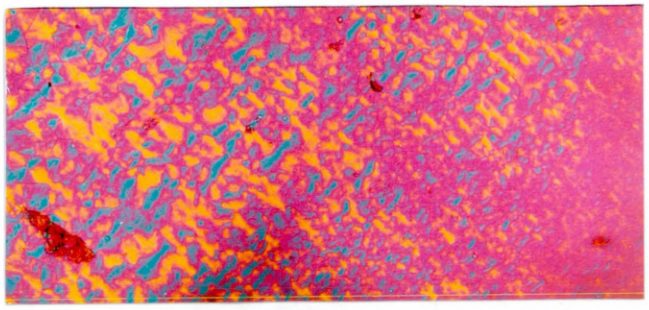

Low Magnification

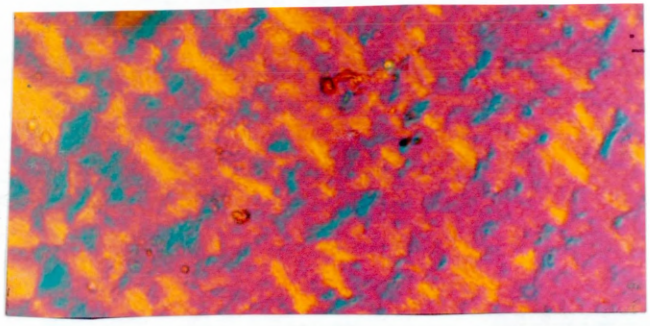

High Magnification

Figure 5.3 Optical micrographs showing spherulites of the Shell : Vest703 blend at high and low magnifications after the 8th co-crystallisation

Co-crystallisation
Run 12

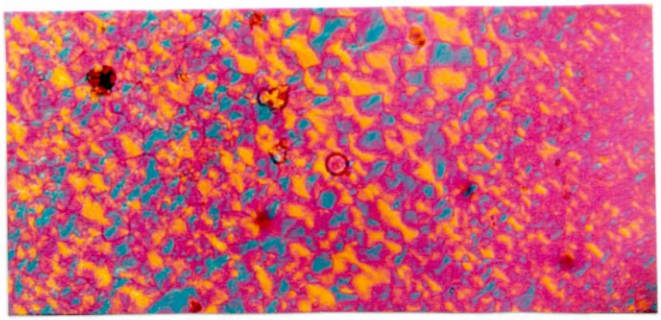

Low Magnification

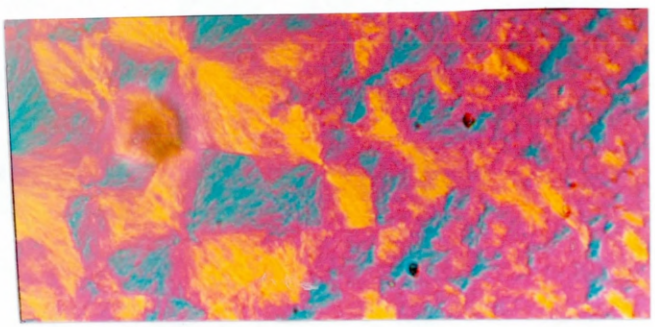

High Magnification

Figure 5.4 Optical micrographs showing spherulites of the Shell : Vest703 blend at high and low magnifications after the 12th co-crystallisation run

Co-crystallisation
Run 14

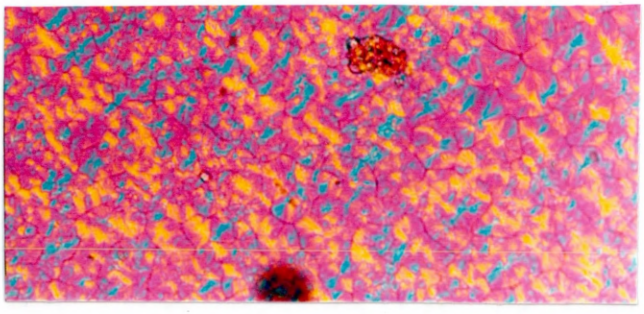

Low Magnification

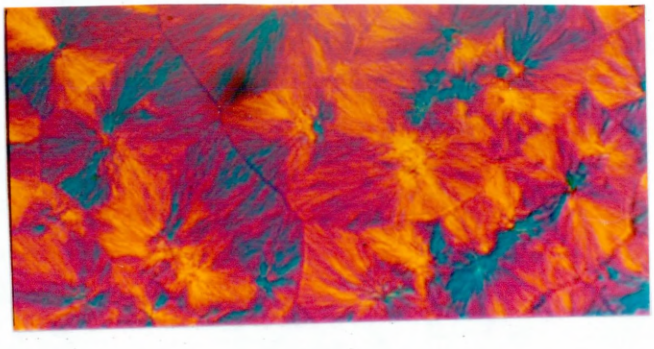

High Magnification

Figure 5.5 Optical micrographs showing spherulites of the Shell : Vest703 blend at high and low magnifications after the 14th co-crystallisation run

5.2.1.2 FTIR Absorption Peak Ratio Analysis (APRA)

FTIR APRA (section 4.3.2) was carried out on the blends in order to assess the effect of blending isotactic polypropylene with the Vest703, 708 and 750 terpolymers on the helical content of the resultant polymer systems.

Triplicate film samples of the blends were prepared according to the procedure described in section 3.2.1 and cooled at room temperature before annealing at 150°C for 10 minutes and slow cooling to 30°C under a nitrogen atmosphere in the vacuum oven.

Data showing mean FTIR APRA results for the A998/A973 and A841/A973 absorption ratios for blends of iPP with Vest703, 708 and 750 are presented in Tables 5.2 - 5.4. The ratio values for 100% Shell iPP and 100% Vest are included in each case. Figures 5.6 and 5.7 show graphs of the A998/A973 and A841/A973 infrared absorption ratios respectively versus blend composition for the various Shell:Vest blends.

Blend Shell:Vest703	Absorption Ratio	
	A998/A973	A841/A973
0 : 100	0.503	0.320
25 : 75	0.802	0.683
50 : 50	0.875	0.790
75 : 25	0.975	0.805
100 : 0	1.000	0.810

Table 5.2 Mean FTIR APRA results for the Shell:Vest703 blends.

Blend Shell:Vest708	Absorption Ratio	
	A998/A973	A841/A973
0 : 100	0.424	0.264
25 : 75	0.719	0.555
50 : 50	0.865	0.721
75 : 25	1.019	0.812
100 : 0	1.000	0.810

Table 5.3 Mean FTIR APRA results for the Shell:Vest708 blends.

Blend Shell:Vest750	Absorption Ratio	
	A998/A973	A841/A973
0 : 100	0.433	0.255
25 : 75	0.727	0.592
50 : 50	0.898	0.763
75 : 25	0.986	0.809
100 : 0	1.000	0.810

Table 5.4 Mean FTIR APRA results for the Shell:Vest750 blends.

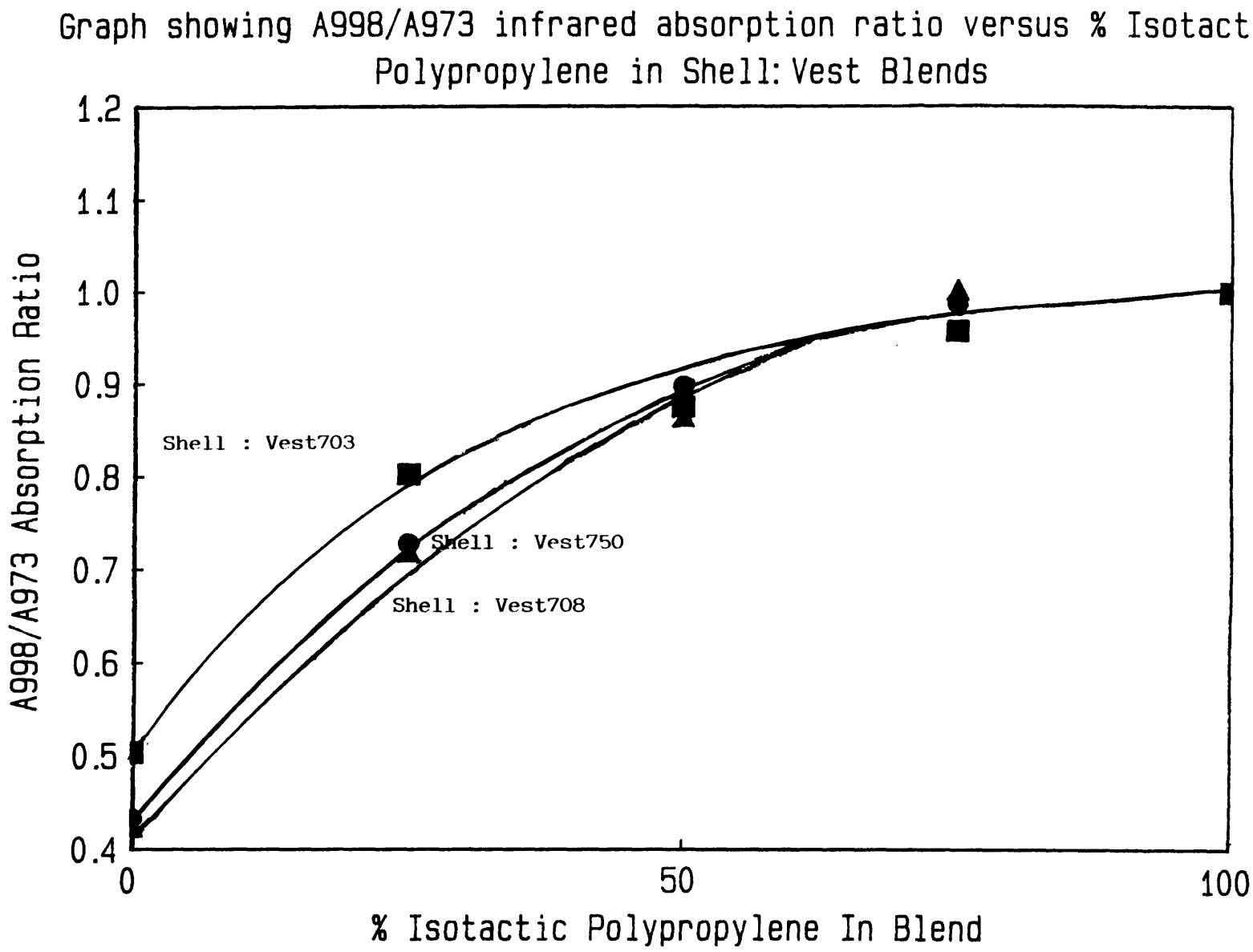
Graph showing A998/A973 infrared absorption ratio versus % Isotactic Polypropylene in Shell: Vest Blends
A998/A973 Absorption Ratio
1.2
1.1
1.0
0.9
0.8
0.7
0.6
0.5
0.4
0
50
100
% Isotactic Polypropylene In Blend
Shell : Vest703
Shell : Vest750
Shell : Vest708

Figure 5.6

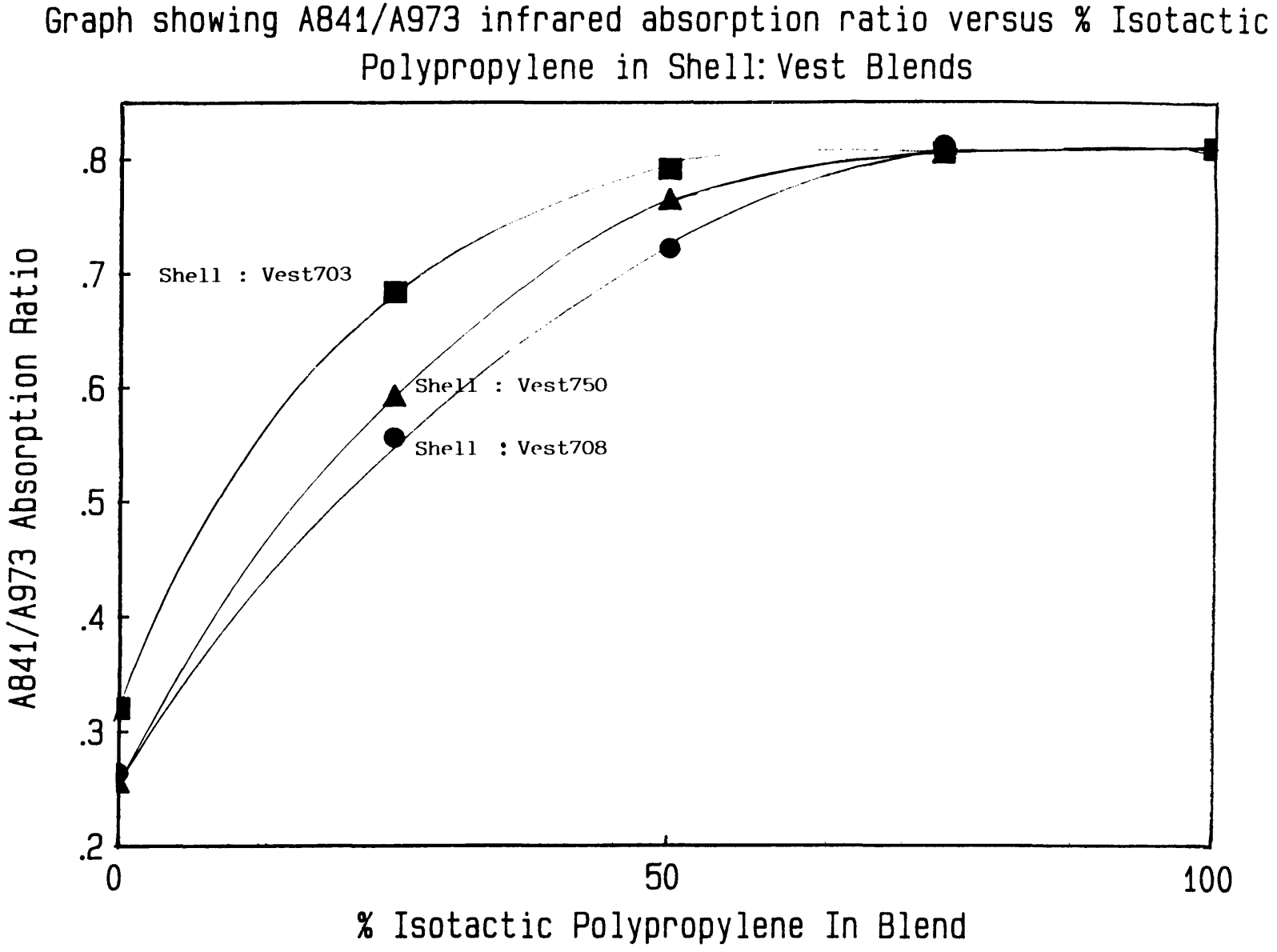
Graph showing A841/A973 infrared absorption ratio versus % Isotactic Polypropylene in Shell: Vest Blends
A841/A973 Absorption Ratio
.8
.7
.6
.5
.4
.3
.2
Shell : Vest703
Shell : Vest750
Shell : Vest708
0
50
100
% Isotactic Polypropylene In Blend

Figure 5.7

5.2.1.3 Density Measurements

Density measurements were carried out in triplicate on the blend samples (annealed at 150°C for 10 minutes and allowed to cool slowly to 30°C under a nitrogen atmosphere in the vacuum oven) using the flotation method as described in section 3.13. Results showing the mean densities for each blend are presented in Tables 5.5 - 5.7. Figure 5.8 shows the relationship between blend composition and density for the blends involving the Vest703, 708 and 750 terpolymers.

Blend Shell:Vest703	Density (g/ml)
0 : 100	0.8818
25 : 75	0.8911
50 : 50	0.9004
75 : 25	0.9072
100 : 0	0.9131

Table 5.5 Mean density results for the Shell:Vest703 blends.

Blend Shell:Vest708	Density (g/ml)
0 : 100	0.8670
25 : 75	0.8803
50 : 50	0.8964
75 : 25	0.9056
100 : 0	0.9131

Table 5.6 Mean density results for the Shell:Vest708 blends.

Figure 5.8

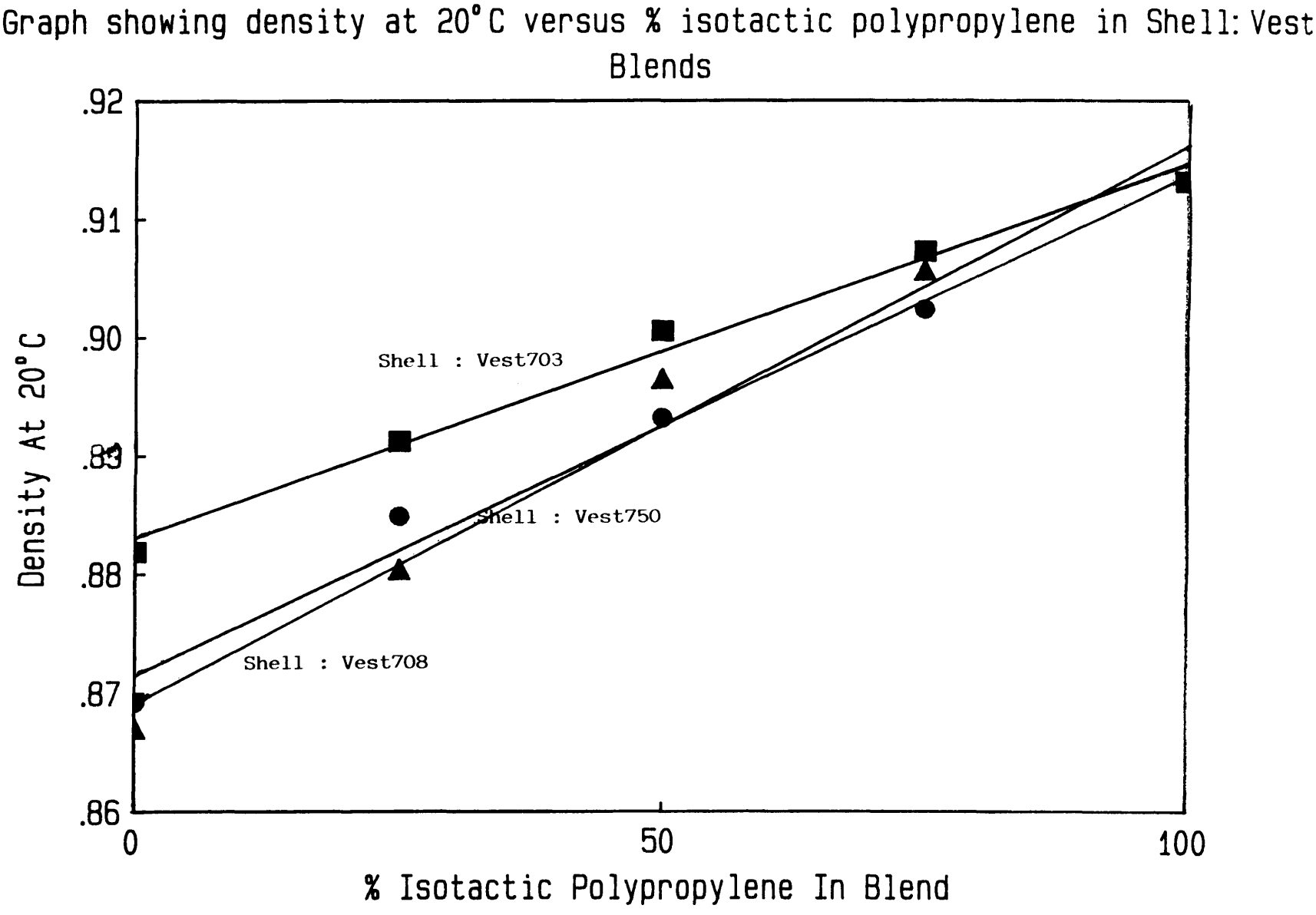
Graph showing density at 20°C versus % isotactic polypropylene in Shell: Vest Blends
.92
.91
.90
.89
.88
.87
.86
Density At 20°C
Shell : Vest703
Shell : Vest750
Shell : Vest708
0
50
100
% Isotactic Polypropylene In Blend

Blend Shell:Vest750	Density (g/ml)
0 : 100	0.8692
25 : 75	0.8848
50 : 50	0.8931
75 : 25	0.9023
100 : 0	0.9131

Table 5.7 Mean density results for the Shell:Vest750 blends.

5.2.1.4 Molecular Weight Measurements

Molecular weight measurements were carried out in duplicate on the blends at 140°C by high temperature gel permeation chromatography according to conditions described in section 2.4.3. Tables 5.8 - 5.10 show molecular weight data for each blend composition for blends involving Vest703, 708 and 750. Molecular weight data for the 100% Shell iPP and 100% Vest samples are included in each case.

Blend Shell:Vest703	$\bar{M}_n/10^3$	$\bar{M}_w/10^3$	$\bar{M}_z/10^3$	$\bar{M}_p/10^3$	$\bar{M}_v/10^3$	$\bar{M}_w/\bar{M}_w$
0 : 100	5.29	42.00	126.25	20.14	34.19	7.942
25 : 75	7.08	104.35	268.55	25.62	81.10	14.738
50 : 50	6.91	109.15	610.90	24.60	84.16	15.788
75 : 25	16.42	231.20	700.65	168.75	196.45	14.085
100 : 0	68.55	342.10	1059.00	203.60	2979.00	5.002

Table 5.8 Mean molecular weight data for the Shell:Vest703 blends.

Blend Shell:Vest708	$\bar{M}_n/10^3$	$\bar{M}_w/10^3$	$\bar{M}_z/10^3$	$\bar{M}_p/10^3$	$\bar{M}_v/10^3$	$\bar{M}_w/\bar{M}_w$
0 : 100	7.52	56.76	216.70	41.99	47.66	7.546
25 : 75	12.31	171.05	640.30	77.18	140.85	13.898
50 : 50	9.93	122.40	573.95	54.43	98.11	12.332
75 : 25	19.66	242.05	728.25	164.10	206.80	12.467
100 : 0	68.55	342.10	1059.00	203.60	297.90	5.002

Table 5.9 Mean molecular weight data for the Shell:Vest708 blends.

Blend Shell:Vest750	$\bar{M}_n/10^3$	$\bar{M}_w/10^3$	$\bar{M}_z/10^3$	$\bar{M}_p/10^3$	$\bar{M}_v/10^3$	$\bar{M}_w/\bar{M}_w$
0 : 100	11.05	90.18	364.15	60.34	75.76	8.176
25 : 75	13.47	126.10	469.75	68.08	105.50	9.364
50 : 50	17.73	179.10	598.70	95.30	151.20	10.104
75 : 25	23.01	231.40	633.85	292.50	199.00	10.057
100 : 0	68.55	342.10	1059.00	203.60	297.90	5.002

Table 5.10 Mean molecular weight data for the Shell:Vest750 blends.

5.2.1.5 Wide Angle X-ray Diffraction (WAXD)

Wide angle x-ray diffraction was carried out for each blend composition (annealed at 150°C for 10 minutes and allowed to cool slowly in an inert atmosphere) involving Shell iPP blends with Vest703, 708 and 750 according to the conditions described in section 2.3.5*(i)*. The x-ray crystallinity was calculated from the relative areas under the crystalline peaks and amorphous scattering regions of the diffractogram. Relative

areas were measured by planimetry (section 4.7.3.8). X-ray crystallinities are presented in Tables 5.11 - 5.13 and graphs showing the relationship between blend composition and x-ray crystallinity are shown in Figures 5.9 - 5.11.

X-ray diffraction profiles of the blends are shown in Figures 5.12 - 5.14 and the corresponding x-ray diffraction angles (2θ) for each composition of each blend are presented in Tables 5.14 - 5.16.

Blend Shell:Vest703	X-ray Crystallinity (%)
0 : 100	15.33
25 : 75	26.27
50 : 50	35.29
75 : 25	47.97
100 : 0	52.96

Table 5.11 X-ray crystallinity values for Shell:Vest703 blends.

Blend Shell:Vest708	X-ray Crystallinity (%)
0 : 100	11.45
25 : 75	20.87
50 : 50	30.00
75 : 25	37.29
100 : 0	52.96

Table 5.12 X-ray crystallinity values for Shell:Vest708 blends.

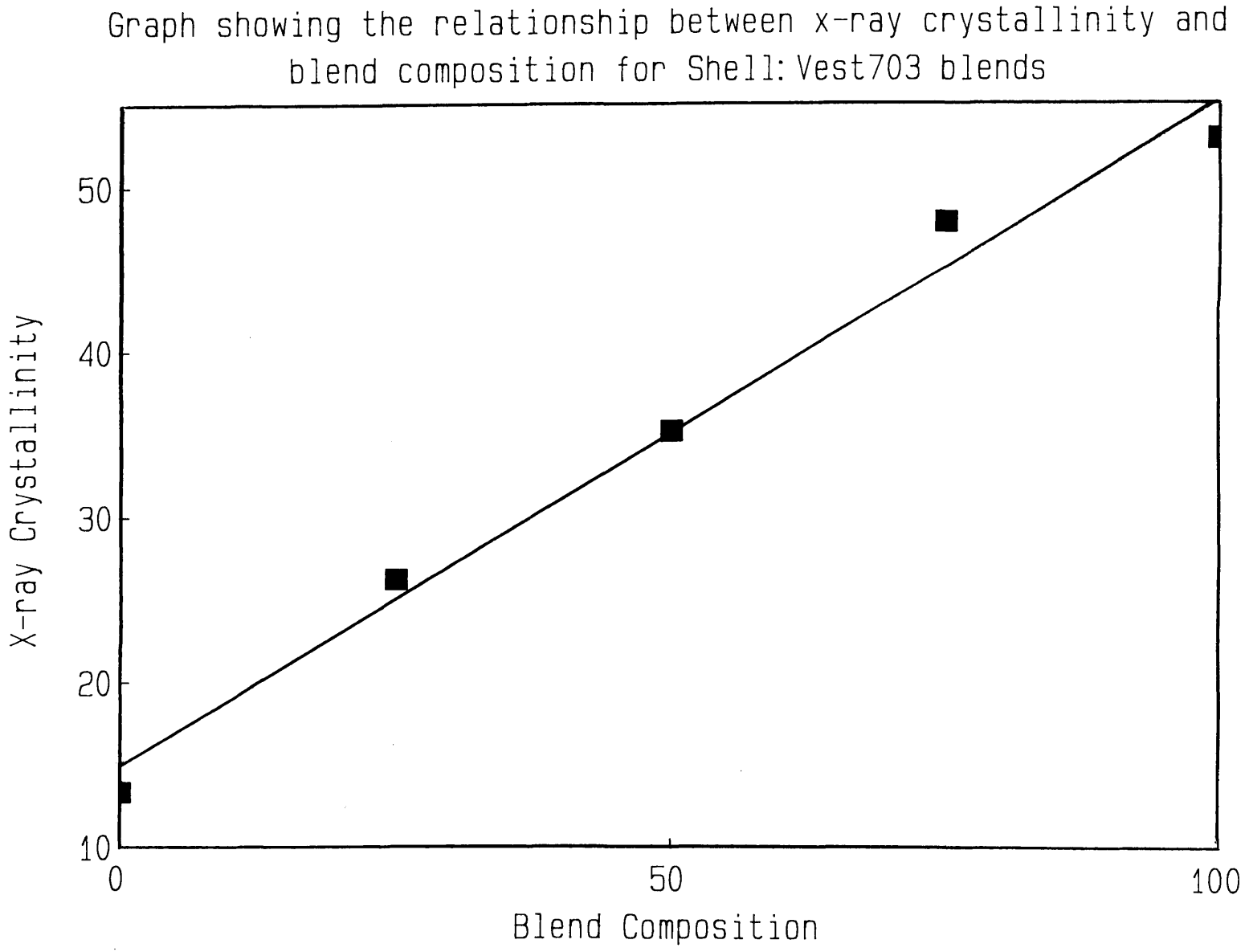
Graph showing the relationship between x-ray crystallinity and blend composition for Shell: Vest703 blends
X-ray Crystallinity
10
20
30
40
50
0
50
100
Blend Composition

Figure 5.9

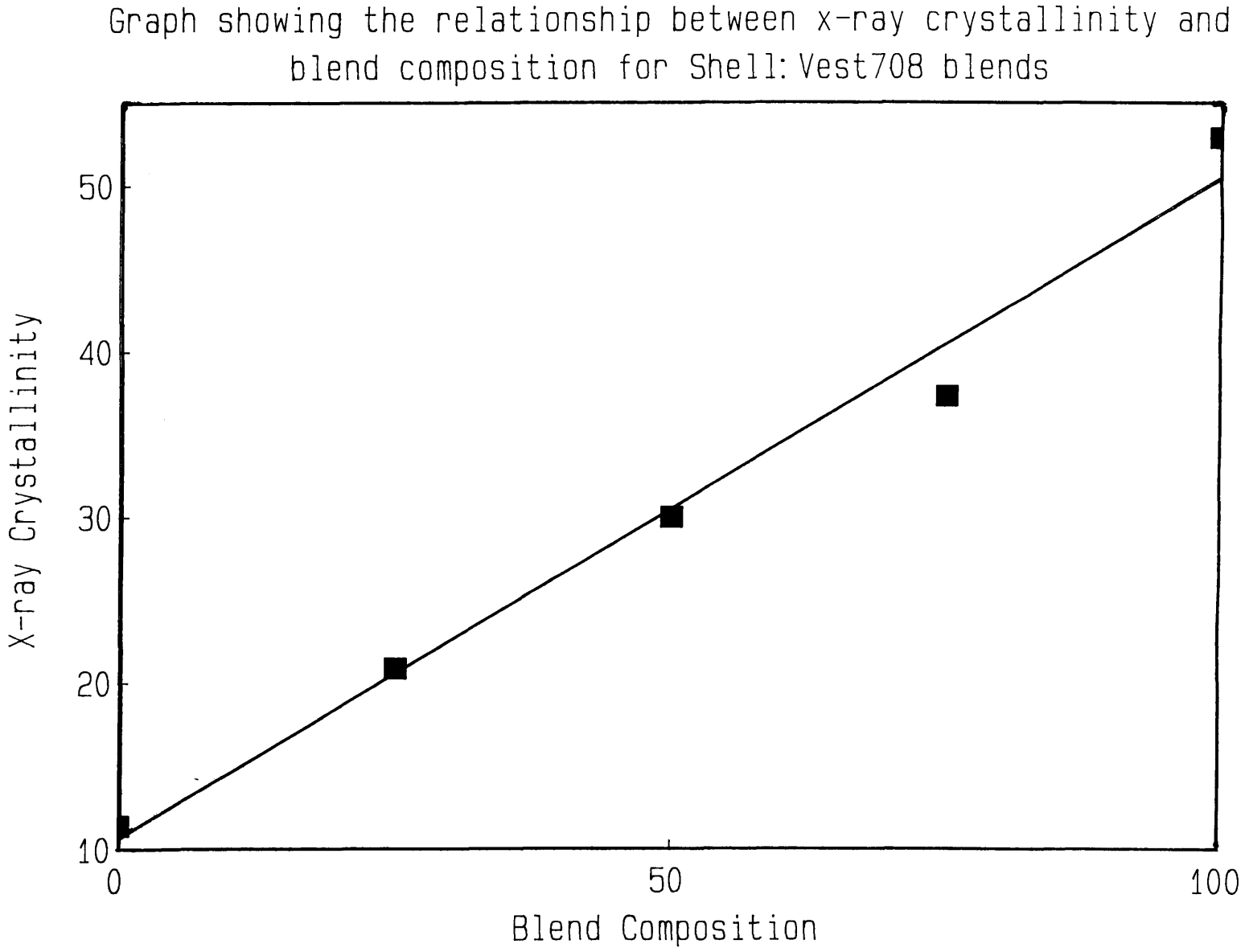
Graph showing the relationship between x-ray crystallinity and blend composition for Shell: Vest708 blends
X-ray Crystallinity
10
20
30
40
50
0
50
100
Blend Composition

Figure 5.10

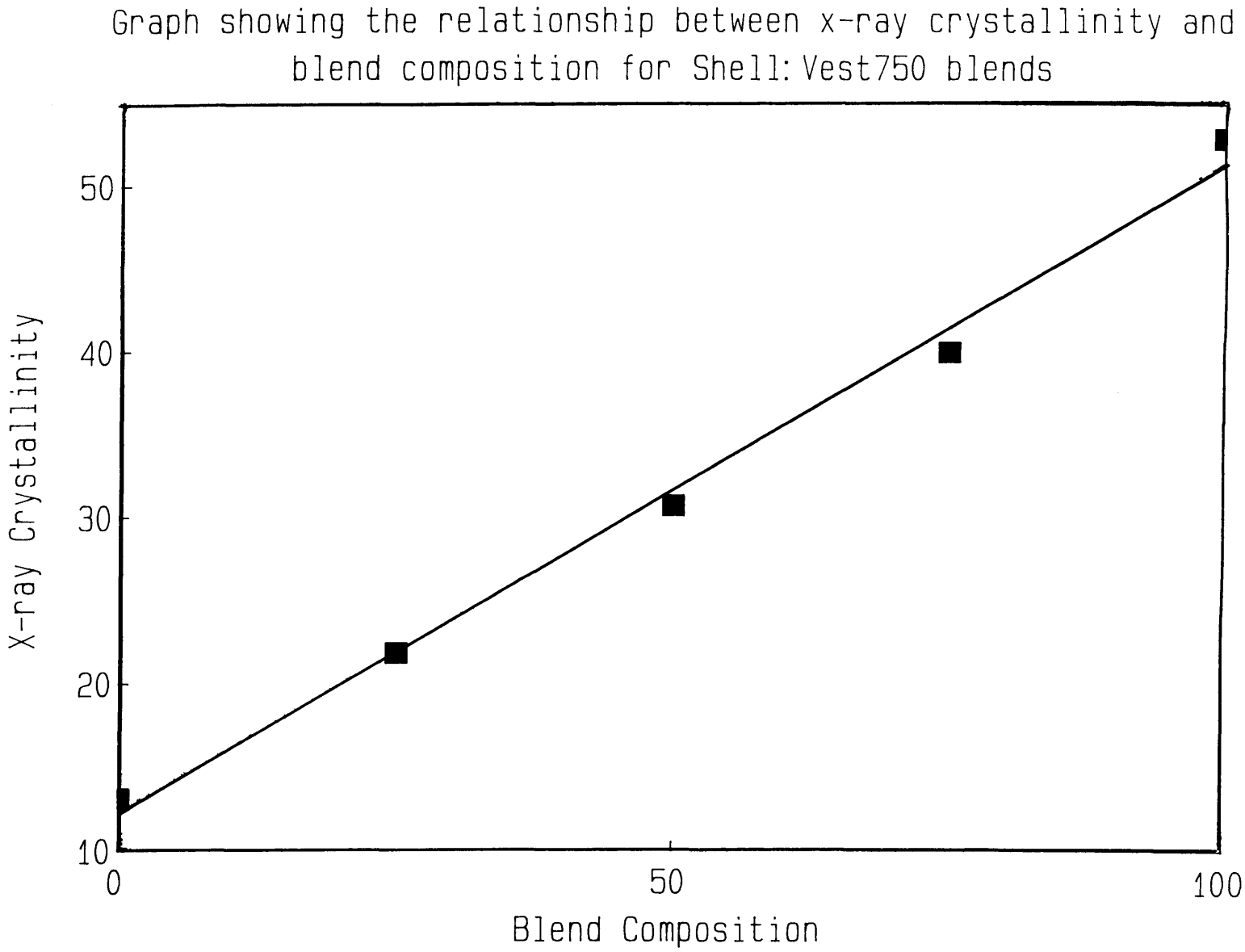
Graph showing the relationship between x-ray crystallinity and blend composition for Shell: Vest750 blends
X-ray Crystallinity
50
40
30
20
10
0
50
100
Blend Composition

Figure 5.11

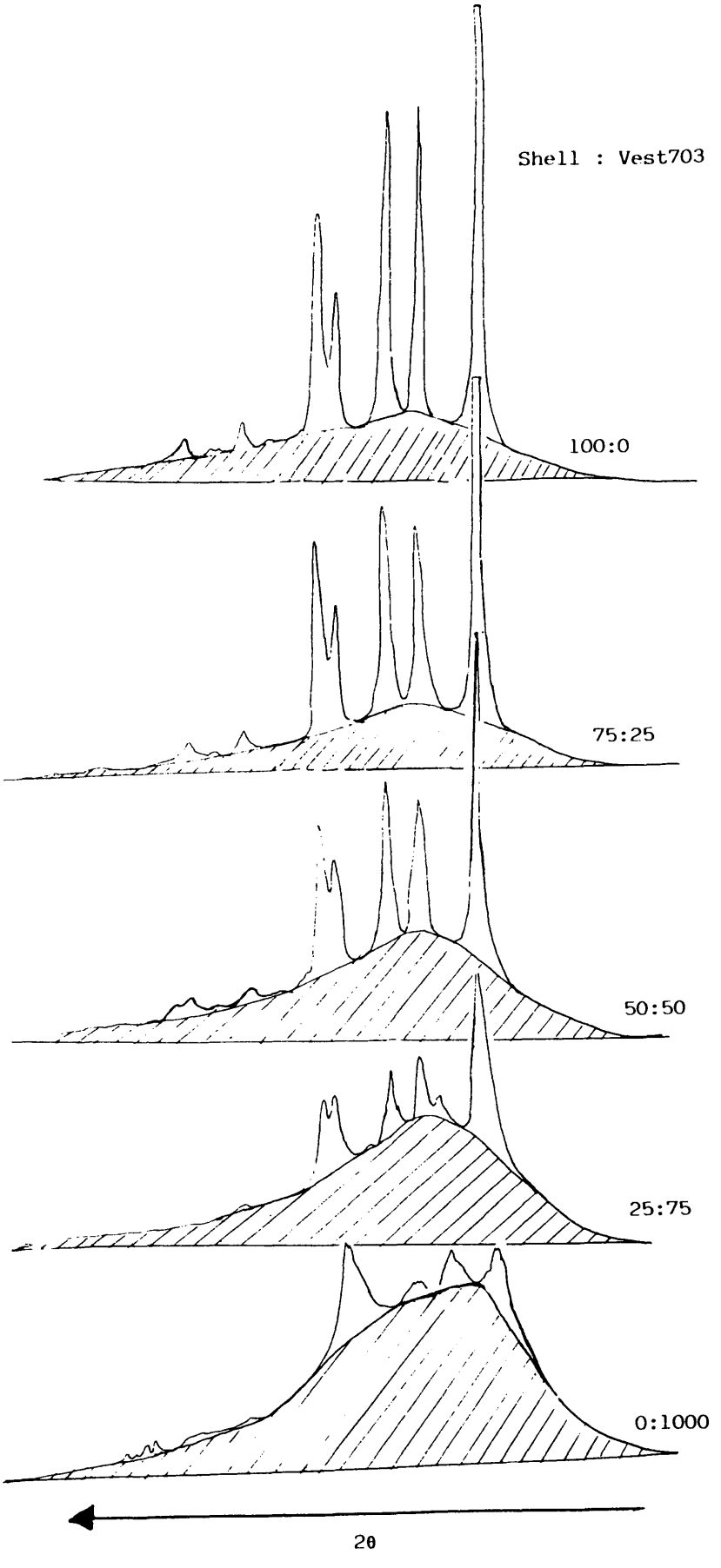

Figure 5.12 X-ray diffractogram profiles for the various Shell : Vest703 blend compositions

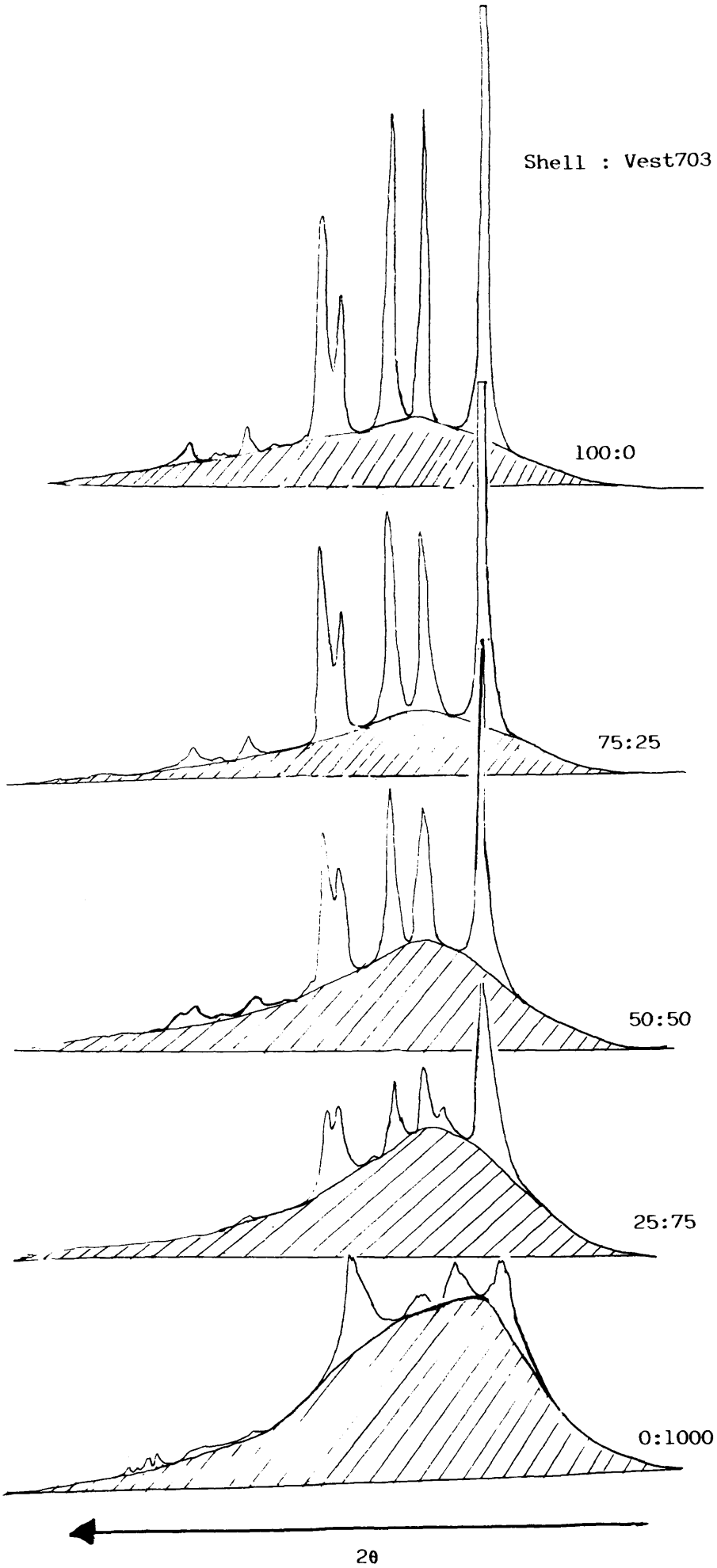

Figure 5.12 X-ray diffractogram profiles for the various Shell : Vest703 blend compositions

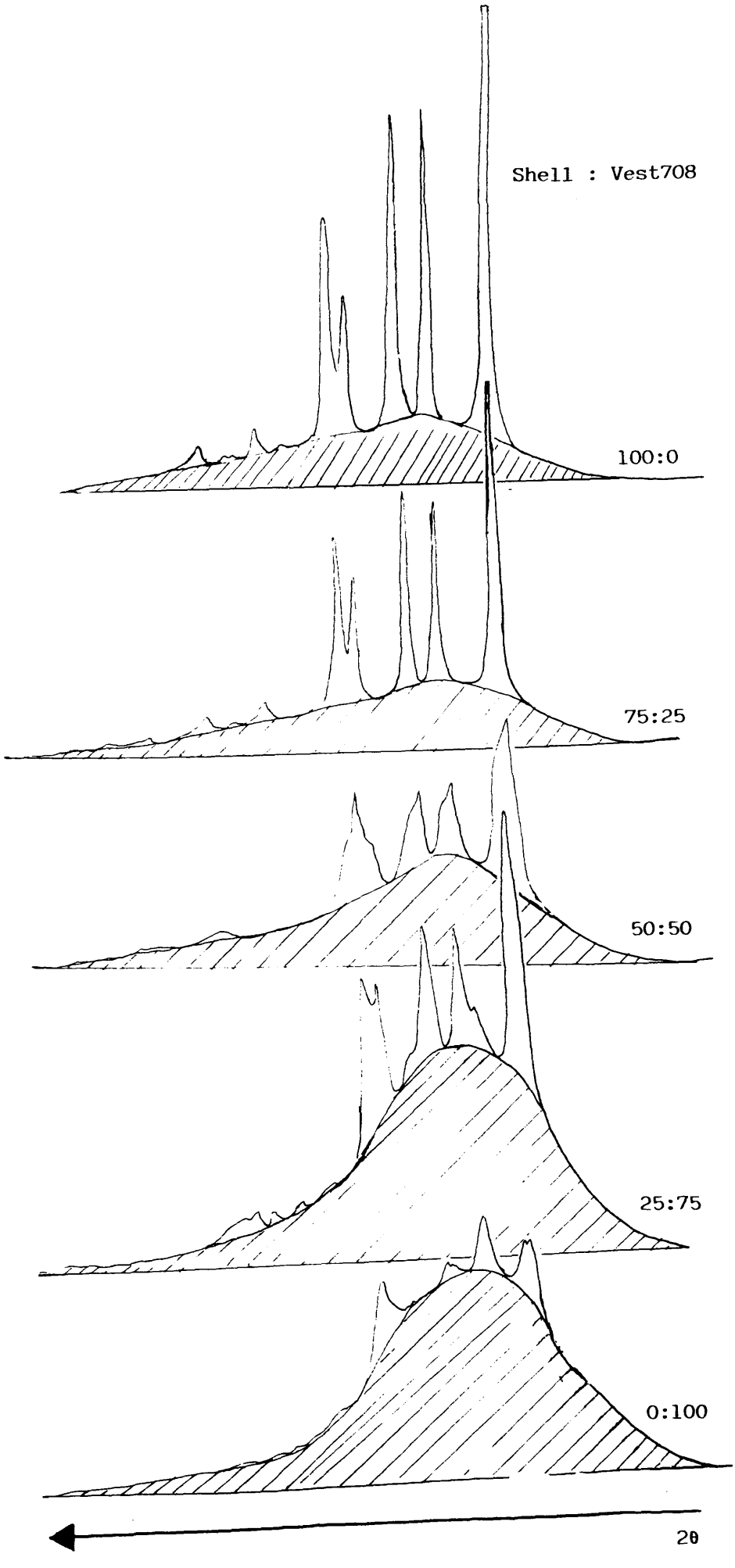

Figure 5.13 X-ray diffraction profiles for the various Shell : Vest708 blend compositions

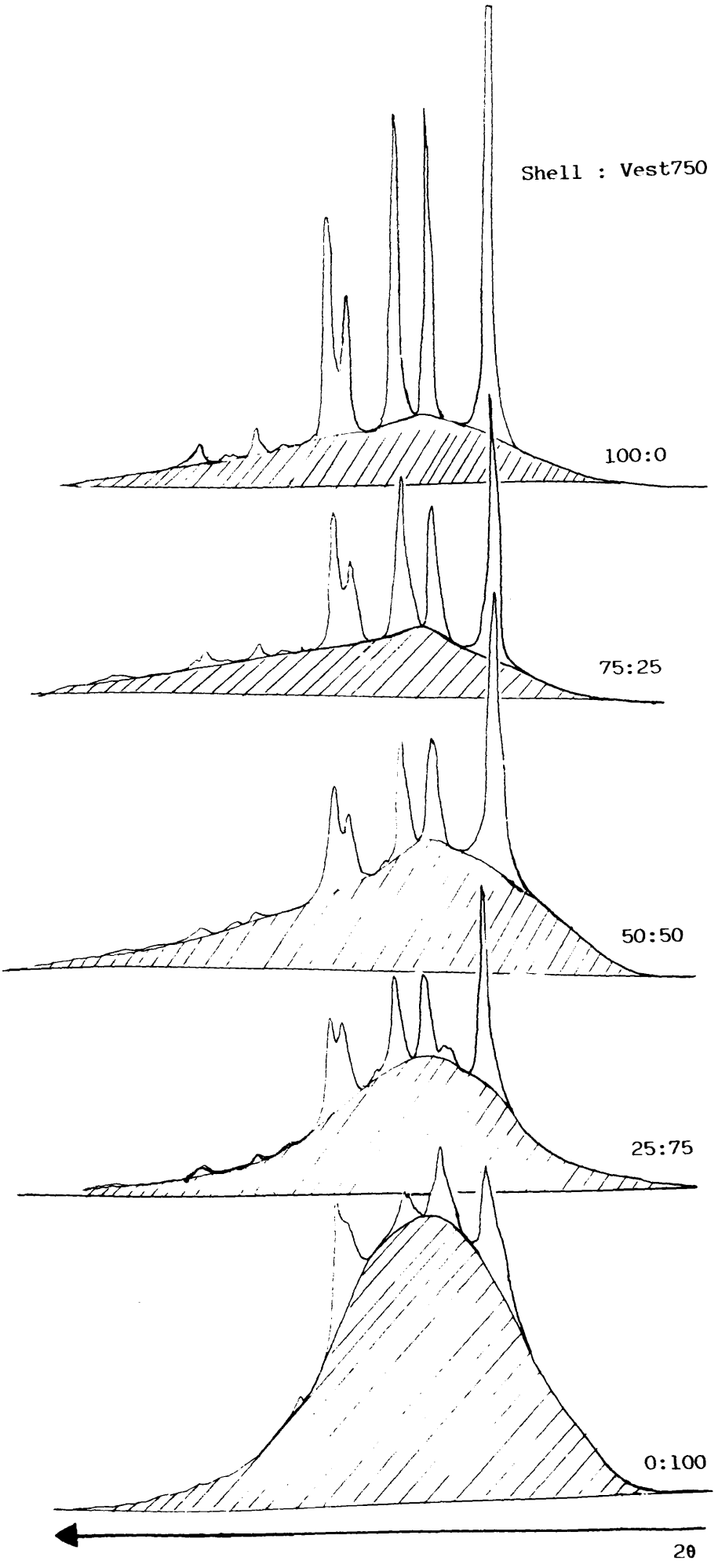

Figure 5.14 X-ray diffractogram profiles for the various Shell : Vest750 blend compositions

Blend Shell:Vest750	X-ray Crystallinity (%)
0 : 100	13.11
25 : 75	21.87
50 : 50	30.72
75 : 25	40.00
100 : 0	52.96

Table 5.13 X-ray crystallinity values for Shell:Vest750 blends.

Blend Shell:Vest703	Diffraction Angle 2θ (degrees)							
0 : 100	13.80	15.85	17.50	---	21.00	---	---	28.50
25 : 75	13.90	15.90	16.85	18.40	21.10	21.80	25.50	28.40
50 : 50	14.10	---	17.00	18.60	21.20	21.90	25.80	28.40
75 : 25	14.00	---	16.90	18.40	21.00	21.80	25.50	28.35
100 : 0	14.20	---	17.00	18.60	21.30	21.90	25.70	28.40

Table 5.14 X-ray diffraction angles (2θ) for Shell:Vest703 blends.

Blend Shell:Vest708	Diffraction Angle 2θ (degrees)							
0 : 100	13.80	16.20	---	18.00	---	21.50	---	---
25 : 75	14.10	16.20	17.00	18.60	21.20	21.80	25.50	28.50
50 : 50	14.00	---	17.00	18.50	21.00	21.80	25.40	28.70
75 : 25	14.20	---	17.10	18.70	21.20	21.90	25.80	28.45
100 : 0	14.20	---	17.00	18.60	21.30	21.90	25.70	28.40

Table 5.15 X-ray diffraction angles (2θ) for Shell:Vest708 blends.

Blend Shell:Vest750	Diffraction Angle 2θ (degrees)							
0 : 100	13.80	16.20	---	18.00	---	21.50	---	---
25 : 75	14.00	15.80	16.90	18.50	21.00	21.80	25.60	28.30
50 : 50	14.05	---	16.90	18.55	21.10	21.85	25.70	28.40
75 : 25	14.30	---	17.30	18.85	21.45	22.20	26.00	28.80
100 : 0	14.20	---	17.00	18.60	21.30	21.90	25.70	28.40

Table 5.16 X-ray diffraction angles (2θ) for Shell:Vest750 blends.

5.2.1.6 DSC Melting and Crystallisation

DSC melting and crystallisation data were recorded in triplicate for the blends. Samples were encapsulated and run according to procedures described in section 3.7.

Prior to melting and crystallisation runs, each sample was heated to 200°C and held for 5 minutes thus providing each sample with a common thermal history. The cooling run was carried out at a rate of 10°C/min from 200°C to 30°C. Subsequent to crystallisation, the samples were heated through their melting range at 10°C/min.

Tables 5.17 - 5.19 show mean melting and crystallisation data. Figures 5.15 - 5.17 show typical melting profiles for the blends whilst Figures 5.18 - 5.20 show typical crystallisation profiles for the blends.

Blend Shell:Vest703	T_m Onset (°C)	T_m Peak (°C)	ΔH_f (J/g)	T_c Onset (°C)	T_c Peak (°C)	$-\Delta H_c$ (J/g)
0 : 100	89.20	107.50	30.32	78.60	72.37	21.27
25 : 75	148.95	160.50	66.13	116.66	110.69	36.33
50 : 50	148.17	161.75	77.80	116.96	112.84	55.03
75 : 25	153.74	160.58	124.85	119.35	115.20	81.88
100 : 0	156.94	161.33	126.66	119.67	115.00	100.64

Table 5.17 Mean melting and crystallisation data for Shell:Vest703 blends.

Blend Shell:Vest708	T_m Onset (°C)	T_m Peak (°C)	ΔH_f (J/g)	T_c Onset (°C)	T_c Peak (°C)	$-\Delta H_c$ (J/g)
0 : 100	60.42	76.91	21.68	39.45	35.46	---
25 : 75	152.90	161.79	46.13	115.02	108.83	33.75
50 : 50	149.28	162.83	68.99	117.56	112.65	53.16
75 : 25	153.08	160.71	109.69	119.31	113.58	81.43
100 : 0	156.94	161.33	126.66	119.67	115.00	100.64

Table 5.18 Mean melting and crystallisation data for Shell:Vest708 blends.

Blend Shell:Vest750	T_m Onset (°C)	T_m Peak (°C)	ΔH_f (J/g)	T_c Onset (°C)	T_c Peak (°C)	$-\Delta H_c$ (J/g)
0 : 100	55.28	76.83	15.22	89.08	61.03	---
25 : 75	152.57	161.30	40.11	110.20	103.75	30.71
50 : 50	149.32	163.12	68.81	117.02	112.42	51.75
75 : 25	152.18	161.08	99.40	118.89	112.82	71.44
100 : 0	156.94	161.33	126.66	119.67	115.00	100.64

Table 5.19 Mean melting and crystallisation data for Shell:Vest750 blends.

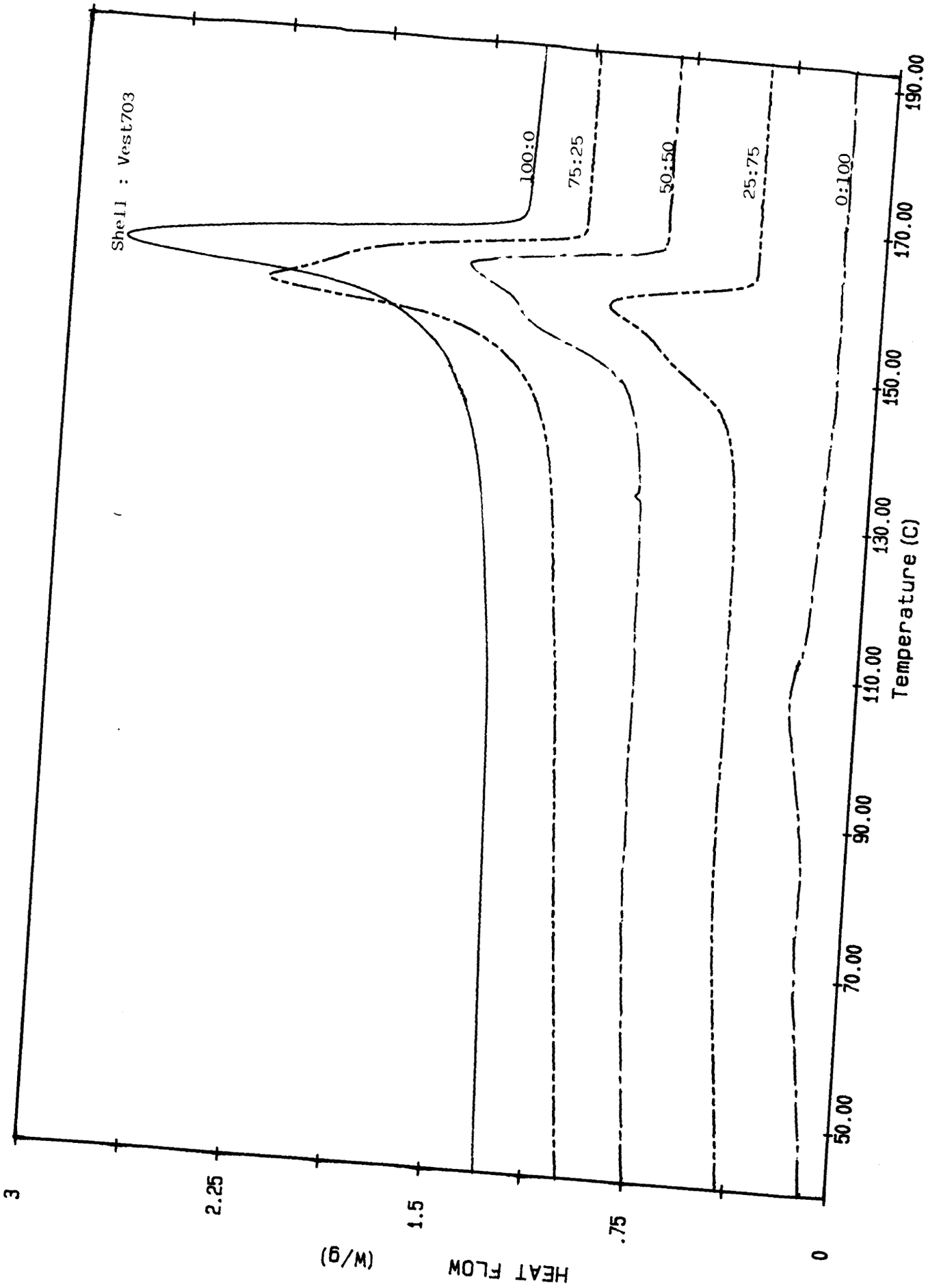

Figure 5.15 Typical DSC melting profiles for the various Shell : Vest703 blend compositions

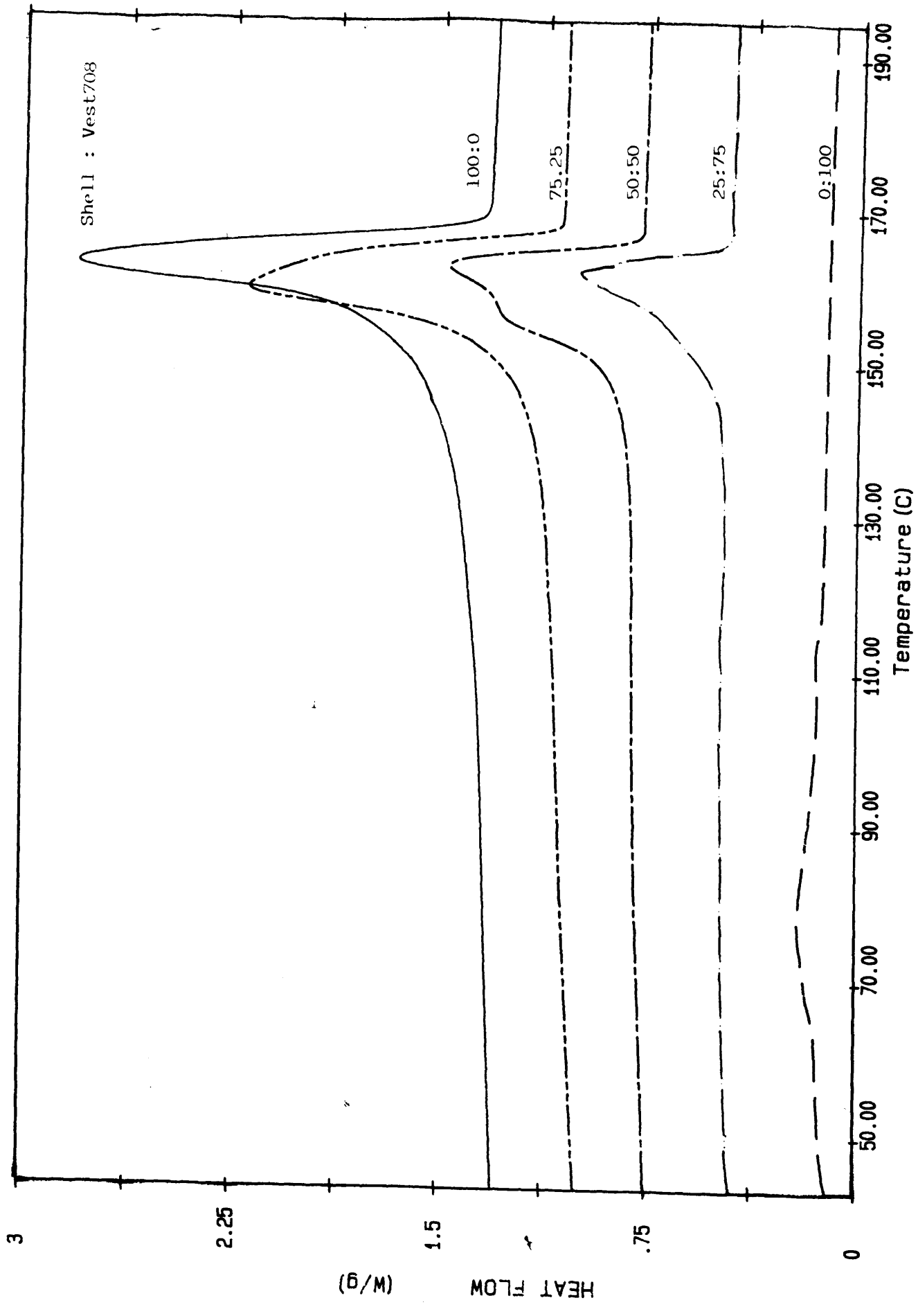

Figure 5.16 Typical DSC melting profiles for the various Shell : Vest708 blend compositions

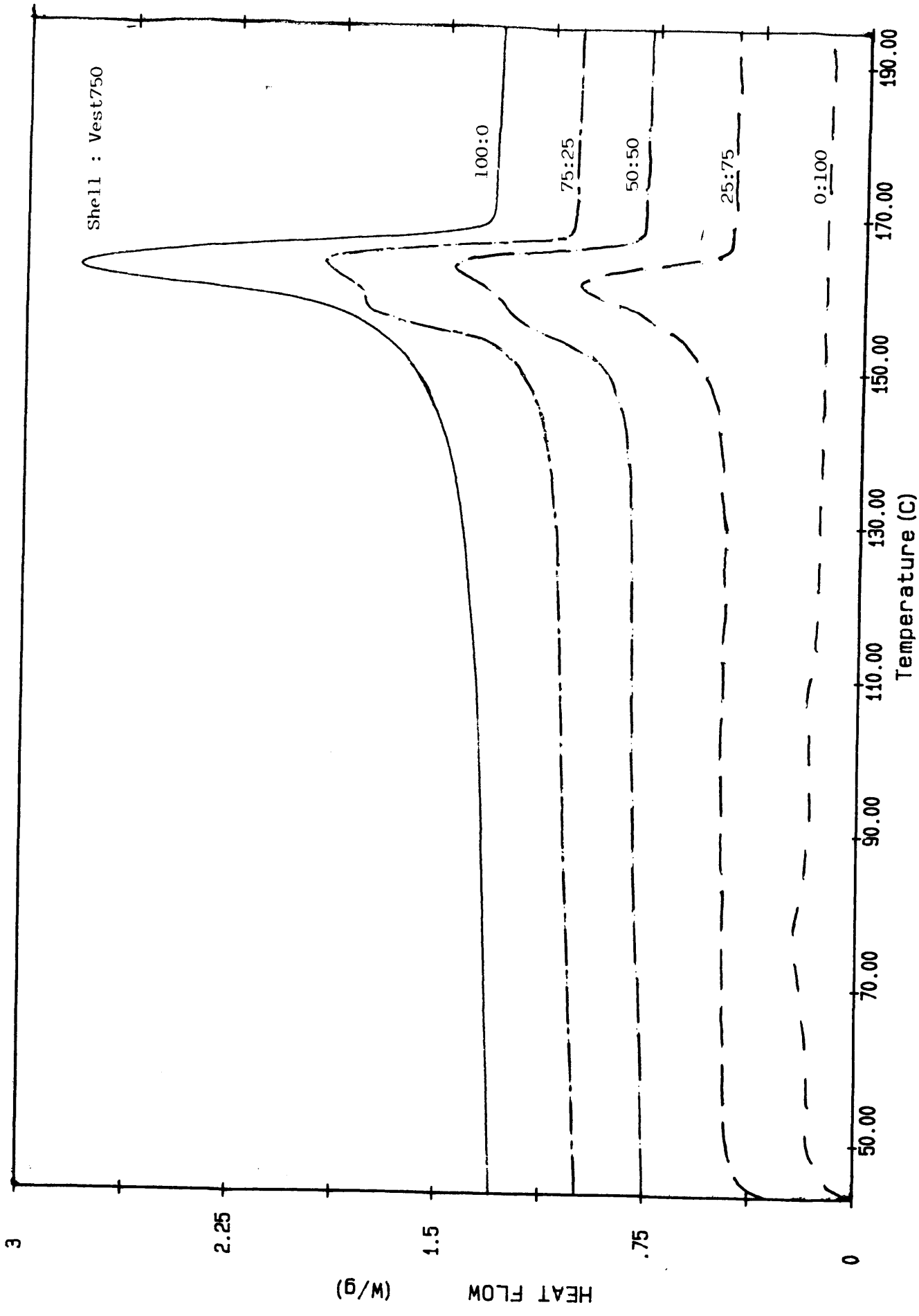

Figure 5.17 Typical DSC melting profiles for the various Shell : Vest750 blend compositions

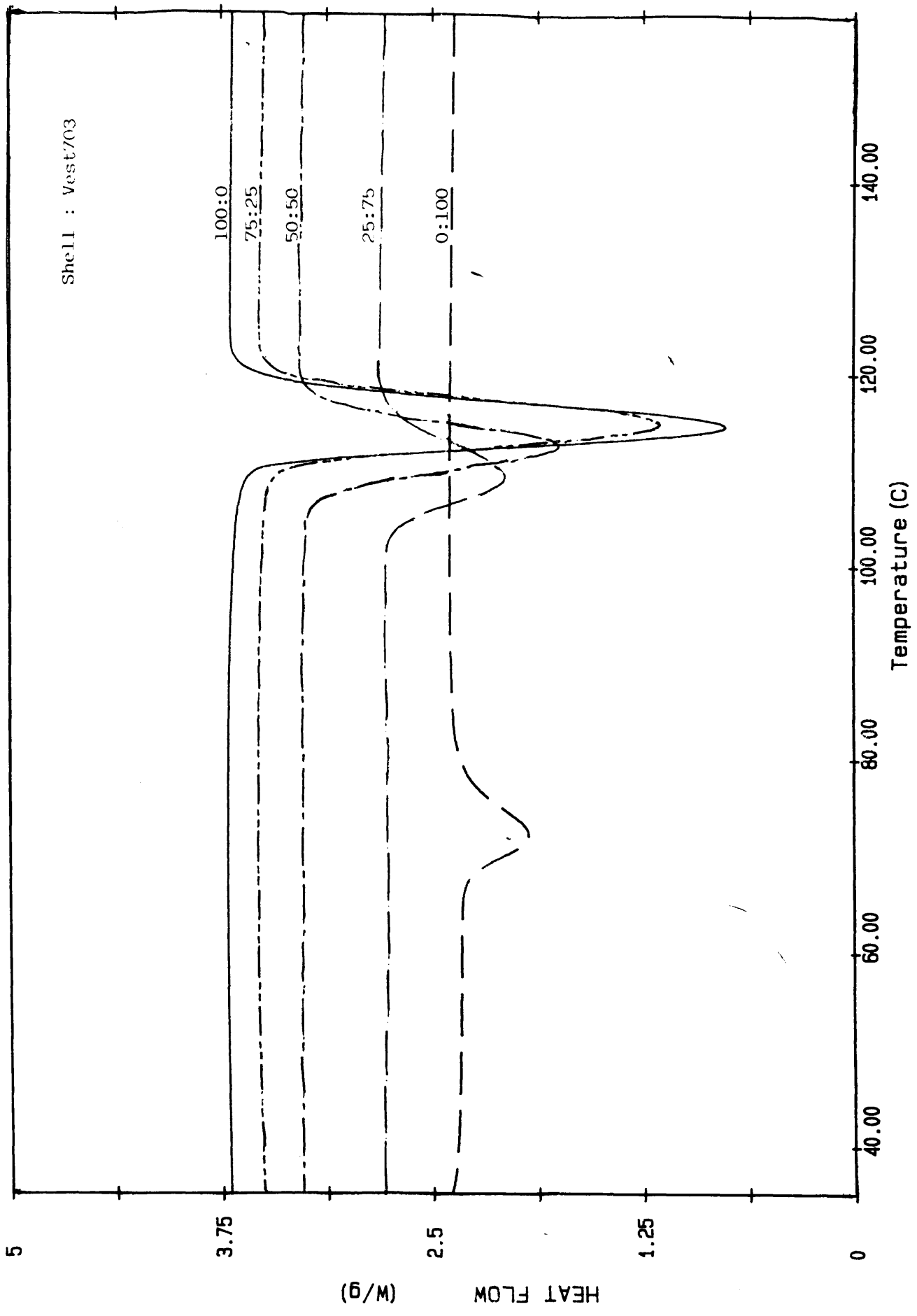

Figure 5.18 Typical DSC crystallisation profiles for the various Shell : Vest703 blend compositions

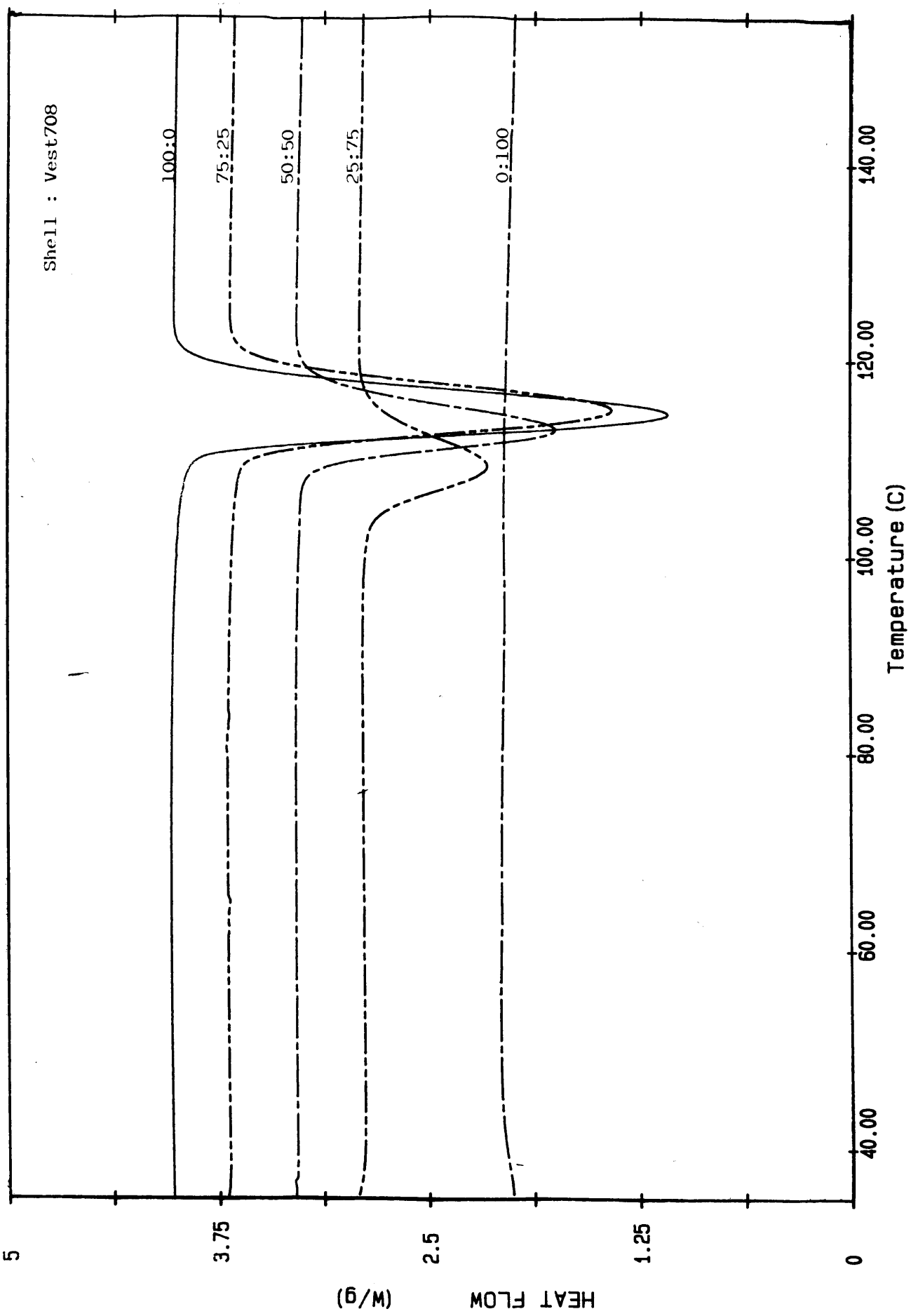

Figure 5.19 Typical DSC crystallisation profiles for the various Shell : Vest708 blend compositions

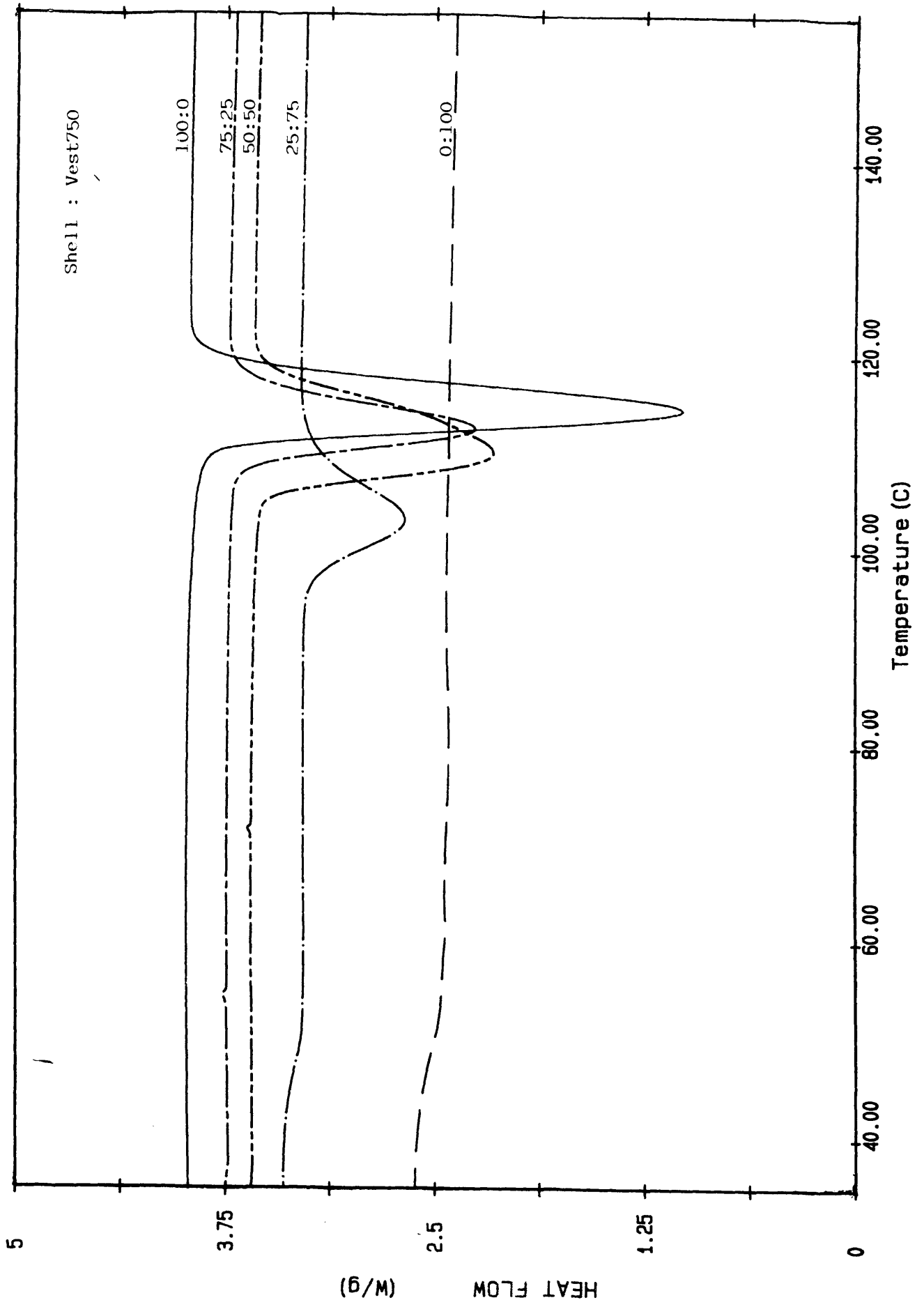

Figure 20 Typical DSC crystallisation profiles for the various Shell : Vest750 blend compositions

5.2.2 Quenching Blends Rapidly From The Melt

FTIR absorption peak ratio analysis (section 4.3.2) involving the use of the A998/A973 and A841/A973 absorption ratios, and density measurements at 20°C (section 3.13), were used to monitor structural changes in the Shell:Vest703 blends when rapidly quenched from the molten state into quench baths at various temperatures. Wide-angle x-ray diffraction was used to examine the structural and crystallinity changes induced by rapid quenching into an ice/water bath at 0°C and a liquid nitrogen at -190°C bath for each blend composition and these were compared to the corresponding samples which had been annealed at 150°C for 10 minutes and allowed to cool slowly in the presence of nitrogen.

Results for the FTIR APRA study for each blend composition quenched into each of the quench media are presented in Tables 5.20 - 5.24 and graphs showing the relationship between infrared ratio and quench temperature for the blends are shown in Figures 5.21 and 5.22. Corresponding density measurements for the same samples are presented in Table 5.25 and the relationship between density and quench temperature is clearly shown in Figure 5.23. X-ray diffractograms of the various blend compositions quenched into ice/water at 0°C and liquid nitrogen at -190°C are shown in Figures 5.24 and 5.25 and a comparison of x-ray crystallinities between the ice/water and liquid nitrogen quenched blends and the corresponding annealed samples are presented in Table 5.26 (x-ray diffractograms of the annealed Shell:Vest703 blends are shown in Figures 5.12 - 5.14).

Figure 5.21

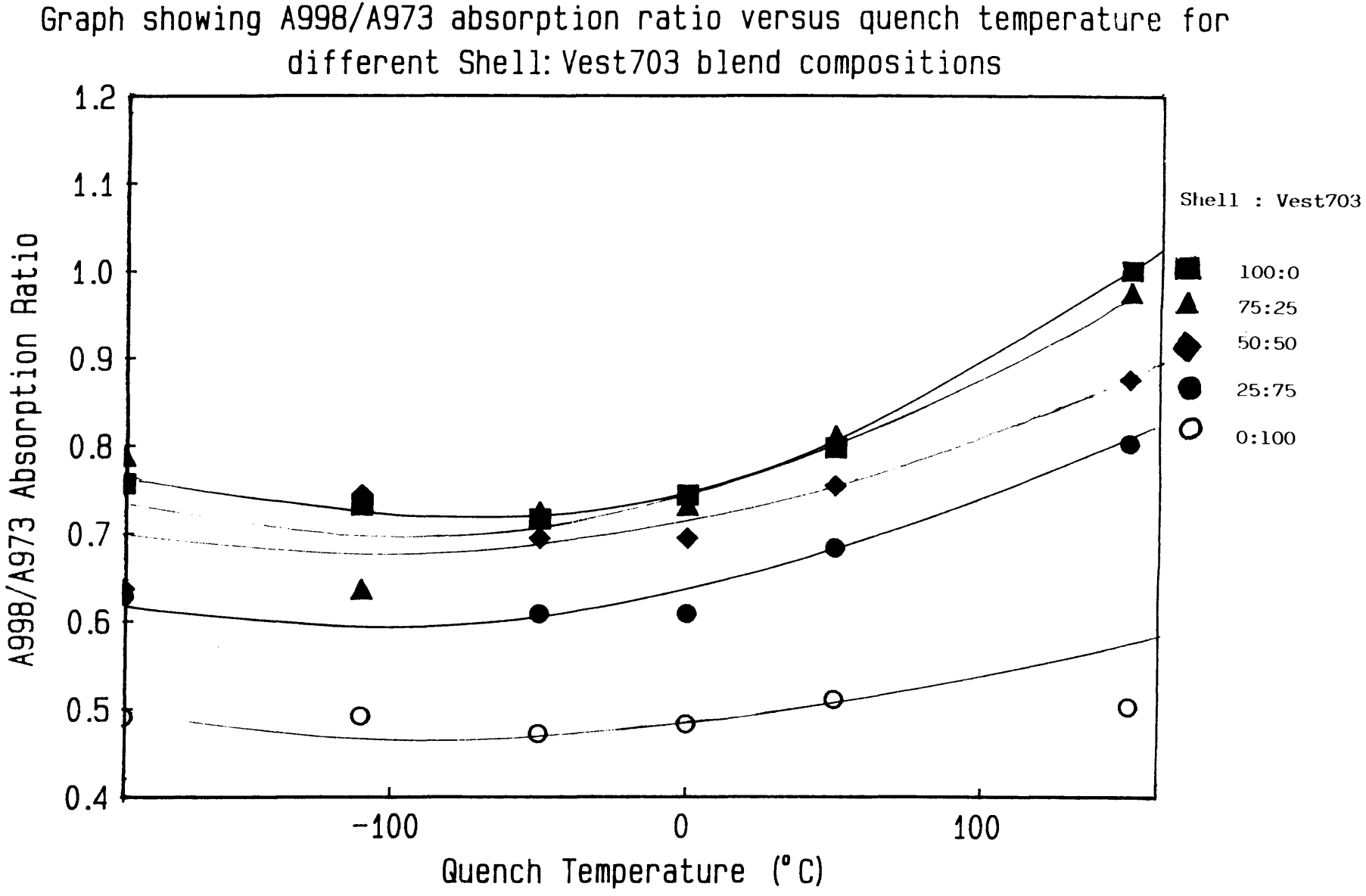
Graph showing A998/A973 absorption ratio versus quench temperature for different Shell: Vest703 blend compositions
A998/A973 Absorption Ratio
1.2
1.1
1.0
0.9
0.8
0.7
0.6
0.5
0.4
-100
0
100
Quench Temperature (°C)
Shell : Vest703
100:0
75:25
50:50
25:75
0:100

Figure 5.22

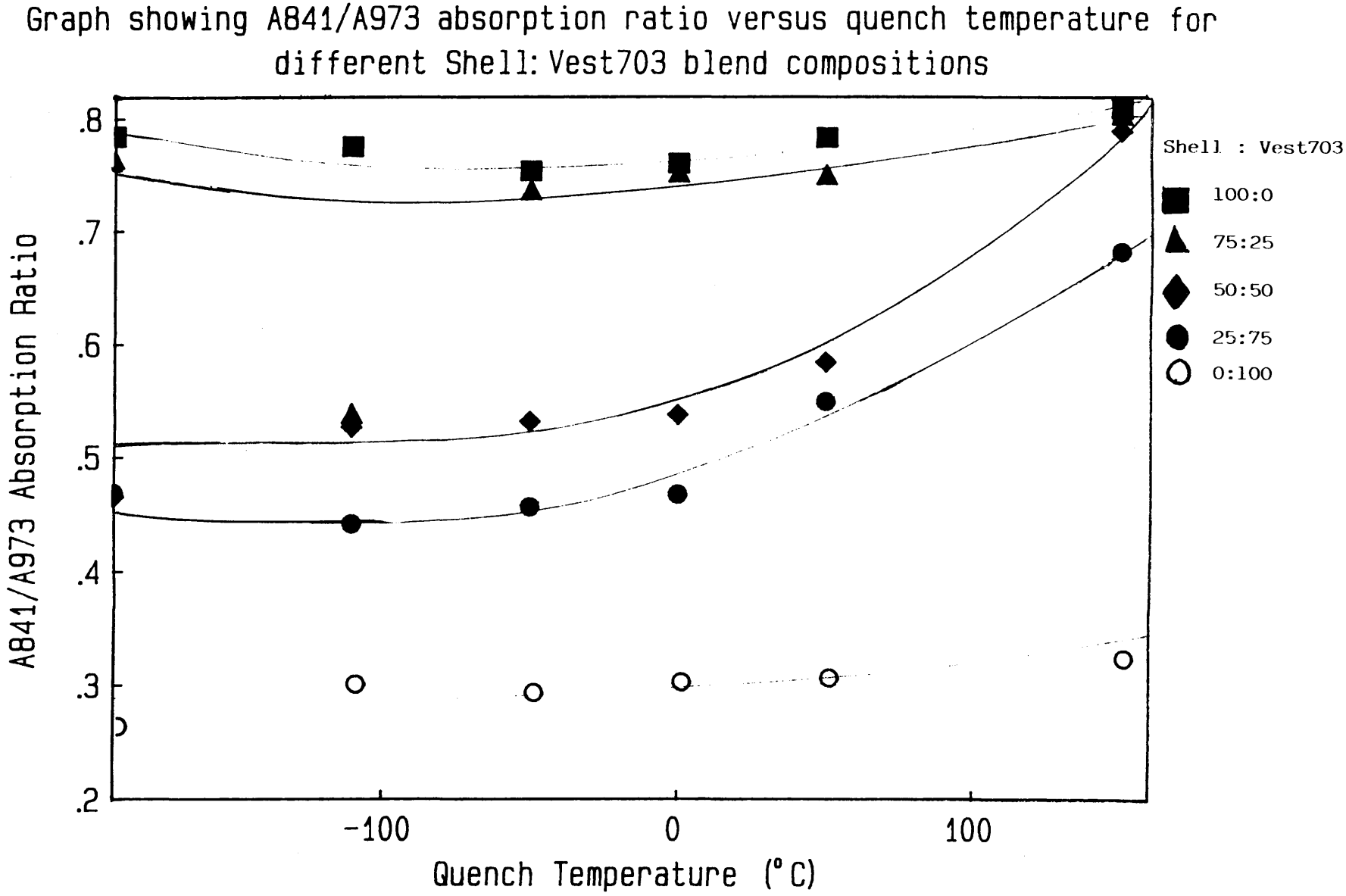
Graph showing A841/A973 absorption ratio versus quench temperature for different Shell: Vest703 blend compositions
A841/A973 Absorption Ratio
.8
.7
.6
.5
.4
.3
.2
-100
0
100
Quench Temperature (°C)
Shell : Vest703
100:0
75:25
50:50
25:75
0:100

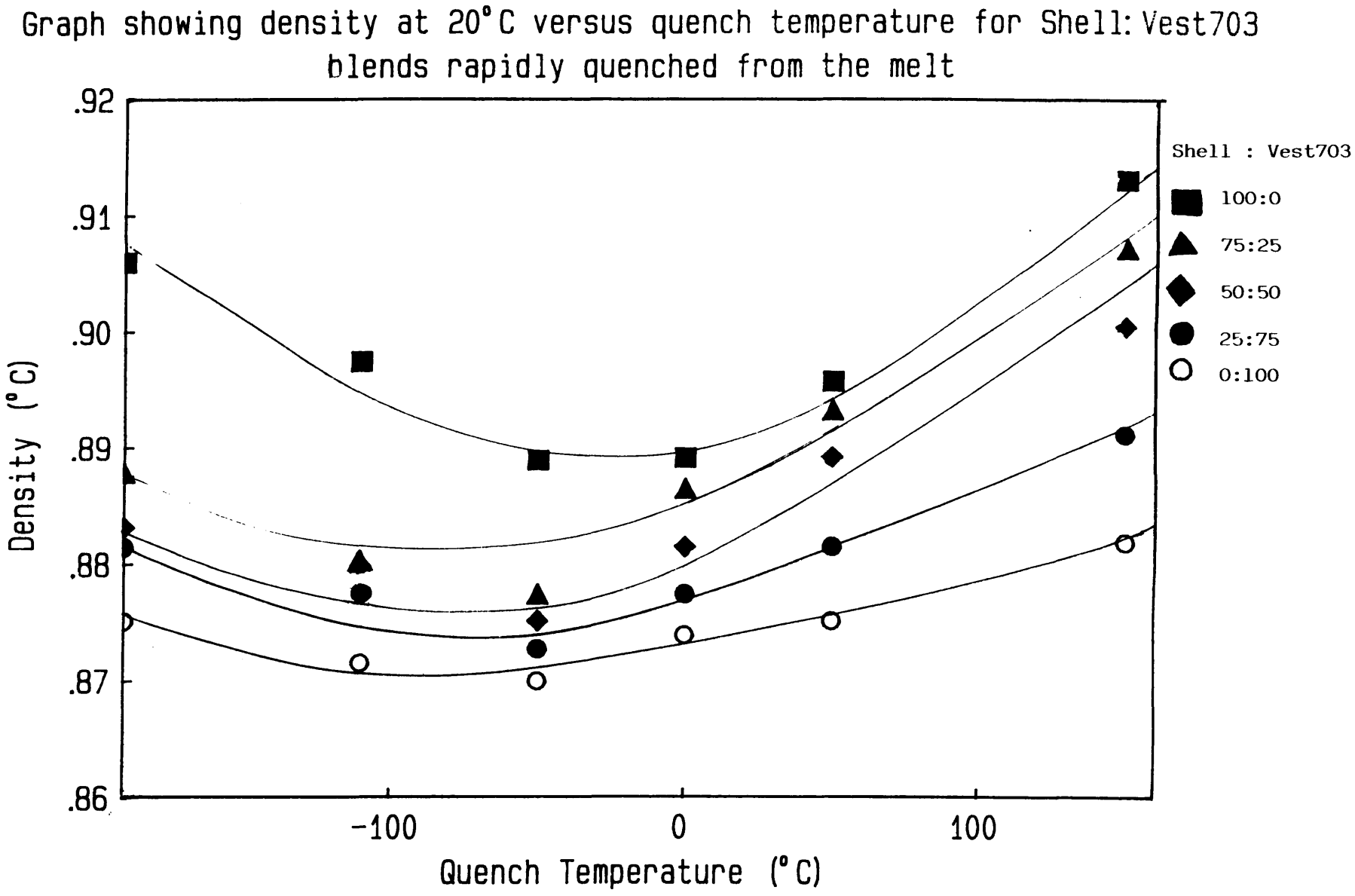
Graph showing density at 20°C versus quench temperature for Shell: Vest703 blends rapidly quenched from the melt
.92
.91
.90
.89
.88
.87
.86
Density (°C)
-100
0
100
Quench Temperature (°C)
Shell : Vest703
100:0
75:25
50:50
25:75
0:100

Figure 5.23

Quench Temperature (°C)	Absorption Ratio	
	A998/A973	A841/A973
Annealed (150°C)	0.100	0.810
Warm water (50°C)	0.796	0.783
Ice/water (0°C)	0.742	0.760
Dry ice/acetone (-50°C)	0.715	0.753
Dry ice/acetone (-110°C)	0.731	0.775
Liquid N_2 (-190°C)	0.756	0.784

Table 5.20 FTIR APRA results for the Shell:Vest703 = 100 : 0 blend rapidly quenched into various quench media.

Quench Temperature (°C)	Absorption Ratio	
	A998/A973	A841/A973
Annealed (150°C)	0.975	0.805
Warm water (50°C)	0.810	0.750
Ice/water (0°C)	0.730	0.752
Dry ice/acetone (-50°C)	0.723	0.736
Dry ice/acetone (-110°C)	0.635	0.538
Liquid N_2 (-190°C)	0.787	0.762

Table 5.21 FTIR APRA results for the Shell:Vest703 = 75 : 25 blend rapidly quenched into various quench media.

Quench Temperature (°C)	Absorption Ratio	
	A998/A973	A841/A973
Annealed (150°C)	0.875	0.790
Warm water (50°C)	0.753	0.584
Ice/water (0°C)	0.693	0.537
Dry ice/acetone (-50°C)	0.693	0.521
Dry ice/acetone (-110°C)	0.661	0.526
Liquid N_2 (-190°C)	0.637	0.465

Table 5.22 FTIR APRA results for the Shell:Vest703 = 50 : 50 blend rapidly quenched into various quench media.

Quench Temperature (°C)	Absorption Ratio	
	A998/A973	A841/A973
Annealed (150°C)	0.802	0.683
Warm water (50°C)	0.682	0.549
Ice/water (0°C)	0.607	0.467
Dry ice/acetone (-50°C)	0.607	0.456
Dry ice/acetone (-110°C)	0.601	0.441
Liquid N_2 (-190°C)	0.611	0.468

Table 5.23 FTIR APRA results for the Shell:Vest703 = 25 : 75 blend rapidly quenched into various quench media.

Quench Temperature (°C)	Absorption Ratio	
	A998/A973	A841/A973
Annealed (150°C)	0.503	0.320
Warm water (50°C)	0.510	0.303
Ice/water (0°C)	0.482	0.300
Dry ice/acetone (-50°C)	0.471	0.291
Dry ice/acetone (-110°C)	0.462	0.276
Liquid N_2 (-190°C)	0.401	0.263

Table 5.24 FTIR APRA results for the Shell:Vest703 = 0 : 100 blend rapidly quenched into various quench media.

Quench Temperature (°C)	Shell:Vest703				
	100:0	75:25	50:50	25:75	0:100
Annealed (150°C)	0.9131	0.9072	0.9004	0.8911	0.8818
Warm water (50°C)	0.8957	0.8932	0.8891	0.8814	0.8751
Ice/water (0°C)	0.8891	0.8864	0.8814	0.8774	0.8739
Dry ice/acetone (-50°C)	0.8889	0.8774	0.8751	0.8727	0.8699
Dry ice/acetone (-110°C)	0.8974	0.8802	0.8798	0.8775	0.8715
Liquid N_2 (-190°C)	0.9060	0.8878	0.8831	0.8814	0.8751

Table 5.25 Mean densities at 20°C for quenched Shell:Vest703 blends.

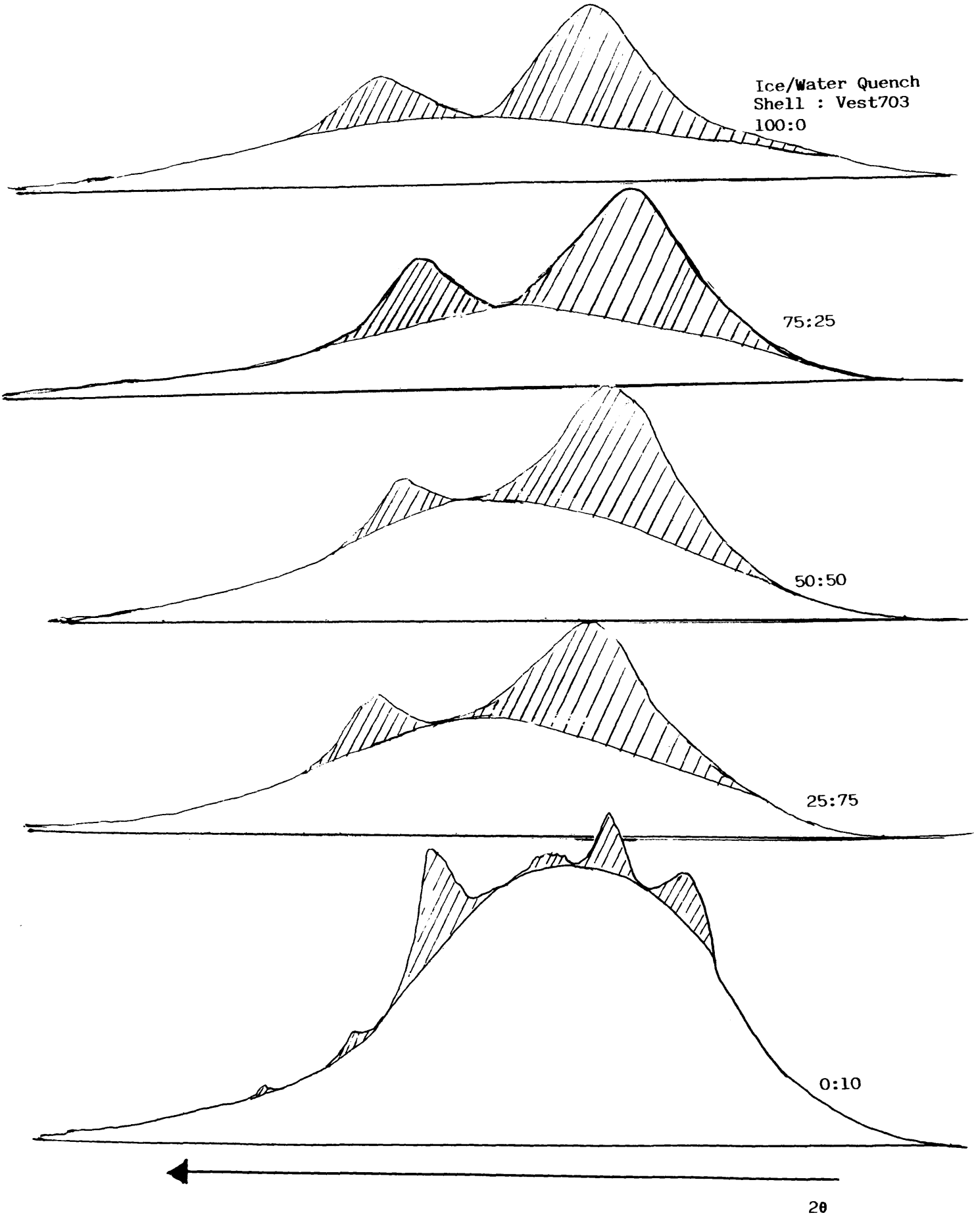

Figure 5.24 X-ray diffractograms for the various Shell : Vest703 compositions rapidly quenched from the melt into ice/water at $0^{o}C$

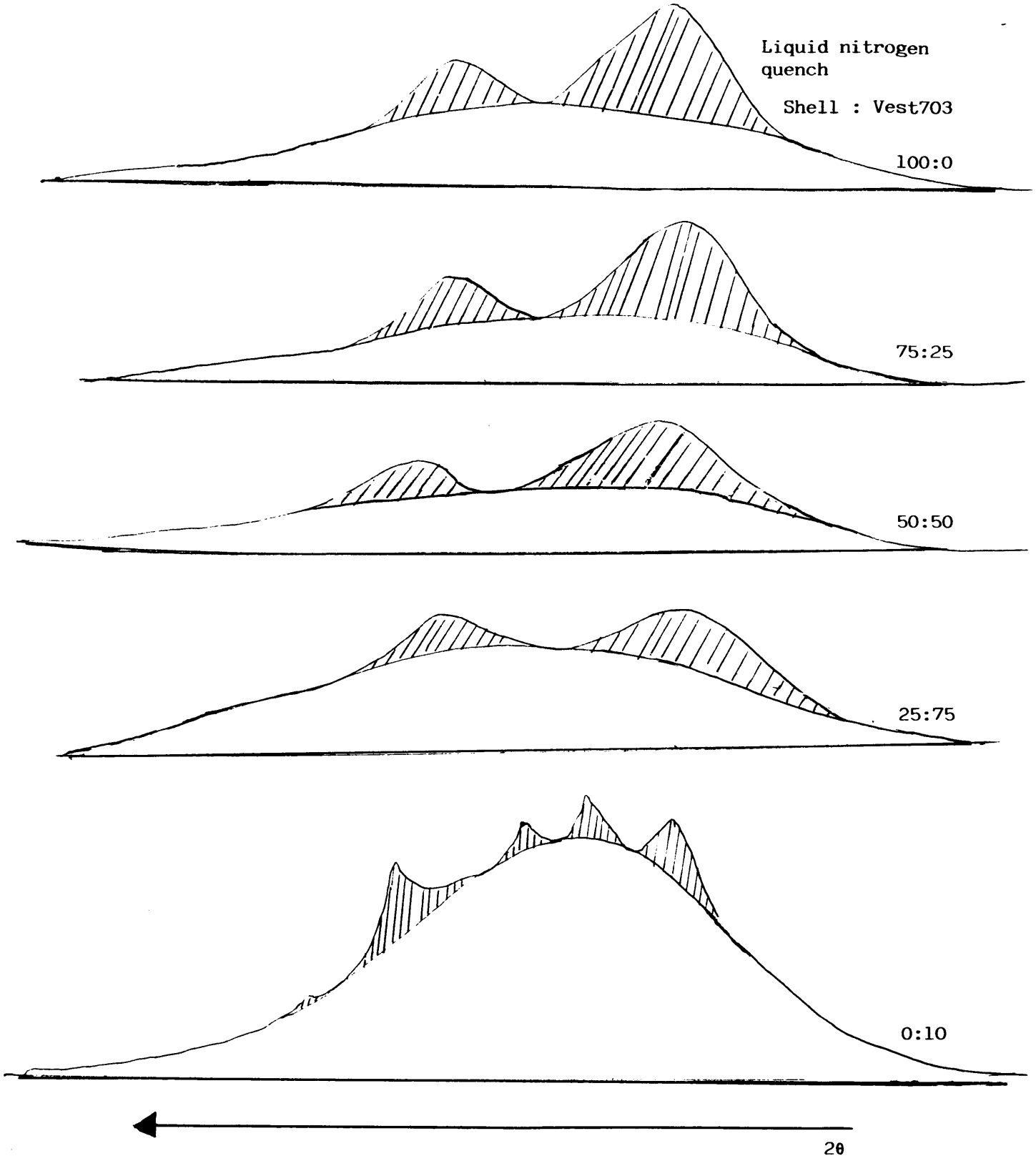

Figure 5.25 X-ray diffractograms for the various Shell : Vest703 blend compositions rapidly quenched from the melt into liquid nitrogen at -190^{o}C

Blend Shell:Vest703	X-ray Crystallinity (%) Quench Media		
	Liquid N_2 (-190)	Ice/water (0°C)	Annealed (150°C)
0 : 100	7.63	9.65	15.33
25 : 75	12.16	12.70	26.27
50 : 50	14.70	14.50	35.29
75 : 25	19.89	18.82	47.97
100 : 0	19.93	18.90	52.96

Table 5.26 X-ray crystallinity data for quenched Shell:Vest703 blends.

5.2.3 Effect Of Temperature On The Infrared Spectroscopy Of The Blends

Infrared spectra of the different Shell:Vest703 blends (annealed for 10 minutes at 150°C and slowly cooled in the presence of nitrogen) were recorded over the range 1300-700 cm^{-1} at increasing temperature increments of 10°C between 30°C and 200°C according to procedures detailed in section 3.6.2 (unless melting prevented further infrared information being obtained).

FTIR APRA was carried out on spectra at each temperature increment using the A998/A973 and A841/A973 absorption ratios. Tables 5.27 - 5.31 show FTIR APRA results for each blend composition. Figures 5.26 and 5.27 show the relationship between temperature and ratio value for the various blends and Figures 5.28 - 5.32 show comparisons between the A998/A973 and A841/A973 ratios for each blend composition.

Shell:Vest703 = 100 : 0

Temperature (°C)	Absorption Ratio	
	A998/A973	A841/A973
30	1.000	0.810
40	0.996	0.820
50	0.977	0.819
60	0.970	0.827
70	0.966	0.830
80	0.948	0.829
90	0.924	0.821
100	0.903	0.817
110	0.899	0.813
120	0.881	0.822
130	0.857	0.813
140	0.840	0.802
150	0.801	0.789
160	0.777	0.770
170	0.718	0.730
180	0.635	0.645
190	0.533	0.561
200	0.395	0.448

Table 5.27 FTIR APRA results for spectra of Shell:Vest703 = 100 : 0 blends taken at increasing temperature increments.

Shell:Vest703 = 75 : 25

Temperature (°C)	Absorption Ratio	
	A998/A973	A841/A973
30	0.957	0.805
40	0.947	0.808
50	0.931	0.797
60	0.914	0.803
70	0.903	0.793
80	0.888	0.793
90	0.866	0.792
100	0.853	0.785
110	0.834	0.782
120	0.804	0.766
130	0.786	0.748
140	0.760	0.735
150	0.731	0.713
160	0.679	0.694
170	0.620	0.631
180	0.534	0.546

Table 5.28 FTIR APRA results for spectra of Shell:Vest703 = 75 : 25 blends taken at increasing temperature increments.

Shell:Vest703 = 50 : 50

Temperature (°C)	Absorption Ratio	
	A998/A973	A841/A973
30	0.875	0.736
40	0.862	0.721
50	0.848	0.711
60	0.825	0.704
70	0.814	0.697
80	0.796	0.695
90	0.776	0.696
100	0.752	0.679
110	0.739	0.680
120	0.718	0.663
130	0.685	0.656
140	0.659	0.643
150	0.641	0.624
160	0.598	0.594
170	0.541	0.552
180	0.481	0.495

Table 5.29 FTIR APRA results for spectra of Shell:Vest703 = 50 : 50 blends taken at increasing temperature increments.

Shell:Vest703 = 25 : 75

Temperature (°C)	Absorption Ratio	
	A998/A973	A841/A973
30	0.802	0.683
40	0.799	0.675
50	0.796	0.673
60	0.808	0.687
70	0.753	0.670
80	0.758	0.669
90	0.735	0.666
100	0.698	0.629
110	0.685	0.618
120	0.674	0.609
130	0.649	0.592
140	0.618	0.571
150	0.611	0.569
160	0.581	0.527
170	0.541	0.505
180	0.499	0.474

Table 5.30 FTIR APRA results for spectra of Shell:Vest703 = 25 : 75 blends taken at increasing temperature increments.

Shell:Vest703 = 0 : 100

Temperature (°C)	Absorption Ratio	
	A998/A973	A841/A973
30	0.503	0.320
40	0.478	0.311
50	0.463	0.293
60	0.448	0.278
70	0.423	0.263
80	0.396	0.244
90	0.372	0.231
100	0.338	0.201
110	0.297	0.170
120	0.233	0.123
130	0.210	0.092
140	0.188	0.069

Table 5.31 FTIR APRA results for spectra of Shell:Vest703 = 0 : 100 blends taken at increasing temperature increments.

Figure 5.26

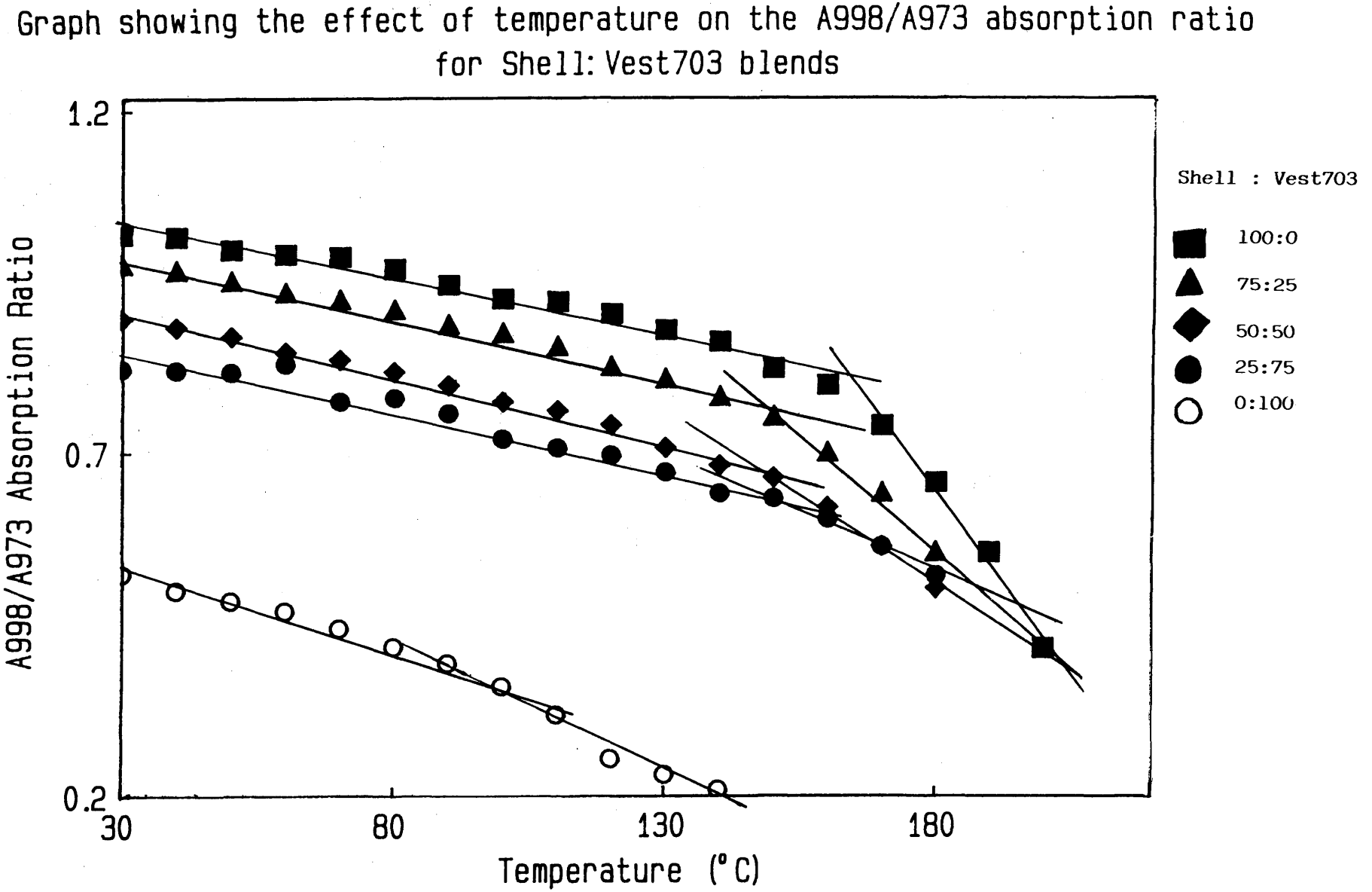
Graph showing the effect of temperature on the A998/A973 absorption ratio for Shell: Vest703 blends
A998/A973 Absorption Ratio
1.2
0.7
0.2
30
80
130
180
Temperature (°C)
Shell : Vest703
100:0
75:25
50:50
25:75
0:100

Figure 5.27

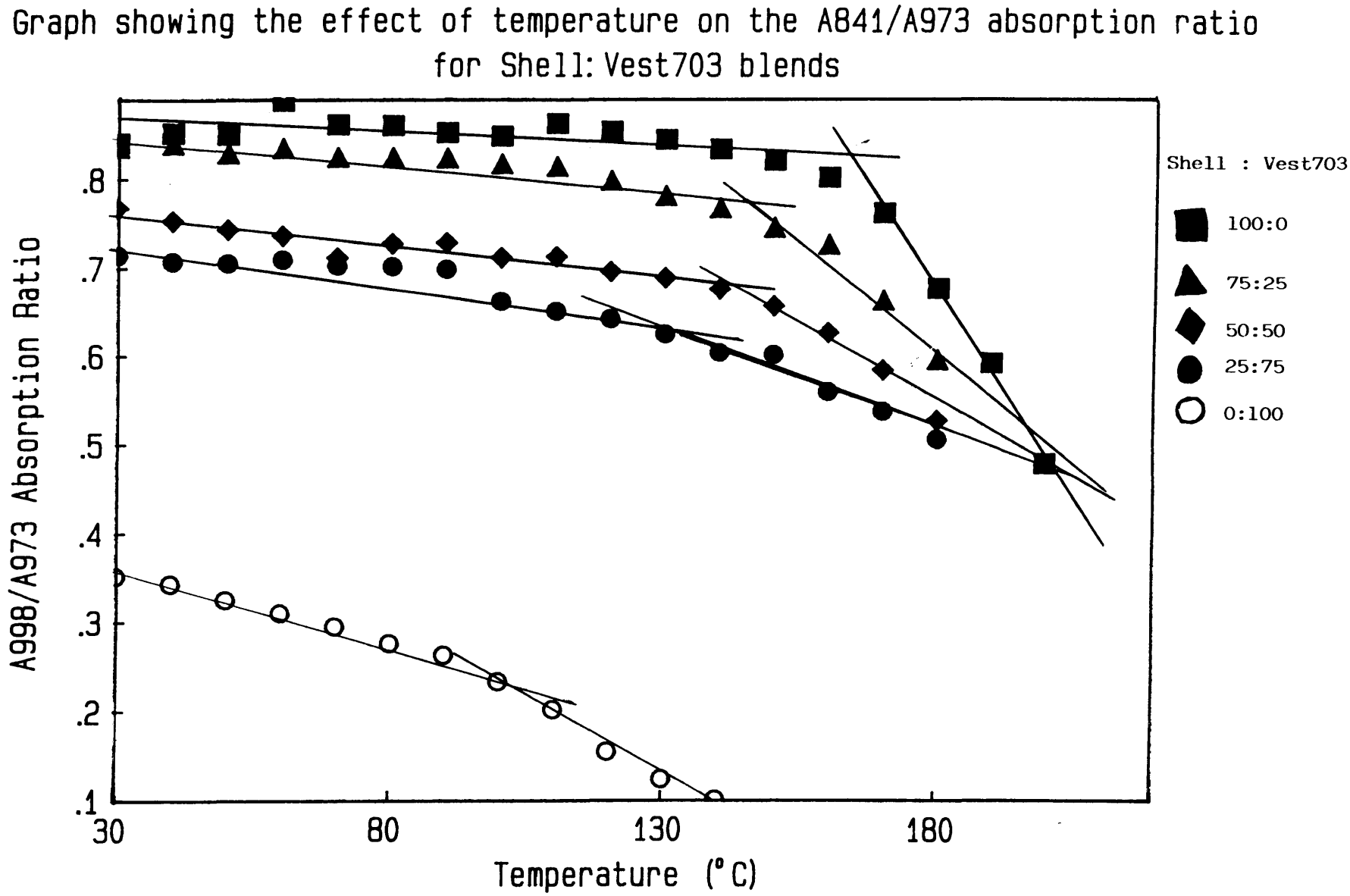
Graph showing the effect of temperature on the A841/A973 absorption ratio for Shell: Vest703 blends
A998/A973 Absorption Ratio
.8
.7
.6
.5
.4
.3
.2
.1
30
80
130
180
Temperature (°C)
Shell : Vest703
100:0
75:25
50:50
25:75
0:100

Graph showing the effect of temperature on the A998/A973 and A841/A973 absorption ratio for Shell: Vest703, 100: 0 blend

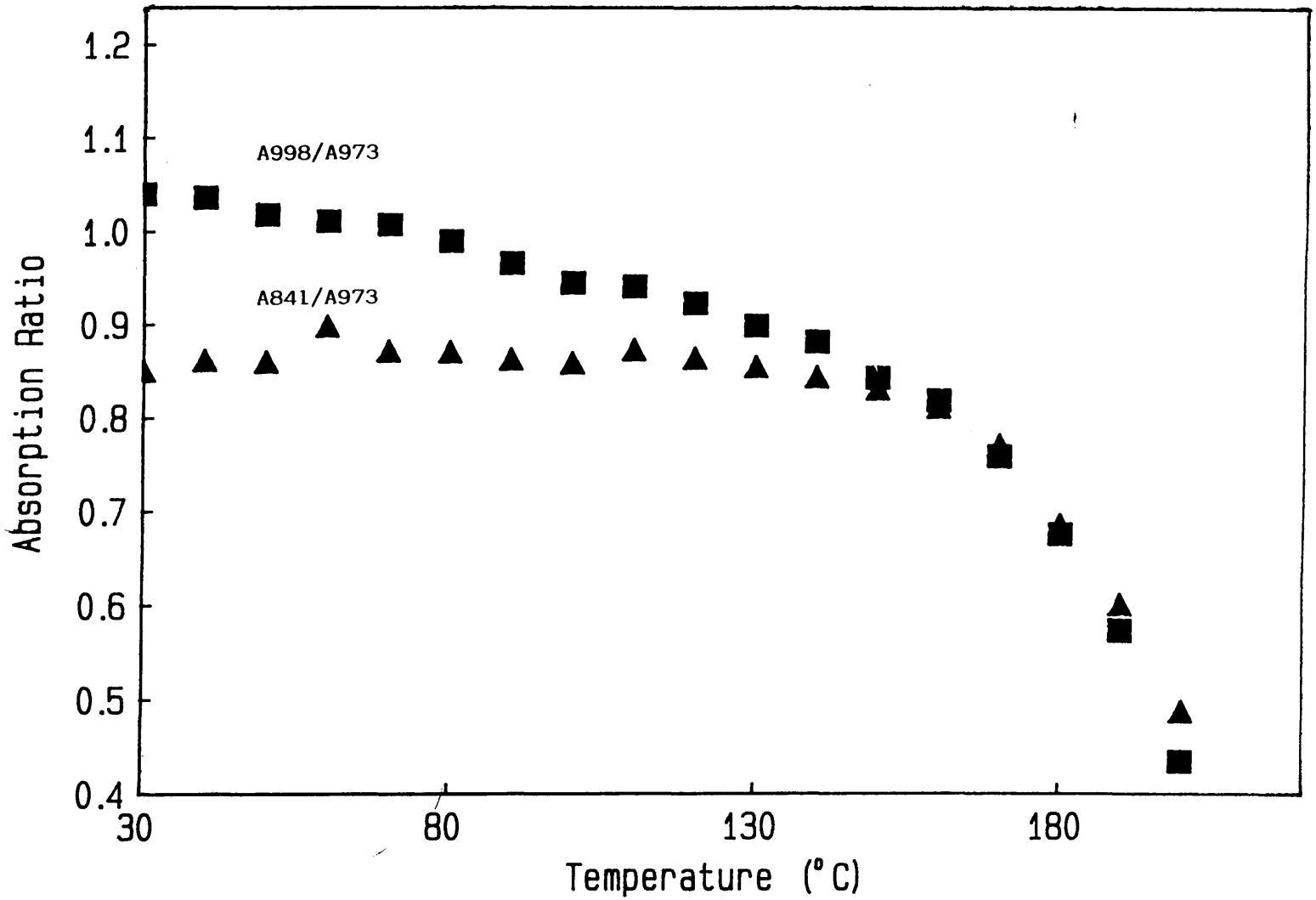

Figure 5.28

Graph showing the effect of temperature on the A998/A973 and A841/A973 absorption ratio for Shell: Vest703, 75: 25 blend

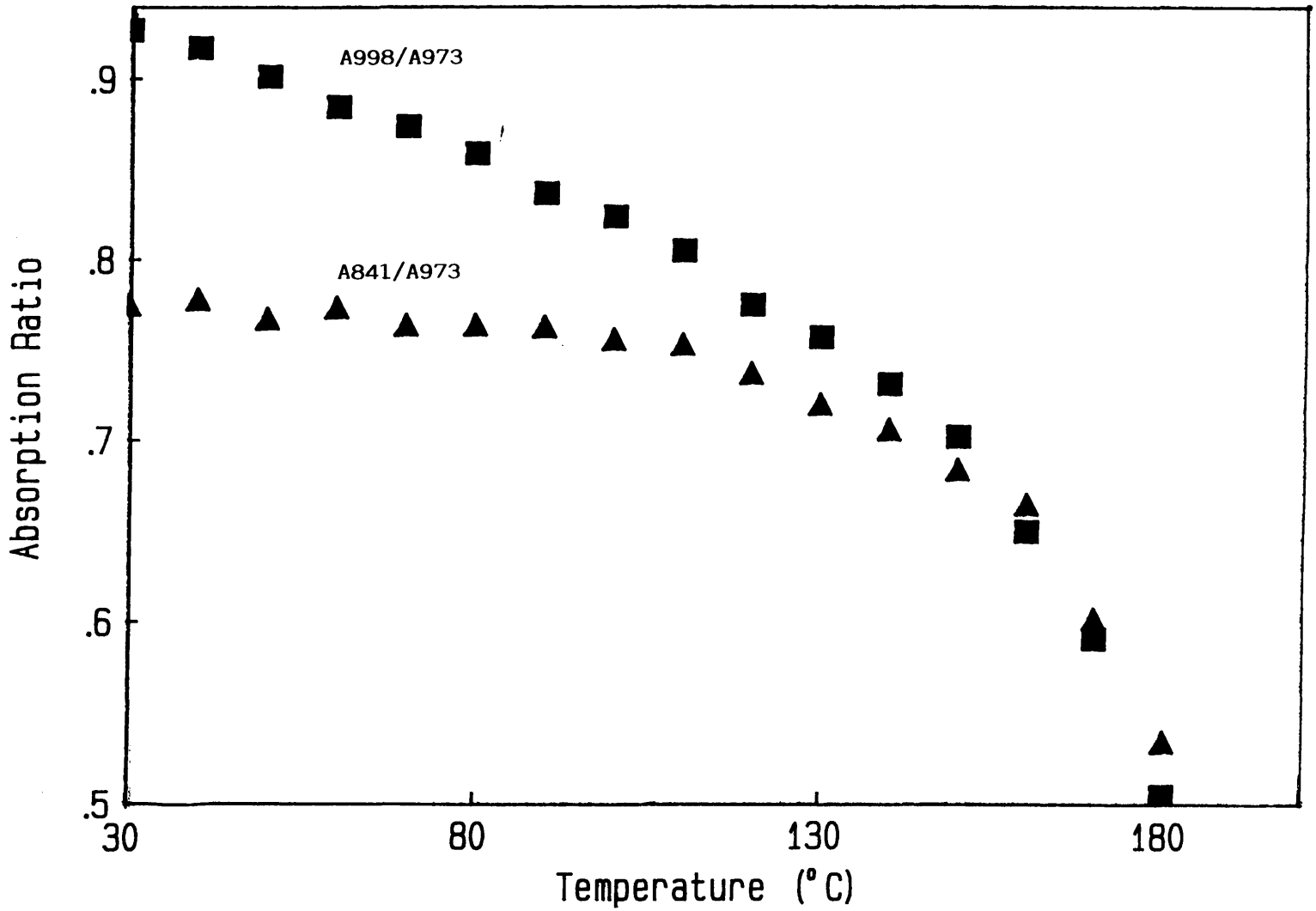

Figure 5.29

Graph showing the effect of temperature on the A998/A973 and A841/A973 absorption ratio for Shell: Vest703, 50: 50 blend

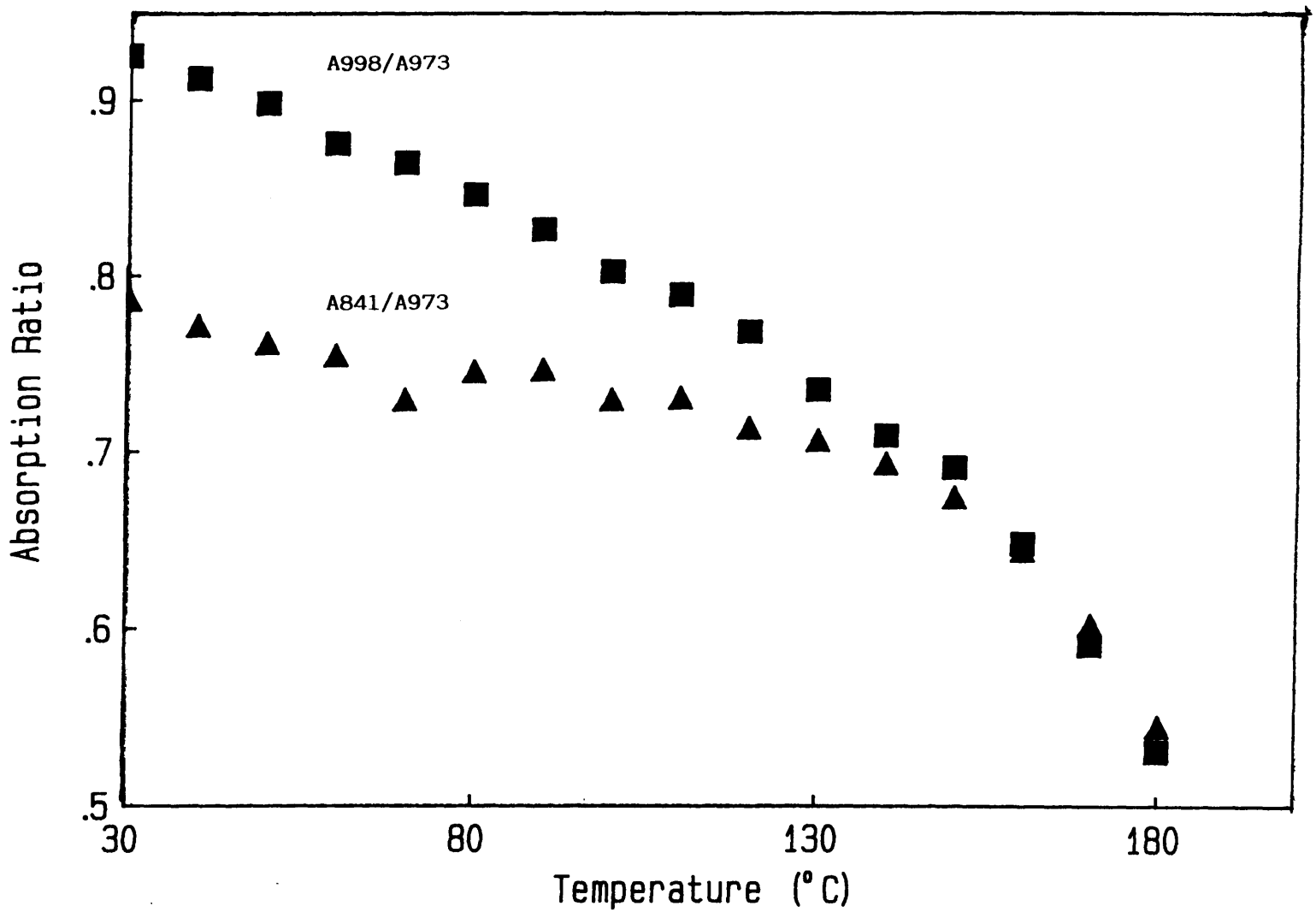

Figure 5.30

Graph showing the effect of temperature on the A998/A973 and A841/A973 absorption ratio for Shell: Vest703, 25: 75 blend

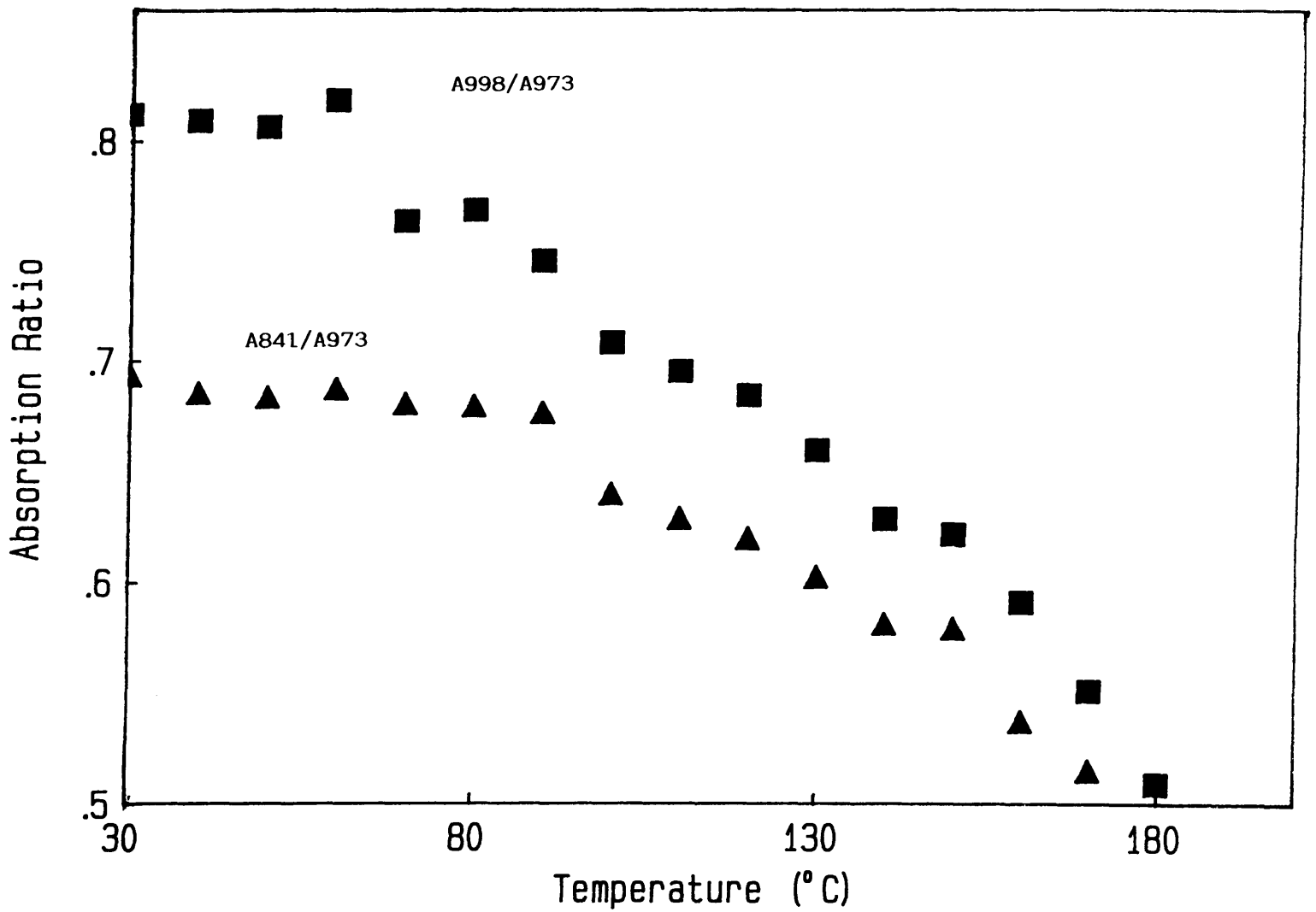

Figure 5.31

Graph showing the effect of temperature on the A998/A973 and A841/A973 absorption ratio for Shell: Vest703, 0: 100 blend

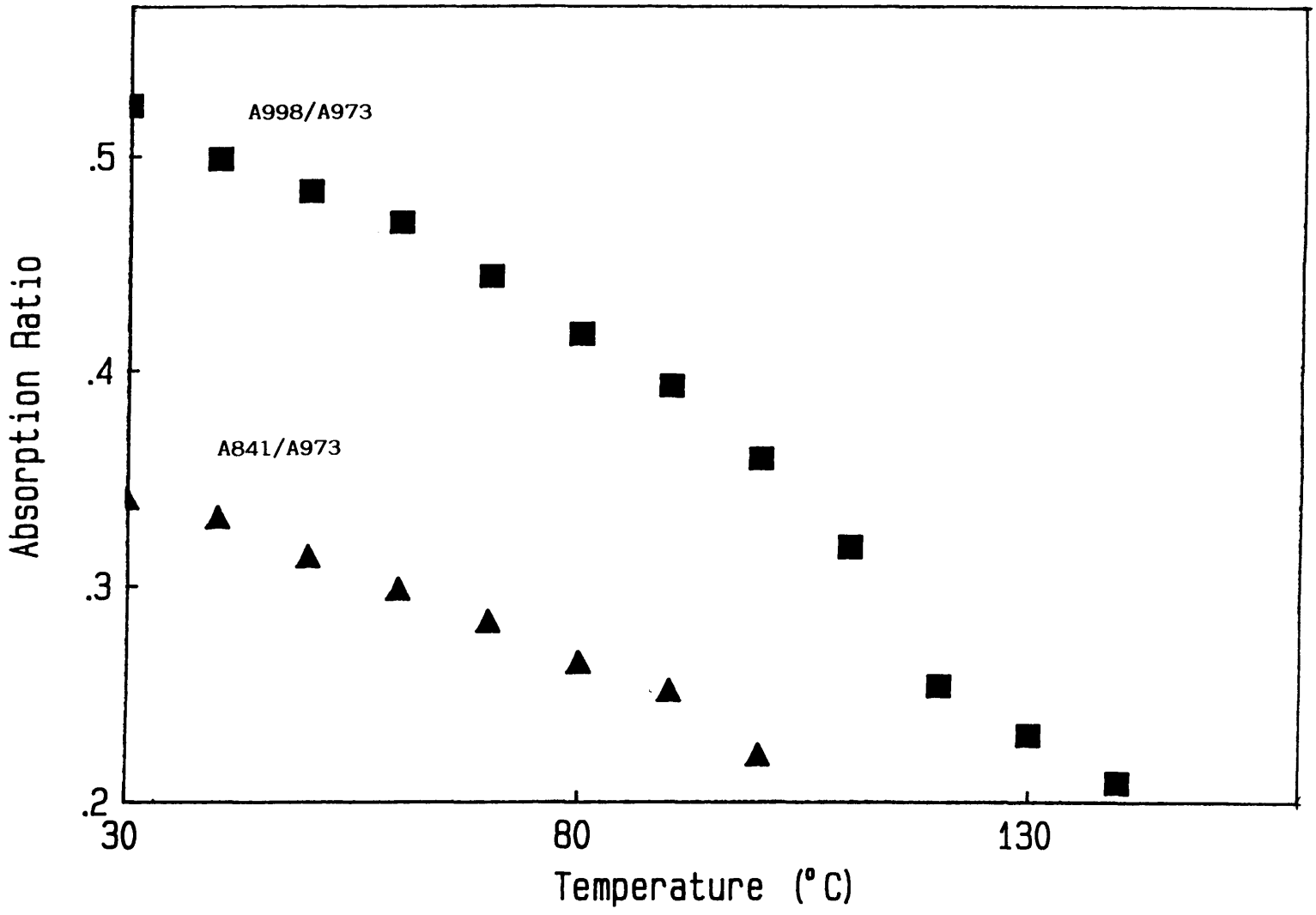

Figure 5.32

5.2.4 Stepwise Downward Annealing Of Shell:Vest Blends

Triplicate samples of 5-10 mg of each composition of blends with Shell isotactic polypropylene involving Vest703, 708 and 750 were encapsulated in aluminium pans for DSC stepwise downward annealing treatment as described in section 4.8.1.

Analyses of the resultant thermograms was carried out by partial area calculations on the multiple peaks as a fraction of the area under the total endotherm. Results for the mean areas and peak positions for each blend are shown in Tables 5.32 - 5.38. Figures 5.33 - 5.35 show the melting endotherms of each blend composition for each blend involving Vest703, 708 and 750 subsequent to multiple downward annealing and Figures 5.36 - 5.38 show the melting endotherms of the 100% Vest703, 708 and 750 samples subsequent to stepwise downward annealing on an expanded scale.

Shell:Vest703

	Total	Partial Areas									
	ΔH_f	1		2		3		4		5	
Blend	(J/g)	Area	%	Area	%	Area	%	Area	%	Area	%
100:0	150.84	1.96	1.30	3.92	2.60	8.60	5.70	25.67	17.02	110.67	73.37
75:25	103.64	1.22	1.18	3.37	3.25	5.91	5.70	16.03	15.47	77.11	74.40
50:50	62.31	0.87	1.40	2.17	3.48	4.34	6.97	25.02	40.16	29.90	47.98
25:75	35.87	0.63	1.75	1.54	4.30	2.36	6.58	25.86	72.11	5.47	15.25
0:100	12.10	9.56	79.01	1.38	11.40	0.76	6.28	0.40	3.31	---	---

Table 5.32 Mean partial areas of each peak for each blend composition of Shell:Vest703 as a percentage of the total heat of fusion (ΔH_f).

Blend Shell:Vest703	Peak Temperature (°C)				
	1	2	3	4	5
100 : 0	130.63	138.83	149.45	159.92	172.07
75 : 25	129.19	140.57	149.83	159.24	171.93
50 : 50	127.75	138.84	149.23	158.70	171.52
25 : 75	126.02	138.96	148.19	158.93	170.94
0 : 100	103.93	127.26	138.26	147.80	---

Table 5.33 Mean peak temperatures in the melting thermograms of successively downward annealed Shell:Vest703 blends.

Shell:Vest708

Blend	Total ΔH_f (J/g)	Partial Areas									
		1		2		3		4		5	
		Area	%	Area	%	Area	%	Area	%	Area	%
100:0	150.84	1.96	1.30	3.92	2.60	8.60	5.70	25.67	17.02	110.67	73.37
75:25	106.53	1.56	1.46	2.77	2.65	5.47	5.13	13.88	13.03	82.81	77.73
50:50	71.11	0.85	1.20	1.66	2.34	3.81	5.36	11.09	15.60	53.69	75.50
25:75	33.65	0.34	1.00	0.71	2.10	2.10	6.23	17.87	53.11	12.64	37.56
0:100	3.49	3.40	97.42	0.09	2.58	---	---	---	---	---	---

Table 5.34 Mean partial areas of each peak for each blend composition of Shell:Vest708 as a percentage of the total heat of fusion (ΔH_f).

Blend Shell:Vest708	Peak Temperature (°C)				
	1	2	3	4	5
100 : 0	130.63	138.83	149.45	159.92	172.07
75 : 25	130.17	139.49	148.81	159.27	171.65
50 : 50	130.59	139.78	148.56	157.96	171.47
25 : 75	127.40	141.15	149.02	158.56	171.35
0 : 100	96.06	123.59	---	---	---

Table 5.35 Mean peak temperatures in the melting thermograms of successively downward annealed Shell:Vest708 blends.

Shell:Vest750

Blend	Total ΔH_f (J/g)	Partial Areas									
		1		2		3		4		5	
		Area	%	Area	%	Area	%	Area	%	Area	%
100:0	150.84	1.96	1.30	3.92	2.60	8.60	5.70	25.67	17.02	110.67	73.37
75:25	96.59	1.10	1.14	2.43	2.52	5.33	5.52	11.49	11.89	76.23	78.92
50:50	68.25	0.61	0.90	1.71	2.50	3.71	5.43	9.23	13.53	52.99	77.64
25:75	34.32	0.46	1.33	0.86	2.51	2.07	6.02	11.51	33.55	19.42	56.59
0:100	2.82	2.79	98.97	0.08	2.94	---	---	---	---	---	---

Table 5.36 Mean partial areas of each peak for each blend composition of Shell:Vest750 as a percentage of the total heat of fusion (ΔH_f).

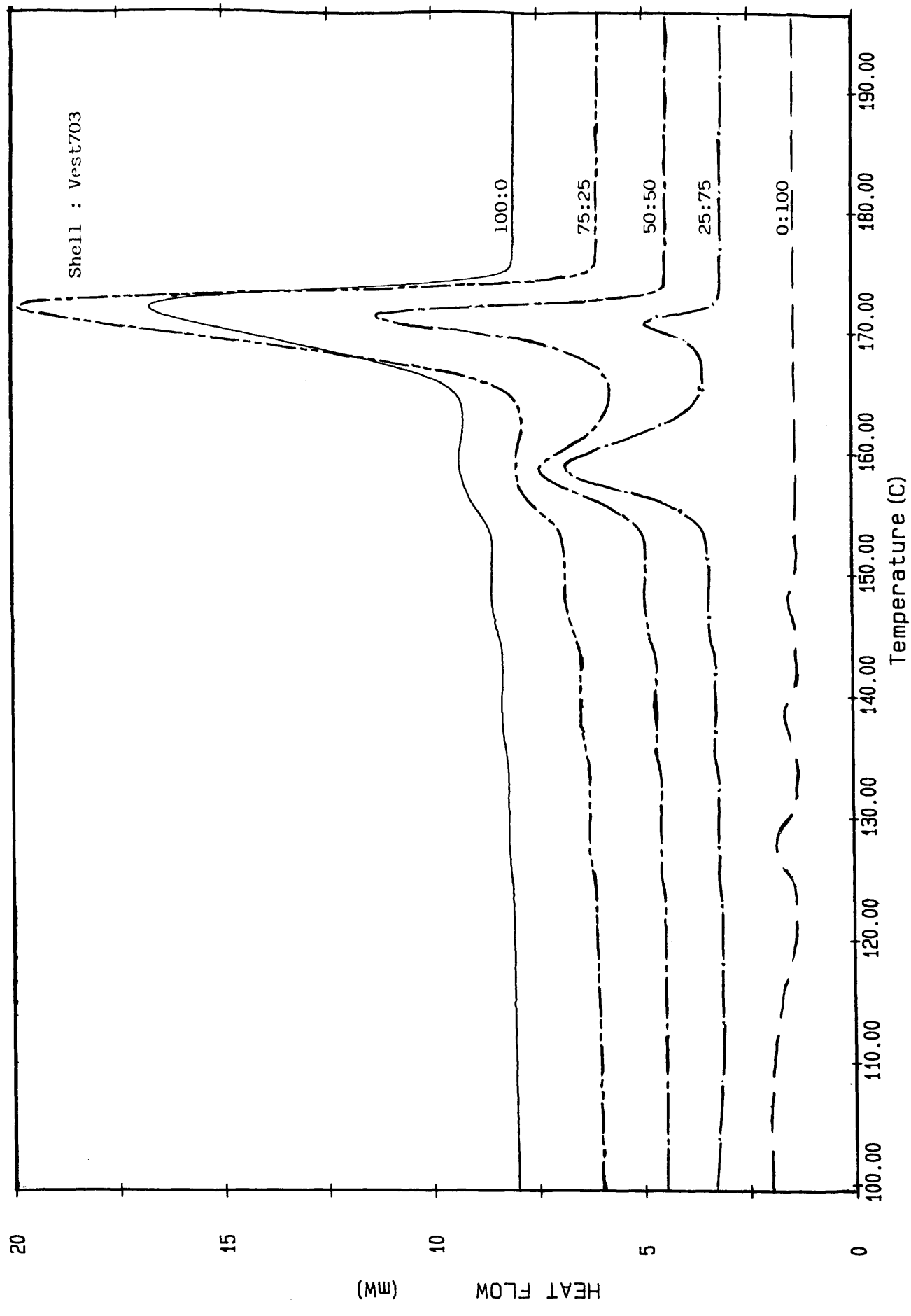

Figure 5.33 DSC melting profiles for the various Shell : Vest703 blend compositions subsequent to stepwise downward annealing

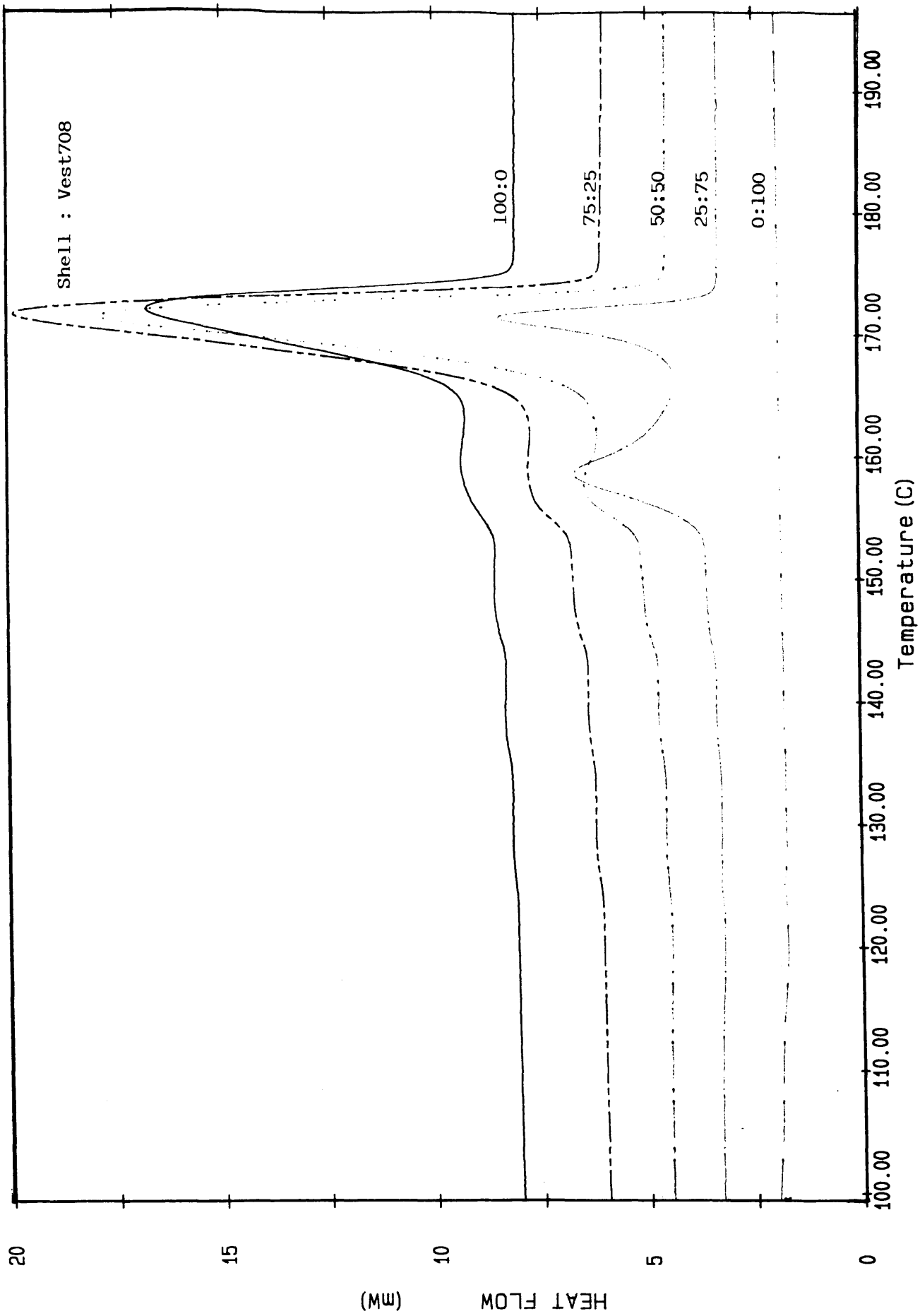

Figure 5.34 DSC melting profiles for the various Shell : Vest708 blend compositions subsequent to stepwise downward annealing

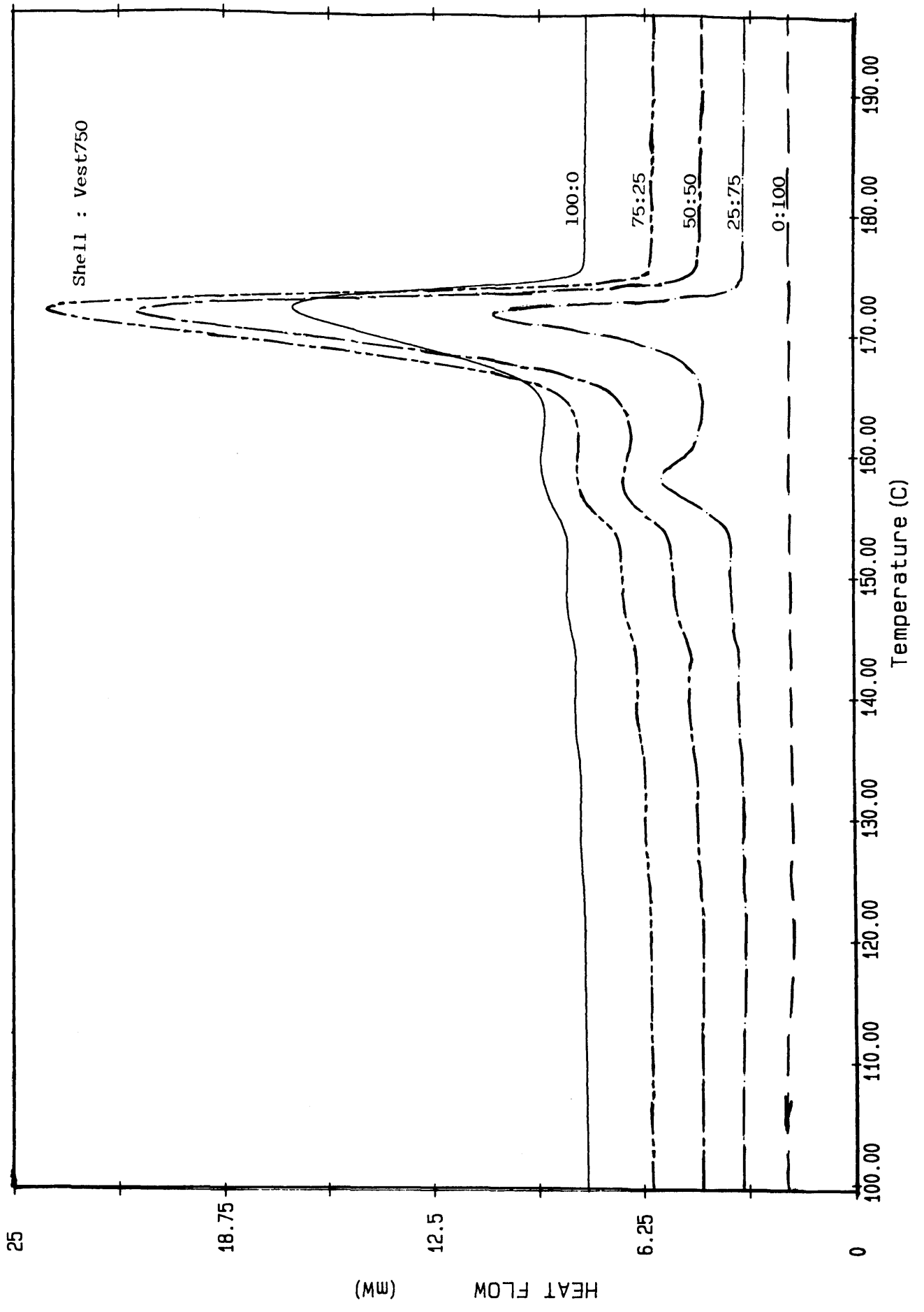

Figure 5.35 DSC melting profiles for the various Shell : Vest750 blend compositions subsequent to stepwise downward annealing

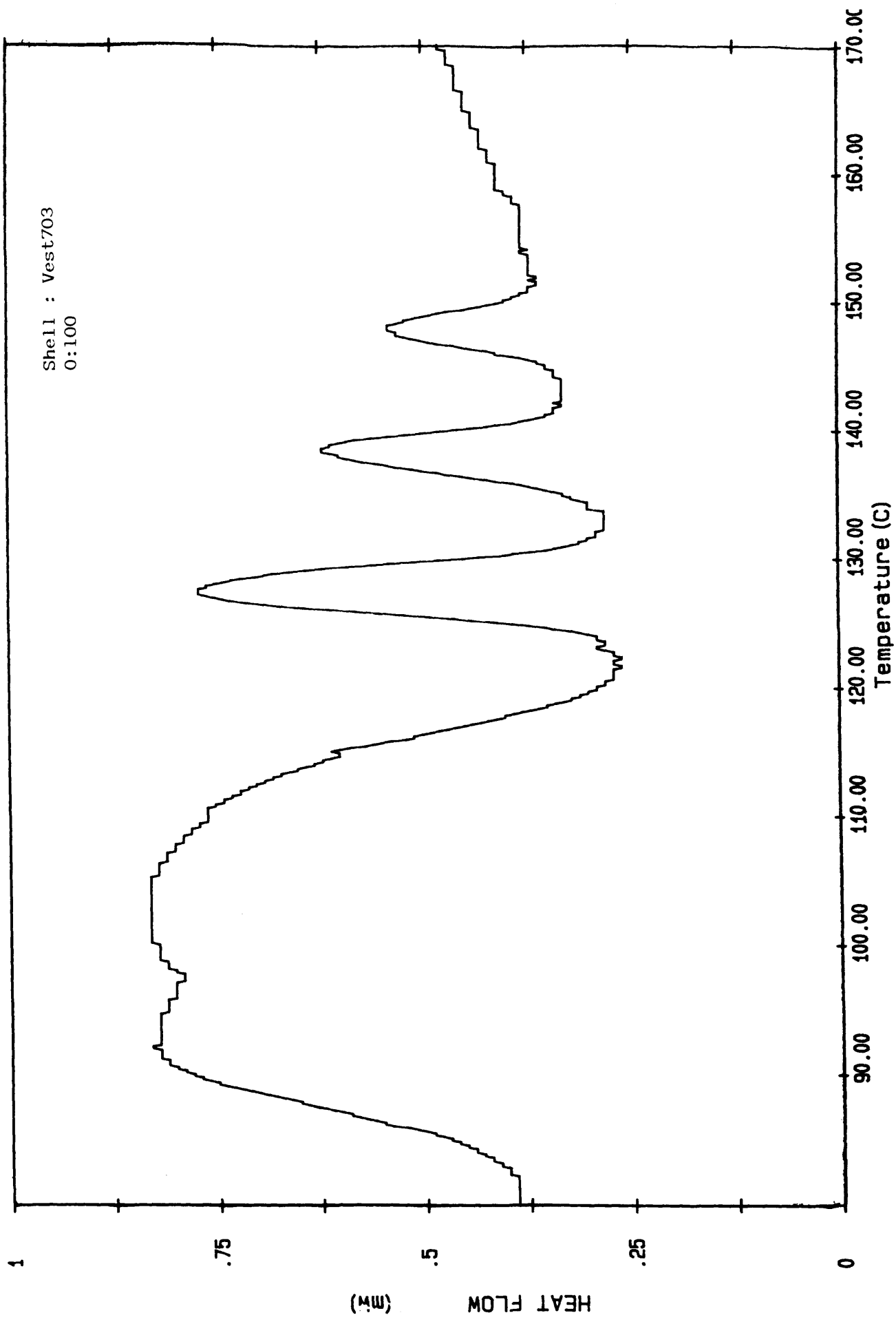

Figure 5.36 DSC melting profile of the Shell : Vest703, 0:100 sample subsequent to stepwise downward annealing shown on an expanded scale

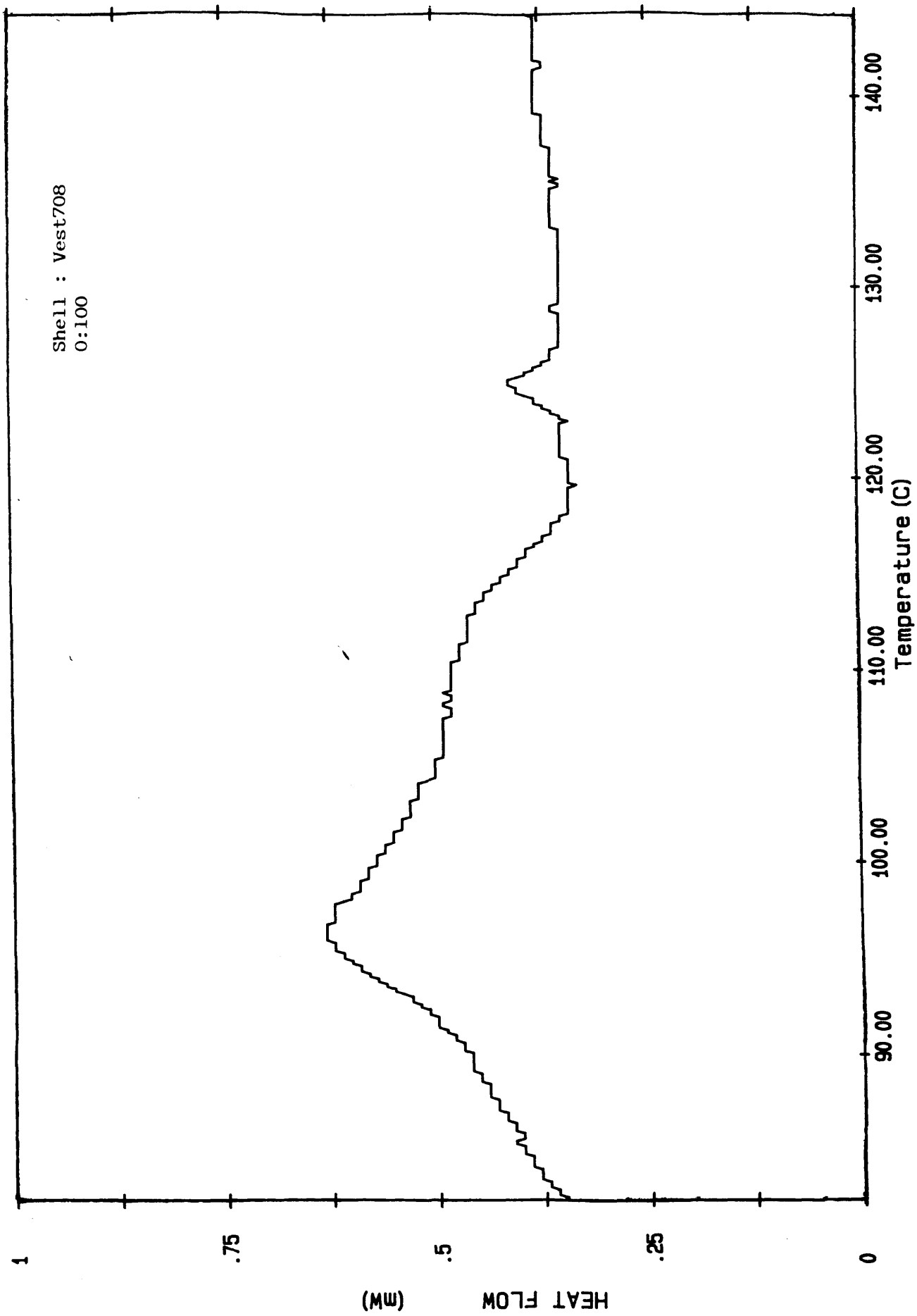

Figure 5.37 DSC melting profile of the Shell : Vest708, 0:100 sample subsequent to stepwise downward annealing shown on an expanded scale

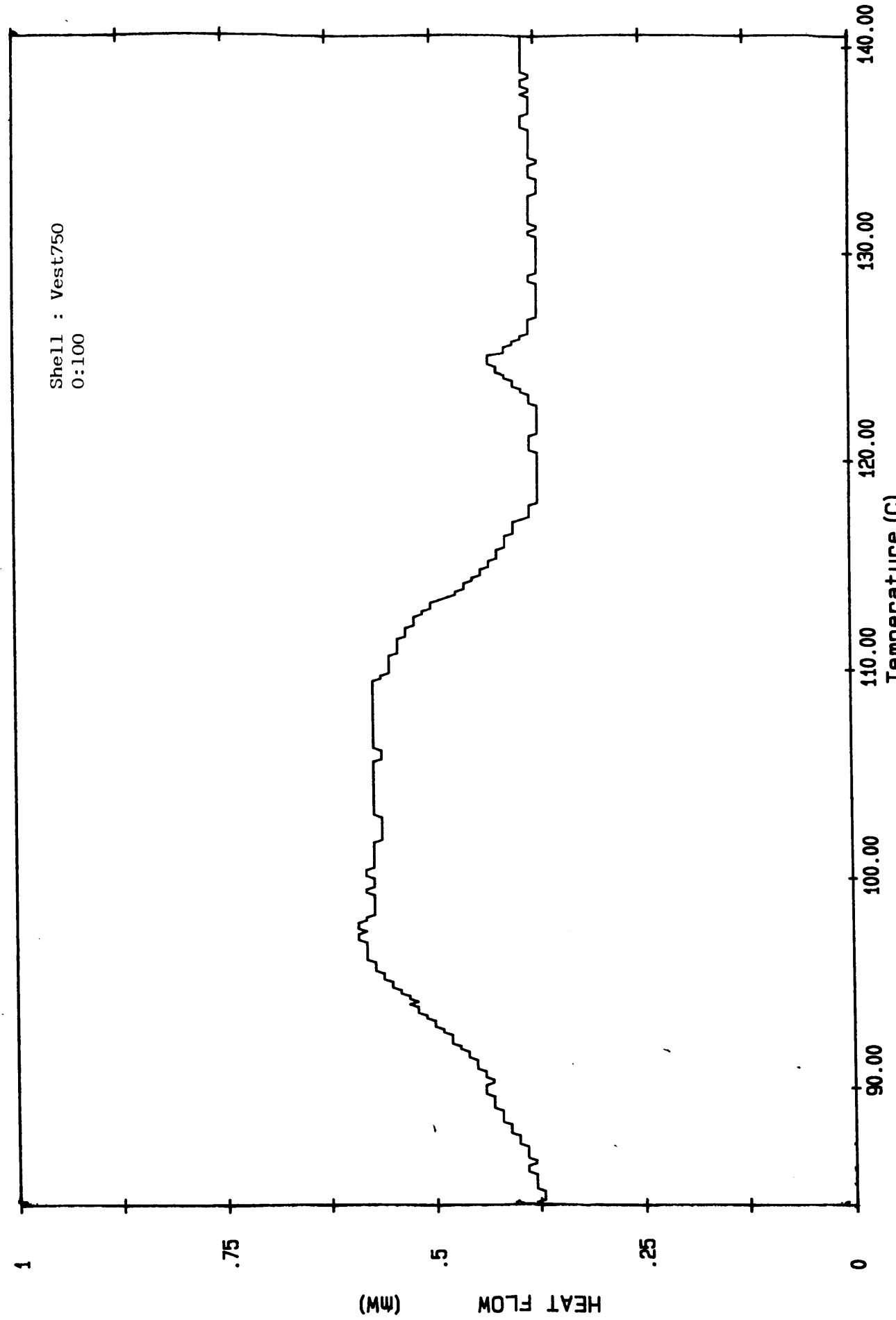

Figure 5.38 DSC melting profile of the Shell : Vest750, 0:100 sample subsequent to stepwise downward annealing shown on an expanded scale

Blend Shell:Vest750	Peak Temperature (°C)				
	1	2	3	4	5
100 : 0	130.63	138.83	149.45	159.92	172.07
75 : 25	130.38	140.96	149.10	159.15	171.76
50 : 50	130.70	140.97	149.99	158.22	171.66
25 : 75	129.50	140.70	150.20	158.25	171.57
0 : 100	97.13	124.73	---	---	---

Table 5.37 Mean peak temperatures in the melting thermograms of successively downward annealed Shell:Vest750 blends.

5.3 Discussion

5.3.1 Miscibility Of Blend Components

Results presented in section 5.2.1.1 show that a considerable degree of miscibility exists in the blends involving the Shell isotactic polypropylene and the Vest703 amorphous terpolymer.

Melting these two components together and allowing them to undergo "self mixing" in the molten condition before cooling at a controlled rate appears to promote a gradual miscibility which increases with each heat/cool cycle. The DSC crystallisation results (Table 5.1 and Figure 5.1) clearly show a tendency towards a single crystallisation exotherm which confirms the miscibility of the two components.

The first crystallisation thermogram exhibits two peaks which correspond to the independent crystallisation of the two components of the blend. This is indicative of very little or no melt mixing of the components. After the eighth heat/cool cycle,

however, a higher degree of "self mixing" is apparent and a corresponding decrease in the ΔH_c and shifting to a higher onset temperature of the lower crystallisation peak is observed. The higher crystallisation peak which is associated with the isotactic polypropylene shifts to a lower crystallisation onset temperature and exhibits a higher ΔH_c value. The depletion of the lower temperature crystallisation peak progresses with further heat/cool cycles and after the twelfth heat/cool cycle, extensive broadening and shifting to a higher onset value and lower ΔH_c is observed. The corresponding higher crystallisation peak exhibits a further increase in ΔH_c as more and more melt mixing occurs. Finally, after fourteen heat/cool cycles, the low temperature peak virtually disappears and is only noticeable by a very slight inflection in the baseline. The higher temperature crystallisation peak by this stage is broader and exists almost exclusively as a single exotherm with a ΔH_c value higher than that of previous heat/cool cycles. It is also interesting to note that the crystallisation onset temperatures of the higher crystallisation peaks after the twelfth and fourteenth heat cycles have increasingly higher onset temperatures. This is possibly due to annealing processess caused by the successive heating and slow cooling of the blend leading to increased perfection in some of the higher melting crystallites which may persist in the melt and as a consequence, nucleate earlier than in previous runs.

In general, as the heat/cool cycles progress (and hence more melt mixing occurs) the lower crystallisation peak onset values appear to move towards that of the higher crystallisation peak. This continues until after complete melt mixing, the components produce only one exotherm characteristic of that particular blend composition. It is proposed that as the degree of melt mixing increases, a greater portion of the isotactic polypropylene segments in the terpolymer are capable of co-crystallising with the Shell isotactic polypropylene when cooled from the molten state and since the terpolymer is inherently high in propylene content, this process is capable of occurring to a relatively high degree.

This raises questions about the fate of the uncrystallisable material present in the terpolymer and its blends with isotactic polypropylene. Lohse and Wissler[171] in a study involving the miscibility of isotactic and atactic polypropylene, suggested that the uncrystallisable or amorphous component can exist in three main regions associated with polypropylene structure:-

(i) Between spherulites (interspherulitic boundaries)

(ii) Between the radial rods which contain stacked lamellae and grow within the spherulite itself

(iii) Between individual lamellae

These regions are represented schematically in Figure 5.39

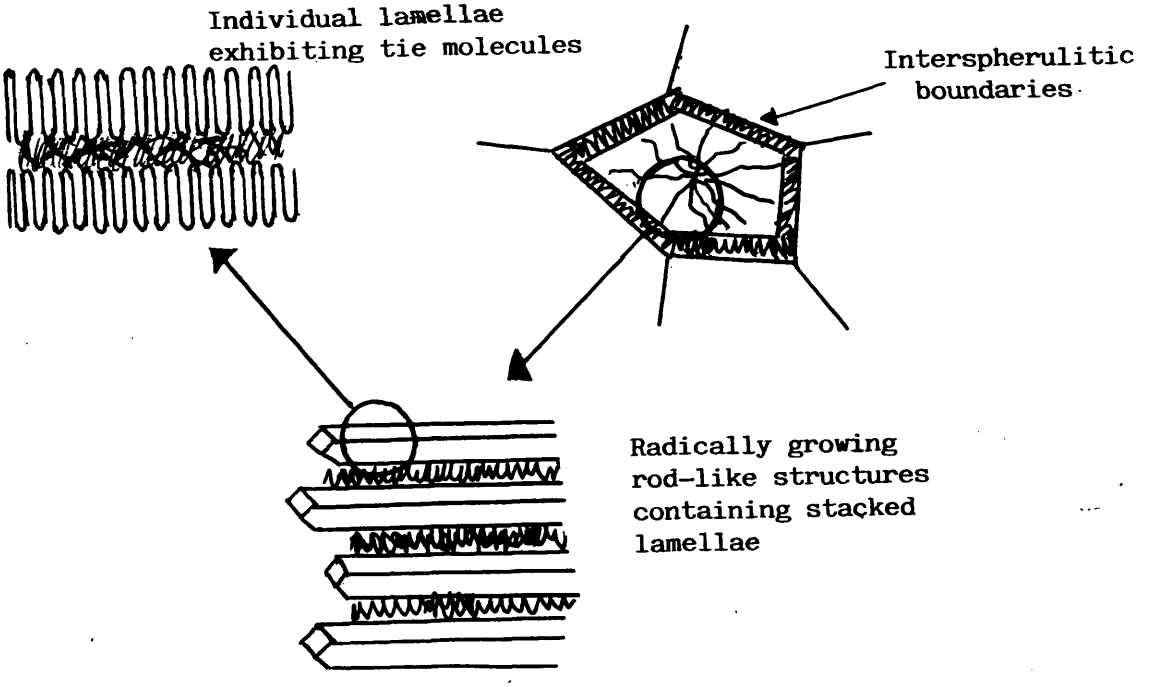

Figure 5.39 Morphological regions capable of accomodating amorphous material.

It is conceivable that the uncrystallisable fraction of the terpolymer is incorporated into the isotactic polypropylene matrix by accomodation in one or all of these morphological regions. This assumes that the components of the system are homogenous in the melt and hence produce an intrinsically determined phase morphology[169].

Further confirmation of the compatibility of the components of the Shell:Vest703 blend can be drawn from the hot-stage polarised light microscopy observations (section 5.2.1.1.2). Figure 5.2 shows optical micrographs of the two components after crystallisation from 200°C at 10°C/min. The interface between the two components is well defined with the isotactic polypropylene showing a well developed spherulitic morphology whilst the poorly crystalline Vest703 terpolymer exibits a largely amorphous character with small regions of crystalline material interspersed throughout. Figures 5.3 and 5.4 show that the interface becomes less well defined after subsequent heat/cool cycles as a consequence of increased melt blending, until finally (Figure 5.5), an almost homogenous picture of spherulitic morphology arises in which isotactic polypropylene spherulites have effectively been "filled" with co-crystallised terpolymer.

5.3.2 General Characterisation Of Shell Isotactic Polypropylene Blends Involving Vest703, 708 and 750 Terpolymers

FTIR, density, molecular weight, wide angle x-ray diffraction and DSC measurements were used to characterise Shell isotactic polypropylene blends with Vest703, 708 and 750.

As expected, the relative concentrations of infrared active isotactic helices in the blend decreased with increasing amorphous terpolymer content. As outlined earlier,

the 998 and 841 cm^{-1} bands are generally believed[20] to be associated with the appearance of isotactic helices of different critical sequence lengths (J_{eff}) in the infrared spectrum of isotactic polypropylene with the 998 cm^{-1} band being associated with relatively smaller (J_{eff} = 11-12 monomer units) isotactic sequence lengths compared to the 841 cm^{-1} band (J_{eff} = 13-15 monomer units).

Figure 5.6 shows that the blends involving the Vest703 terpolymer contain a higher concentration of short isotactic helices than the blends involving the Vest708 and 750 terpolymers which possess similar concentrations of short isotactic sequence lengths to each other. For the longer isotactic sequences (Figure 5.7), the blends involving Vest703 also appear to have higher concentrations. The blends involving the Vest750 contains less longer sequences than blends involving Vest703 but more than blends involving Vest708.

In general, as the isotactic polypropylene content of the blend increases, the differential between the helical concentrations in the blends becomes less and tends towards a maximum saturation value.

Similar trends appear in plots of the density results for the various blends (Figure 5.8). From these results it can be seen that the different base terpolymers generally exhibit different degrees of crystallisability in the order:-

Vest703 > Vest750 $\gtrsim$ Vest708

The x-ray crystallinities of the blends (Figures 5.9 - 5.11) show a linear relationship with blend composition and the x-ray diffractograms of the blends (Figures 5.12 - 5.14) all seem to be of isotactic polypropylene in origin. The small peak at a 2θ value of around 16.00° present in the 100% Vest samples diminishes as the isotactic

polypropylene content increases and the peak at a 2θ value of 17.00° becomes a singlet. The single peak at a 2θ value of 21.50° which is exhibited in the 100% Vest samples splits to form a doublet characteristic of isotactic polypropylene in the 21.00°-22.00° 2θ range.

The x-ray data shows that as the content of Vest increases the diffractograms, although primarily isotactic in nature, become less well defined and, not surprisingly, contain a larger proportion of amorphous scattering.

The GPC data obtained for Shell:Vest blends (Tables 5.8 - 5.10) followed expected trends in so much as molecular weight averages were found to increase with increasing Shell isotactic polypropylene content in the blend. It was also apparent that, in general, the values of the molecular weight averages in the blends involving the Vest 750 were higher than those involving Vest708 which in turn were higher than those involving Vest703. This result is seen in Figure 5.40 which shows $\overline{M}_w$ versus percent isotactic polypropylene content in the terpolymer blends. Considering that the manufacturer's specifications for the Vest703, 708 and 750 terpolymers have $\overline{M}_v$ values of 35000, 45000 and 70000 respectively, which are in good agreement with data obtained in this study, it is not surprising that the molecular weight averages for the blends are dependent on which terpolymer is used.

It is also noticeable that the polydispersity index of the various blends is much higher than that of the 100% Vest or 100% isotactic polypropylene samples with the blends involving Vest703 having the highest values for this, then the blends involving Vest708 followed by the blends involving Vest750 which have the lowest polydispersity index. Again this result is not entirely surprising since blending a relatively low molecular weight polymer with a relatively high molecular weight polymer will inevitably increase the breadth of the molecular weight distribution.

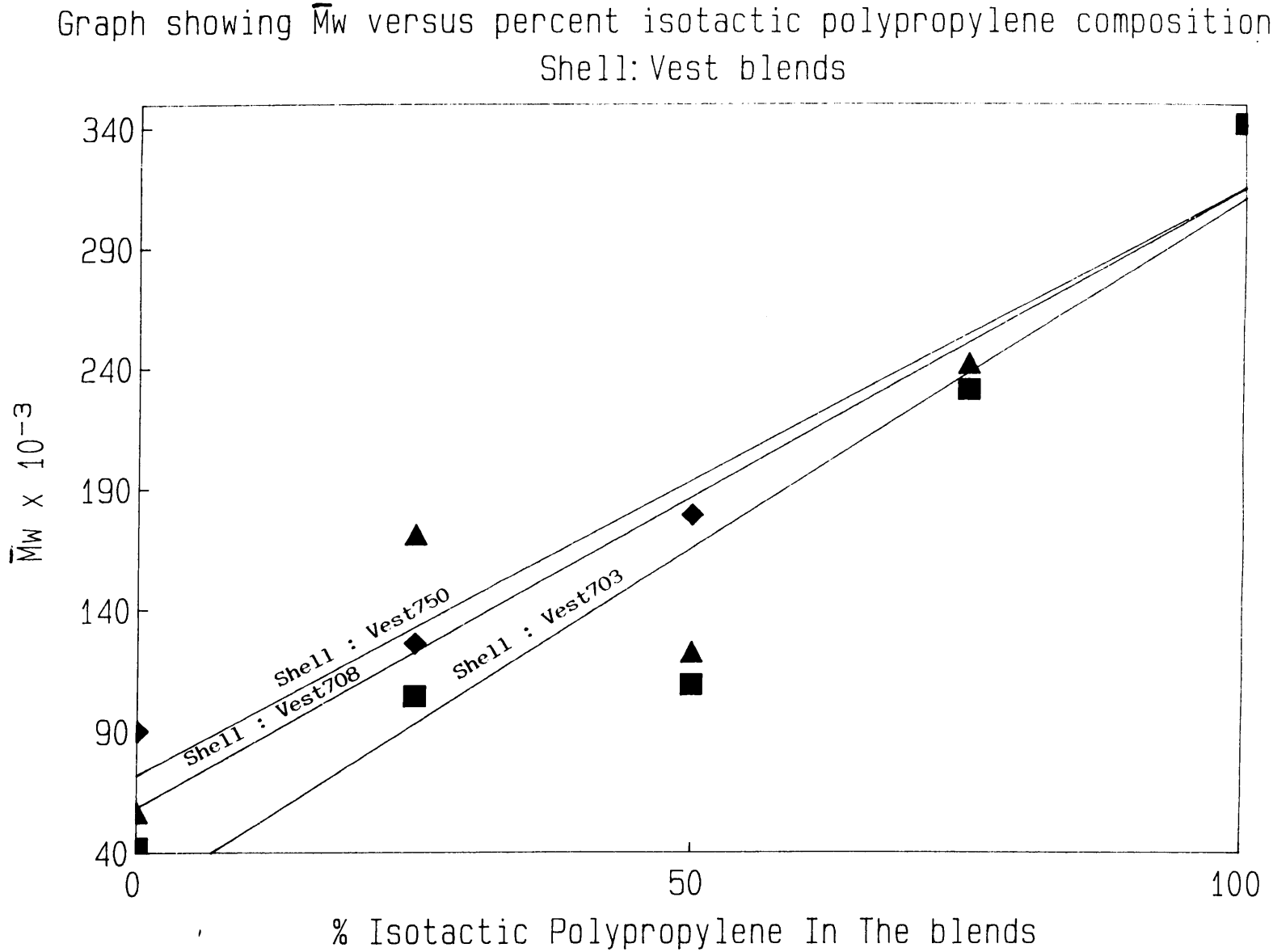
Graph showing $\bar{M}w$ versus percent isotactic polypropylene composition in Shell: Vest blends
340
290
240
190
140
90
40
$\bar{M}w \times 10^{-3}$
0
50
100
% Isotactic Polypropylene In The blends
Shell : Vest750
Shell : Vest708
Shell : Vest703

Figure 5.40

The DSC results presented in section 5.2.1.6 show that the blends exhibit interesting melting and crystallisation behaviour. The melting behaviour of the blends (Table 5.17 - 5.19 and Figures 5.15 - 5.17) involving Vest703, 708 and 750 is similar throughout the various blend compositions although there are differences in the melting of the 100% Vest terpolymers. These differences are small between the Vest708 and 750 terpolymers but the Vest703 clearly shows a higher melting temperature relative to the other two terpolymer grades.

For the 100% Shell isotactic polypropylene homopolymer, a single relatively sharp peak is observed with its peak temperature at about 161°C. For all blend compositions, the melting onset temperatures are lower than that of the isotactic polypropylene homopolymer. The Shell:Vest, 75:25 melting profiles for the blends involving the Vest703 and 708 terpolymer exhibit a main peak temperature which is lower than that of the corresponding main peak temperature in the Shell:Vest750, 75:25 blend. All three melting endotherms, however, clearly consist of two overlapping melting regions. This scenario becomes more apparent as the Vest terpolymer content of the blend is increased.

For the Shell:Vest, 50:50 blend compositions, the melting profiles exhibit a broad low temperature shoulder which is merged with a more intense higher temperature peak which occurs at a temperature corresponding to the melting isotactic polypropylene homopolymer. As the Shell:Vest ratio reaches 25:75, the melting profiles tend towards a single broad endotherm which has its peak at a temperature intermediate between the two overlapping peak temperatures observed in the 75:25 and 50:50 blend compositions. Despite the relatively high content of Vest terpolymer in the blend, this broad melting peak occurs closer to the temperature region normally associated with the melting of isotactic homopolymer than that of the pure Vest terpolymer which suggests that even the addition of small amounts of isotactic

polypropylene vastly increases its crystallinity content. On the other hand, the Shell:Vest, 75:25 blend compositions are very close in character to the melting of the entirely isotactic sample which suggests that adding a small amount of Vest to the isotactic polypropylene homopolymer has a relatively small effect on its thermal properties. These results reinforce the argument for compatibility of the components of the blend and present an argument for the occurrence, to a certain degree, of co-melting in the blends.

It has been suggested[172,173] that blending isotactic polypropylene with an elastomer results in a decrease of the size and perfection of the isotactic crystallites in the blend or in otherwords, the presence of an elastomer hinders crystallisation. In the light of this, the origin of the lower temperature shoulder in the endotherms of the blends may be due to the melting of relatively poorly formed crystallites which stem from the co-crystallisation of isotactic polypropylene segments from the Vest terpolymer with the Shell isotactic polypropylene homopolymer. As the Vest terpolymer content in the blend is increased, more co-crystallisation occurs which results in a broader distribution of relatively poorly formed crystallites. Subsequent melting of these crystallites occurs over a broader range and at a lower temperature hence the tendency towards a broad peak at a lower temperature as the Vest content in the blend is increased. There is also a corresponding decrease in the ΔH_f values which is what would be expected when an increasing amount of isotactic polypropylene is being substituted by a less crystalline polymer.

The crystallisation results for the Shell:Vest blend compositions (Tables 5.17 - 5.19 and Figures 5.18 - 5.20) reinforce the above hypothesis. Again the blends all behave similarly with only small differences being observed with respect to the terpolymer grade. All crystallisation profiles exibit the presence of only one peak which varies in position depending on blend composition.

The 100% Shell isotactic polypropylene, not surprisingly, has the highest crystallisation peak temperature and ΔH_c and the 100% Vest has the lowest values of crystallisation peak and ΔH_c. With increasing Vest content in the blend there is a tendency towards a broader less intense peak which is shifted to a lower temperature. The difference in crystallisation temperature between the 100% Vest and the Shell:Vest, 25:75 is large, which corroborates the findings of the melting study which suggest that even small amounts of isotactic polypropylene added to Vest terpolymer markedly increases its crystallinity. The difference between the 100% isotactic polypropylene and the Shell:Vest, 75:25 is small which, again, is in agreement with the findings of the melting study for this end of the blend composition scale.

The increase in breadth of the profile and shifting of the peak to a lower temperature as the Vest terpolymer content is increased reinforces the argument for the formation of a distribution of less perfect co-crystallised crystallites in the blends. This is also emphasised by the fact that only one crystallisation peak is observed in the profile with no discontinuity whatsoever in the temperature region associated with the crystallisation of the 100% Vest terpolymer.

5.3.3 Quenching Of Blends Rapidly From The Melt

FTIR APRA results for Shell:Vest703 blends rapidly quenched from the molten state into media of various temperatures show a clear decrease in helical content with decreasing quench temperature.

For the shorter isotactic helices, as measured by the 998 cm^{-1} band, there appears to be a steady decrease in the concentration of infrared active isotactic ternary helices with respect to quench temperatures down to -50°C (Figure 5.21). At quench

temperatures lower than this, the helical content remained constant or in some cases increased in value from that obtained at the previous quench temperature. One explanation for this curious behaviour at the very low quench temperatures (-110°C and -190°C) may be that when the hot molten polymer is plunged into the quench medium, it immediately causes a gas to form around it which acts as an insulator from the true temperature of the medium and hence limits the degree of quenching.

The extent of helical loss is indicated by steepness of the slope in the curve and, as might be expected, is moreso in the blends containing a larger fraction of isotactic polypropylene. As the content of isotactic polypropylene in the blend decreases, the initial helical content is shifted to a lower value and the gradient of the quench curve becomes shallower. It should also be noted that there is a significantly large difference between the values for the initial helical content of the quenched 100% Vest703 and that of the Shell:Vest703 25:75 blend. At the other end of the scale, there is only a minor difference between the 100% Shell isotactic polypropylene and the Shell:Vest703 75:25 blend. Once more, this suggests that even relatively small amounts of isotactic polypropylene when blended with Vest703 results in a considerable increase in the crystallinity of the blend and at the other end of the scale, a relatively small amount of Vest703 when blended with isotactic polypropylene has a much smaller effect on the overall structure of the blend.

The relatively longer isotactic helices as measured by the 841 cm^{-1} band are affected by rapid quenching in much the same way (Figure 5.22) although gradients of the curves are not nearly so pronounced. This suggests that there is not such a high concentration of longer isotactic helices present initially as there are short ones.

The fact that the blends are affected in much the same way as isotactic polypropylene homopolymer is under similar quenching conditions again highlights the compatibility of the blends. It suggests that the isotactic polypropylene segments of the Vest703 terpolymer which co-crystallise with the isotactic polypropylene homopolymer are involved in the structural disordering of the ternary helices in the overall blend.

Further evidence for this behaviour is reflected in the density measurements (Figure 5.23) of each blend composition subsequent to rapid quenching from the melt into quench media of various temperatures. Each successively lower quench temperature results in a corresponding decrease in sample density (except in the case of samples quenched at the very low quench temperatures for reasons already discussed).

X-ray crystallinity measurements for blends quenched from the melt into liquid nitrogen and ice/water are compared with the x-ray crystallinities of the annealed blends (Table 5.26). It can be seen that quenching changes the structure of the blends in a way which significantly affects the sample crystallinity. The x-ray diffractograms of the liquid nitrogen and ice/water quenched blends (Figures 5.24 and 5.25) exhibit profiles characteristic of the conformationally disordered smectic state of polypropylene[112]. The x-ray diffractogram of quenched 100% Vest703 is very similar to that of of the annealed 100% Vest703 terpolymer which suggests that rapid quenching from the melt has little effect on the structure of the pure terpolymer. This is in agreement with the FTIR APRA results (Figures 5.21 and 5.22) which show only a very slight gradient in the plot of absorption ratio versus quench temperature for the 100% Vest terpolymer.

The peaks characteristic of the pure terpolymer are not present in the x-ray diffractograms of the blends, even in the blend containing 75% Vest703 terpolymer. This again highlights the ability of the terpolymer isotactic polypropylene segments to co-crystallise with, and assume similar behavioural traits as the isotactic polypropylene homopolymer under rapid quenching conditions.

Another interesting feature which can be seen in Figure 5.41 is that the effect of rapid quenching from the melt on the subsequent x-ray crystallinities of the liquid nitrogen and ice/water quenched samples are very similar. This supports the argument that the film samples are not being quenched to the full extent in the liquid nitrogen medium due to nitrogen gas insulation and, in fact, are being quenched at temperatures closer to 0°C, hence the discrepencies in the density and FTIR APRA results for this particular quench temperature.

5.3.4 Effect Of Temperature On The Infrared Spectra Of Blend Samples

Studying the effect of temperature on the infrared spectra gave further insights into the structure of the blends. FTIR APRA results (Tables 5.27 - 5.31) for the various blend compositions of Shell:Vest703 between 30°C and their melting temperatures were used to gain an understanding of structural changes associated with heating in the blends.

Graphs of absorption ratio versus temperature (Figures 5.26 and 5.27) were plotted for the 841 cm^{-1} and 998 cm^{-1} regularity bands ratioed against the 973 cm^{-1} non-helical reference band. Since these regularity bands result from the presence of 3_1 helical structure in polypropylene, they therefore disappear from the infrared spectra of polypropylene when it is melted leaving only the bands which have been assigned to the shortest helices.

Graph showing the relationship between x-ray crystallinity and Shell: Vest70: blend composition for annealed, ice/water and liquid N_2 quenched samples

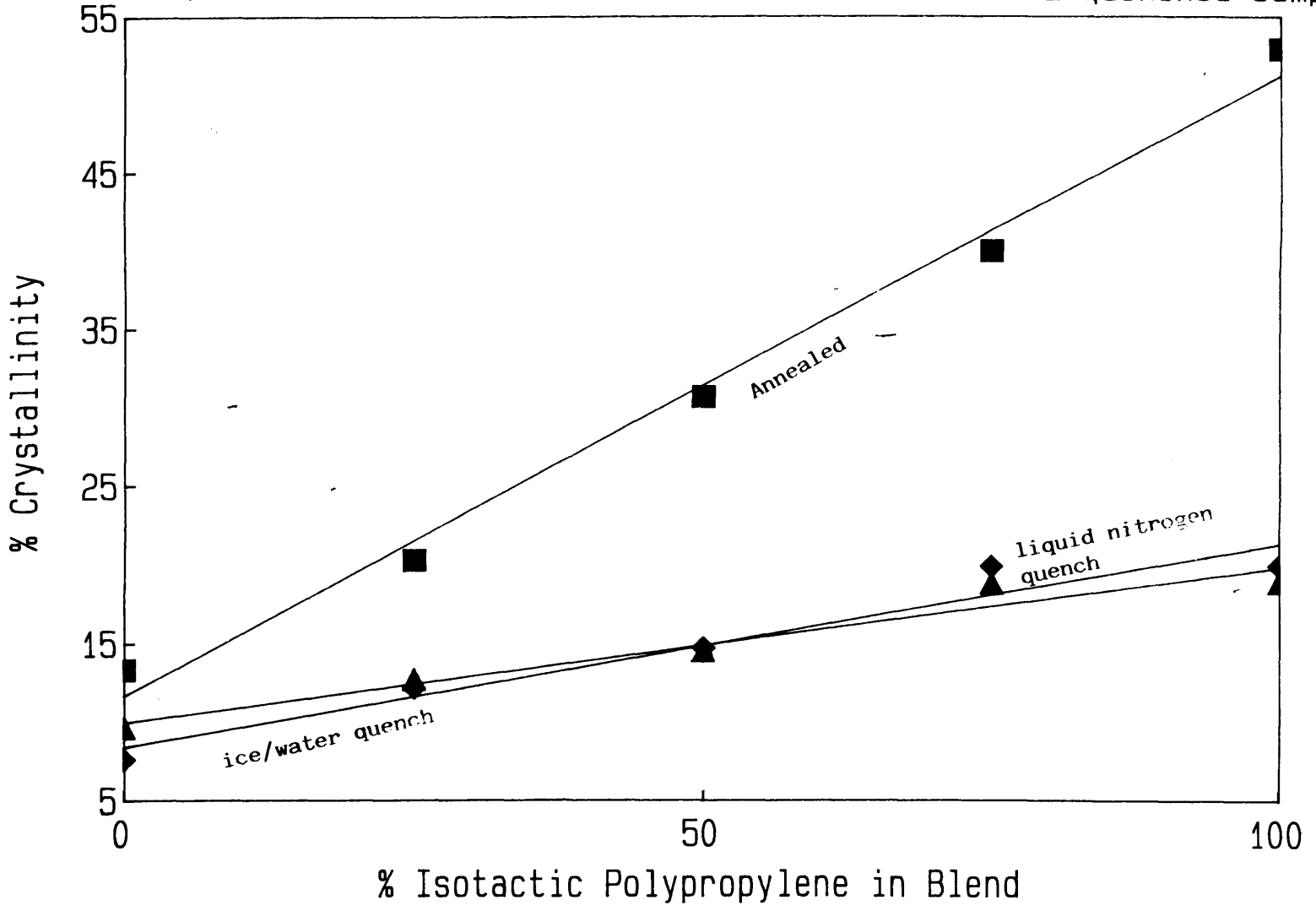

Figure 5.41

For the 100% Shell isotactic polypropylene (Figure 5.26), the plot of A998/A973 ratio versus temperature shows a linear decrease in absorption ratio values as the temperature increases. At a temperature 30-40°C below that at which melting of the film samples prevents further infrared spectroscopic readings, the absorption ratio values fell rapidly with increasing temperature. This is in agreement with work carried out by Hanna and co-workers[174] who used infrared spectroscopy, amongst other techniques, to characterise a transition which occurs some 30°C below the melting point of annealed isotactic polypropylene, above which the decrease in the helical concentration occurred at a higher rate.

When Vest703 terpolymer is blended with Shell isotactic polypropylene, the linear relationship which was observed in the 100% Shell iPP sample is maintained as is the transition 30-40°C below the melting temperature in the infrared spectra of the films. From Figure 5.26, however, it can be seen that as the fraction of Vest703 in the blend increases, the rate of decrease in the concentration of helical material in the sample after the transition temperature, becomes increasingly less as indicated by shallower line gradients. (Again the difference in the helical content between the pure Vest703 and the Shell:Vest703, 25:75 blend is noticeably large).

The results for the A841/A973 absorption ratio (Figure 5.27) which is representative of the longer helices, showed similar behaviour. The pre-transition linear behaviour of the blends for this ratio, however, shows less of a gradient than the corresponding linear portions for the A998/A973 ratio. Figures 5.28 - 5.32 show a comparison of the results for the two ratios. For the Shell:Vest703 100:0, 75:25 and 50:50 blend compositions, this feature of the pre-transition linear portion of the curves is clear. Another noticeable feature of these curves is that after the transition, the values for both ratios and the rates of helical extinction as indicated by the line gradients are virtually identical. For the Shell:Vest703, 25:75 and 0:100 blend compositions, the

pre-transition line gradients show the same trend as found in all other compositions for both ratios. The post-transition slopes, however, show that although the rate of decrease in helical concentration appears to be similar there is a clear separation of ratio values between the A998/A973 and A841/A973 absorption ratios.

These results show that the behaviour of the blends when heated is characterised by a decrease in helical concentration which is not unexpected since heating leads to an increase in disorder in polymers. Helical material in polypropylene exists mainly as well packed ordered unit cell structures. It is known, however, that some helically coiled material which is not arranged in the unit cell structure can exist in polypropylene and therefore there are two structures which must be considered when interpreting the results. In otherwords both the crystalline and non-crystalline helical material may be affected by temperature.

The rate of decrease in the concentration of the shorter helices appears to be higher than that of the longer isotactic helices in the pre-transiton temperature region in all blend compositions. Also the transition temperature becomes lower with a higher Vest703 content, which is not unexpected since the melting temperature of these blends also becomes lower with a higher Vest703 content. As the Vest703 content is increased it is reasonable to assume that the presence of non-crystalline helical material also increases and hence there is relatively less helical material arranged in the well packed unit cell structure. If this is the case, it is likely, from energetic considerations that the non-crystalline material would disappear first leaving only a small concentration of crystalline material left to undergo the transition at 30-40°C below melting.

Since co-crystallisation with the Vest703 terpolymer lowers the melting temperature of the resultant blend structure the transition takes place earlier. This may also explain the increasing shallowness of the transition line gradient because as more Vest703 is present in the blend then more of the Shell isotactic polypropylene is involved in co-crystallisation and hence a higher concentration of relatively poorly perfected cystalline structures are present leaving less highly ordered crystalline helices to be extinguished. These poorly ordered structures would be similar to one another in perfection and take less energy to extinguish and hence would disappear from the infrared spectra at a more gradual rate and lower temperature than those blends which have a higher concentration of well packed unit cell structures. This inevitably leads to a corresponding decrease in the transition line gradient as more Vest703 is present in the blend.

5.3.5 Stepwise Downward Annealing Of The Blends

Stepwise downward annealing was carried out on the Shell:Vest703, 708 and 750 blends in order to gain further insights into the behaviour of the blend structure.

Each blend composition was subjected to the stepwise downward annealing process and from the results (Tables 5.32 - 5.37 and Figures 5.33 - 5.38) it can be seen that for all blend compositions five peaks were resolved (except for the pure Vest703 which produced four peaks and the pure Vest708 and 750 each of which produced two peaks) which correspond to each annealing temperature and provide information on the crystallite distribution in the samples. The total ΔH_f values for the various blends, not unexpectedly, decrease with increasing Vest terpolymer content.

Applying Gray and Casey's discontinuous crystallite distribution model[163] as previously discussed in section 4.8.2.1, to the Shell:Vest blend stepwise downward annealing results, it was possible to obtain information on the crystallite distribution behaviour as a consequence of melt blending Shell isotactic polypropylene homopolymer with the various Vest terpolymer grades.

From the partial area results (Tables 5.32 - 5.37) it can be seen that the 100% Shell isotactic polypropylene sample produces five peaks with a total ΔH_f of 150.84 J/g. The highest temperature peak at 172°C which represents melting of crystallites which have grown in size and perfection as a consequence of high temperature annealing at 160°C constitutes 73.37% of the total ΔH_f. The remaining peaks at around 160°C, 150°C, 139°C and 131°C represent the melting of crystallites which achieve greater perfection at annealing temperatures of 150°C, 140°C, 130°C and 120°C respectively and account for 17.02, 5.70, 2.60, and 1.96% respectively. Clearly, then, the majority of crystallites in the isotactic homopolymer are able to achieve an annealing induced higher order at the top annealing temperature of 160°C.

All the blends behave in a manner similar to isotactic polypropylene homopolymer, that is, having a majority of crystallites being perfected at the highest annealing temperature but to different degrees depending on compostition (except the Shell:Vest 25:75 and 100% Vest terpolymer samples for blends involving Vest703 and Vest708; and the 100% Vest750 sample). As the fraction of Vest in the blend increases, a corresponding decrease in the percentage of crystallites able to achieve perfection at the highest annealing temperature is observed. This decrease is offset by an increase in the percentage of crystallites obtaining higher order at the 150°C annealing temperature.

The peaks associated with the perfection of crystallites at annealing temperatures of 140°C, 130°C and 120°C represent roughly 5-7%, 2-4% and 1-2% of the total ΔH_f respectivley but changes in the percentage of total ΔH_f attributed to the melting of crystallites achieving perfection at the two highest annealing temperatures show that these are the main areas of the thermogram which are most sensitive to increasing Vest content in the blends. A noticeable feature in all the blends is that for the Shell:Vest, 75:25 composition an increase in the percentage of total ΔH_f attributed to crystallites melting at temperatures corresponding to an annealing temperature of 160°C over the corresponding percentage for the 100% Shell isotactic polypropylene sample is observed.

Furthermore, in the blends involving the higher molecular weight terpolymers, even the 50:50 blend has a higher percentage of its total ΔH_f attributed to the melting of crystallites perfected at the highest annealing temperature. The fact that this does not occur in the Vest703 blends to such a great extent even though it appears to exhibit the highest degree of crystallisable material, highlights the role of molecular weight as well as crystallisablity in the ability of the blends to produce highly ordered, high melting perfected crystallites. This would also explain why the Shell:Vest750 and 708, 25:75 blends have a higher percentage of the total ΔH_f attributed to the melting of crystallites achieving perfection at an annealing temperature of 160°C than the corresponding 25:75 blend composition for the Shell:Vest703 .

Crystallites achieving a higher degree of order at 150°C for the various blends show a general increase in percentage of the total ΔH_f as the Vest content of the blend increases. At the same time, however, the blends again exhibit a molecular weight dependency with those involving the lower molecular weight Vest703 terpolymer showing a relatively higher proportion of perfected crystallites being formed at this annealing temperature compared to the blends involving the Vest708 terpolymers

which, in turn, have a higher proportion of crystallites developing perfection at this annealing temperature than blends involving the Vest750 terpolymer.

For the stepwise downward annealing of the 100% Vest703, 708 and 750 samples, the profiles were relatively featureless due to the majority of the molecules being in the molten state at even the lowest annealing temperature. The 100% Vest703 sample (Figure 5.36), however, showed that it was capable of producing perfected crystallites which melt at temperatures associated with annealing at 140°C, 130°C and 120°C. The large broad peak at around 104°C for this sample is attributed to the melting of crystallites which remained in the liquid state at the 120°C annealing temperature and hence could not improve in structural properties. Vest708 and 750 (Figures 5.37 and 5.38) exhibited a very small proportion of crystallites capable of melting at temperatures attributed to annealing at 120°C but from their respective large broad main melting peaks it is evident that the majority of crystallites in these samples were still in the molten state at 120°C

The 100% Vest results reflect previously discussed characterisation results in so much as they show the Vest703 to be the most crystalline and the Vest708 and 750 to be similar to one another in that respect.

Once more it is interesting to note that even small amounts of isotactic polypropylene added to Vest terpolymers vastly increases its crystallisability and its ability to exhibit a relatively large amount of highly perfected crystallites which melt at correspondingly high temperatures.

The stepwise downward annealing procedure has again been useful for the investigation of polymer crystallite distribution. These results reinforce the conclusions of experiments discussed in section 4.8.2.1 concerning the molecular

weight/tacticity dependency on annealing induced perfection in the polypropylene crystallites and highlight the remarkable ability of the blends to assume behaviour typical of polypropylene homopolymer. This in turn must be attributed to the large degree of co-crystallisation apparent in the blends and the compatability of the components.

CHAPTER 6

6.0 CONCLUSIONS AND SUGGESTIONS FOR FURTHER WORK

6.0 CONCLUSIONS AND FURTHER WORK

Experimental work presented in this thesis consists of two main sections, both of which share the common aim of investigating the implications of thermal treatments on structural aspects of isotactic polypropylene and its blends with amorphous poly-α-olefin terpolymers.

6.1 STUDIES ON ISOTACTIC HOMOPOLYMER

This work is centred around investigations concerning the isotactic polypropylene homopolymer and involved five main areas of study:-

(i) Effect of quenching rapidly from the melt on the infrared spectra of several commercial grade polypropylene homopolymers.

(ii) Effect of quenching rapidly from the melt on the DSC endotherms of commercial polypropylene.

(iii) Effect of rapid quenching at a controlled rate in the DSC furnace itself.

(iv) Fractionation of isotactic polypropylene homopolymer and subsequent characterisation of the fractions.

(v) Role of molecular weight/tacticity in the thermal behaviour of polypropylene.

These investigations progressively develop from each other and collectively, present a picture of isotactic polypropylene structure as it behaves under different thermal environments and treatments. Taking each in turn, the conclusions drawn from these studies are presented in the following pages.

(i) Effect Of Quenching Rapidly From The Melt On The Infrared Spectra Of Several Commercial Grade Isotactic Polypropylene Homopolymers

This study was set up in order to determine any differences in structural behaviour between several commercial grade polypropylene homopolymers with respect to quenching rapidly from the melt whilst simultaneously appraising the use of infrared spectroscopy as a technique for investigating such changes.

A preliminary investigation involving the use of x-ray diffraction, scanning electron microscopy and density measurements established that structural changes taking place in the polypropylene samples on rapid quenching from the molten state were dependent on the temperature of the quench medium.

X-ray diffraction profiles for samples quenched into quench media at -50°C and -190°C exhibit only two broad peaks with a relatively large amounts of underlying amorphous background which is indicative of the formation of the conformationally disordered smectic phase in the polypropylene samples. The x-ray profile of the highly crystalline quenched and annealed sample shows well defined peaks characteristic of the monoclinic phase of polypropylene. X-ray photographs, show the -50°C quenched film to possess more Debye-Scherrer lines than the -190°C quenched film which exhibits a diffuse pattern consisting of only two broad lines. This confirms that as the quench temperature is lowered, more isotactic ternary helices are converted to the disordered smectic state.

Scanning electron microscopy results support this trend showing that structural differences exist in the polypropylene samples as the quench temperature decreases whilst density measurements and pseudo crystallinities show a linear decrease with

respect to quench temperature. Annealing studies show that the structural changes observed are reversible with degree of recovery from the smectic state being more dependent on annealing temperature than annealing time.

FTIR APRA results in the preliminary study revealed statistically significant differences between samples quenched at different temperatures. The findings of this preliminary study are as follows:-

(a) For a given polypropylene grade (GSE18, GYE41, PLZ772), infrared absorption ratios vary and are dependent on quench temperature.

(b) Samples quenched at temperatures below 0°C have statistically similar absorption ratio values which are significantly different to those quenched at temperatures above 0°C.

(c) There are statistically significant differences in ratio values for a given infrared absorption ratio and quench temperature between sample grades (GSE18, GYE41 and PLZ772).

These conclusions show that infrared spectroscopic methods are capable of detecting quench induced structural differences (i) at different quench temperatures within a particular sample grade; and (ii) between sample grades. A second study was initiated to further assess the ability of FTIR APRA in detecting structural changes occurring in quenched polypropylene samples between several commonly used commercial grades. The results obtained in this study corroborated the conclusions of the preliminary study. Furthermore, Tukey's Pairwise Comparison carried out on the results revealed that certain grades of polypropylene are affected differently from others at each quench temperature. It was also found that, of the ratios used, the

A998/A973 and A841/A973 were the most affective for detecting these differences. Differences between results obtained from each of these ratios are attributed to differences in the sensitivity to rapid quenching from the melt of short and long isotactic ternary helices respectively.

In general, this study has shown that infrared spectroscopy can be used to detect quench induced structural changes in commercial isotactic polypropylene, although the sensitivity of the method to structural changes induced in samples at quench temperatures below 0°C is limited in comparison to other techniques such as x-ray diffraction or density measurements. FTIR APRA has also been shown to be capable of detecting differences between commercial polypropylenes but as a routine analysis method it is time consuming and laborious and as such is perhaps not the most ideal method.

(ii) Effect Of Quenching Rapidly From The Melt On The DSC Endotherms Of Commercial Polypropylene

Studies involving the structural changes occurring in polypropylene on rapid quenching from the melt were extended to include thermal analysis investigations. DSC melting of quenched polypropylene samples (ie. the same samples as used in the preliminary infrared experiments) exhibit a small broad exothermic peak at around 80°C which confirms the formation of the smectic phase on rapid quenching and is attributed to the smectic → monoclinic phase transition. Another feature of the melting endotherm is a is a double peak phenomenon which, on subsequent heat cycles disappears from the thermogram, leaving only one relatively sharp endotherm occurring at 4-8°C higher than that of the original melting onset temperature for the quenched samples. The double peak, therefore, is considered to be a direct consequence of the quench induced structural changes in the polypropylene.

Furthermore, the intensity of the higher temperature peak is higher in the samples quenched at the lower temperatures. The ΔH_f values for the first heat cycle of the quenched polypropylene samples are lower than those of heat cycles 2-5 which, again confirms a decrease in crystallinity on rapid quenching from the melt.

X-ray studies show that the occurrence of a double peak could not possibly be attributed to the presence of other polypropylene polymorphs and the continuous nature of the Debye-Sherrer lines in the x-ray photographs eliminate the possibility of orientation effects having a role in the formation of the double peaks. It is also doubtful that sample oxidation could be a contributing factor because the double peak profile disappeared on subsequent heating cycles.

It is proposed that the double peak is caused by a partial melting and subsequent recrystallisation process during the heating run. It is thought that the origin of the high temperature peak stems from the behaviour of the smectic material. When smectic phase material crystallises to the monolinic phase, it is proposed that this newly transformed material undergoes a further partial melting and recrystallisation process more easily than the bulk material before it finally melts at a higher temperature. This process involves transformation from the α_1-limiting modification, to the higher order, lower energy α_2-limiting modification. Since more smectic material forms at lower quench temperatures, then this also explains the increase in intensity of the higher melting peak as the quench temperature is decreased.

Crystallisation endotherms recorded during thermal cycling show no dependency on quench temperature but differences in onset temperatures between different polypropylene grades are thought to reflect inherent tacticity differences between them.

(iii) Effect Of Quenching From The Melt At A Controlled Rate In The DSC Furnace

The appearance of more than one peak in the melting profiles of quenched polypropylene was further investigated by extending the study to include the *in situ* quench cooling of the molten polypropylene at a controlled rate in the DSC furnace itself.

It was found that quenching polypropylene from the melt at 200°C/min in the DSC furnace induces structural changes in the samples which are reflected in the subsequent melting profiles which exhibit four distinct melting peaks. X-ray diffraction of these samples shows that only the monoclinic phase is present and therefore this quench rate is considered insufficiently fast to induce formation of the smectic phase.

In studying this quadruple endotherm a variety of conditions were employed in order to establish its origin. These were, effect of different melt times prior to quenching, the effect of different heating rates subsequent to quenching, different quenching rates from a melt temperature of 200°C and annealing of samples quenched from the melt at 200°C/min. From these results the following conclusions can be drawn:-

(a) Different holding times in the melt at 200°C has very little effect on the resultant quadruple endotherm and it was found that holding for 5 minutes at this temperature was sufficient to destroy any previous thermomechanical history and provide samples with a new common thermal history.

(b) At very slow heating rates subsequent to quenching (1°/min and 5°C/min), there is a tendency towards a single broad melting endotherm which occurs at a higher temperature (165°C). A single endotherm is also obtained using higher heating rates (20°C and 30°C) but the melting endotherm in this instance is relatively sharp in nature and occurs at a slightly lower temperature (160°C). The intermediate heating rate of 10°C/min appears to be the optimum rate at which resolution of the quadruple endotherm is produced since, unlike the fast heating rates, it is slow enough to enable partial melting and recrystallisation and, unlike the slowest heating rates, is fast enough to obtain a signal for this process in the DSC thermogram.

(c) High quenching rates (350°, 300°, 250°, 200° and 150°C/min) from a melt temperature of 200°C exhibit the customary quadruple endotherm which becomes less resolved with decreasing quenching rate. At quench rates of 20°C/min and 15°C/min, three relatively poorly resolved peaks are obtained and at a quenching rate of 10°C/min, two peaks are obtained (although the high temperature peak now exists mainly as a slight shoulder). At a quenching rate of 5°C/min, only a single relatively sharp endotherm is resolved. X-ray results show that the structure of the samples quenched at various rates consists of molecules in the monoclinic unit cell arrangement only and hence even the fastest of these quench rates is unable to induce smectic phase formation. At the lower quench rates, the crystallites have time to form stable, ordered structures during cooling and therefore undergo less recrystallisation and partial melting on reheating whilst at the higher quench rates there is more disorder in the crystallites which consequently leads to a higher degree of recrystallisation and partial melting which ultimately results in the quadruple melting endotherm.

(d) Annealing of samples quenched from the melt at 200°C/min at increasing increments of 10°C from 30°C to 150°C results in the progressive disappearance of the quadruple endotherm. Annealing temperatures of 30-70°C, have very little effect on the appearance of the quadruple endotherm. At T_a = 80-100°C, three peaks are observed with the highest temperature peak appearing shoulder-like in nature. At T_a = 110-140°C, two peaks remain which tend towards a single endotherm as T_a increases until, finally, at T_a = 150°C, only a single relatively sharp endotherm remains. As T_a increases, then, the disordered crystallites formed on quenching are able to undergo structural reorganisation from the disordered α_1-limiting modification towards the more stable, higher order α_2-limiting modification.

It is believed, then, that the origin of the quadruple endotherm lies in a quench induced distribution of metastable crystallites in the α_1-limiting modification which on reheating at an intermediate heating rate, strive for perfection towards the α_2-limiting modification by undergoing a partial melting and recrystallisation process.

(iv) Fractionation Of Isotactic Polypropylene

Having established that quench induced structural changes in polypropylene lead to multiple endotherms in subsequent melting profiles, it was decided to investigate this further by separating polypropylene into its component molecular weight/tacticity fractions by a stepwise solvent extraction procedure. These fractions were to be used in order to establish the role of molecular weight/tacticity in the behaviour of crystallites, subsequent to a special annealing process which was capable of inducing very reproducible distinct multiple endotherms in the melting profile of polypropylene.

In these studies, two fractionation procedures were investigated, namely, the Soxhlet extraction and the reflux extraction procedures. Due to the reproducibility of good quality fraction yields using the reflux fractionation method, this became the preferred method which, although simple in concept, proved to be very efficient.

Several techniques were employed in order to assess the quality of the fractionated polypropylene in terms of separation on the basis of molecular weight and tacticity. These included GPC, ^{13}C-nmr, FTIR APRA, density measurements, DSC melting and crystallisation, x-ray diffraction and hot-stage polarised light microscopy. From the results the following conclusions can be made about the polypropylene fractions obtained:-

(a) Molecular weight averages for the fractions increase in an exponential manner with respect to fractionation temperature. The molecular weight averages for the GSE18 homopolymer were found to be higher than those of even the highest molecular weight fraction obtained. It is feasible that this may be due to thermal breakdown of high molecular weight chains during fractionation since it is the $\overline{M}_w$ and $\overline{M}_z$ values which are most affected

(b) ^{13}C-nmr results show a progressively higher degree of peak splitting in the methylene, methine and methyl regions of the spectra of the polypropylene fractions as the molecular weight of the fractions decreases. Analysis of the methyl region peak integrals showed that as the fractionation temperature increases, the relative concentration of *mmmm* isotactic pentads stereosequences becomes higher whilst the concentration of non-isotactic and less regular pentad stereosequences decreases. The supposedly atactic ether fraction and the poorly crystalline pentane fraction were found to consist of a relatively large proportion of *rrrr* syndiotactic polypropylene stereosequences which were interspersed in a distribution of stereoblock sequences.

(c) FTIR APRA analysis of the fractions revealed a general increase in the concentration of both short and long isotactic helices (as measured by the A998/A973 and A841/A973 absorption ratios respectively) as the fractionation temperature increased. This corroborates the ^{13}C-nmr results which suggest that fractionation proceeds on the basis of both molecular weight and stereoregularity.

(d) Further confirmation of fractionation on the basis of stereoregularity is provided by relative crystallinities derived from density, DSC and x-ray results.

(e) Hot-stage polarised light microscopy photographs show clear differences in the crystallisation behaviour in terms of spherulitic growth and degree of perfection of sherulites between the fractions obtained at low fractionation temperatures and those obtained at higher fractionation temperatures.

In general, these results show quite clearly that fractionation by the reflux extraction procedure provides good quality and reproducible fractions which are separated on the basis of both molecular weight and stereoregularity which seem to possess a high degree of interdependence. Furthermore, results from the various characterisation methods used show good correlation with ^{13}C-nmr results (which is generally accepted to be an absolute technique for structure determination).

(v) Role Of Molecular Weight/Tacticity Fractions In The Thermal Behaviour Of Polypropylene

Samples of fractionated GSE18 polypropylene were subjected to a stepwise downward annealing procedure which reproducibly induces the formation of discontinuous crystallite clusters and results in several discrete melting regions in the DSC thermogram of polypropylene, the number of which is dependent on the number of annealing steps.

This multiple endotherm DSC profile arises as a consequence of crystallite clusters which would ordinarily have melted at a temperature a few degrees higher than the annealing temperature (T_a) being able to grow in perfection and undergo lamellar thickening. On subsequent reheating runs, these discrete crystallite clusters melt at a temperature which is approximately 10°C higher than the corresponding annealing temperature. Armed with this knowledge, the crystallite distributions in the polypropylene fractions were used to reveal information on the role of molecular weight/tacticity on the appearance of multiple peaks in polypropylene.

The conclusions from this study are as follows:-

(a) The relative percentage of discrete crystallite clusters formed at the various annealing temperatures is highly dependent on the molecular weight/tacticity of the sample.

(b) The high molecular weight/tacticity octane and toluene fractions exhibit a structure modification in which the majority of crystallites are able to achieve perfection at the highest annealing temperature of 160°C and hence melt at around 172°C.

(c) The intermediate molecular weight/tacticity heptane fraction shows a higher proportion of its crystallites achieving perfection at annealing temperatures below 160°C, the majority of which melt at temperatures corresponding to T_a = 150°C and 140°C.

(d) The low molecular weight/tacticity hexane fraction has only one small annealing induced cluster of perfected crystallites which melt at a temperature corresponding to an annealing temperature of 120°C. All other crystallites for this fraction are considered to be in the molten state at this temperature and hence unable to grow or achieve increased order. The molecular weight and isotacticity content of this fraction, then, is insufficiently high to enable the formation of discrete crystallite clusters at higher annealing temperatures than 120°C.

(f) The very low molecular weight/tacticity ether and pentane fractions produced very weak signals and as such were considered to be composed entirely of molecules incapable of producing multiple peaks subsequent to stepwise downward annealing.

(g) Stepwise downward annealing carried out on the GSE18 polypropylene homopolymer exhibited a profile similar to that of the toluene and octane fractions but had relatively less crystallite clusters achieving perfection at T_a = 160°C. This is due to the fact that it represents all of the fractions mixed together, hence the intermediate nature of its crystallite distribution.

Successive downward annealing of the fractions has therefore highlighted the role of molecular weight and stereoregularity in the formations of crystallites which possess different degrees of order and which are capable of forming discrete clusters which melt in a discontinuous manner at temperatures corresponding to the annealing temperature.

6.2 STUDIES ON BLENDS OF ISOTACTIC POLYPROPYLENE WITH AMORPHOUS POLY-α-OLEFIN TERPOLYMERS

Studies reported in this thesis involving isotactic polypropylene homopolymer have shown it to be susceptible to various thermally induced structural changes, some of which may ultimately affect the polymer properties. Since polypropylene is often modified by melt blending with other polymer systems to obtain desired properties (such as blending with an elastomer in order to enhance impact properties), it was decided to investigate the effect of some of the thermal treatments, previously discussed on such a system. The blends studied were those involving a commercial isotactic polypropylene manufactured by Shell with amorpous ethylene-propylene-butene-1 terpolymers high in propylene content. This provided an alternative morphology to that of the polypropylene homopolymer in which to investigate the effects of thermal treatment.

Investigations into the miscibility of the blend components and general characterisation of the various blends and blend compositions were carried out. The effect of rapid quenching from the molten state on the blends was studied as was the effect of temperature on the infrared spectra of the blends. Finally the behaviour of the co-crystallised crystallite distribution of the blends was investigated using the stepwise downward annealing procedure.

(i) Miscibility Of The Blends

Equal weights of Shell isotactic polypropylene and Vest703 encapsulated side by side in a DSC sample pan were found to undergo a considerable degree of "self-mixing" in the molten state as evidenced by the crystallisation behaviour on subsequent heat/cool

cycles. Hot-stage polarised microscopy was also used to investigate this behaviour. From these studies, the following conclusions can be made:-

(a) Successive heat/cool cycles in the DSC reveal a tendency towards a single crystallisation exotherm as more and more "self-mixing" occurs. After 14 heat/cool cycles the low temperature crystallisation peak disappears and a single endotherm which suggests co-crystallisation remains.

(b) Hot-stage polarised microscopy of the two components melted side by side on a microscope slide show that on successive heat/cool cycles, "self-mixing" occurs. This is evidenced by a depletion of the interface between the highly crystalline and well formed isotactic polypropylene spherulites and the poorly formed Vest703 terpolymer spherulites which eventually leads to a homogenous mix exhibiting the formation of "blend spherulites".

From these results the compatibility of the blends is seen to be very good. It is proposed that this is aided by the fact that isotactic polypropylene segments from the terpolymer are capable of becoming part of the isotactic polypropylene matrix by co-crystallising with the isotactic helices from the homopolymer. It is suspected that the amorphous terpolymer material is accomodated at either spherulitic boundaries, between radial rods which contain the stacked lamellae, between individual lamellae or, indeed, in all of these morphological regions. The homogeneity of the blends means that no compatibilisers are necessary and the system is therefore considered to have an intrinsically determined morphology.

(ii) General Characterisation Of Shell:Vest Blends

Several techniques including FTIR, density, x-ray diffraction and DSC were used to characterise the Shell:Vest blends involving all three terpolymer blends. From the results the following conclusions can be made:-

(a) FTIR APRA and density results show that the densimetric crystallinity of the blends increases as the concentration of both short and long isotactic helices in the blends increases. This is reflected in the crystallisability of the 100% Vest terpolymer samples which was found to decrease in the following manner:-

Vest703 > Vest750 $\geqslant$ Vest708

(b) X-ray diffraction profiles of the various blend compositions are all of isotactic polypropylene origin. As the proportion of isotactic polypropylene in the blend increases, the terpolymer peak at 2θ equal to 16.00° diminishes and the peak at 2θ equal to 17.00° becomes a singlet. Furthermore, the terpolymer peak at 21.50° splits to form a doublet as the isotactic polypropylene content increases. Adding even small amounts of isotactic polypropylene has a marked affect on the x-ray diffractogram of the blends.

(c) Molecular weight averages increase with increasing isotactic polypropylene content in the blends. Also, in terms of terpolymer type in the blends, the molecular weight averages increase in the order:-

Vest703 < Vest708 < Vest750

Polydispersity ratios were much higher for the blends compared to the corresponding 100% Shell isotactic polypropylene and 100% Vest terpolymers. This is due to the fact that blending a low molecular weight polymer with a relatively high molecular weight polymer leads to an increase in the breadth of chain length distribution.

(d) Blending Shell isotactic polypropylene with Vest terpolymer leads to a decrease in DSC melting onset and the appearance of a shoulder-like profile which tends towards a single broad melting endotherm as the Vest content of the blend increases. The peak temperature occurs at a temperature intermediate between the the main peak and the shoulder exhibited in the previous blend compositions. Even when a relatively high proportion of Vest terpolymer is present in the blend, the melting temperature is found to be nearer that of isotactic polypropylene than that of the pure Vest terpolymer. This suggests that a degree of co-melting of the components takes place. The shoulder-like profile is attributed to the melting of poorly formed crystallites which stem from the co-crystallisation of terpolymer isotactic polypropylene segments with the isotactic polypropylene homopolymer. As expected, ΔH_f values decrease with increasing Vest terpolymer content of the blends.

(e) All crystallisation profiles exhibit only one exothermic peak suggesting that complete co-crystallisation of the components has taken place. Increasing Vest terpolymer content of the blend leads to a broader, less intense peak which is shifted to a lower temperature. Again, a relatively small amount of isotactic polypropylene

homopolymer added to the 100% Vest terpolymer results in a large increase in its crystallinity. The broad crystallisation peak in the samples having a relatively high Vest terpolymer content reflect the results for the corresponding melting endotherm and support the argument for the formation of a distribution of less perfect co-crystallised crystallites on blending of the two components.

In general, these characterisation results corroborate the results of the miscibility study and suggest a high degree of compatibility. Properties exhibited by the blend obviously depend to a large extent on the blend composition and the grade of terpolymer used.

(iii) Quenching Of The Shell:Vest703 Blends Rapidly From The Melt

FTIR APRA, density and x-ray diffraction were used to investigate the behaviour of the Shell:Vest703 blend structures when rapidly quenched from the molten state into quench media of various temperatures. From the results, the following conclusions can be made:-

(a) No separation via a process of preferential crystallisation of blend components occurs on rapid quenching from the molten state.

(b) Long and short isotactic helices in the blends are affected in much the same way with respect to quench temperature, that is, they show a decrease in concentration as the quench temperature is decreased.

(c) The rate of helical loss is indicated by the steepness of the slope in the graph of absorption ratio versus temperature and, in general, blends containing a higher proportion of isotactic polypropylene have steeper gradients than those blends containing a high Vest terpolymer content, which tend to exhibit rather shallow gradients.

(d) At quench temperatures less than -50°C, there appears to be no further decrease in helical content and in some cases the absorption ratio value increases over that obtained for the previous quench temperature. This behaviour is attributed to a pocket of gas which is formed around the hot sample as it is plunged into quench baths at temperatures of -110°C and -190°C and which insulates it from the true temperature of the quench medium. X-ray crystallinities for the various blend compositions quenched into ice/water (0°C) and liquid nitrogen (-190°C) show very similar absorption ratio values. This suggests that the "gas insulated" samples quenched into liquid nitrogen experience a true quench temperature of not much less than 0°C. Density measurements also show an increase in values below temperatures of -50°C which corroborates this theory.

The behaviour of the blends when rapidly quenched form the melt, then, is very similar to that of the isotactic polypropylene homopolymer in that the co-crystallised ternary helices are converted to the conformationally disordered state and the extent of change in the concentration of isotactic helices with respect to quench temperature is dependent on blend composition and grade of terpolymer used.

(v) Effect Of Temperature On The Infrared Spectra Of Shell:Vest703 Blend Samples.

Further insights into the behaviour of the isotactic helices in the Shell:Vest703 blends were obtained from the study of the infrared helical bands at increasing temperature increments of 10°C between 30°C and the temperature at which film melting prevents further infrared spectroscopic measurements being recorded. Graphs of absorption ratio (A998/A973 and A841/A973) were plotted against temperature and from the results, the following conclusions can be made:-

(a) A linear decrease in absorption ratio value is exhibited for both the A998/A973 and A841/A973 ratios with respect to temperature. At 30-40°C below the temperature at which film melting prevents further infrared measurements, a transition exists which is characterised by a rapid increase in the rate of helical loss as the temperature increases. This transition occurs at a progressively lower temperature as the Vest703 content of the blend increases. The pre-transition linear portion of the graph shows a higher rate of disappearance of shorter isotactic helices as measured by the A998/A973 ratio than the longer isotactic helices measured by the A841/A973 ratio.

(b) The rate of decrease in helical material after the transition becomes less as the Vest703 terpolymer content of the blend is increased. This is indicated by the appearance of shallower post-transition gradients and is attributed to the fact that the relatively poorly formed co-crystalline structures in these samples are more easily extinguished.

(c) Comparisons of the plots of A998/A973 and A841/A973 versus temperature for each blend composition, in general, show that the post-transition rate of decrease in both short and long isotactic helices is almost identical.

(d) Both crystalline and non-crystalline helices may be affected by temperature. As the Vest703 content increases, it is likely that the presence of non-crystalline helical material also increases. This non-crystalline helical material will be preferentially extinguished leaving an increasingly smaller concentration of crystalline helices to be extinguished at the transition temperature, hence the shallower gradient.

(v) Stepwise Downward Annealing Of The Blends

Using stepwise downward annealing on the various blends, it was possible to obtain information on the behaviour of the co-crystallised structures in terms of crystallite distribution. Blends involving Shell:Vest703, 708 and 750 were subjected to the stepwise downward annealing procedure and from the results, the following conclusions can be made:-

(a) All blends behave similarly to the isotactic homopolymer in terms of the amount and positioning of seperate melting peaks induced by the annealing program.

(b) Shell:Vest, 75:25 blends for all Vest terpolymer grades show an increase in the percentage of the total ΔH_f being attributed to crystallites melting at a temperature corresponding to an annealing temperature of 160°C over the corresponding percentage for the 100% Shell isotactic polypropylene. This difference becomes larger as the molecular weight of the Vest terpolymer used is increased and is therefore attributed to the perfection of crystallites formed by co-crystallisation with higher molecular weight Vest terpolymer.

(c) The peaks associated with annealing temperatures of 140°C, 130°C and 120°C are relatively constant throughout the various blends and constitute 5-7%, 2-4% and 1-2% of the total ΔH_f respectively.

(d) The peaks associated with annealing temperatures of 150°C and 160°C are the most sensitive to changes in blend composition and grade of Vest terpolymer in the blends. The relative percentage of total ΔH_f attributed to the melting of crystallites perfected at T_a = 160°C decreases with increasing Vest terpolymer content in the blends and a corresponding increase in the percentage of the total ΔH_f attributed to the melting of crystallites perfected at T_a = 150°C is also observed as the Vest content of the blend is increased. The blend compositions involving the highest molecular weight terpolymer grade, Vest750, show a higher tendency towards the perfection of crystallites at T_a = 160°C than that of the blends involving the Vest708 terpolymer which in turn shows a higher tendency toward this behaviour than the blends involving the Vest703 terpolymer. This further confirms previously discussed conclusions stressing the dependency of the resultant profile of stepwise downward annealed samples on molecular weight.

(e) The subsequent melting profiles of stepwise downward annealed 100% Vest703, 708 and 750 terpolymer samples are relatively featureless compared to those of the blends. The Vest703 sample did show the presence of crystallites capable of forming clusters which melted at temperatures corresponding to annealing temperatures as high as 140°C but the Vest708 and 750 samples show no crystallites capable of perfection at any of the annealing temperatures used. This is because the samples are completely molten even at temperatures as low as 120°C. These results support

previously discussed characterisation results showing the crystallisability of the three Vest terpolymers to be highest in the Vest703 terpolymer followed by the Vest750 and Vest708 which have similar crystallisabilities.

The most striking feature of the Shell:Vest terpolymer blends is the remarkable ability of the components to co-crystallise. Results show that the behaviour of the blends is very similar to isotactic polypropylene in origin even in blends with high Vest terpolymer contents. This surely has implications as to the use of these blends for processing into commercial products although further testing on mechanical properties would be required.

6.3 SUGGESTIONS FOR FURTHER WORK

Polymer research is relatively new at Dundee Institute of Technology and this project is the first of what is hoped will be many research projects involving polypropylene and which will ultimately provide a service to local polypropylene processors. As such this project forms the very first building blocks on which to establish a solid base for continued research.

This project has concentrated on aspects of thermal treatment of polypropylene and gaining an understanding of consequent structural behaviour. Much of this research has focussed on the rapid crystallisation of the polymer whether it be directly from the melt or from a predetermined annealing temperature. Thermally induced structural changes are a very important area of study in polypropylene since melting and subsequent cooling are fundamental features of processing.

Possibilities for further work would be to extend the study of structural changes in polypropylene rapidly quenched from the melt by investigating the effect on the

polypropylene subsequent to flat-tape extrusion in a laboratory extruder. In this form a degree of orientation would be present and the dimensions of the samples would allow the study of mechanical properties of the thermally treated polypropylene samples.

Results reported in this study have shown a dependence of quench induced structure on molecular weight and tacticity of polypropylene. Using reactive degradation of polypropylene to control the molecular weight and presumeably the tacticity of the material during extrusion it would be interesting to examine quench induced structural changes in controlled molecular weight, oriented tapes. Molecular weight could be monitored by the recent development of a modular high temperature GPC system in the laboratories of the Molecular and Life Sciences Department at Dundee Institute of Technology. Furthermore, the crystallisation kinetics of controlled molecular weight polypropylene samples could be investigated using both DSC and hot-stage polarised microscopy.

Extensions of this work could involve the assessment of the processability and thermal properties of isotactic polypropylene/amorphous ethylene-propylene-butene-1 blends. Optimum blend compositions for the enhancement of mechanical properties could be investigated. Melt rheology of the blends would undoubtedly play a large role in their processability. Using a laboratory rheometer to study this would therefore provide useful insights into the flow properties of the material.

Polypropylene tapes produced under conditions of varying quench temperature, orientation, blend composition, degrees of molecular weight control and annealing could be investigated for mechanical properties and optimum processing conditions defined.

7.0 REFERENCES

7.0 REFERENCES

1. H.F. Mark, Preface in *History of Polyolefins*, Eds. R.B. Seymour, T.Cheng, Reidel Publishing Co, Dordrecht, Holland, (1985).

2. A.M. Butlerov and V. Goryainov, *J. Russ. Chem. Soc.*, **5**, 302, (1873).

3. A.M. Butlerov and V. Goryainov, *J. Russ. Chem. Soc.*, **9**, 38, (1877).

4. R.B. Seymour in *Advances In Polyolefins. The World's Most Widely Used polymers.*, eds. by R.B. Seymour and T. Cheng; Plenum Press, New York, (1987).

5. C.M. Fontana and G.A. Kidder, *J. Am. Chem. Soc.*, **70**, 3745, (1948).

6. C.M. Fontana, G.A. Kidder and R.J. Herold, *Ind. Eng. Chem.*, **44**, 1688, (1952).

7. C.M. Fontana, R.J. Herold, E.J. Kinney and R.C. Miller, *Ind. Eng. Chem.*, **44**, 2955, (1952).

8. C.M.Fontana, *J. Phys. Chem.*, **63**, (1959).

9. G.Natta, P.Pino, P. Corradini, F. Danusso, E. Mantica, G. Mazzanti and G. Moraglio, *J. Am. Chem. Soc.*, **77**, 1708, (1955).

10. Interference No. 89,634, initiated by the *U.S. Patent and Trademark Office*, Sept. 9, (1958).

11. G.Natta, *U.S. Pat.* 3,715,344 assigned to Montecatini Corp, (1972).

12. *U.S. Patent Quarterly*, P:676 Civil Action Suit 4319, January 11, (1980).

13. J.P. Hogan and R.L. Banks, *U.S. Pat.* 4,376,851 (1983) assigned to Philips Petroleum Co.

14. R.B. Seymour, *Pop. Plast. Packag.*, **34**, 51-3, (1989).

15. G. Natta, I. Pasquon and E. Giachetti, *Chem. Ind. (Milan)*, **39**, 993, (1957).

16. *Brit. Plastics*, **38**, 213, (1965).

17. Montecatini, *Belg. Pat.* 538,782 (1954).

18. J.A. Brydson, *Plastics Materials*, 4th Edition, Butterworth Scientific, (1982).

19. S.I. Shah, *Chem Age India*, **38**, 111, (1987).

20. Y.V. Kissin, *Isospecific Polymerisation Of Olefins With Heterogenous Zeigler-Natta Catalysts*, Springer-Verlag, New York, (1985).

21. G.W. Parshall, *Homogenous Catalysis, The Applications and Chemistry Of Catalysis By Soluble Transition Metal Complexes*, Wiley, New York, (1980).

22. A. Zambelli in *Coordination Polymerisation*, Ed. by J.W.C. Chien, Academic Press,New York, (1975), p15.

23. G. Natta, I. Pasquon, A. Zambelli, *J. Am. Chem. Soc.*, **84**, 1488, (1962).

24. N.J. Mills, Plastics: Microstructure, Properties And Applications (Metallurgy And Materials Science Series), Eds. R.W.K. Honeycombe and P. Hancock, Edward Arnold, London, (1986).

25. F.W. Billmeyer Jr., *Textbook Of Polymer Science*, 3rd Edition, Wiley, New York (1984).

26. F. Rodriguez, *Principles Of Polymer Systems*, McGraw-Hill, New York, (1970).

27. J. Frados, *Plastics Engineering Handbook*, Van Nostrand Rheinhold, New York, (1976).

28. *Comprehensive Polymer Science: The Synthesis, Characterisation, Reactions And Applications Of Polymers*, Pergamon Press, (1989), Vol. 7.

29. *Films, Woven And Non-Woven Fabrics Made From Polypropylene*, Verlag, Bonn, (1979).

30. Hans-Georg Elias, *Macromolecules: Synthesis, Materials And Technology*, 2nd Edition, Plenum Press, New York, (1984).

31. C. Hall, *Polymer Materials: An Introduction For Technologists And Scientists*, 2nd Edition, MacMillan, (1989).

32. C.T. Greenwood and W. Banks, *Synthetic High Polymers*, Oliver and Boyd Ltd, Edinburgh, (1968).

33. H. Staudinger, *Die Hochmolekurene Organischen Verbindungen, Springer-Verlag*, Berlin, (1932).

34. T. Alfrey, A. Bartovics and H. Mark, *J. Am. Chem. Soc.*, **65**, 2319, (1943).

35. M.L. Huggins, *J. Am. Chem. Soc.*, **66**, 1991, (1944).

36. C.E. Schildknecht, S.T. Gross, H.R. Davidson, J.M. Lambert and A.D. Zoss, *Ind. Eng. Chem.*, **40**, 2104, (1948).

37. C.E. Schildknecht, S.T. Gross and A.O. Zoss, *Ibid.*, **41**, 1998, (1949).

38. G. Natta and P. Corradini, *J. Polym. Sci.*, **20**, 251, (1956).

39. G. Natta, *Ibid.*, **16**, 143, (1955).

40. G. Natta, *Makromol Chem*, **16**, 213, (1955).

41. R.B. Seymour and C.E. Carraher, *Structure-Property Relationships In Polymers*, Plenum Press, New York, (1984).

42. G. Natta and P. Corradini, *J. Polym. Sci.*, **39**, 29, (1959).

43. G. Natta and P. Corradini, *Suppl. Nuovo. Cimento.*, **15**, 40, (1960).

44. T. Shimanouchi, *Pure Appl. Chem*, **12**, Pt 1-4, 287, (1966).

45. P. Corradini, *Proc. Robert A. Welch Found., Conf. Chem. Res.*, **10**, 91, (1966).

46. R.K. Agarwal, J. Horska, J. Stejskal, O. Quadrat and P. Kratochvil, *J. Appl. Polym. Sci.*, **28**, 3453, (1983).

47. D.R. Morrow, *J. Macromol. Sci. Phys.*, **3**, Pt. 1, 53, (1969).

48. E.J. Addink and J. Bientema, *Polymer*, **2**, Pt.2, 185, (1961).

49. H.D. Keith, F.J. Padden Jr., N.N. Walter and H.C. Wyckoff, *J. Appl. Phys.*, **30**, 1485, (1959).

50. G. Natta, *Irish Patent Application*, 430/60, (filed June 1960).

51. R. Napolitano, B. Pirrozi and V. Varriale, *J. Polym. Sci. Pt B., Polym Phys*, **28**, 139, (1990).

52. A. Turner-Jones, J.M. Aisleswood and D.R. Beckett, *Makromol. Chem.*, **75**, 134, (1964).

53. M. Hikosaka and T. Seto, *Polym. J.*, **5**, 111, (1973).

54. A. Turner-Jones and A.J. Cobbold, *Polym. Letters*, **6**, 539, (1968).

55. S.V. Meille, S. Bruckner and W. Porcio, *Macromolecules*, **23**, 414, (1990).

56. A. Turner-Jones, *Polymer*, **12**, 487, (1971).

57. B. Lotz, S. Graff and J.C. Wittmann, *J. Polym. Sci., Pt. B, Polym. Phys.*, **24**, 9, 2017, (1986).

58. M.R. Morrow and B.A. Newman, *J. Appl. Phys.*, **39**, 4944, (1968).

59. W.R. Thompson, *Modern Plastics*, **63**, 10A, (1986).

60. B. Greek, *Chem Eng News*, **64**, 17, (1986).

61. W.R. O'Donnel, *Am Dyestuff Reporter*, **54**, 25, (1965).

62. A.G. Mash, *European Plastics News*, **July/August**, p11, (1991).

63. Plastics And Rubber Institute, *4th Int. Conf. On Polypropylene Fibres And Textiles*, **23-25 Sept.**, p1/4, (1987).

64. Unpublished private discussions with R.G. Hillier, ICI Wilton, (Sept. 1991).

65. *European Plastics News*, **July/August**, 13, (1991).

66. Unpublished private correspondence with D. Raspin, ICI Wilton, (Sept. 1991).

67. S. Bhagavantam and T. Venkatarayudu, *Theory Of Groups And Its Application To Physical Problems*, 3rd Edition, Andhra University, Waltair, (1962).

68. L.A. Woodward, *Introduction To The Theory Of Molecular Vibrations And Vibrational Spectroscopy*, Clarendon Press, Oxford, (1972).

69. G. Turrell, *Infrared And Raman Spectra Of Crystals*, Academic Press, London, (1972).

70. W.H. Steel, *Interferometry*, 2nd Edition, Cambridge University Press, (1983).

71. P.R. Griffiths, *Transform Techniques In Chemistry*, Heydon and Sons Ltd, (1986).

72. P.R. Griffiths and J.A. De Haseth, Fourier Transform Infrared Spectroscopy, Wiley, New York, (1986).

73. R.B. Cassel, *Am. Lab.*, **7**, 9, (1975).

74. S.L. Boersma, J. Am. Ceram. Soc., **38**, 281, (1955).

75. J.L. McNaugton and C.T. Mortimer, *Differential Scanning Calorimetry*, Reprint **L604**, Perkin-Elmer Corp.

76. D.R. Burfield, P.S.T. Loi, Y. Doi, and J. Mejzik, *J. Appl. Polym. Sci.*, **41**, 1095, (1990).

77. D.R. Burfield and P.S.T. Loi, *Macromolecules*, **16**, 702, (1983).

78. D.R. Burfield, and Y. Doi, *Polymer Communications*, **24**, 48, (1983).

79. M. Mucha, *J. Polym. Sci., Polym. Symp.*, **69**, 79, (1981).

80. J. Varga, J. Therm. Anal., **35**, 1891, (1989).

81. T.A. Blazer and R.L. Blaine, *Therm. Anal. Proc. Int. Conf.*, **7th**, 1368, (1982).

82. J.M. O'Neill, *Anal. Chem.*, **38**, 1331, (1966).

83. D.R. Gee and T.P. Melia, *Makromol. Chem.*, **132**, 195, (1970).

84. M. Eder and A. Wlochowicz, *Polymer*, **24**, 1593, (1983).

85. M. Nural Huda, H. Dragaun, S. Bauer, H. Muschik, and P.Skalicky, Colloid and Polym. Sci., 263, 730, (1985).

86. B.D. Cullity, *Elements Of X-ray Diffraction*, Addison and Wesley, (1956).

87. M.M. Woolfson, *An Introduction To X-ray Crystallography*, Cambridge University Press, (1970).

88. W.H. Bragg and W.L. Bragg, *The Crystalline State*, Vol 1, Bell, London, (1949).

89. S.Z.D. Cheng, J. Janimak, A. Zhang and E.T. Hsieh, *Polymer*, **32**, 648, (1991).

90. A.J. Lovinger, J. Polym. Sci. Phys. Ed., **21**, 97, (1983).

91. J.C. Moore, *J. Polym. Sci.*, Pt A, **2**, 835, (1964).

92. *Comprehensive Polymer Science: The Synthesis, Characterisation, Reactions And Applications Of Polymers*, Pergamon Press, Vol. 1, p190 (1989).

93. H. Mark in *Der Fest Korper*, edited by R. Saenger, Hirzel, Leipzig, p103, (1938).

94. I. Sakurada, *Kasen-Koenshu*, **5**, 33, (1940).

95. R. Houwink, *J. Prakt. Chem.*, **157**, 15, (1940).

96. J. Brandrup and E.H. Immergut, Polymer Handbook, 3rd Edition, Wiley, New York, (1989).

97. Unpublished private discussions with A. Titterton, ICI Wilton, (May 1989).

98. Unpublished private discussions with S. Holding, RAPRA Technology Ltd., (March 1989).

99. S. Matsuoka, *Polym. Eng. Sci.*, **7**, 142, (1965).

100. R. Greco and F. Coppola, *Plast. Rubb. Proc. Appl.*, **6**, 35, (1986).

101. R.H. Olley and D.C. Basset, Polymer, **30**, 399, (1989).

102 T. Mulvey and R.K. Webster, *Modern Physical Techniques In Materials Technology*, Oxford University Press, (1974).

103. *Comprehensive Polymer Science: The Synthesis, Characterisation, Reactions And Applications Of Polymers*, Pergamon Press, Vol. 1, Chapter 34, (1989).

104. F. Rybnikar, *J. Appl. Polym. Sci.*, **30**, 1949, (1985).

105. F.C. Schilling and A.E. Tonnelli, *Macromolecules*, **13**, 270, (1980).

106. J.C. Randall, *J. Polym. Sci., Polym Phys. Ed.*, **14**, 2083, (1976).

107. A. Bunn, M.E.A Cudby, R.K. Harris, K.J Packer and B.J. Say, *Polymer*, **23**, 64, (1982).

108. J.C. Randall, *J. Polym. Sci., Polym. Phys. Ed.*, **13**, 1975 (1975).

109. D.R. Burfield and P.S.T. Loi, *J. Appl. Polym. Sci.*, **36**, 279, (1988).

110. V. Vittoria and F. Riva, *Macromolecules*, **19**, 1975, (1986).

111. F. De Candia, R. Russo and V. Vittoria, J. Appl. Polym. Sci., **34**, 689, (1987).

112. G. Natta, M. Peraldo and P. Corradini, *Rend. Acc. Naz. Lincei.*, **26**, 14, (1959).

113. R.I. Miller, *Polymer*, **1**, 135, (1960).

114. J.A. Gailey and R.H. Ralston, *SPE Trans.*, **4**, 29, (1964).

115. D.M. Gezovich and P.H. Geil, *Polym. Eng. Sci.*, **8**, 202, (1968).

116. C.C. Hsu and P.H. Geil, *J. Polym. Sci., Pt B: Polym. Phys.*, **24**, 2379, (1986).

117. G. Bodor, M.Grell and A. Kallo, *Faserforsch. Textil-Tech.*, **15**, 527, (1964).

118. P.B. McAllister, T.J. Carter and R.M. Hinde, *J. Polym. Sci, Polym. Phys. Ed.*, **16**, 49, (1978).

119. B. Wunderlich, and J. Grebowicz, *J. Adv. Polm. Sci.*, **60/61**, 1, (1984).

120. M.A. Gomez, H. Tanaka, and A.E. Tonelli, *Polymer*, **28**, 2227, (1987).

121. P. Corradini, C. De Rosa, G. Guerra and V. Petraccone, *Polymer Communications*, **30**, 281, (1989).

122. P.J. Hendra, J. Vile, H.A. Willis, V. Zichy and M.E.A. Cudby, *Polymer*, **25**, 785, (1984).

123. A. Fichera and R. Zannetti, *Makromol. Chem.*, **176**, 1885, (1975).

124. F. De Candia, R. Russo, V. Vittoria and P. Iannelli, *Polym. Eng. Sci.*, **28**, 974, (1988).

125. K. Abe and K. Yanagisawa, *J. Polym. Sci.*, **36**, 536, (1959).

126. W. Heinen, *J. Polym. Sci.*, **38**, 545, (1959).

127. J. Majer, *Coll. Czechoslov. Commun.*, **26**, 1756, (1961).

128. J.P. Luongo, *J. Appl. Polym. Sci.*, **9**, 302, (1960).

129. S. Krimm, *Adv. Polym. Sci.*, **2**, 51, (1960).

130. J. Brader, *J. Appl. Polym. Sci.*, **3**, 370, (1960).

131. R.H. Hughes, *J. Appl. Polym. Sci.*, **13**, 417, (1969).

132. M.P. McDonald and I.M. Ward, *Polymer*, **2**, 341, (1961).

133 G. Zerbi, F. Ciampelli and V. Zamboni, *J. Polym. Sci.*, **7**, 141, (1964).

134. H. Tadokoro, M. Kobayashi, M. Ukita, K. Yasufuku, S. Murahashi and T. Torii, *J. Chem. Phys.*, **42**, 1432, (1965).

135. V. Vittoria and A. Perullo, *J. Macromol. Sci. Phys.*, **B25(3)**, 267, (1986).

136. V. Vittoria, *J. Macromol. Sci. Phys.*, **B28(1)**, 97, (1989).

137. V. Vittoria, R.H. Olley and D.C. Basset, *Colloid Polym. Sci.*, **267**, 661, (1989).

138. G. Farrow, *J. Appl. Polym. Sci.*, **9**, 1227, (1965).

139. B. Ke, *J. Polym. Sci.*, **42**, 15, (1960).

140. K.D. Pae and J.A. Sauer, *J. Appl. Polym. Sci.*, **12**, 1901, (1968).

141. K. Kamide and K. Yamaguchi, *Makromol Chem*, **162**, 219 (1972).

142. R.J. Samuels, *J. Polym. Sci, Polym. Phys. Ed.*, **13**, 1417, (1975).

143. G. Guerra, C. De Rosa, V. Petraccone and A. Tuzi, *J. Therm. Anal.*, **30**, 1337, (1985).

144. P. Corradini, R. Napolitano, L. Oliva, V. Petraccone, B. Pirozzi and G. Guerra, *Makromol. Chem. Rapid. Commun.*, **3**, 753, (1982).

145. C. Passingham, P.J. Hendra, M.E.A. Cudby, V. Zichy, and M. Weller, *Eur. Polym. J.*, **6**, 631, (1990).

146. J.G. Fatou, *Eur. Polym. J.*, **7**, 1057, (1971).

147. P. Jacoby, B.H. Bersted, W.J. Kissel and C.E. Smith, *J. Polym. Sci., Pt. B, Polym. Phys.*, **24**, 461, (1986).

148. V.I. Selikhova, A.O. Baranov, Yu. A. Zubor, and N.F. Bakeyev, *Polym. Sci. USSR*, **31**, 804, (1989).

149. V. Petraccone, C. De Rosa, G. Guerra and A. Tuzi, *Makromol. Chem.*, **5**, 631, (1984).

150. G. Guerra, V. Petraccone, P. Corradini, C. De Rosa, R. Napolitano and B. Pirozzi, *J. Polym. Sci., Polym. Phys. Ed.*, **22**, 1029, (1984).

151 P. Corradini, G. Giunchi, V. Petraccone, B. Pirozzi and H.M. Vidal, *Gazz. Chim. Ital.*, **110**, 413, (1980).

152. K. Yamaguchi, H. Kojima and A. Takahashi, *Int. Chem. Eng.*, **5**, 169, (1965).

153. D.E. Thomas and R.L. Tobias, *J. Polym. Sci.*, **50**, 227, (1961).

154. J.E. Guillet, R.L. Combs, D.F. Slonaker, J.T. Summers and H.W. Coover, *SPE Trans.*, **2**, 164, (1962).

155. G. Natta, G. Mazzanti, G. Crespi and G. Moraglio, *Chim. e Ind.*, **39**, 275, (1957).

156. A. Nakajima and H. Fujiwara, *Bull. Chem. Soc. Japan*, **34**, 909, (1964).

157. H. Kawamura, T. Hayashi, Y. Inoue and R. Chujo, *Macromolecules*, **22**, 2181, (1989).

158. F.A. Bovey, *Polymer Conformation and Configuration*, Academic, New York, (1969)

159. T. Hayashi, A. Nishoika, R. Chujo and T. Asakura, *Polymer*, **29**, 139, (1988).

160. A. Zambelli, P. Locatelli, A. Pravasoli and D.R. Ferro, *Macromolecules*, **13**, 267, (1980).

161. Yu. V. Kissin, V.I. Tsvetkova and N.M. Chirkov, *Eur. Polym. J.*, **8**, 529, (1972).

162. G. Shi, B. Huang and J. Zhang, *Makromol. Chem., Rapid Commun.*, **5**, 573, (1984).

163. A.P. Gray and K. Casey, *J. Polym. Sci. B*, **2**, 381, (1964).

164. L. Bianchi, S. Cimino, A. Forte, R. Greco, E. Martuscelli, F. Riva, and C.J. Silvestre, *J. Mater. Sci.*, **20**, 895, (1985).

165. J. Karger-Kocsis, A. Kallo, A. Szafner, G. Bodor, and Zs. Senyei, *Polymer*, **20**, 37, (1979).

166. A.J. Tinker, *Polym. Commun.*, **25**, 325, (1984).

167. G. Heufer, *Kunststoffe*, **68**, 145, (1978).

168. K.C. Dao, *Polymer*, **25**, 1527, (1984).

169. J. Lohmar and K. Meyer, *Makromol. Chem., Makromol Symp.*, **16**, 161, (1988).

170. A. Kuhlne and L. Gross, *Technical Lecture, Lecture at the Eurobondex '89*, London, June 19-21, (1989).

171. D.J. Lohse and G.E. Wissler, *J. Mat. Sci.*, **26**, 743, (1991).

172. B. Pukanszky, F. Tudos, A. Kallo and G. Bodor, *Polymer*, **30**, 1399, (1989).

173. A. Wlochowicz and M. Eder, *Polymer*, **25**, 1268, (1984).

174. L.A. Hanna, P.J. Hendra, W. Maddams, H.A. Willis, V. Zichy and M.E.A. Cudby, *Polymer*, **29**, 1843, (1988).

8.0 APPENDICES

APPENDIX 1

Scheffé's S Test

Analysis of variance tests whether there is a difference between the mean levels of factors. A Scheffé S test can investigate where such differences occur.

Scheffé S test allows the analysis of a contrast and gives confidence limits valid for all contrasts.

If $\phi = \Sigma C_i\beta_i$ then we reject that there is no difference in levels if:

$$\hat{\phi} > (I-1)F_{\alpha(I-1),(h-1)(g-1)}\,\sigma_\theta$$

When ϕ = contrast

C_i= coefficients of β_i

β_i= theoretical population mean at level i

$F_{\alpha(I-1),(h-1)(g-1)} = F_{critical}$

I = no. of levels of the factor under consideration

$\hat{\phi}$ = estimates of $\phi = \Sigma C_i\beta_i$

β_i= estimates of $\beta_i = \Sigma Y_i/n_i$

σ_θ= standard error of $\hat{\phi} = \Sigma C_i^2\sigma^2/n$

σ^2= estimate of variance of residual error

APPENDIX 2

Tukey's Pairwise Comparison

In comparing k averages, supposing we wish to state the confidence interval for $\beta_i - \beta_j$, taking account of the fact that all possible comparisons may be made. It has been shown by Tukey that the confidence limits for $\beta_i - \beta_j$ are given by:-

$$(\bar{y}_i - \bar{y}_j) \pm q_{kv,v,\alpha/2}/\sqrt{2} \,.\, \sqrt{(1/n_i + 1/n_j)} \,.\, s$$

where q_{kv}, us the appropriate upper significant level of the studentized range for k means and v the number of degrees of freedom in the estimate s^2 of variance σ^2. This formula is exact if the numbers of observations in all the averages are equal and approximate if the averages are based on unequal numbers of observations.

For the preliminary study, $n_i = n_j = 10$, therefore differences were significant if:-

$$(\bar{y}_i - \bar{y}_j) > q_{k,v} \times 0.3162 \times s$$

In this case $q_{k,v} = 3.31$ and $s = \sqrt{0.000309}$

For the detailed study, $n_i = n_j = 5$, therefore differences were significant if :-

$$(\bar{y}_i - \bar{y}_j) > q_{k,v} \times 0.4472 \times s$$

In this case, $q_{k,v} = 4.29$ and $s = \sqrt{0.000875}$

NB. Values for $q_{k,v}$ and s were obtained from statistics tables and ANOVA tables respectively.